MEDICAL ULTRASOUND: MIRROR TRANSDUCER SYSTEMS FOR HIGH RESOLUTION IMAGING

JEREMY JOHN NICOLL.

PhD. University of Edinburgh. 1984.

This thesis has been composed by myself.
The work is my own and acknowledgement gratefully given
to those who have contributed to it.

Mr. R. Borthwick made the air-backed copper mirrors developing the necessary techniques himself and performed other mechanical work.

Messrs. T. Anderson and R. McHugh helped with electronic design and provided the transmitter and receiver circuits for the test tank.

Dr. J.M. Piggins designed the breast scanner and built it with the aid of Mr. G. Campbell.

Dr. Piggins and I shared the clinical scanning duties.

Dr. Piggins developed the ultrasonic method for aligning mirror systems.

The Special Techniques Laboratory of the Physics Department silvered the araldite mirrors.

I developed the numerical models from the sources given, wrote and ran the programs.

I performed the experiments described here.

Jeremy J Nicoll

"Our echoes roll from soul to soul,

And grow for ever and for ever."

The Princess.

Tennyson.

ABSTRACT

Resolution in medical ultrasound images depends largely upon beam width. Mirror systems are investigated as a means of strongly focussing beams in water bath scanners. Numerical models based on continuous wave theory were developed to aid development of a suitable system. Initially, the model was confined to simulating concave spherical bowl transducers but it was developed to simulate more complex shapes of mirror.

The design of air-backed, thin copper mirrors enabled the building of systems which are more sensitive than previous designs and which have a short pulse length for good axial resolution.

Several types of known mirror systems have been studied in depth to assess their suitability in medical imaging. A new design of modified Cassegrain mirror system was developed to give a pointed secondary reflector. This eliminates the reverberation of pulses between mirror components which has arisen in all previously described systems. This device gives a sharp focus over a limited depth of field and has sufficient dynamic range for studying small regions in great detail.

The numerical models are used to investigate possible developments of mirror systems. Particularly, methods of increasing the focal range are considered.

ACKNOWLEDGEMENTS

I wish to express my thanks to the many people who made this work possible.

Mr. R. Borthwick made the copper mirrors. Without his enthusiasm, skill and patience, the work would not have been possible.

Messrs. T. Anderson and R. McHugh helped with electronic design and provided transmitter and receiver circuits for the test tank. The Special Techniques Laboratory of the Physics Department silvered the araldite mirrors.

Doctors W. N. McDicken and J.M . Piggins provided help and guidance throughout.

Professor J. R. Greening supported the project from its inception.

I thank my friends David and Steve Pye for their comradeship in the Students Lab.

Finally I thank my mother for her forebearance while typing the manuscript.

THESIS SUMMARY

CHAPTER 1.

INTRODUCTION

This chapter introduces the thesis and the work contained in it.

The quality of an ultrasound image and the detail which may be seen in it depend upon the shape of the ultrasound beam. A decrease in beam width may be achieved by focussing. Increased resolution may be achieved by increasing the Numerical aperture or by increasing the frequency of the probe used. However a sharply focussed beam will give high lateral resolution only over a short depth. This short beam length is acceptable in C-scanning where only a short length of the beam is used. A short depth of focus may be sufficient for small parts scanning. In breast scanning it must be overcome in order to obtain the high resolution necessary for the early detection and identification of breast disease. If ultrasound is to make a contribution to breast examination generally it must be able to detect abnormalities $\sim$2 mm diameter.

An experimental water-bath breast scanner proves a good test-bed for a high resolution probe. Although easily accessible, breasts present a variety of scanning problems and great variation in ultrasonic appearance. The scanner is a research tool and is very adaptable mechanically and electrically. It is software controlled by a micro-processor but may be reprogrammed or used manually.

A summary of the principal probes discussed is given in section 1.4 and shown in figure 1.2. Two commercial probes, one a concave bowl transducer, one a planar transducer focussed by an epoxy lens are described. These serve as comparison both with the experimental results of the devices built and with the numerical result of the models used to study the effects of different parameters upon the transmitted field. A mirror system based on the design of a Cassegrain telesoope is considered but suffers from pulses reverberating between different components. A novel modification to the Cassegrain design overcomes this problem. A Herschel style mirror system is considered as a future development, as is an axicon mirror system which might overcome the problems associated with a short depth of field.

CHAPTER 2. APPROACHES TO A HIGH RESOLUTION TRANSDUCER

This is the base from which the work of the subsequent chapters develops. All the early decisions and the basis of them are presented here. The chapter is split into three main parts. The first deals with the constraints imposed on the devices both by the resolution desired and by the envisaged experimental application (the breast scanner); the second with possible transducer designs or systems and the third with the use of numerical models to assist in the design and development of such systems.

Numerical apertures up to, and perhaps beyond 0.25 will give improvements in resolution even in a heterogeneous organ like the breast (Foster and Hunt 1978, 1979). Water-bath scanning requires a long transducer to skin distance in order that reverberations of the skin echo do not interfere with the image. Using a focal length of 150 mm to allow for this together with a frequency of 5MHz, Fraunhofer diffraction theory suggests a resolution of 1 mm would be obtained with a Numerical Aperture of 0.185 corresponding to an aperture of diameter 55.5 mm.

Many approaches to such a device are possible and must be considered. A concave bowl transducer would be the simplest to understand but in practice it would be difficult to obtain and work with a large, fragile ceramic bowl. A plane disc transducer would be easier (but still difficult) to obtain. A good practical lens material is however not known. A stepped lens might be easier to design than a conventional lens but there would be secondary foci in the field which would make it unsuitable for pulse-echo scanning. The field from a Fresnel zone transducer would be similarly affected. Electronically focussed annular arrays are not suited to such large apertures. The largest aperture devices described to date have been mirror systems based upon the Cassegrain telescope. These offer very large apertures, great flexibility and are ideally suited to a water bath scanner. It is with the development and assessment of the style of device that the work is concerned.

The use of mirror systems offers great flexibility of design. A numerical model is required to demonstrate the effects of different parameters of the device upon the ultrasonic field. To do this usefully the model must be available quickly. An impulse response model, while offering, in a developed form, the most accurate mathematical representations of a device, would take a long time to develop. An analytical description of the transfer functions may not be available for most mirror shapes (e.g. a cone (Foster et al, 1981)), and such a complicated model may take prohibitively long to evaluate. A simple continuous wave (CW) model could be available quickly to assist device design. Initially simulating a concave spherical bowl with a circular aperture and a circular centre block (to simulate a secondary mirror) and written on a flexible program base it might be developed for a more detailed analysis of mirror geometry or to consider finite pulse lengths. It can be used to test different possible boundary conditions for the model itself

CHAPTER 3.

NUMERICAL MODELLING OF SIMPLE SPHERICAL BOWL TRANSDUCERS

This chapter describes the first and most basic of the numerical models. It meets the criteria derived in section 2.3. It is quickly available, it is quick to execute and is built on a flexible software base. It will demonstrate the general performance of large apertures, particularly it will show the effect that a central block, due to the secondary reflector of a mirror system, will have upon lateral beam shape. On the debit side it is a continuous wave (CW) model and the algorithms can only evaluate points on the system axis or in a plane through the geometrical focus.

Although this model is referred to as a spherical bowl transducer, this is a conceptual not a mathematical idea. The Green's function is the same whether the source is a uniformly transmitting or a uniformly reflecting spherical surface. Physically the same is true of the resulting field.

The mathematical interpretation of the surroundings will however affect the result and sections 3.1.1 and 3.1.2 describe the algorithm with Huygen's and Kirchoff's boundary conditions respectively. The evaluation of the two algorithms for large numerical apertures (section 3.4) shows the difference to be trivial and so the simpler Huygen's conditions may be used.

The shortcomings of the model are (i) it describes a continuous wave beam where in fact a pulsed wave (PW) beam is used; (ii) although the model can include some effects of apodisation by including the centre block due to the secondary of a mirror system, it does not model the geometry completely. Particularly since a mirror system cannot be made from spherical elements it does not allow for the non-uniform distribution of flux lines across the aperture which will result from the use of conic mirrors in a real system. Published work comparing CW and PW fields is considered in sections 2.3 and 3.5. Although no comparison is available for highly focussed devices it is concluded that the PW beam profile will be flatter topped than the CW and will be broader for the same decibel levels. The sidelobe structure seen in the CW beam will be smoothed out in the PW, the magnitude of the sidelobes being increasingly reduced as the pulse shortens. These published results are used to interpret the significance of CW results for PW fields. This model is used and discussed in Chapters 7 and 8 and in section 9.3

CHAPTER 4.

NUMERICAL MODELLING OF A POINT SOURCE/SINGLE MIRROR COMBINATION

This chapter describes a development of the model discussed in Chapter 3. The model is of a point source, placed on axis reflected by a single mirror. This mirror may have any analytic form but the improvement is intended to accommodate an accurate description of the primary reflector of a mirror system. Such a mirror would inevitably be based upon a conic, most probably an ellipsoid of revolution (prolate spheroid). This would result in the field being concentrated towards the outer edge of the aperture and this effect should be investigated in this thesis. This model can evaluate the field at any point. Huygen's boundary conditions, validated in Chapter 3, are used.

The model however is still CW and its representation of the geometry over-simplified. The transducer and secondary combined are seen as a point source. This means that the calculated field will not contain the spherical aberration that will be present in the experimental field. Beam width will be underestimated because of this.

This algorithm takes longer to evaluate than the previous one since a numerical, two-dimensional integration is required. Various approximations are considered which speed the execution of the program.

The model is used and discussed in Chapters 7 and 8.

A development of the program for studying Herschel style mirror system is described. It is employed in section 9.1.

CHAPTER 5.

EXPERIMENTAL BEAM PLOTTING

The experimental work is described and discussed in this chapter.

The first section describing the hardware built and used for beam plotting. The plotter is based on a 60 cm x 60 cm square water tank. A stepper motor is used to scan a target laterally across the beam. This is controlled by TTL logic and the result is output by an x-y plotter. Any axial movement of the target must be made manually. The transmitter and receiver circuits are of conventional design and may be used either for pulse-echo or for transmission field plotting. Peak capture is achieved by placing a sample and hold gate around the peak.

A bi-laminar PVDF hydrophone with an active area of 1 mm diameter is used for transmission field plotting. It is good for examining pulse shapes but is too big for plotting highly focussed beams. Spheres, because of their non-directional shape are good targets for pulse-echo plotting. A 2 mm diameter stainless steel ball is found to be sensitive enough to plot devices useful for diagnostic imaging. This is the smallest sphere that can be mounted rigidly enough for plotting. Although the plot is a convolution of ultrasonic field and target which may not be readily resolved, in general smaller targets show smaller beam widths. Comparison of Weyns (1980b) theoretical results and pulse-echo plots suggest the 2 mm target may still overestimate beam width by a factor of 1.7 (-6dB level) to 2.2 (-20dB level).

In order that they may be assessed in the light of the experimental technique results for the two commercial large aperture probes are given here. Comparison between the CW numerical model and experiment shows a factor of 2.7 difference in beam width. This is the combination of the difference between CW and PW models ($\sim$ 1.3) and between the PW model and the 2 mm diameter target pulse-echo plots ($\sim$ 2.2) found in section 5.2.

CHAPTER 6.

DESIGN AND CONSTRUCTION OF MIRROR SYSTEM COMPONENTS.

This chapter draws together all the practical problems and techniques required for constructing the mirror system. Although the need for all the techniques is not apparent from the mirror systems discussed in section 2.2.6 the summary of systems investigated (section 1.4) shows the basic designs. The techniques are presented in their final, most useful form.

A program using interactive graphics was written to assist with the design of mirror systems. It displays and produces hard copy of two conic sections, as well as listing coordinates of the curve. It uses the methods described in Appendix 1 for the description of conics and makes use of the fact that successive elements of conic mirror systems must share a common reference point. Because of this flexible base, principally the use of the eccentricity to describe the curves, the program proved readily adaptable to developing mirror designs.

Hollow, air-backed mirrors may be made by pressing thin copper sheets between male and female moulds in a process of repeated heating and annealing. Mirrors made in this way are highly reflective and do not seriously degrade the pulse. Other mirrors are made of a tungsten powder (2 mm diameter) epoxy resin (2.7:1 by weight) mixture using a wax moulding technique.

Three techniques, an optical method, an acoustical method (using the breast scanner) and a visual method (using a graticle) for aligning mirror system components are described.

CHAPTER 7.

A CASSEGRAIN MIRROR SYSTEM.

The first mirror system is built in the style of a Cassegrain telescope. Its purpose is to explore the viability of a mirror system and to test construction materials and techniques. It is designed with construction techniques as well as the final ultrasonic field in mind.

The primary mirror is ellipsoidal. The internal (common) reference point lies in the plane of the aperture (diameter 100 mm) and the external reference point is 66.7 mm from that. The secondary may be ellipsoidal or paraboloidal depending on whether a focussed or plane transducer is used. A hyperboloidal secondary is used if the mirror is to focus on reception only.

The two numerical models (spherical and elliptical mirrors) show widely different fields because of the different distribution of sound across the aperture. Both main lobes are well behaved responding as expected to apodisation and to increasing outer aperture diameter although the elliptical mirror main lobe is smaller initially and responds less to either effect. Neither are seriously enlarged by a 25 mm diameter central block.

The sidelobes predicted by ellipsoidal mirror model increase rapidly as the outer diameter of the aperture approaches its limit (the minor axis of the ellipse). Deep ellipsoidal mirrors must be avoided. A pulse-echo dynamic range of approximately -20dB is predicted.

Beam and pulse shape were investigated experimentally. Pulse shape was good (figure 7.24(b). No significant non-linear effects were observed. The two models show the 'perfect' wavefront from an ellipsoidal mirror (i.e. without spherical aberration) and a uniform spherical wavefront from the same aperture. In practice, the wavefront will be a combination of the two. If allowance is made for the error due to the use of a CW model and that due to the plotting target (as assessed in section 5.2), the beam shape is a compromise between these two limits.

Although in many respects the design and construction have been a success, in practice the system is not suitable for pulse-echo scanning. This is because of echoes reverberating between mirror components, mainly between the secondary and the transducer.

CHAPTER 8.

A MODIFIED CASSEGRAIN MIRROR SYSTEM.

A novel modification of the Cassegrain mirror system was developed. The common (internal) reference point of the two mirrors is offset from the system axis. Generation of the mirror surfaces by rotation about the axis gives rise to pointed mirrors. Pulses will not then reverberate between the secondary and the transducer.

The primary of this system has a design aperture of 88 mm diameter and the distance from transducer face to final focus is 150 mm.

Once again the numerical models are used to represent extreme cases of the wave front and to explore the response to changes in the size parameter describing the aperture. Since the Numerical Aperture of this device is smaller than the Cassegrain design (0.42) the difference in beam width between the two models is greater. A secondary mirror greater than 25 mm diameter will reduce the pulse-echo dynamic range to less than 20 dB.

Many experimental problems are found when aligning the new system and widespread variation in axial beam shape. Pulse length and amplitude are in close agreement (figure 8.24). The spherical bowl model and experimental results are closer than with any of the devices plotted previously and within the limits estimated previously.

A mirror system was made with an experimental -10dB beam width of 0.84 mm and a 20 dB dynamic range. It is a successful imaging device with sufficient sensitivity for clinical use and a short pulse. It does not suffer from reverberations. It's focal zone however is only about 1 cm long.

CHAPTER 9.

FUTURE DEVELOPMENTS

This chapter summarises early investigations of three possible lines of development for mirror transducers.

A smaller, more manoeuverable system is considered and the possibilities of a single reflector system based on the Herschel design of telescope are studied. While the Herschel system is appealing, because it is a simpler design, a suitable transducer to drive it will be difficult to produce. Numerical results demonstrate significant aberrations which would be difficult to control.

An axicon mirror system is described. For this design the Cassegrain system is modified by moving the external reference point of the primary mirror off axis. This gives a converging wavefront which is partly conical and partly spherical resulting in a real line focus on the axis and a real annular focus in the plane of the external reference point. Theory suggests that the line focus will be narrower than that due to a purely conical wavefront. Early experimental results show an extended focal zone with a -10dB beam width of 1.1mm The focal zone shows large variation in amplitude (13dB) and in places the sidelobes are large. Variations in alignment and different combinations of transducer and secondary mirror should be tried to improve the field. Foster et al (1981,1983) suggest that axicons may be best used focussing on reception only.

An alternative method of extending the focal zone is suggested by the behaviour of the systems during alignment. Although the position of the focus was influenced by small movements of the secondary mirror its size was not appreciably affected. Investigation with a spherical mirror model is encouraging. The increase in beam width is not marked and the relative amplitude of the first sidelobe is little affected. More theoretical work should be done using the ellipsoidal mirror model. Detailed experimental investigation is required. This would seem to be a promising, practical solution to extending the focal zone.

CONTENTS

CHAPTER 1. INTRODUCTION

1.1. High Resolution Transducers

Ultrasound imaging has expanded rapidly over recent years. Advances in electronics have made sensitive grey-scale imaging widespread. Real-time scanning has overtaken conventional B-scanning in most applications (Wells, 1977; Kossoff, 1976, 1978; McDicken, 1981; Whittingham, 1981; Kobayashi, 1977; Babcock, 1977).

However the quality of an image and the detail which may be observed in it, still depend ultimately on the shape of the ultrasound beam. Axial resolution depends on pulse length; lateral resolution on beam main lobe width. Contrast resolution will depend on side lobe size as well as on the speckle pattern generated by the tissue being scanned and on image noise. Thus a highly focussed probe is required to give high resolution in the image

A narrow beam may be achieved by the use of a high frequency and a large aperture. Both these present constructional problems. Both present problems in use since a large transducer will be difficult to couple to the patient and the attenuation of ultrasound in tissue increases with increasing frequency. A sharply focussed beam has a short focal depth. In practice an ultrasound beam used for imaging will be distorted by mixtures of tissues and by complicated biological structures. A need remains, however, for high resolution, especially in small parts or breast imaging or in C-scanning.

Highly focussed transducers have been studied and built. An experimental water-bath breast scanner has been used for the clinical evaluation of these transducers. Computer models have been developed and used to design and compare the ultrasonic fields of large aperture probes. New techniques have been developed for the construction of efficient ultrasonic mirrors.

1.2. Objectives

1) Decide on a transducer style which will offer the greatest practical potential for high resolution ultrasound, water-bath scanning.

2) Develop mathematical models which will guide the design of such a transducer by demonstrating the effect of transducer parameters on the transmitted field.

3) Build a beam plotting system which will measure experimentally the field of such transducers.

4) Develop the necessary construction techniques to manufacture such a transducer.

5) Design, build and test a high resolution device.

6) Evaluate the transducer for clinical ultrasound scanning of the breast.

1.3. Application of High Resolution Probes - Breast Scanning

1.3.1. Background to Ultrasound Breast Examination

Breast cancer is the most common malignant disease of women (Crymes, 1979). It is associated with great psychological distress as well as with the deformity of mastectomy. Prognosis for the individual patient remains uncertain (Stewart, 1980). It is a major medical problem and much effort is devoted to the early detection and to identification of breast disease as well as treatment.

The possibilities of ultrasound diagnosis of the breast have long been considered. This is both because of the medical importance of the breast and because being a readily accessible soft tissue organ it is, in many ways, an ideal subject for ultrasonic examination. Early A-scan studies (Wild and Reid, 1952) and the first medical pulse-echo B-scans made in 1950 (Howry et al, 1954), were of the breast and breast carcinoma.

Since the early pioneers, continued attempts have been made to exploit the potential of ultrasonic breast examination (Hayashi, 1962; Laustela, 1966; Wells and Evans, 1968; Kelly-Fry et al, 1969; Jellins et al, 1971; Kelly-Fry et al, 1972). Efforts were directed both to a better understanding of the physical interaction of ultrasound and breast tissue (Frucht, 1953; Kossoff et al, 1973) and to identifying diagnostic criteria in the images (Kobayashi et al, 1972 a and b). The technical developments of the seventies, especially grey-scale imaging, have led to increasing success and an upsurge in research and application.

In 1978 Kossoff reviewed the general field of diagnostic ultrasound and identified breast scanning as an area for attention and investigation. An area in which automated waterbath scanning was showing an important role for ultrasound.

Since 1979, dedicated ultrasonic breast scanners have become available commercially. These place emphasis on the automated collection and rapid review of a large number of images (Elliot, 1981; Carmen, 1981). The images tend to be in an arbitary plane and the operator has little choice.

The principal method of breast imaging is X-ray mammography. While ultrasound is in most ways a complimentary technique (Feig et al, 1977; Harper et al, 1981) if it is to play a useful role in breast diagnosis, it must be able to resolve tumours 2 to 3 mm in diameter.

This is true not only of conventional B-scan imaging but also of computed tomography (e.g. Dick et al, 1977; Greenleaf et al, 1975; Glover and Sharp, 1977; Clemant and Alais, 1981; Whiting et al, 1981).

In 1978 the construction of an experimental, water-bath breast scanner started in Edinburgh. This machine was used to evaluate the imaging potential of the transducers described here.

1.3.2. A Water-bath Ultrasound Breast Scanner

A schematic diagram of the breast scanner designed is shown in figure 1.1. The patient lies on a couch over the water-bath with one breast hanging into it. The water is kept at 37°C and is continually circulating through a feeder tank system (not shown). It is possible to immerse the whole breast and axillary tail. Inside the tank there is a rotating probe arm: the whole tank may be rotated or moved transversely as shown. All these movements may be controlled by a microprocessor. If coronal sections are desired the patient couch may be raised or lowered. Images are collected on a scan convertor and stored on video tape.

The scanner was designed as a research tool: a very flexible machine with as few in-built limitations as possible. The tank is rectangular but the axis of rotation of the probe arm is at about 30° to the tank wall. The transverse motion is parallel to the rotation axis. The probe arm may carry a fixed or rotating probe.

No work has been published on scanning patterns, yet it seems likely that an organ with a strong, if unpredictable, pattern of milk ducts and Cooper's ligaments, with a well-defined shape with a very attenuating areola, will present different penetration and different echo patterns to different scanning actions.

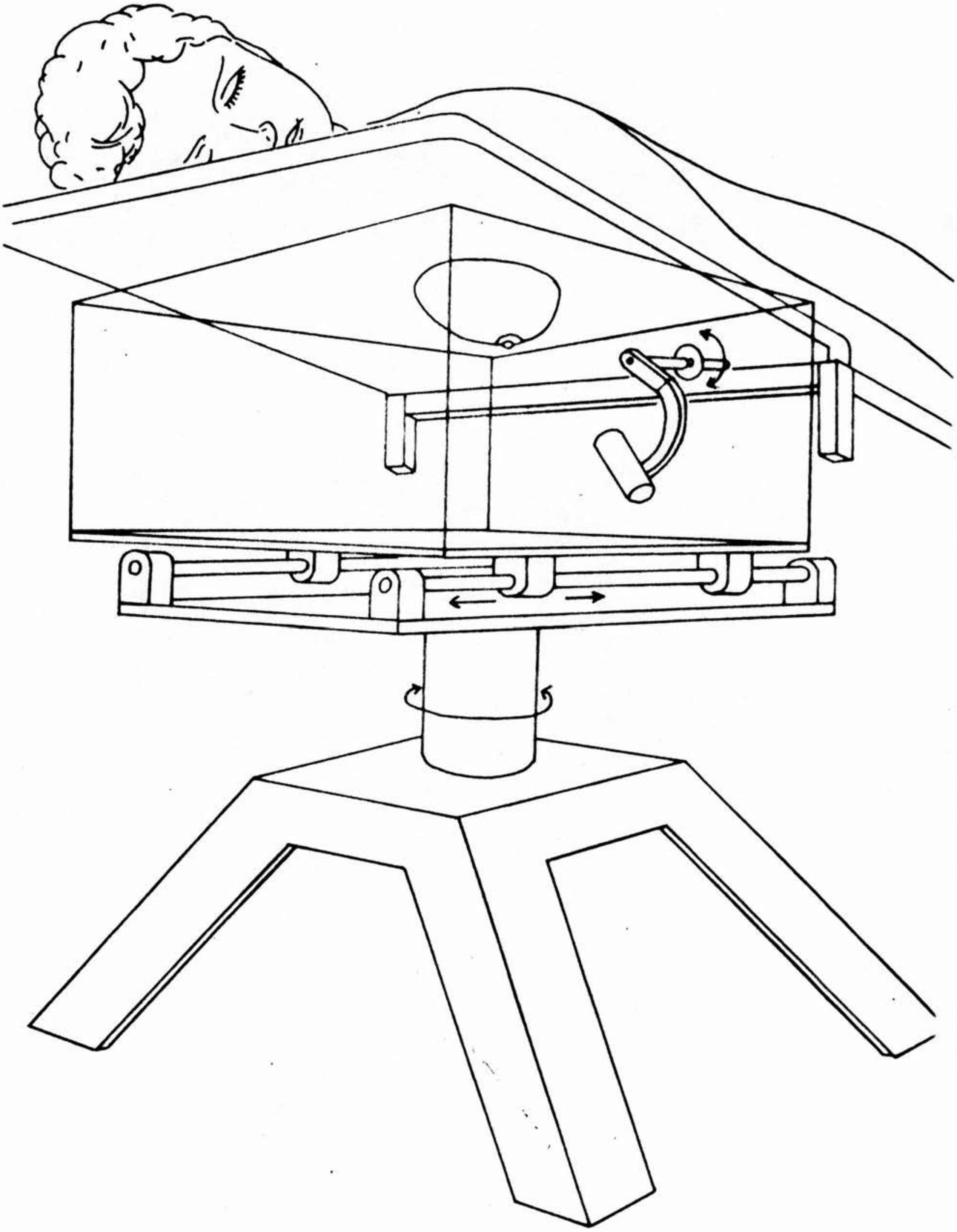

Figure 1.1. A schematic diagram of the Ultrasonic Breast Scanner.

Initially envisaged scanning patterns were

1) B-scanning by rotation of the probe arm about its horizontal axis. The scan may be compounded by oscillating the probe. By rotation of the tank on its turntable, the plane of scan may be chosen to be transverse, sagittal or oblique. Linear movement of the tank provides for selection of the plane of scan.

2) B-scanning in a coronal plane with the probe arm horizontal, the couch being raised or lowered to select the desired plane.

For automatic scanning of the whole breast volume, the microprocessor may be instructed to scan with any of the three movements and stepping between scans on either of the others.

Only the probe arm and the breast intrude into the tank. Space remains for other probes, perhaps real-time or sharply focussed, which may contribute to some or all examinations.

In addition to the general requirement of scanning the whole breast volume, it was recognised that there would be a requirement to examine with high resolution, areas which were of particular interest following clinical examination, x-ray mammography or a standard ultrasound scan. For examining small areas, high resolution could be achieved at the expense of a long depth of field. Standard EMI (now GL Ultrasound) Diasonograph transmitter and receiver circuits are used.

1.3.3. Water-bath Breast Scanning Problems

The problems associated with the experimental application of the probes will influence the parameters chosen.

The possibilities of ultrasound diagnosis of the breast have long been considered. This is both because of the medical importance of the breast and because being a readily accessible soft tissue organ it is, in many ways, an ideal subject for ultrasonic examination. Early A-scan studies (Wild and Reid, 1952) and the first medical pulse-echo B-scans made in 1950 (Howry et al, 1954), were of the breast and breast carcinoma.

Since the early pioneers, continued attempts have been made to exploit the potential of ultrasonic breast examination (Hayashi, 1962; Laustela, 1966; Wells and Evans, 1968; Kelly-Fry et al, 1969; Jellins et al, 1971; Kelly-Fry et al, 1972). Efforts were directed both to a better understanding of the physical interaction of ultrasound and breast tissue (Frucht, 1953; Kossoff et al, 1973) and to identifying diagnostic criteria in the images (Kobayashi et al, 1972 a and b). The technical developments of the seventies, especially grey-scale imaging, have led to increasing success and an upsurge in research and application.

In 1978 Kossoff reviewed the general field of diagnostic ultrasound and identified breast scanning as an area for attention and investigation. An area in which automated waterbath scanning was showing an important role for ultrasound.

Since 1979, dedicated ultrasonic breast scanners have become available commercially. These place emphasis on the automated collection and rapid review of a large number of images (Elliot, 1981; Carmen, 1981). The images tend to be in an arbitary plane and the operator has little choice.

The principal method of breast imaging is X-ray mammography. While ultrasound is in most ways a complimentary technique (Feig et al, 1977; Harper et al, 1981) if it is to play a useful role in breast diagnosis, it must be able to resolve tumours 2 to 3 mm in diameter.

A very large echo will occur at the water:skin interface. There will be a tendency for part of the pulse to reverberate between the transducer and the skin. This will lead to 'ghost echoes' appearing in the image. To overcome this, the water path from transducer to skin must be greater that the depth of tissue to be imaged. Thus such reverberations will fall beyond the image area. To place the focus in the centre of a 100 mm depth of tissue a focal length of 150 mm is required.

There will be an acoustic mismatch between the water (1520 ms^{-1} at $35^{\circ}C$) and breast (between 1.445 ms^{-1} and 1,575 ms^{-1}). If the beam is not normal to the skin, a part of it will be specularly reflected and part will be refracted, resulting in reduction in the strength and in registration errors.

Ultrasound problems are presented by the organ itself. There is wide variation in size, shape and tissue content. An individual's breasts will change with pregnancy, obesity, menstrual cycle, age and disease. The acoustic properties of breast tissues have been summarised by Chivers and Parry (1978), the macroscopic effects on a beam by Halliwell (1976, 1978).

Any transducer design must allow for the ultrasound effects. Any application must allow for the physiological variations and changes.

1.4. Summary of Transducers considered in this Thesis.

The letters refer to figure 1.2.

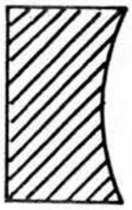

A. A concave bowl transducer.(Section 5.3.1.)

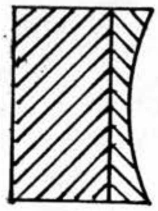

B. Plane disc transducer with epoxy lens.(Section 5.3.2.)

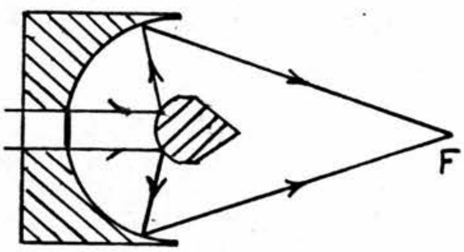

C. A Cassegrain mirror system.(Chapter 7).

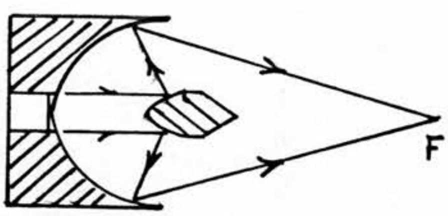

D. A novel modification of the Cassegrain mirror system. Off-setting the common reference point of the mirror surfaces from the system axis results in a pointed secondary mirror.(Chapter 8)

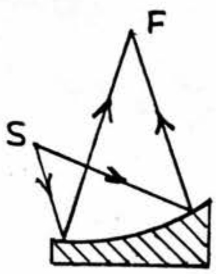

E. Herschel mirror system using a diverging source. (Section 9.1).

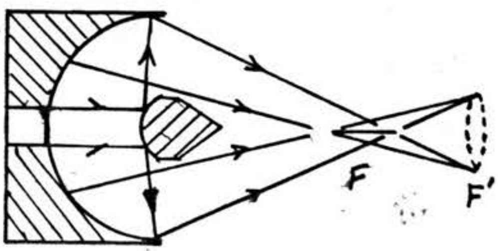

F. An axicon mirror system to give a line focus. (Section 9.2).

Figure 1.2. Transducers considered in this thesis.

1.4.1. Commercial Transducers

Two commercial transducers are considered here for comparison with the systems which were built. These are the transducers used routinely for breast scanning and are the best which could be obtained when breast scanning was initiated.

Transducer A: Panametrics V307, 1" diameter concave bowl transducer focussed at 150 mm range. Described in section 5.3.1.

Transducer B: S. and I 2" diameter plane disc transducer focussed by an epoxy lens at a range of 150 mm. Described in section 5.3.2.

1.4.2. Mirror Systems

Transducer C: A mirror system built using the techniques described in Chapter 6 and following the traditional Cassegrain telescope design. Described in Chapter 7.

Transducer D: A novel mirror system design using the Cassegrain geometry modified by moving the common reference point of the mirror surfaces off the system axis. This results in the mirrors being pointed and eliminates reverberations between components. Described in Chapter 8.

Transducer E: Mirror systems based on the Herschel telescope geometry are investigated theoretically in Section 9.1.

Transducer F: A mirror system based on the Cassegrain geometry with the external reference point of the primary moved off-axis resulting in an axicon system with a line focus.

Described in section 9.2.

CHAPTER 2.

APPROACHES TO A HIGH RESOLUTION TRANSDUCER.

The definition of resolution is complicated. In the complicated echo patterns of an ultrasound image, some balance must be reached between point resolution and contrast resolution, that is dynamic range. Similarly a compromise may be struck between point resolution and depth of field. This will depend on the application. Sharp focussing will result in large variations of resolution and intensity through a B-scan image.

Any frequency in the range employed in medical ultrasound is of interest. In the case of breast scanning with long focal lengths, the range is likely to be 3 to 5 MHz.

The problems of focussing through tissue have been considered by Foster and Hunt (1978, 1979). Even in a heterogenesus organ like the breast, they found Numerical Apertures of 0.17 to be valuable and advise of improvement in resolution up to, and possibly beyond, a Numerical Aperture of 0.25. In a water bath, this could be an aperture of 75 mm (or 250 wavelengths) diameter.

This chapter considers the possible options for high resolution transducers and for theoretical models which would facilitate the design of such a device by theoretically evaluating the effects of design parameters.

2.1. Design considerations and constraints.

The requirement of high lateral resolution indicates good focussing combined with a large aperture. The size of an aperture is taken relative to the focal length of the device. Commonly used to describe this relationship are f-number and Numerical Aperture. I will use the latter as defined by Driscol (1978)

$$\text{Numerical Aperture, NA} = n \sin u \qquad - 2.1$$

where n = refractive index
= 1
u = halfangle of extreme ray
a = radius of aperture

The refractive index is used to correct for the medium in which the element is focussing, comparing with reference conditions. Conventionally for optical systems this is the speed of light in vacuum. More appropriately the reference medium used here is deionised water as $35^{\circ}C$ with a sound velocity of 1520 ms^{-1}. Thus $n = 1$ for the water tank under normal conditions but a new Numerical Aperture may be readily calculated for different tissues or if the water velocity is altered, e.g. by a different operating temperature or by the addition of impurities.

The Numerical Aperture is used to derive other beam shape parameters. Franhofer diffraction conditions are assumed. Of use in preliminary considerations will be

$$\text{Depth of focus} = \frac{k\lambda}{(NA)^2} \qquad - 2.2$$

Where λ is wavelength
k is a constant $k \simeq 1.8$ for half-maximum (-3dB) intensity
$k \simeq 2.4$ per half-maximum (-6dB) amplitude

and the diffraction limit of resolution is given by

$$\Delta x = \frac{k\lambda}{NA} \qquad - 2.3$$

Where k is a constant
The constant comes from the 1st order Bessal function which describes the diffraction pattern and the criterion involved to judge separation.

For the Rayleigh Criterion for resolving two images of equal intensity (that is the peak of one diffraction pattern co-incides with the first minimum of the other) k = 0.61. If Sparrow's Criteria is used k = 0.5. The limited value of such criteria to ultrasonic imaging is recognised. It is possible to modify the criteria to accommodate sources of different intensity (Longhurst, 1977) but even this is little related to the complex signal patterns which will be encountered in echoes from human tissues. They are, however, of use as a point of comparison between devices.

The assumptions associated with the derivation must be considered. The pattern is caused solely by diffraction. It is assumed that the focussing devices had no aberrations whatsoever. In a spherical bowl of large aperture for instance, the effects of spherical aberrations will become apparent. A uniformly transmitting, circular aperture is assumed. Again it is unlikely that such an aperture could be achieved in practice. A mirror system would have a block in the centre due to the secondary, a lens will not be of uniform thickness and the effect of attenuation within its material will vary across the aperture. The last assumption is the homogeneity of the medium. The effect of tissue on the beam is discussed in section 2.1.3.

2.1.1. Waterbath Scanning

In a water bath there is little loss of signal due to attenuation in water (2.2×10^{-3} dB cm^{-1} (MHz)^2 - Wells, 1977) and part of the pulse will be reflected by the skin. This reflection will tend to reverberate between transducer and skin. This will lead to the reappearance of the skin and other structures as ghost echoes deeper in the image. To avoid this, the pathlength between transducer and skin must be long so that such echoes fall beyond the region being imaged. Thus to place the focal zone in the centre of a 100 mm depth of tissue a focal length of 150 mm is required if such artifacts are not to obscure the image.

2.1.2. Lateral Resolution

Considering a focal length of 15Ø mm with a frequency of 5MHz and a velocity of sound of 1500 ms^{-1} a lateral resolution of 1 mm indicates a Numerical Aperture of Ø.185 corresponding to a diameter of 55.5 mm.

Driscoll (1978) has described qualitatively the effects of apodisation. Generally if transmission is reduced at the centre of the aperture, then the diameter of the first off-axis minimum is reduced but the energy in the rings off-axis is increased at the expense of the main lobe. Likewise if the energy at the outside of the aperture is reduced, then the size of the main lobe is increased and that of the other lobes decreased. More specifically Weyns (1980b) considered smaller focussed transducers. He describes the change from circular aperture to a thick annulus as reducing the spread of the beam beyond the focus but with a corresponding increase in the size of the sidelobes.

2.1.3. Depth of Focus and Axial Resolution

It is recognised that for a conventional focussing system high lateral resolution is inevitably accompanied by a short depth of focus. It is recognised that this will limit the usefulness of such a probe but the immediate application envisages examining only a small volume of tissue with such a probe.

Using equation 2.2 and the same parameters as in section 2.1.2 a depth of focus $\pm$ 6.1 mm is found.

Axial resolution is determined by pulse length. An axial resolution of 1 mm corresponds to a pulse length of 0.66 ms or 3 cycles at 5 MHz. A suitable transducer would require a pulse length of this order or shorter in the focal zone.

2.1.4. Large Aperture Transducers and the Breast

A large angle subtended by the transducer at the target increases sensitivity to isotropically reflecting targets and increases the probability of receiving echoes from objects with other reflecting properties. Although focussing will limit the volume insonified, sensitivity to off-axis isotropically reflecting targets will fortunately be reduced by different acoustic path lengths to different parts of the transducer.

However because echoes follow different paths through tissue, they will encounter tissues with different velocities. This could lead to echoes with the same origin but different paths arriving out of phase - resulting in destructive interference. At 5 MHz a difference of 100 ns would cause a phase shift of π. If the path length in tissue is 100 mm at 1520 ms^{-1} the time of flight in breast is 6.6×10^{-5}s, and the difference only 0.15%.

Increasing the aperture would increase the averaging of local effects but also increase the possibility of there being a significant velocity gradient across the beam.

Rays following different paths through tissue will be refracted by differing amounts. This would lead to blurring.

The conical structure of the breast would result in the beam distortion being dependent on the angle of approach.

The effects of breast tissue on ultrasound beams have been described by Foster and Hunt (1978, 1979) and by Halliwell (1976, 1978). They may be summarised as

(1) Beam diverges through the breast.
(2) Beam may be deviated and may be split - possibly 20 mm between maxima.
(3) Beam may reflect from chestwall/ribs.
(4) A beam parallel to the chestwall will tend to bend towards it. (This may be explained by the conical structure of the breast.)
(5) Velocity and attenuation show 'large' <u>local</u> variations as well as variations between patients. Generally as age increases, the amount of fatty tissue increases and velocity decreases.
(6) Velocity increases towards the nipple (more glandular tissue).

Particularly Foster and Hunt attribute defocussing to two mechanisms: (a) attenuation (b) phase distortion of the wavefront. Most commonly attenuation is the more important, although it may be controlled by frequency bandwidth. However, breast tissue is very heterogeneous and the second mechanism may remove a large proportion of energy from the beam.

In all tissues they find a Numerical Aperture greater than 0.17 to be of benefit to focussing although the beam focussed less well in breast than in the same depth of liver tissue. They also observed that defocussing was very dependent on position in the breast. This has been discussed in Section 1.3. They conclude that Numerical Apertures up to and perhaps beyond NA = 0.25 will improve point resolution.

2.2. Selection of a Transducer Type for a large Aperture Device.

Several approaches are possible to the design of a large aperture water-bath transducer

Generally the constraints used are those discussed in section 1.3. Initially the frequency considered will be 5 MHz although it must be possible to execute any design in 3.5 MHz if 5 proves unsatisfactory as discussed in Section 1.3.

2.2.1. Concave Bowl Transducer

Purchase of a sufficiently large bowl would be difficult and time consuming, if possible. Neither a commercial transducer nor a PZT ceramic bowl of sufficient size is a standard item for any supplier known to us.

Local techniques exist for the manufacture of transducers. These have been described by Bow (1979). The technique, however, would require some development to handle a crystal larger than 29 mm or as fragile as 5 MHz ceramic. An entirely new wave plating technique would be required for a bowl or a large diameter. The largest device made by this method is 15 mm diameter.

A bowl transducer is unlikely to achieve as large an aperture as recommended by Foster & Hunt. It would however be simplest to predict in terms of performance.

Wells (1977) gives a formula for the intensity Gain, G

$$G = \frac{I_f}{I_o} = (kh)^2 \qquad - 2.4$$

where I_f = intensity at focus.

I_o = intensity at transducer face.

k = wave number = $\frac{2\pi}{\lambda}$

h = depth of bowl

The geometry is shown in figure 2.1. The increase in G with $(\text{frequency})^2$ will help compensate for the increase in attenuation with $(\text{frequency})^2$ at least in the focal zone. The point of greatest intensity lies on the axis closer to the bowl than the centre of curvature and approaches the centre as kh increases. The intensity difference between peak and centre is small unless kh is small. It would be manoeuverable and easy to use in the breast scanner. Preliminary experiments demonstrated the difficulties in manufacturing such a device locally. Our technique is based on the work of Kossoff (1966) but it was not practical to develop this to keep pace with increasingly sophisticated designs. (Desilets et al, 1978; Bainton & Silk, 1980; Smith & Awojobi, 1979; Martin, 1977).

Two commercial bowl transducers with Numerical Apertures 0.08 and 0.14 were purchased for breast scanning and they are discussed in Section 5.4.

2.2.2. Plane, disc transducer focussed by a conventional lens.

The construction of a disc transducer would be considerably simpler than a bowl. A large piece of 5MHz ceramic would be very fragile but backing and matching problems would be greatly eased by its being flat.

Good lenses are, however, difficult to produce. The problems have been discussed Wells (1977). The ideal lens material may be summarised as having

(i) an absorption coefficient = Ø.

(ii) the same characteristic impedance as its load.

(iii) the maximum possible refractive index.

The absence of such a material is unfortunate. A change in characteristic impedance between lens and load means that sound pulses will be reflected within the lens. Therefore, the lens must absorb to prevent these

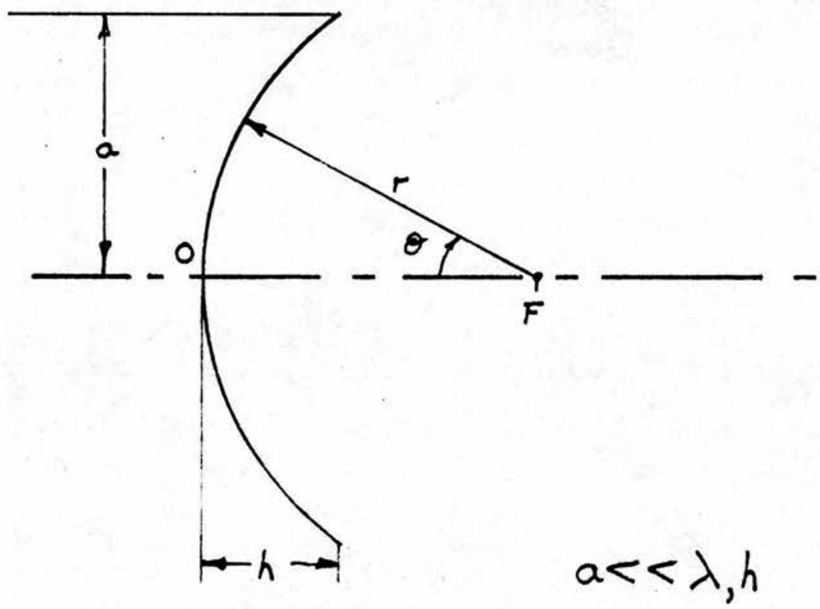

Figure 2.1. Geometry of a concave bowl transducer.

reflected pulses from reverberating within it. This increases the need for a large refractive index in order that the lens is thin. A thick lens not only would reduce the signal but also apodise the aperture since transmission and sensitivity at any point in the aperture will depend on the lens thickness at point. Transmission through a lens whose characteristic impedance differs from its surroundings will also be controlled by interference. Maximum transmission will be when the lens thickness is an integral number of half-wavelengths. Wells observes that this leads to variations of about 3 dB across a polymethylmethacrylate lens. Exploiting this effect is discussed in 2.2.3. The demands of characteristic impedance and refractive index are contradictory since both depend linearly on sound velocity in the lens. Thus the high velocity in the lens must be balanced by its having a low density to maximum transmission through the lens load surface.

Seeking a high refractive index begs the question of whether a concave or convex lens should be used. In a water bath, both are possible. Driscoll (1978) describes the effects of such variation in transmission over the aperture. A convex lens would increase the size of side lobes; a concave one would effectively reduce the size of the aperture. Although some concave lens materials, i.e. those with sound velocities less than that of water (e.g. 'silastic' rubber, Freon (Foster & Hunt, 1979)) have been used, none met the absorption and impedance requirements well enough to be employed at such large apertures.

The choice of refracting surface also poses problems. At the large apertures being considered spherical aberration will become appreciable spreading out the focal cone. Design of an aspheric element would be difficult.

Consider a concave spherical lens. The geometry if shown in figure 2.2 The focal length, F, is given by

$$F \simeq \frac{R}{1 - \frac{1}{n}} \qquad - 2.5$$

where R = radius of curvature

n = refractive order

$$= \frac{c_{lens}}{c_{load}} = \frac{\text{sound velocity in lens}}{\text{sound velocity in load}}$$

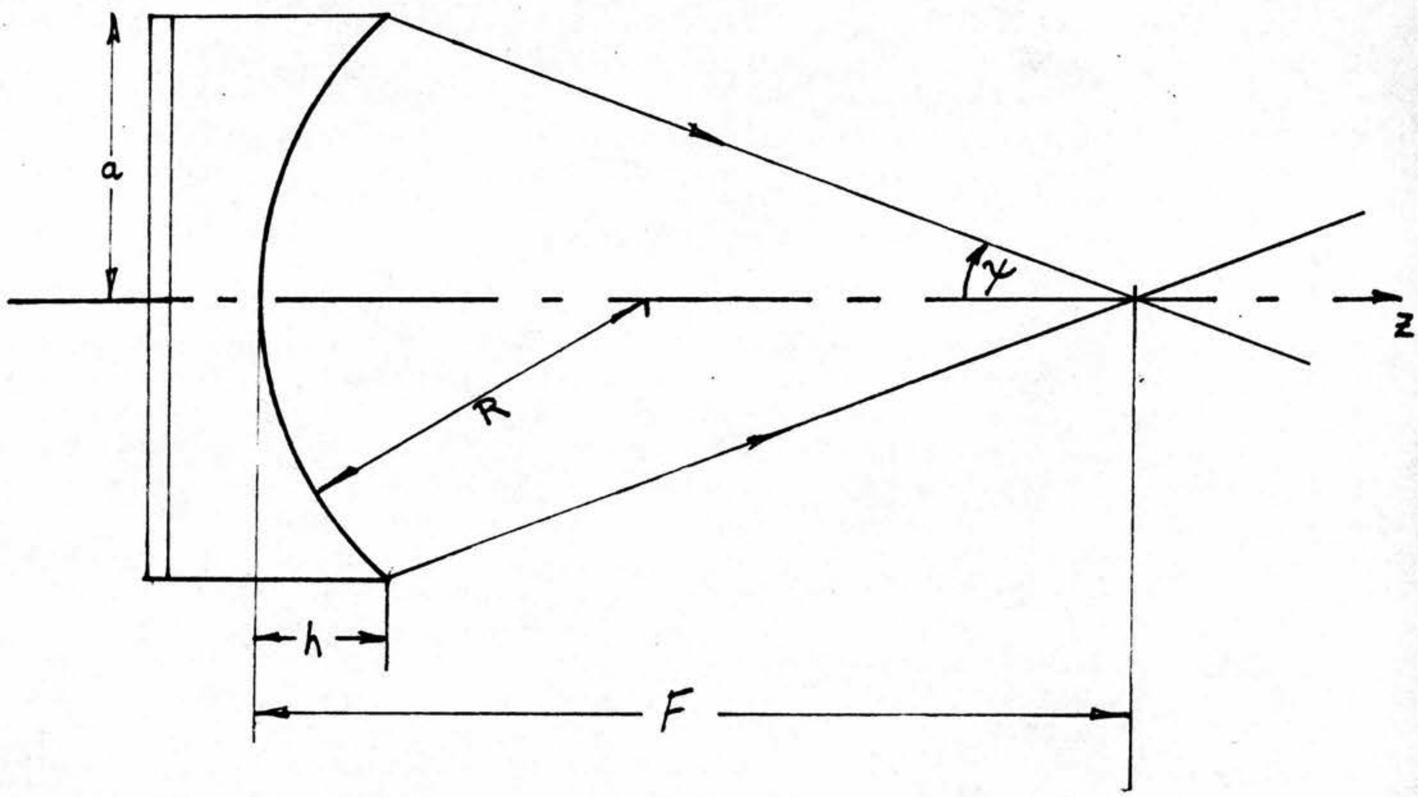

Figure 2.2. Geometry of a flat transducer with a spherical concave lens.

This uses the small angle approximation, i.e. assumes that angles of incidence and refraction are small and hence $\sin\theta \simeq \tan\theta$. This is reasonable for $h < 0.1R$.

Rays leaving the spherical surface all converge at a distance F along the axis. Rays from zones of different radii are out of phase and this limits the useful aperture possible.

If the aperture limit is chosen such that rays do not arrive at the focus more than $\lambda/2$ out of phase then

$$\lambda_{load} \simeq \frac{F^2 \tan^4 \chi}{2R\, n\, (n-1 + n \tan^2 \chi)} \qquad -2.6$$

These equations may be used to calculate restraints on the refractive index, n, and hence on the lens material.

Equation 2.5 gives

$$Rn = F(n-1) \qquad - 2.7$$

Assume speed $c_{load} = 1520\ ms^{-1}$ (Water at 35^oC)

Focal length $F = 150$ mm

frequency $f = 5 \times 10^6$ Hz

and combine equations 2.6 and 2.7.

$$\frac{c_{load}}{f} \simeq \frac{F \tan^4 \chi}{2(n-1)(n-1+n \tan^2 \chi)} \qquad - 2.8$$

Consider a Numerical Aperture, NA = 0.25

then $\tan\chi \simeq 0.25$

Equation 2.8 becomes $$\frac{C_{load}}{f} \leqslant \frac{F}{512(n-1)\ (n-1+ \frac{n}{16})}$$

$$\frac{c_{load}}{f} \leqslant \frac{F}{32(n-1)\ (17n-16)}$$

$$(n-1)\ (17n-16) \leqslant \frac{Ff}{32c_{load}}$$

$$17n^2 - 33n + 16 - \frac{Ff}{32c_{load}} \leqslant 0$$

Solving this as a quadratic equation gives roots 1.923 and 1.776 x 10^{-2}.

Reject second solution since $n < 1$ (i.e. a convex lens)

$$\underline{n \leqslant 1.92}$$

Since $n = \frac{c_{lens}}{c_{load}}$

this means a material with speed of sound $\leqslant 2918\ ms^{-1}$

Using equation 2.5 this implies a radius of curvature R = 72 mm. This is inaccurate because of the failure of the small angle approximation here ($h \simeq 0.15\,R$).

The acoustic velocity and characteristic impedence of a number of possible materials is shown in table 2.1. This illustrates the contradictory requirements of refractive index and impedence. Various plastic materials have been used although aluminium was the first material used (Bez-Bardilli, 1935) and is still in use especially for high power applications although it tends to attenuate the signal more than plastics, (Golis, 1968). Polymethylmethacrylate has also been used successfully for a long time (e.g. Sette, 1949; Tarnócry, 1965). Such plastic materials, however, will not meet the restrictions placed on refractive index by spherical aberrations. Workers interested only in focussing continuous wave radiation will not encounter problems due to pulses reverberating within the lens.

Focal Region

The size and shape of the focal region depends upon wavelength, λ , and Numerical Aperture, NA. Wells (1977) gives approximate formula to describe the -3dB contour of the focal spot. The Focal region is roughly a prolate spheroid about the geometrical focus with transverse diameter D_r and axial length, D_z.

$$D_r \simeq \frac{kt\lambda}{2.NA} \qquad - 2.9$$

where kt is dimensionless and dependant on γ.
If $\gamma < 50^\circ$ then the solution is correct to 20% if $kt \simeq 1.0$.

MATERIAL	Velocity, C ms^{-1}	Characteristic Impedance, Z $\times 10^6$ Nsm^{-2}
Water (35°C)	1520	1.5
Aluminium	6400	17.3
Araldite (MY753:HY951)	1470	1.7
Copper	4760	42.0
Lexan	2230	2.7
Nylon	2680	3.1
Platinum	3260 — 4075	70 - 87
Polyethylene	2000	
Polymethylmethacrylate	2680	3.2
Silver	3650	38.0
Tin	3320	24.2
Titanium	5990	27.0

Data from Kaye and Laby (1957).

CRC Handbook of Chemistry and Physics (Weast, 1969).

The Practicing Scientist's Handbook (Moses, 1978).

Table 2.1. Acoustic Properties of possible lens materials.

$$D_z = k_a D_y \qquad - 2.10$$

if $\gamma < 50^\circ$, then solution is correct to $< 15\%$ in k_a if $k_a = 15(1-0.01\gamma)$ (γ in degrees)

For a system of NA = 0.25 and with the same conditions as previously $\lambda = 0.3$ mm

$$D_r \simeq 0.61 \text{ mm}$$

$$D_z \simeq 7.8 \text{ mm}$$

This promise of good performance will only be met if a lens can be manufactured in a suitable material as determined earlier. The short depth of field is demonstrated.

Such a transducer would be of great potential in this application and a commercially manufactured device was purchased. This had a crystal diameter 50 mm giving it a nominal Numerical Aperture of 0.17 and is discussed in Section 5.5.

2.2.3. Stepped Lenses

Another style of lens is suggested by the dependence of transmission through a layer on interference and hence the thickness of the layer.

At normal incidence intensity transmissions, T, is given by

$$T = \frac{4 Z_m Z_c}{(Z_m + Z_c)^2 \cos^2(K_L t_L) + (Z_L + \frac{Z_m Z_c}{Z_L})^2 \sin^2(k_L t_L)} \qquad -2.11$$

where k = wave number

t = thickness

z = characteristic impedance

and the subscript c indicates the crystal

L indicates the lens

M indicates the outside medium

If $t_L \ll \frac{L}{4}$ or $t_L = \ell \frac{\lambda L}{2}$

where ℓ is an integer

Assuming $Z_L \not\ll Z_C$ OR $Z_L \not\ll Z_M$

then $$T \simeq \frac{4 Z_M Z_C}{(Z_M + Z_C)^2}$$ - 2.12

Hence transmission is independent of lens properties when the lens is an integer number of half-wavelengths thick.
Alternatively, midway between these points

$$t_L = (\frac{2l - 1}{4})\lambda_L \text{ and}$$

$$T = \frac{4(Z_m Z_C)(Z_L)^2}{(Z_m Z_C + (Z_L)^2)^2}$$

These equations explain the variation of intensity across the surface of a lens and give the possibility of minimising the quarter-wavelength losses by using a lens with its thickness stepped in half-wavelength increments (Tarnóczy, 1965). Such a lens would be less lossy, would not suffer from reverberations and would be easy to machine.

Golis (1968) compared at 800kHz conventional and zone lenses of aluminium and of plastic 'Textolite'. Looking at solely the focal zone (-6dB width) he observed that either might perform better - depending on the focal lengths. At the longer focal lengths (and correspondingly smaller Numerical Aperture) the lens gave a narrower focus, the crossover point being dependent on the material (or its refractive index) and the frequency. The zone lens always gave a narrower peak for a given focal length. However, his schlieren images showed the field, due to the zone lens, to be very broken. Higher order focii appeared on axis but more significantly large off-axis lobes were apparent.

2.2.4. Fresnel Zone (Phase) Plate Focussing

The idea of a Fresnel zone plate is well known and discriptions may be found in standard optics texts, e.g. Jenkins and White (1976). They attribute the invention to Lord Rayleigh in 1871. The geometry is shown in figure 2.3.

Focussing is achieved by transmitting waves that arrive at the focus in phase. Therefore, if alternate zones do not transmit the signals from

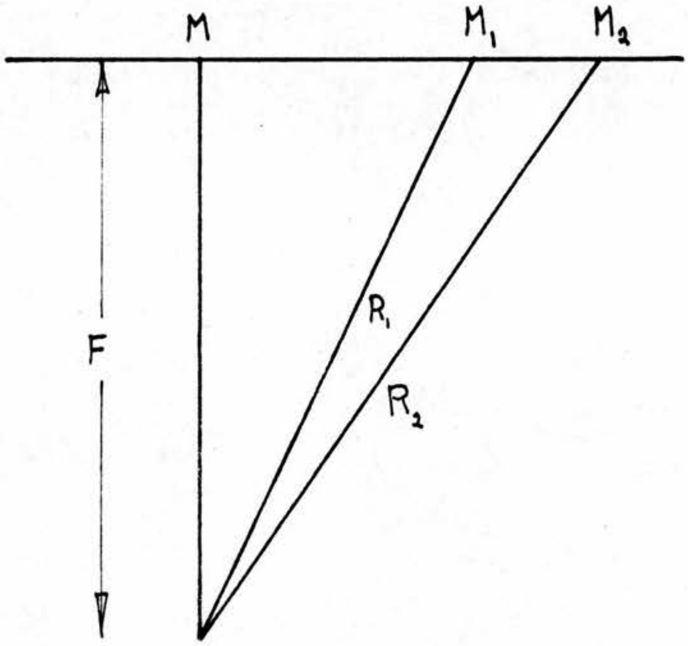

Figure 2.3. Fresnel zones. $R_1 = F + \frac{1}{2}\lambda$

$R_2 = R_1 + \frac{1}{2}\lambda$

the other zones will arrive in phase at the focus. This constructive interference will occur elsewhere in the field where smaller groups of zones meet in phase. Thus fainter foci will occur at $F/_3$, $F/_5$, $F/_7$, etc.

The radius r_n, of the nth zone is given by

$$r_n^2 = n\lambda\,(F + \frac{n\lambda}{4}) \qquad - 2.13$$

For the specifications being considered where F >> n,

$$r_n^2 \simeq n\lambda F \qquad 2.14$$

10 active zones would be required for a good focus. According to Jenkins and White, this would give an intensity Gain, G = 400. Either odd or even numbered zones may be used with the same effect.

Equation 2.14 gives r_{20} = 30.2 mm. Using the formula given by Wells (1977) for the Intensity gain of a conventional lens focussing system of these dimensions.

$$G \simeq 0.8 \;\left(\frac{2r}{D_r}\right)^2$$

$$G \simeq 5000$$

Such a transducer would present all the constructional problems of a plane disc transducer plus those of producing and exciting a suitable array of annuli. The marking of a suitable array of zones on a crystal electrode would not be trivial. Scribing would be unsuitable (Pye, 1983). The difference between r_{19} and r_{20} is only 0.76 mm.

If a crystal 60 mm diameter could not be obtained then either the number of zones or the focal length would need to be reduced or the frequency increased.

Quate (1976) discussing the work of Farrow and Auld (1975) suggests a transducer could operate on all zones at once if alternate zones of the piezoelectric are poled in opposite directions. The productions of such a device would be difficult and many electrical and mechanical difficulties would be encountered. It is not possible to determine magnitude of the sidelobes from Quate's paper although the lateral resolution at 10MHz is about 0.25 mm for a numerical aperture of 0.32 and 20 zones. The asymmetry of the transverse beam plot shows some production difficulties. The principal claims made for the device are its insensitivity to objects not in the focal plane and the ability to vary focal length by altering the frequency. Perhaps a device suited to ultrasonic microscopy but not for B-scanning.

2.2.5. Annular Arrays and Electronic Focussing

A lot of work has been published in this field (e.g. Vilkomerson, 1974; Macouski, 1975; Dietz et al, 1978) which presents a lot of promise since swept electronic focussing can increase the depth of field, something of exceptional value in B-scanning techniques. Most relevantly annular arrays have been used by Arditi, et al (1981, 1982) for breast scanning. Lately the same group have employed an annular array as part of a hybrid transducer, incorporating a mirror system (Patterson et al, 1983).

Pye (1983) has described the determination of size parameters for annular arrays. Focussing is best achieved in the far field of the annulus. Assuming that the nearest point at which we desire to focus is 100 mm away, then for a 50 mm diameter device at 5 MHz this gives a ring width of 0.344 mm. This is close to the wavelength and the theoretical limit of how narrow a ring may be. Thus Numerical Aperture would be limited to 0.25 at the nearest point of focussing and 0.167 at the mean focal depth.

For a seven ring system at these dimensions only 20% of the area of the aperture would be involved in transmitting and receiving with a consequent loss of sensitivity.

2.2.6. Mirror Systems

A traditional solution to focussing when refractive elements are unsatisfactory is to use reflective surfaces instead. Early telescopes employed mirrors because of the dispersion displayed by refractive elements and the basic designs bear the names of early astronomers and physicists e.g. Newton, Gregory, Herschel, Cassegrain.

Mirrors have been used as an alternative focussing to the shaping of quartz crystals (e.g. Griffing & Fox, 1949; Fox & Griffing, 1949).

Olofsson (1963) described a system based on the Cassegrain telescope for pulse-echo imaging. Such applications are inevitably limited to water-bath scanning but have been used by investigators who require high resolution. Olofsson for the heart, Fry et al (1967) for the brain. Wells (1977) describes a system based on a parabola with a cone shaped secondary. All other systems have been based on second degree conic surfaces.

A comprehensive study of conic mirrors has been published by Bruggemann (1968). He establishes conventions for the description of conics of revolution and these have been summarised in Appendix 1.

Olofsson's mirror system is shown in figure 2.4. The large mirror labelled 'E' in the figure will be termed the primary reflector and the smaller labelled 'W', the secondary. This is in keeping with the conventions used for optical systems although it may be inappropriate where transmission as well as reception is focussed in other mirror systems.

Since the size of aperture is not limited by the crystal itself, mirror systems offer potentially large apertures. Of all the imaging transducers in the literature mirror systems have the largest apertures, both Olofsson and Fry et al, using Numerical Apertures of 0.4.

For these very large apertures conic surfaces are used to reduce spherical aberration. This is the only on-axis aberration and is therefore, critical to pulse-echo imaging where the commensurate increase in off-axis aberrations is not important. Mirror systems are constructed by combining conic elements with common reference points. Thus Olofsson's system may be understood. A pulse is transmitted from the plane transducer T. It is reflected by a target at F_1. This is the external reference point of the elliptical primary mirror as well as the accoustical focus of the mirror system. The reflected wave, diverging from F_1, is reflected by the primary towards its internal reference point F_2. This is the common reference point of the two mirror elements being also the internal reference point of the hyperboloidal secondary. The secondary reflects waves directed at its internal reference point towards its external reference point, F_3, where the receiver crystal, R, is placed.

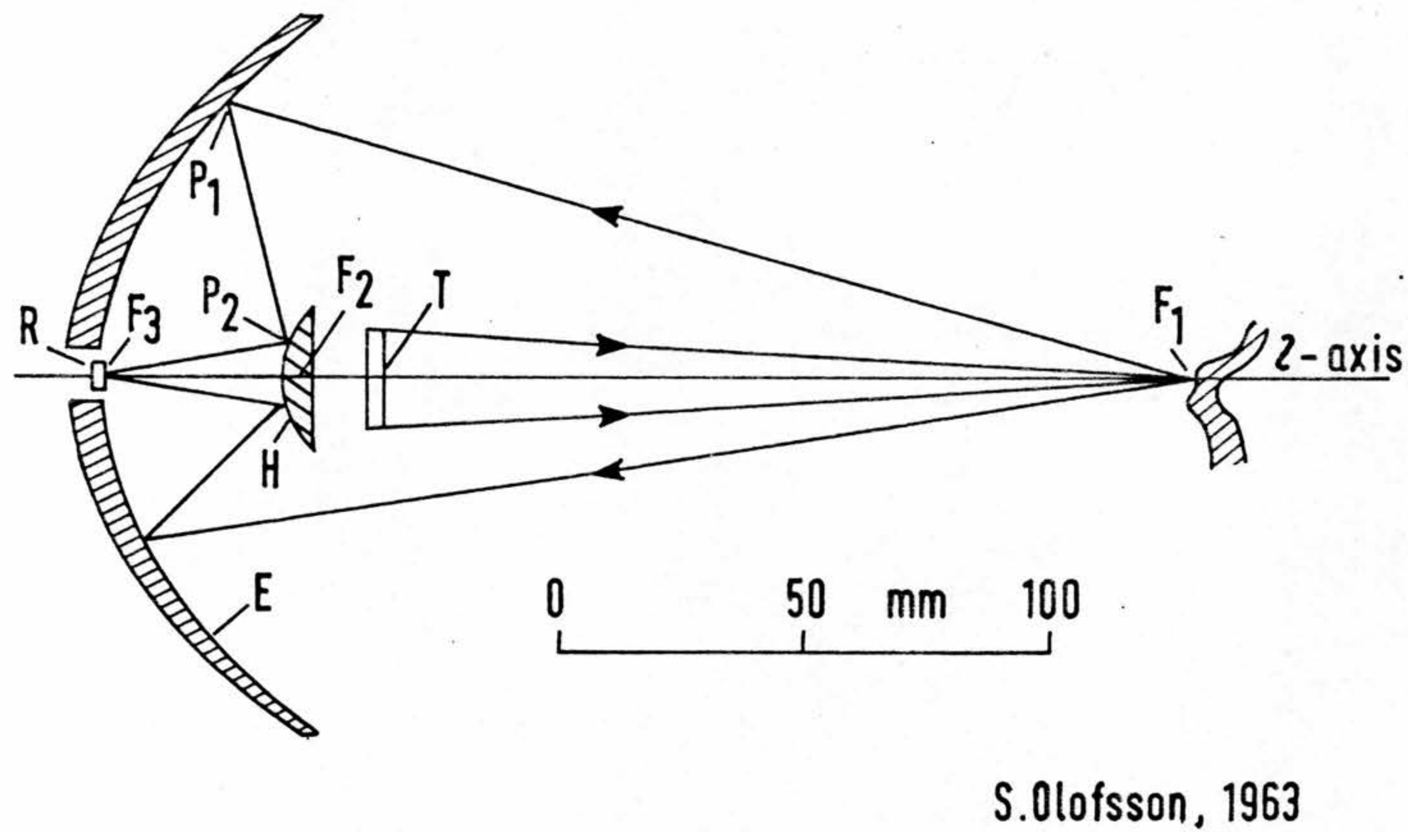

Figure 2.4. An ultrasound mirror system.

The criteria laid down by Olofsson for the design were that the amplitude must not be diminished by reflection nor must the pulse length be increased.

The demands made by a mirror on its material are less than those placed on a lens. It must have a high reflectivity to maintain the signal strength. It must absorb that portion of the signal which is not reflected so that there are no reverberations within the system. Olofsson tried both brass and wood before settling on an araldite epoxy resin: tungsten powder mix. The design used by Fry et al for studying monkey brains was very similar.

Olofsson with a focal length 180 mm and a Numerical Aperture = 0.4 achieved a revolving power of (2.3 ± 0.2) mm at 1 MHz. He found experimentally that this was largely independent of the size of the receiver crystal provided the main lobe of the directivity function encompassed all of the secondary within its - 3db limits. The ± 10 mm usable depth of field was sufficient to encompass the heart structures of interest.

The system of Fry et al was very similar except that they focussed the transmitting transducer with an epoxy lens and operated at a frequency of 3 MHz. They achieved resolution of approximately 1.25 mm. The scanning system described in this paper is very complex and depth of field problems were overcome by gating the focal zone on the A-scan and combining many scans with a transducer in different positions to give the image.

The agreement between Olofsson's theory and experiment was good but imperfect. He failed to predict that resolution was independent of receiver diameter. His estimate of focal length was over optimistic. The transverse plot through the focal zone shown by both him and Fry et al do not actually zero at the minima nor are they symmetrical. This Olofsson attributes to aberrations for which he did not allow and to irregularities in the mirror surfaces. It seems likely, however, that misalignment of mirror elements would also contribute. Fry et al show a further asymmetry. The supports for their secondary, further disturb the focus making mutually perpendicular transverse plots substantially different.

2.2.7. Summary.

Of the options considered mirrors offer the largest apertures. The demands on the material are less than for a lens. The separation of the systems into three elements gives advantages as well as disadvantages. The elements would be difficult to align well but makes it possible to vary different elements. It would be possible to use standard transducers to energise the systems thus making a change of frequency, for instance, simple. It would be possible with a paraboloidal secondary to focus on transmission and reception. Other designs than the Cassegrain are possible. Mirror systems will be large and bulky. Scanning with them will be difficult. However, the breast scanner has been designed for experiment and there is room in it for such devices. The pulse will be reflected twice within the system and if the mirror focusses both transmission and reception, the water path of the sound pulse will be considerably greater than the mirror to skin distance. It is interesting to speculate on why Olofsson focussed only on reception. Was this to achieve a desired focal shape or was he unable to transmit through his system?

It will be necessary to predict and compare the performance of possible designs and this may be difficult. As has been seen from the work of Olofsson and Fry et al, it is likely that constructional and alignment problems will cause any device to fall short of its theoretical performance. Allowance for conic mirrors and for the apodisation due to the location in the centre of the aperture of the secondary mirror may be important.

2.3. Selection of a Mathematical Model for the detailed design of a Large Aperture Transducer System.

There are two basic approaches to the theoretical description of ultrasound transducers. The more 'traditional' approach is a continuous wave (CW) solution. The field due to a single frequency is soluble analytically in certain special cases or the numerical solution fairly readily obtained. The CW solution may then be used to develop qualitatively the pulsed field, over a limited area. The single frequency may be expanded over a limited band width to give a quantitative pulse solution. The increased availability of computing power has led to the recent development of pulsed wave (PW) solutions. The most powerful PW approaches have used an impulse response approach which leads directly to a solution for any pulse shape or even for a continuous wave. Foster and Hunt (1978) have also approached PW solutions by using Fourier transforms. However it seems to have been slow to evaluate and they concentrate on special cases. More recently they have employed the impulse response method (Arditi et al, 1981; Foster et al, 1981).

All theoritical approaches make the same simplifications to the transducer environment. Various boundary conditions have been used with CW models (these are discussed in section 3.2) and although all the impulse responses in the literature have used Huygen's boundary conditions, this is not a theoretical limit. In addition the transmitting medium is assumed infinite (or semi-infinite) homogeneous, isotropic, and loss-less with constant acoustic velocity. The vibration is usually taken to be uniform over the transducer surface.

The physical development of appropriate theories and parameters is described by Rayleigh (1945), the mathematical development by Coulson and Jeffrey (1977), p.158 onwards.

CW solutions have been employed for a long time, e.g. H.T. O'Neil (1949); Griffing and Fox (1949). More recently the CW solution of large aperture highly focussed transducers has been described by Archer-Hall and his co-workers (1979), (1980), (1980b). It is considered to give insight into the variations in ultrasound beams with frequency, diameter etc. since some of the CW beam parameters may be described analytically, especially for plane pistons. See, for example, Kossoff (1968), Wells (1977), Kinser and Frey (1965), Zemanek (1971). The CW model continues however to be an imperfect model of a pulsed transducer. Much work has been published on PW solutions in the past decade, e.g. Beaver (1974), Stephanishen (1971), Weyns (1980 a and b), Duck (1981), Weight and Hayman (1978). The whole history and status of transient field solutions has been summarised by Harris (1981) in a comprehensive and illuminating review.

The Rayleigh Integral in its frequency or time domain forms (Rayleigh, 1945) describes the field at a point P, located by the position vector $\bar{x}$ and at time t.

$$\bar{\phi}(\bar{x}, s) = \frac{1}{2\pi} \int_S \nu_n(s) \frac{e^{-s\frac{r}{c}}}{r} \, dS \qquad - 2.15$$

$$\phi(\bar{x}, t) = \frac{1}{2\pi} \int_S V_n\left(t - \frac{r}{c}\right) \cdot \frac{1}{r} \, dS \qquad - 2.16$$

where ϕ is the velocity potential

$\bar{\phi}$ its Laplace transform

ν_n the Laplace transform of the normal velocity, V_n

Pressure may be derived from the velocity potential using the first order approximation (Duck, 1981).

$$p(\bar{x}, t) = \rho \frac{\partial \phi}{\partial t} \qquad - 2.17$$

This is also used in the derivation of pressure using the impulse response.

This may be solved for any vibration defined by the time varying function V_n.

This approach is closely related to the continuous wave solution of chapters 3 and 4 taking special cases of V_n. Weyns (1980a and b) evaluated it for a sine modulated Gaussian pulse and a variety of wave-fronts. Weyns evaluated the integral numerically. Unless an analytic expression for the transform is available the high-speed method of Lockwood and Willette has no advantage.

The impulse response in its developed form is described well by Weight & Hayman (1978) and by Duck (1981) in his article on field description. The field pressure is proportional to the temporal convolution of $V_n(t)$ the time varying normal velocity of the vibrator and what Weight & Hayman term the pressure impulse response, $h^1(\bar{x}, t)$ i.e.

$$p(\bar{x}, t) = \rho V_n(t) * h^1(\bar{x}, t) \qquad - 2.18$$

where * denotes a temporal convolution

p is pressure

ρ is density

$\bar{x}$ is the position vector

t is time

$$h(\bar{x}, t) = \int_S \frac{\delta(t - \frac{r}{c})\, dS}{2\pi r} \qquad - 2.19$$

h^1 is the first time derivative of h

C = velocity

r = ct

h has the same form as the Rayleigh integral but containing the delta function, δ, instead of V_n.

This has the very useful quality of separating the description of the pulse from the geometry of the transducer. The temporal convalution is achieved numerically with a computer.

Impulse response functions have been published by several authors (e.g. Beaver, 1974; Stephanishen, 1974; Arditi et al, 1981). Arditi and Lockwood and Willette (1973) go on to obtain CW solutions from the Fourier transform of $h(\bar{x}, t)$. The Toronto group (Hunt, Foster, Arditi, Patterson) use the impulse response to investigate annular arrays. Indeed they use the combination of annuli to approximate shapes for which they are unable to derive an impulse response,(Foster et al, 1980). Also in this paper they extend the impulse response and the assumptions to evaluate echo pulses thus enabling them to model a device which transmits, and receives on different transducers. This has also been demonstrated by Chivers & Duck(1977) and Weight and

Hayman (1978).

All solutions describe the interference between different components of the beam. The CW interference spreads through all space and was described by Schoch (1941) as two components; one due to the face of the piston, one due to its edge. The case of a plane circular piston is illustrated in figure 2.5.

Freedman (1970) developed the replica pulse theory which applies to pulses where interference will only occur over a limited part of the field. The edge wave will be in anti-phase with that due to the piston surface. The pulse from a transducer will, therefore, consist of three components which will interfere with each other.

These are the possible approaches to beam descriptions. The most complete is the impulse response. It can describe beams over their full length and give an accurate presentation of pulse shape anywhere in the beam. Once the impulse response of a geometry has been found the effect of various pulse shapes may be obtained. However, much of this may be wasted. The transducer is for water-bath scanning. This will necessitate a 'stand-off' distance between source and subject to prevent reverberations falling within the image. Thus the field close to the transducer is not important. Pulse shape is arbitary and in mirror systems will not be short (e.g. less than one wavelength). Even if a half or one cycle pulse could be obtained, reflection from the mirror elements would almost inevitably lengthen and weaken it. A suitable model must be able to explore complex (e.g. conic sections) forms which are likely to be adopted for mirror transducers. Analytical expressions for the impulse response have only been published for a limited number of geometries. For most they will not exist. Approximations, such as that used by Patterson and Foster (1982) to describe conical transducers may not always be possible.

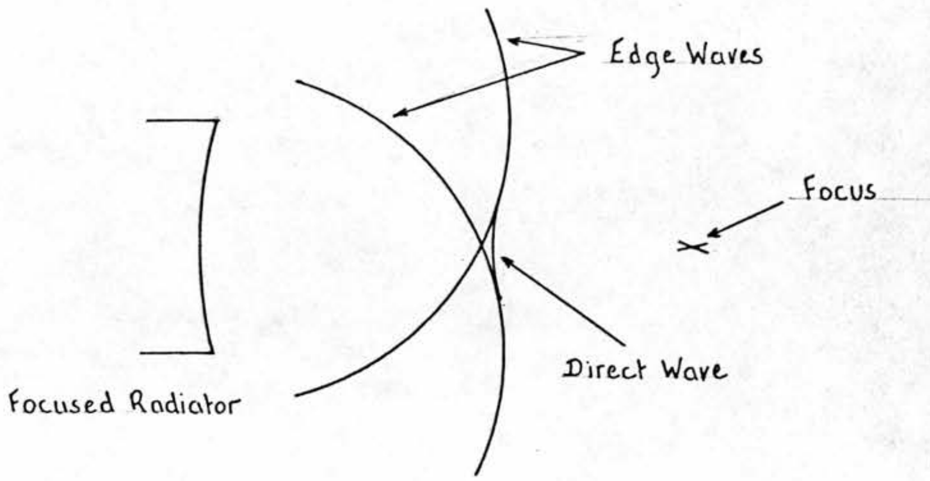

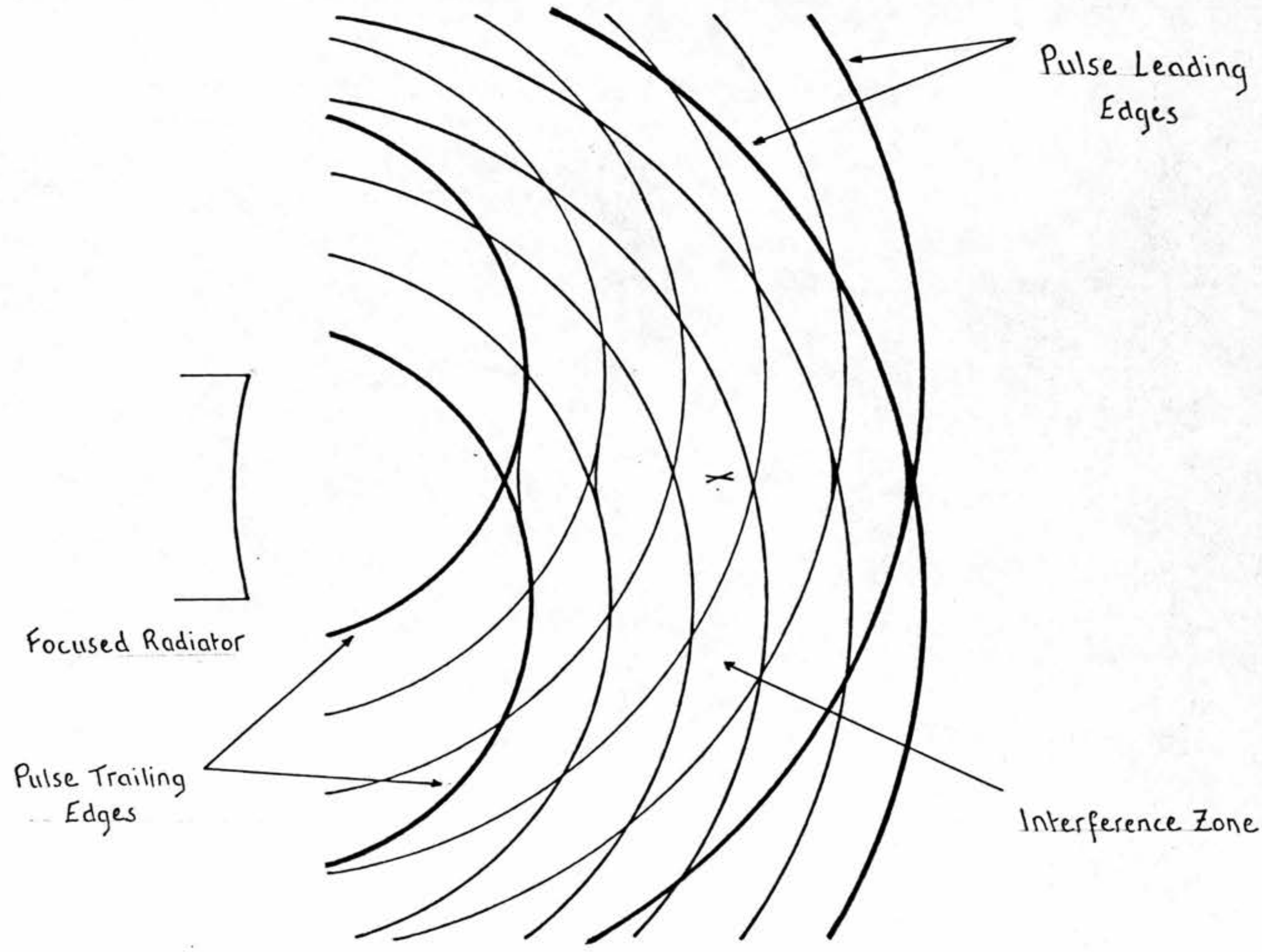

Figure 2.5. Edge and direct wave components of an ultrasound pulse.

The combination of numerical integration and numerical convolution would be time consuming to evaluate.

It is more important to be able to compare different designs than predict absolute values of field parameters. Before developing mirror systems the effect of important parameters such as the apodisation of the aperature by the secondary mirror must be evaluated.

This reasoning would indicate the simplest (i.e. CW) solution as the most desirable if its description of the field is adequate. Such an algorithm could be expanded to equation 2.16 to give the field due an arbitary pulse shape. However, will it be an adequate description of the field? Although pulsed information for large focussed apertures is not available, several authors have compared CW and PW solutions.

Beaver (1974) looked at the radial pulse shape four arbitary pulse lengths with rectangular and half-sine envelopes. For pulses four wavelengths long or at distances greater than 100 wavelengths from the transducer the PW field was close to the CW. Only close to the transducer was there great change. However, his transducers were small (radius $\leqslant 10\lambda$) and unfocussed.

Foster & Hunt (1978) looked at a 12.7 mm diameter 3.5 MHz disc with a single cycle pulse. In the far field (at a range of 350 mm) they found the PW profile to be more peaked at the axis with a full width, half maximum of 8.8 mm for the pulsed and 12.2 mm for CW. As might be expected the two differ more radically along the axis. The PW and CW solutions correspond well only in the far field. There is a broader, lower peak corresponding to the last axial maximum of the CW. The near field of the pulsed beam lacks the fine structure caused by interference in the CW beam although it does have one small minimum.

Weyns (1980b) describes spherical bowls excited by a sine modulated Gausian pulse. His bowls were of 15 mm diameter, 2MHz and with radius of curvature in the range 20 to 60 mm. Kossoff et al (1968) gave a formula for the theoretical diameter between the first off-axis zeros of focussed bowls. For comparison with his PW beams, Weyns multiplies this by a constant to give the -3dB and -10dB contours. He found Kossoff's estimates to be remarkably good although generally pessimistic, more so for strongly focussed devices. The field shapes are, however, complicated and strongly dependent on pulse shape. For radii of curvature less than 110 mm, the two solutions gave the same values. Weyns also found that the transition from 'pulsed' to 'continuous' fields occurred at pulses 6 cycles long. The pulsed field showed a reduction in the near field structure, in the size and number of side lobes and in the constrictive effect. He also compared the pulsed field of discs with spherical bowls and annuli. He concludes that spherical bowls focus without augmenting the side lobes but increase the beam spread after the focus and introduce a far field interference structure. Spherical rings maintain the quality of the far field and the focussing principal increases the side lobes.

These results combine with the experimental requirement to guide the selection of a suitable algorithm. The development of the project requires that model should principally be able to demonstrate the effect of varying parameters, that it should be capable of development to investigate the increasingly complex designs that are likely to evolve or to provide more detailed information. It should be available quickly and its algorithm must be validated.

An important factor influencing the evaluation of the field will be the boundary conditions used. The effect of choice of boundary conditions on a highly focussed large aperture water bath transducer is unknown. The model should also be able to test them. This is discussed in chapter 3.

An impulse response model is complicated and will take some time to construct. It may not be able to evaluate analytically complicated designs. It will not yield a quick CW solution.

A CW model on the other hand may be developed (after Weyns) to give a pulsed field if required or to accommodate complicated geometries. The only published work on such highly focussed large bowls is the work of Archer-Hall and Ali Bashter (1980) using a CW model. This, however, would be at the expense of the ability to investigate pulse shapes.

It seems however that practically it may not be possible to manufacture a desired pulse shape. The greatest weakness of a CW model is the difference between the continuous interference over all space and the coincidence of the replica pulses described by Freedman (1971) in the pulsed field. This is shown by the differences in axial beam shape found by Foster and Hunt. Although they found the far fields to be alike for both fields this is likely to change as focussing introduces interference patterns there as described by Weyns. If a CW model is used to study the effect of apodisation on the trade-off between side lobe size and far field structure, then beam spread rather than interference must be used.

The application, however, recognises that devices will have a limited focal depth. An estimate from classical optical theory is likely to be a little pessimistic (due to apodisation).

It is recognised that a CW model will principally yield information only about the focal regions, traditionally within only a pulse length (probably about 1.3 mm axially) of it although as suggested previously, it will probably be sufficiently accurate beyond that. As a starting point, the initial algorithm is based on the simple, single integral of Archer-Hall and Ali-Bashter, which will give radial fields only through the centre of curvature of the bowl. This simple model facilitates program development as well as transducer design and development. It may be used to test possible developments of the model itself. Different boundary conditions may be tried. Numerical evaluation of the surface integral would permit points anywhere in the field to be calculated. Pulse shape might be added to give the PW field.

CHAPTER 3.

NUMERICAL MODELLING OF SPHERICAL BOWL TRANSDUCERS.

INTRODUCTION.

Since the focal qualities of a breast scanning transducer are of such importance and since several approaches to beam design are possible, it was important to develop mathematical models which would permit the comparison of focussing devices and, if possible, prediction of the beam shape of an individual transducer.

The model considered here is a starting point. There are many possible models. There are many possible transducer designs. The following features are important.

(1) Both the algorithm and the program that evaluates it should be capable of development and of evaluating a variety of systems.

(2) The model should be simple so that the direction of design and model development may be established early.

(3) The model is capable of plotting large aperture sources and of showing the effect that apodisation has on such fields; thus indicating if it may be worthwhile pursuing the design and construction of mirror systems and the constraints which will be placed on such devices.

(4) Simplicity and the use of external functions to describe the algorithm make it suitable for assessing the lines of development for algorithms intended to describe such devices more fully.

(5) In the context of large apodised apertures, different boundary conditions may be explored and the relevance of a continuous wave (steady state) solution to a field which will in practice be pulsed wave (transient) investigated.

The algorithm is described in Section 3.1 and possible alternative boundary conditions discussed.

The program itself is described in Section 3.2. It is built on a flexible base designed to accommodate readily, expansion of algorithm, parameters and facilities for the manipulation and output of data once it has been calculated. The verification of coding and algorithm is dealt with in section 3.3.

The application and validity of the algorithm are considered in section 3.5. The role of a continuous wave model is discussed; pulsed and continuous wave results compared.

3.1. ALGORITHM

The analysis of a steady state diffraction pattern involves solving an integral of the form

$$\phi_p = \int_S A \quad G \quad dS \qquad - 3.1$$

where A = arbitary constant.

S = transmitting surface or aperture.

G = any Green's function.

The theory of such surface integrals is given by Coulson and Jeffrey (1977). The choice of Green's function employed depending on the boundary conditions employed. This will be discussed later.

The physical constraints are placed on the model to maintain simplicity. The source is seen as a uniformly transmitting concave bowl. The case of a focussing mirror illuminated by an incident beam is directly analogous (Griffing and Fox, 1949). Since it is intended in any design that only sound focussed by the mirror should be present at the focus an incident beam is not evaluated. The aperture may be apodised by an obstruction, representing the secondary mirror of any reflector system, at the centre. The surface integral may be reduced to an analytical solution for points on the axis or to a single integral for points in the plane of the geometric centre of the bowl by using the techniques described by Archer-Hall and Ali-Bashter (1980). This restraint greatly assists the evaluation of the integral but also restricts its utility. Most relevantly diffraction will lead to the field maximum, the 'acoustic focus' being displaced from the geometric focus inwards towards the bowl. This effect will decrease for increasing Numerical Aperture. Study of the axial plot, shows the field maximum to be close to the geometrical focal plane for $N \geqslant 0.26$. The medium is infinite or semi-infinite, homogeneous and loss-less. The greatest departure of the model from the physical situation it simulates, is that it is a steady state (continuous wave) solution of a transient (pulsed wave) field.

This problem is considered in section 3.5.

Several options exist in the selection of boundary conditions. The more common are those attributed to Huygens. The transducer is located in a plane, infinite rigid baffle and transmits into a semi-infinite loss-less medium as shown in figure 3.1(a). How extensive the baffle must be to approximate well to infinite is debated. Archer-Hall and Gee (1980) suggest a sonar device in the side of a ship as a close approximation. More generally a baffle several wave-lengths thick is considered sufficient. Huygen's boundary conditions have been widely used Rayleigh (1945), O'Neil (1949) for continuous wave, Stephenishan (1971), Duck (1981), Weyns (1980) for pulsed wave. Archer-Hall and Ali-Bashter (1980) have used these boundary conditions in their detailed study of highly focussed bowls in a watertank. Foster and his co-workers (1981, 1982) have used them when studying unusual conical wavefronts. The associated Green's function is

$$G_H = \frac{e^{-jks}}{s} \qquad - 3.2$$

where k = wave number

s = path length

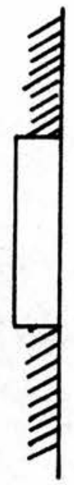

a) Huygen's: infinite, rigid, planar baffle.

b) Kirchhoff: totally immersed transducer with perfectly rigid back face.

c) Radiating Dipole: totally immersed, unbaffled, freely suspended transducer. (Archer-Hall and Gee (1980))

Figure 3.1. Transducer boundary conditions

Kirchhoff's boundary conditions have also been used over a long period (e.g. Baker and Copson (1939), Archer-Hall et al (1979, 1980)). These boundary conditions are appropriate to a completely immersed traducer with a thin rigid case isolated from it by a completely absorbing medium (figure 3.1b). The medium is infinite and loss-less. This is a good description of a mirror in a water bath. However the differences between the two models will be confined to the near field (Fresnel region) (Archer-Hall and Gee (1980)) and may not be important. The associated Green's function is:-

$$G_k = \frac{e^{-jks}}{s} \quad (jk(1 + \frac{z}{s}) + \frac{z}{s^2}) \qquad - 3.3$$

In their investigation of boundary conditions for medical ultrasound transducers, Archer-Hall and Gee (1980) introduced the boundary condition of zero acoustic pressure in the plane of the transducer aperture. They assumed the transducer suspended in an infinite loss-less medium enabling it to transmit both forwards and backwards. Summing up the effect of these two waves gives zero pressure in the plane of the disc. This is illustrated on figure 3.2(c). They called these the radiating dipole boundary conditions and the resulting Green's function is

$$G_D = \frac{e^{-jks}}{s} \cdot \frac{z}{s} \cdot (jk + \frac{1}{s}) \qquad - 3.4$$

This condition is appropriate for a transducer applied to an air:liquid or air:solid interface. This is close to the conditions normally found in medical ultrasound. Archer-Hall and Gee describe the resulting CW field. It is not likely that this will be an appropriate solution for water bath scanning and only the Huygen and Kirchhoff functions are investigated here. Kirchhoff's solution is the average of the Huygen's and Radiating Dipole solution and the result of this comparison would indicate if the radiating dipole solution should be investigated in this context.

3.1.1. USING HUYGEN'S BOUNDARY CONDITIONS.

Two different expressions are used to evaluate the ratio P/P_o where P is the acoustic pressure at the field point and P_o that at the geometrical focus, i.e. in this case the centre of curvature of the bowl. Both model a round spherical bowl source and use cylindrical polar co-ordinates with Z axis of symmetry of the bowl and with the origin where the axis intersects the spherical surface.

The geometry is shown in figure 3.2. The surface is not a complete bowl but is masked in the centre by a disc of radius b_1. This is to allow for the shadow caused by a secondary mirror.

The acoustic pressure at a point, P, in the field, is given by the formula

$$P = A \int_S \frac{e^{-jks}}{s} . \, dS \qquad - 3.5$$

using Green's function of equation 2.2 where

A is an arbitary constant.

S is the surface area of the bowl.

s the pathlength to P from dS.

k is the wave number

At the geometric centre of the bowl

$$P_o = 2\pi A a e^{-jka} \left[\frac{\sqrt{a^2 - b_1^2} - \sqrt{a^2 - b_2^2}}{a} \right] \qquad - 3.6$$

where a is the radius of curvature.

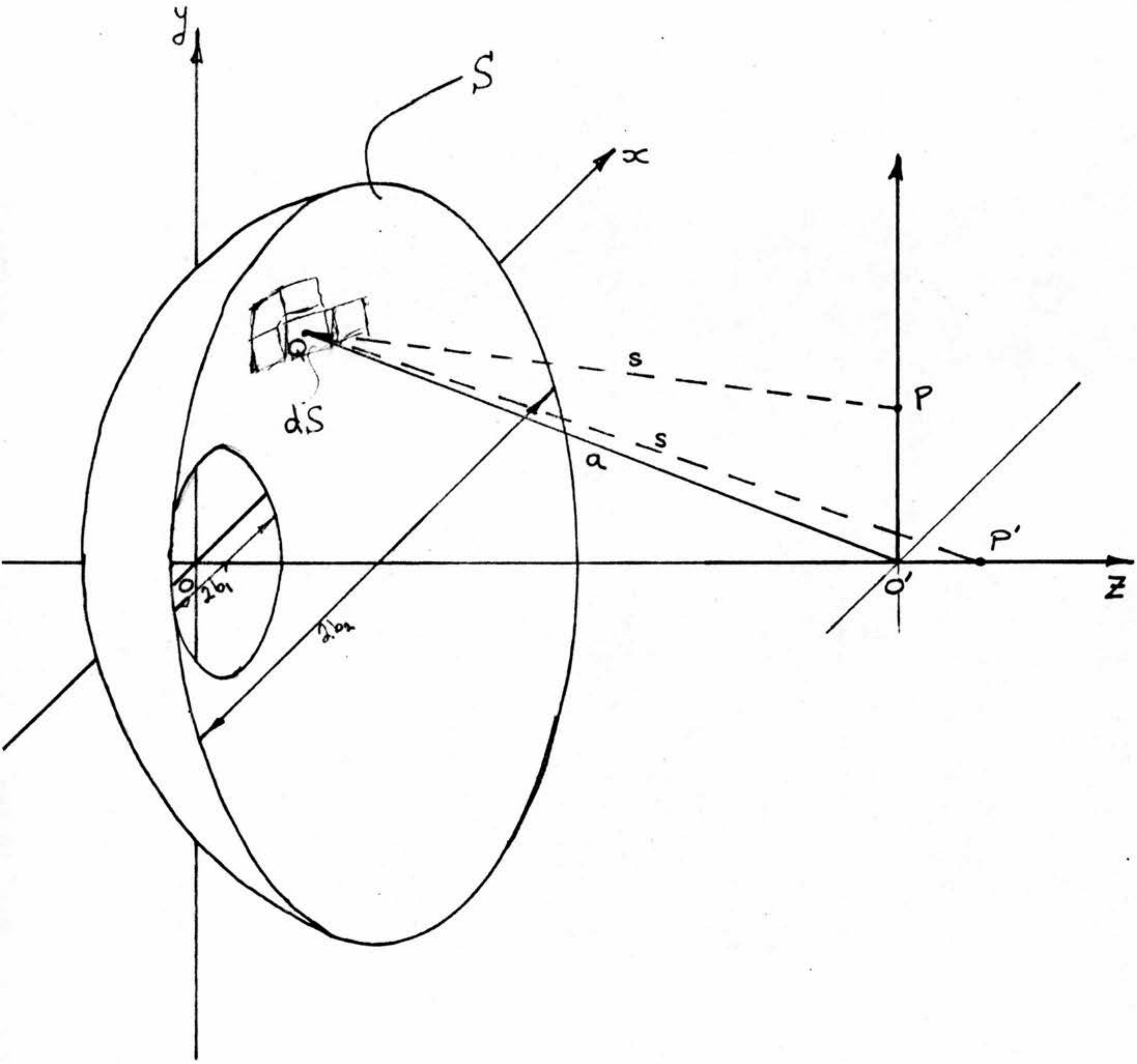

Figure 3.2: PLOTBCW geometry.
The field point P is confined to the O′ plane or the Z-axis.

On axis solution

For other points on the axis an analytic solution is possible. The geometry is shown in figure 3.3.

From geometrical considerations

$$s^2 = a^2 + p^2 - 2ap \cos\beta$$

$$\text{Hence } s\,ds = -ap \sin\beta \; d\beta \qquad - 3.7$$

$$P = \frac{2\pi Aa(-j)}{kp} \left[e^{-jks} - e^{-jks} \right] \qquad - 3.8$$

$$\text{where } s_1 = (a^2 + p^2 + 2p\sqrt{a^2 - b_1^2})^{\frac{1}{2}}$$

$$s_2 = (a^2 + p^2 + 2p\sqrt{a^2 - b_2^2})^{\frac{1}{2}}$$

$$p = (z - a)$$

The relative acoustic pressure at points on the axis of symmetry is therefore:-

$$\frac{P}{P_o} = \frac{-j}{kp} \left[\frac{a}{\sqrt{a^2 - b_1^2} - \sqrt{a^2 - b_2^2}} \right] \left[e^{jk(a-s_2)} - e^{jk(a-s_1)} \right] \qquad - 3.9$$

This may be split into real and imaginary components

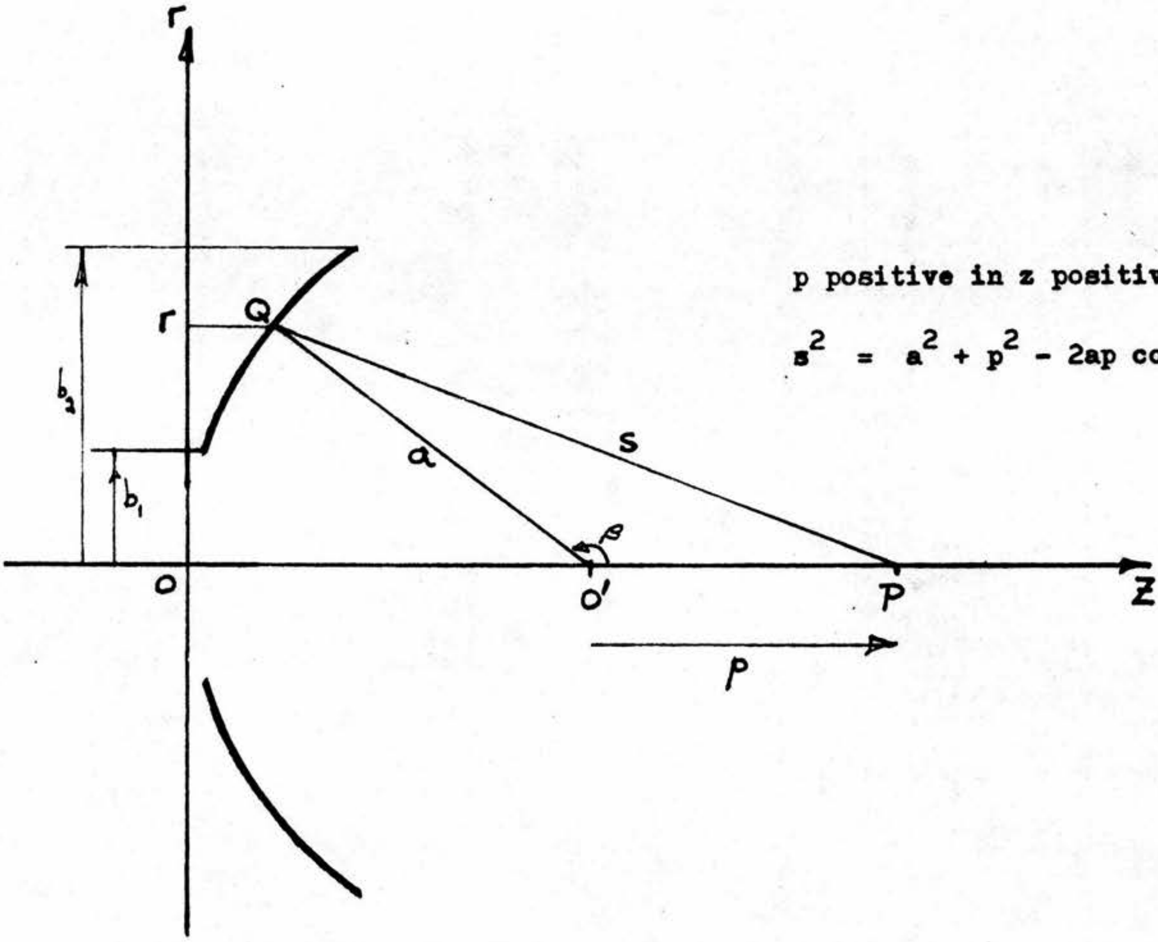

p positive in z positive direction

$$s^2 = a^2 + p^2 - 2ap\cos\beta$$

Figure 3.3. PLOTBCW geometry:

Field point on axis.

$$R\left[\frac{P}{P_o}\right] = \left[\frac{a}{\sqrt{a^2 - b_1^2} - \sqrt{a^2 - b_2^2}}\right] \frac{1}{kp} \left(\sin(k(a-s_2)) - \sin(k(a-s_1))\right) \qquad \text{— 3.10a}$$

$$I\left[\frac{P}{P_o}\right] = \left[\frac{a}{\sqrt{a^2 - b_1^2} - \sqrt{a^2 - b_2^2}}\right] \frac{1}{kp} \left(\cos k(a-s_1) - \cos k(a-s_2)\right) \qquad \text{— 3.10b}$$

These are evaluated separately.

Focal plane solution

Equation 3.5 is not so readily solved for off-axis points. However it may be reduced to a single integral for points in a plane through the centre of curvature of the bowl and orthogonal to the axis. A method is described by Archer-Hall and Ali Bashter (1980).

Figure 3.4 shows the geometry. Since all the transducers being considered are axisymmetric the field point, P, may be considered only on the y^1 - axis without loss of generality.

From geometrical considerations only.

$$s^2 = a^2 + y_1^2 - 2yy_1 \qquad \text{- 3.11}$$

$$\text{therefore } dS = a\,d\alpha\,dy \qquad \text{- 3.12}$$

Substituting in equation 2.5 gives

$$P = A \int_{-b}^{+b} \int_{-\alpha_{max}}^{+\alpha_{max}} \frac{a}{s} e^{-jks} \, d\alpha \, dy$$

since $-\alpha_{max} < \alpha < +\alpha_{max}$

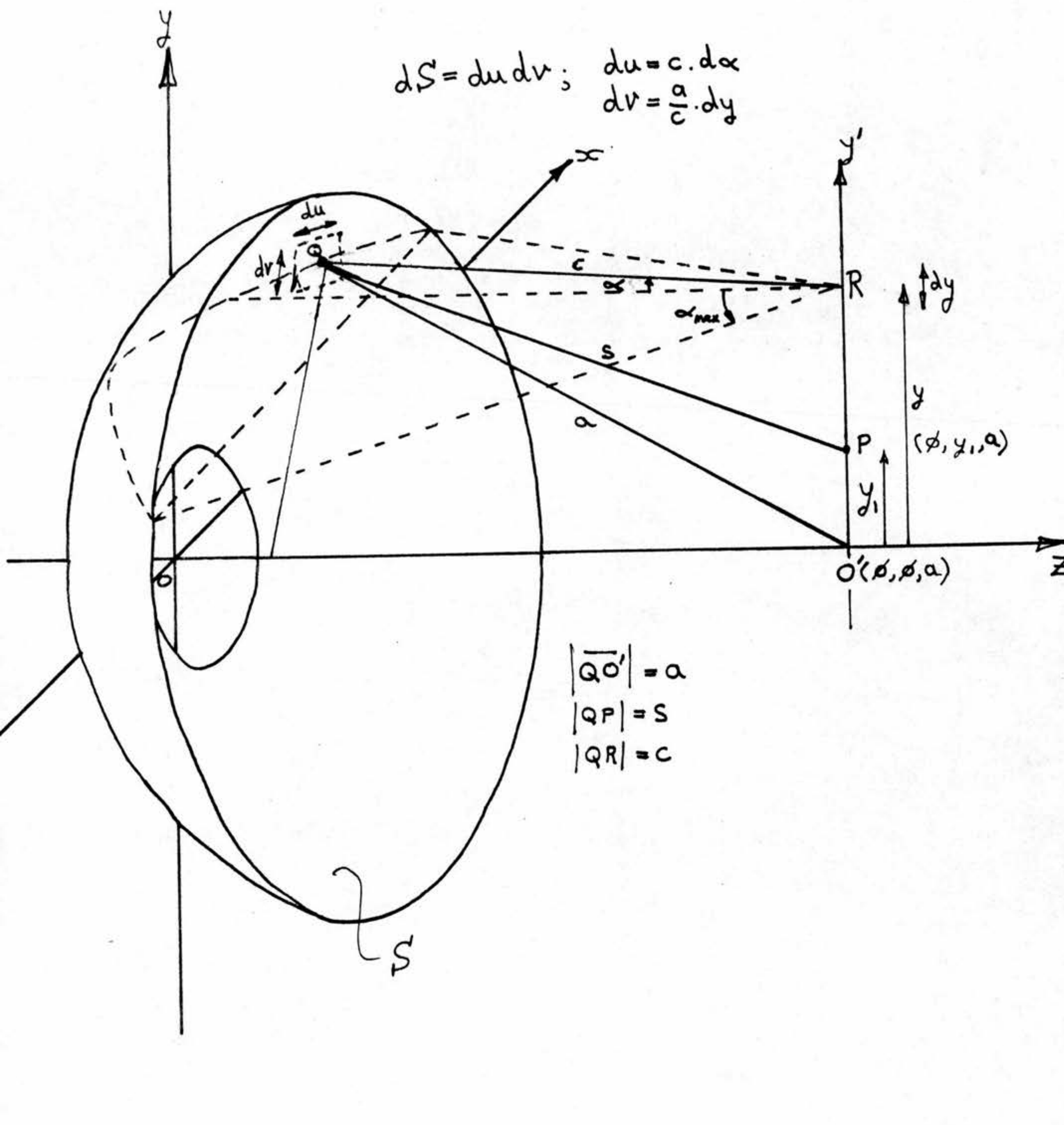

Figure 3.4. PLOTBCW geometry.

Field point in focal plane.

$$P = 2Aa \int_{-b}^{+b} \alpha_{max} \frac{e^{-jk(a^2 + y_1^2 - 2y_1)^{\frac{1}{2}}}}{(a^2 + y_1^2 - 2y_1)^{\frac{1}{2}}} dy \qquad - 3.13$$

since S is independant of α

Also from geometry only

$$\alpha_{max} = \cos^{-1}\left[\left(\frac{a^2 - b^2}{d^2 - y^2}\right)^{\frac{1}{2}}\right] \qquad - 3.14$$

Substituting this and equations 3.11 in 3.13 gives an expression which, while clumsy to look at may be evaluated numerically. This is normalised to the peak geometrical pressure by dividing by equation 3.6.

The real and imaginary fields due to a complete source of the given outer diameter ($2b_2$) are evaluated. Then the components due to a source the diameter of the obstruction ($2b_1$) are calculated and subtracted before the resultant field is obtained. It is simpler to do this than to evaluate the integral with different limits for α when $y < b_1$.

3.1.2. USING KIRCHOFF'S BOUNDARY CONDITIONS

Kirchoff's boundary conditions simulate a transducer backed by a rigid baffle. As with Huygen's boundary conditions, different solutions are found for points on the axis of symmetry and for the plane perpendicular to this axis and through the geometrical focus.

The geometry is shown in figure 3.2. The Kirchhof solution Green's function (Equation 3.3) is substituted in equation 3.1. The pressure at the field point is given by

$$P = A \int_S \frac{e^{-jks}}{s} \left[jk(1 + \frac{z}{s}) + \frac{z}{s^2} \right] dS \qquad - 3.15$$

using the Green's Function of equation 3.3.
where A is an arbitary constant
S is the surface of the bowl
s the path length to P from dS
k is the wave number
z is the axial co-ordinate

At the geometric centre, C

$$P_o = 2\pi A \left[2jk + \frac{1}{a} \right] e^{-jka} \left[\sqrt{a^2 - b_1^2} - \sqrt{a^2 - b_2^2} \right] \qquad - 3.16$$

where a is the radius of curvature

<u>On-axis solution</u>

For other points on the axis. (The geometry is shown in figure 3.3 using equation 3.7.)

$$P = \frac{2\pi Aa}{-p} \left[(1 + \frac{z}{s_1}) \; e^{-jks_1} - (1 + \frac{z}{s_2}) \; e^{-jks_2} \right] \qquad - 3.17$$

where $s_1 = (a^2 + p^2 + 2p\sqrt{a^2 - b_1^2})^{\frac{1}{2}}$

$s_2 = (a^2 + p^2 + 2p\sqrt{a^2 - b_2^2})^{\frac{1}{2}}$

as before

The relative pressure on axis is given by

$$\frac{P}{P_o} = \frac{+1}{p(2jk + \frac{1}{a})} \left[\frac{a}{\sqrt{a^2 - b_1^2} - \sqrt{a^2 - b_2^2}} \right] \left[(1+\frac{z}{s_2}) e^{jk(a-s_2)} - (1+\frac{z}{s_1}) e^{jk(a-s_1)} \right]$$

- 3.18

As with equation 3.9, the real and imaginary components are evaluated separately.

Focal Plane Solution

The Kirchoff solution Green's equation (3.15) is

$$P = A \int_S \frac{e^{-jks}}{s} \left(jk(1 + \frac{a}{s}) + \frac{a}{s^2} \right) dS$$

The geometry shown in figure 3.4 gives equations 3.12 and 3.11 which substitute for the elemental area dS and path length s respectively giving

$$P = Aa \int_{-b}^{+b} \int_{-\alpha max}^{+\alpha max} \frac{e^{-jks}}{s} \left(jk\,(1 + \frac{a}{s}) + \frac{a}{s^2} \right) d\alpha \; dy$$

$$= 2Aa \int_{-b}^{+b} \alpha_{max} \frac{e^{-jk(a^2+y_1^2-2yy_1)^{\frac{1}{2}}}}{(a^2 = y_1^2 - 2yy_1)^{\frac{1}{2}}} \left[jk(1+ \frac{a}{(a^2+y_1^2-2yy_1)^{\frac{1}{2}}}) + \frac{a}{a^2+y_1^2-2yy_1} \right] dy$$

- 3.19

3.2. Program Structure

The program is written in Fortran IV and run under the EMAS operating system used by the Edimburgh Regional Computing Centre on a twin processor ICL 2972 installation. It uses NAG Library subroutines for integration as well as ERCC Graphpack subroutines for output. The structure of the program is shown in figure 3.5.

The program caters for 3 curves of up to 100 points each. Once the first curve has been calculated subsequent processing and calculations are centred on an 'Instruction' node from which various options may be selected. This node may be readily enlarged to cope with an increased number of possible options. These options mainly take the form of subroutines which may be altered without affecting the main program. Parameters are passed as common blocks or as subroutine parameters; data in a common block.

The program is 'user friendly' and checks for unsuitable, inconsistent parameters; giving an error message and the opportunity to confirm that they are correct and to provide a label.

The algorithm used is housed in the sub-program called in the central loop of the main program. These sub-programs are called many times and this is the time consuming part of the program. Therefore these elements are written in the most efficient, rather than the most elegant, Fortran. After debugging they were recompiled using options to give an efficient object code at the expense of helpful error messages. The error flags set by the NAG integration routine DOIAGF are monitored to check for any failure to converge to the specified accuracy. Program efficiency is considered in section 4.2.7.

The CPU time used by the principal loop of the program between statement labels 160 and 230 is output at the end of the loop.

All the curves must be of the same type, either axial or radial, and if one of the other type is required the instruction 'NNEW' must be

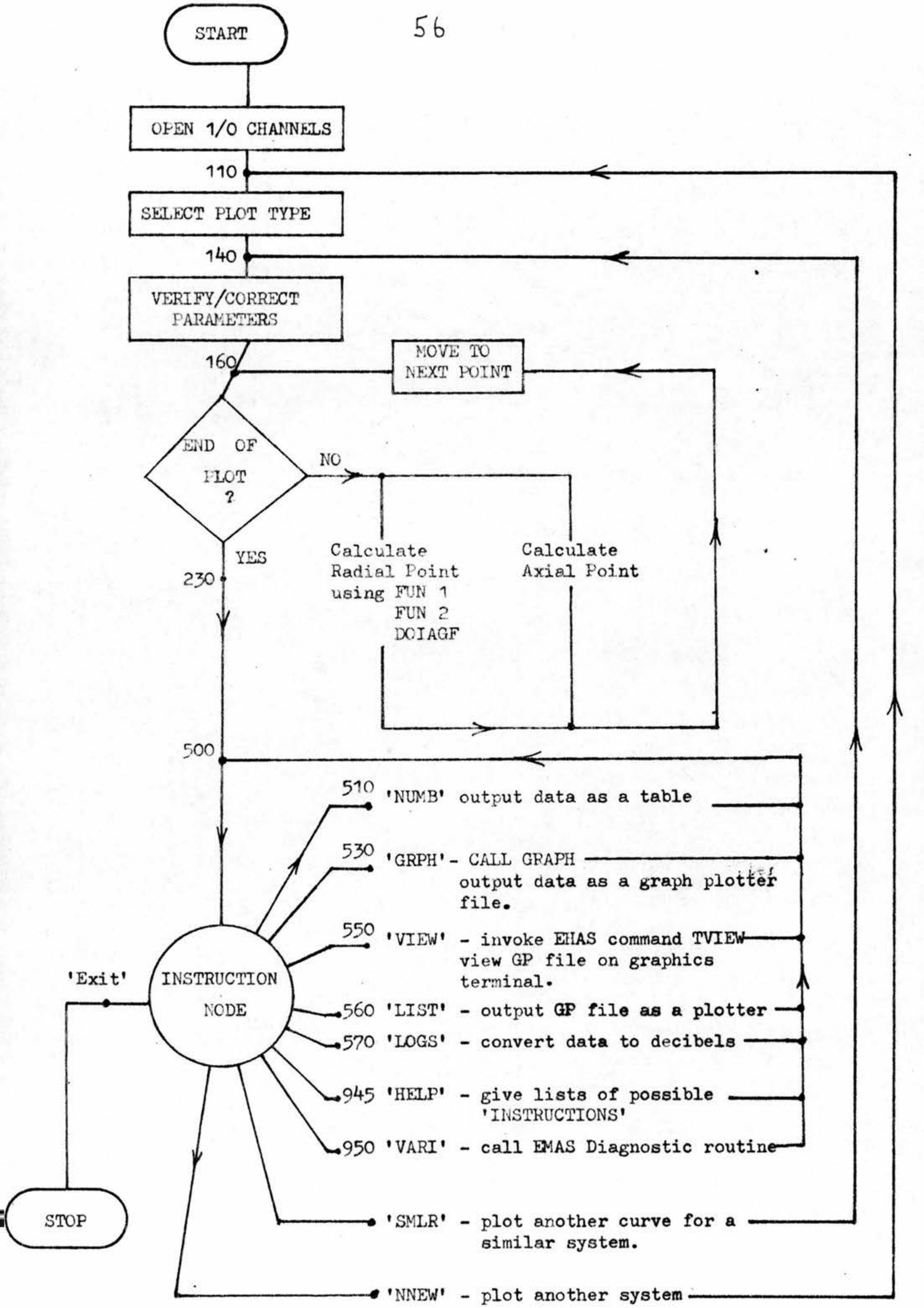

Figure 3.5: Flow diagram of PLOTBCW

used and the current curves lost. If an attempt is made to calculate a 4th curve, a check is made before overwriting curve 3. Likewise any attempt to discard data which has not been output in some form, either as numbers or as a graph is queried.

The 'NUMBERS' subroutine (invoked by the Instruction 'NUMB') deals with a specified curve but the other Instructions will be applied to all the curves which exist when they are called.

'LOGS' converts data to decibel form and if another curve is calculated subsequently the graphical output will be inhibited until the new data is in decibel form also.

The Instruction 'GRPH' creates a graph plotter file which may be subsequently 'VIEW'ed or 'LIST'ed. It will not be lost if the program is stopped or crashes. These data files, named 'PLOTSTOREn' may be viewed or listed from outside the program or those created at previous use of the program may be handled while it is running.

Use of the Instruction 'VIEW' which invokes an interactive graphic package, requires that a graphics terminal is being used.

An ERCC subroutine is used to enter the 'GRAPHPACK' interactive package TVIEW directly from the program. After using TVIEW the user is transferred directly back to the program instruction node without loss of any program flags or parameters.

Important parts of the program listing are given in Appendix 2.

3.3. Verification of PLOTBCW

The program evolved in a series of steps. Each new version was checked by comparing its output with simple theory for small apertures or plane transducers, with published data and with earlier versions. Similarly PLOTCW (see Chapter 4) was compared against PLOTBCW.

The material, theoretical and experimental, published for systems is limited. That of Archer-Hall and Ali-Bashter (1980) is useful. Unfortunately the measurements of Olofsson (1963) and Kelly-Fry et al (1968) cannot be used since they transmit and receive on different crystals.

Kinsler and Frey (2965) give the formula for the relative intensity on axis for a plane, CW piston radiator. Since intensity is proportional to pressure squared, this may be expressed as

$$\text{Relative Pressure} \quad \frac{P}{P_o} = \sin \frac{\pi}{\lambda} \left[\left(\left(\frac{b}{2} \right)^2 + Z^2 \right)^{\frac{1}{2}} - Z \right] \qquad - 3.20$$

where λ = wavelength

b = diameter of piston

Z = axial distance

This was compared with PLOTBCW for the same transducer as plotted by Wells (1972) that is $b/\lambda = 10$ at a frequency of 3MHz and a water velocity of 1500 ms^{-1}. Also compared was a larger aperture, b = 50 mm at a frequency of 5MHz and a sound velocity of 1520 ms^{-1} (water at 35°C). A radius of 9.99 m was taken as close to infinity. The plots evaluated by PLOTBCW are shown in figure 3.6. There is perfect agreement with equation 3.20 over the ranges shown.

O'Neil (1949) gives axial fields for small focussed CW bowls. It is however, Archer-Hall and Ali-Bashter who provide an axial plot for a large Numerical Aperture (0.25). No detectable difference from this was found.

Radial plots are compared with the traditional Airy pattern. This assumes Fraunhofer diffraction conditions from which there will be some departure for large Numerical Apertures. This is due to the wavefront impinging on the aperture, being spherical not planar. Archer-Hall and Ali-Bashter (1980) have shown this quantitatively for large unapodised bowls with Numerical Apertures of 0.75 and 1.0.

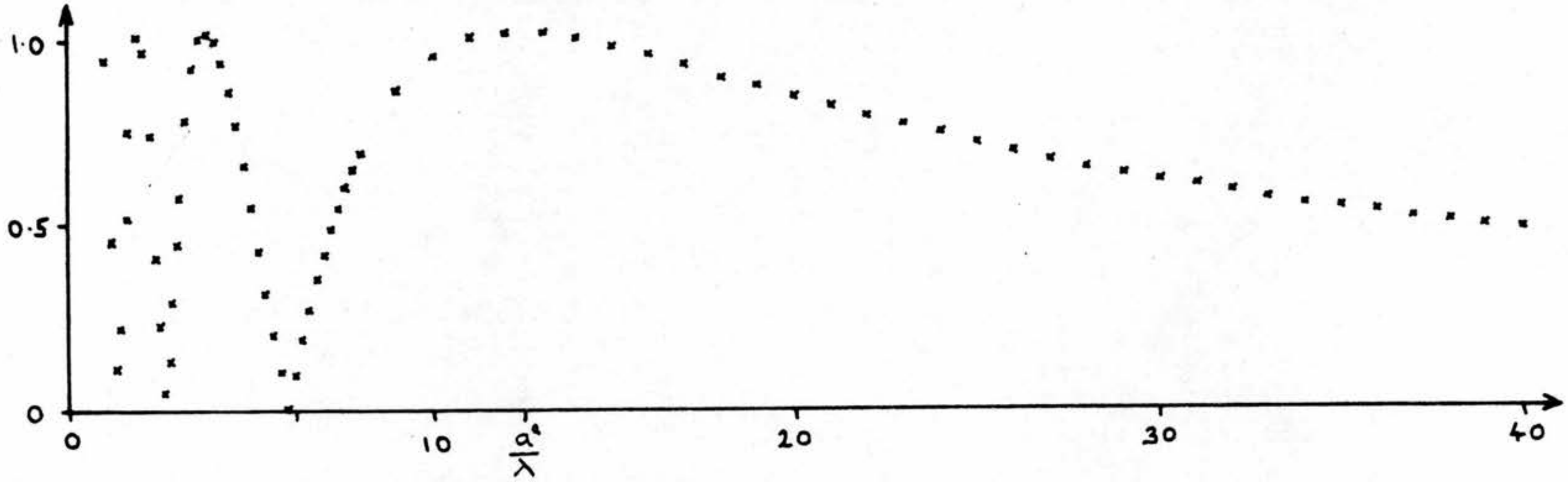

Figure 3.6(a) Comparison with flat disc axial field (equation 2.20)
Wells (1977) dimensions. Diameter = 5 mm
λ = 0.5 mm

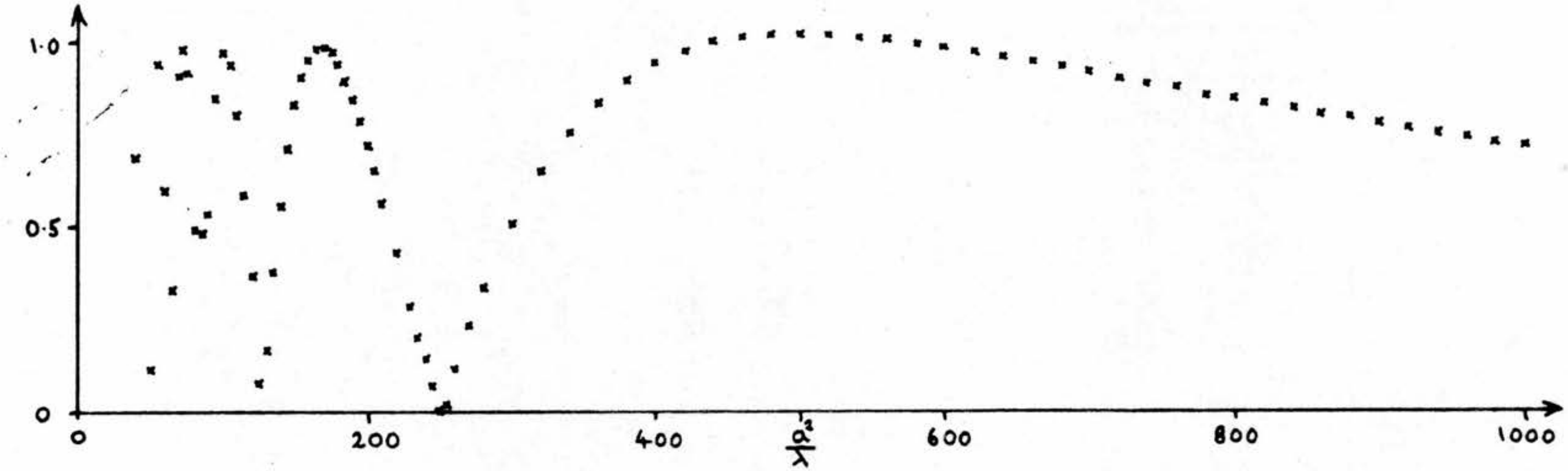

Figure 3.6(b). Comparison with flat disc axial field (equation 2.20)
Diameter = 25 mm; λ = 0.304 mm.

Using Airy's theory, the normalised pressure diffraction pattern is given by:-

$$\frac{P}{P_o} = \frac{2 J_1 (m)}{m} \qquad - 3.21$$

where $J_1(m)$ is the first order Bessel function of the first kind.

m = normalised radial coordinate
$= k.b^1 . (NA)$

k = wave number $= \frac{2\pi}{\lambda}$

b^1 = radial position of field point

NA = numerical aperture

Minima will occur at m = 3.832,7.061,10.173, 13.324 and so on. This may be readily compared with the side lobe structure calculated by PLOTBCW. This was checked and found to be in good agreement for a variety of bowls including these discussed by Weyns (1980).

Comparison was made with the radical plots of Archer-Hall and Ali-Bashter for Numerical Apertures of 0.75 and 1.0. No detectable variation from these results was found.

3.4. Comparison of boundary conditions

The boundary conditions described in section 3.1.1 and 3.1.2 are compared for a variety of transducer parameters in the range of interest.

i) A 35 mm diameter, 125 mm focus (NA = 0.13) 5MHz transducer

ii) A 50 mm diameter, 150 mm focus (NA = 0.167) 5MHz transducer corresponding to the lens focussed probe in section 5.4.1.

iii) A 100 mm diameter, 100 mm focal length (NA = 0.5) 5MHz bowl apodised by blocks of 0, 20 and 40 mm. This will demonstrate if apodisation affects the results.

iv) The two bowls described by Archer-Hall and Ali-Bashter (1980). These are 7.5 MHz, 100 mm radius of curvature. The diameters are 150 mm and 200 mm (a complete hemisphere) giving Numerical Apertures of 0.75 and 1.

The Kirchoff model took approximately three times as long as Huygen's to evaluate.

There were no significant differences between the two sets of boundary conditions.

Radial Plots

The radial plots were all identical except for the hemisphere, where there was a very slight variation in the side lobes. The Kirchoff boundary conditions showed the side lobes about 0.002 mm closer to the axis. This case is shown in figure 3.7.

Axial Plots

There were no significant differences between the two axial plots in the region of the focus or field maximum. Only transducer i) demonstrated a slight variation (1% of the actual value, 0.1% of the field maximum) in the amplitude of a peak at about 52 mm range (compared to a focal length of 125 mm). This is 5 maxima closer to the transducer from the field maximum.

Conclusion

There is no benefit in using Kirchoff's boundary conditions for highly focussed devices, even when they are apodised by a central obstruction. The Huygen's conditions are preferable since they may be evaluated much faster.

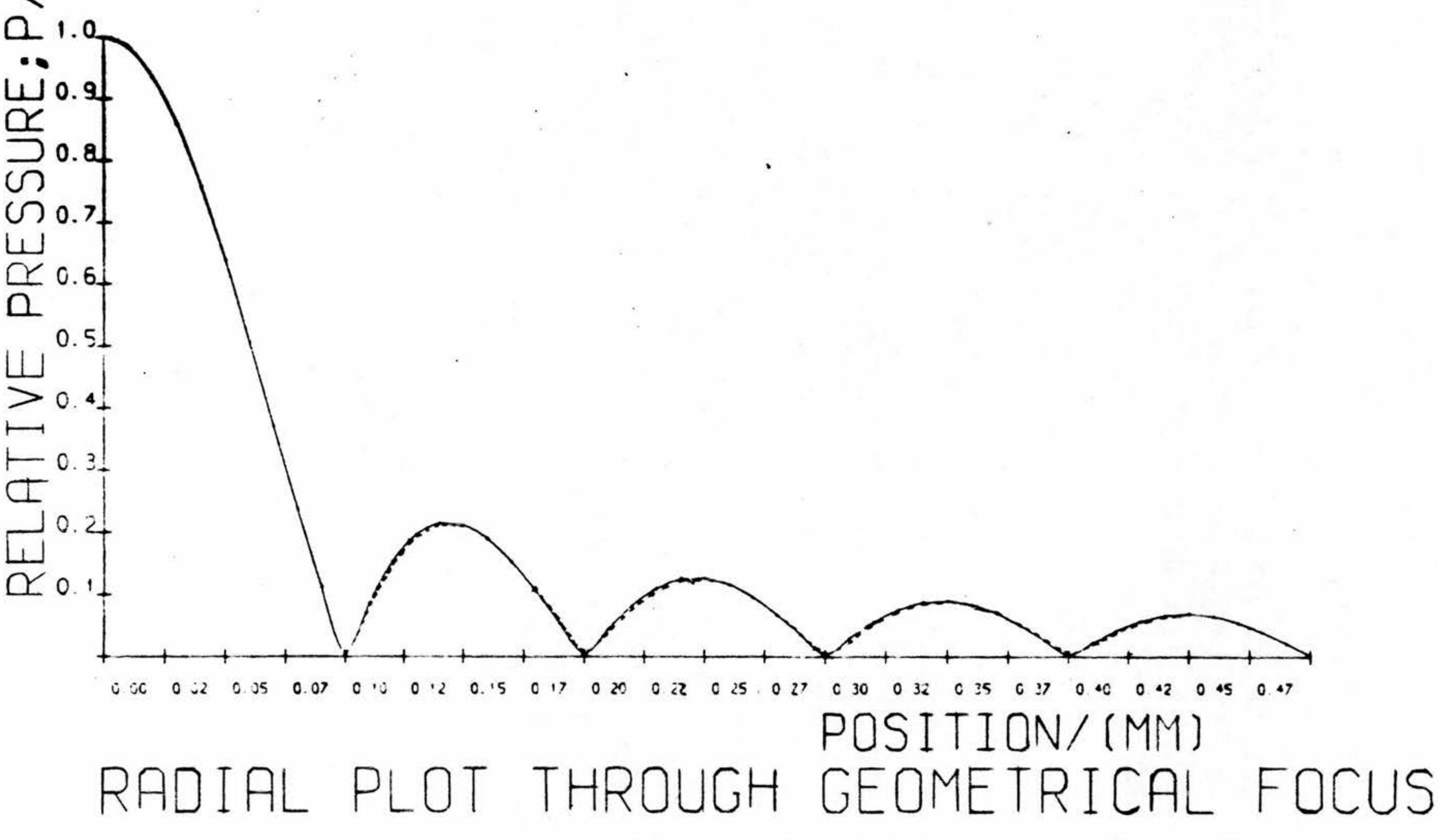

Figure 3.7. Radial field due to a 100 mm radius of curvature, 7.5 MHz hemisphere.

The broken line indicates the Kirchhoff solution.

3.5. Application of a CW solution to a Pulsed Field

Weyns (1980a) looked at the theoretical effect of pulse length on beam shape for plane discs observing that the field depended strongly on the number of cycles in a pulse. Above 6 cycles the field was very similar to CW but as the number decreases from 6 the near-field structure begins to disappear, the side lobes becoming reduced in size and number and the constrictive effect of interference on beam width being reduced. Considering the -3 dB contour, Weyns observed the point of maximal constriction moved away from the transducer. This effect is appreciable at 6 and less cycles. The -3 dB minimum width also increases but this effect is only appreciable for 1 and 2 cycle pulses. Beaver (1974) published beam profiles, comparing half-cycle, one cycle and four cycle pulses with rectangular and half-sine envelopes with CW for small (10 wavelength diameter) planar discs. He demonstrated a tendancy to smooth out the off-axis interference structure. The side lobes appeared and increased in size as the pulse became longer. The four cycle pulses coming close to the CW field, both in shape and amplitude of maxima. The four cycle pulse in the rectangular envelope could not be distinquished from CW in the plane of the last axial maximum. The four cycle pulse in the half-sine envelope was within 5% of the CW amplitude. The shorter pulses, however, did not achieve the same peak amplitude as the CW (-2.8 dB for the one cycle pulse). The focal zone itself is less peaked, giving the same amplitude at about 2 wavelengths off-axis and -6 dB of the CW peak amplitude. At two wavelength radius in the plane of the last axial maximum, the one-cycle pulse is -2.6 dB of its own maximum, -5 dB of the CW maximum. Axially it is only -3 dB of its own peak amplitude at the last axial zero of the CW field.

The pulsed beam profile is, therefore, flatter topped than the CW. Contours taken relative to this peak would, therefore, be broader than a CW beam shape might indicate.

Weyns (1980b) considers focussed bowl transducers. With a two cycle pulse length he shows the -3, -10 and -20 dB beam widths at the focus drawing closer as the Numerical Aperture increases. This effect becomes more marked for Numerical Apertures greater than 0.2. This would slightly negate the effects of the flatter beam profile.

Hunt et al (1983) show the Airy distribution modified by increasingly short pulse length (as represented by bandwidth) for the pressure distribution of a focussed beam and of an annular aperture. The pulse shapes used are typical of what might be achieved in practice. They show no change of the main lobe shape until -15 dB of peak amplitude below which it becomes broader and the zero disappears. The first off-axis side lobe is about 3 dB less than predicted by CW.

Conclusion

A CW model will yield valuable information about the beam shape of various systems relative to one another. The pulsed field will be generally smoothed relative to the CW since the interference effects will be limited in their extent. The maxima caused in the CW field far from the focal zone. The effect will also exist in the focal zone where the PW peak will be broader relative to its own maximum than will the CW.

A CW model will be a powerful tool because of its speed of execution and its ability to explore variations in Numerical Aperture and the effects of apodisation. The expansion of the algorithm to investigate different mirror surfaces would be valuable in assessing mirror systems.

This model is used in Chapter 7 and 8 and in sections 9.1 and 9.3.

Numerical and experimental results for mirror systems are compared in Sections 7.4.6, 7.6, 8.4.4 and 8.6.

CHAPTER 4. NUMERICAL MODELLING OF A POINT SOURCE/SINGLE MIRROR COMBINATION.

A more flexible numerical model than that of the preceding chapter is required to consider sources with non-spherical wavefronts such as would be generated by more sophisticated mirror designs and for field points which are not confined to the principal axis or the focal plane. The conventions used in reference to mirror systems are described in Appendix 1.

4.1. ALGORITHM

The geometry is shown in figure 4.1. Cylindrical polar co-ordinates are used. The mirror is considered as being placed in an infinite planar baffle, (Huygen's boundary conditions). Other boundary conditions are discussed in Section 3.1. The field amplitude at the point P due to a point source, S, reflected in a mirror, M, is given by

$$U_p = \frac{jk}{2\pi} \iint_S \frac{e^{-jk(SQ + PQ)}}{\overline{SQ}.\overline{QP}} \, dS \qquad - 4.1$$

Where P is the point $(r, 0, l')$

l' is the distance of the origin of the field plane, O' from the origin O.

P will always lie in the $\chi = 0$ plane.

This causes no loss of generality for axi-symmetric mirrors.

S $(0,0,l)$ is the location of the point source. It is confined to the z-axis.

Q (ρ,x,z) is the point of reflection in the mirror.

Mirror. The mirror is described by the function

$$Z = M(\rho) \qquad - 4.2$$

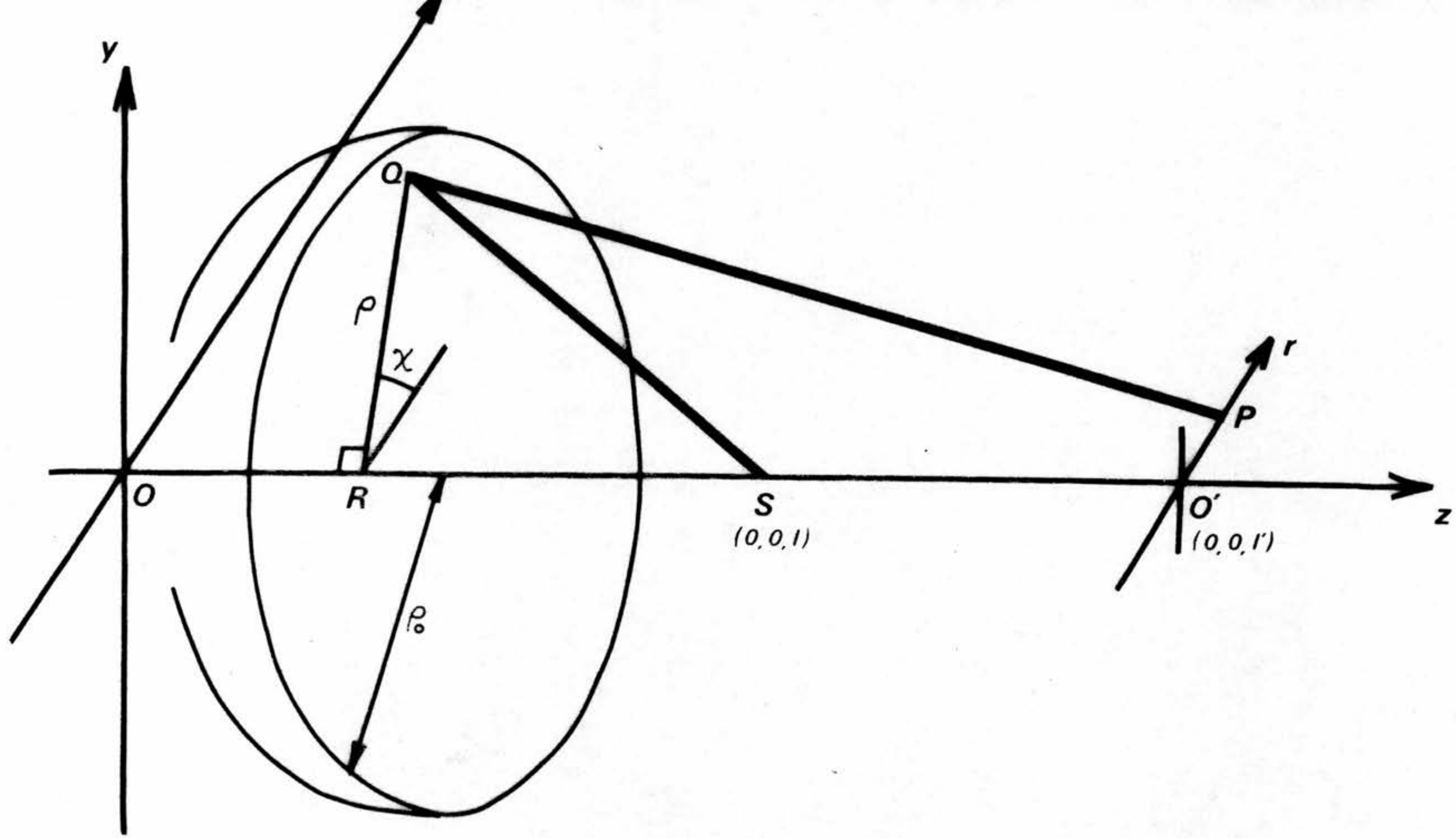

Figure 4.1. Geometry used by PLOTCW.

It is symmetrical about the z-axis. Integration is performed over its surface, S.

Restriction of circular symmetry

All point focus mirror shapes possess circular symmetry about a principal axis, even if not all of the mirror surface which is used is symmetric about that axis (see section 9.1). It is also a property of all axicons, McLeod (1954).

In his consideration of optical axicons, Fujiwara (1962) confined his analysis to cones: he considered the effect of moving the source off-axis. He made several approximations to reduce the surface integral to an expression which, while not soluble analytically, permitted him to use a technique (The Method of Stationary Phase) to get a close approximation. While his procedure was valid for his optical experiment with a very flat cone ($\alpha = 1.5 \times 10^{-3}$ radian) an aperture of 100 mm, a focal length of 20m and a wavelength of 5.5×10^{-7} m, they are unsuitable for the long wavelengths (0.3 mm) and short focal lengths (150 mm) of water bath ultrasound.

4.1.1. Substitutions and Approximations in the double integral

a) Substituting for elemental area, dS
The area element, dS is shown in figure 4.2.

$$dS = \frac{\rho}{\sin(\frac{\pi}{2} - \alpha)} \; d\chi \, d\rho \qquad - 4.3$$

$$dS = \frac{\rho}{\sin\alpha} \; d\chi \, dz \qquad - 4.4$$

2 small angle approximations are worth considering.

i) the angle α is small

hence $\sin\alpha \rightarrow \tan\alpha$

then $dS \simeq \rho \, d\chi \, d\rho \qquad - 4.5$

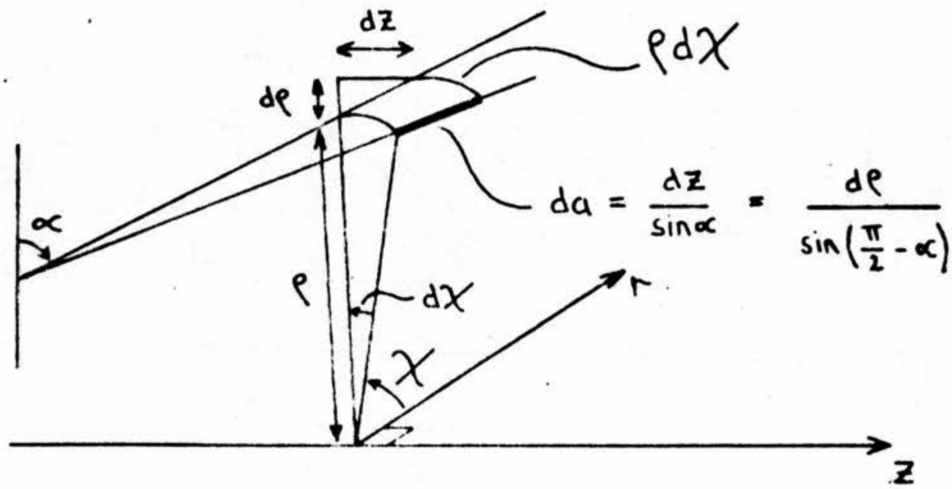

Figure 4.2. The area element, dS.

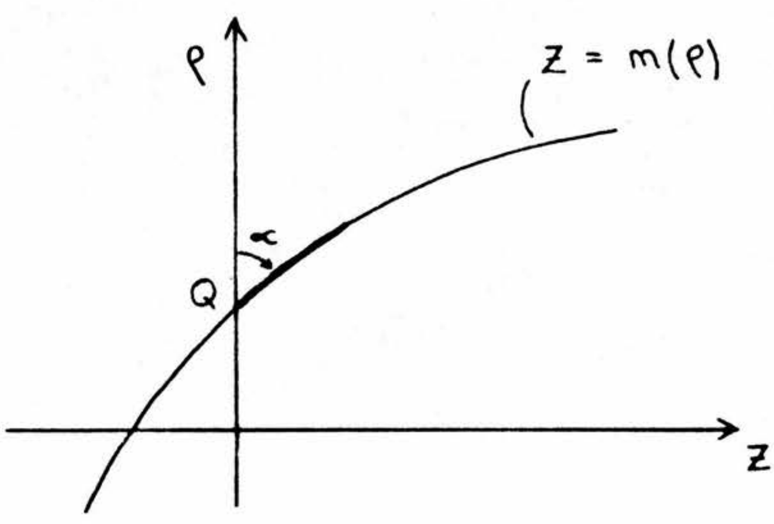

Figure 4.3. Angle of incidence of mirror surface.

This approximation would be suitable for relatively flat mirrors.
The error would be 1.6% for $\alpha = 10^\circ$; 6% for $\alpha = 20^\circ$.
It was used by Fujiwara.
It is applied in subroutine POINT6 (Section 4.2.3).

ii) the angle $\alpha \to \frac{\pi}{2}$

that is $\sin(\frac{\pi}{2} - \alpha) \to \tan(\frac{\pi}{2} - \alpha)$.

then $dS \simeq \rho \, d\alpha \, dz$ - 4.6

This approximation will suit better very deep highly focussed bowls, e.g. those studied by Archer-Hall et al (1980)

It is used by subroutines POINT1 and POINT2 (Section 4.2.3)

4.1.1(b) <u>Determining $\sin\alpha$ or $\sin(\frac{\pi}{2} - \alpha)$</u>

The angle of incidence α of the mirror element, dS is shown in figure 4.3.

The mirror is described by equation 4.2.

$$z = M(\rho)$$

$$\frac{dz}{d\rho} = M'(\rho) = \tan(\alpha)$$

and $\frac{d\rho}{dz} = \tan(\frac{\pi}{2} - \alpha)$

therefore $$dS = \frac{\rho}{\sin(\tan^{-1}\frac{d\rho}{dz})} d\rho \, d\alpha$$ - 4.7.

$$dS = \frac{\rho}{\cos(\tan^{-1} \frac{dz}{d\rho})} \quad d\rho \, d\chi \qquad - 4.8$$

See section 4.2.3, subroutine POINT4

$$dS = \frac{\rho}{\sin(\tan^{-1} \frac{dz}{d\rho})} \quad dz d\chi \qquad - 4.9$$

See 4.2.3 subroutine POINT5

4.1.1(c) Evaluating the magnitude of vectors $\overline{SQ}$ and $\overline{QP}$

SQ with S confined to the z-axis

$$|SQ| = (\rho^2 + (z - l)^2)^{\frac{1}{2}} \qquad - 4.10$$

(Movement in the direction of increasing z is considered positive).

Approximation: The expression may be expanded as a power series and a sufficient number of terms evaluated to give the desired accuracy. Fujiwara (1962) used only the first term.

In a numerical technique, there is a speed advantage (c.f. straight forward evaluation of the above equation) in only using the 1st term. This advantage is lost if any more terms are evaluated.

Hence $$|SQ| \simeq l - Z + \frac{\rho^2 + z^2}{2l} \qquad - 4.11$$

QP with P confined to $\chi = 0$ plane

$$|QP| = (r^2 + \rho^2 - 2r\rho\cos\chi + (l' - z)^2)^{\frac{1}{2}} \qquad - 4.12$$

Approximation: Use a power series expansion as for SQ.

$$|QP| \simeq l' + \frac{r^2 + \rho^2 + z^2}{2l'} - \frac{r\rho\cos\chi}{l'} - z \qquad - 4.13$$

The scalar product.

$$\overline{SQ}.\ \overline{QP} = r\rho\cos\chi - \rho^2 - z^2 + z(l + l') - ll' \qquad 4.14$$

This is exact. It is always used for the scalar product.

4.2. The program suite, PLOTCW

The program layout is based on PLOTBCW (section 3.2)
The basic algorithm is as described in section 4.1. Six different versions of the algorithm were tried, employing different combinations of the substitutions and approximations described in section 4.1.1. These variations of the algorithm are invoked by calling the appropriate subroutine from the range POINT1 to 6.

The program itself evolved, based on the basic two dimensional plotting routine. One version included the option of two or three dimensional plots. This proved a poor arrangement. The program was unwieldy. Long computation times made interactive three dimensional plots impractical. The program could not be optimised without losing the flexibility desired for two dimensional plots. Two and three dimensional plots could not share the same INSTRUCTION set, (see Appendix 3). Therefore two separate programs evolved.

The definitive two-dimensional plotting program is stored in the file PLOTCW. It calculates and stores up to three independant linear plots (maximum 100 points each) which may run axially outwards from the mirror or radially outwards, orthogonal to the axis at any point in the field. This is designed for interactive use along the same lines as PLOTBCW.

PLOTCWX prepares only three dimensional plots. It calculates field points on a two dimensional rectangular grid. The plots may be subsequently presented using the SYMAP, SYMVU and ASPEX packages of the Laboratory for Computer Graphics and Spatial Analysis, Harvard University. This program is designed primarily for batch running because of the large processing times required.

The INSTRUCTION set of the two variations differs but both are able to store and re-read plot data to enable re-analysis on later occasions. This becomes important as the computer time required to evaluate the field points becomes greater. Possible INSTRUCTIONS are listed in Appendix 3.

The mirror shape is supplied and selected from outside the program as described in section 4.2.2.

The shape of the mirror being unknown and variable, no attempt is made to reduce the integral from two dimensions. The NAG subroutine D01DAF is used and implemented as described in section 4.2.4.

The increased complexity of the algorithm and the necessity of a two dimensional, iterative integration will inevitably lead to an increase in the time required for evaluation.

To explore the possibility of minimising this a number of possible approximations were explored. These are described in section 4.1.1. their implementation in 4.2.3.

Calls to subprograms are made dynamically and they are only loaded if required.

4.2.1. The Main Program

a) Linear plotting, PLOTCW

This is the mirror equivalent of the concave bowl programs described in section 3.2. The flow diagram is shown in figure 4.4. Its functioning is essentially similar to PLOTBCW. The enlarged INSTRUCTION set is described in appendix 3.

b) Rectilinear plotting, PLOTCWX

This version differs in two principal ways. The flow diagram is shown in figure 4.5.

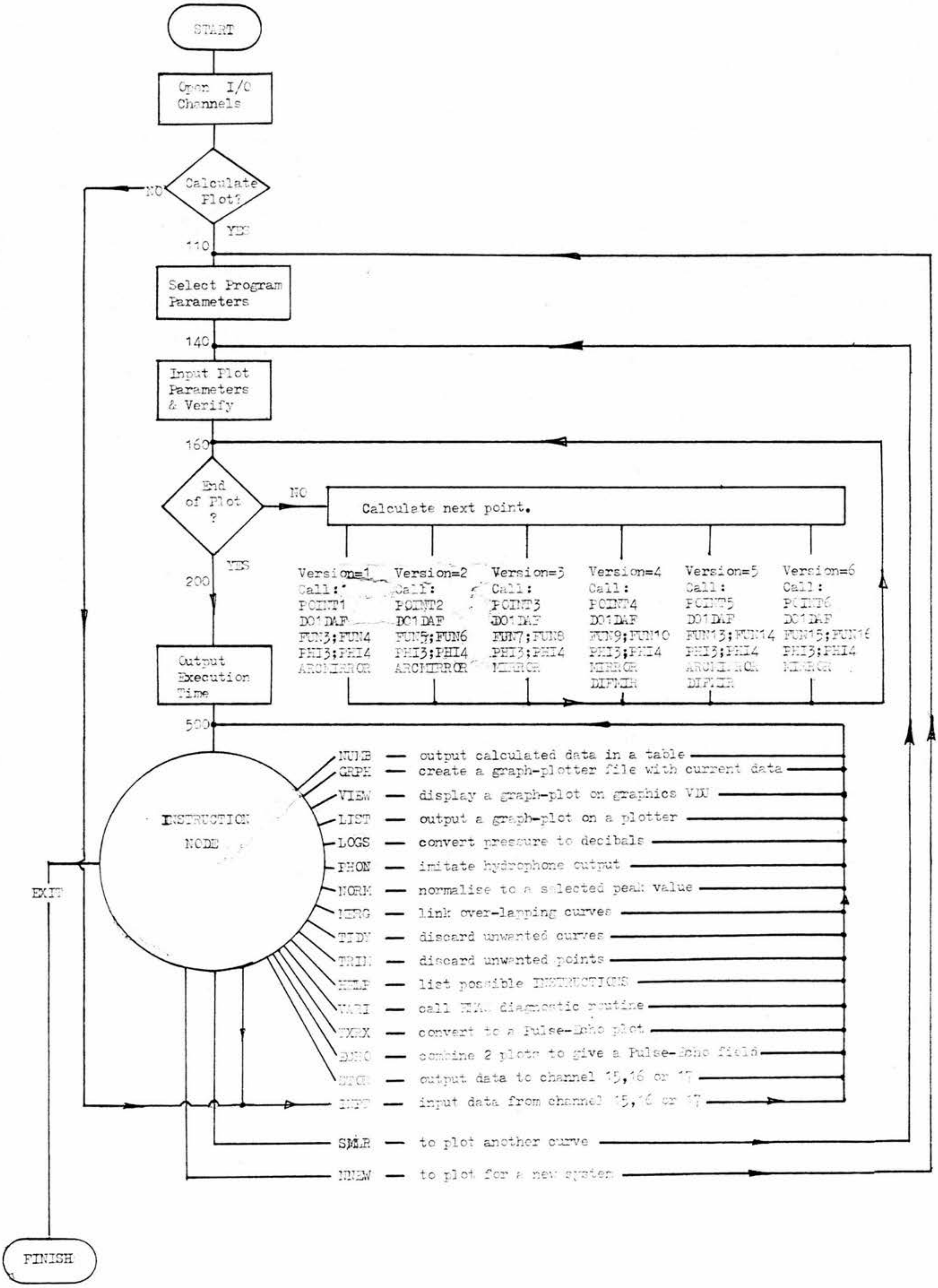

Figure 4.4: PLOTCW flow diagram.

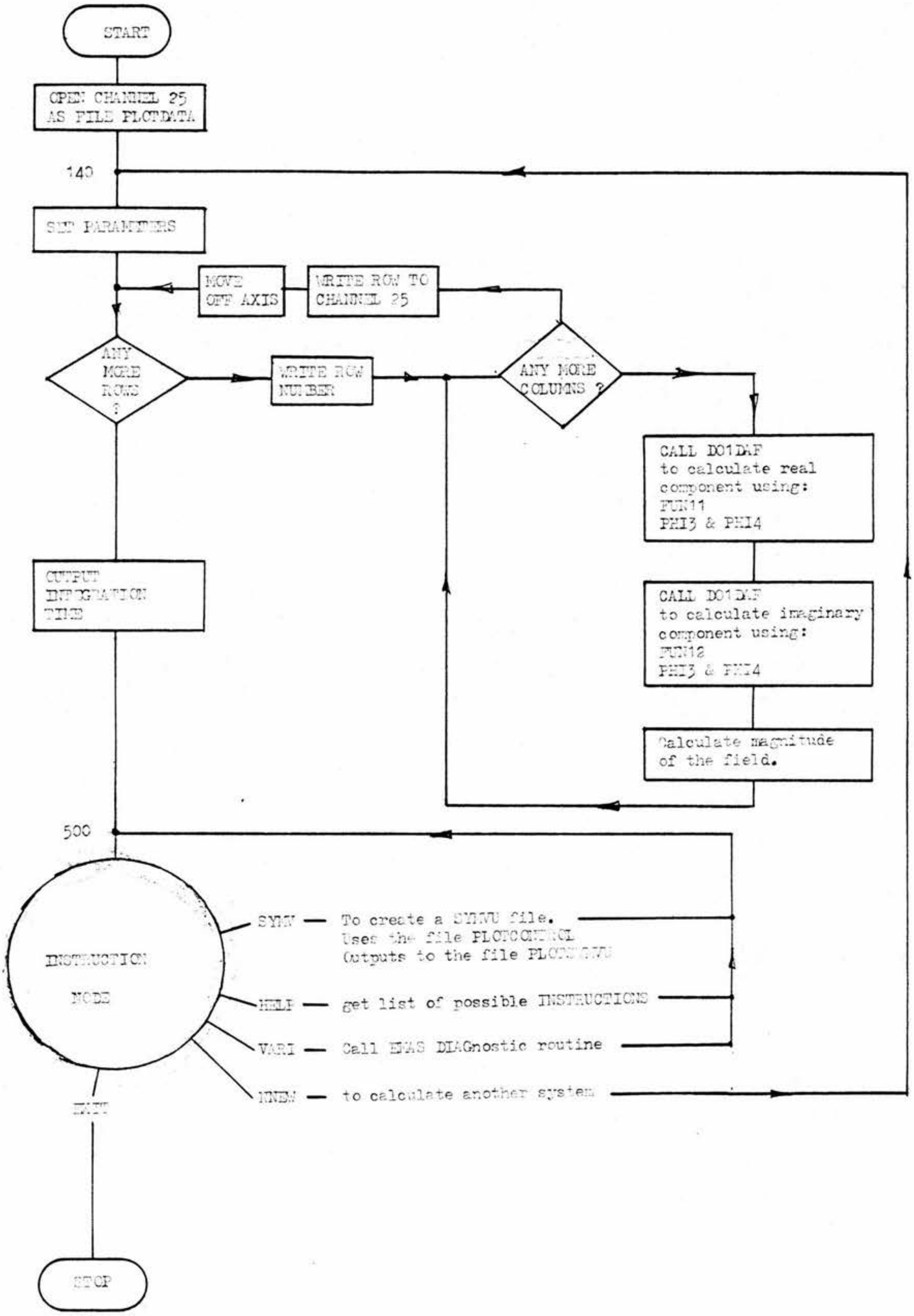

Figure 4.5: PLOTCWX flow diagram.

Firstly the core of the program has a double loop and it evaluates points on a rectangular grid. This grid is normally set to 25 x 15 points. It may be changed by altering the source program. Associated programs for handling the matrix, e.g. PLOTCONTROL will also have to be changed to match. PLOTCWX evaluates points along lines parallel to the system axis and moves radially outwards from the axis. The points are stored outside the program row at a time. Thus they are not lost if the program is stopped for overrunning its pre-set time limit or because of a system crash.

Secondly, the program is designed primarily for batch, not interactive, use. The requirement for input and verification of parameters is simplified and the instruction node reduced and matched to batch input. Most manipulation and presentation of data is done by external programs. Plots may be calculated in parts and subsequently added together. This is useful if uncertain about how far off-axis the field should be calculated.

Channel 25 is required for output.

All parts of the program are kept together in one file PLOTCWX. The mirror function is no longer an independant subroutine and appropriate expressions appear where required in the program. All these must be altered to change the mirror. The functions FUN11, for the real integral and FUN12 for the imaginary, evaluate the expressions exactly. The value for wave number (normally calculated from the frequency and velocity of sound) and the source position are set in each function. This will save some execution time. Experience has shown that these are rarely altered. There is only one 'correct' position for the source for any given mirror.

If any parameters are altered by editing the source program, care should be taken to recompile with the compiler parameters set to OPT (see section 4.2.7).

4.2.2. The Mirror Function, $M(\rho)$.

The partitioned file MIRROR (see EMAS Users' Guide, October 1983 for a description of partioned files) contains source and object files for every mirror design considered. New mirrors may be added or existing ones altered. Before running the main program, PLOTCW, the desired mirror object file is copied to the object file MIRRORO, which is already entered in the directory. This simplified call leads to more efficient running of the main loop of the program. Mirrors are readily altered or new ones added without altering the main program or leaving it exposed to calls to undefined mirror functions. However, it is not possible to change the mirror while PLOTCW is running. When PLOTCW is called it introduces itself and describes the mirror currently in use.

For mirror design 'n' the source programs are in MIRROR_Sn and the object programs in MIRROR_On. Each mirror has the following subroutines:

a) MIRNUM: called by PLOTCW at the beginning of a run, this returns the mirror number 'n' and a short description and the current value of parameters.

b) MIRROR: contains the function $Z = M(\rho)$ - 4.15

c) ARCMIRROR: contains the function $\rho = M^{-1}(Z)$ - 4.16

d) DIFMIR: contains the function $\frac{dZ}{d\rho} = M^{1}(\rho)$ - 4.17

e) DIFAMIR: contains the function $\frac{d\rho}{dz} = (M^{-1})^{1}(Z)$ - 4.18

Efficiency considerations in writing and compiling are discussed in section 4.2.7.

Since the mirror function is at the very core of the program and may be called even more often than the integral functions themselves, care is taken to make them as fast as possible. To get fastest evaluation of the functions, the parameters are supplied in DATA statements and must, therefore, be entered before compiling and loading the program.

The mirrors currently in use are:

1) A simple cone; apex at the origin. It is described by the angle α between its surface and a plane orthogonal to the axis.

2) A hemisphere of radius, R, passing through the origin. 2R125 is a hemisphere of radius 125mm passing through the origin.

3) The mirror surface used in the extended focus system described in section 9.2.

4) An ellipsoidal mirror with the internal reference point at the origin and specified by the semi-major and semi-minor axes squared. Only the left hand half of the ellipse is considered. It is described to the user by the semi-major and semi-minor axes.

5) A hemisphere, centred at the origin, specified by the radius squared but described to the user by the radius.

6) A plane mirror, passing through the origin.

4.2.3. The Subroutines POINTn: applying different approximations

There are six POINT subroutines and any one of them may be selected. Each POINTn contains the algorithm with different approximations (4.1.1).

POINTn is at the core of the program and is called to evaluate the field at every point in the plotting loop. POINTn in its turn calls the NAG Library Subroutine DO1DAF to perform the surface integration. DO1DAF is called twice - once for the real and once for the imaginary components. DO1DAF requires other subroutines - two to describe the limits of the inner integral and one the function being integrated - either the real or the imaginary. The integration functions are stored in the same object program as the POINTn subroutine.

Certain mirror designs (e.g. some of those described in section 9.1) may not have unique radial co-ordinates and will require axial coordinates for limits. As the inner integral may be called as often as 255 times, a complicated function and an additional call to the mirror function are to be avoided. A version of the algorithm (POINT5) is, therefore, designed to use axial limits and when it is in use the program will prompt for axial limits to the mirror surface.

Relationships between the different 'versions' may be readily identified. POINT5 is identical to POINT4, except that the independent variable is the axial co-ordinate, Z, instead of the radial, ρ . POINT4 and POINT5 are both exact. POINT2 has the same appeoximation for the differential of the mirror surface as has POINT1 but evaluates the vector magnitudes correctly. POINT3 is the same as POINT4 except a numerical approximation is tried as an alternative to evaluating the derivative of the mirror curve.

The subroutine POINT1.

Stored in the files PLOTPT1#.
Uses the NAG subroutine D01DAF
which calls the functions PHI3 and PHI4. for integration limits.

Functions FUN3 and FUN4 (also held in PLOTPT1) which describe the real and imaginary expressions for the field. They in turn use the mirror functions which are 'active' in MIRROR0.

Approximations.

i) $\alpha \rightarrow \frac{\pi}{2}$ Hence $dS = \rho\, d\chi dz$. - 4.6

(This is approximation (i) in section 4.1.1(a) and is best suited to deep mirrors).

ii) 1st order approximations for SQ and QP. Only the first terms of the power series expansions are used.

$$|SQ| = l - z + \frac{\rho^2 + z^2}{2l} \qquad - 4.11$$

$$|QP| = l' - z + \frac{r^2 + \rho^2 + z^2}{2l'} - \frac{r\rho\cos X}{l'} \qquad - 4.13$$

Hence

$$Up = \frac{ik}{2\pi}\iint_S \frac{\exp\left[-ik\left(l+l'-2z + \frac{\rho^2 + z^2}{2l} + \frac{r^2+\rho^2+z^2}{ll'} - \frac{r\rho\cos X}{l'}\right)\right]}{r\rho\cos X - \rho^2 - z^2 + z(l + l') - ll'}\,\rho\, dz\, dX \qquad - 4.19$$

Integration limits.

Outer integral: 0 → 2π for a symmetrical system. Symmetrical about zero for the Herschel systems discussed in sections 4.5 and 9.1.

Inner integral: Function PHI3 specifies the lower limit.
Function PHI4 specifies the upper limit.

The limits are user input to the main program as axial coordinates in millimetres. Since this function is of the axial coordinate, Z, PHI3 and PHI4 supply these in metres.

Subroutine POINT2

Stored in files PLOTPT2 # .
Uses D01DAF
which calls the functions PHI3 and PHI4 for integration limits.

FUN5 and FUN6 to describe the real and imaginary parts of the expression respectively. They in turn use the MIRROR functions which are active in MIRRORO.

Approximations

i) As with POINT1 $\alpha \rightarrow \frac{\pi}{2}$. Hence $dS = \rho\, dz d\chi$ - 4.6

(This is approximation in section 4.1.1(a). Best suited for deep mirrors.

ii) SQ and QP are evaluated correctly using equations 4.10 and 4.12 respectively.

Hence

$$Up = \frac{1k}{2\pi}\iint_S \frac{\exp -ik\left((\rho^2+(z-l)^2)^{\frac{1}{2}} + (r^2+\rho^2-2r\rho\cos\chi + (l'-z)^2)^{\frac{1}{2}}\right)}{r\rho\cos\chi - \rho^2 - z^2 + z\,(l+l') - ll'}\,\rho\, dz d\chi$$

- 4.20

Integration limits

Outer integral: $0 \rightarrow 2\pi$ for a symmetrical system. Symmetrical about zero for the Herschel systems discussed in sections 4.5 and 9.1.

Inner integral: Function PHI3 specifies the lower limit. Function PHI4 specifies the upper limit. The limits are user input to the main program as axial coordinates in millemetres. Since this function is of the axial coordinate, z, PHI3 and PHI4 supply these in metres.

Subroutine POINT3

Stored in the files PLOTPT3
Uses the NAG subroutine DO1DAF
which calls the functions PHI3 and PHI4 for integration limits.
FUN7 and FUN8 (the integrals). They
in turn use the Function MIRROR.

Approximations

i) Using the geometry shown in figure 4.6 a linear approximation is made for the gradient of the mirror. $\delta\rho$ is arbitarily set to 5×10^{-5}m and other mirror coordinate evaluated either side of the point Q.

$$\delta Q = (\delta z^2 + \delta\rho^2)^{\frac{1}{2}}$$

$$\cos\alpha_q = \frac{\delta\rho}{\delta q}$$

$$= \frac{\delta\rho}{\left((M(\rho + \frac{\delta\rho}{2}) - M(\rho - \frac{\delta\rho}{2}))^2 + \delta\rho^2\right)^{\frac{1}{2}}} \qquad - 4.21$$

$$\text{Use} \quad dS = \frac{\rho}{\cos\alpha} \quad d\rho d\chi$$

ii) Evaluate SQ and QP are evaluated correctly using equations 3.10 and 3.12 respectively.

Hence

$$U_p = \frac{ik}{\pi 2}\iint_S \frac{\exp -ik(SQ+QP)}{\overline{SQ}.\overline{QP}} \; \frac{\rho\left((M(\rho + \frac{\delta\rho}{2}) - M(\rho - \frac{\delta\rho}{2}))^2 + \delta\rho^2\right)^{\frac{1}{2}}}{\delta\rho} \; d\rho \, d\chi \qquad - 4.22$$

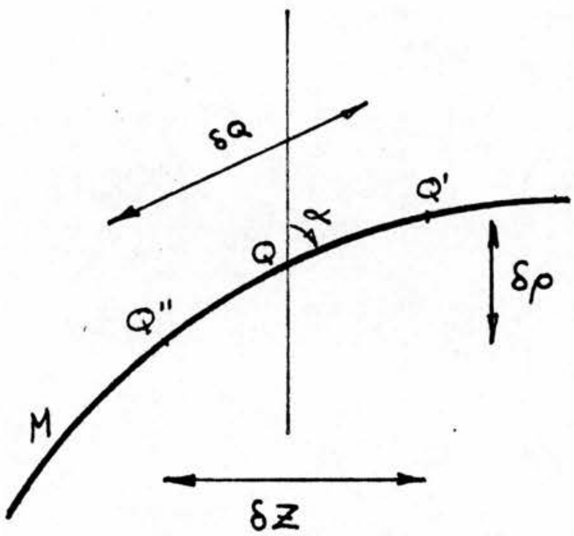

Figure 4.6. Linear approximation of $\frac{dz}{d\rho}$ for subroutine POINT3.

The Subroutine POINT4

Stored in the files PLOTPT4#
Uses the NAG subroutine DO1DAF
which calls the Functions PHI3 PHI4 for integration limits
FUN9 and FUN10 for the real and imaginary integrals respectively.
They in turn call MIRROR to describe the mirror and DIFMIR for its derivative.

Approximations

No approximations are used in this sub-program.
The surface element is given by equation 4.8.

$$dS = \frac{\rho}{\cos(\tan^{-1} \frac{dz}{d\rho})} \quad d\rho \, d\chi$$

The vectors $\overline{SQ}$ and $\overline{QP}$ are evaluated exactly using equations 4.10 and 4.12 respectively.

Hence

$$Up = \frac{ik}{2\pi} \iint_S \frac{\exp -ik(SQ + QP)}{\overline{SQ}.\overline{QP}} \quad \frac{\rho}{\cos(\tan^{-1} \frac{dz}{d\rho})} \quad d\rho \, d\chi \qquad - 4.23$$

Integration limits

Outer integral: Normally 0 → 2π

Inner integral: These limits are user supplied to the main program as diameters and converted to radii in metres.

PHI3 and PHI4 supply these constant values for the lower and upper limits respectively.

The subroutine POINT5

Stored in the files PLOTPT5#
Uses the NAG subroutine DO1DAF
which calls the functions: PHI3 and PHI4 for integration limits
FUN13 and FUN14 for the real and imaginary integrals respectively. They in turn call ARCMIRROR and DIFMIR to get the curve of the mirror and its derivative.

Approximations

No approximations are used by this sub-program.
The surface element is given by equation 4.9.

$$dS = \frac{\rho}{\sin(\tan^{-1} \frac{dz}{d\rho})} \quad dz d\chi$$

The vectors $\overline{SQ}$ and $\overline{QP}$ are evaluated exactly using equations 4.10 and 4.12 respectively.

Hence

$$Up = \frac{ik}{\pi 2} \iint_S \frac{\exp -ik\,(SQ+QP)}{\overline{SQ}.\overline{QP}} \quad \frac{\rho}{\sin(\tan^{-1} \frac{dz}{d\rho})} \quad dz d\chi \qquad - 4.24$$

Integration limits

Outer integral: Normally $0 \rightarrow 2\pi$ for a symmetrical system. For a Herschel system (see section 4.4) they should be symmetrical about zero.

Inner integral: These limits are user supplied to the main program as axial coordinates in millimetres and are converted to metres. PHI3 and PHI4 supply these constant values for the lower and upper limits respectively.

The Subroutine POINT6

Stored in the files PLOTPT6
Uses the NAG subroutine DO1DAF
which calls the Functions PHI3 and PHI4 for integration limits
FUN15 and FUN16 for the real and imaginary integrals respectively. They in turn use the function MIRROR to get the shape of the mirror.

Approximations

This sub-program applies the same approximations as were used by Fujiwara (1962).

i) $\alpha \rightarrow \emptyset$
Hence equation 4.5.
$dS = \rho \, d\rho \, d\chi$

This approximation is discussed in section 4.1.1(a)(i) and is best suited to shallow mirrors.

ii) First order approximations are used of the magnitude of the vector SQ and QP.

Equation 4.11. $|SQ| \simeq l - z + \dfrac{\rho^2 + z^2}{2l}$

and Equation 4.13 $|QP| \simeq l' - z + \dfrac{r^2 + \rho^2 + z^2}{2l'} \quad \dfrac{r\rho \cos\chi}{l'}$

These are discussed in section 4.1.1 (c)

Hence

$$U_p = \frac{ik}{2\pi} \iint_S \frac{\exp -ik\left(l - l' - 2z + \dfrac{\rho^2 + z^2}{2l} + \dfrac{r^2 + \rho^2 + z^2}{2l'} - \dfrac{r\rho\cos\chi}{l'}\right)}{r\rho\cos\chi - \rho^2 - z^2 + z\,(l + l') - ll'} \, \rho \, d\rho \, d\chi$$

- 4.25

Integration limits

Outer integral: Normally $\emptyset \rightarrow 2\pi$

Inner integral: These limits are user supplied to the main program as diameters in millimetres and converted to radii in metres. PHI3 and PHI4 supply these constant values for the lower and upper limits respectively.

4.2.4. The NAG Subroutine DØ1DAF

DØ1DAF attempts to evaluate a double integral to a specified absolute accuracy by repeated applications of Patterson's Quadratures method, (Patterson, 1968). It is fully described in the NAG Library Manual, Vol. 1.

It attempts to evaluate

$$I = \int_a^b \int_{\phi_1(y)}^{\phi_2(y)} f(x,y) \;\; dxdy \qquad - 4.26$$

The limit of the outer integral, a and b, are constants, ϕ_1 (y) and ϕ_2 (y) are functions of the variable y.

First the inner then the outer integral is evaluated. Evaluation is repeated with an increasing number of pivots until two successive results agree within the specified accuracy up to a maximum of 255 points in each. An accuracy of 1×10^{-3} was specified throughout. In addition to the estimate of the integral DØ1DAF returns the total number of function evaluations, a useful indicator of whether the integral is behaving reasonably and an error indicator to show if any of the integrals failed to converge. This was used to trigger an error message but not to interrupt the program since it may well not be significant.

4.2.5. Integration Limits PHIn

DØ1DAF requires that the limits of inner integral be supplied as Fortran Function sub-programs. Speed of execution is important, therefore, PHI3 and PHI4 simply return a constant. This is communicated to the sub-program from the main program in the common block PHI.

4.2.6. Program Efficiency

The greater part of the program is written to give it a clear, logical structure. However, the central loop may be executed very many times. For each field point evaluated the real and imaginary functions may be called a maximum of 255 times for the inner integral which may be performed for 255 pivots of the outer. Thus effort was made to optimize the coding of the POINTn subroutines and the functions they call. This was done based on the advice of the Edinburgh University Program Library Unit, which is derived from that of Scarborough (1978).

All program units are small, less than 8kbyte. Those in the central loop are compiled using the 'OPT' compiler parameter which give an efficient object program at the expense of diagnostics in the event of failure. These sub-programs are limited to those required by DØ1DAF. In practice, using the 'OPT' parameter at compilation, gave an improvement of 28 to 38% in computation time. Arguments are passed in common. Constants do not appear as arguments or in common. There are no intermediate temporary variables.

All PLOTCWX program units are stored together in one file and all are normally compiled with the 'OPT' parameter.

4.3. Verification of PLOTCW

As with PLOTBCW (section 3.3) the algorithm and coding of PLOTCW was verified by reference to published results and simple CW results.

Comparison was also made to PLOTBCW results.

The verification was complicated by the existence of six sets of approximations. Comparison between the different approximations is made in section 4.4.

Not all of the 'MIRROR' functions could be compared with published work. Care was taken in manually checking these program units. When run, they were checked for reasonable behaviour, e.g. excessive or very short computation times, failure to achieve the specified integration precision and for compatible results from 'POINT' subroutines using different subroutines from 'MIRROR'.

4.4. Comparison of the different approximations, POINTn

The different approximations contained in the various sub-programs POINTn were compared for two devices.

4.4.1. A deep concave spherical transducer

Radius of curvature = 100 mm
Chord = 150 mm - no apodisation
Wavelength= 0.2 mm
e.g. frequency = 7.6 MHz
velocity = 1520 ms^{-1}

This is the device described by Archer-Hall and Ali-Bashter (1980). It is a deep mirror best suited to the approximation (i) in POINT1 and POINT2 (section 4.2.3).

The system was plotted from 0 to 0.5 mm off-axis in steps of 0.01 radially in the focal plane.

The results are shown in figure 4.7.

Similarly the field was plotted axially for 5 mm through the geometric focus with a step size of 0.1 mm. These results are shown in figure 4.8.

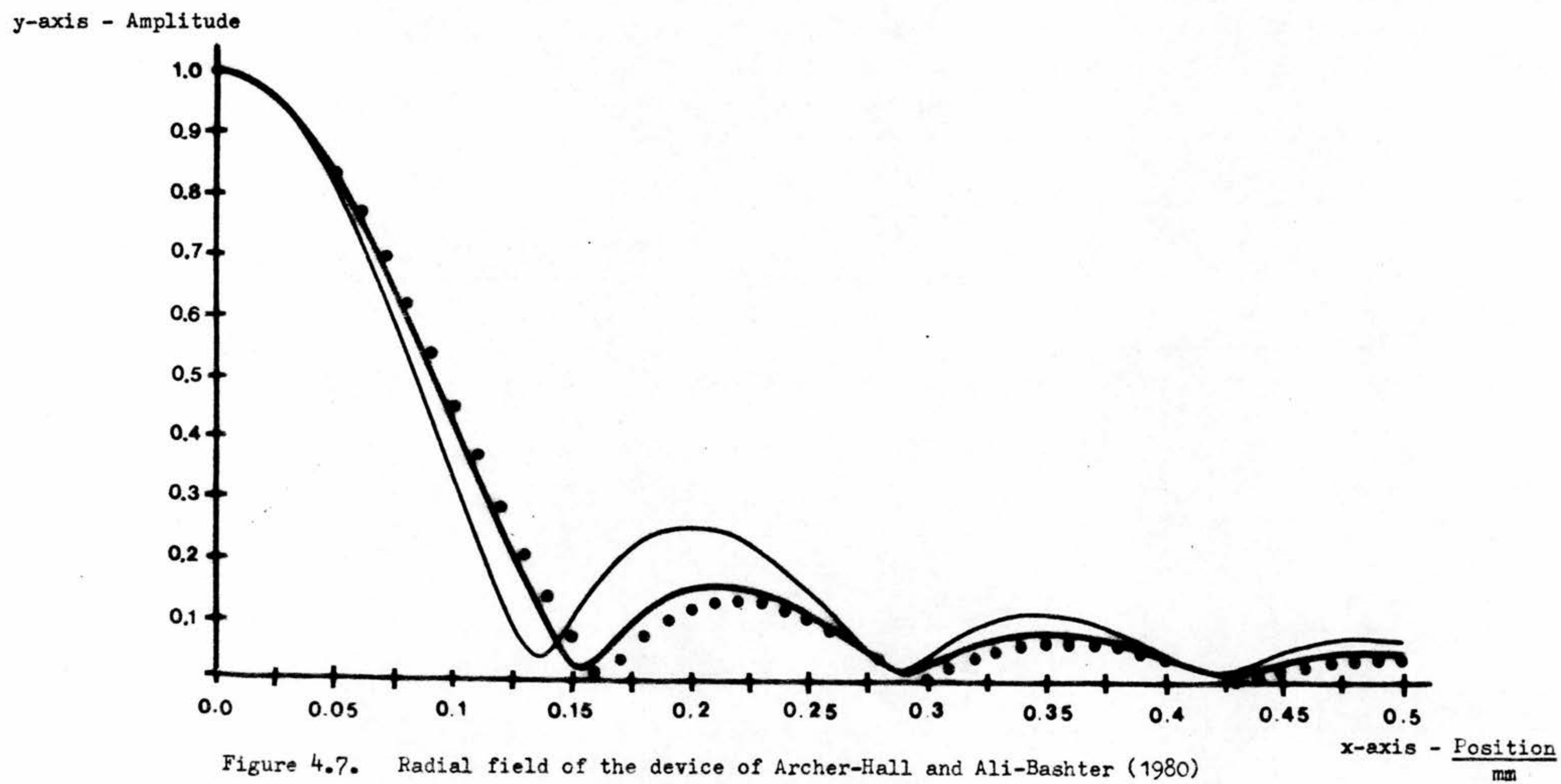

Figure 4.7. Radial field of the device of Archer-Hall and Ali-Bashter (1980) using different approximations (see section 4.4.1.

The narrow line is POINT1 and 2. The broad line is POINT3,4,5 and PLOTBCW.

The dotted line is POINT6.

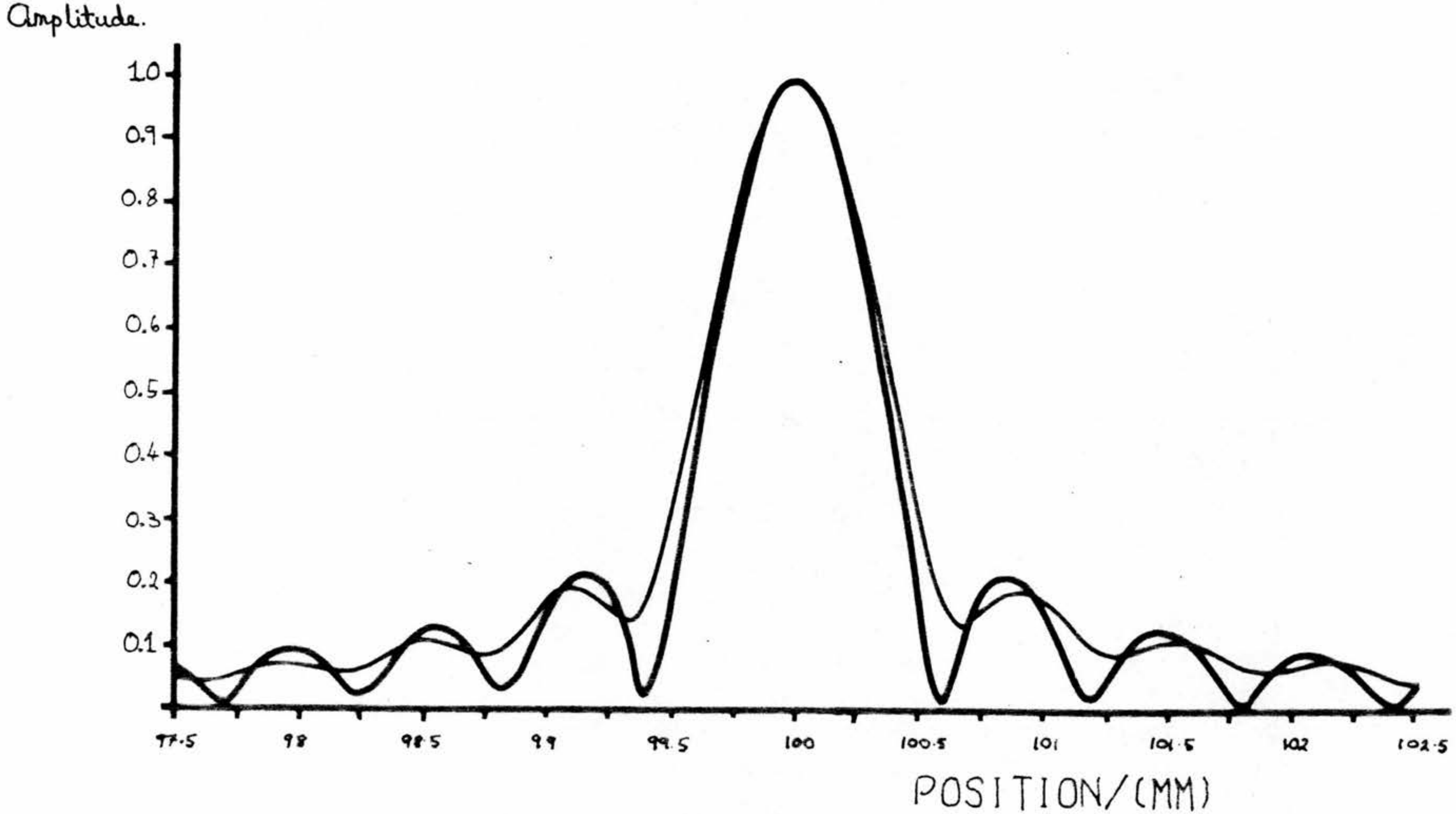

Figure 4.8. Axial field of the device of Archer-Hall and Ali-Bashter (1980) using different approximations (see section 4.4.1.) The narrow line is POINT1, and POINT2. the broad line is all the other models.

Both MIRROR2 and MIRROR5 were used in this comparison. MIRROR5 was slightly, but not significantly, faster.

The evaluation times for the various approximations are given in Table 4.1.

4.4.2. A shallow concave spherical transducer

Radius of curvature	=	150 mm	
Chord	=	50 mm	- no apodisation
Wavelength	=	0.304	
e.g. frequency	=	5 MHz	
velocity	=	1520 ms^{-1}	

This represents the S and I transducer which is described in section 5.3.2. It is a shallow bowl well suited to the approximation (i) of POINT6 (section 4.2.3).

The system was plotted from 0 to 3 mm off-axis in steps of 0.1 mm radially in the plane of the geometric focus. These results are shown in figure 4.9.

Similarly the field was plotted axially from 100 mm through the geometric focus with a step size of 2 mm. The results are shown in figure 4.10.

The evaluation times are given for the various approximations in Table 4.2.

4.4.3. Conclusions

i) All the algorithms work well.

ii) Approximation (i) of POINT1 and 2 is the furthest removed from the devices considered here. It may have some application in Herschel style systems. (Section 4.5, 9.1.)

Algorithm	Evaluation Times S	
	Radial Plots (51 pts)	Axial Plot (51 pts)
PLOTBCW	20.55	4.06×10^{-2} *
POINT1	66.19 **	4.30
POINT2	73.84	4.47
POINT3	85.94	8.62
POINT4	70.27	6.96
POINT6	49.88	5.16

Table 4.1: Computation times for different approximations to the device of Archer-Hall and Ali-Bashter (1980). See section 4.4.1.

* This does not involve numerical integration.

** For one point the integral failed to converge to the preset precision. This failure was not serious.

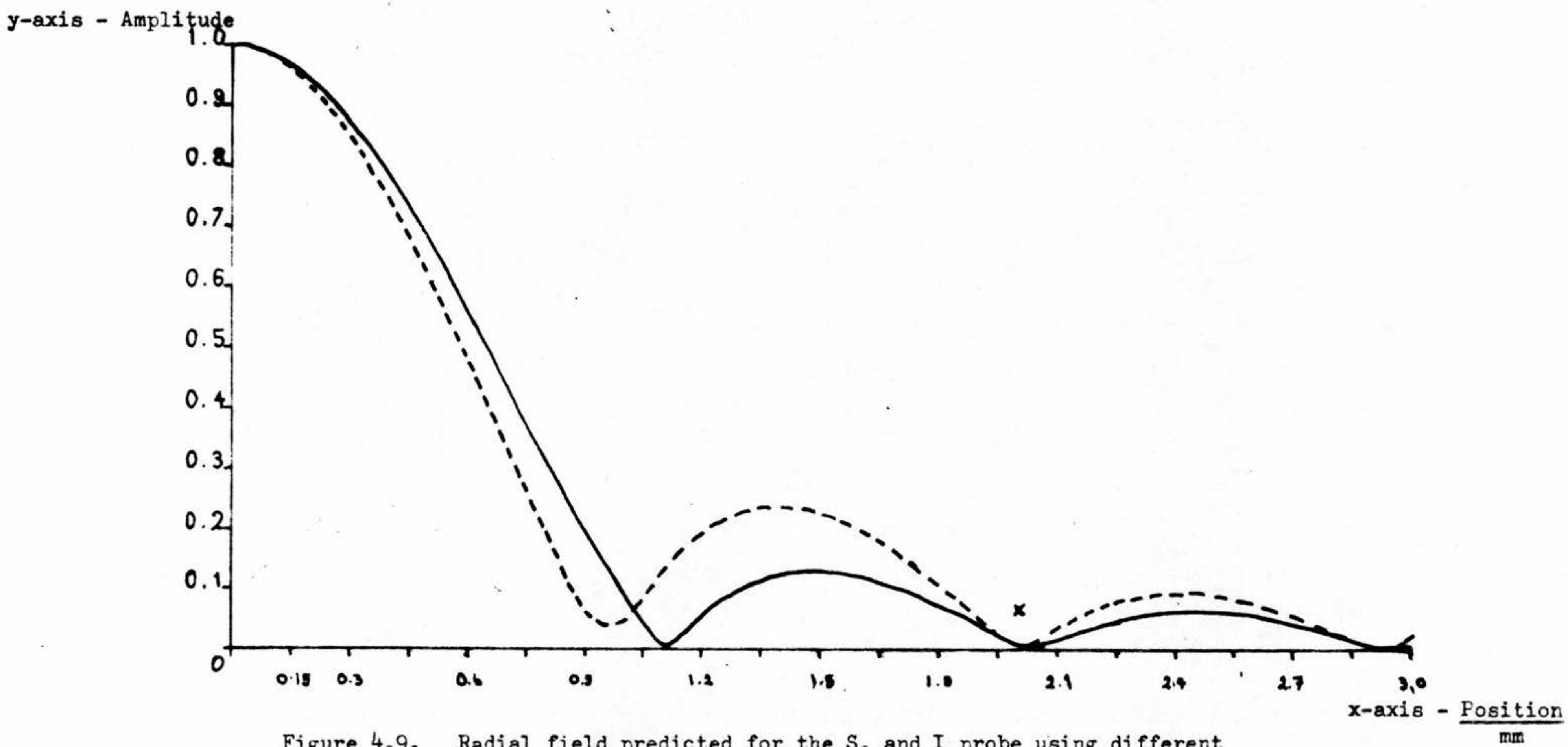

Figure 4.9. Radial field predicted for the S. and I probe using different approximations (see section 4.4.2).
The broken line is POINT1 and 2. The solid line is all the other models.

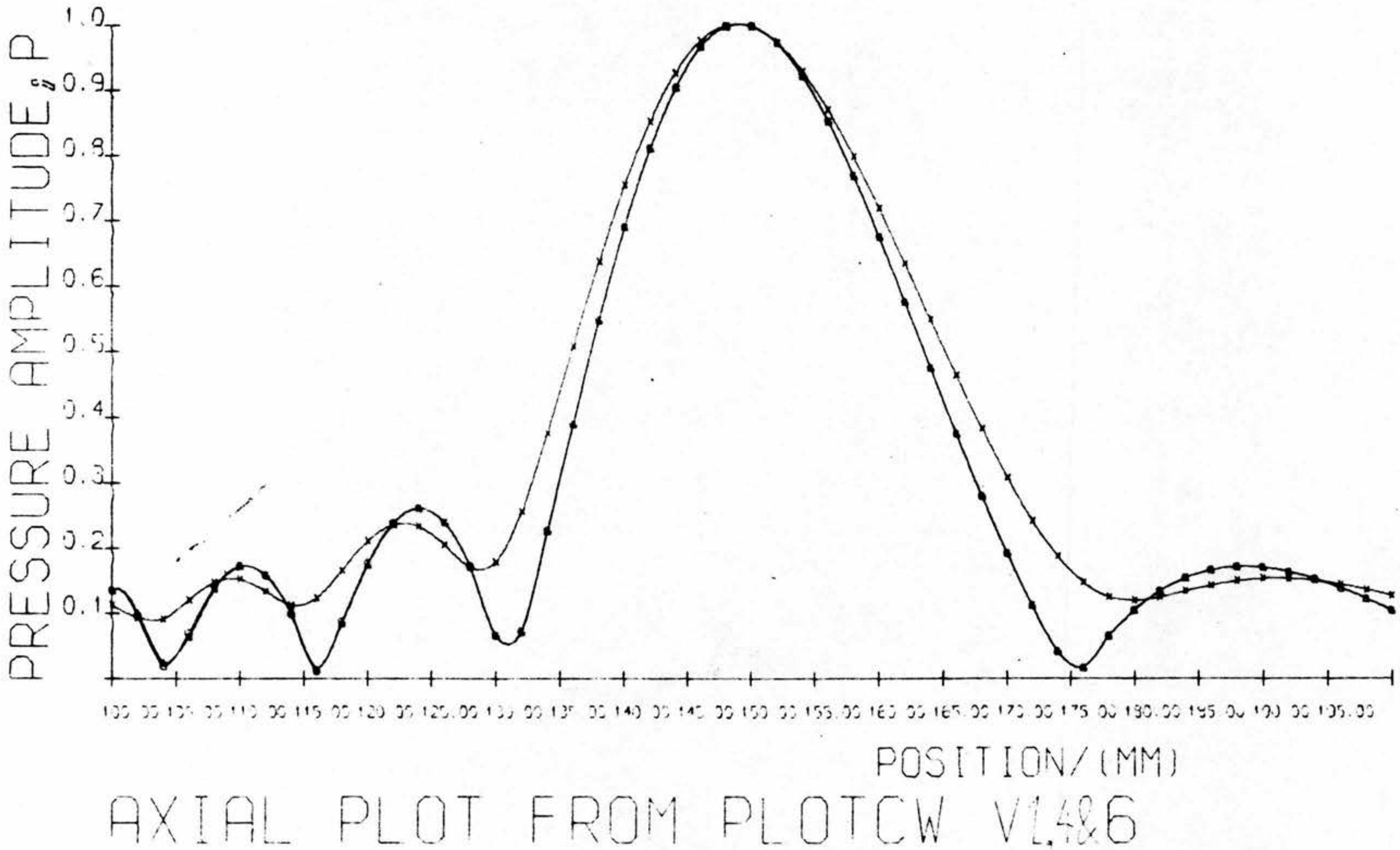

Figure 4.10. Axial field predicted for the S. and I probe using different approximations (see section 4.4.2.). The points marked X are due to POINT1 and 2. The other line represents all the other models.

Algorithm	Evaluation Times S	
	Radial Plot (31 pts.)	Axial Plot (51 pts.)
PLOTBCW	8.84	3.97×10^{-2} *
POINT1	9.36	2.00
POINT2	10.47	2.16
POINT3	19.86	4.96
POINT4	17.12	4.01
POINT6	11.44	3.06

Table 4.2. Computation times for different approximations to the model of the S and I probe (see section 4.4.2.).

* This does not involve numerical integration.

iii) The first order approximation of the length of vectors $\overline{SQ}$ and $\overline{QP}$ (appeoximation (ii) in POINT2 and POINT6) increases the speed by $\sim$10% but does not result in increased error.

iv) The numerical approximation of the first derivative of the mirror surface (used in POINT3) does not result in error but, since it generally takes longer to evaluate, has no value when the derivative is available.

v) The accidental convergence of quadrature routines is discussed in the NAG Library Manual. This occurs when two estimates of the integral agree within the specified precision but, in fact, both differ considerably from the true result. An example is the point marked 'X' in figure 4.9. This is due to such an error in POINT2. These errors may be associated with either an unusually quick or slow evaluation of that point. This was found to occur in the algorithms containing approximations. These errors are readily recognised as apparent discontinuities in the field which may be investigated using another algorithm.

iv) Failures to converge also occurred more frequently with the approximations. This results in the quadrature routine using a great number of pivots and thus increasing the computation time. When the use of an approximation resulted in a large number of such failures, the computation time was often found to exceed that of the unapproximated algorithm. This occurs only rarely.

The algorithms used most commonly were POINT4 and POINT6.

This model is used in Chapter 7 and 8. Numerical and experimental results for mirror system are compared in sections 7.4.6, 7.6, 8.4.4 and 8.6.

4.5. Modelling Herschel Mirror Systems

This design of mirror system is discussed in section 9.1. The mirror is not symmetrical about the co-ordinate axis used by the program and may be modelled only if certain modifications are made to the POINTn sub-program before it is loaded.

Only MIRROR 4 or 5 may be used for these systems since the algorithm for plots along the principal ray depends on a knowledge of the geometry and it may not be readily used for other reflector shapes. The mirror parameters (semi-major and semi-minor axes squared (AA and BB) for MIRROR4; radius squared (RR) for MIRROR5) must be inserted correctly before the MIRROR_Sn is compiled as MIRRORO.

The description of a circular section off-axis would be difficult. The mirror surface is, therefore, limited by the angle it subtends to the Z-axis and by the axial or radial projection of its edges. The desired integration limits to define the angular extent of the mirror must be calculated and inserted in calls to DØ2DAF. This requires that the limits are set (and reset) twice - once for the real and once for the imaginary components. The limits whould be symmetrical about zero so that the principal ray lies in the $\rho = 0$ plane of the program's cylindrical polar co-ordinate system. It may not be possible to describe such a section of the mirror surface uniquely using radial co-ordinates. POINT5 which accepts axial limits instead may be used as an alternative to POINT4 in such cases.

The program also requires that the 'system angle', α , (see figure 4.11) in radians be entered at run time.

4.5.1. Radial Plotting

For radial plots the field point, P (u,v) is described by the intersection of the scan plane AB with the Z-axis at the point I (Ø,l); the system angle, α , and the distance /IP/ = r' , l is user input as LGTH at run time.

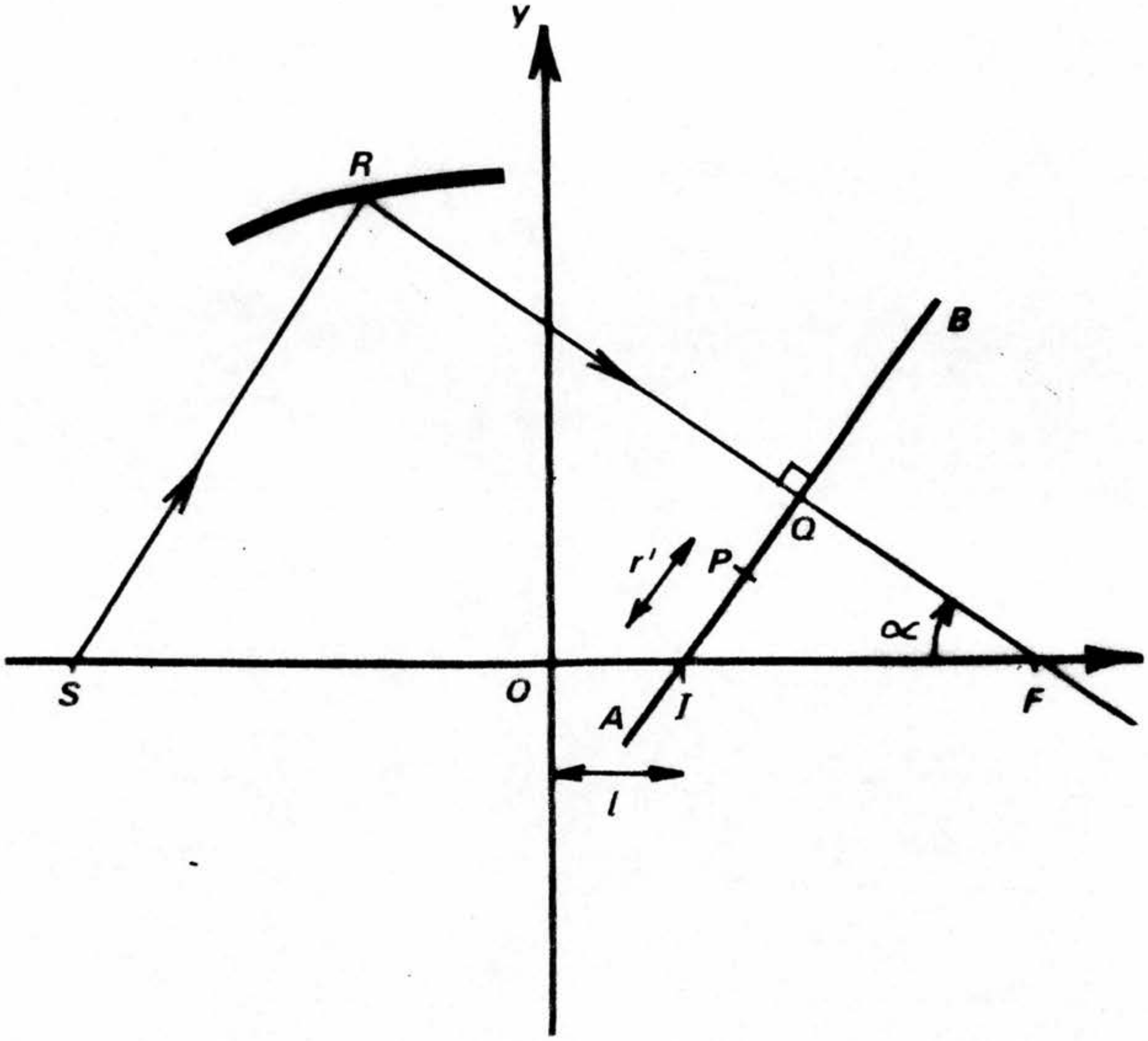

Figure 4.11. Geometry of a ellipsoidal mirror Herschel system.

4.5.2. Axial Plotting

The calculation of field points, Q, for plots along the principal ray of Herschel systems depends on the mirror being used, since a different geometry applies for ellipsoidal and spherical mirrors.

The point Q is positioned relative to the 'geometrical focus' that is the point where the principal ray crosses the axis of symmetry (marked, F, in figures 4.11 and 4.12).

4.5.2.1. An Ellipsoidal Mirror (MIRROR4)

In this case (the geometry is shown in figure 4.11) the source is placed at S, the 'internal' reference point, and the focus occurs at, F, the 'external' reference point. The program assumes the source is correctly placed and positions, F, opposite the source.

4.5.2.2. A Spherical Mirror (MIRROR5)

The geometry is shown in figure 4.12. With the spherical mirror, the point F is not known exactly and /OF/ is determined by applying the Sine Rule to the triangle ORF. To do this the fact that $\overline{OR}$ bisects the angle β is combined with known constraints to the system i.e. the fixed length /RF/ and angle β . As described in section 9.1.1. for the breast scanner /RF/ =125 mm and β = 0.768 radians.

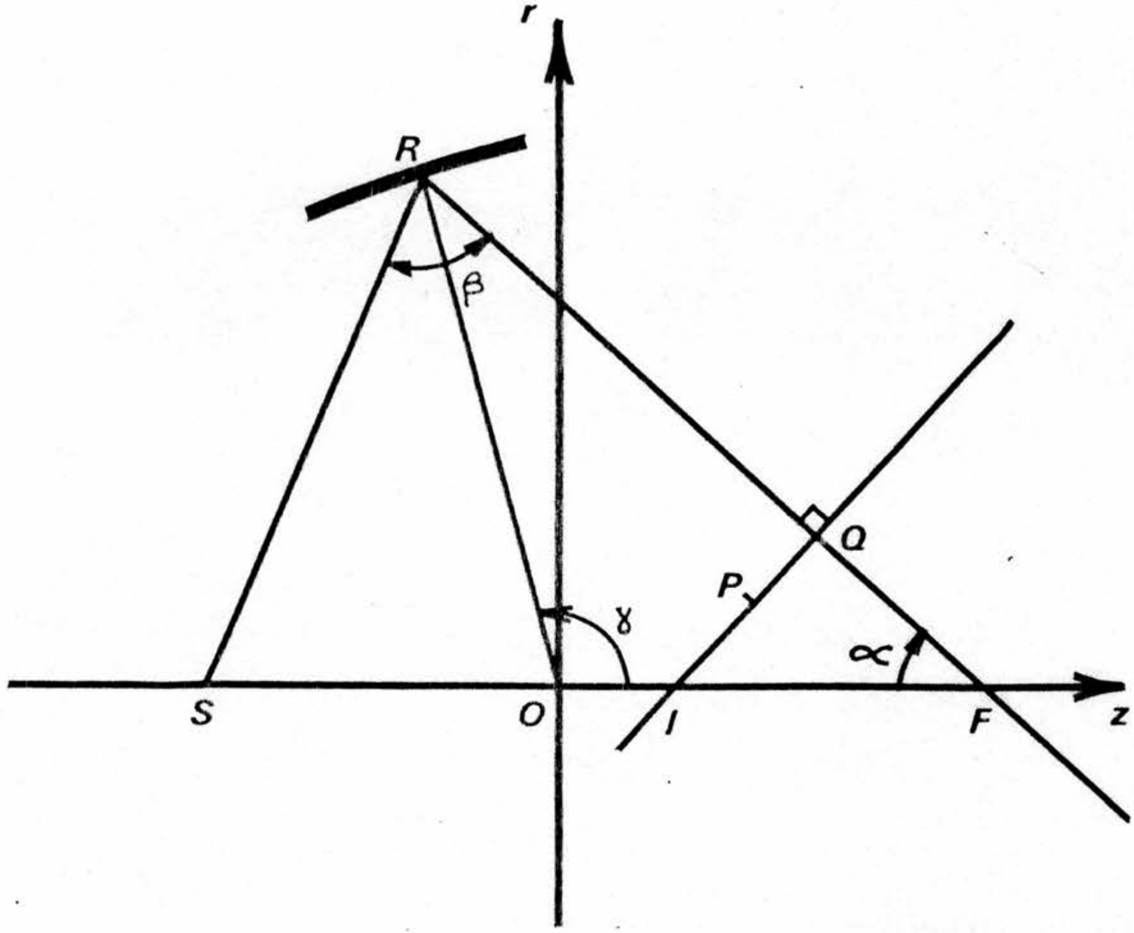

Figure 4.12: Geometry of a spherical mirror based Herschel system

CHAPTER 5

EXPERIMENTAL BEAM PLOTTING

5.1. Beam Plotting System

In order to determine experimentally the beam shape of the systems developed and for comparison with commercially manufactured probes a beam plotting system was developed.

Overview

The plotting system is based on a 600 mm square water tank. A rigid aluminium frame carries orthogonal sets of rails which enable two carriages to be placed anywhere over the tank. The movement of one carriage is partially automated and it may be used to plot single lateral beam shapes on an x, y-plotter. It incorporates a pulse transmitter as well as linear and logarithnic receiver amplifiers. Various targets may be used including stainless steel balls and monofilament nylon wires for pulse echo plotting; a bi-laminar shielded PVDF hydrophone and a thick PZT block for transmission field plotting or examining pulse shapes.

The system has a dynamic range of 30 dB.

The plotting tank is shown in figure 5.1.

5.1.1. Design and Description

The perspex tank is 600 mm x 600 mm x 300 mm deep. The 1" square aluminium frame supports 2 carriages permitting them to be placed and locked over any point in the tank. Brass posts on the carriages carry either probes or targets, which may be adjusted vertically.

One of the carriages may be scanned horizontally by a stepping motor. Steps of either 5×10^{-4} inch (1.27×10^{-2} mm) or 1×10^{-3} inch (2.54×10^{-2} mm) are possible. The usual scan length is 2 inch (50.8 mm). Scan lengths are in Imperial units because the drive screw has a pitch of 0.2"/rev. This carriage also carries a high

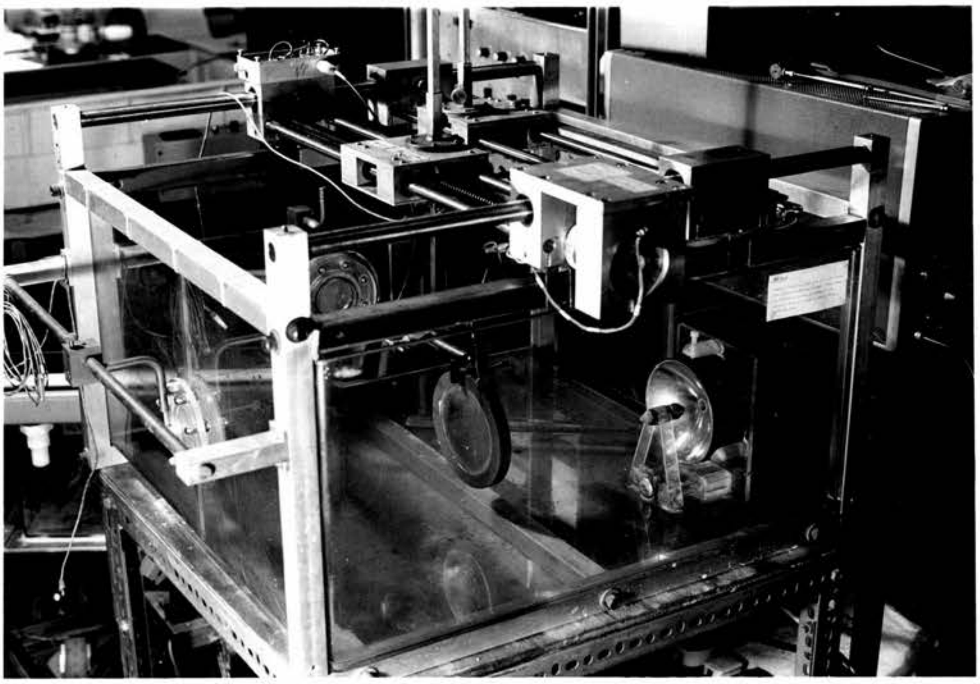

Figure 5.1: the transducer test tank.

input impedance (2.7 MΩ) FET preamplifier for the hydrophone. Scanning is controlled by TTL logic.

Mounting of transducers and targets on the carriages is variable and they may be adjusted to make the beam axis orthogonal to the plane of scan. The mirror systems were unsuited to mounting in this way and a milled plate is fitted to the base of the tank to permit the reproducible placing of these devices.

Tap water, de-aeriated by boiling and standing, was used. No benefit was found to accrue from using de-ionised water.

Block diagrams of the arrangements used for pulse-echo plotting and for transmission field plotting are shown in Figures 5.2 and 5.3 respectively.

Electronics

The letters indicate the boxes marked on figures 5.2 and 5.3.

a) Transmitter: generates a sharp pulse of maximum amplitude 180V. On-board attenuator reduces this by 10 or 20 dB.

b) Receiver: containing a linear amplifier with a time controlled gain circuit.

The transmitter and receiver are mounted in a box with a trigger circuit so that they may be used independently of the plotter. Both circuits were designed and made in the Department and are employed in various experimental scanners (e.g. Pye, 1983).

c) Attenuator: a standard Marconi TF1073A. r.f. attenuator is used. A 50Ω feed-through termination must be used on its output.

d) Logarithmic Amplifier: The characteristic is shown in figure 5.4.

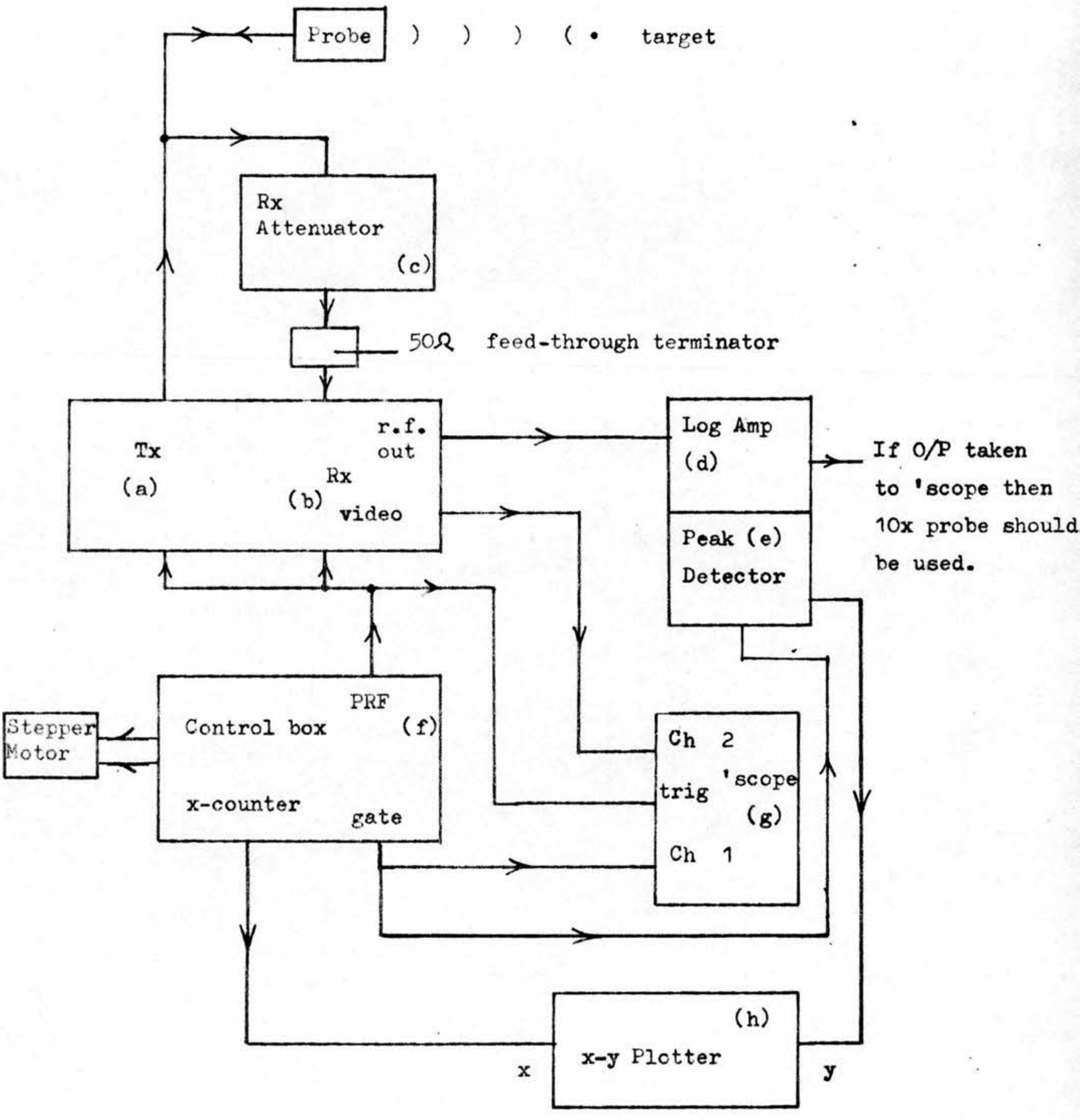

Figure 5.2. Test tank electronics: configuration for pulse echo plotting.

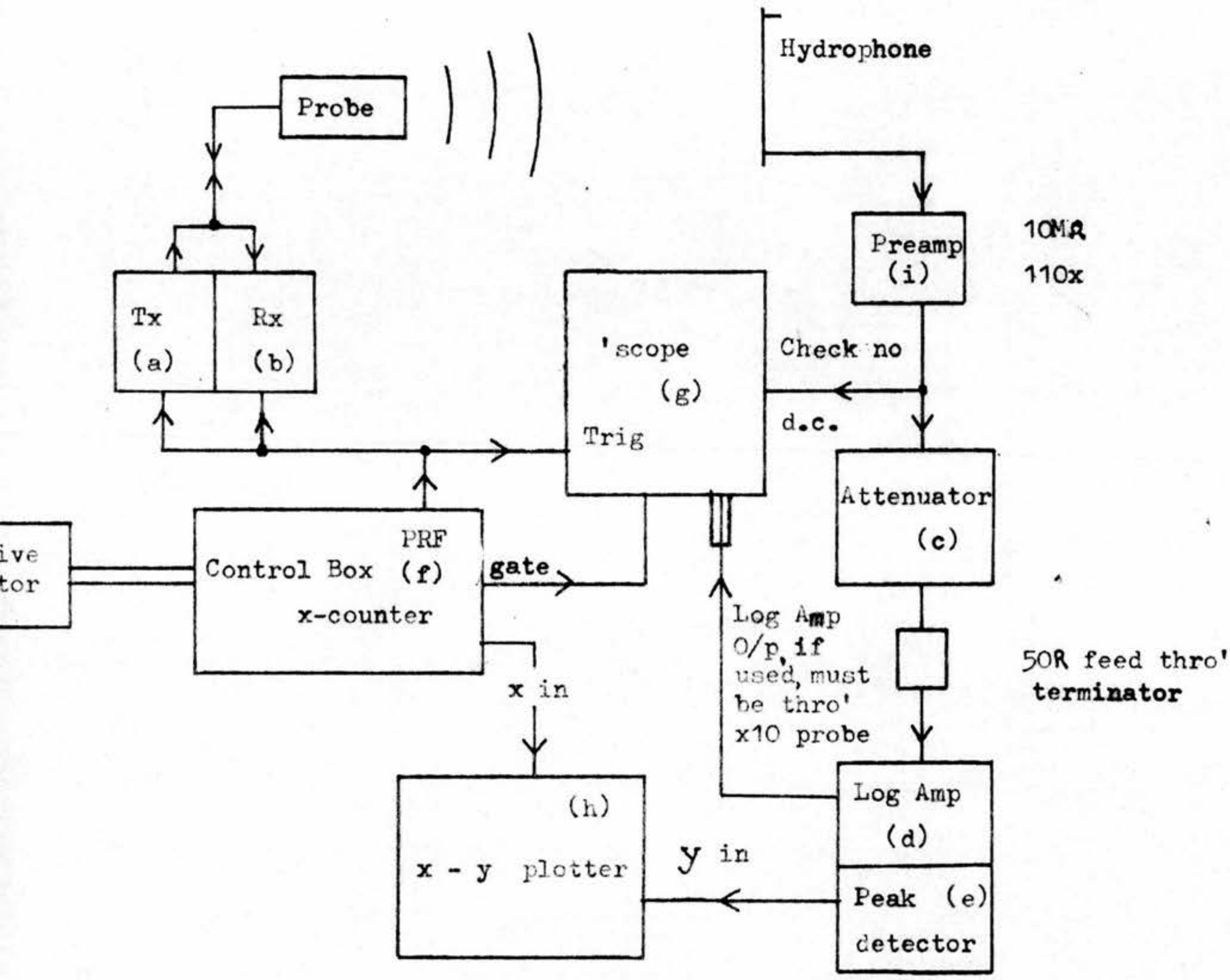

Figure 5.3. Test tank electronics: configuration for hydrophone plotting.

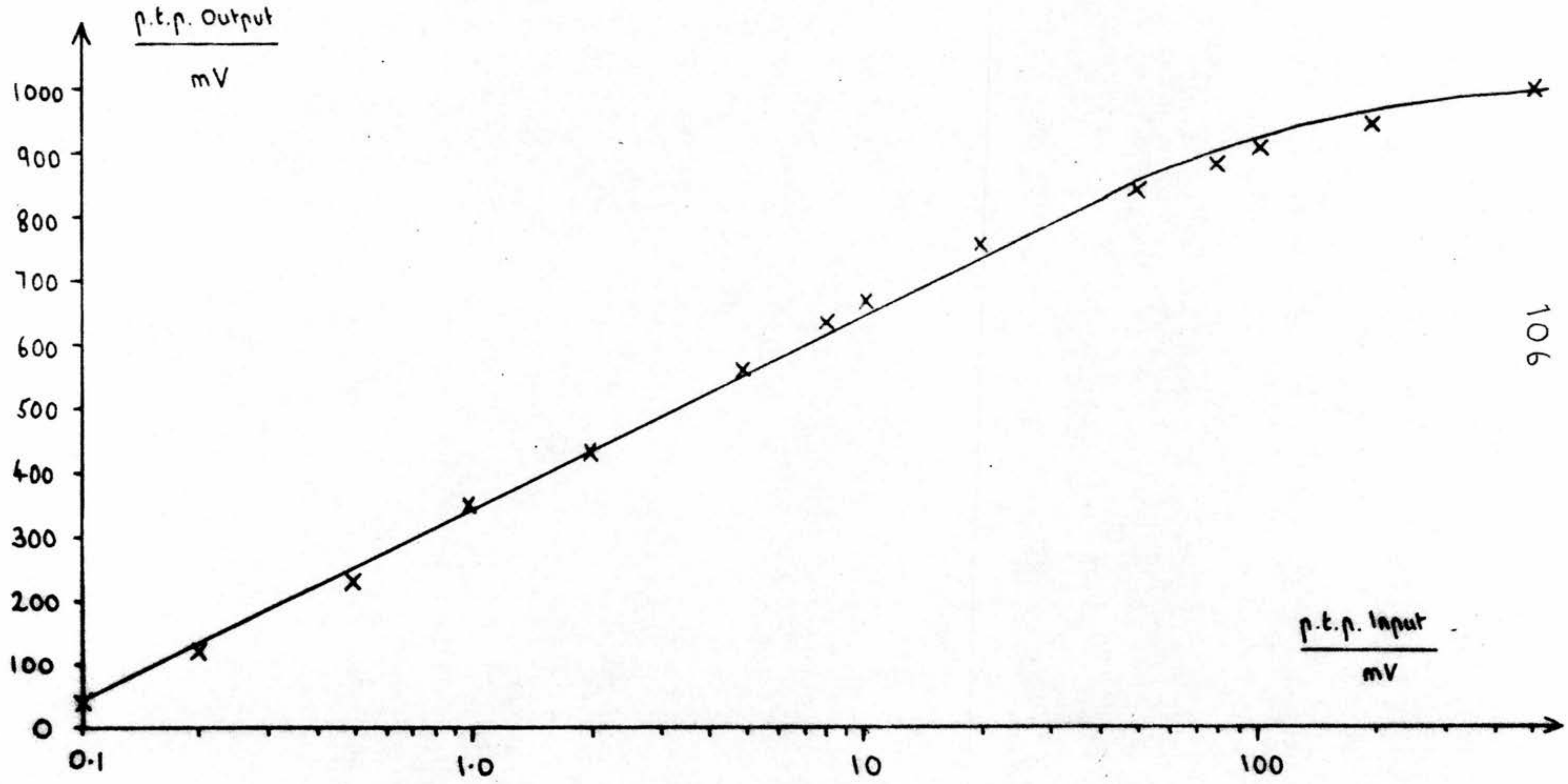

Figure 5.4: Characteristic of Receiver logarithmic amplifier.

e) 10 MHz peak detector: This unit rectifies the r.f. signal and captures the highest peak within a 4 μs gate. A DG181 analogue switch is used to charge and discharge a capacitor.

f) Control box: This houses the TTL logic which controls the stepper motor together with its drives and power supplies. It clocks the system, provides the peak detector gate and generates and sets the position signal. This is obtained by counting the stepper motor pulses.

The system also incorporates Tektronix 7603 dual trace, delayed timebase oscilloscope and a Bryans 26000 x-y-t chart recorder.

The system has been used to generate axial plots, single lateral plots and multiple lateral plots to show the overall field by performing lateral plots at increasing range.

5.1.2. Operation

When a transducer is to be plotted a target must be selected. Target selection is discussed in section 5.2.

i) The transducer is mounted in the tank. The transducer is normally mounted on the non-scanning carriage. The orthogonality of the beam to the plotting system is established by adjusting it on its mount to maximise the echo from the back wall of the tank. A mirror system placed in the mount of the floor of the tank will be aligned with the plotter. The beam, however, may not be. Such misalignment is due to a misalignment between mirror components.

ii) The beam is explored with the target until the greatest signal to be plotted is detected. This would normally be the field maximum. The 'gate' is placed over this signal. The transmitter and receiver attenuation are adjusted until the y-signal is the largest that the system can handle without saturation effects. This peak signal is set to a 10 cm deflection on the x-y plotter. The sweep centre is set on the beam axis, the sweep size is set most commonly to 2 inches. A vertical scale is marked by using the attenuator.

iii) The system is switched to 'auto' and the target moved to the start position by pressing the 'scan' button. In practice, no mechanical backlash was found in the target drive and scans in either direction were identical.

Two dimensional field plots were achieved by drawing a line of starting points on the plotter paper and manually moving the track carrying the plotter carriage and adjusting the x and y positions on the x - y recorder. All movements on the tank have scales and cursors to facilitate this.

Axial plots may be obtained in a similar manner. The target is left on axis and its position and the x position on the recorder adjusted in step. At each position the gate is swept across the signal to generate a spike on the plot.

5.2. Selection of a Target

The system offers two types of plotting. The transmission field only may be plotted using the PVDF hydrophone. A reflective target may be used to produce a plot of the pulse echo field.

5.2.1. Transmission Field Plotting

A bi-laminar shielded PVDF membrane hydrophone (Marconi Research Laboratories) was used to examine the field. These devices have been described by Shotton et al (1980) and Bacon (1982).

They are useful for examining pulse shape as well as field shape. Such plots might be expected to resemble most closely the theoretical fields predicted by the models described in Chapters 3 and 4 since it was only the transmission field which was calculated. However the hydrophone used has an active area of 1 mm diameter and this is large compared with the focal zones of some of the highly focussed probes being considered.

5.2.2. Pulse-Echo Plotting

This method produces a representation of the beam actually used in scanning. It incorporates the transmission and reception fields of the transducer. The bandwidth will incorporate the characteristics of the transmitter, the transducer and the receiver circuits. All of this will effectively alter the beam shape (Wells, 1977). It will also contain the convolution of the beam with the target used.

Various targets have been used. Wires and spheres predominate. Łypacewicz and Hill (1974) have considered the suitability of targets. Spheres, because of the non-directional shape, present similarly to the beam, independent of their location in it. They are secured by their rear surface often to a hypodermic needle (Foster et al, 1981). Burchhardt et al (1973) simply rounded the end of a 2 mm diameter rod. Lypacewicz and Hill consider that the sphere should be as small as possible while still giving a sufficiently strong echo and be capable of being rigidly fixed in position. At low megahertz frequencies a diameter of 3 mm is considered satisfactory.

5.2.3. Experiment

Three 5 MHz transducers of similar Numerical Aperture but of differing aperture diameters and hence beam shape were plotted in the plane of their axial peak pressure with three reflective targets and with the PVDF hydrophone. The reflective targets were stainless steel ball bearings with diameters of 2, 5 and 10 mm, mounted on hypodermic needles.

Probe A is a Diagnostic Sonar MD 3106 handheld 5 MHz probe with a diameter of 6 mm and a peak 28 mm from its face.

Probe B is a Nuclear Enterprises NE 4353 5MHz, MIF Diasonograph probe (Serial No. 48673 H) 13 mm diameter with a peak 56 mm from its face.

Probe C is a Panametrics V307, 5MHz immersion transducer (serial no. 45892). 25 mm diameter with a focal length of 150 mm.

The results are shown in Table 5.1.

The larger targets are more sensitive. However only the hydrophone sensitivity shows any strong dependence on beam shape. All the beam shapes are a convolution of the target and the true beam shape. This is an effect that will vary with amplitude in the beam and depend upon beam shape. Targets larger than the beam alter its shape, flattening its peak. Thus the width at high amplitudes is exaggerated. The effect at lower amplitudes is less marked but is more dependent on the radius of curvature of the target.

5.2.4. Conclusions for Plotting Highly Focussed Probes.

The hydrophone will not indicate well the shape of a narrow beam. This will become especially critical for $NA > 0.16$, this corresponding to the limits of the main lobe of the hydrophone's directivity function at 5 MHz.
Applying the Kossoff (1968) formula used by Weyns (1980b) the pulse:echo beam width is overestimated by a factor of 1.4 at the -6dB level and 1.7 at the -20dB level. Weyns demonstrates the Kossoff CW result to be an overestimate of 1.3 compared to his PW model, thus suggesting an overall overestimate of 1.8 at the -6dB level and 2.2 at the -20dB level.
A 2 mm diameter steel ball will be used as a target for pulse:echo plotting. A spherical target is required because of its insensitivity to target orientation thus giving reproducible results. 2 mm is the smallest diameter which may be fixed rigidly for scanning. It will give a sufficiently large echo with any probe sensitive enough for clinical use.

5.3. Breast Scanner Transducers

Two commercial transducers were purchased for breast scanning. Both were 5MHz devices. One was a concave bowl with Numerical Aperture of 0.09. One was a flat transducer with a concave plastic lens and a notional Numerical Aperture of 0.167.
The theoretical and experimental performance of the devices is described here so that they may be compared to the mirror system results in Chapters 7 and 8.

5.3.1. Panametrics 1" Immersion Probe.

Panametrics V307, 5MHz immersion transducer (Serial number 45892) 25 mm diameter radius of curvature 150 mm. This transducer is a concave bowl device purchased through Diagnostic Sonar Ltd., Livingston. It is transducer C in Section 5.2.3.

	TARGET				
	Stainless steel ball bearing			Hydrophone	
	2mm diam	5mm diam	10mm diam		
Probe A Attenuation	-10 dB	-15 dB	-20 dB	-20 dB	
-6 dB	1.9 mm	2.5 mm	2.3 mm	2.1 mm	-3 dB
NA=0.11 -10 dB	2.5 mm	3.1 mm	2.9 mm	2.9 mm	-5 dB
-12 dB	2.9 mm	3.3 mm	3.2 mm	3.1 mm	-6 dB
-20 dB	4.0 mm	4.4 mm	4.2 mm	4.3 mm	-10 dB
-30 db	5.8 mm	6.0 mm	5.8 mm	6.2 mm	-15 dB
Probe B Attenuation	-10 dB	-17 dB	-22 dB	-15 dB	
-6 dB	1.6 mm	1.8 mm	1.8 mm	1.9 mm	-3 dB
NA=0.12 -10 dB	2.0 mm	2.2 mm	2.2 mm	2.3 mm	-5 dB
-12 dB	2.2 mm	2.4 mm	2.3 mm	2.5 mm	-6 dB
-20 dB	3.0 mm	3.1 mm	3.1 mm	3.3 mm	-10 dB
-30 dB	4.6 mm	4.4 mm	4.7 mm	5.1 mm	-15 dB
Probe C Attenuation	-10 dB	-16 dB	-20 dB	-25 dB	
-6 dB	4.0 mm	3.9 mm	4.1 mm	3.8 mm	-3 dB
NA=0.09 -10 dB	5.0 mm	5.2 mm	5.1 mm	4.8 mm	-5 dB
-12 dB	5.5 mm	5.7 mm	5.8 mm	5.2 mm	-6 dB
-20 dB	8.0 mm	8.5 mm	8.2 mm	7.4 mm	-10 dB
-30 dB	10.6 mm	11.2 mm	10.7 mm	10.0 mm	-15 dB

Table 5.1. Experimental Beam Shapes:
Dependance of full width on choice of target.

The theoretical field is shown in figure 5.5. An axial plot, made with the PVDF hydrophone and the corresponding prediction using PLOTCW is shown in figure 5.6. Agreement is good in the region of the peak but some of the CW nearfield interference pattern is seen. The actual field loses sensitivity more quickly in the farfield.

Figure 5.7 shows the transverse field. Figure 5.7(a) compares the theoretical transverse field at the axial maximum (range 138 mm) and the test tank hydrophone plot through the experimental peak (range 142 mm). The two agree well on shape but badly on actual size. This is shown in figure 5.7(b) where the scale for the theoretical plot has been expanded by a factor of 2.67. As expected the PW field does not show the CW interference maxima and minima. Weyns (1980a) analysis of the effect of pulse length on beam width might account for a factor of 1.3 based on the manufacturer's pulse length test which suggest a pulse length of little more than two cycles. This analysis also suggests a mean frequency of 4.4 MHz. Observations of the pulse with the PVDF hydrophone (Figure 5.7(c)) show a single cycle with a frequency of 4.2 MHz (based on the downward slope) and some lower frequencies. Neither this reduction in frequency nor a lower velocity in the test tank water (at room temperature, about 17°C, giving a velocity of 1475 ms^{-1}) account for this difference in beam width. Using Weyns results, a single cycle pulse would result in significant broadening, a factor of 2.2 for flat discs. This effect, together with broadening, due to the hydrophone, could account for the differences.

This transducer displayed a shift to lower frequencies, presumably due to a failure of internal tuning components and was eventually returned to the manufacturer for repair.

5.3.2. S. and I. 2" transducer with lens.

Supplied by Systems and Instrumentation Ltd., agents for Transducer Manufacturing Services, this device was a 2" diameter disc focussed by a concave epoxy lens.

The lens surface is spherical and its thickness varies from zero in the centre to approximately 4 mm at the edge. It's performance will,

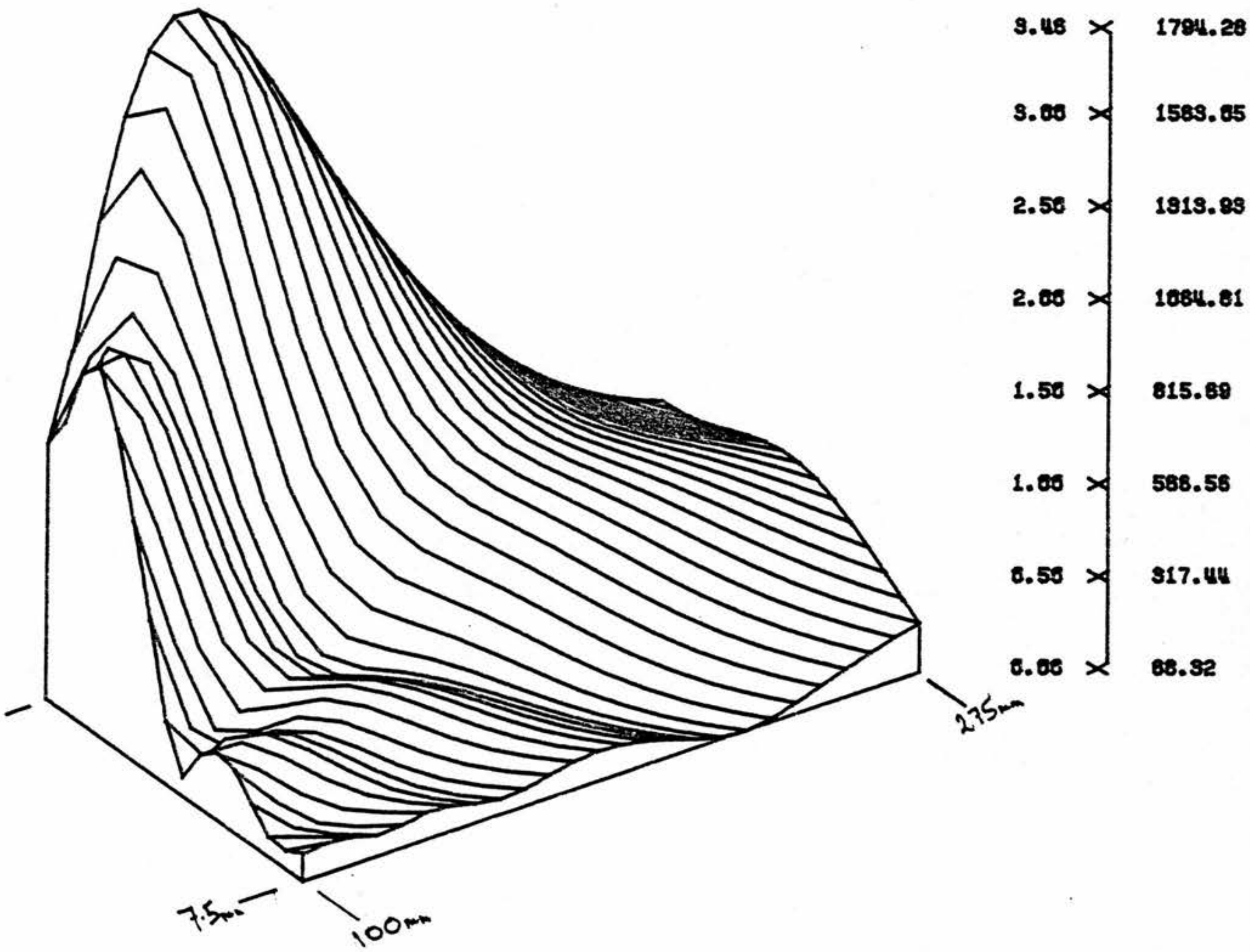

PANAMETRICS 25MM PROBE(MIRROR2);AXIAL STEP 7MM,

Figure 5.5: Theoretical plot of Panametrics V307 1" dia., 5MHz probe.

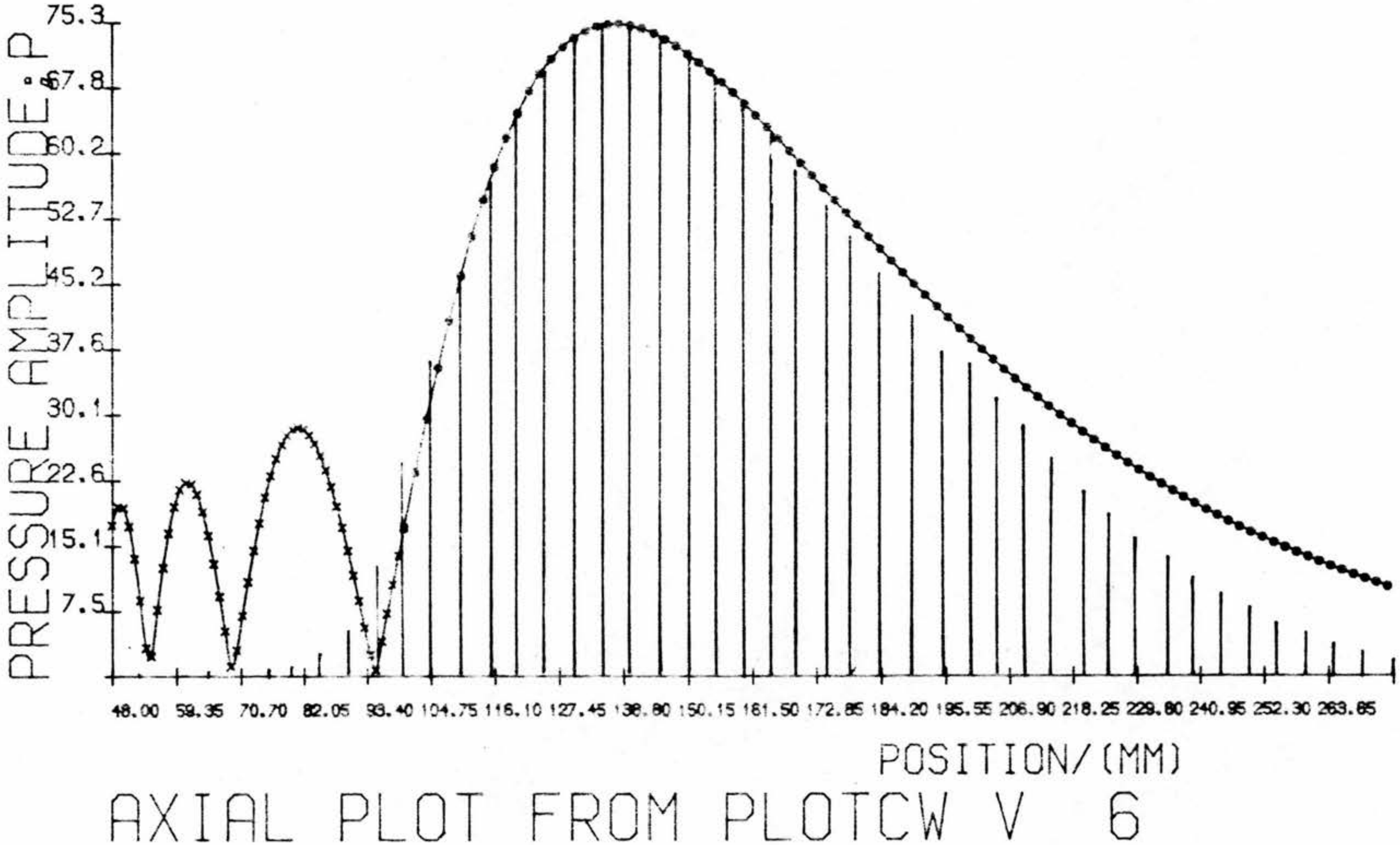

Figure 5.6. Theoretical (PLOTBCW) and experimental axial fields of the 1" diameter 5 MHz Panametrics probe. The vertical bars are the experimental results.

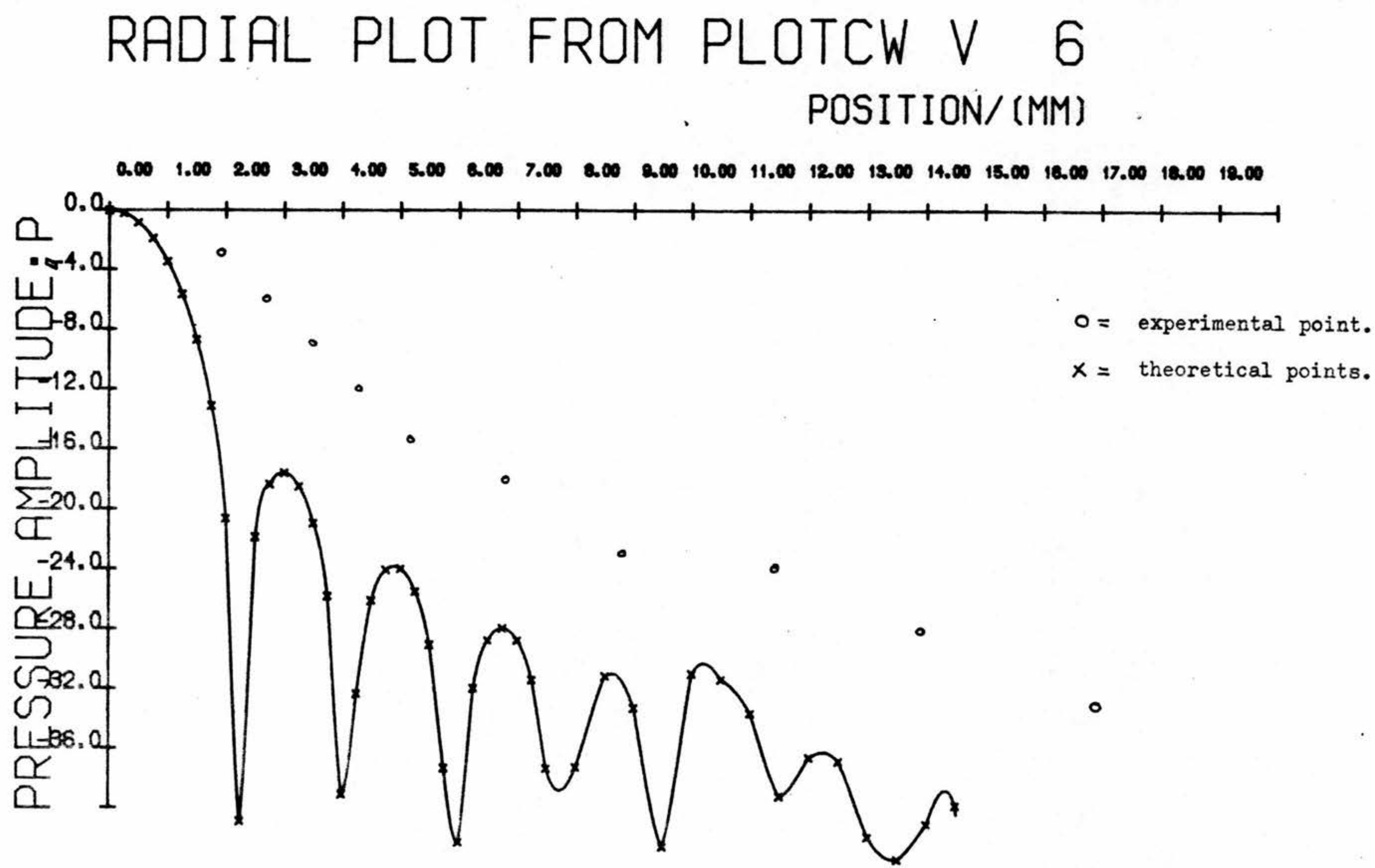

Figure 5.7(a). Theoretical and experimental plots through the peak of the ¾" Panametrics probe.

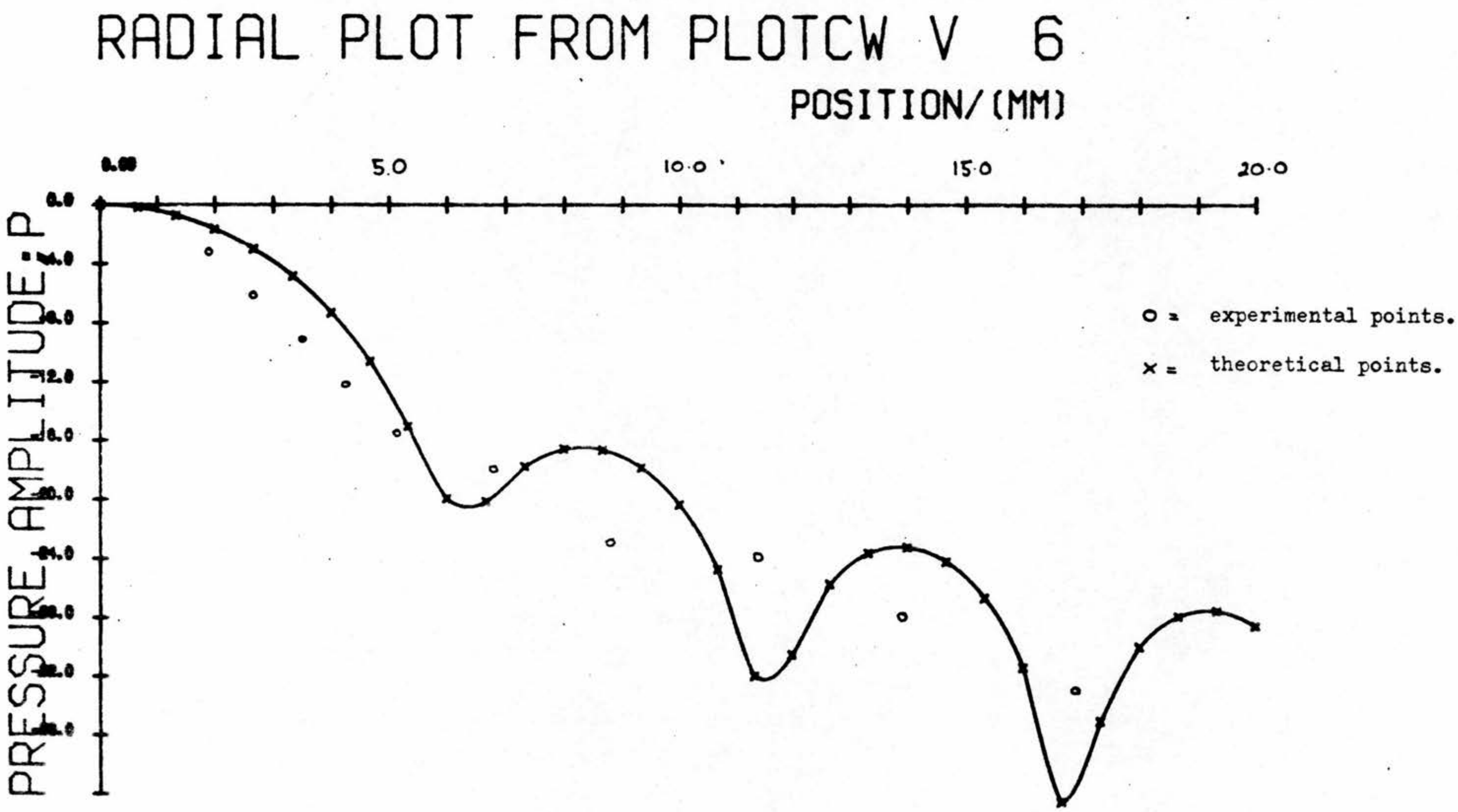

Figure 5.7(b). Theoretical and experimental plots through the peak of the 1" Panametrics probe.

Radial scale of theoretical plot expanded by a factor of 2.67.

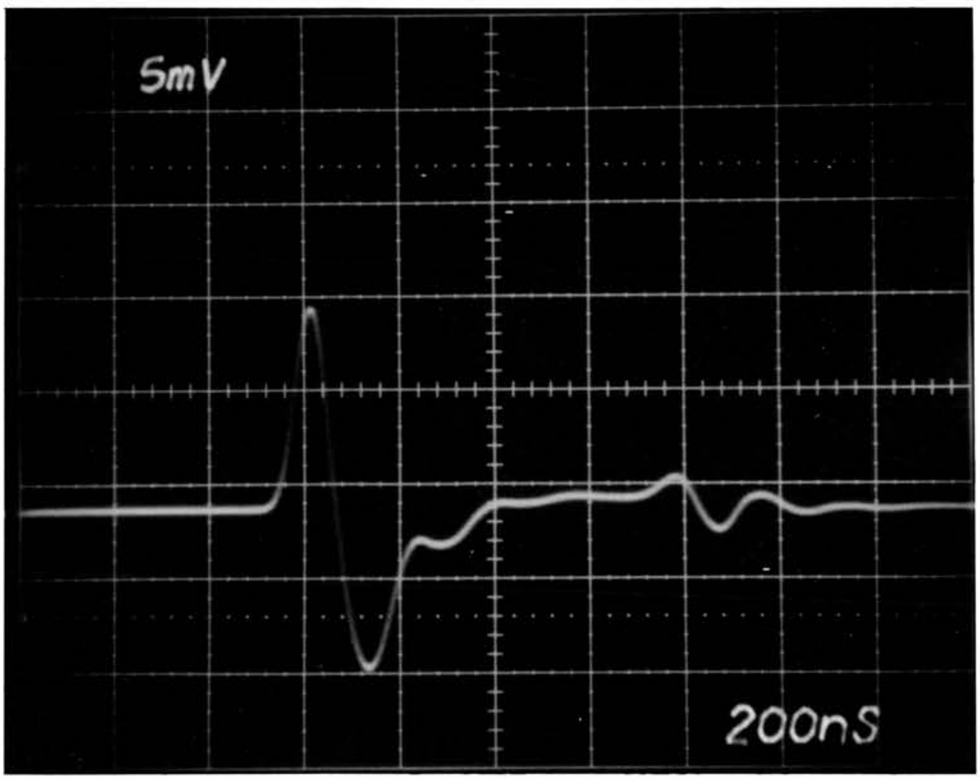

Figure 5.7(c): Parametrics V307 1" probe pulse-shape using PVDF Hydrophone (T_x-10dB)

therefore be degraded both by spherical aberration and by apodisation caused by varying attenuation in the lens.

A CW field plot is shown in figure 5.8; separate radial and axial plots in figure 5.9. The radial plot is in the plane of the geometrical focus but in this case (NA = 0.177) theoretically the peak pressure is displaced inwards by only 0.7 mm.

Figure 5.10 shows the test plot with the CW model results superimposed as broken lines. The differences are obvious. Agreement on the transverse shape is good but the experimental width is 3.5 greater.

However, many factors which contribute to this divergence are visible. The axial plot would not usually indicate the focal length well and this will be exacerbated by spherical aberration. Spherical aberration will also lead to beam widening. The apodisation due to lens attenuation will effectively reduce the aperture, enhancing these effects. The field maximum is at 160 mm, 10 mm beyond its intended position. This is contrary to the effect of spherical aberration and the lens apodisation and can only be attributed to a design failure. It is not possible to assess the lens theoretically since its acoustic properties are not known. The pulse shape is shown in figure 5.11. It is difficult to assess. It shows a dependance on excitation energy. There is a second component - apparently a reverberation within the lens.

This transducer failed several times during its service. This was caused by the front face electrode coming away from the crystal, perhaps pulled loose by the lens. Repair times became longer as the manufacturer sought a solution. It was eventually replaced

It was used to scan some 90 patients as it offered better resolution than the probe described in section 5.3.1. (-20 dB experimental beam width of 5.3 mm compared with 8.0 mm) although it did lack sensitivity. An example scan is shown in figure 5.12.

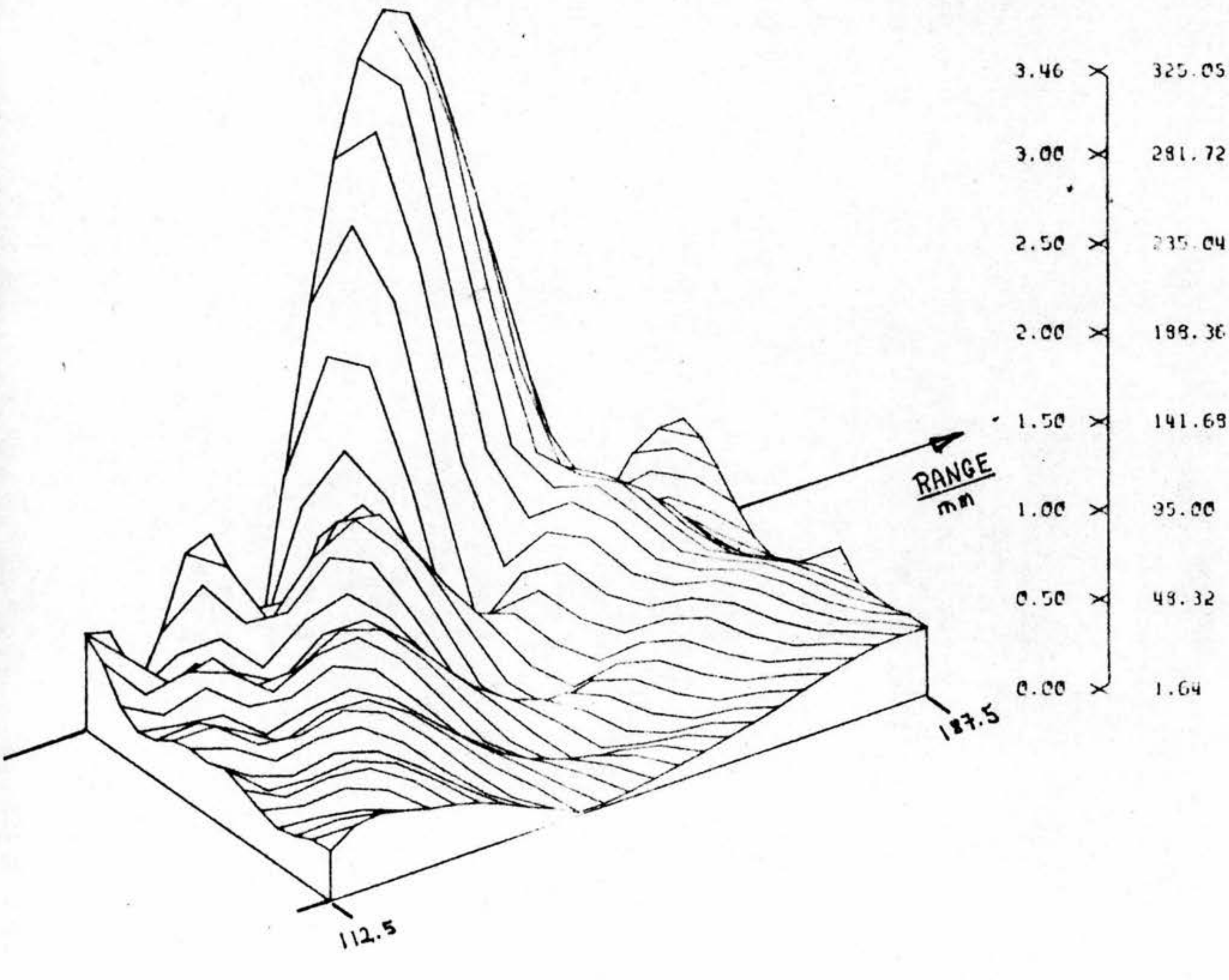

S & I PROBE: 112.5 TO 187.5 MM, 3MMSTEPS

Figure 5.8. Theoretical plot of lens focussed, 2" diameter transducer.

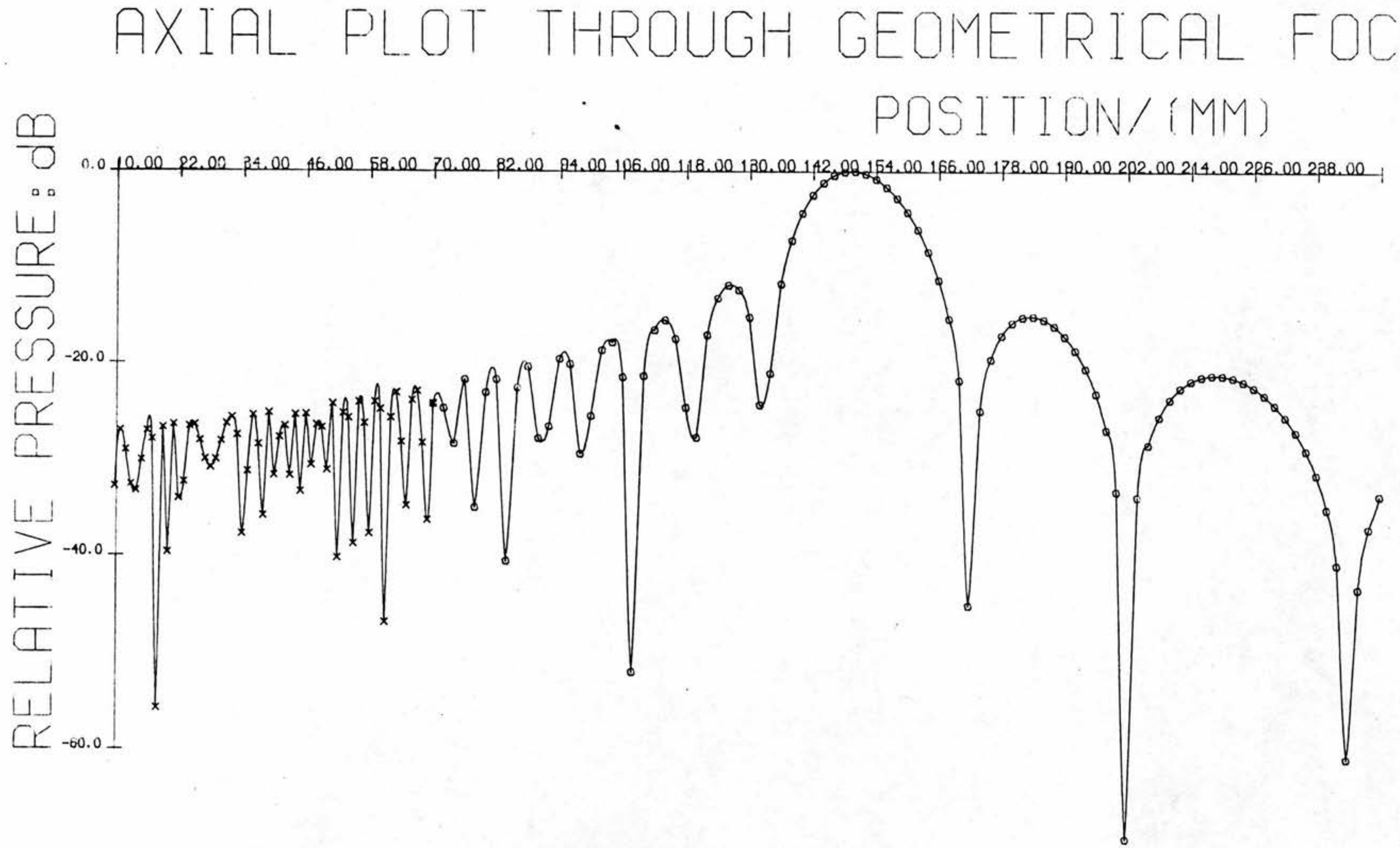

Figure 5.9: CW bowl (PLOTBCW) model of the axial field of the S & I 2" dia. probe.

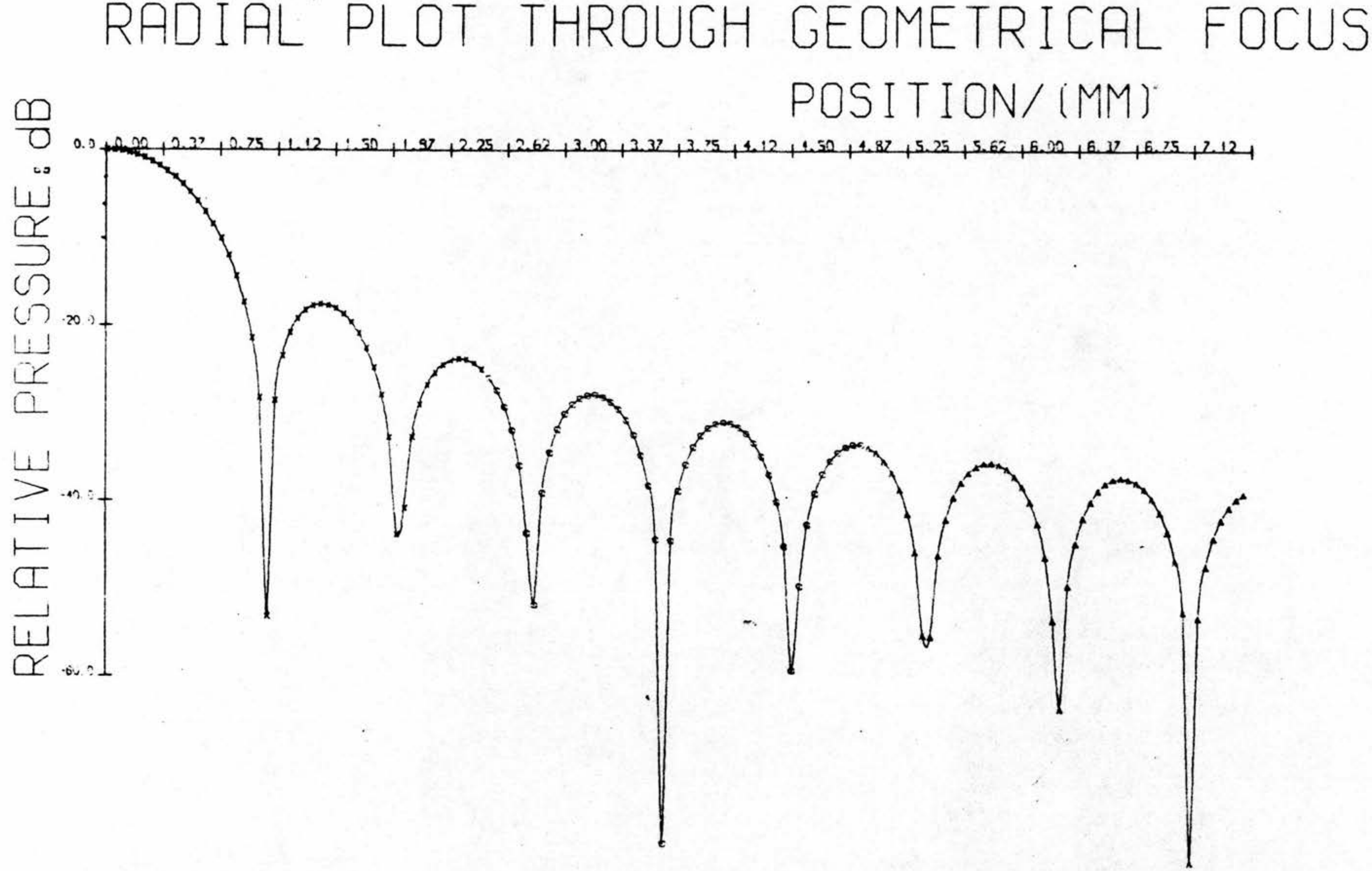

Figure 5.9(a). Theoretical radial plot for 2" lens focussed transducer.

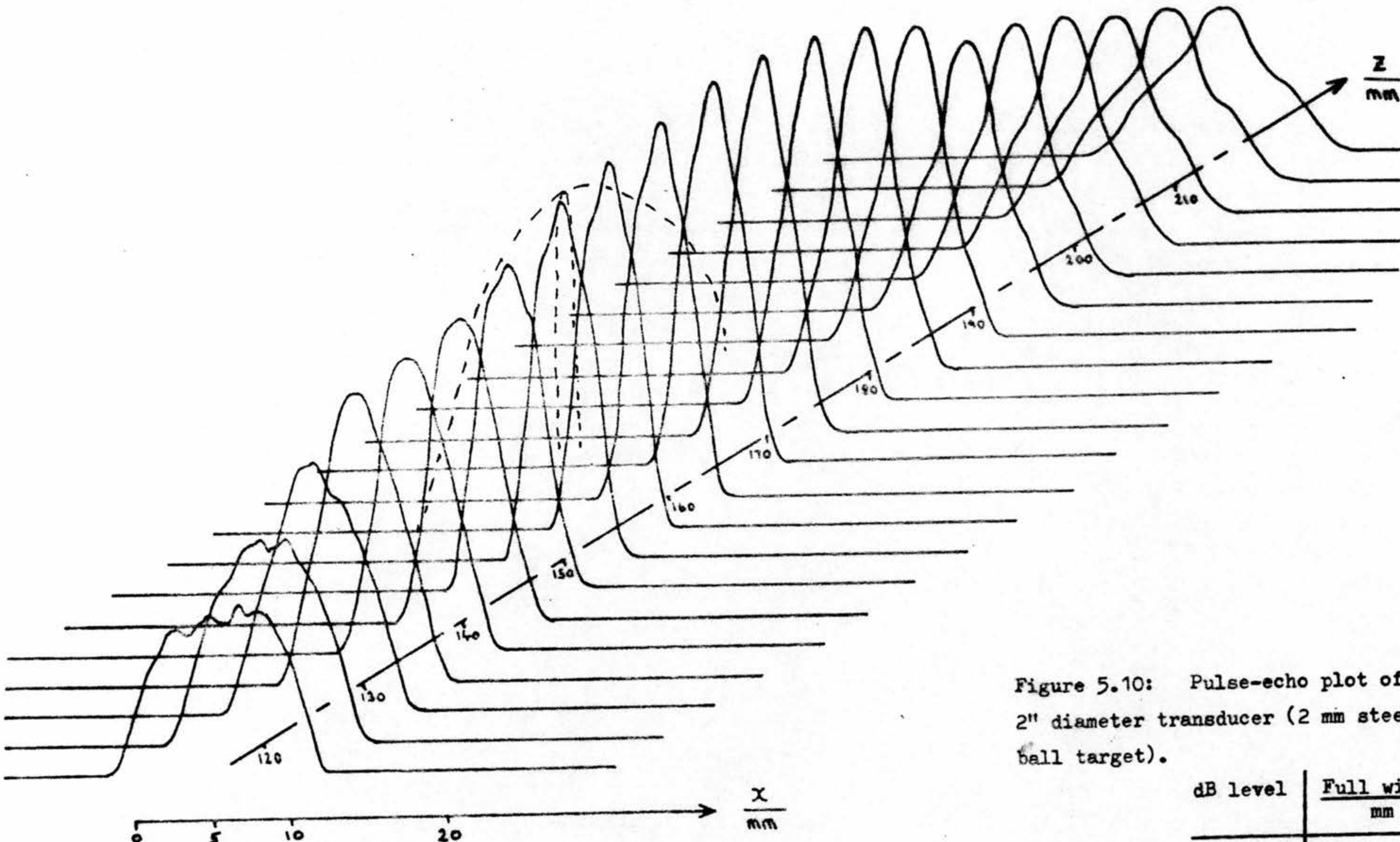

Figure 5.10: Pulse-echo plot of S and I 2" diameter transducer (2 mm steel ball target).

dB level	Full width mm
-6	2.4
-12	4.25
-20	5.3

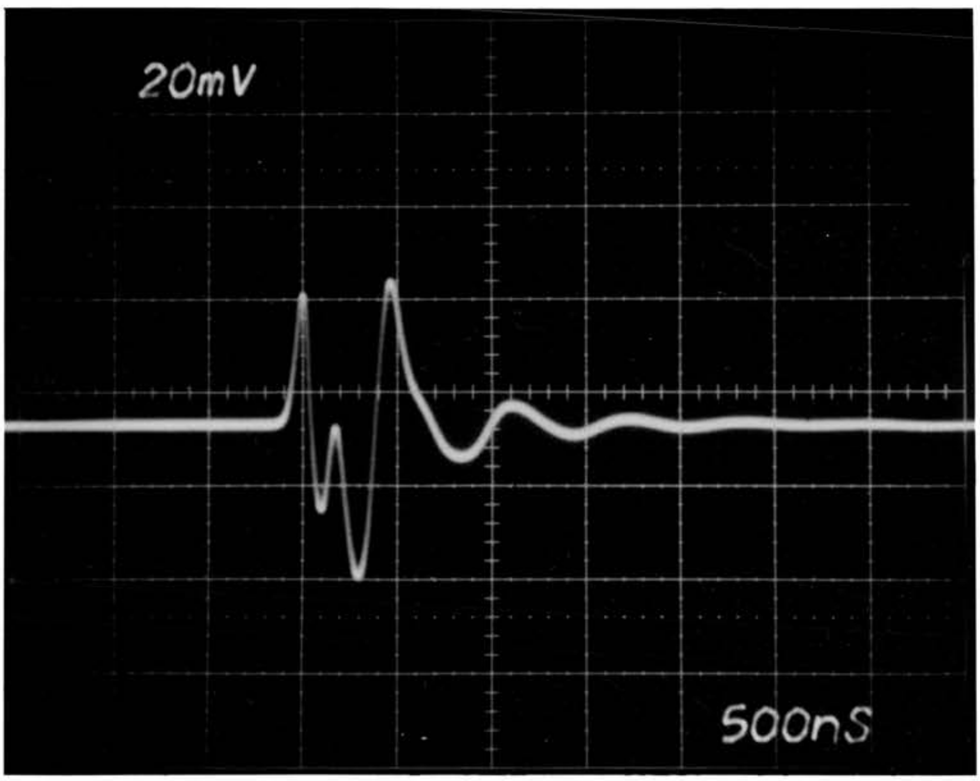

Figure 5.11. S and I probe pulse shape using PVDF Hydrophone (T_x-0dB)

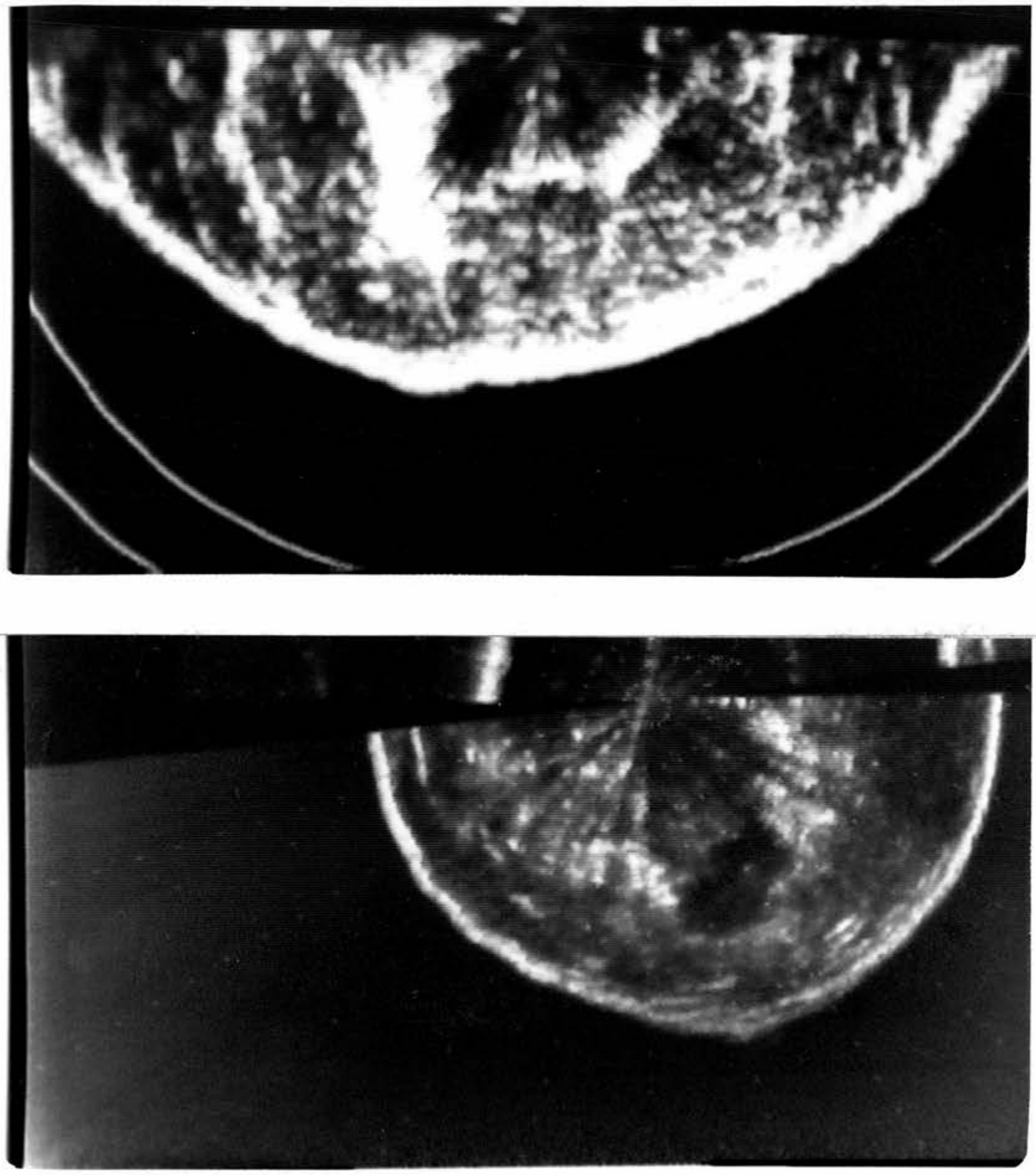

Figure 5.12: Example breast images using the S & I 2"dia. probe.

CHAPTER 6. DESIGN AND CONSTRUCTION OF MIRROR SYSTEM COMPONENTS.

This chapter discusses the techniques used to manufacture and assemble the various mirror components. A design program using interactive graphics was employed to assist in the choice of mirror shapes. The two different techniques used to construct mirrors are explained, the choice of materials discussed and the transducers used to energize them analysed. Alignment of the mirror systems is described.

6.1. The Mirror Design Aid Program.

To facilitate the design of mirror systems, a program was written to use interactive graphics to produce a qualitatively acceptable design. The mirror curves can then be printed on a matrix plotter and the curves themselves listed as a series of x and y coordinates, or differences in SI or Imperial units. The latter is required because the lathes used to turn the mirror surfaces are not metric.

The program itself does not insert any ray plotting on the mirror shapes. This must be done manually.

The program itself is written in Fortran lV.

A flow diagram is shown in figure 6.1. The geometry used is shown in figure 6.2.

It is assumed that any mirror system will be based on two conics sharing a common reference point. The terminology used in discussing conics is explained in Appendix 1. The system will be circularly symmetric about a common axis (shown as AB in figure 6.2). The common reference point (marked as F_2) is at the origin of the cartesian co-ordinates used. The two singular reference points are both expected to lie on the system axis and have the same 'y' co-ordinate but it is possible to move F_3 off-axis.

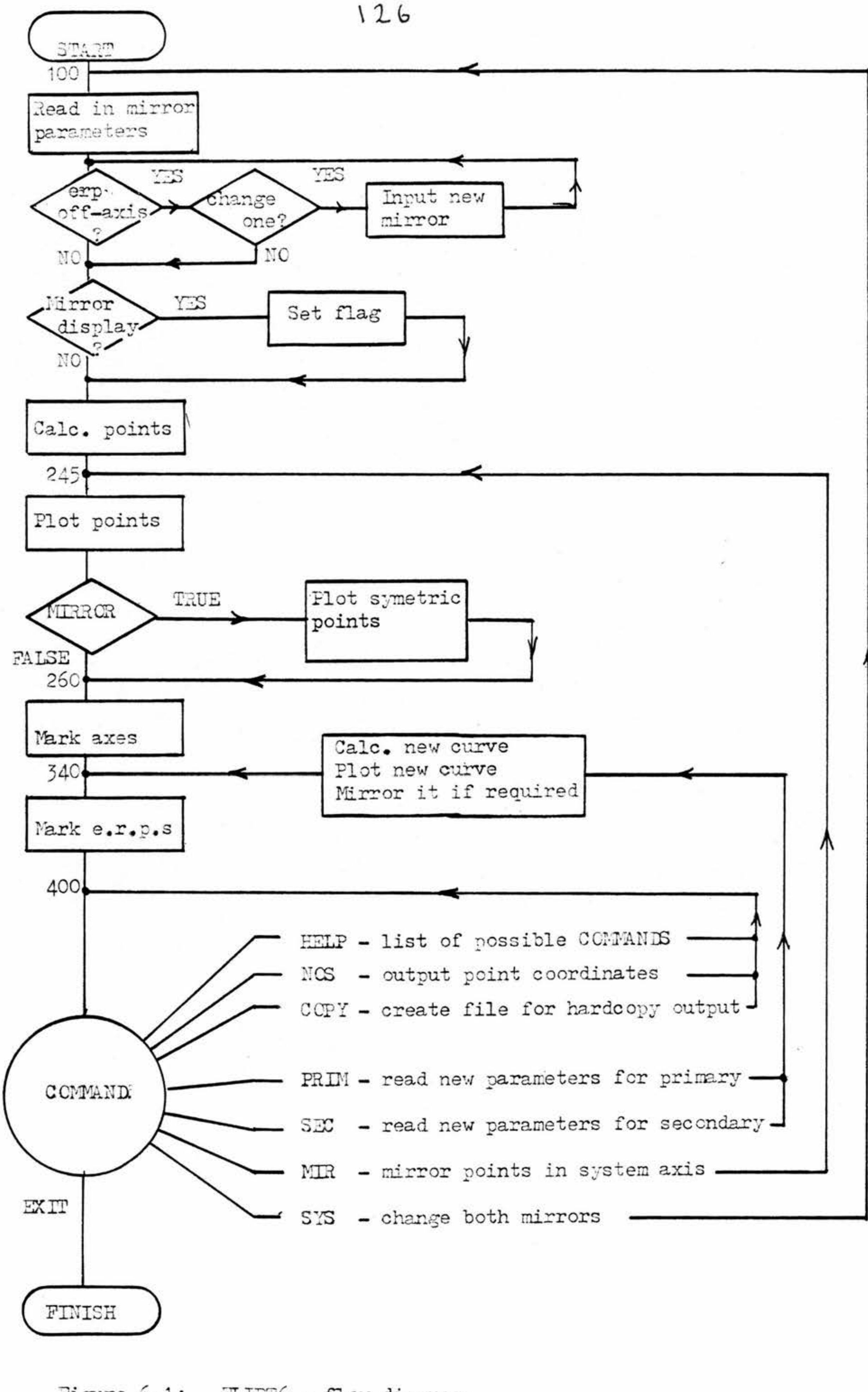

Figure 6.1: ELIPT6 - flow diagram.

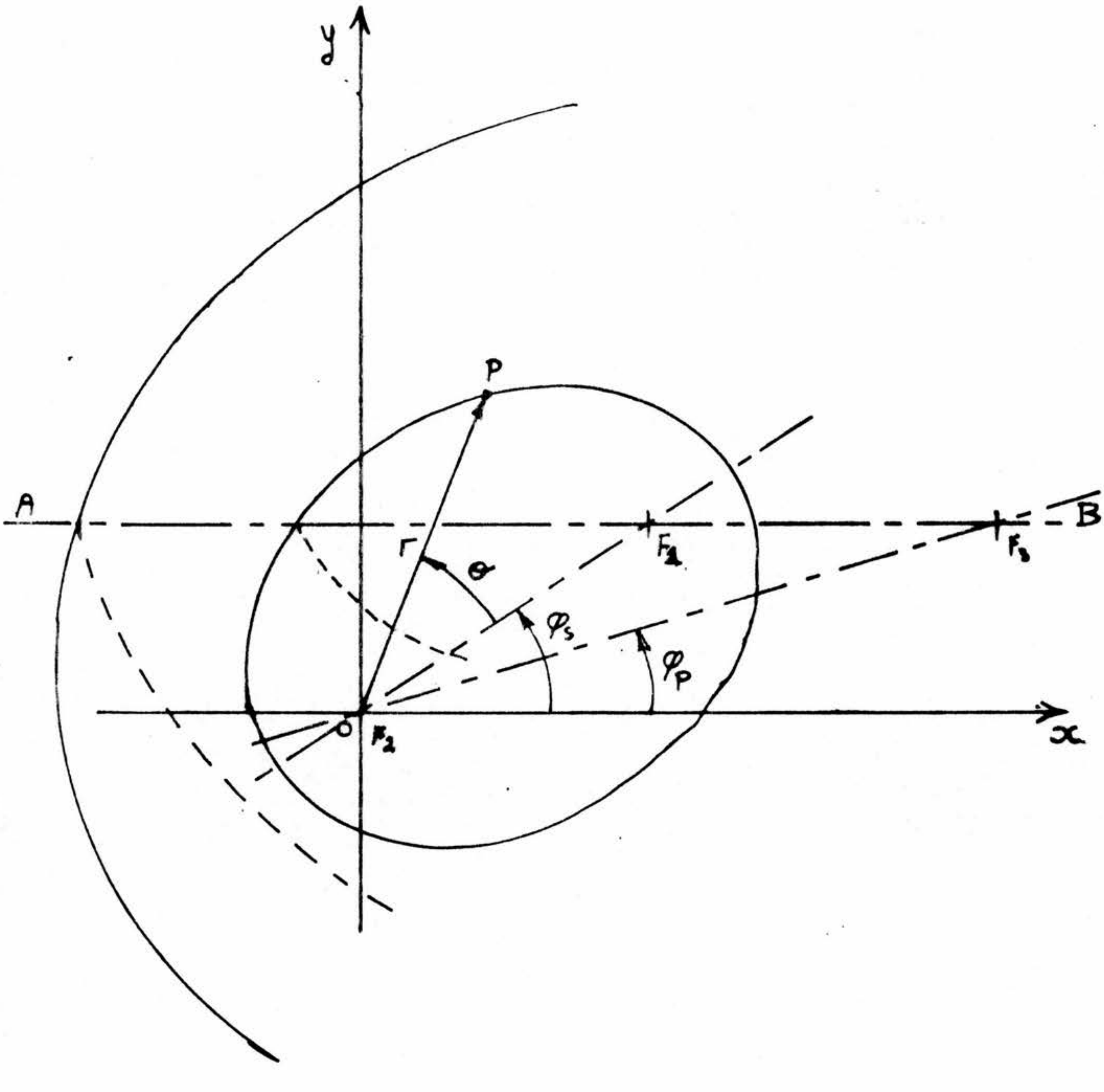

Figure 6.2. Mirror design geometry.

The operator describes a mirror by the cartesian location of its singular focus (F_1 for the secondary, F_3 for the primary) and the length of its semi-major axis. Points are calculated as polar co-ordinates (r, θ) with origin at F_2 and $\theta = 0$ axis, the major axis of the conic. The equation used is

$$r = \frac{k\, e}{1 - e \cos \theta} \qquad 6.1$$

where e = eccentricity = $\frac{c}{a}$

$k = -\frac{a}{e}$

a = semi-major axis length

c = half-distance between reference points

$= \frac{1}{2}\left|F_2F_1\right|$ or $\frac{1}{2}\left|F_2F_3\right|$

The program will display or print the points as they are, or reflected in the axis AB if this is different from the x-axis. An example output is shown in figure 6.3.

6.2. Mirror Construction

Two types of mirrors were made to meet different design needs.

6.2.1. Air Backed Mirrors: Hollow Copper

A high degree of mismatch of acoustic impedance between water and mirror material is required to achieve a good reflectivity. In the past, this high acoustic reflectivity has been achieved by use of a dense metal (e.g. Thurstone and McKinney, 1965) or a dense metal powder: epoxy resin mix (e.g. Olofsson, 1963). Both these materials have an acoustic impedance much higher than that of water. A

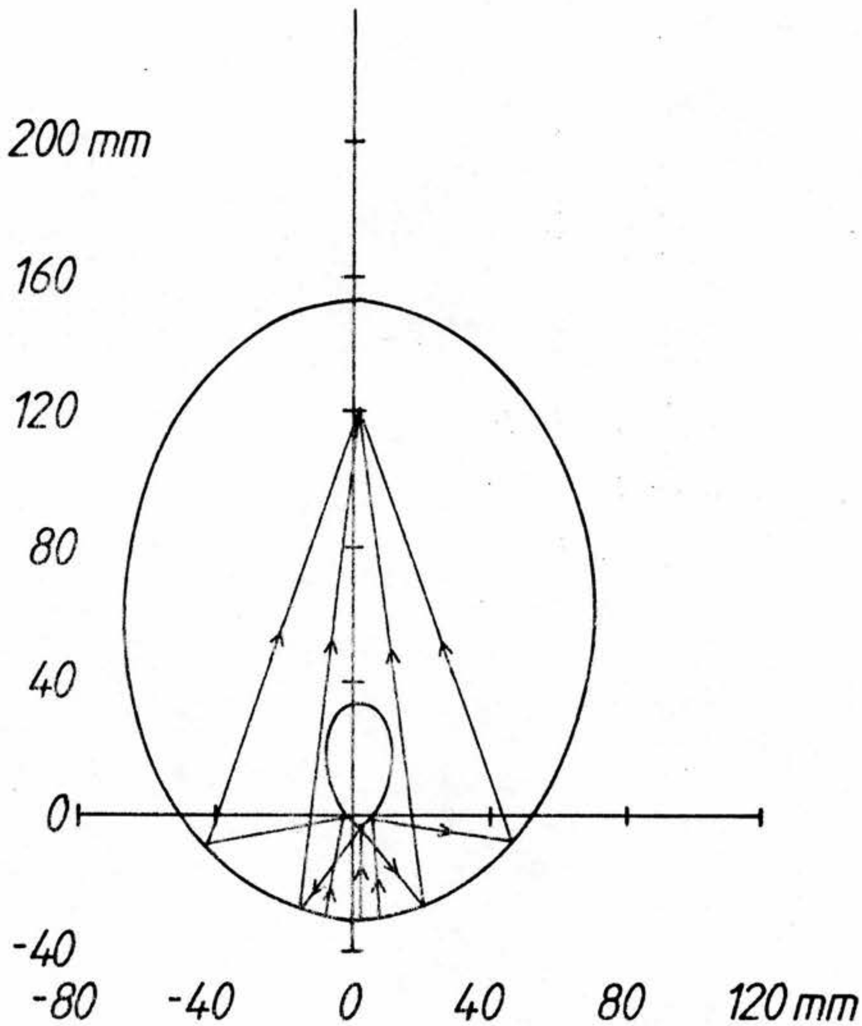

Figure 6.3: Example output of design aid.

disadvantage of metals is that their attenuation is relatively low and therefore reverberations can occur between front and rear surfaces.

An alternative means of achieving a high degree if mismatch would be to use a material with a much lower impedance than that of water. Air serves this purpose admirably, as there is virtually total reflection at a water/air interface. Unfortunately, air requires to be contained. However, if the containing walls are very thin, we have effectively an air reflector. The walls must also be rigid. Thin walled air-backed copper mirrors were manufactured.

The mirrors were selected using the design assistance program described in section 6.1. This program output the curves as a list of Imperial (thousandths of an inch) co-ordinates and differences. These were used as instructions to turn both male and female brass moulds to the form of the required reflecting surface. This was done on a manual lathe. Next, from a circular piece of 22 swg (0.71 mm) copper sheet, a hole was cut for the transducer aperture at the centre of the mirror. The copper was then annealed by repeated heating and quenching and pressed to shape between the brass bowl moulds. This produced a thin (less than 0.68 mm after stretching) copper bowl with a central aperture. This was glued at its inner and outer edges to hollow copper cylinders which formed the walls of the final structure and finally the back was closed by soldering on a flat, annular copper sheet.

There are limits to the technique. The copper plate must maintain its shape after being stretched. It is unlikely that a mirror much deeper than that described in Chapter 8 could be produced by this method without development.

Pulse lengthening.

Although the reflective copper surface is thin (< 0.64 mm) it is not ideally thin when compared to the wavelength in copper (0.95 mm).

Figure 6.4 shows the pulse before and after reflection. Using the pulse length criterion of the transducer manufacturer, the reflected pulse is 0.5 cycles longer but 2 μs after its start, the pulse is still only -27 dB (c.f. -35 dB for the original pulse). The degradation is not considered to be serious for present purposes. The ultimate effect is shown in figure 7.24(b).

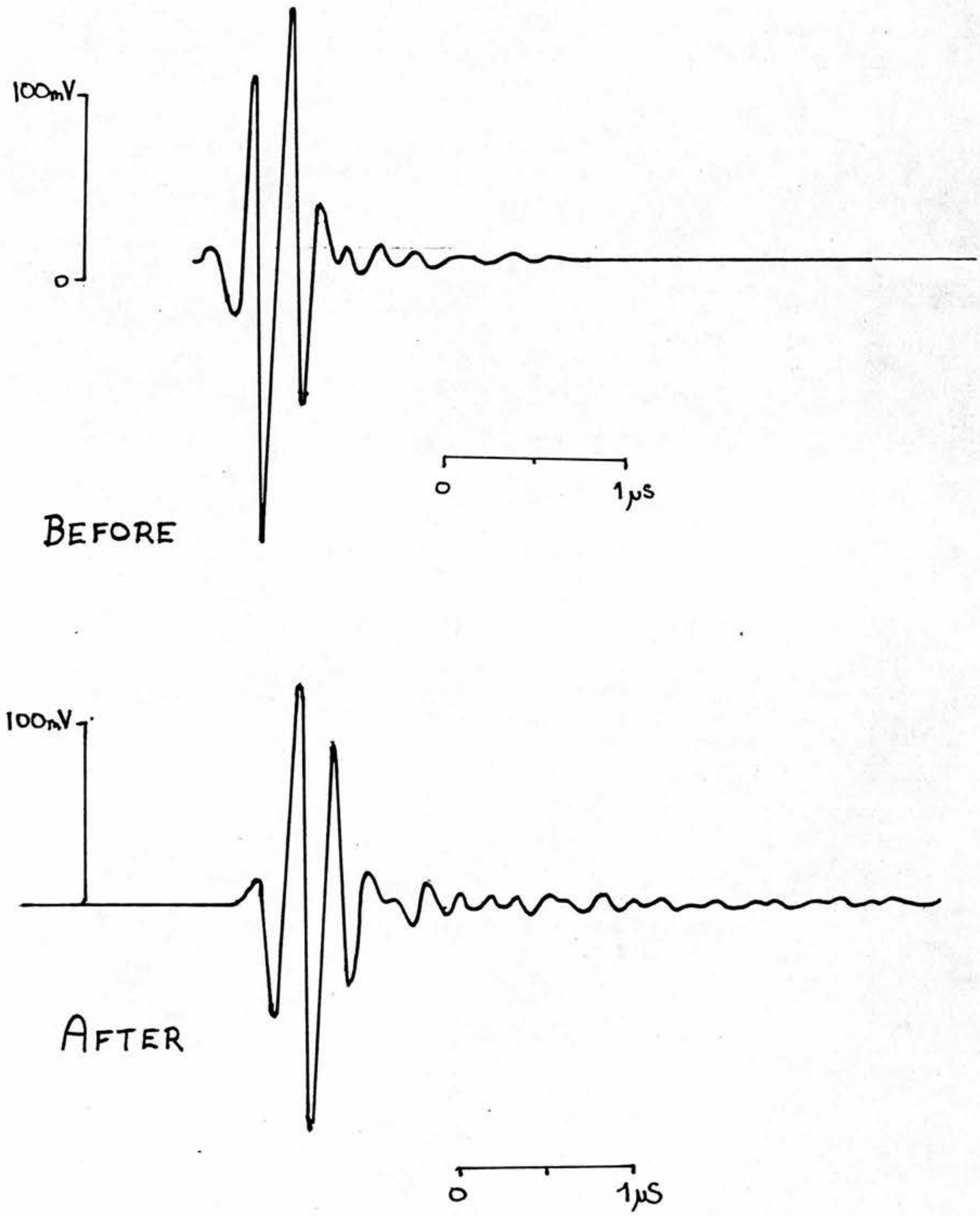

Figure 6.4: Pulse before and after reflection from an
air-backed, thin copper reflector.

6.2.2. Moulded Mirrors: Tungsten-Epoxy Composites.

The same technique could not be used to make all of the small secondary mirrors, because it is impossible to press a metal sheet to the sharp point which is required. A solid brass reflector (as tried by Thurstone and McKinney, 1965) was found unsatisfactory because of internal reverberations. A better reflector of reasonably high acoustic impedance can be made from a composite of grains of high-density metal embedded in a matrix of attenuating material. The composite has a high attenuation not only because of the absorbing matrix but also because of the scattering effect of the grains. Epoxy resin filled with powder has frequently been used in transducer manufacture (e.g. Kossoff, 1966) or in mirror manufacture (e.g. Kelly-Fry et al, 1968). Acoustic properties of some mixes have been given by Pelmore (1977).

For his mirror Olofsson (1963) used a mix of 6 : 1 (Tungsten : Araldite) by weight. Fry et al (1967) used the same ratio but added a polymer (not included in the mass of resin) to the mix. They also specify the tungston powder as being a mixture of 1 - 2 μm and 4 - 5 μm diameter particles. Burckhardt et al (1973) however used a ratio of only 3 : 1.

The acoustic impedance of various tungsten : araldite ratios are shown in figure 6.5. A composite of Araldite (Resin MY 753 + hardener HY 951, CIBA - Geigy Ltd) and 1μm diameter tungsten powder was used. These results are in good agreement with those of Bainton and Silk (1980). The addition of the tungsten powder makes the mix increasingly viscous. However it was found to be beneficial to evacuate the mixes before they set to remove air trapped during mixing; bubbles set in the composite being echogenic. It was also difficult to mix the very viscous mixturesthoroughly. Thinning with isopropyl alcohol and with additional amounts of the hardener (HY 951) was tried. Both decreased the acoustic impedance slightly. Isopropyl alcohol had the worse effect, in addition to which it took a long time (approximately 3 months) for the material to achieve its final acoustic properties.

Even with the addition of twice the recommended amount of hardener, high tungsten : araldite ratios could not be worked reliably. Therefore in spite of the potentially increasingly high returns for increasingly

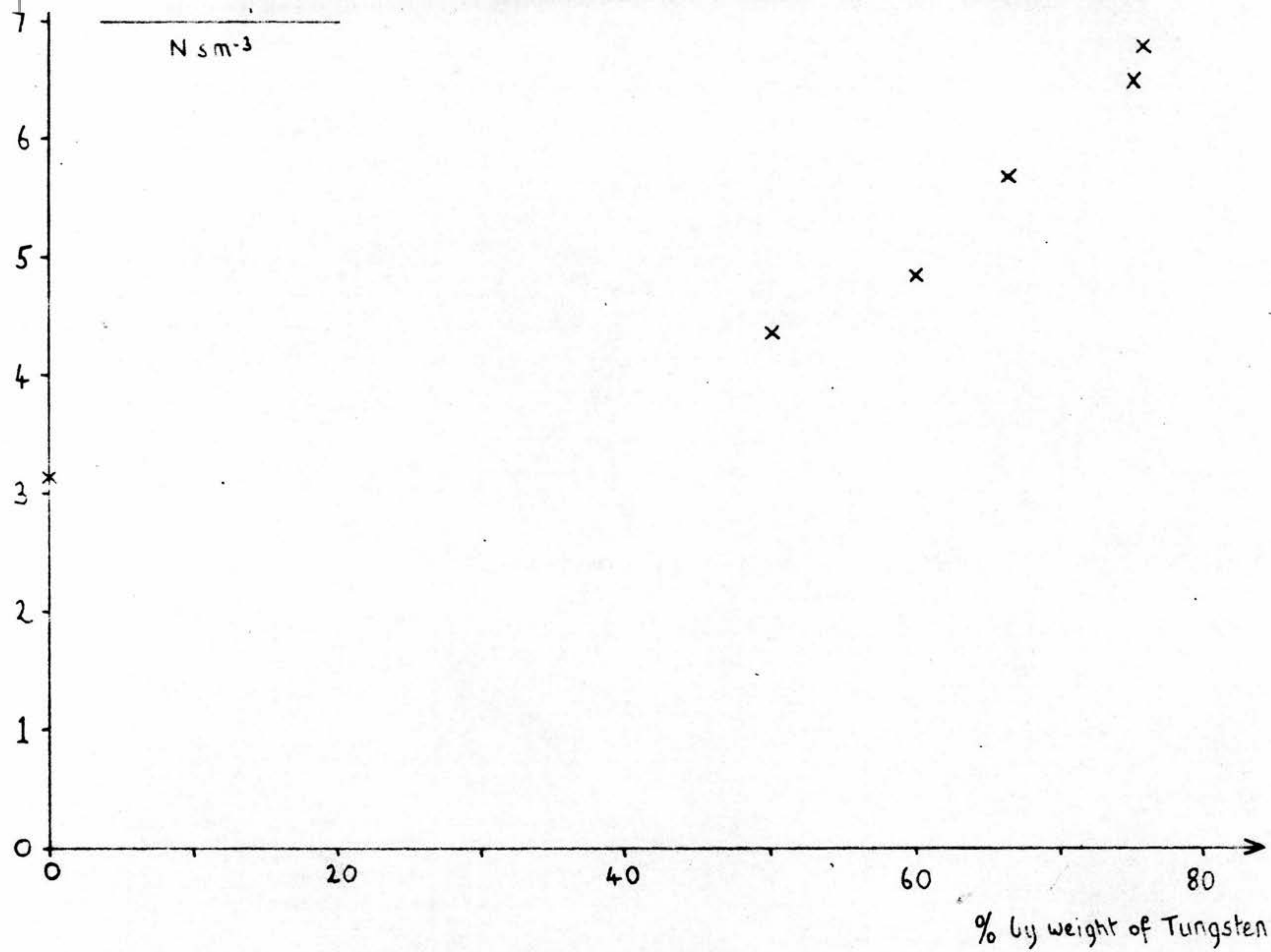

Figure 6.5: Acoustic Impedance of epoxy:tungsten powder composites.

dense mixes, a ratio of 2.7 : 1 by weight with twice the recommended hardener was used.

The resulting material is homogeneous and attenuating. Figure 6.6 compares reflected pulses from this and other materials. The composite material has a comparatively low reflectivity but is attenuating.

The composite material did not machine well and reflectors made in it were moulded. Because of the difficulty in machining small concave moulds, secondary mirrors were moulded in wax moulds using a 'ciré perdu' method. The moulding technique is illustrated in figure 6.7.

The desired mirror shape is turned in brass. This positive mould is located at the bottom of a tube (figure 6.7(a)). A release agent (aerosol silicone grease) is used to prevent the mould from sticking to the perspex. No release agent is put on the mirror surface of the mould. The assembly is heated in an oven to approximately 75°C and a high melting point (68°C) wax is poured in. The assembly is permitted to cool slowly. Slow cooling is essential as the wax contracts as it cools and will part from the brass if cooled too quickly. The brass mould is removed leaving a wax negative of the mirror which is filled with the tungsten powder : epoxy mix. A similar mix with tufnol shavings added to increase the attenuation is added on top and the mould is placed in a vacuum chamber to remove trapped air. Once air bubbles have been removed, the epoxy is set in an oven at 45°C, the wax is melted away, the tube removed by parting in a lathe if need be, and the back of the mirror turned to a 60° cone. This cone shaped back surface will refract any pulses transmitted through the mirror away from the beam axis.

As an aid to alignment of the system, the mirror surface is silvered. A light layer of aerosol varnish is applied while the mirror is being spun in a lathe. Silver is vacuum deposited on top of this.

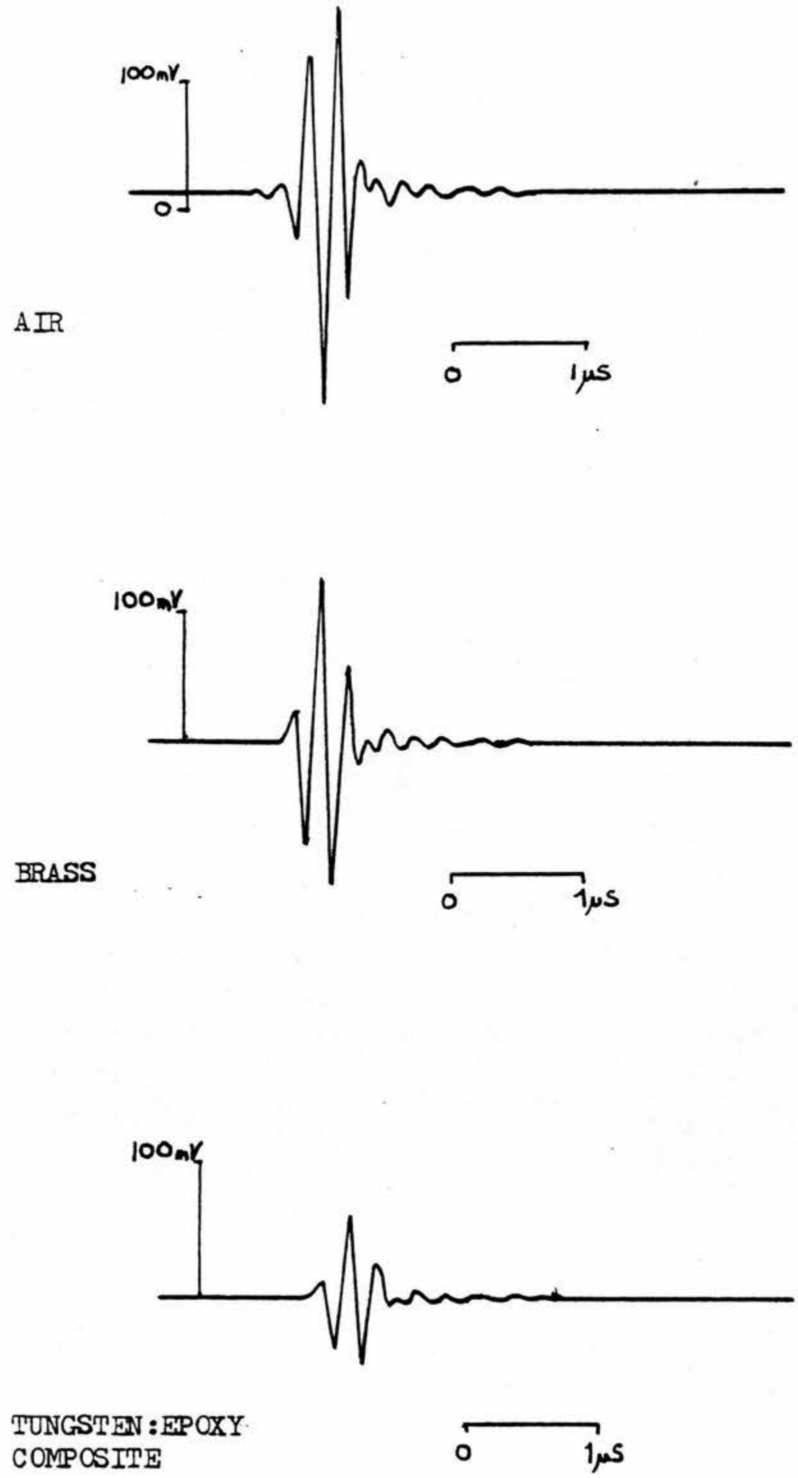

Figure 6.6: Reflected pulses from some materials.

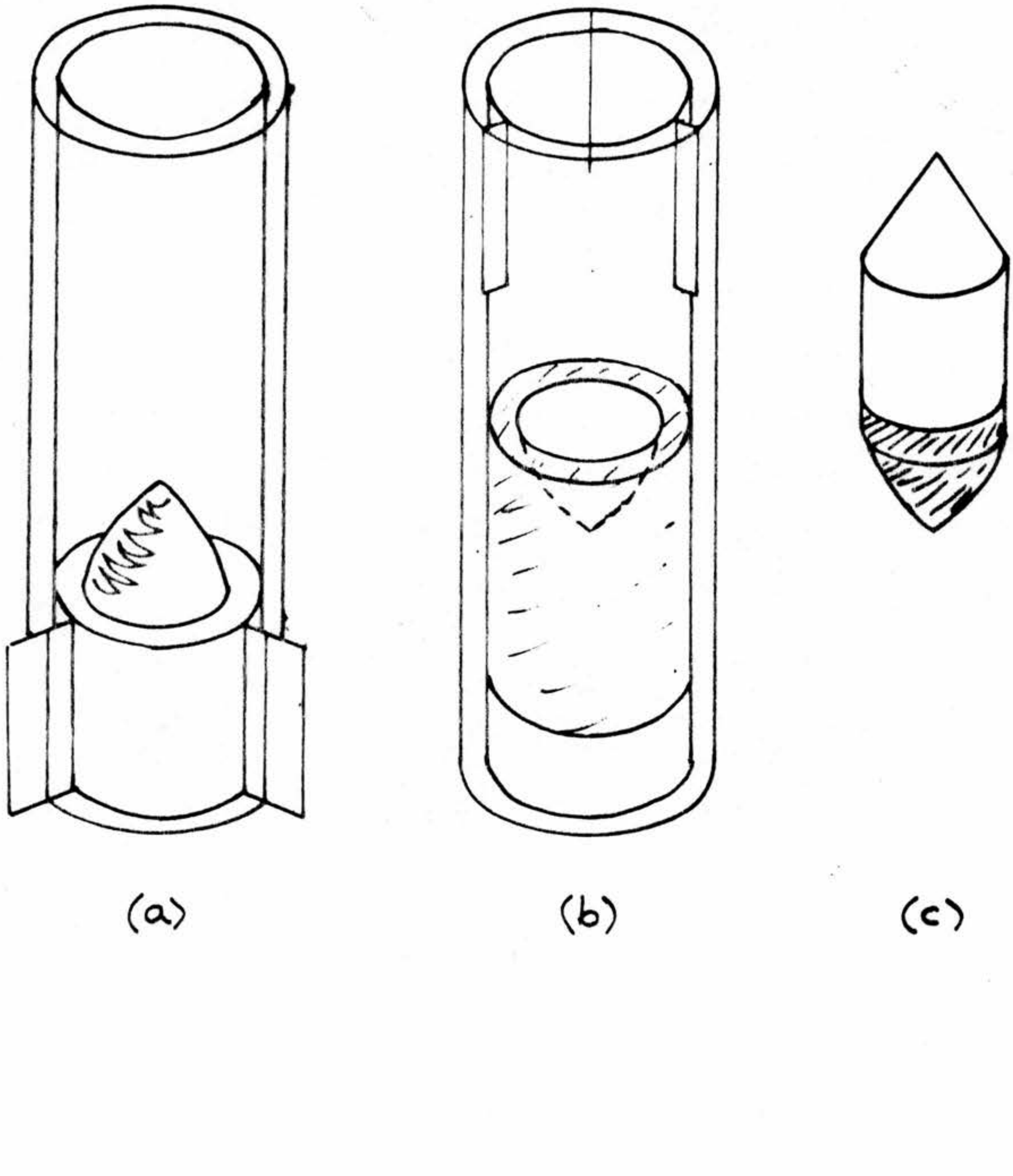

Figures 6.7. Ciré perdu wax moulding technique.

6.3. Transducers used with Mirror Systems

Five transducers were used with mirror systems.

i) A laboratory manufactured, unfocussed 12 mm diameter 2.5 MHz disc. The manufacture of this was based on the work of Kossoff (1966) and Bow (1979). A test tank plot is shown in figure 6.8.

ii) Nuclear Enterprises NE4376 2.25MHz 13 mm diameter Medium Internal Focus transducer Serial no. 34281H. A test tank plot is shown in figure 6.9.

iii) Nuclear Enterprises NE4352, Serial no. 48673H. Similar to ii) but operating at 5MHz. A test plot is shown in figure 6.10.

iv) Diagnostic Sonar MD3500. A 5 MHz 13 mm diameter probe made specially for use in mirror systems. It was a special order on account of its external dimensions. Its axial peak is at 60 mm range and its pulse shape is shown in figure 6.11, a test tank plot in figure 6.12. This is the probe most commonly used to drive mirror systems.

v) Diagnostic Sonar MD3106 5MHz 6mm diameter Medium Focus Serial no. 27803. A smaller probe to ensure shadowing by the secondary reflector. A plot through the spatial peak is given in figure 6.13.

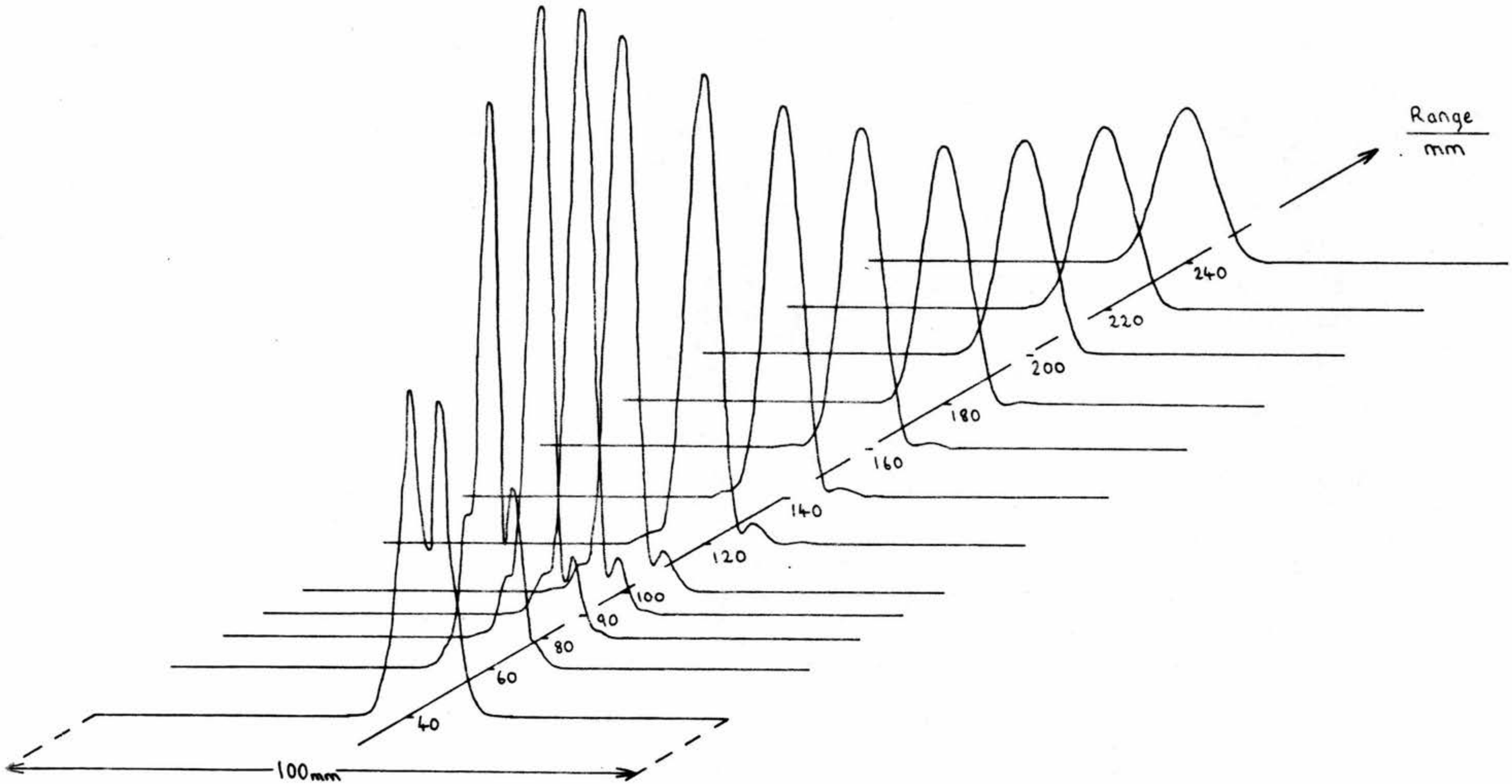

Figure 6.8. Pulse-echo plot of 12 mm diameter, 2.5MHz plane disc transducer.

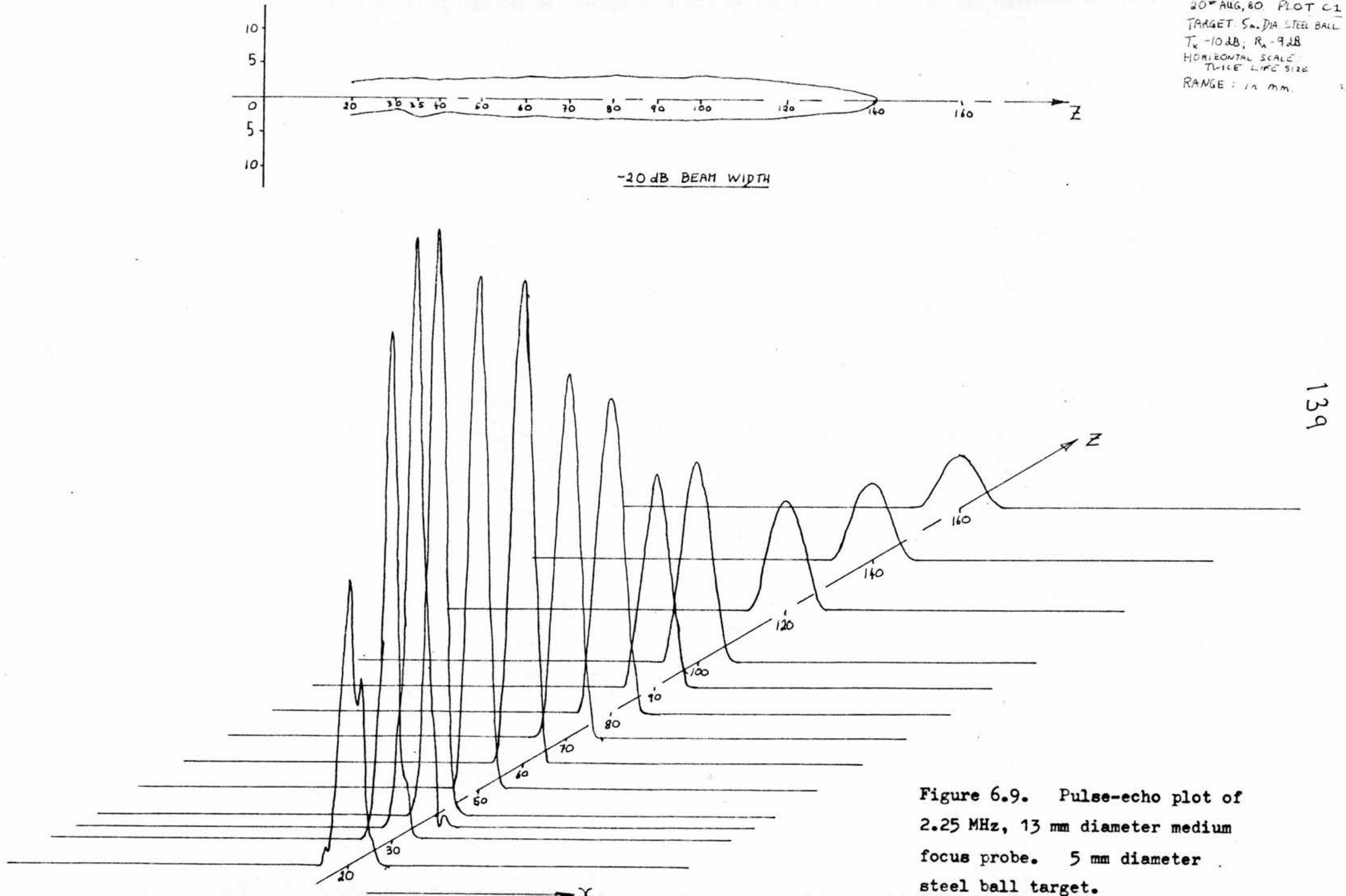

Figure 6.9. Pulse-echo plot of 2.25 MHz, 13 mm diameter medium focus probe. 5 mm diameter steel ball target.

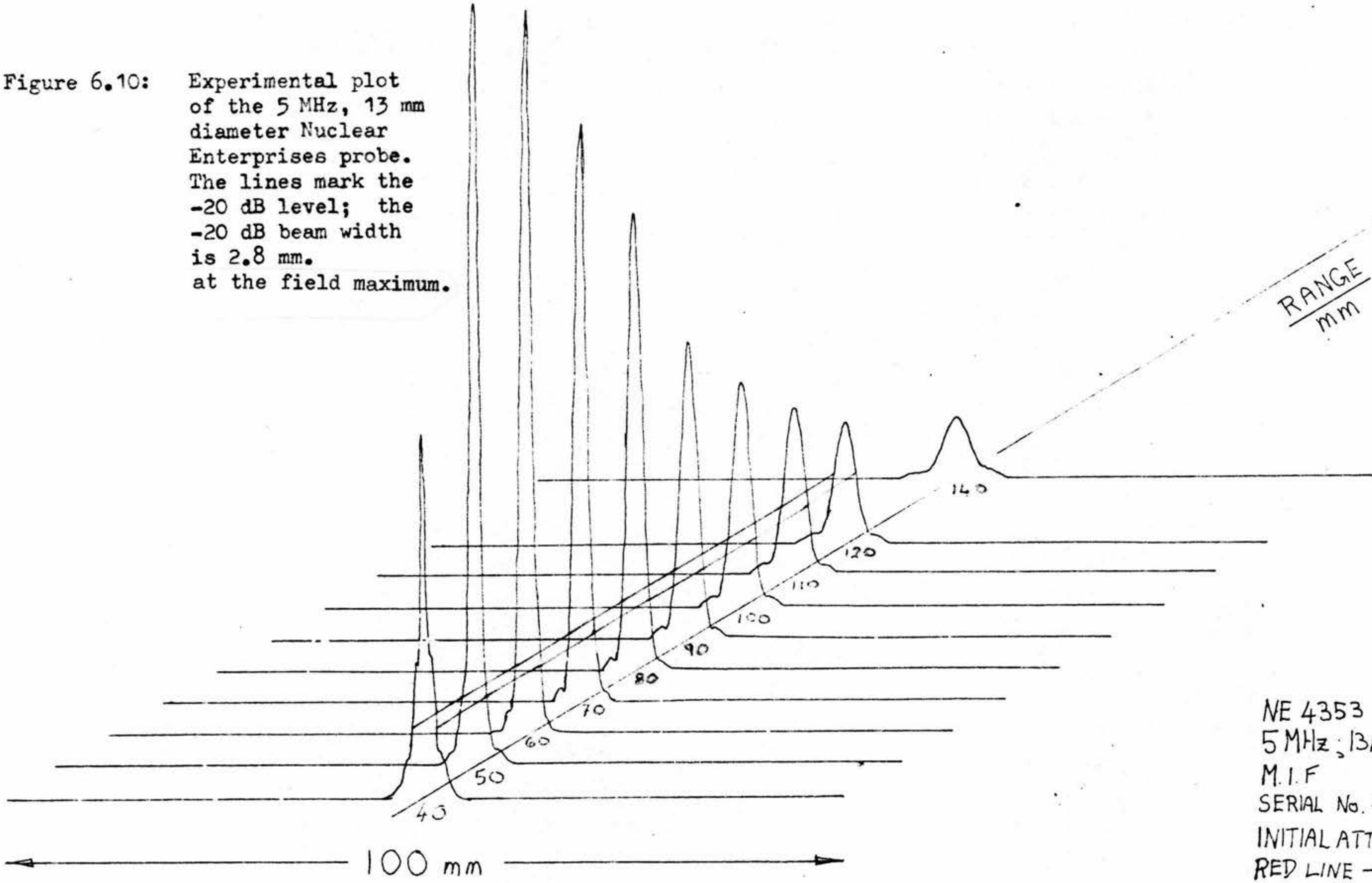

Figure 6.10: Experimental plot of the 5 MHz, 13 mm diameter Nuclear Enterprises probe. The lines mark the -20 dB level; the -20 dB beam width is 2.8 mm. at the field maximum.

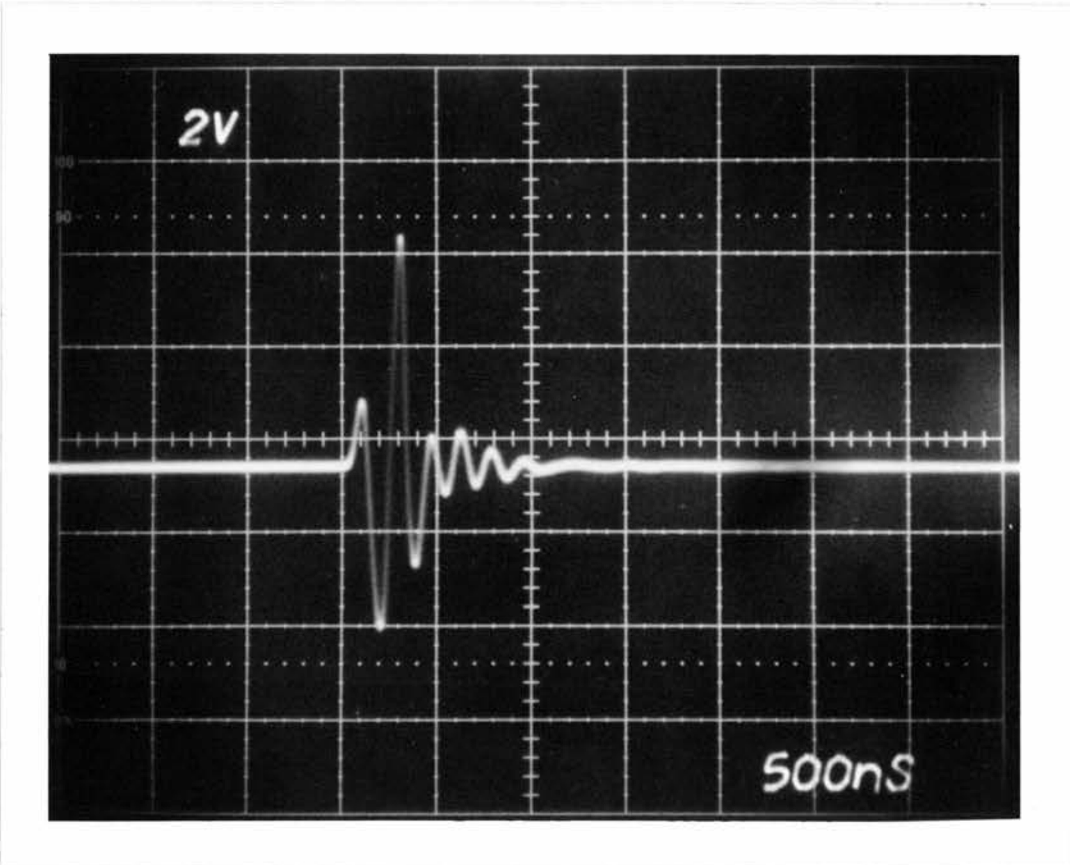

Figure 6.11: Pulse shape of the Diagnostic Sonar 5MHz, 13mm dia. transducer.

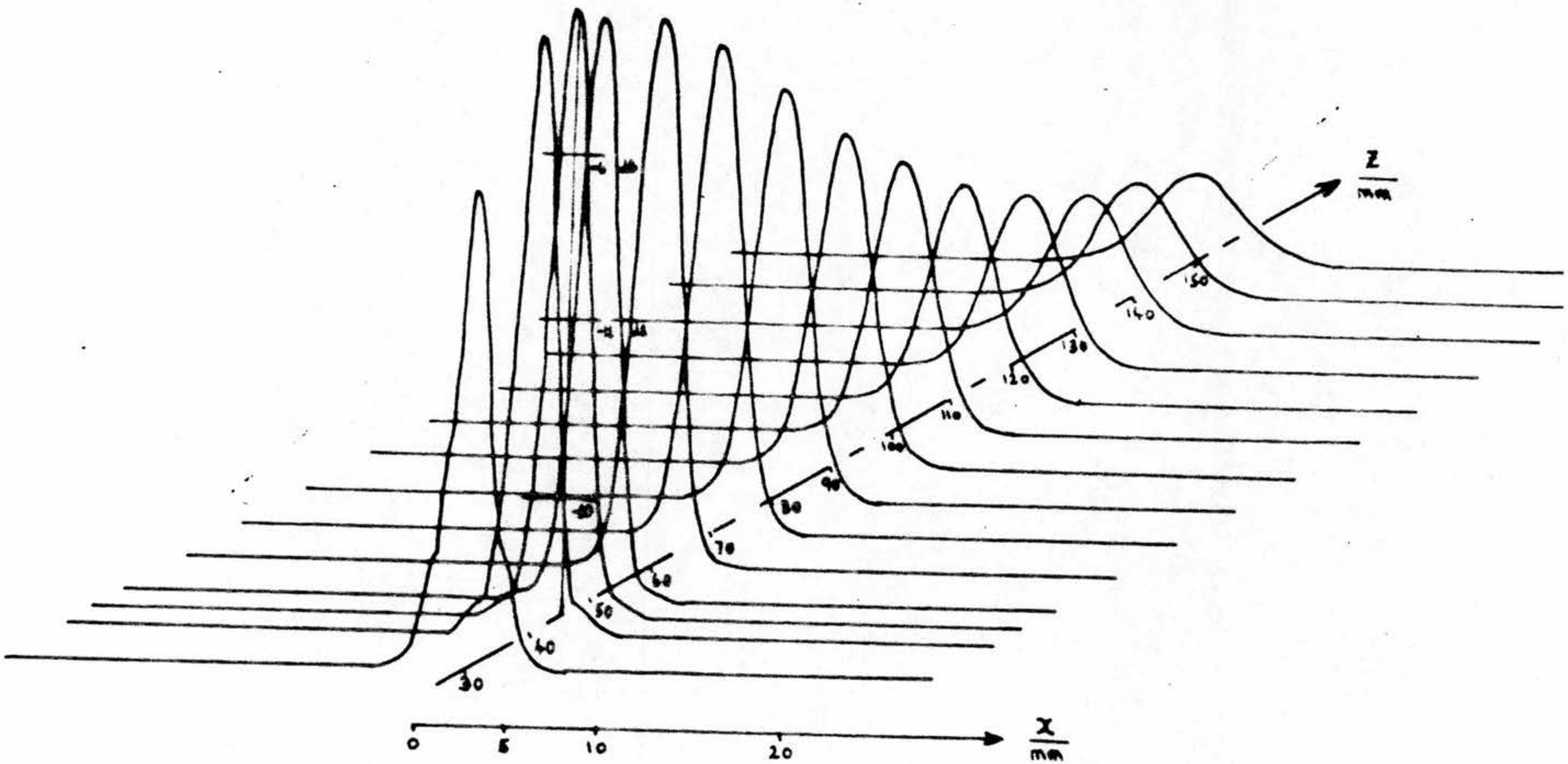

Fogire 6.12. Field due to the 5 MHz, 13 mm diameter. Diagnostic Soner MD3500 probe.
(T_x -20dB; R_x -3dB)

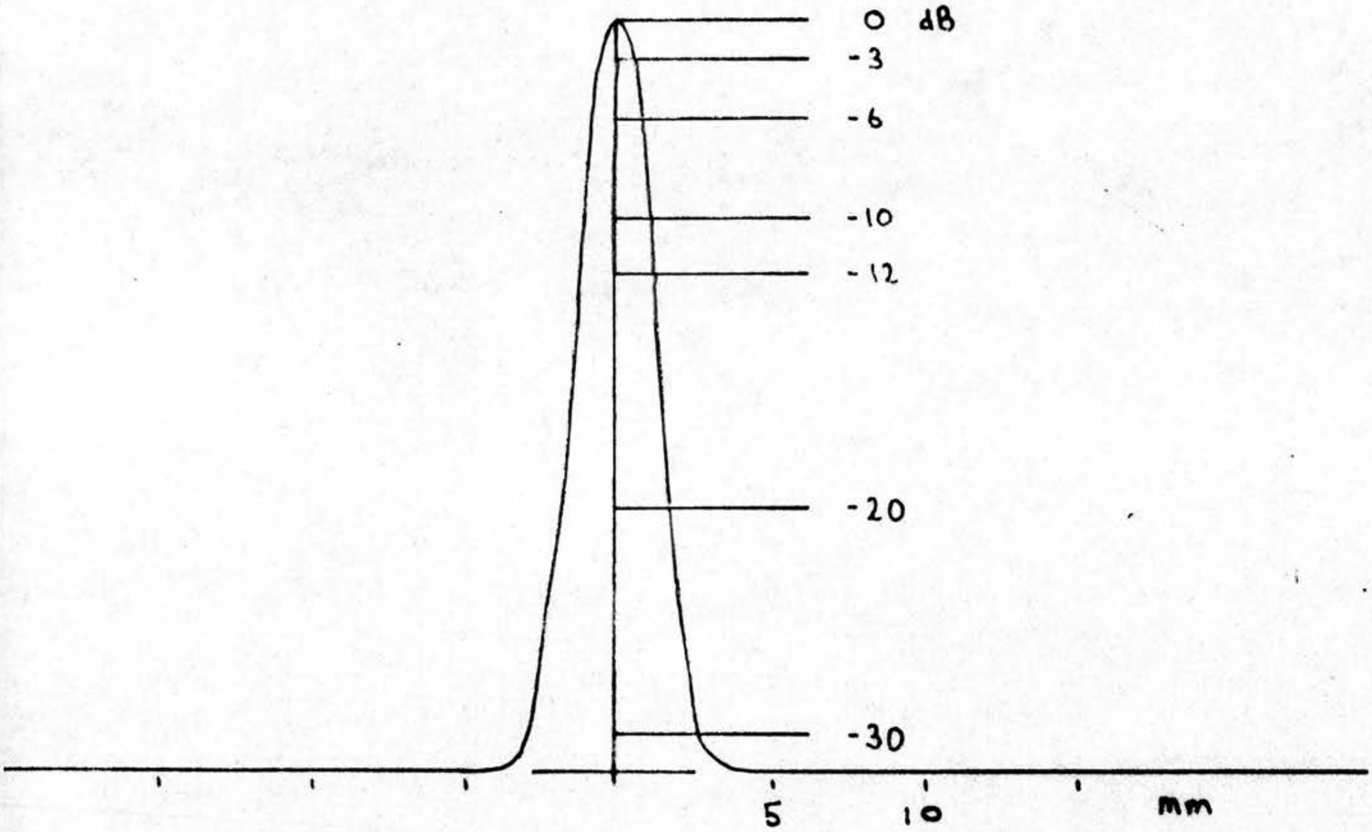

Figure 6.13: Traverse pulse:echo plot through the field maximum of 6 mm diameter 5MHz probe. Range 23 mm, 2 mm steel ball target.

6.4. Aligning Mirror System Components.

Alignment of the three mirror system components, transducer, primary and secondary, is delicate but important. Three different techniques have been employed.

The complete mirror assembly is shown in figure 6.14. In order to facilitate alignment, the hollow copper primary sits on a polymethyl-methacrylate (Perspex, trade mark of Imperial Chemical Industries Ltd.) baseplate between three equally spaced adjusting screws. These allow the position of the primary mirror to be accurately set so that its central axis coincides with that of the secondary mirror suspended in front of it. The secondary mirror is mounted by way of two sliding rods whose position is controlled by a lead screw, so that the distance of the secondary mirror from the primary can be adjusted. Although this distance has a correct theoretical value in accordance with the design calculations, in practice it was found that small variations here varied the position of the final focus F_3 without noticeable degradation of the size of the focal zone.

6.4.1. Optical Alignment

The optical technique is shown in figure 6.15. Advantage is taken of the optically reflective surface of the copper primary. The tungsten : araldite composite secondaries were silvered to make them optically reflective. A point source (pinhole) and a small lens are used to simulate the transducer. The focal spot is observed on a white card and focussed by adjusting the mirror elements.

This method was successful but time consuming. It aligned only two of the three elements. Although a good parallel beam could be produced, a focussed transducer could not be simulated well.

6.4.2. Acoustical Alignment.

This was done by attaching the mirror to the water-tank breast scanner and observing the B-scan image of a wire target as the mirror

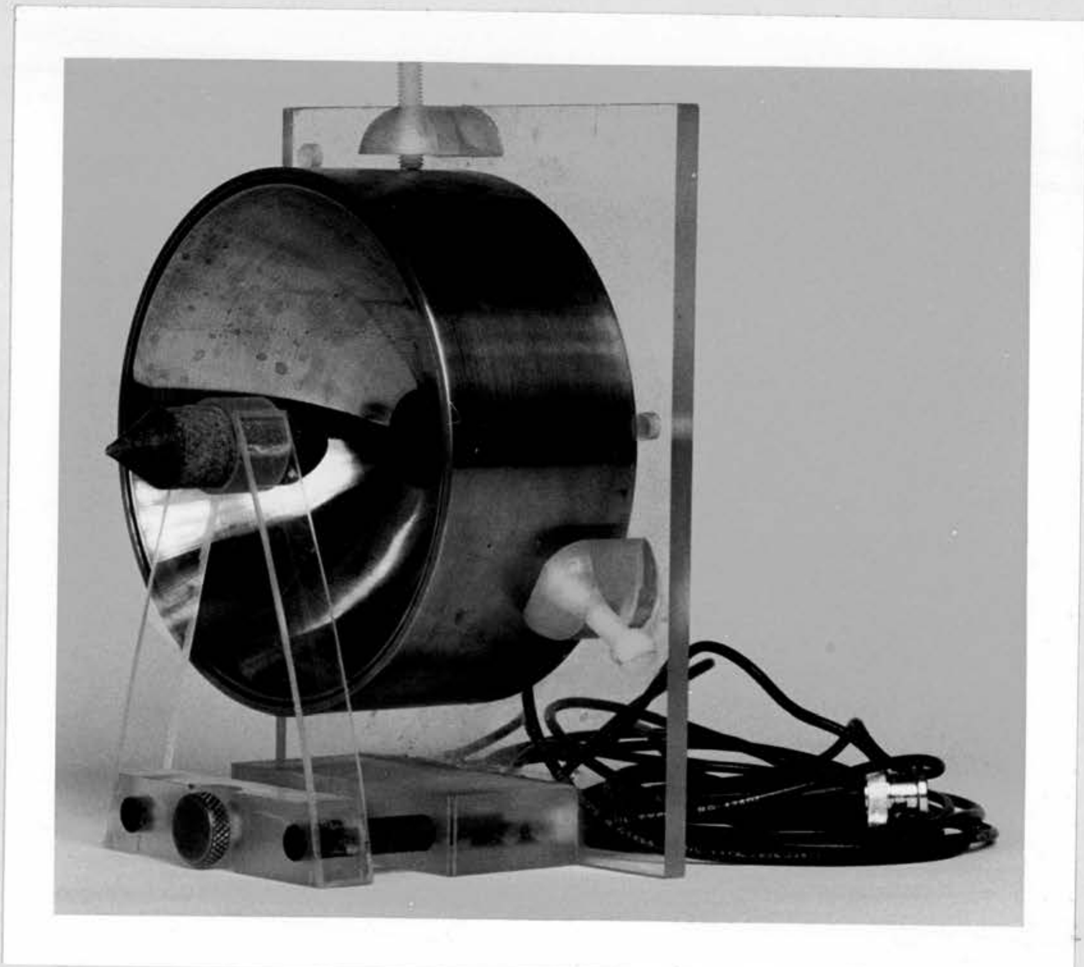

Figure 6.14: A Cassegrain mirror system in the perspex mount.

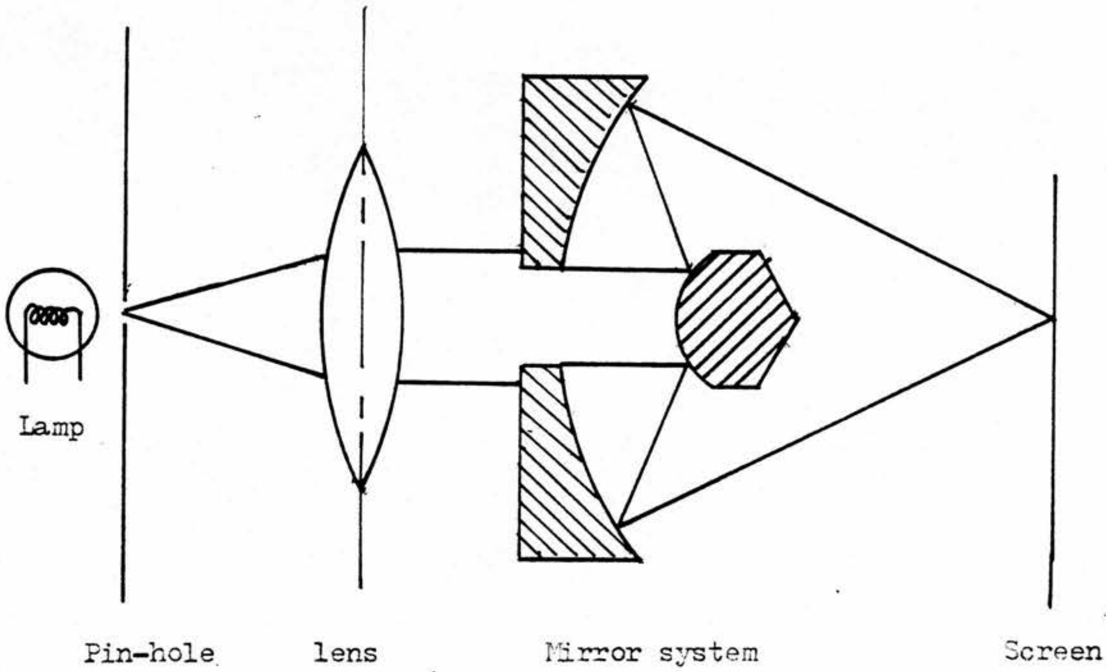

Figure 6.15: Optical alignment of mirror systems.

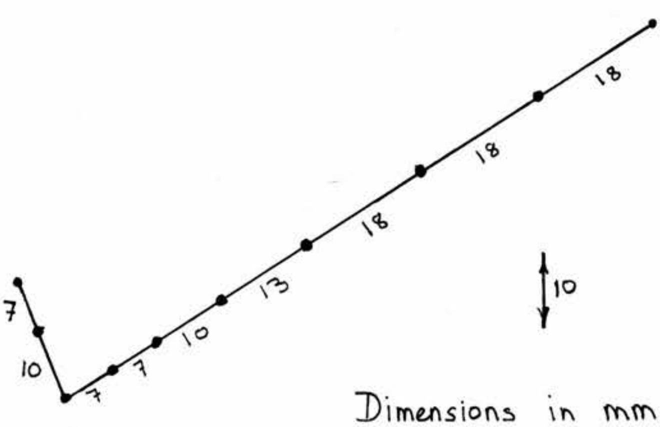

Figure 6.16(a) Wire target for ultrasonic alignment.

scanned across it. The target consists of ten 18 swg tinned copper wires arranged as shown in figure 6.16(a). The focal region is placed to cross the centre of the target and the transmitter power adjusted to give echoes from both the main and side lobes of the beam. Figure 6.16(b) shows the image obtained when the primary mirror was deliberately offset by a few millimetres; the asymmetry of the echoes from individual wires is apparent, particularly for wires not at the focal distance. By adjustment of the mounting screws, the primary mirror was moved sideways until a symmetrical response pattern as in figure 6.16(c) was obtained. The whole mirror assembly was then rotated by 90° and the procedure repeated to obtain correct alignment in the orthogonal direction.

6.4.3. Visual Alignment.

The system described in Chapter 8 proved particularly difficult to align, the pointed form of the mirrors making it particularly sensitive to axial misalignment. The point of the secondary gives a reference point and in practice it was found that visual alignment, using the graticule shown in figure 6.17, produced as good a result as the acoustical technique but very much more simply. The transducer is removed and the graticule centred in the aperture at the back of the primary. Primary and secondary are then adjusted until they appear symmetrical. The graticule is removed and transducer inserted.

(b)

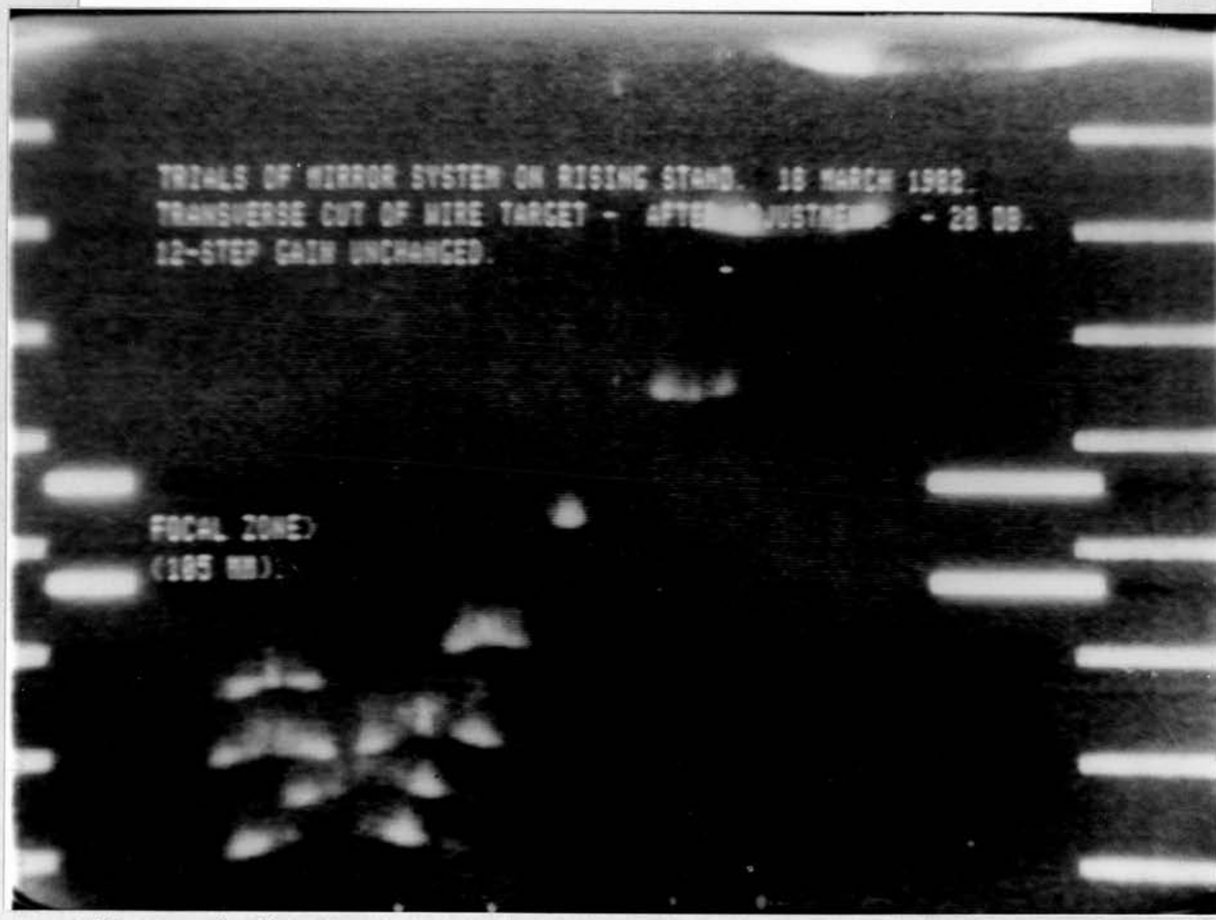

(c)

Figure 6.16: B-scan of multiple wire target by Cassegrain Mirror System.

(b) before adjustment

(c) after adjustment

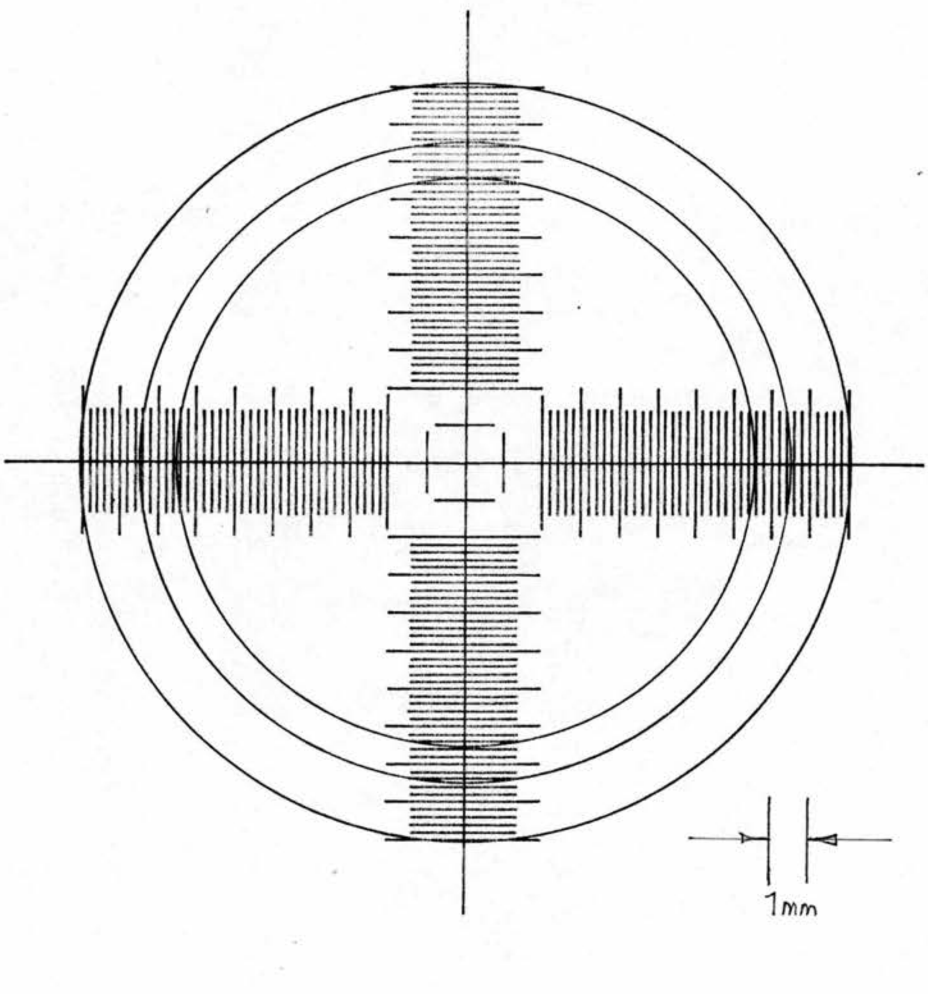

Figure 6.17. Visual alignment graticule for the modified Cassegrain mirror system.

CHAPTER 7. A CASSEGRAIN MIRROR SYSTEM.

Introduction

The first mirror system was built in the style of the traditional Cassegrain telescope. It is shown in figure 7.1. It is not a 'true' Cassegrain (as defined by Bruggemann, 1968, p.69) but is the same in concept and all but the details of the conics used. Its purpose was to explore the viability of a mirror system, to test construction materials and techniques. Thus the dimensions were chosen to see what could be built as much as to see what focus could be achieved.

7.1. Initial Design

The design is based on that of a Cassegrain telescope. It is shown in figure 7.1.

7.1.1. The Primary Reflector.

The primary surface is an ellipsoid of revolution (prolate spheroid). The aperture was chosen as the plane of the internal reference point, that is the latus rectum. The dimensions were chosen to give as large an aperture as was ever likely to be required, a diameter of 100 mm. The dimensions were also constrained to place the external reference point (the ultrasound focus) 100 mm from the transducer face (the apex of the ellipse). This completely defines an ellipse with the following properties.

Semi-latus rectum	r_k	=	50 mm
Semi-major axis	a	=	$\frac{200\text{ mm}}{3} = 66.7$ mm
Semi-minor axis	b	=	$\frac{100}{\sqrt{3}}$ mm
Eccentricity	e	=	0.5
Semi-inter focal distance	c	=	$\frac{100}{3}$ mm

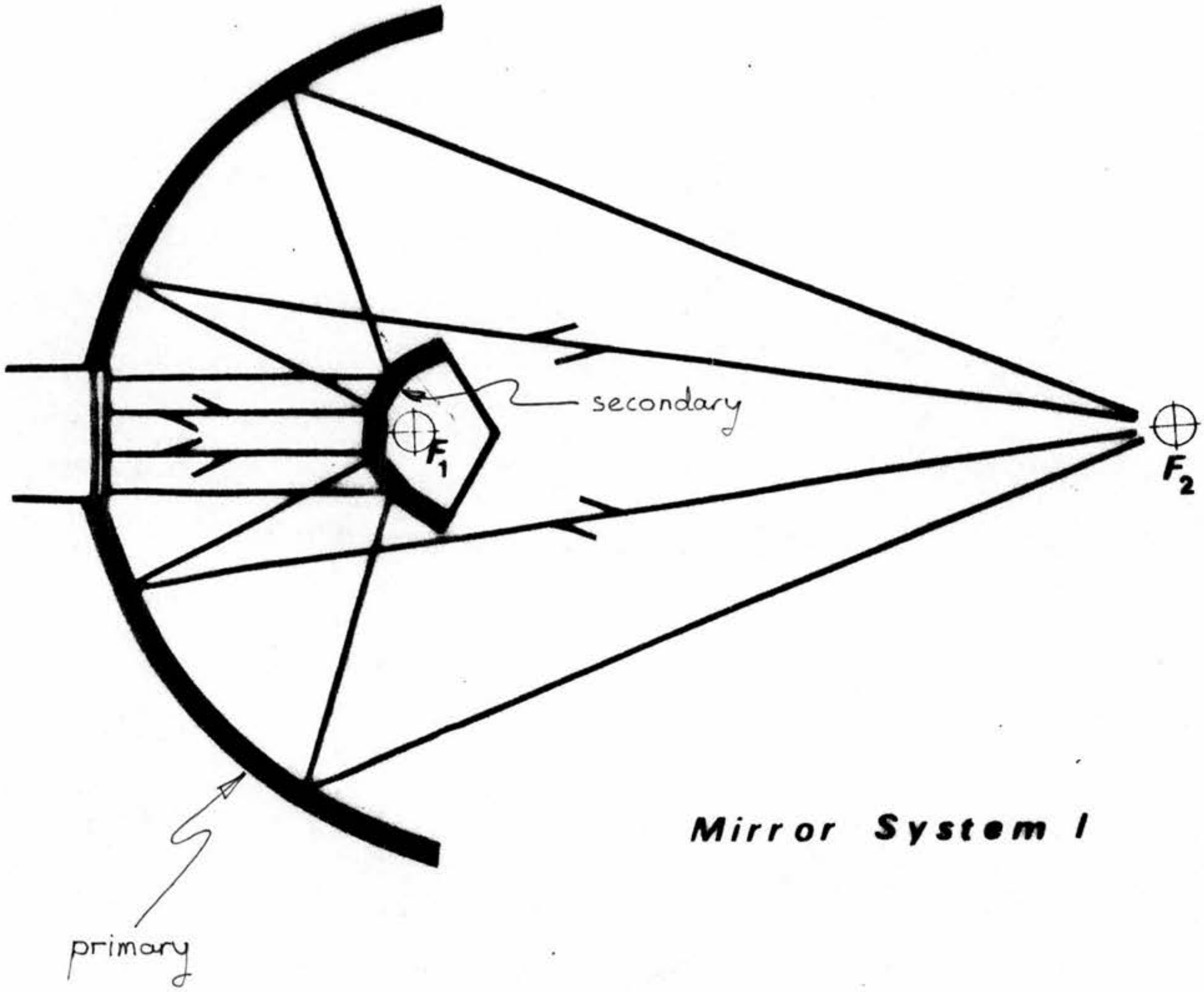

Figure 7.1(a). Cassegrain Mirror with plane disc transducer for transmission and reception.

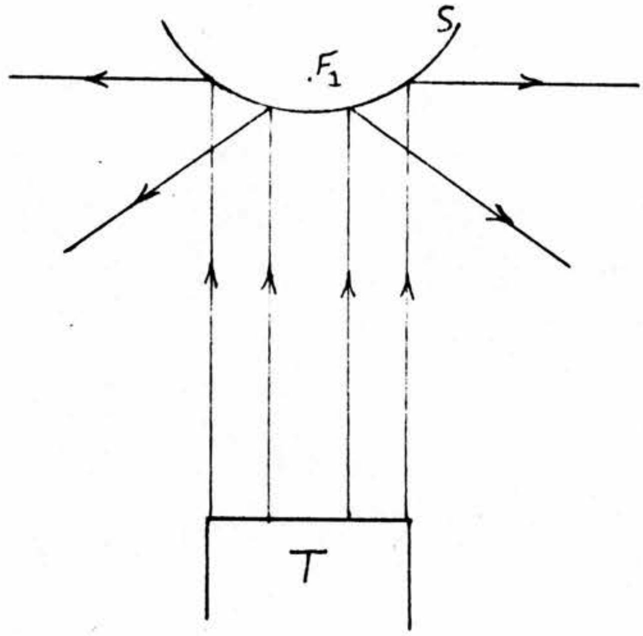

Figure 7.1(b) Paraboloidal secondary mirror with latus rectum equal to the transducer diameter.

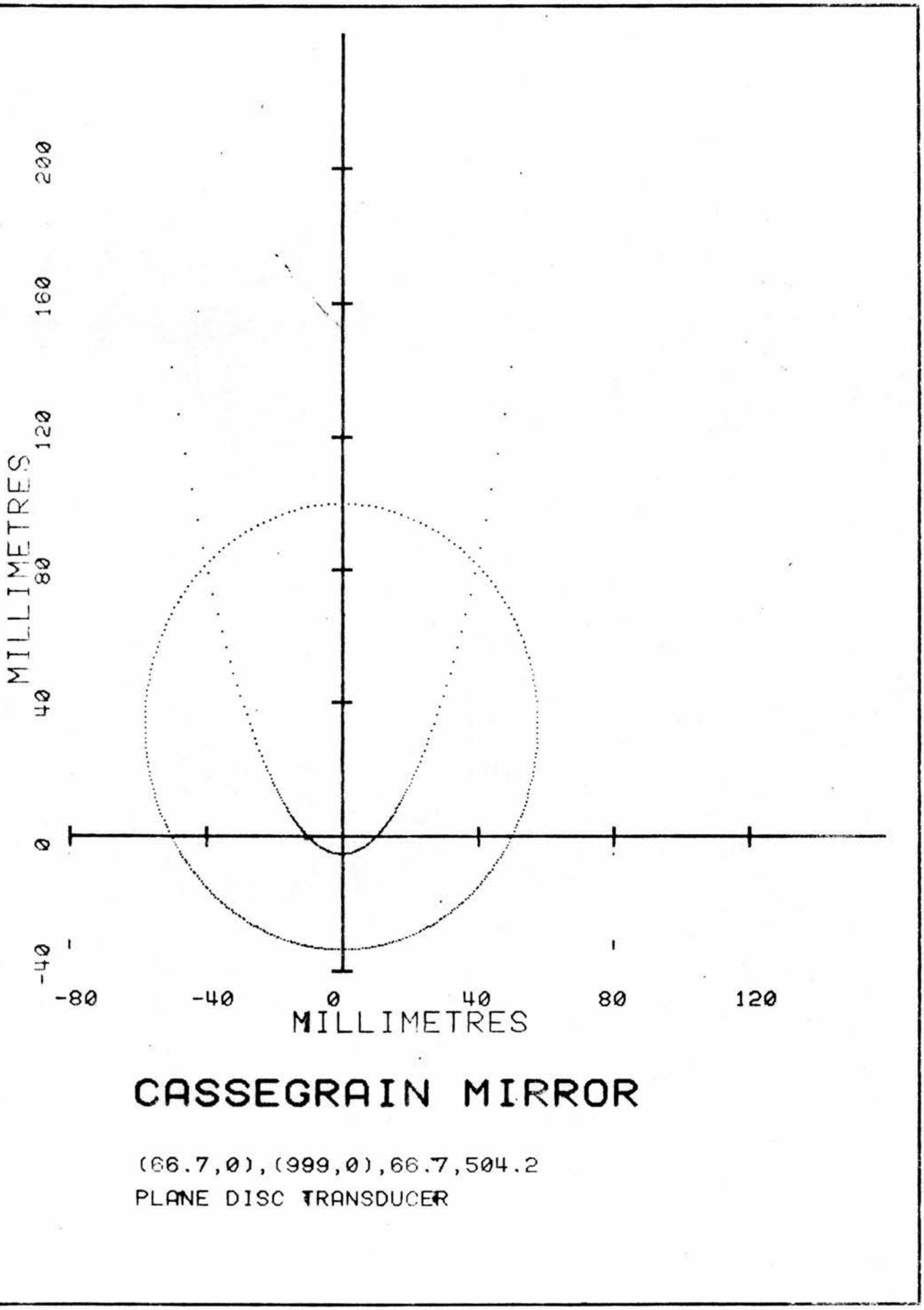

Figure 7.1(c). Design program output.

Equation: (Assuming co-ordinate origin at the centre of the ellipse).

$$\frac{9}{4} x^2 + 3y^2 = 100 \qquad - 7.1$$

The mirror surface is generated by rotating the ellipse about its major axis and that part of the surface from the apex to the first reference point used as the mirror.

The mirror will have a Numerical Aperture = 0.6. The aperture is very large compared to the wavelength.

7.1.2. The Secondary Reflector

Three possible conic surfaces may be used as the secondary mirror. All share the same internal reference point and major axis as the primary. They too are generated by rotation about that axis. The conic is chosen to match the transducer. The latus rectum must be great enough to block the entire beam; the eccentricity is chosen to spread the beam over the primary mirror. The external reference point is placed at the transducer focus. This gives a parabolic secondary for an unfocussed probe, an ellipsoid for a focussed transducer, a hyperboloid where the mirror system focusses only on reception. This defines the choice of conic and its actual dimensions. Normally a secondary will be chosen to spread the beam over all of the primary but a smaller spread may be estimated by ray tracing on the design program output.

i) A Paraboloidal Secondary. This is illustrated in figure 7.1(a). A plane disc radiator is assumed to produce plane, parallel wavefronts which strike the secondary and are spread by the paraboloid as though they diverge from its internal reference point F_1. This is also the internal reference point of the primary reflector so the wave front is focussed to F_2, its external reference point.

A parabola is chosen such that its semi-latus rectum is equal to the diameter of the beam - assumed to be the diameter of the disc. This is shown in figure 7.1(b). This will spread the beam over 2π steradian and illuminate the whole of the primary.

With co-ordinate origin at its vertex, the parabola is described by

$$y^2 = 15x$$

In these co-ordinates the reference point is at (3.5, 0) Units

ii) An Ellipsoidal Secondary. This style is shown in figure 7.2(a). Like the system described in section 7.1.2(i), it focusses on transmission and reception but the energising transducer is also focussed and therefore the secondary is ellipsoidal with the transducer focussed at its external reference point. The ray model of a small transducer is an inappropriate guide to its focus. Diffraction leads to the axial peak being well displaced from the centre of curvature of the bowl. The focus of the energising transducer is taken to be in the region of the last axial maximum i.e. at a range of about 60 mm. If the transducer is placed at the apex of the primary, this gives a value for the distance between the secondary reference points of 2c = 27 mm. The relative positions of the transducer and the secondary may be adjusted to optimise the focus. Any axial spread in the focus of the transducer at F_1 will result in spherical aberration in the virtual focus at F_2 and in turn in the final focus at the external reference point of the primary at F_3. This has been described analytically by Brueggeman, (1968).

The geometry for a 15 mm transducer (shown in figure 7.2(b)) indicates a latus rectum of 7 mm. The beam plot shown in Chapter 6, however, shows that the beam is appreciably wider at that range, giving a width of some 12 mm. Thus, an ellipse was chosen which would block that beam entirely. The conic equation may be derived from the expression:

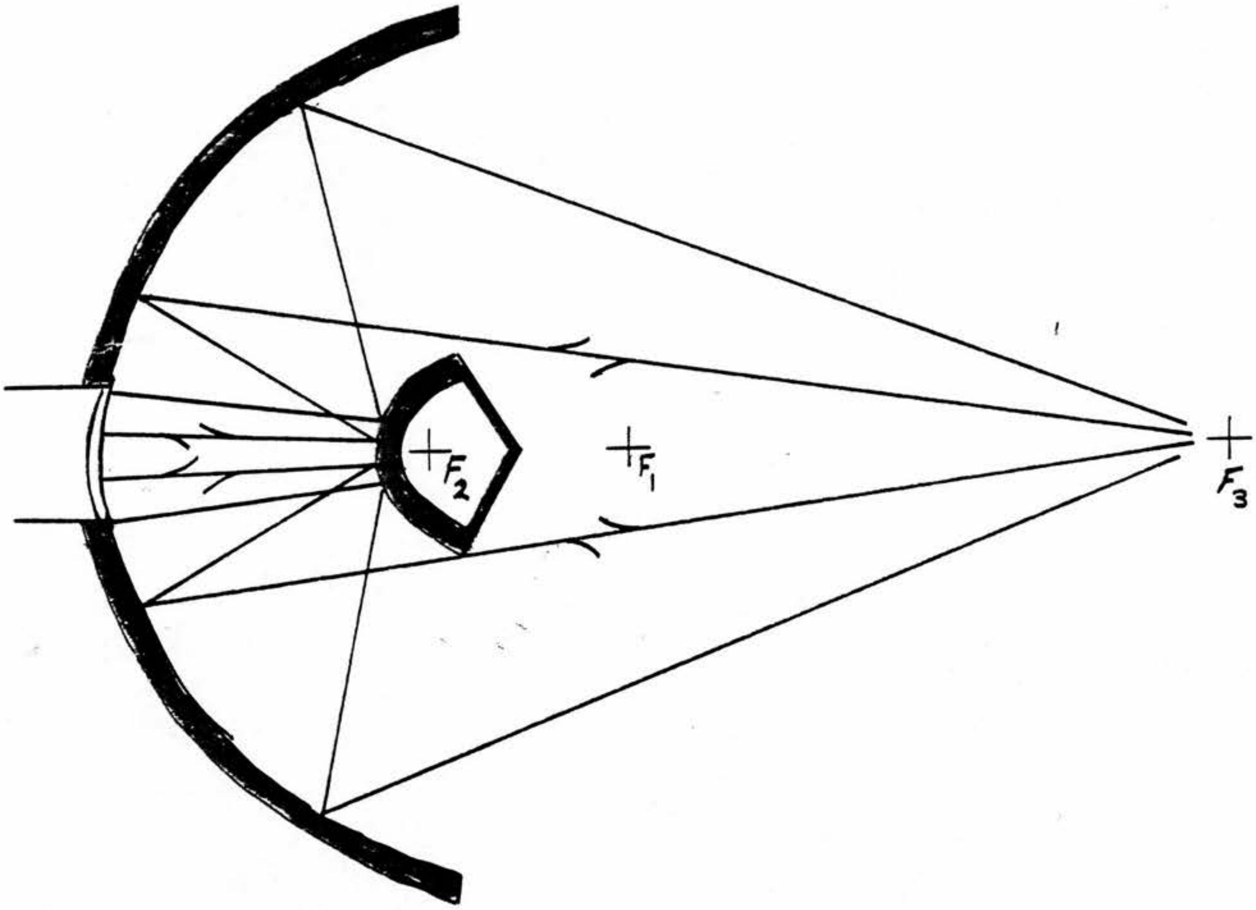

Figure 7.2(a): A Cassegrain mirror design with a focussed transducer used for transmission and reception and an ellipsoidal secondary reflector.

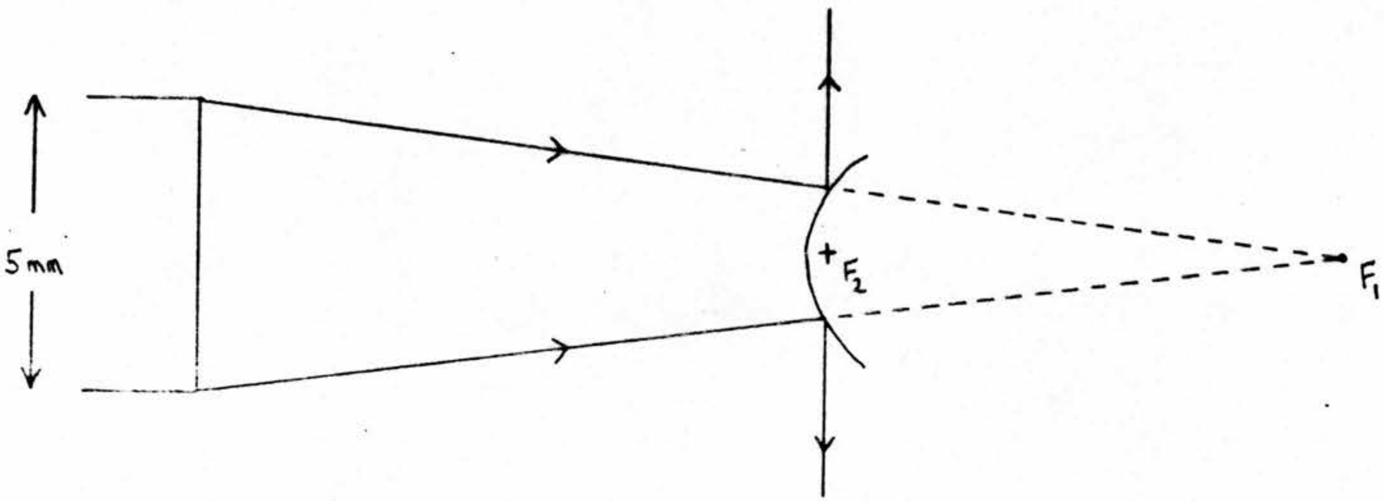

Figure 7.2(b): Cassegrain Mirrors System, ellipsoidal secondary for 15 mm focussed Transducer.

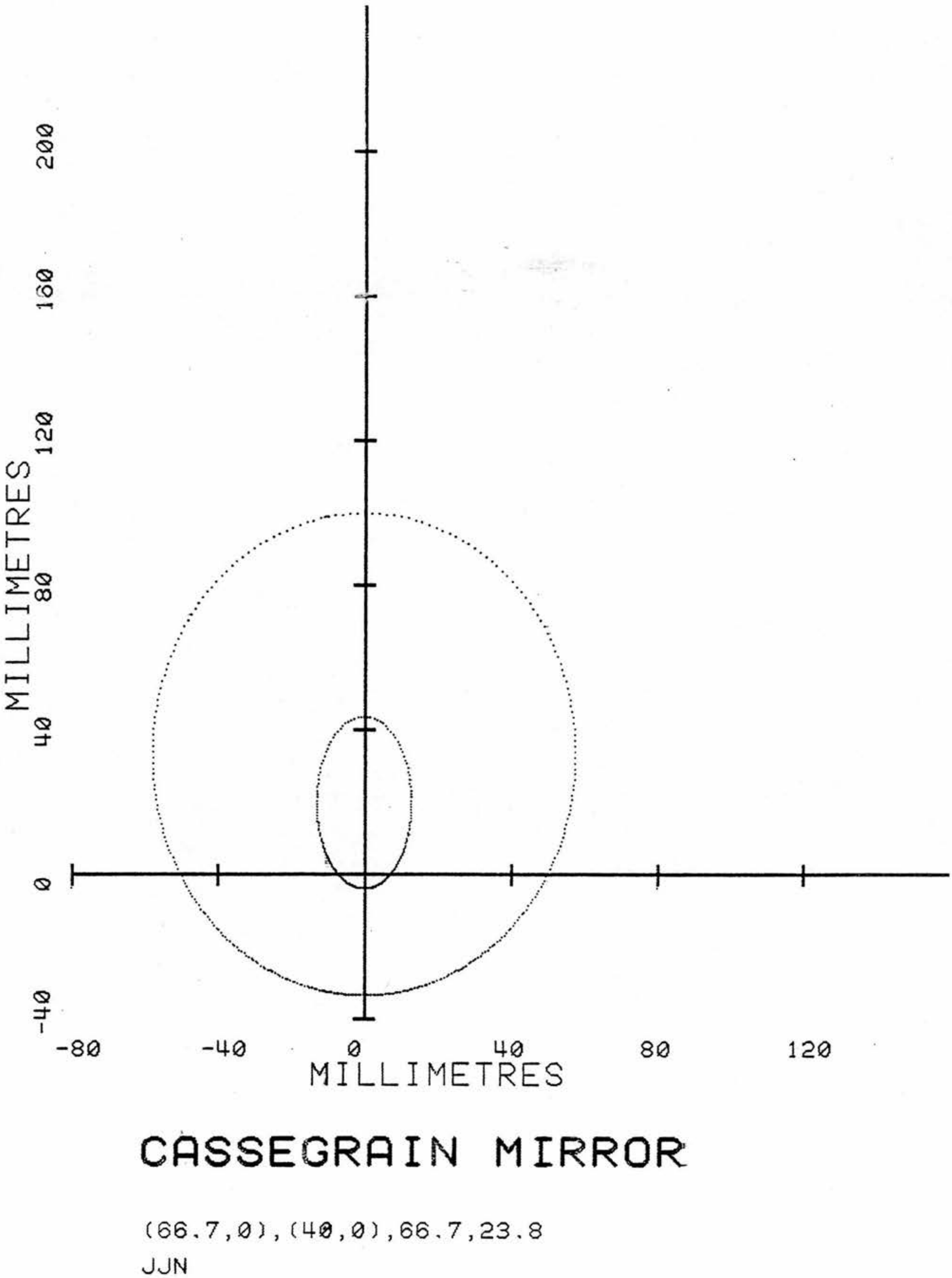

Figure 7.2(c): Design program output for the Cassegrain mirror system with an ellipsoidal secondary.

$$r_k = a(1 - e^2) \qquad - 7.3$$

where the variables are as defined in section 7.1.1. together with $c = ae$ this gives

$$a = \frac{1}{2}(r_k \pm \sqrt{r_k^2 + 4c^2}) \qquad - 7.4$$

The two solutions will yield an ellipse and a hyperbola.

In the case chosen a semi-latus rectum of 7 mm will give a semi-major axis a = 17.45 mm. The design program output is shown in figure 7.2(c)

iii). A Hyperboloidal Secondary. This is shown in figure 7.3(a). It is in the same style used by Olofsson (1963) and Fry et al (1968). The mirror focussed the received echoes only. The secondary is a hyperbola which concentrates the incoming echoes onto the receiving crystal. Its design is simpler than the other conics. The external reference point is on the face of the receiving crystal. It must be broad enough to totally occlude the receiver so that it may not pick up echoes directly. A semi-latus rectum of 10 mm is chosen, the distance between the reference points is 33.3 mm if the receiver is placed at the apex of the primary, then the semi-major axis $a = -12.4$.

7.2. Investigation of design parameters using Numerical Models.

The prospective design was investigated using the numerical models described in Chapters 3 and 4. The principal feature of interest is the effect of apodisation upon focal size. The field due to the device modelled as a spherical bowl is shown in figure 7.4; that due to a ellipsoidal mirror in figure 7.5. It should be noted that the radial scale in 7.4. is larger. The differences in the field are clearly seen. These are further investigated below. The field due to the conic mirror seem to be substantially confined to the focal plane. However, in practice, spherical aberration at the virtual focus, F_2 leading to further aberration at F_3 would spread the focus axially.

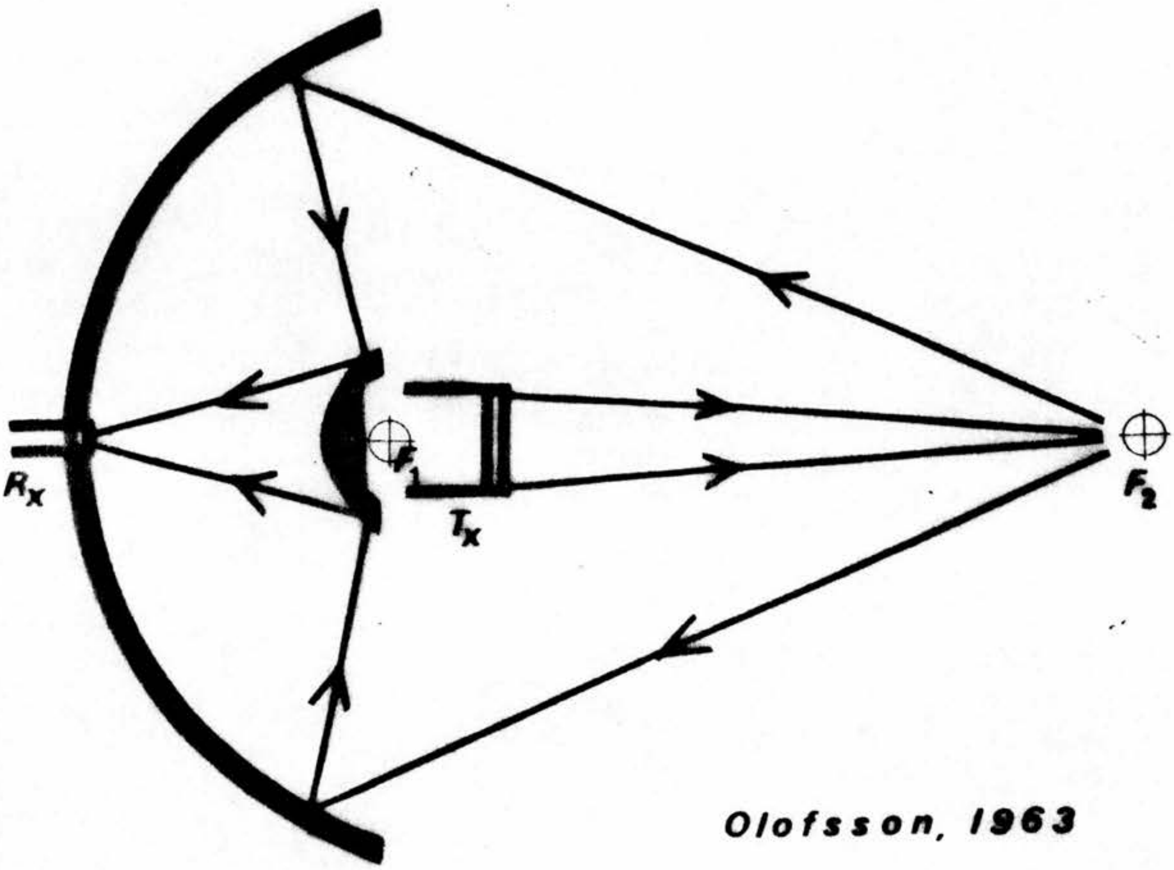

Figure 7.3(a) An Oloffson style system focussed on reception only.

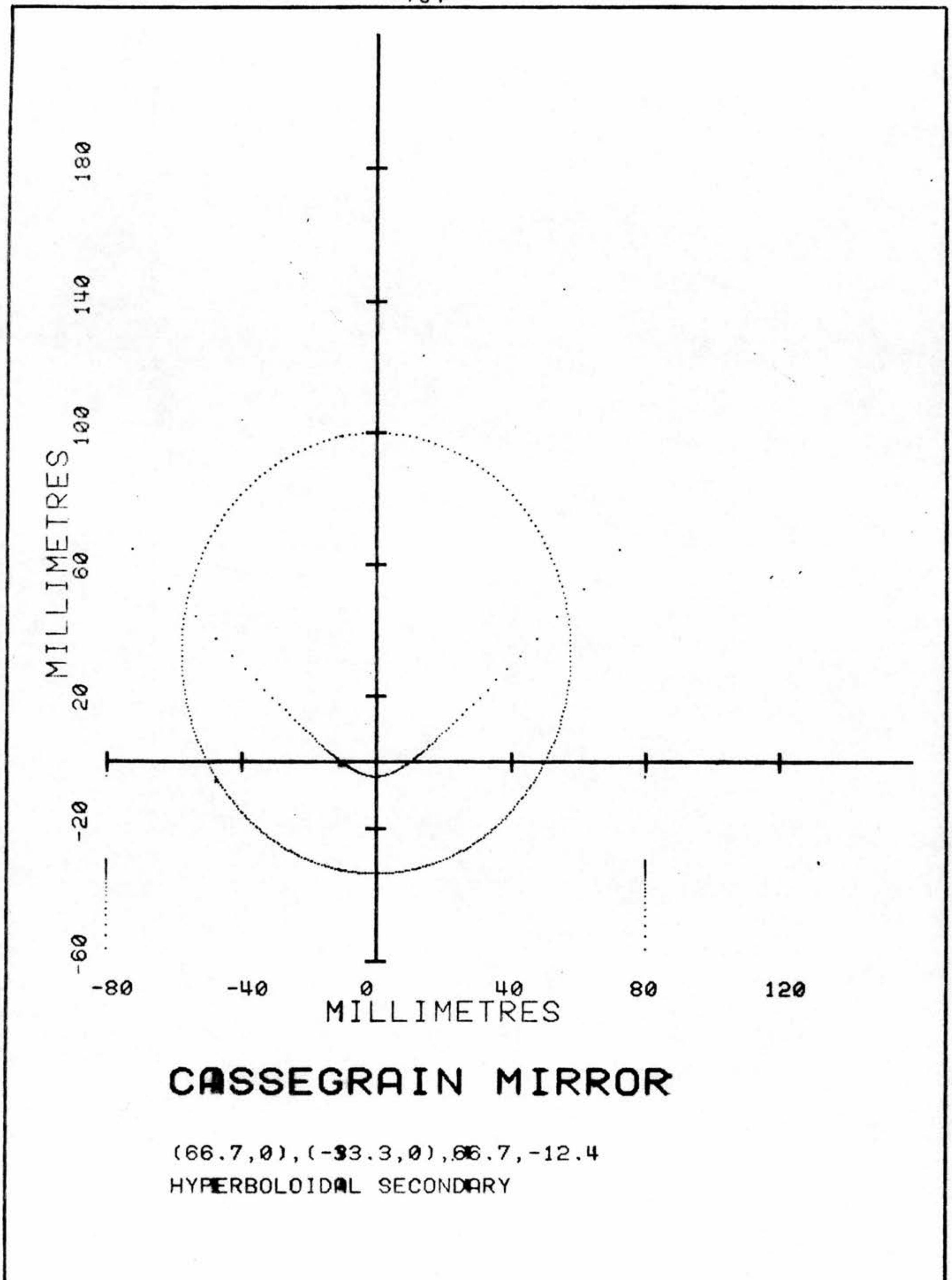

Figure 7.3(b). Design program output.

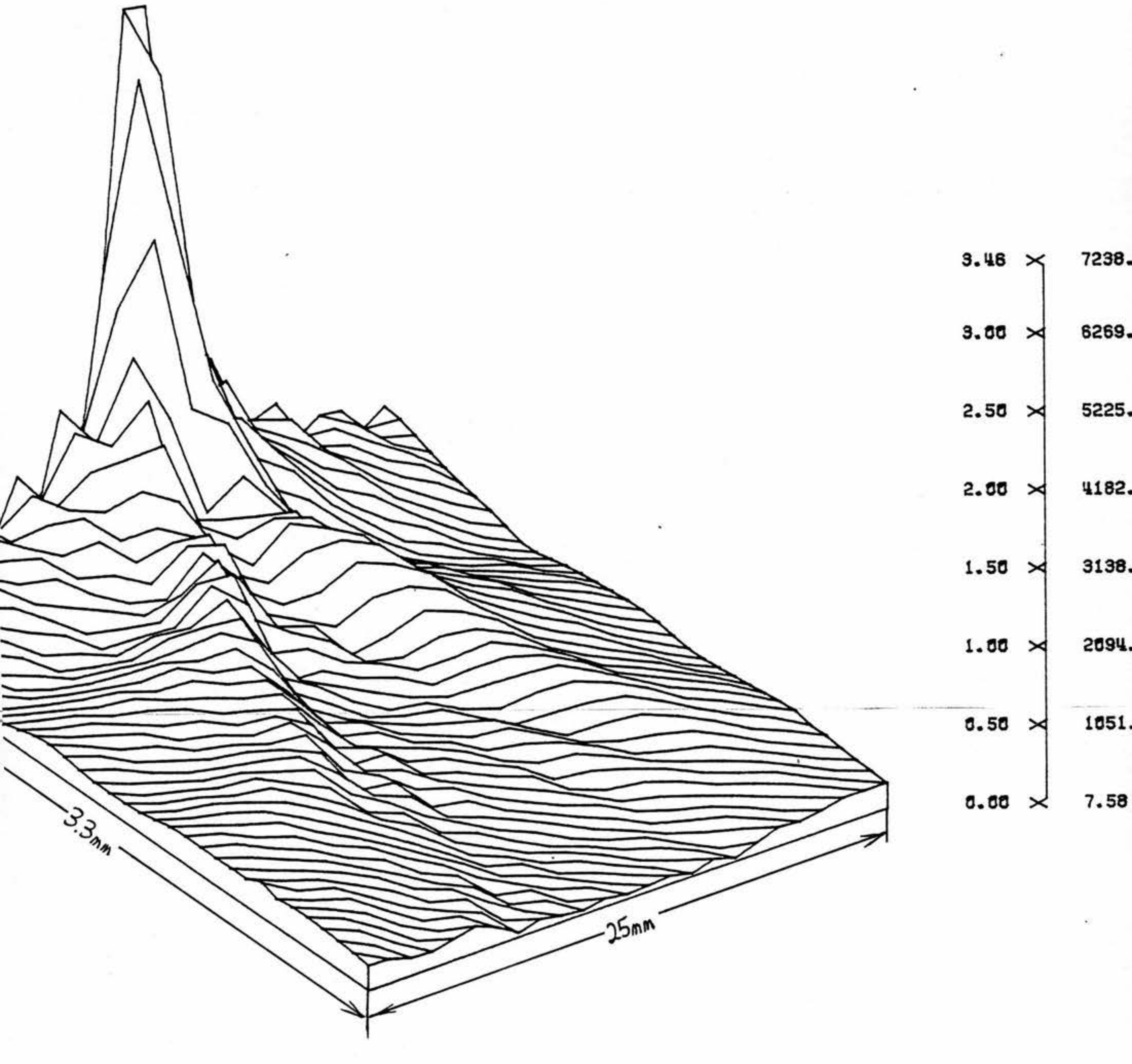

MS#1 (MIRROR2) ; AXIAL STEP 1MM, RADIAL STEP 0.1MM TO 3.3MM

igure 7.4: CW model of the Cassegrain mirror system using a spherical mirror.

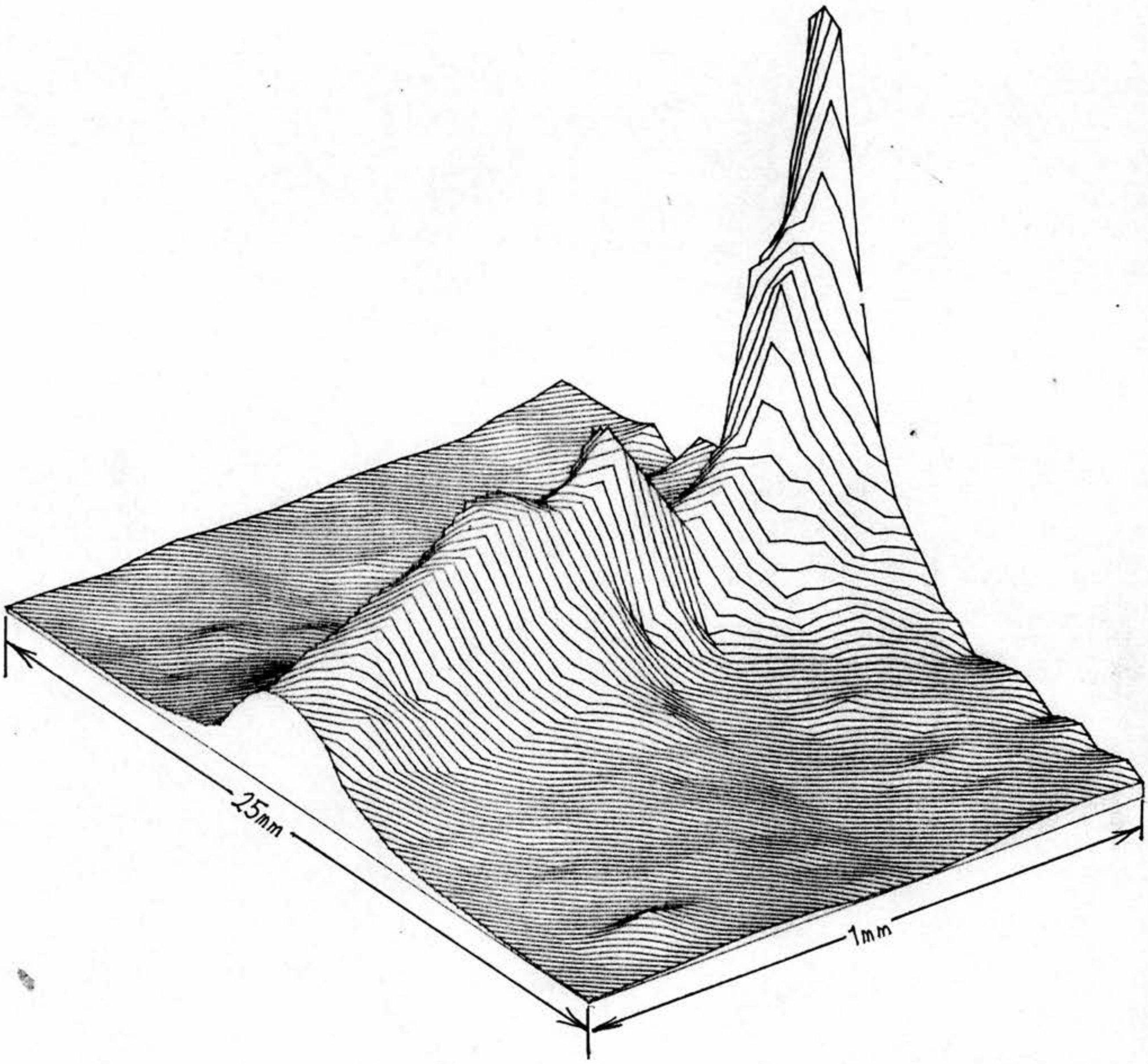

MS#1 (MIRROR4) ; FOCUSSED AT 100MM:AXIAL STEP 1MM

Figure 7.5. Cassegrain Mirror modelled as an ellipsoidal reflector

7.2.1. The Concave Bowl Model (using PLOTBCW)

A concave spherical bowl nodel of the Cassegrain Mirror was investigated for the effect of apodisation upon the beam shape. Beam size parameters are tabulated in Table 7.1 and are shown graphically in figures 7.6 and 7.7. The main lobe, particularly lower down, is narrowed slightly and the radius of the Airy disc decreases slightly. There is no detectable movement of the first off-axis maximum if the apodisation $\leqslant$ 25 mm diameter. The only appreciable effect is upon the height of the first off-axis maximum which increases steadily at 0.175 $dB.mm^{-1}$ for apodising discs in the range 10 to 40 mm diameter.

The effect of varying the outer diameter of the aperture while keeping the apodising disc 20 mm diameter is shown in figure 7.8. This is quantified in Table 7.2 and shown graphically in figure 7.9. All the beam width parameters decrease although the effect is less marked for the larger apertures. The amplitude of the sidelobes also decreases steadily. This may be attributed to the decrease in relative size of the apodising disc.

7.2.2. The Ellipsoidal Mirror Model (using PLOTCW)

The Cassegrain system was modelled using the function Mirror 4 (described is section 4.2.2) to describe the mirror surface.

The field calculated was greatly different from that predicted by the spherical mirror model. This has been shown qualitatively in figures 7.4 and 7.5.

The effect of variation in the size of the disc apodising a 100 mm diameter aperture upon the width of the main lobe width and upon the amplitude of the first off-axis maximum is given quantitatively in Table 7.3 and graphically in figures 7.10 and 7.11. The main peak described by this model is substantially narrower than that predicted by the spherical bowl model. It responds similarly to blocking the centre of the aperture showing a slight but not significant narrowing. The predicted effect on the first off-axis maximum is also similar. This peak however is some 5.6 dB larger for the full aperture but apodisation causes it to increase at a slower rate, 0.07 dB, mm^{-1}

Diameter of Apodising disc. mm	Main lobe half-width mm				1st off-axis maximum	
	-3dB level	-5dB level	-6dB level	1st off-axis minimum	radius mm	height dB
0	0.153	0.193	0.212	0.361	0.49	-17.0
10	0.153	0.193	0.210	0.360	0.49	-16.4
20	0.151	0.190	0.206	0.350	0.49	-14.9
25	0.149	0.188	0.204	0.340	0.49	-14.0
30	0.147	0.186	0.200	0.336	0.48	-13.1
40	0.143	0.180	0.194	0.320	0.475	-11.4

Table 7.1. Effect of apodisation upon the spherical bowl model of the Cassegrain Mirror System.

Outer diameter = 100 mm

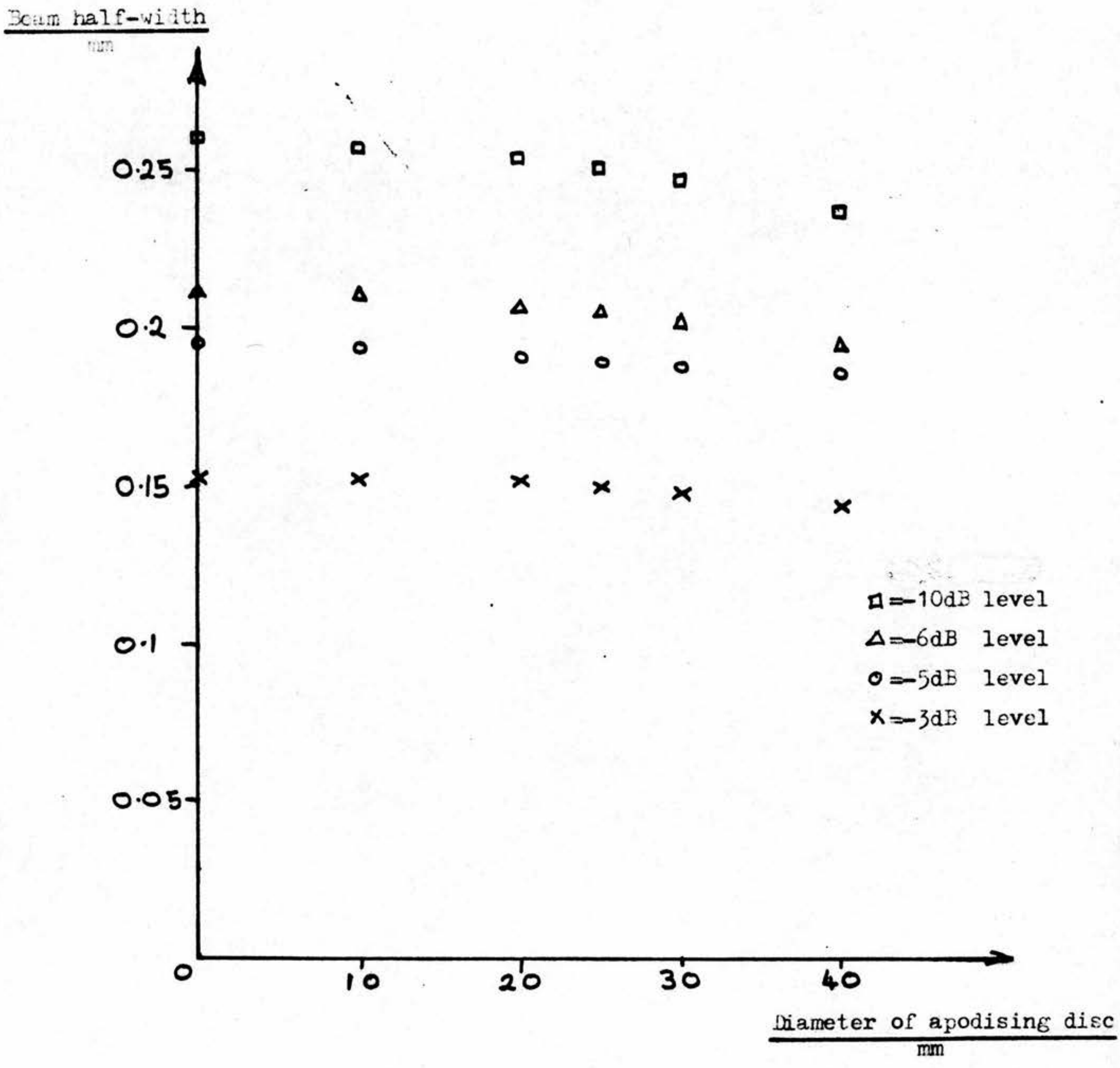

Figure 7.6: Effect of apodisation on the spherical bowl model of the Cassegrain mirror system.

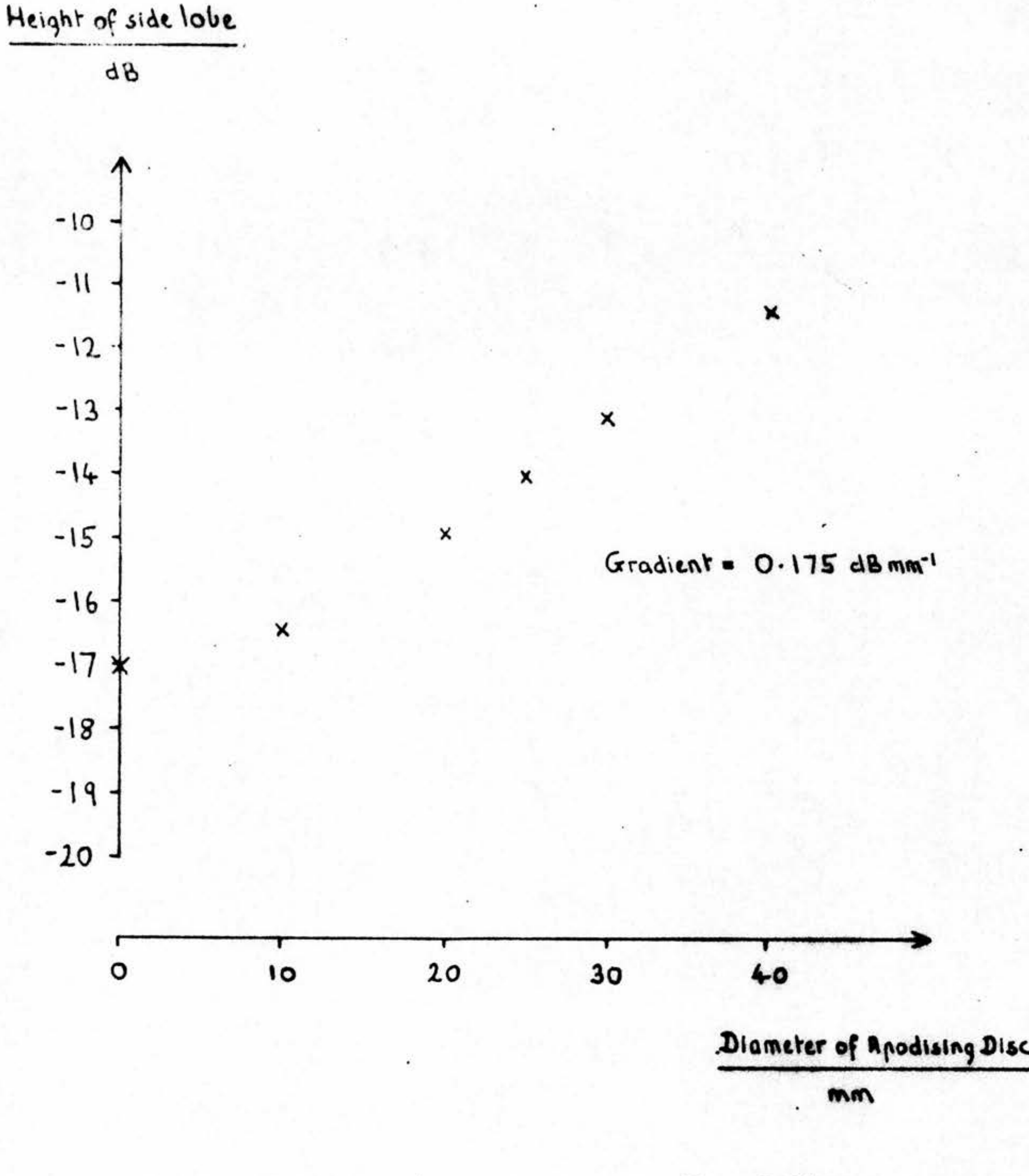

Figure 7.7: Effect of apodisation upon the relative height of the first off-axis maximum using a spherical bowl model of the Cassegrain Mirror System.

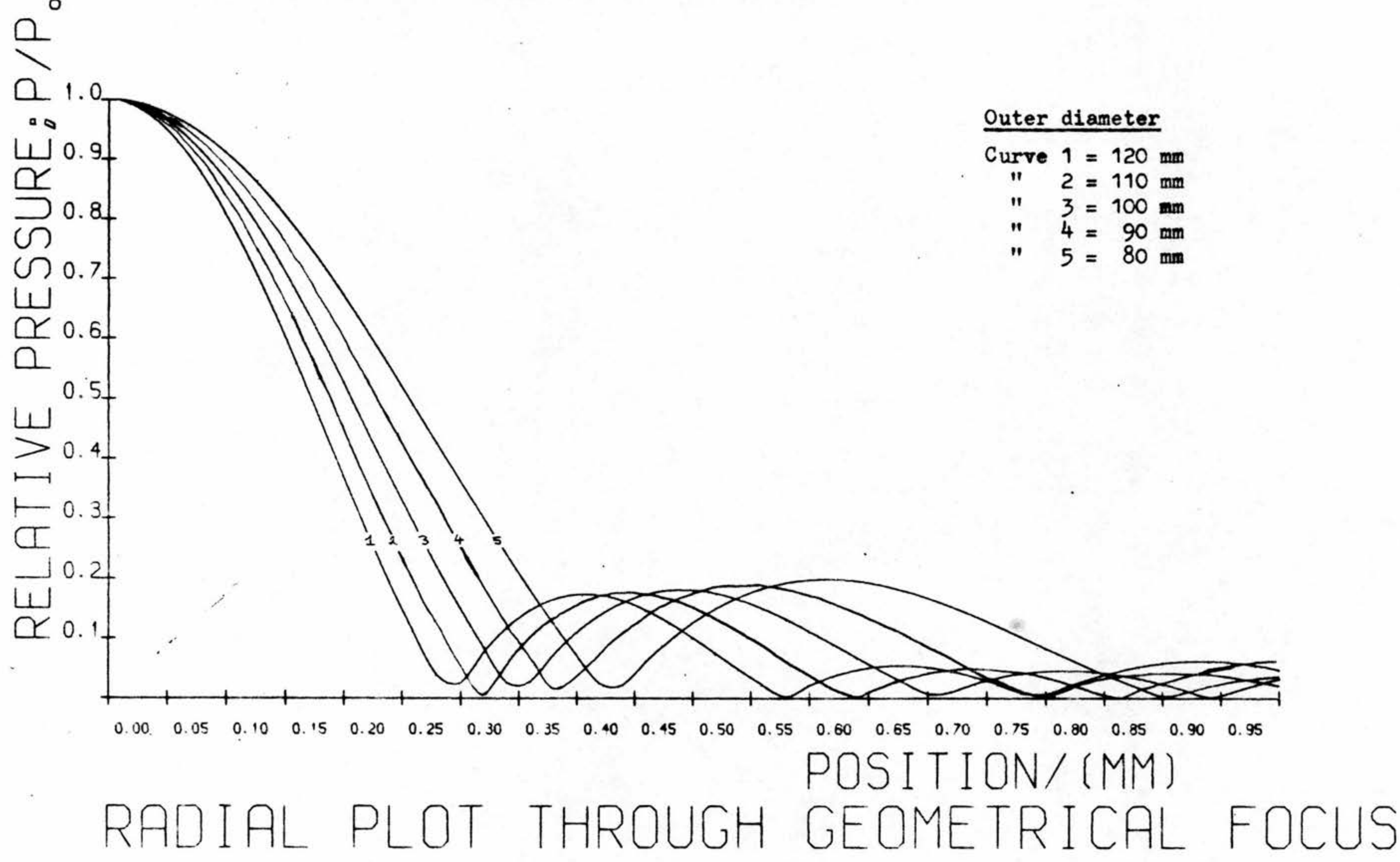

Figure 7.8. Effect of increasing the outer diameter upon the spherical bowl model of the Cassegrain Mirror.

Outer Diameter mm	Main Lobe half-width mm					1st off-axis maximum	
	-3dB level	-5dB level	-6dB level	-10dB level	1st off-axis minimum	radius mm	height dB
80	0.187	0.236	0.256	0.314	0.42	0.615	-14.0
90	0.167	0.221	0.228	0.281	0.38	0.54	-14.5
100	0.151	0.190	0.206	0.254	0.35	0.49	-14.9
110	0.137	0.173	0.187	0.231	0.31	0.44	-15.1
120	0.125	0.159	0.172	0.211	0.305	0.41	-15.2

Table 7.2. Effect of outer-diameter upon the spherical bowl model of the Cassegrain Mirror System (apodising disc of 20 mm diameter)

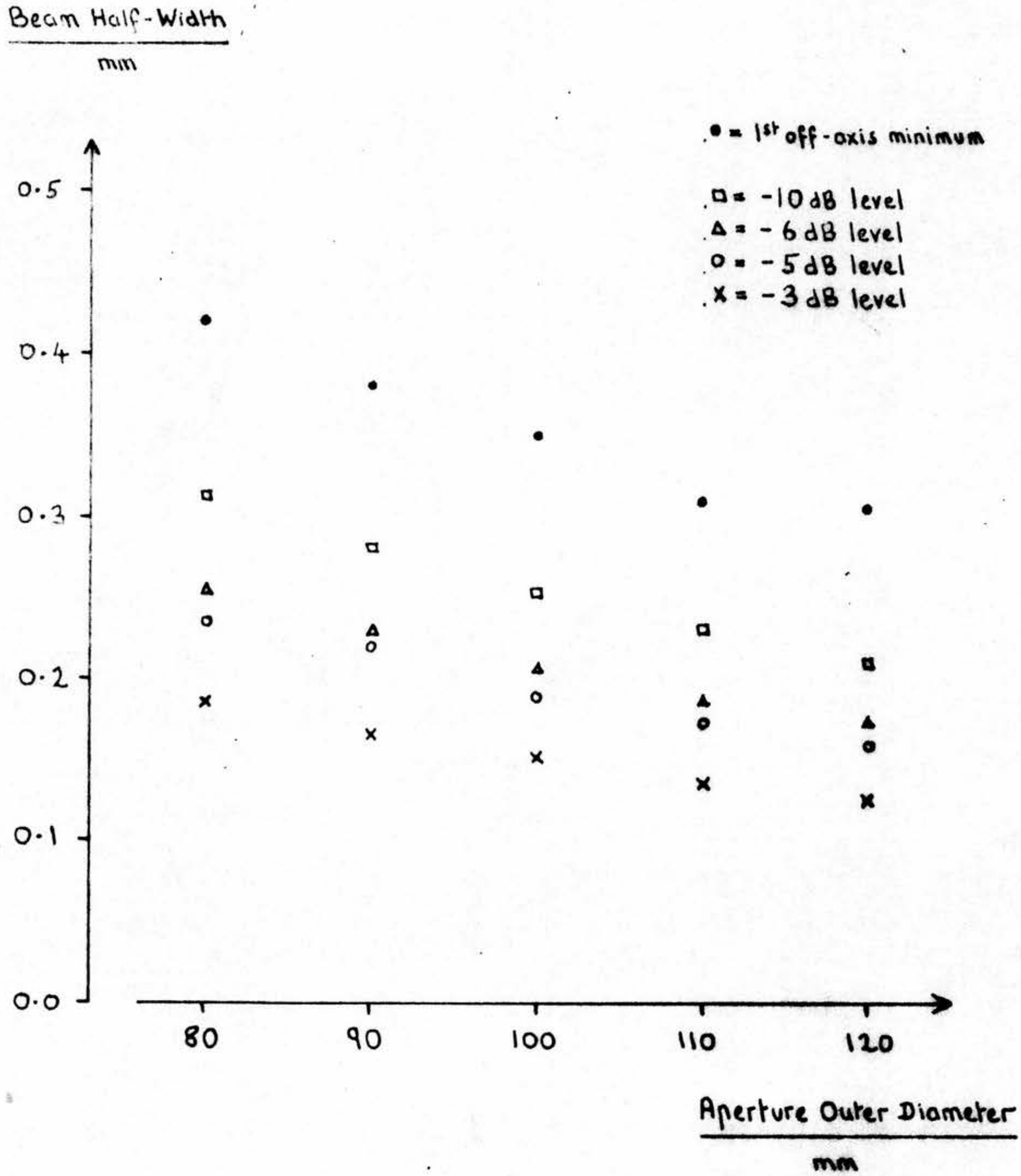

Figure 7.9: Effect of increasing the aperture upon the spherical bowl model of the Cassegrain Mirror System (Apodising disc 20 mm diameter).

Diameter of Apodising Disc mm	Main lobe half-width mm					1st off-axis maximum	
	-3dB level	-5dB level	-6dB level	-10dB level	1st off-axis minimum	radius mm	height dB
0	0.0622	0.0785	0.0843	0.103	0.14	0.22	-11.4
10	0.062	0.078	0.084	0.102	0.14	0.205	-10.9
20	0.0615	0.0773	0.0832	0.101	0.14	0.20	-10.3
25	0.0612	0.0766	0.0827	0.101	0.14	0.20	-9.9
30	0.061	0.076	0.082	0.100	0.14	0.20	-9.6
40	0.060	0.0742	0.0808	0.098	0.13	0.205	-8.9

Table 7.3. Effect of apodisation upon the elliptical mirror model of the Cassegrain Mirror System.

Outer diameter = 100 mm

Diameter of Apodising disc mm	-10dB Beam half-width mm	2nd off-axis peak Amplitude dB
0	0.103	-15.1
10	0.102	-15.3
20	0.101	-15.5
25	0.218	-15.4
30	0.221	-15.0
40	0.227	-13.7

Table 7.3A. Beam width and 2nd off-axis peak of the ellipsoidal mirror model. outer diameter = 100 mm

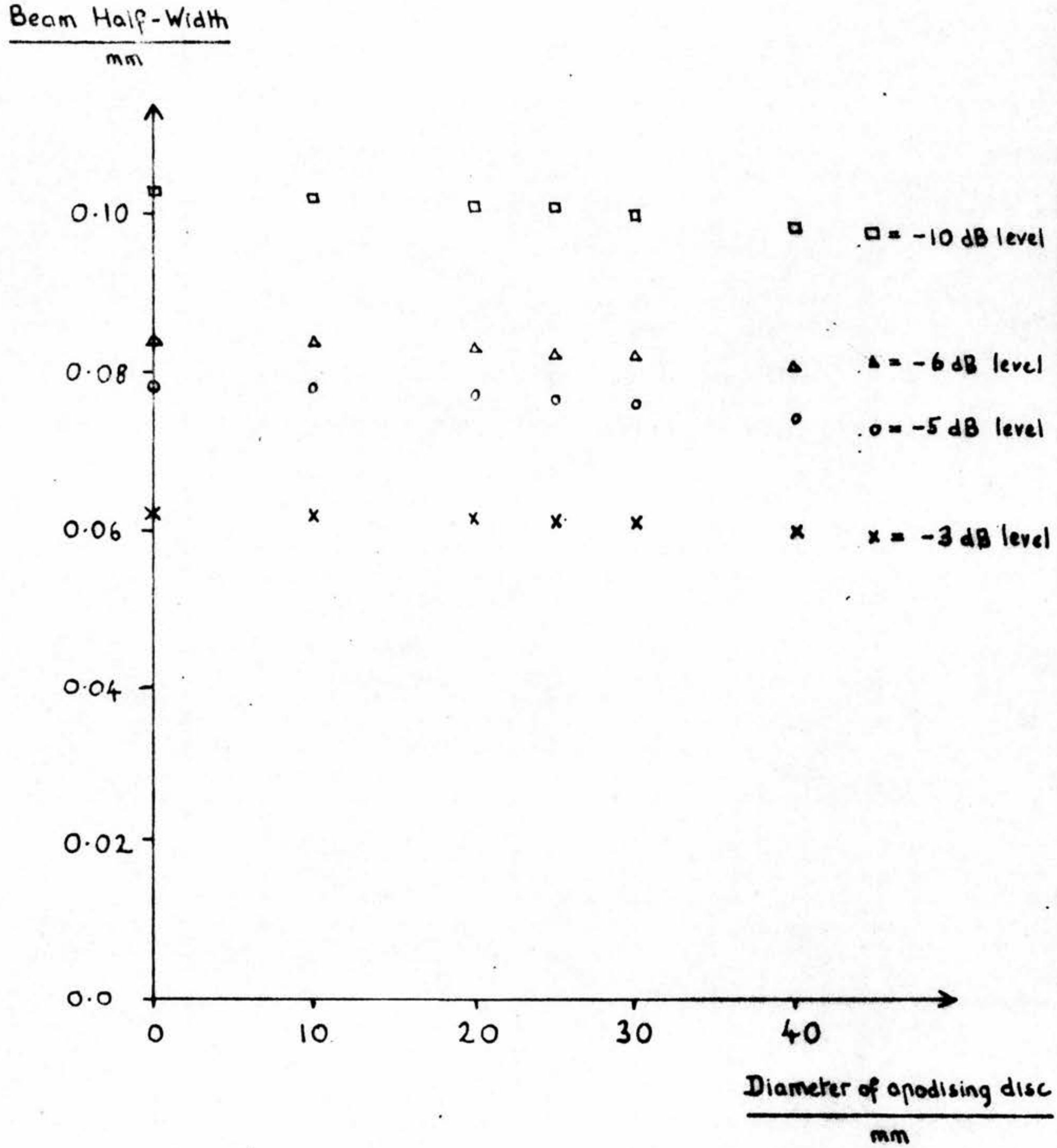

Figure 7.10: Effect of apodisation upon beam width using an ellipsoidal mirror model of the Cassegrain Mirror System.

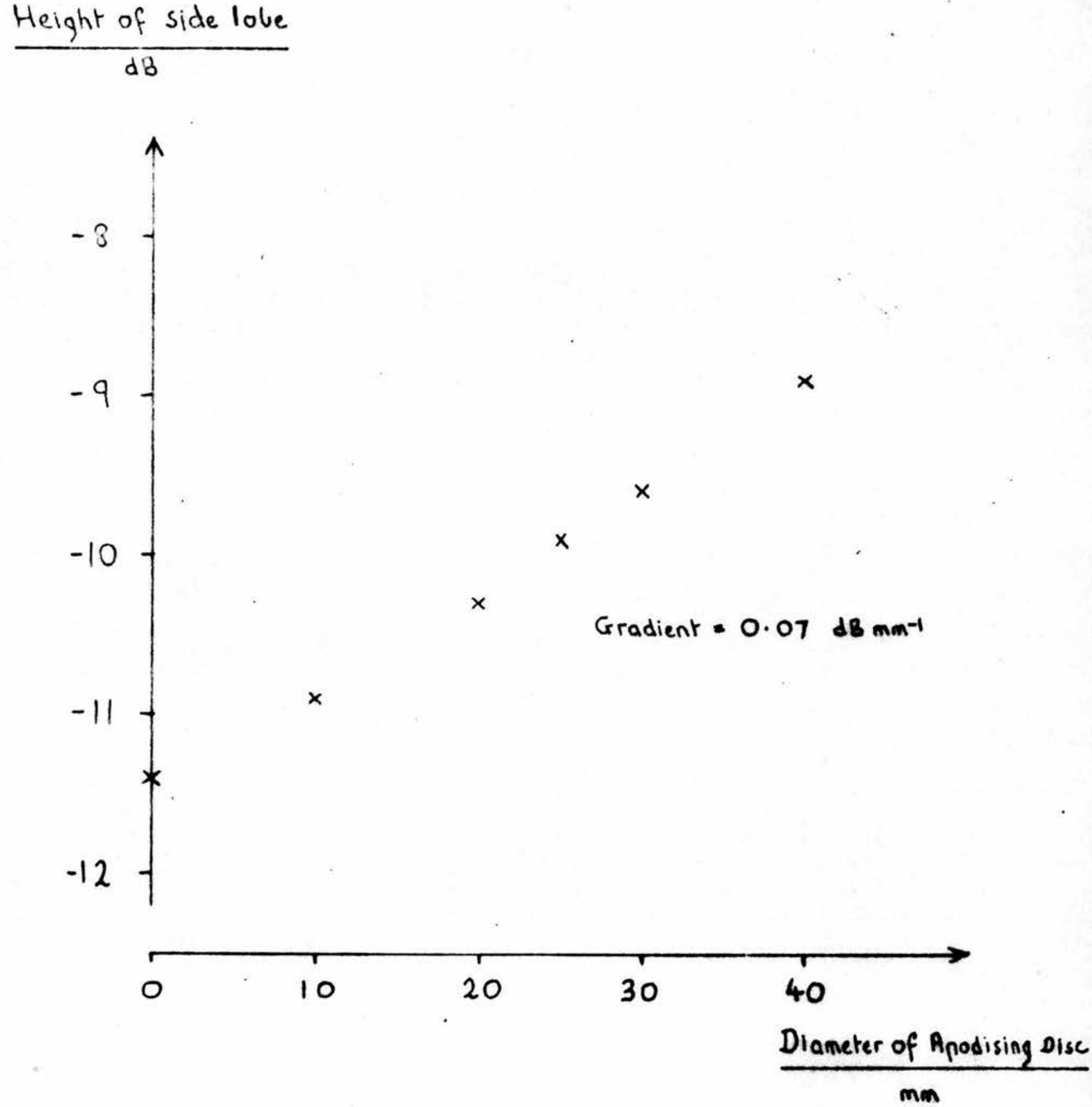

Figure 7.11: Effect of apodisation upon the relative height of the first off-axis maximum using an ellipsoidal mirror model of the Cassegrain Mirror.

for apodising discs between 10 and 40 mm diameter. The first side lobes, however, are large enough to be included in the usable dynamic range. Table 7.3A gives the actual beam half-widths and the amplitude of the second off-axis peak. The total beam width is still less than for the spherical bowl model and the next side lobe is comparable to the first with the spherical bowl. It must be realised that if such a fine focus could be achieved the plotting targets described in Chapter 5 would be unable to resolve it.

The effect of increasing the outer diameter of the aperture while keeping the apodising disc fixed at 20 mm diameter is quantified in Table 7.4 and shown graphically in figures 7.12 and 7.13 Radial fields to the same scale for outer diameters of 80, 90 and 110 mm are shown in figure 7.14. The peak amplitude increases faster than the increase in area of the aperture. It increases with the surface area of the primary mirror. Figure 7.13 shows the increasing amplitude of the sidelobes with the widening aperture. In the region of 100 mm outer diameter the rate of increase is 0.05 $dB.mm^{-1}$ but the rate is increasing with the size of the aperture.

7.2.3. Discussion of the Theoretical Results

Modelling the mirror as a sphere and as a prolate spheroid results in two widely different fields. Both the axial and the radical characteristics differ greatly. Physically the difference between the fields is due to the different distribution of sound acress the aperture, it being concentrated towards the edge in the ellipsoidal mirror. Qualitatively this would be expected to result in a smaller main lobe and increased side lobes. The numerical results confirm this.

Both the main lobes are well behaved, responding as expected to apodisation and to increases in the aperture outer diameter. The main lobe due to the ellipsoidal mirror is smaller and narrows less in response to apodisation. Neither are seriously enlarged by 25 mm diameter central block.

The sidelobes are also different in size and behave differently in response to increasing aperture outer diameter. The ellipsoidal

Outer diameter of aperture mm	Main lobe half-width mm					1st off-axis maximum	
	-3dB level	-5dB level	-6dB level	-10dB level	1st off-axis minimum	radius mm	height dB
80	0.0703	0.0886	0.0962	0.1177	0.16	0.24	-11.2
90	0.0650	0.0823	0.0883	0.1076	0.14	0.22	-10.8
100	0.0615	0.0773	0.0832	0.101	0.14	0.20	-10.3
110	0.060	0.0734	0.0803	0.097	0.13	0.20	-9.54

Table 7.4. Effect of outer diameter upon the ellipsoidal mirror model of the Cassegrain Mirror System (Apodising disc 20 mm diameter).

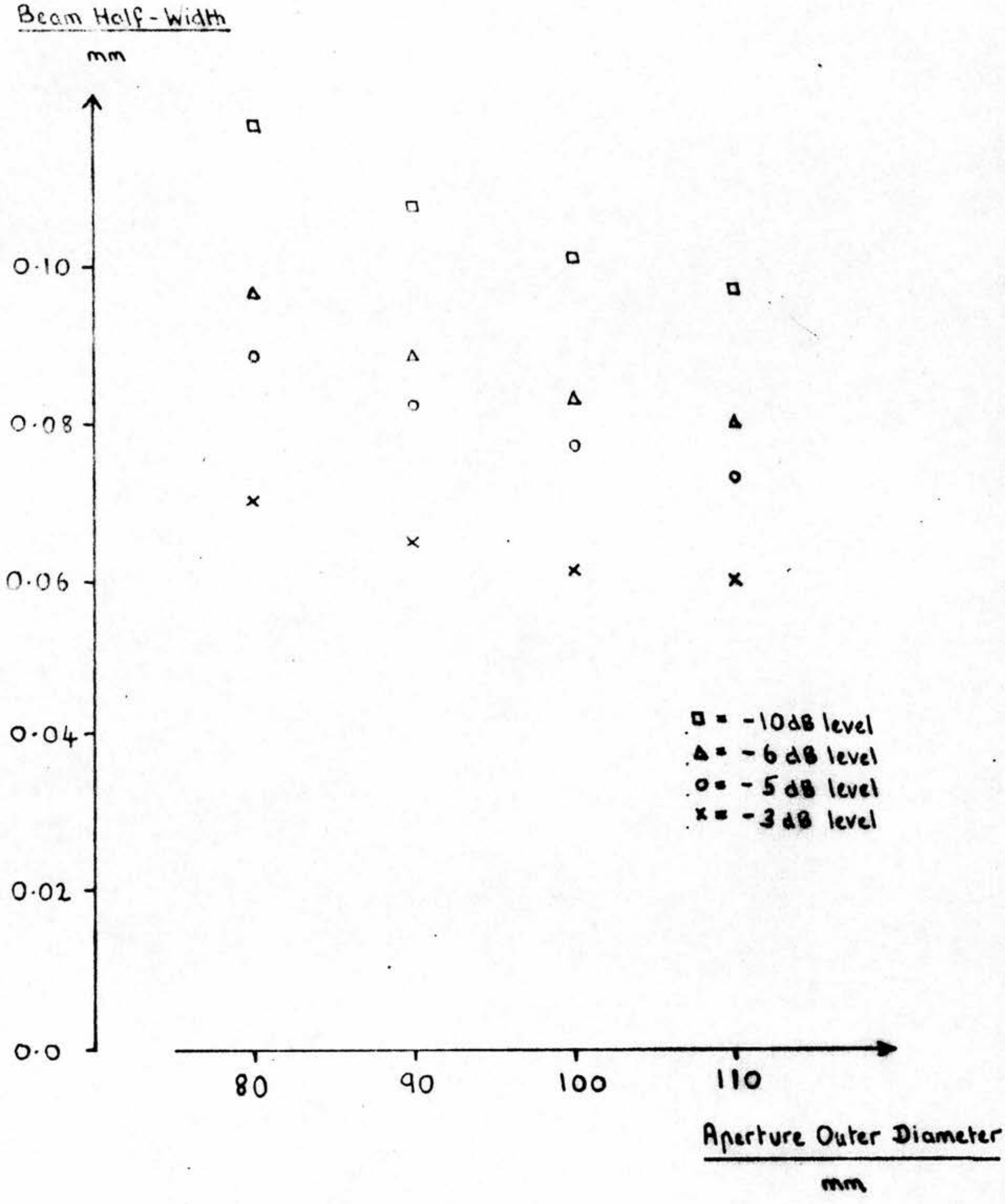

Figure 7.12: Effect of increasing the aperture upon the elliptical mirror model of the Cassegrain Mirror System (Apodising disc 20 mm diameter).

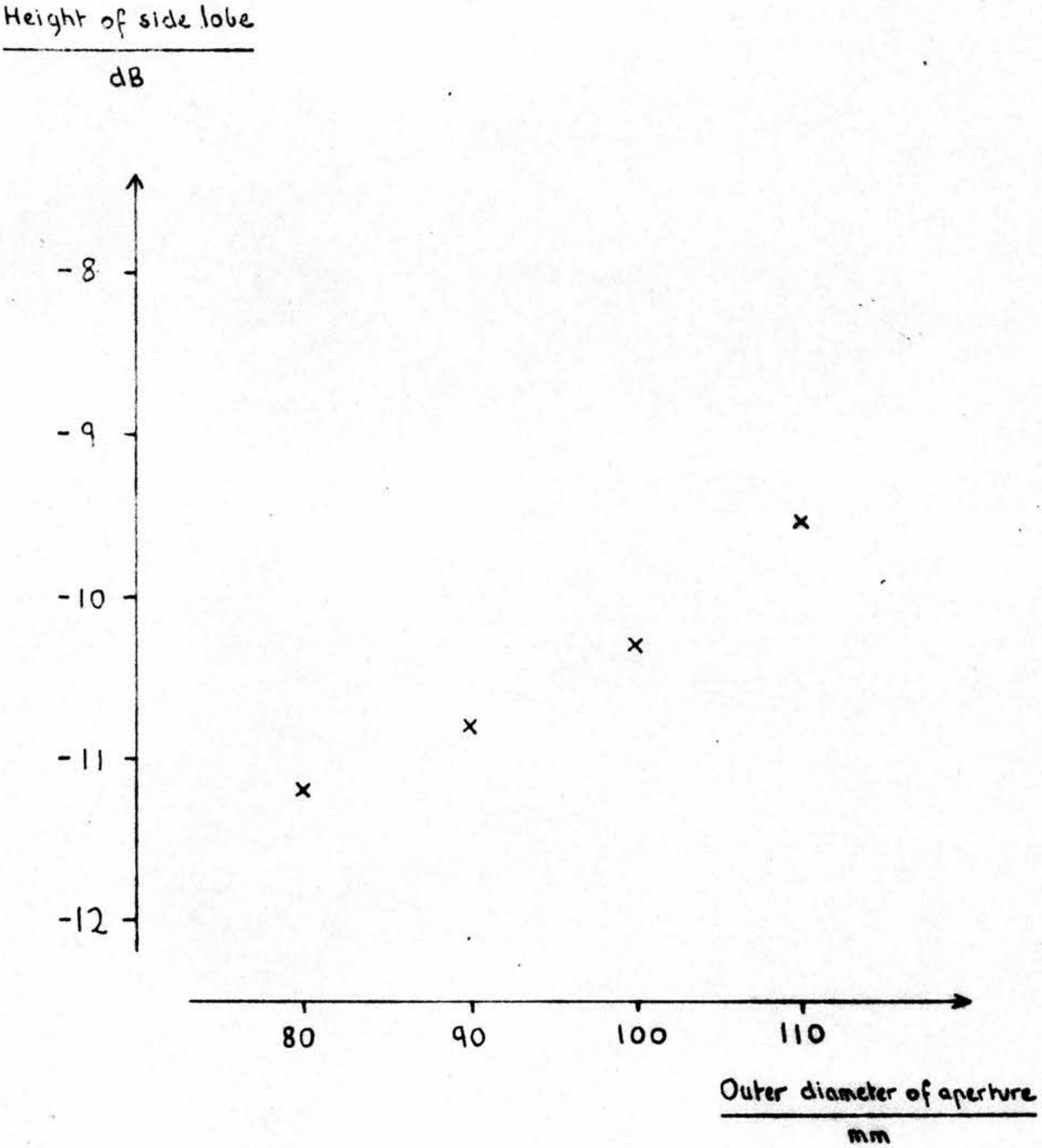

Figure 7.13: Effect of increasing the aperture outer diameter upon the relative height of the first off-axis maximum using an ellipsoidal mirror model of the Cassegrain Mirror.

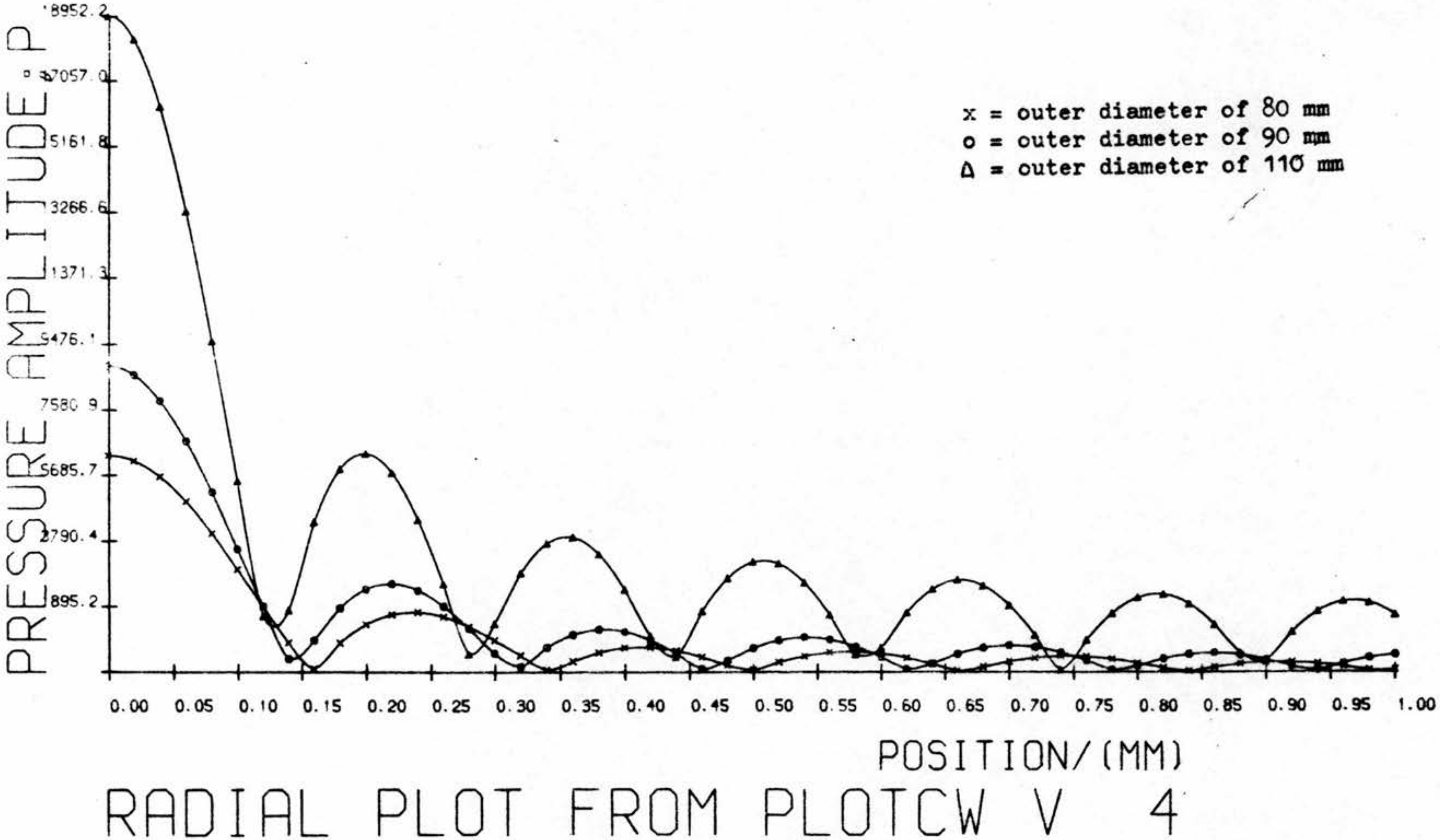

Figure 7.14. Radial plot of the ellipsoidal mirror model of the Cassegrain Mirror

model shows larger sidelobes, although they increase more slowly, they become large enough to interfere with the dynamic range. However the beam is considerably narrower than that predicted for the spherical bowl. Indeed the first side lobe could be incorporated in the main lobe of the spherical bowl. The second lobe is comparable to the first in the spherical bowl field.

The behaviour of the ellipsoidal mirror with increasing aperture (figure 7.13) is important. The side lobes increase and can become large enough (> - 10 dB) to interfere with the desired dynamic range even for a 20 mm diameter centre stop. This occurs when the outer diameter approaches the minor axis of the ellipse (here 110 mm compared to 115.5 mm).

Any practical mirror system will be based on an ellipsoid not a sphere. Equally any practical field will contain spherical aberration since the source will be an axially distributed transducer beam reflected by the secondary mirror, not a perfect point source. This will result in a depth of focus considerably longer than that predicted by the ellipsoidal mirror. The beam width will also be increased. However the model shows that wide, deep ellipsoidal mirrors must be avoided since improved beam shape will not result.

A limited dynamic range is also shown. The demands upon the dynamic range of this device will, however, be less than those upon a device with a large depth of field which may be required to image a large variety of tissues at one time. A dynamic range of the order of 20 dB in the image (i.e. transmission and reception together) should be sufficient to image the variety of tissues found in the small areas of interest for which this probe is being considered. This dynamic range can be achieved but the limits of the ellipsoidal mirror diameters must be recognised.

Experiment will demonstrate how close to the predicted fields the actual beam will be.

7.3. Final Design and Manufacture of a Cassegrain Mirror.

The system described in section 7.1. was produced.

The primary is an ellipsoid of revolution (a prolate spheroid) based on an ellipse with a semi-major axis of 66.7 mm and a separation of 66.7 mm between the reference points. The ellipse is truncated at a diameter of 100 mm which is through the plane of the internal reference point. This design was executed in araldite, araldite and aluminium powder composite and in thin air-backed copper.

The increase in sidelobe size with increasing aperture demonstrated by the ellipsoidal mirror suggests a disadvantage in too large an ellipsoidal mirror. The numerical model, however, considers only the primary mirror. The practical design of the secondary sheds much light on the nature of mirror systems.

The system may be altered by changing only one element. Thus the secondary mirror or the transducer may be chosen so as not to 'illuminate' the whole of the aperture.

The situation of having a virtual point source at the internal reference point of the primary is idealised. In practice the transducer will have a finite focal zone. The rotational symmetry of the primary about its major axis will lead to this axial distribution resulting in spherical aberration in the final acoustic focus. This effect is described analytically by Bruggemann (1968), p 54. This will prevent the field being substantially confined to the focal plane as predicted by the ellipsoidal model.

7.4. Experimental Observations

Several experiments were performed with the Cassegrain system. Those concerned with pulse shapes and echoes are described in Section 7.4.3. The field plots with the PVDF hydrophone and with ball bearing targets are discussed in sections 7.4.1 and 7.4.2 respectively.

A general feature of the systems was a sensitivity to radial rather than to axial misallignment. Axial displacement of the secondary relative to the primary and to the transducer caused the focal peak to shift axially but with little effect upon its amplitude. The axial spread of the transducer field must contribute to this effect. Unless otherwise stated the results that follow are based upon the 5 MHz, 13 mm diameter MD3500 probe and the ellipsoidal secondary. The optimum result was achieved for this configuration with the focal peak at an estimated range of 80 mm from F_2. This range measurement contains an inaccuracy because of the difficulty in estimating the position of F_2 but the precision of range measurements is 0.25 mm.

Little work was done with the Olofsson style systems since sufficient sensitivity could be achieved transmitting and receiving through the mirror system when the hollow copper primary was used.

The combination of plane disc transducer and parabolic secondary did not work well in practice because the secondary failed to completely shadow the transducer permitting it to transmit and receive directly as well as through the mirror system. Although these problems were ameliorated by alterations to the design and by the introduction of additional absorbing blocks it remained a poor option. The reverberation problems discussed in section 7.4.3 were more marked with this configuration.

7.4.1. Hydrophone Field Plots

An axial plot with a transmitter attenuation of -6 dB and with the focal peak at 80 mm range is shown in figure 7.15. Transverse plots at ranges of 70, 80 and 95 mm are shown in figures 7.16 (a), (b) and (c) respectively. The beam widths of the peak plot are marked on the plot. The sidelobes are -13 dB of the transmitted field peak. A similar axial and transverse plot for the system adjusted to place the peak at 57 mm range are given in figures 7.17 and 7.18 respectively. The transverse plot shows an increased beam width but slightly reduced sidelobes at -16 dB. Both transverse plots (figure 7.16(b) and 7.18) show a distinct asymetry attributable to imperfect alignment.

It should be considered that the hydrophone may be unable to resolve sidelobes which it may incorporate with what is apparently the main lobe.

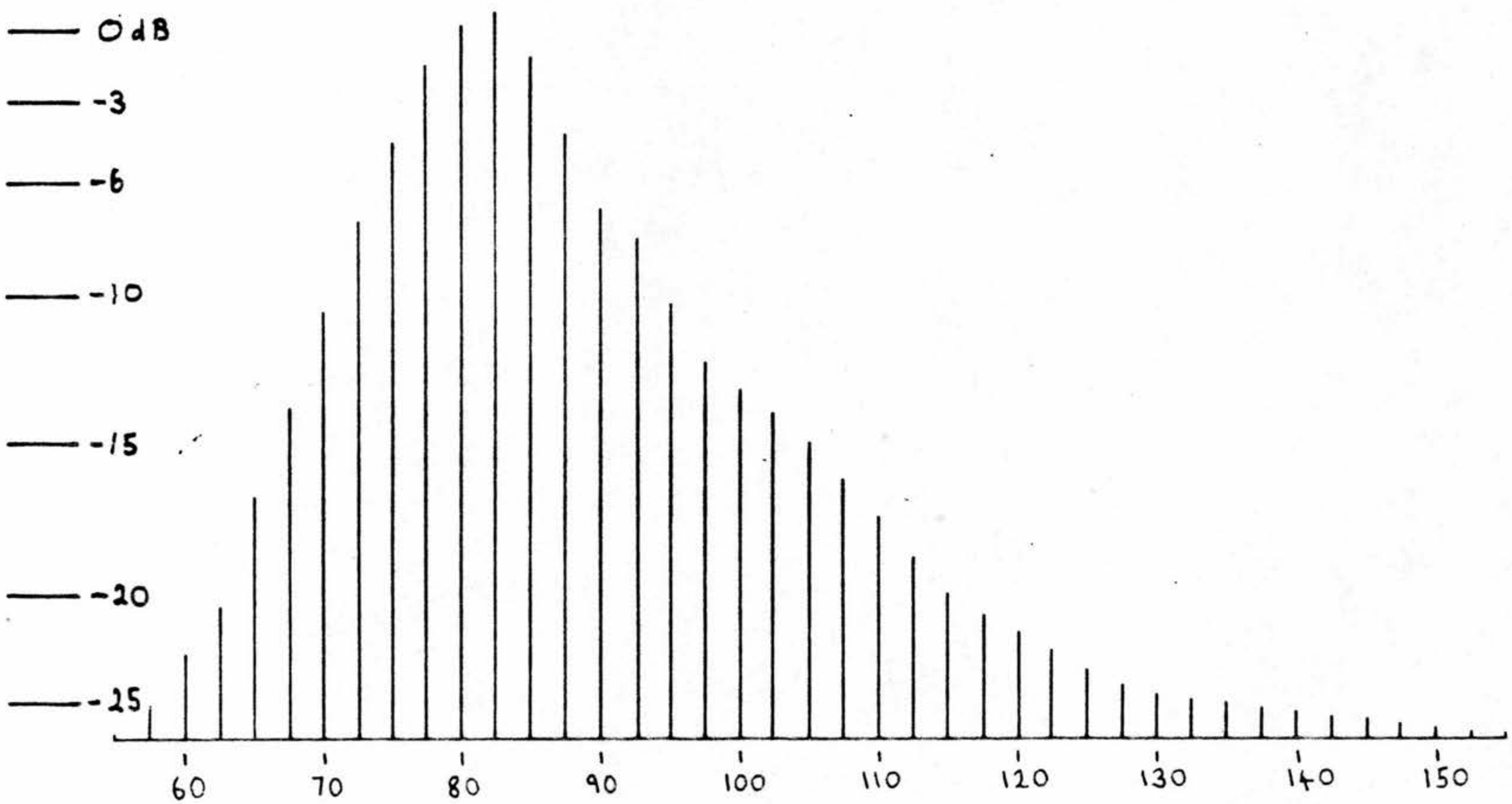

Figure 7.15. Axial plot of the Cassegrain Mirror system using the PVDF Hydrophone
Peak at 80 mm. Focal length -3dB = 10 mm. -6dB = 15 mm. -10dB = 22 mm.

Figure 7.16: Transverse plots of the Cassegrain mirror system using the PVDF hydrophone.

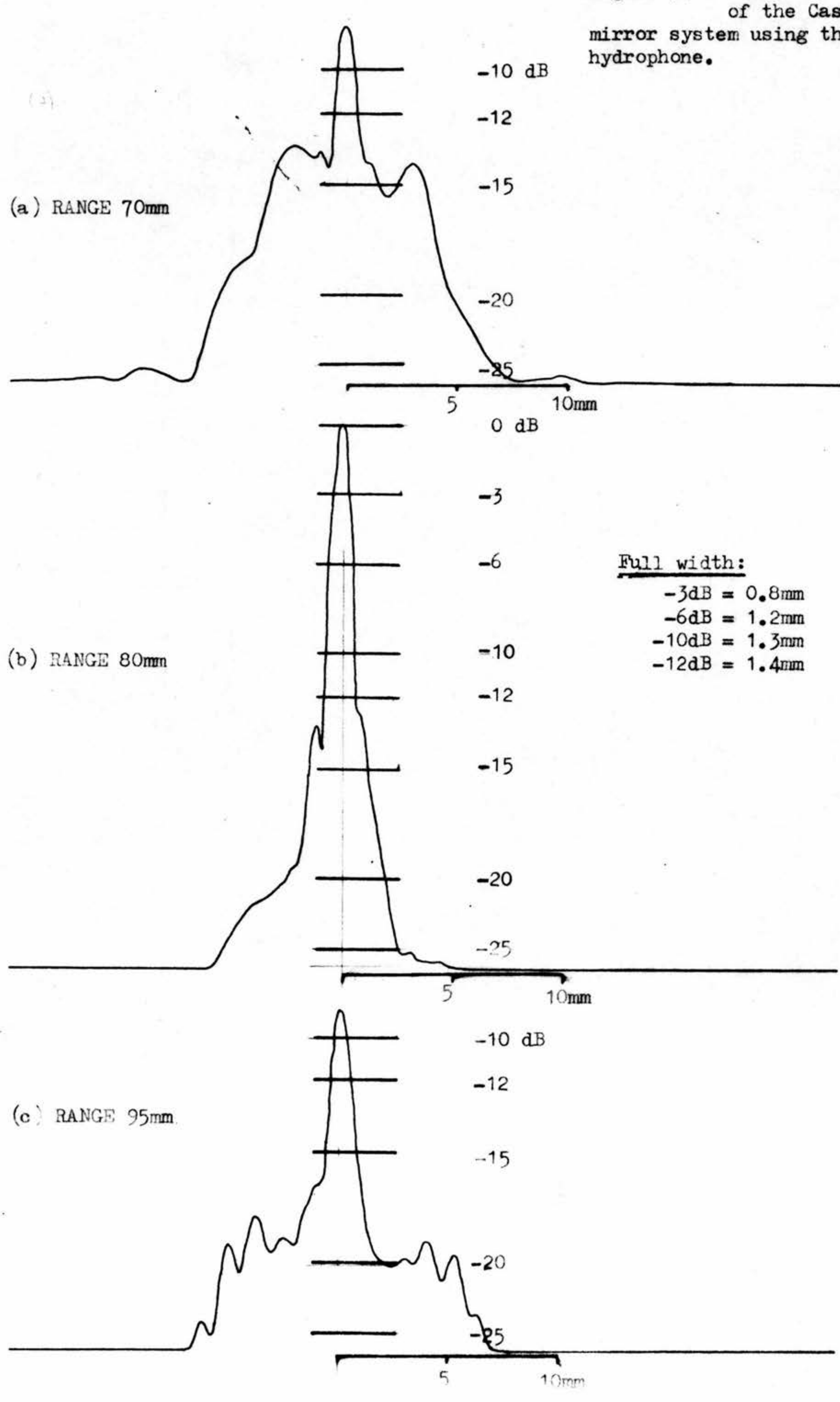

Figure 7.17: PVDF Hydrophone axial plot of the Cassegrain mirror system (Peak at 57mm).

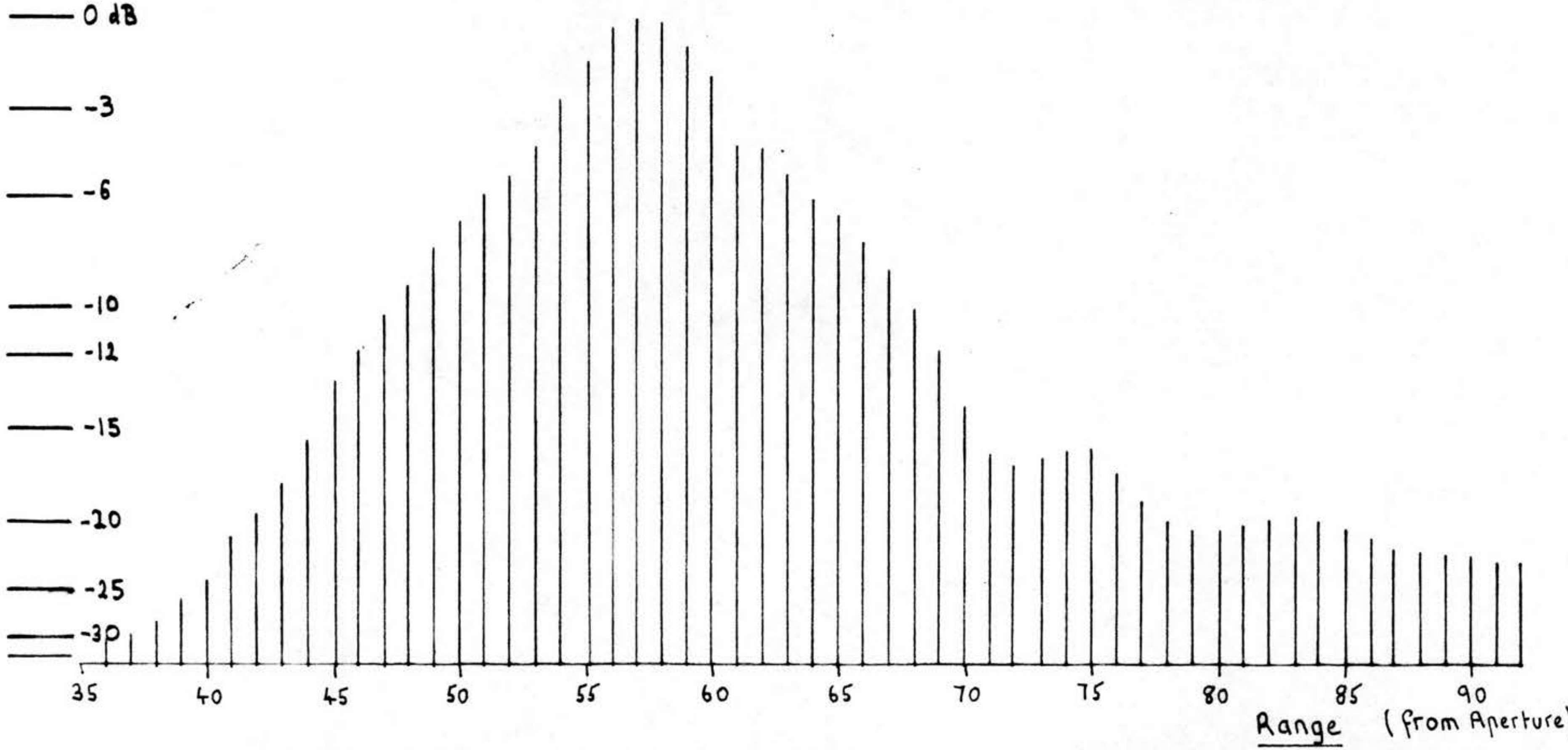

Figure 7.18: PVDF Hydrophone transverse plot through the field maximum (range 57mm) of the Cassegrain mirror system.

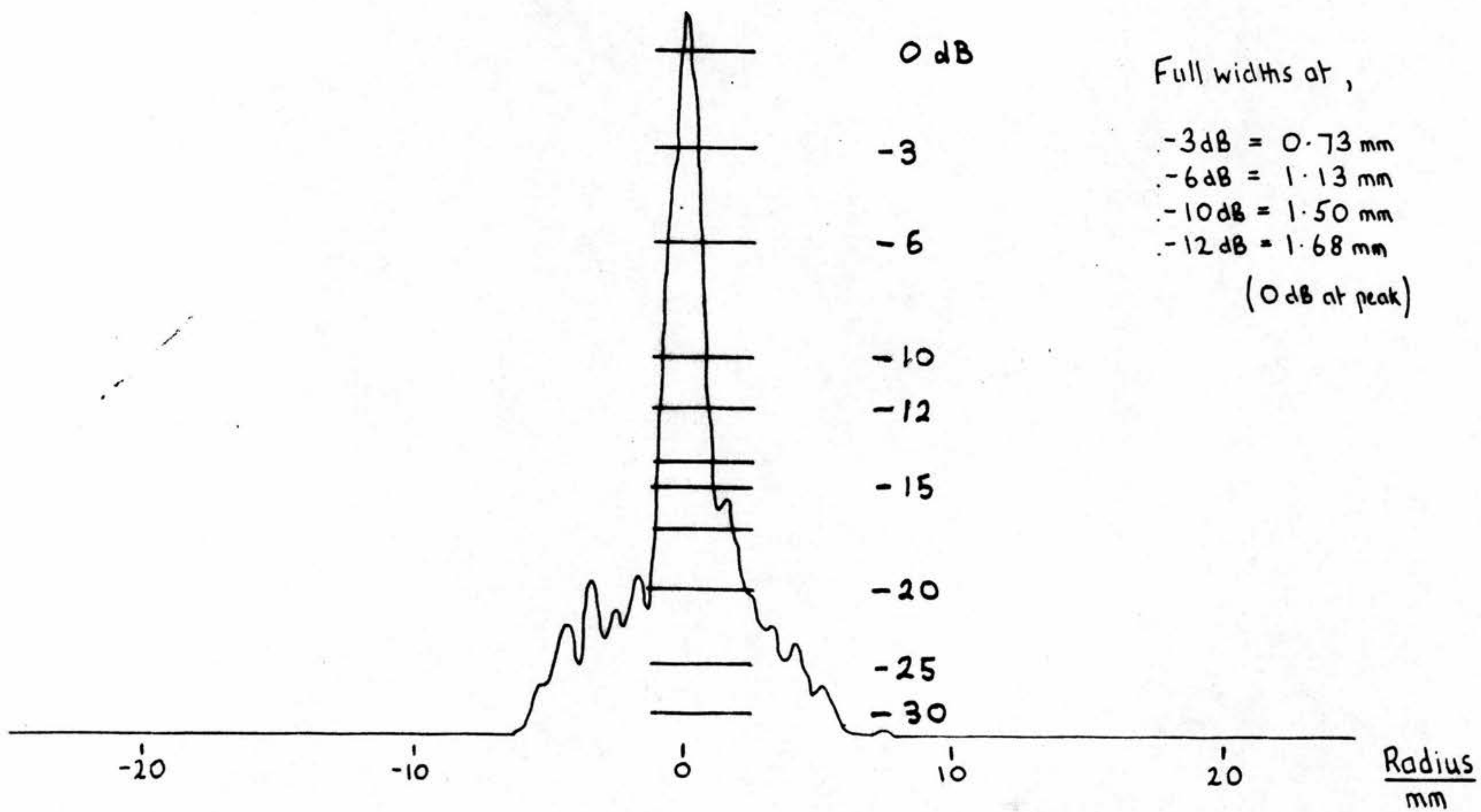

7.4.2. Pulse-Echo Field Plot

Pulse-echo transferse plots through the 80 mm range focal peak are shown in figure 7.19. (a) is the plot using a 2 mm diameter spherical target, (b) a 5 mm sphere and (c) a 10 mm sphere. The 10 mm ball offers an increase of only 4 dB in sensitivity compared to the other two targets.

The same configuration but using a 2.25 MHz 13 mm diameter transducer is shown in figure 7.20. A 6 mm diameter 5 MHz probe was used with the paraboloidal secondary to produce the plot shown in figure 7.21. The transverse plot through the field maximum is shown in figure 7.22.

7.4.3. Pulse Shapes and Reverberations

The transducer primarily used with the mirror systems, MD3500 5MHz, was aimed at a variety of surfaces and the returned pulse examined. The target was placed at a range of 90 mm, the transmitter attenuation -20 dB and although the received echo was examined directly, the system was loaded by connecting the receiver as usual. The transducer orientation was adjusted to maximise the echo. Some of these pulses are shown in figure 7.23. (a) is the echo from an air-backed thin ($<$ 0.01 mm) plastic film ("snap-wrap" cling film). This was taken as the best attainable echo (b) is the echo from front surface of the air-backed, thin copper primary (c) is the echo from a similar primary mirror moulded in araldite (d) is the primary moulded in an Aluminium powder: araldite mixture. No primary was manufactured in the tungsten powder: araldite composite but flat surfaces of epoxy resin composite using the different powders gave indistinguishable echoes. There is no reason to believe that they would behave differently when moulded to the curved surface.

There is a little degradation in the pulse reflected by the copper mirror but the performance of this mirror is excellent. The amplitude of the pulse is maintained well. There are no reverberations from within the mirror.

The PVDF Hydrophone was used to examine the pulses transmitted by

Figure 7.19: Pulse-echo plots through the field maximum (range 80mm) of the Cassegrain mirror system using various target sizes.

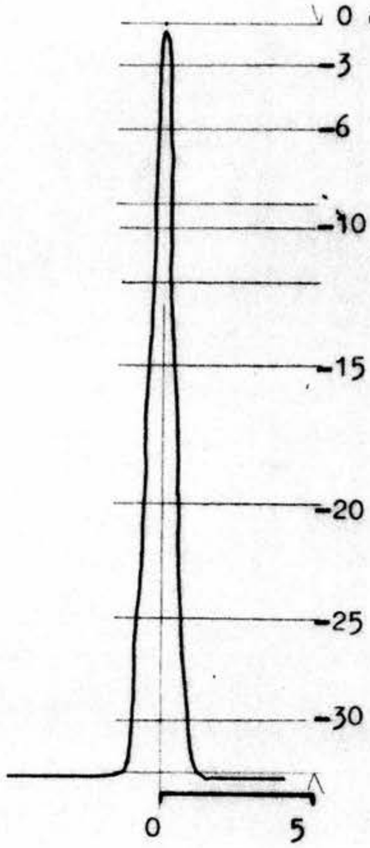

(a) 2mm dia. steel ball target

Full widths:

-6 dB = 0.4mm
-10dB = 0.5mm
-12dB = 0.6mm
-20dB = 1.1mm
-35dB = 2.4mm

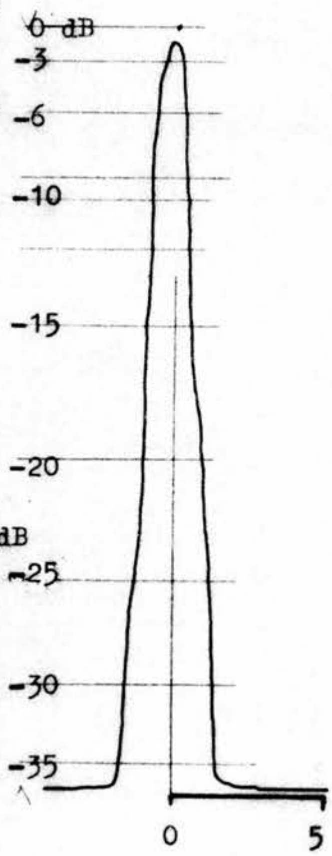

(b) 5mm dia. steel ball target

Full widths:

-6 dB = 0.9mm
-10dB = 1.2mm
-12dB = 1.3mm
-20dB = 1.9mm
-35dB = 3.15mm

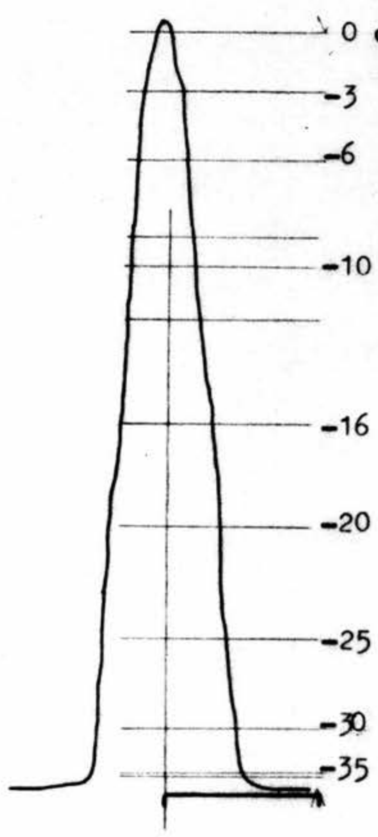

(c) 10mm dia. steel ball target

Full widths:

-6 dB = 1.6mm
-10dB = 2.1mm
-12dB = 2.35mm
-20dB = 3.7mm
-35dB = 4.9mm

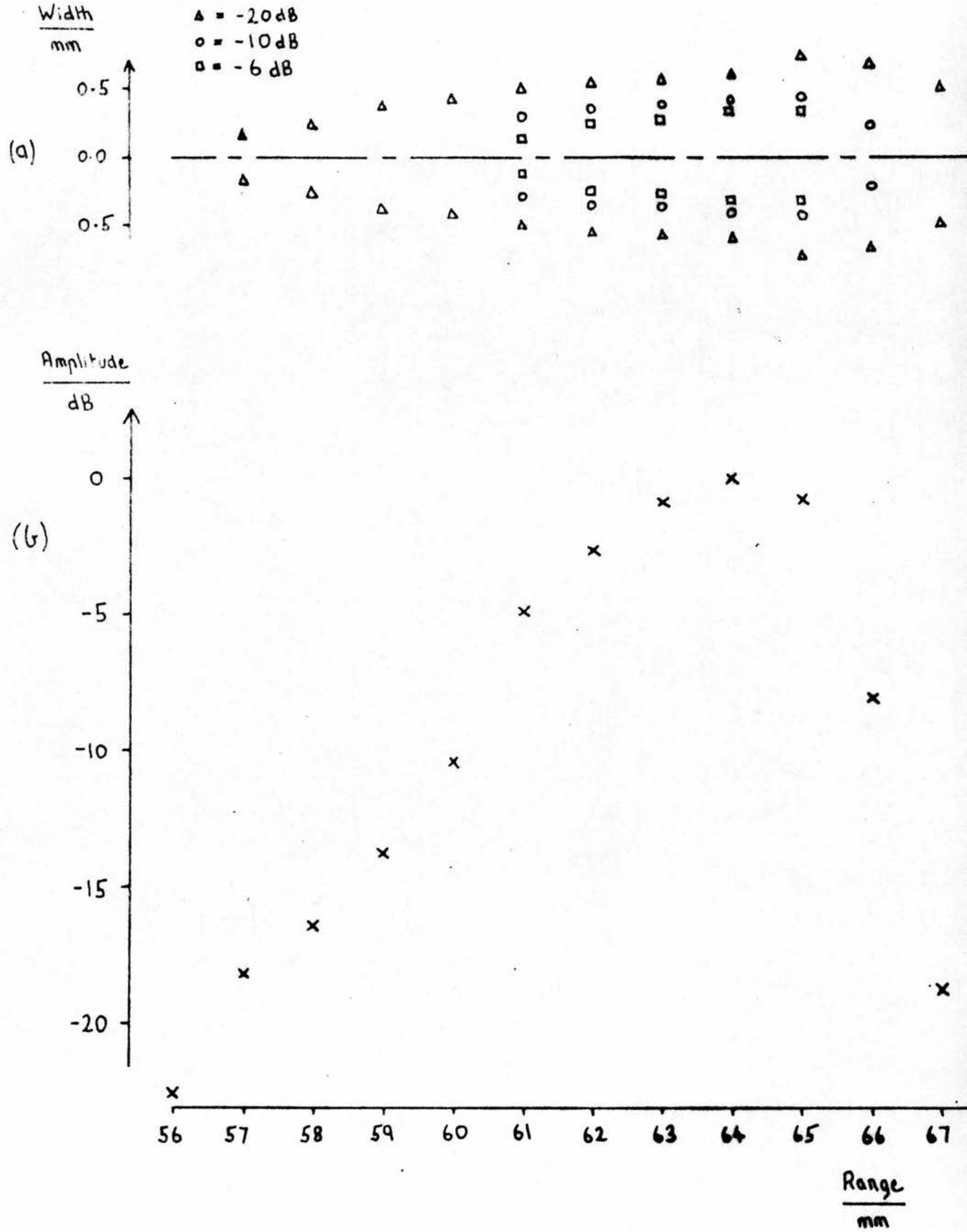

Figure 7.20: Beam shape of Cassegrain Mirror
with 2.25 MHz, 13 mm diameter transducer
a) Beam width contours.
b) Axial profile.

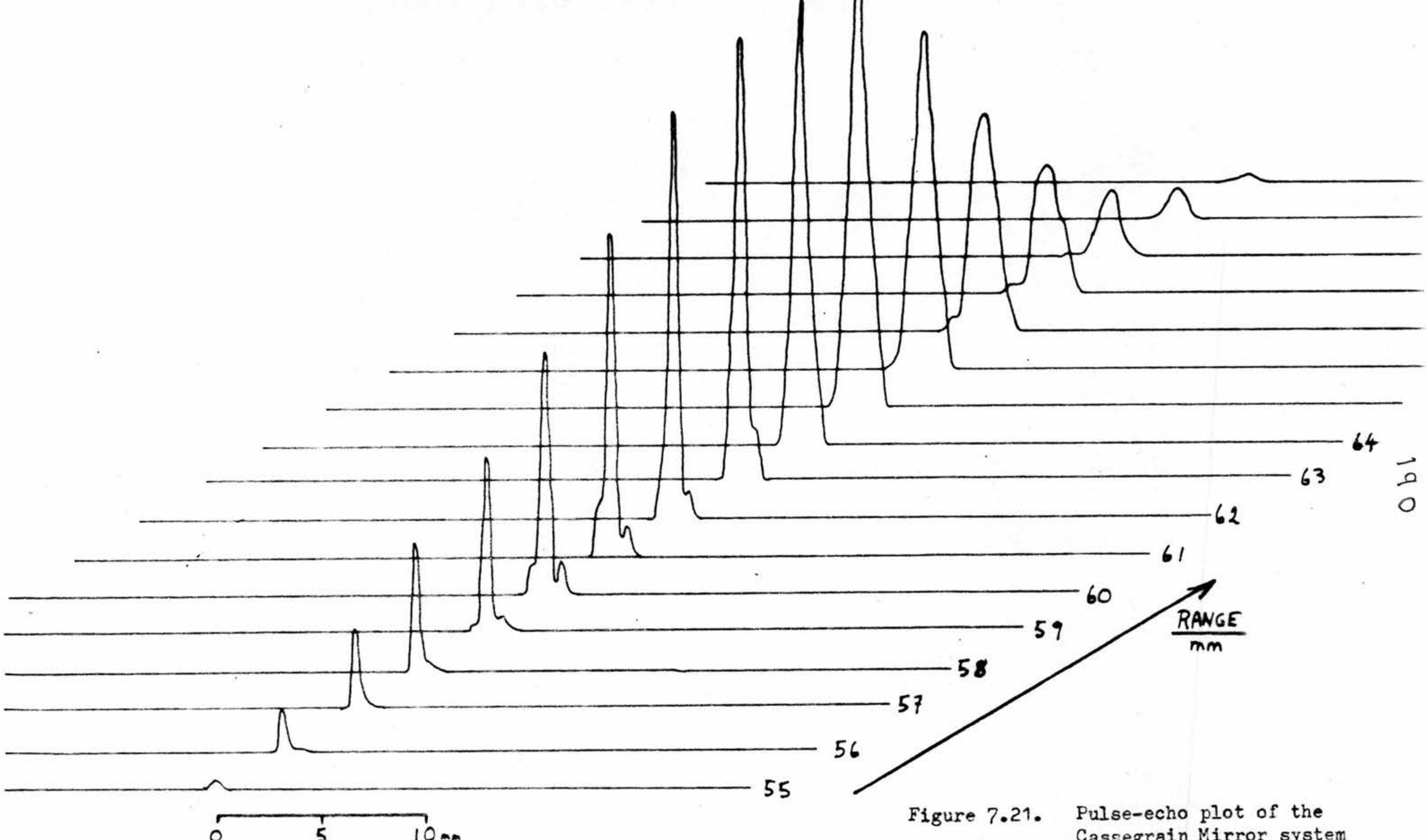

Figure 7.21. Pulse-echo plot of the Cassegrain Mirror system with 6 mm diameter, 5MHz transducer. (5 mm diameter steel ball target.)

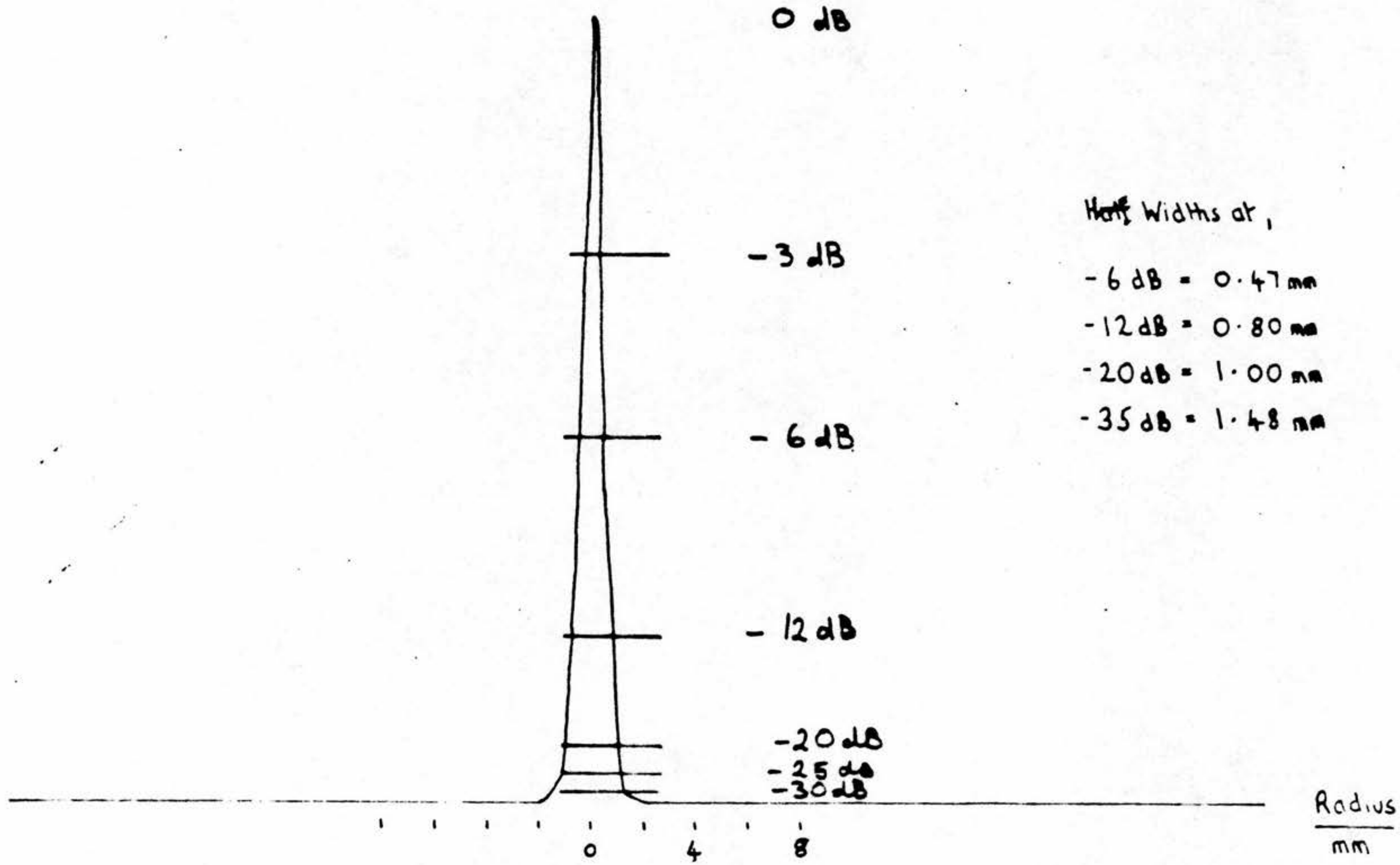

Figure 7.22. Peak, transverse plot of the Cassegrain Mirror system, range 64 mm using the 6 mm diameter 5MHz transducer. The target is a 5 mm diameter steel ball.

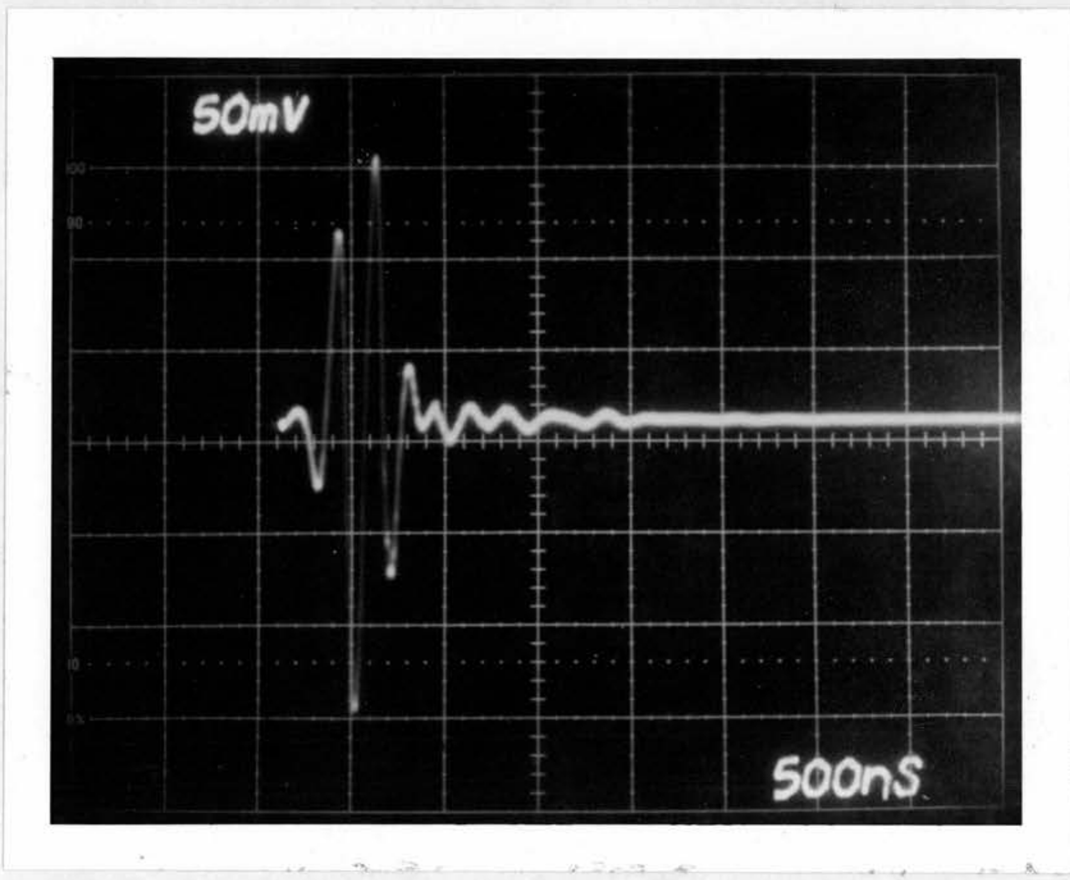

Figure 7.23(a): Echo pulse from an air interface.

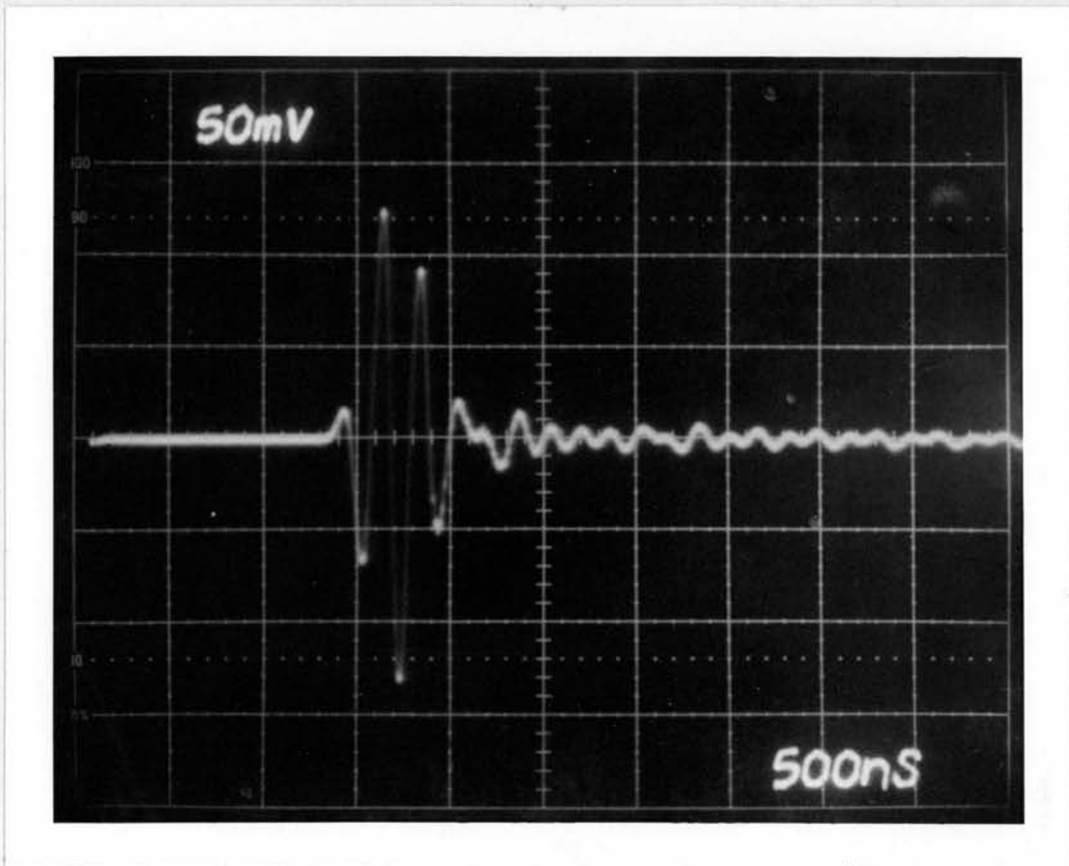

Figure 7.23(b): Echo pulse from the air backed, thin copper primary mirror.

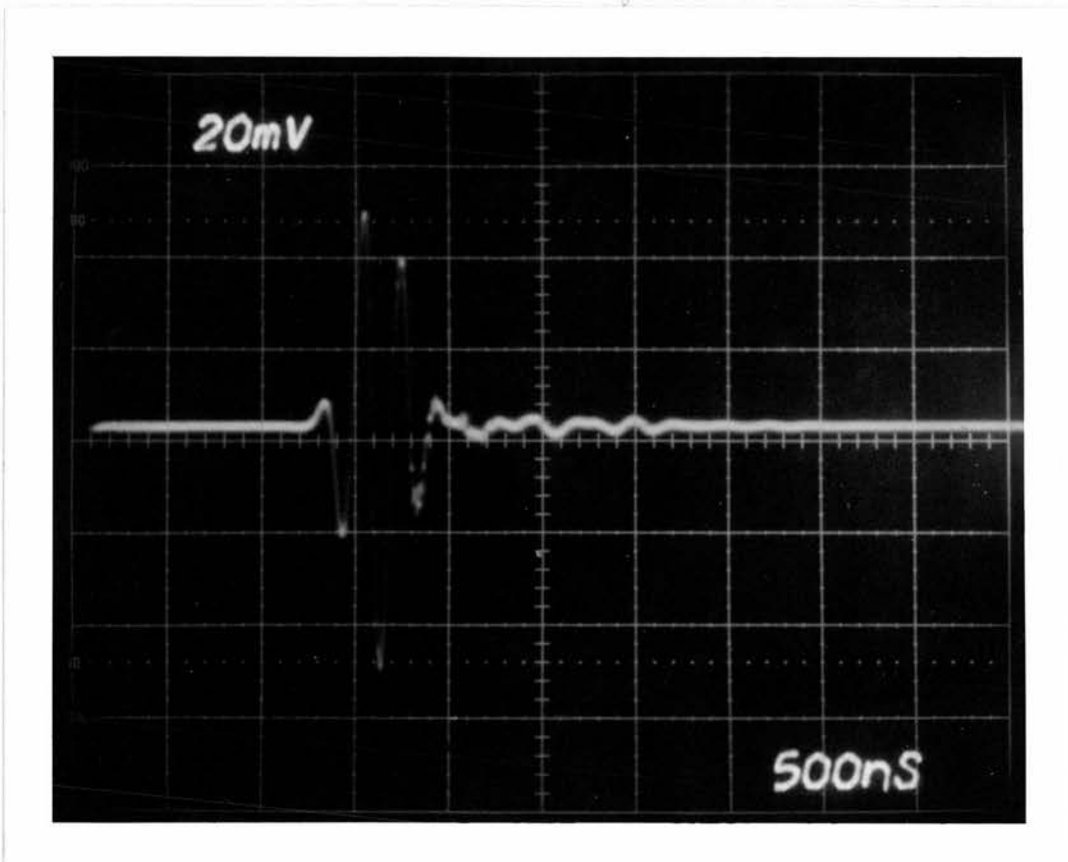

Figure 7.23(c): Echo pulse from an araldite primary mirror.

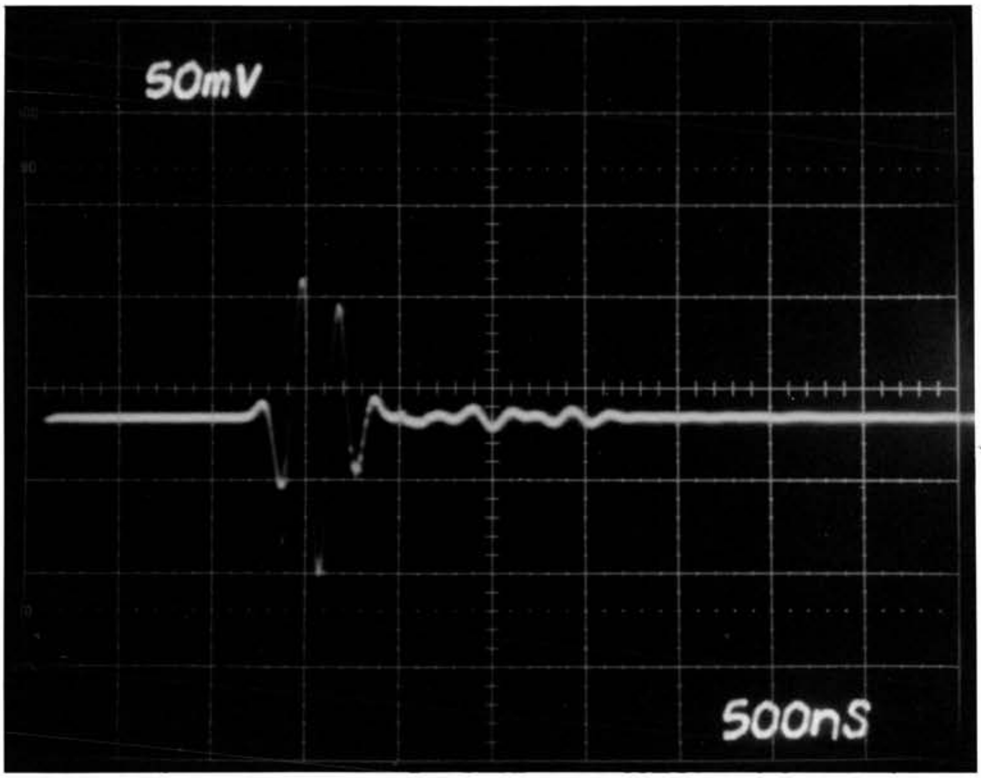

Figure 7.23(d): Echo pulse from tungsten:epoxy composite mirror.

the Cassegrain system. Figure 7.24 (a) to (c) shows the pulse shapes associated with the transverse plots given in figure 7.16 (a) to (c). The two -10 dB pulses show lengthening due to edge wave effects.

The hydrophone also shows a more serious problem. The peak pulse with a slower timebase is shown in figure 7.25. 36 μs behind the main pulse there is a second pulse. This is a result of part of the transmitted pulse reverberating between the primary and secondary mirror. The effect is seen again on the video output of the receiver shown in figure 7.26. The reverberation is only some 17 dB less than the peak. It will appear some 50 mm from the peak, i.e. within the breast image and in an area where the field amplitude will be much less than the peak amplitude.

Another manifestation of this is shown in figure 7.27. This is the video signal in the absence of any target. 'A' marks the transmitter spike; 'B' is a reflection from the front of the secondary. Part of the transmitted pulse enters the tungsten: araldite composite secondary mirror and in turn some echoes from the back surface of the secondary giving the pulse marked 'C', 'D' and 'E' are due to subsequent reverberations between the secondary and the transducer or the primary. 'F' marks the region of the focal zone.

This effect was amplified by the use of the air-backed copper secondary.

7.4.4. Non-Linear Effects in Pulse Propagation

Significant non-linear effects will appear with pulses whose amplitude is great enough for a large change in density to accompany the change in pressure. this is due to the inertia of the fluid particles. This leads to a progressive steepening of the pressure front and, when the pressure front becomes abrupt (i.e. its depth is of the same order as the mean free path of the fluid particles), a shock wave. These effects more commonly occur in gases since these are much more compressible than liquids.

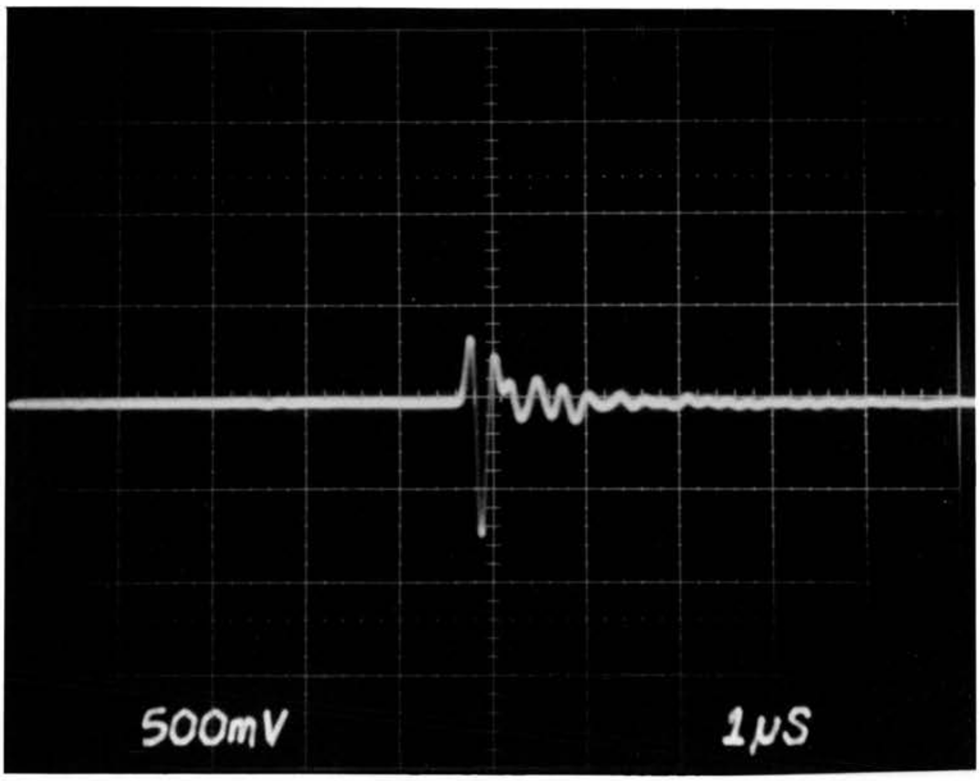

Figure 7.24: Pulse from the Cassegrain mirror system
(PVDF hydrophone)
(a) at 70mm range (-10dB from peak).

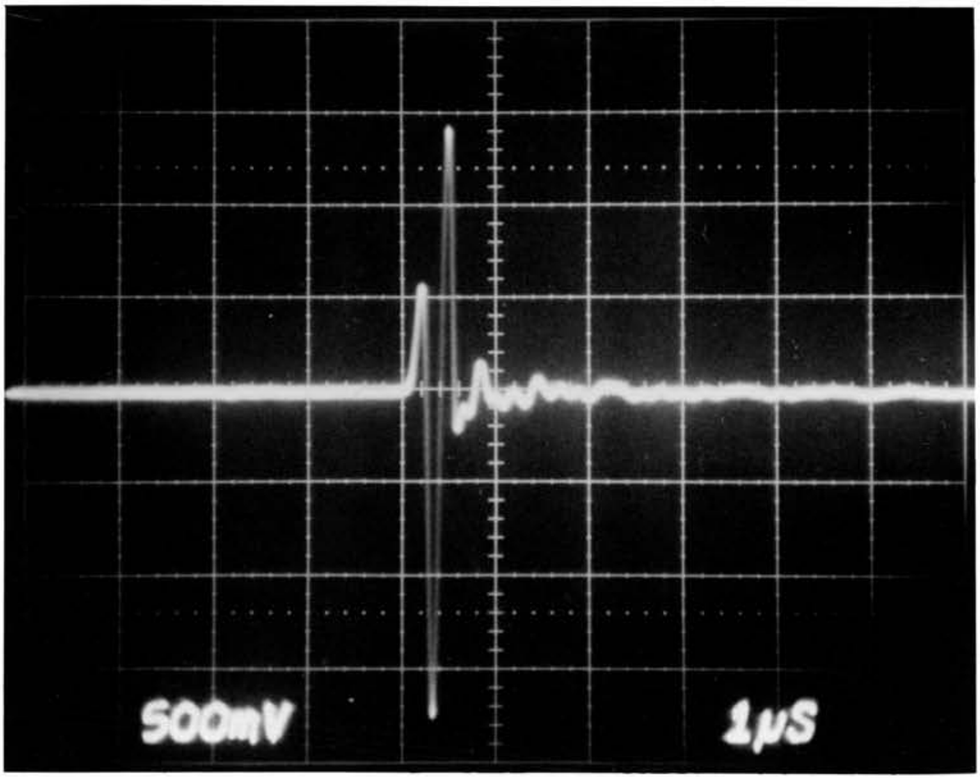

Figure 7.24: Pulse from the Cassegrain mirror system (PVDF hydrophone)
(b) at 80mm range (peak).

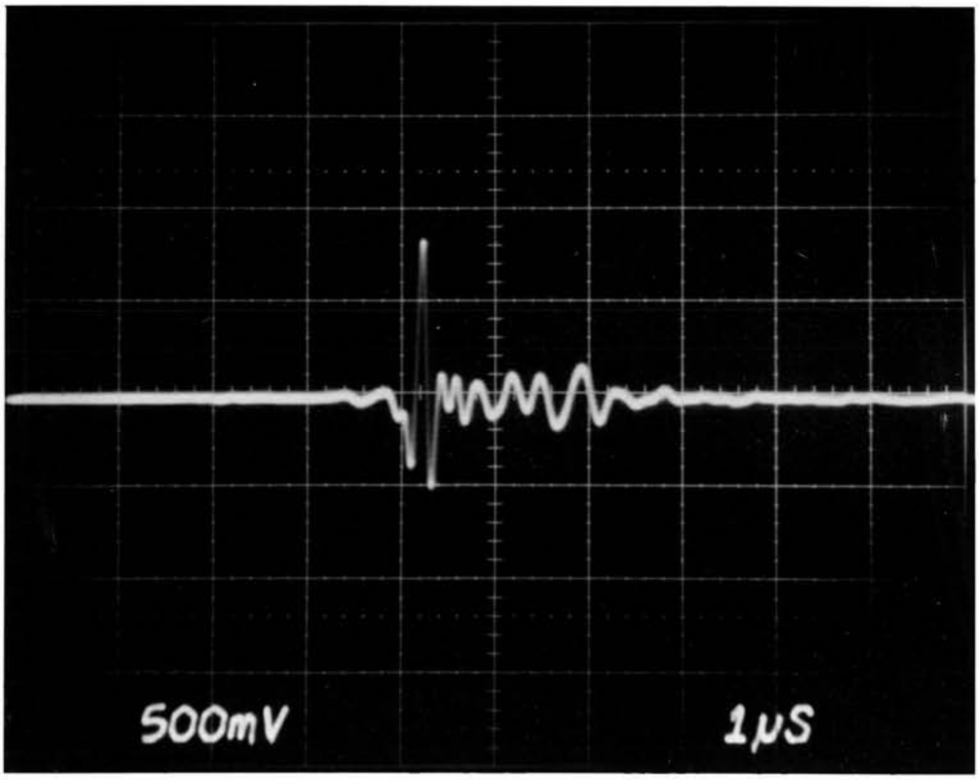

Figure 7.24: Pulse from Cassegrain mirror system
(PVDF hydrophone)
(c) at 95mm range (-10dB from peak).

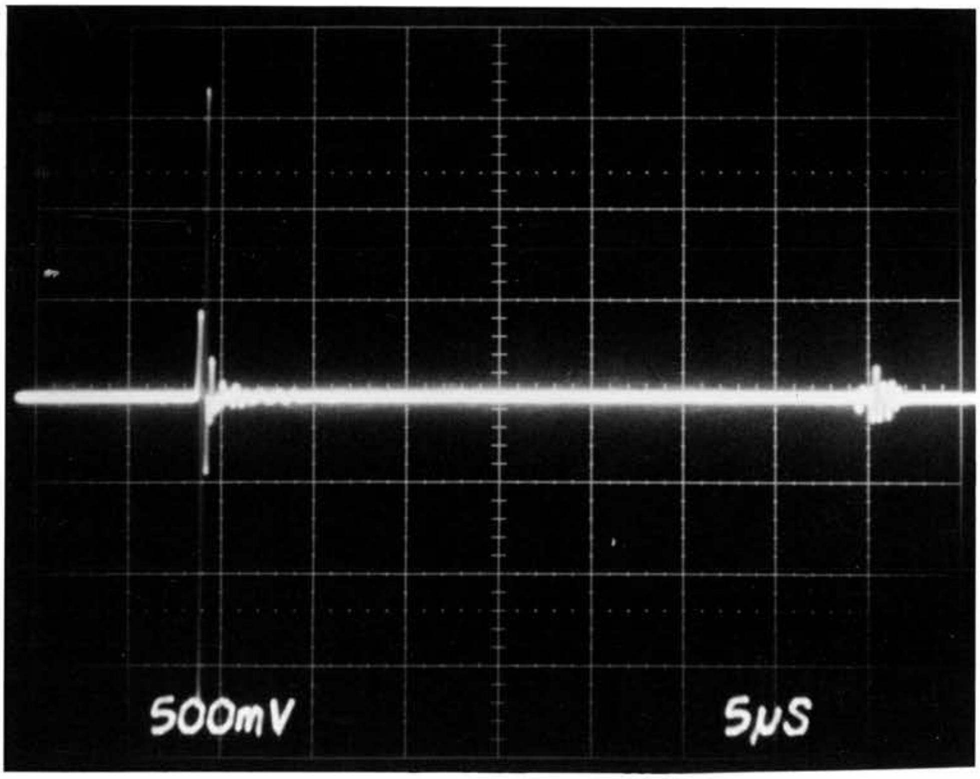

Figure 7.25: Pulses from Cassegrain mirror system showing ghost signals.

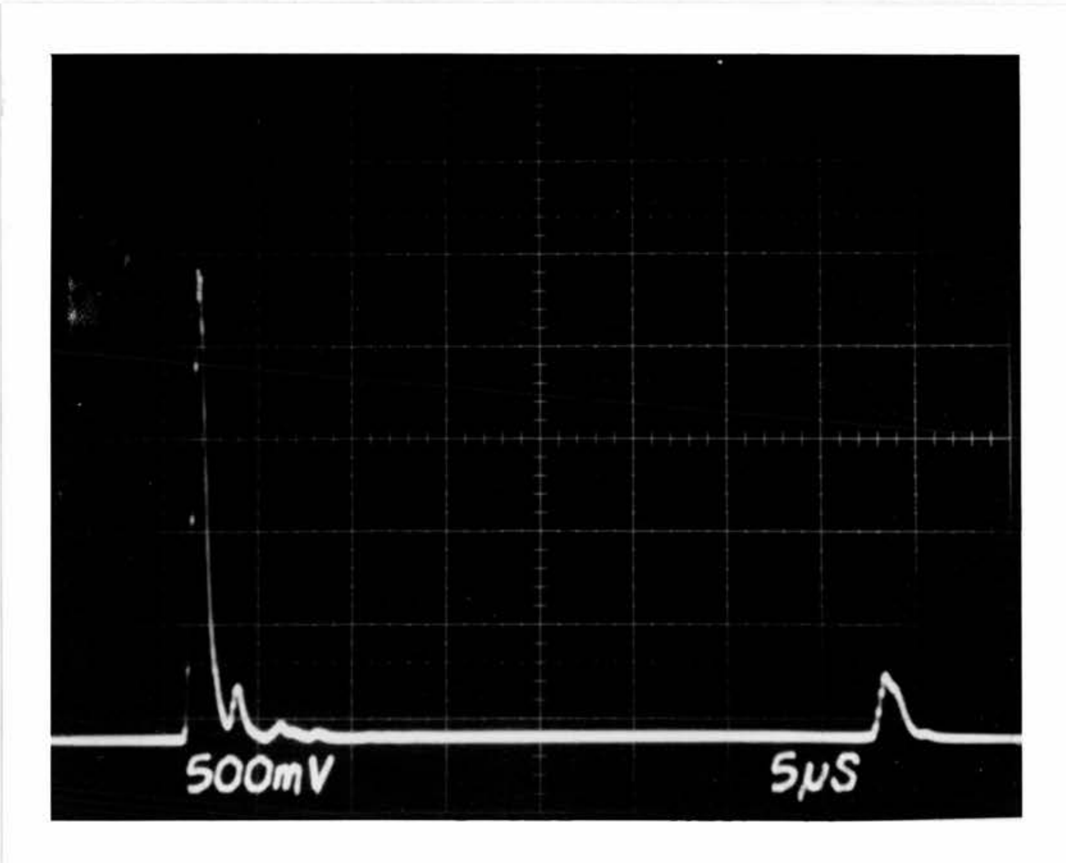

Figure 7.26: Video signal from Cassegrain mirror system showing ghost echos.

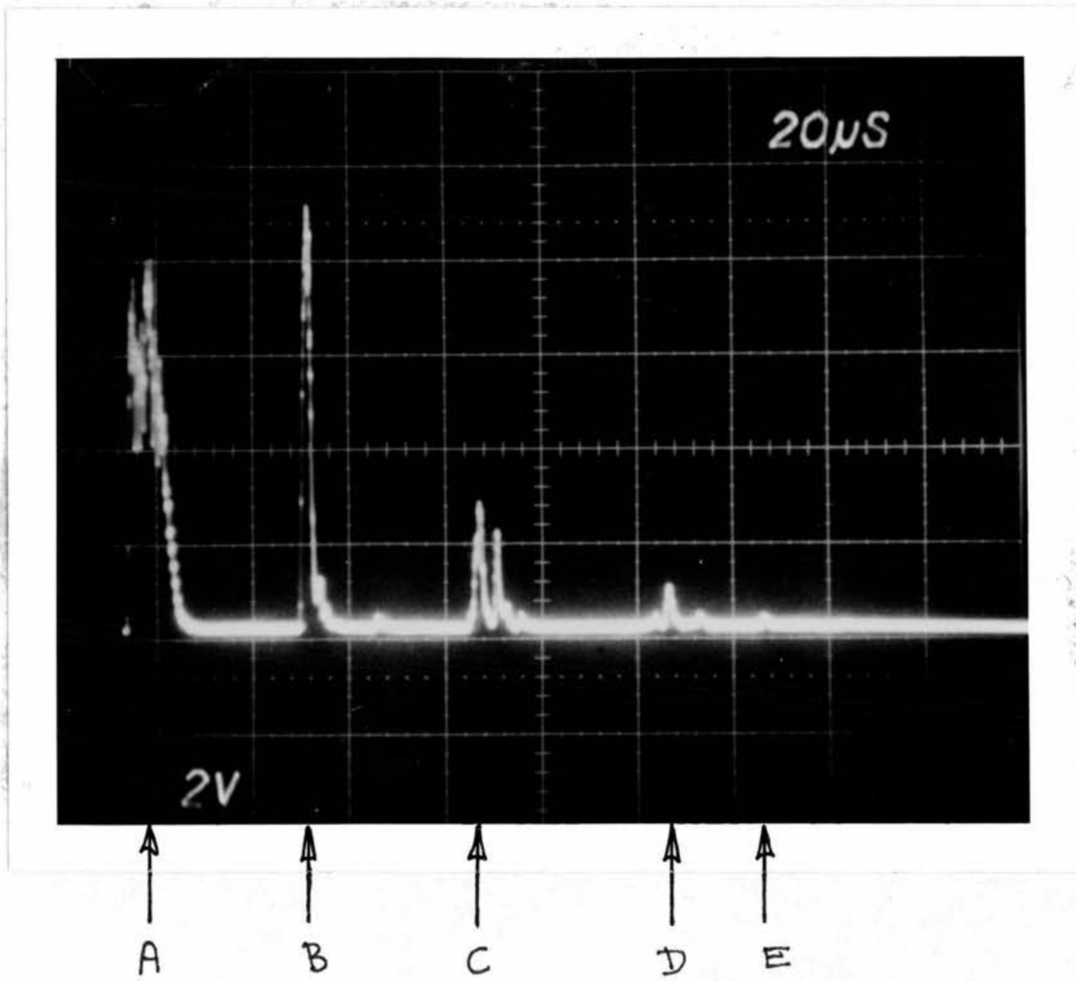

Figure 7.27. Video signal from the Cassegrain Mirror System.

Shockwaves may be appreciated qualitatively as the adiabatic compression of the transmitting medium by the positive pressure component of the wave leading to a localised increase in temperature and hence velocity (e.g. Feynman, 1963). Quantitative solution requires close physical restraints. Early theory was by W.F.B. Reimann (1826-66) and developed by W.J.M. Rankine (1820-72). Lighthill (1978) describes the development of 'excess' velocity by components of a simple pulse in an ideal gas.

Recent work (Horan and Cook, 1983) with PVDF hydrophones has revealed evidence of these non-linear effects created in water tanks by diagnostic transducers. This distortion of waveform increases with distance as the wave propagates and with frequency, peak acoustic pressure at the transducer face, the propagating medium and the degree of focussing (Preston, 1983). Examination of the pulses transmitted by the Mirror System and by the transducers described in Chapter 5, however, showed no indications of these non-linear effects. This was the case even when the 20 cm co-axial cable of the hydrophone was input directly to the 25 MHz y-amplifier of the Tektronics oscilloscope. This may be due to a combination of factors. The transducers were found to be slightly insensitive. This may indicate a lower than usual peak acoustic pressure at the surface. The transducers also responded badly to high power transmitter pulses giving very distorted output pulses for electro-mechanical reasons. In the case of the mirror system the pressure from a small transducer is spread over a large area, usually about 56 times greater than the transducer surface. This will result in a low peak acoustic pressure across the mirror. This is coupled with very sharp focussing which will lead to significant pressures existing only in the focal region. This may not be long enough to form shock waves. The pulse shape changes markedly with axial position. This effect might conceal developing non-linear effects.

7.4.5. Safety of highly focussed beams.

In discussion of the safe use of sharply focussed transducers the following points must be borne in mind:

a) The transmitter used in the breast scanner is a Nuclear Enterprises Ltd. (now G.L. Ultrasound Ltd.) circuit board as used in the Diasonograph scanner.

b) The receiving amplifier is likewise a circuit board used in the Diasonograph but it has been modified to give a small but useful increase in its gain. Hence the receiving sensitivity is actually better than that in the commercial scanner and so there is no requirement for increased power output because of poor receiving sensitivity.

The largest probe presently used has a 2 inch diameter active element focussed at 150 mm nominal range in water. Its nominal frequency is 5 MHz.

Carson et al (1978) studied a number of commercial pulse-echo scanners and found a typical intensity at the probe face of 3 mW cm^{-2} (temporal average). Figures measured by Fischer Ultrasound using one of their probes and their transmitter circuit indicate a similar value. These measurements relate to pulse repetition frequencies (p.r.f.) of 1000 Hz, whereas at the scanning speeds used in the breast scanner a p.r.f. of about 330 Hz is adequate. Therefore, a reasonable figure to assume for the temporal average intensity at the transducer face is 1 mW cm^{-2}.

Applying this to the largest probe described in chapter 5 gives an ultrasonic intensity at the focus of 537 mW cm^{-2}.

This figure is likely to an overestimate because the transducer relies for its focussing on a lens attached to its front face. In order to avoid troublesome reverberations, this lens must be made of an attenuating material, so that the assumed intensity of 1 mW cm^{-2} at probe face is almost certainly an overestimate.

Furthermore, the calculation above applies in water. In the application of the transducer to the breast, its focus will lie at a depth of typically 4 cm below the skin. The attenuation of normal breast tissue at 5 MHz is of the order of 3 dB cm^{-1} so that there is a total attenuation of typically 12 dB or a factor of 16. This reduces the intensity at the focus to around 34 mW cm^{-2}.

Now comparing these figures with the recommendations of the A.I.U.M. Bio-Effects Committee (1976). These state that there have been no demonstrated significant effects in mammalian tissues exposed to intensities below 100 mW cm^{-2}. Furthermore, for ultrasonic exposure times less than 500s and greater than 1 s, such effects have not been demonstrated even at higher intensities, when the product of intensity and exposure time is less than 50 J cm^{-2}.

According to this criterion, the estimated intensity when the probe is focussed within the breast is well within the accepted safe limits.

Even if the probe were accidentally focussed at the skin, an exposure time of 93 s, would be required before the possibility of hazard arose. As scanning is normally carried out continuously, the likelihood of the probe remaining stationary and focussed at the skin for this length of time is remote.

The Cassegrain Mirror system is driven by a transducer at most 13 mm in diameter, so that the total power is less by a factor of about 15 than in the foregoing calculations. Also there are losses in the reflections at the mirrors. Therefore, despite the sharper focus, the intensity at the focus is considerably less than the limiting value computed above for the directly focussed transducer. Indeed comparison of the peak pulse seen by the hydrophone for the transducer alone (figure 6.11) and for the mirror system (figure 7.24 (b)) shows the mirror system peak pressure some 7 dB less. (Transmitter -10 dB; copper primary; Tungsten; epoxy secondary;MD 3500 probe).

7.4.6. Comparison of Theoretical and Experimental Plots

Figure 7.28 shows both experimental and theoretical transverse beam shapes. Experimental half-widths were obtained by halving the full

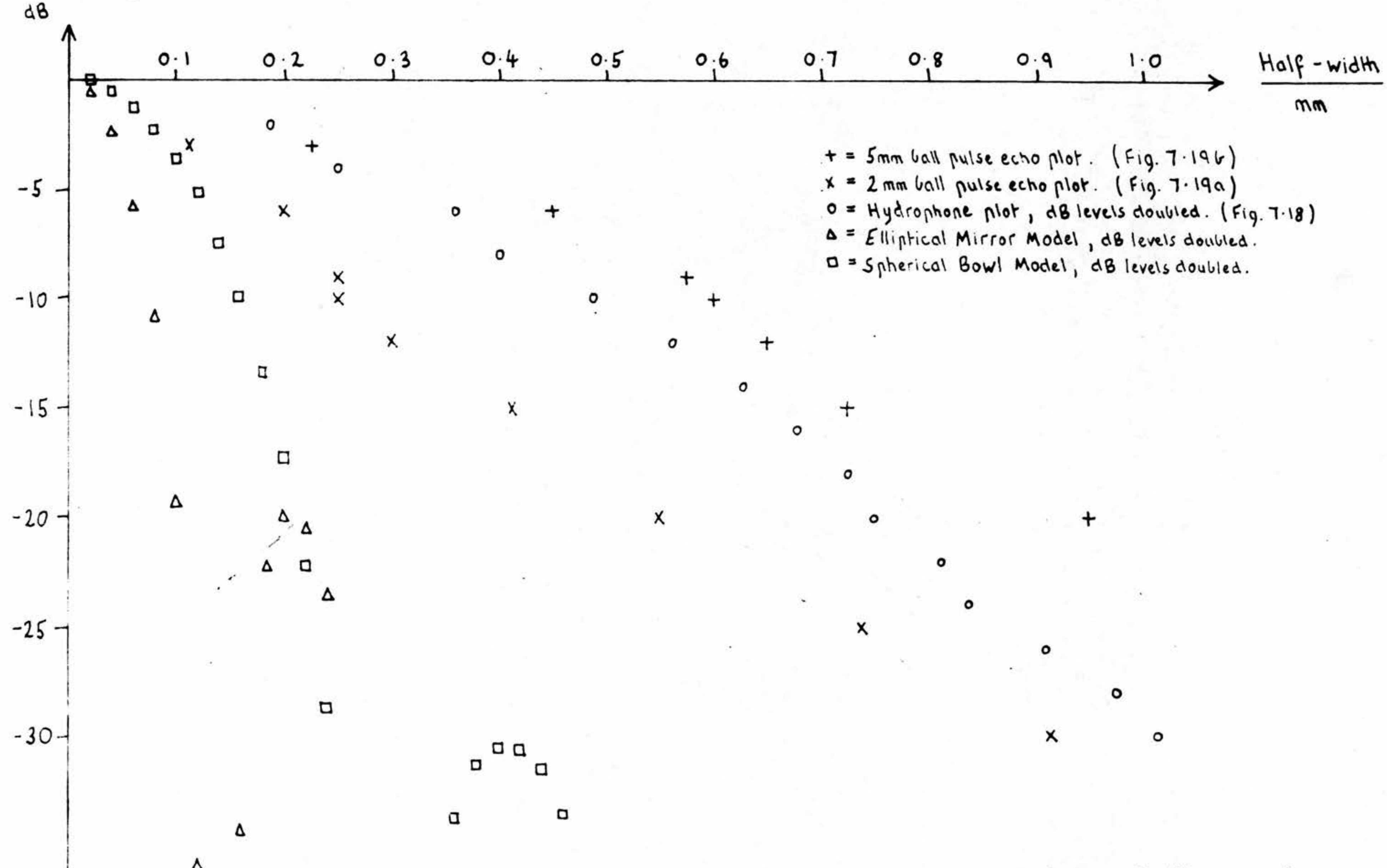

Figure 7.28. Theoretical and experimental beam shapes for the 5MHz Cassegrain Mirror system.

width and ignoring any asymmetry. The theoretical and hydrophone plots are compared to the pulse-echo field by squaring the amplitude (i.e. doubling the decibel level).

As predicted from the comparison of CW and PW models of small bowls (see sections 2.3 and 3.5) the experimental (PW) field is flatter topped than the CW models predict. The experimental results show that a smaller target resolves the beam shape better. The relative sizes of the beam and of the target suggest the true beam shape is still not being seen. The experiments of section 5.2 suggest that the experimental beam widths may differ from PW theory by a factor of 2.2 at the -10dB level. Weyn's (1980b) results suggest that the difference between CW and PW models may be a factor of 1.35. Thus the difference in -10dB beam width between the ellipsoidal mirror model and the 2 mm target pulse:echo plot (a factor of 3.1) might be expalined by the combination of these two factors (3.0). In practice, although the ellipsoidal model demonstrates the apodisation effects which will occur in practical mirror systems which must be based on conic sections, it will over estimate the resolution possible since, because the geometry is simplified and the transducer and secondary modelled as a point source, spherical aberration due to the axial distribution of the source is omitted from this field. In addition imperfect construction and alignment of the mirrors will broaden the beam. The side lobes are smoothed out in the experimental plot but how much of this effect is due to the PW field departing from the CW model and how much to the plotting target is not known. The differences due to the incomplete modelling of the mirror geometry and to the lack of a small enough plotting target are greater than those due to the use of a CW model.

7.5. Imaging

Images were produced with the Cassegrain mirror system by simple B-scanning, using the breast scanner. Figure 7.29 shows the wire target used for aligning the mirrors. The 'ghost' images are clearly demonstrated. It was generated by a single horizontal scan.

The system was reasonably manoeuvreable in practice. Alignment was stable. Anchoring the system to the tank floor proved satisfactory for horizontal scanning but the vertical motion, by raising and lowering the patient couch was clumsy and unworkable. A small jack was designed to fit in the tank and position the focus by raising and lowering the mirror.

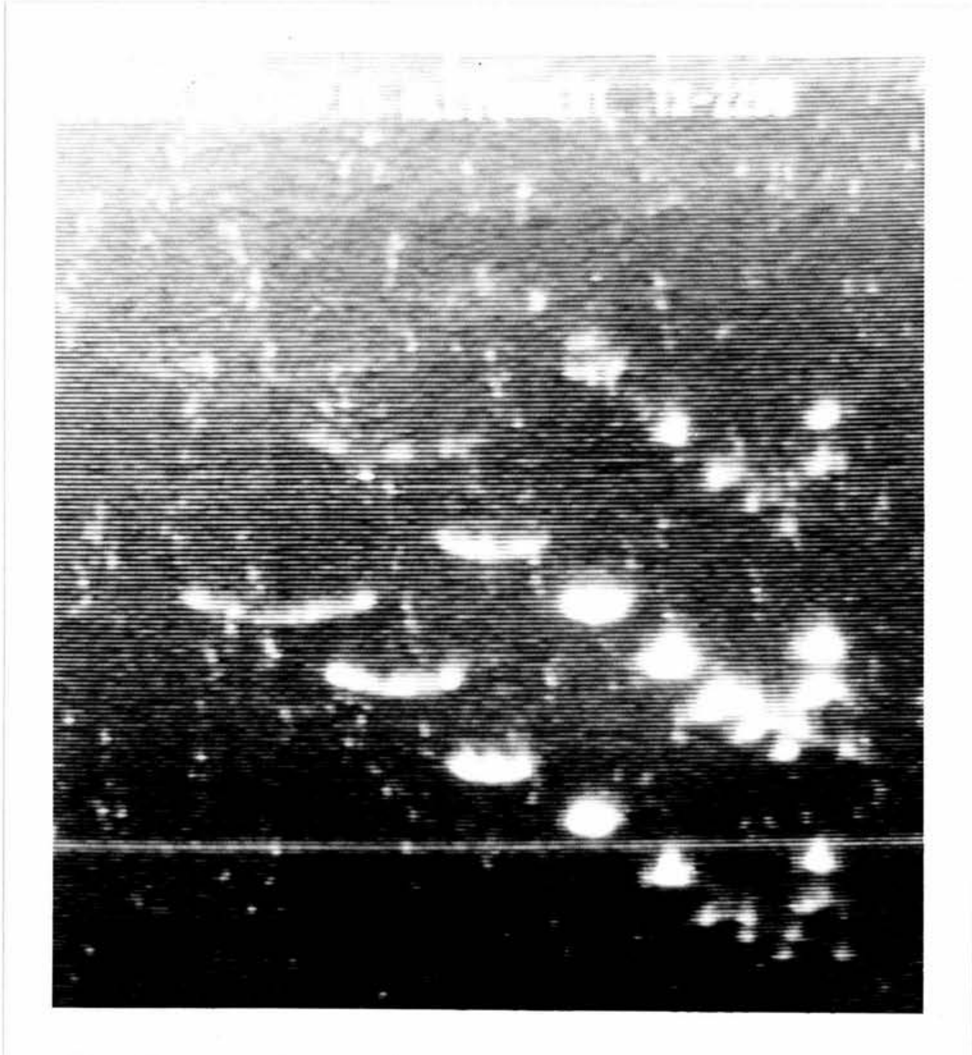

Figure 7.29: Image of a multiple wire target (in the shape of a single tick) using the Cassegrain mirror system and showing several 'ghosts' due reverberations between mirror elements.

7.6. Conclusions.

i) Highly focussed ultrasound beams can be achieved using mirror systems.

ii) A sufficient dynamic range for scanning small regions of interest can be achieved.

iii) The use of air-backed thin copper reflectors results in minimum distortion to the pulse shape and low losses in reflection. This results in a system sensitive enough to be used in transmission and reception; producing a short pulse with consequent good axial resolution. Figure 7.24(b)

iv) Thin air-backed copper mirrors can be manufactured even for quite deep mirrors. These are robust and do not distort or relax towards their former shape even over long periods.

v) A focussed transducer should be used to ensure that the beam is blocked completely by the secondary. Alternative solutions, e.g. the use of a smaller transducer or the addition of absorbing material around the secondary are less satisfactory since they reduce sensitivity or increase apodisation.

vi) Although the performance is degraded by apodisation, due to the secondary mirror blocking the centre of the aperture, side lobes can be maintained at an acceptable level for imaging small regions of interest.

vii) The numerical models have proved useful for predicting the effects of variations in the field across the aperture. The spherical bowl model (PLOTBCW) predicts the general performance of large numerical apertures with central blocks. In practice a mirror system will employ conic mirrors and PLOTCW demonstrates the effect on field parameters of an ellipsoid primary which will concentrate flux lines towards the outer rim of the aperture.

viii) Variation between theoretical and experimental fields can be attributed to the limitations of both the models as well as to imperfect construction or alignment of the mirrors. The main limitation of the numerical models is that even the more sophisticated (PLOTCW) does not include a complete description of the mirror system geometry. The use of a point source in place of the transducer and secondary reflector means that the axial (and lateral) distribution of sound about the internal reference point of the primary reflector is omitted. The effects of this, particularly the introduction of spherical aberration, are thus not seen in the numerical model. These effects are practically important. The field predicted by PLOTCW, free of on-axis aberration (i.e. spherical aberration) would not be useful for B-scanning because of the very short focal length. The main limitation of the experimental plotting is the lack of a small enough spherical target to examine these very small focal zones.

ix) The Cassegrain design is unsuitable for an imaging transducer. This is because of reverberations between components giving rise to spurious echoes. This occurs principally between the transducer and the secondary. The use of a tungsten:epoxy secondary reduced this but also reduced sensitivity. Attempts at further reduction by drilling out the centre of the secondary or by placing absorbing material on its apex and around the transducer were only partially successful. For a mirror system to be practical, a design must be sought which would not give rise to these reverberations. Such a design would be based upon a pointed secondary mirror.

CHAPTER 8. A MODIFIED CASSEGRAIN MIRROR SYSTEM

Introduction

The studies of the Cassegrain Mirror system indicate potential for such a system if the problem of reverberations between components could be overcome. Particularly a system employing a pointed secondary would not suffer from reverberations between it and the transducer. The Cassegrain configuration was modified to meet this criterion.

8.1. Initial Design

8.1.1. The Modification

The basic modification to the Cassegrain is the moving of the common reference point from the system axis. The development of the geometry is shown in figure 8.1. Figure 8.1(a) shows a half-section through the system with the outer ray shown. This ray is initially aimed at F, but is redirected by reflection from the secondary and then the primary to cross the axis at F_3. As described before, this may be achieved if F_1 and F_3 are the external reference points of two ellipses sharing a common internal reference point, F_2. Such a situation is shown in figure 8.1(b). Unlike previously, the common reference point F_2 does not sit upon the system axis, that is the axis of the transducer field, which also passes through F_1 and F_3. The ellipses generated about F_1 and F_2, and F_2 and F_3 have therefore their major axis tilted relative to the system axis. Both the ellipses therefore, but importantly the secondary, will cross the system axis at an acute angle. Circular symmetry is introduced by rotating the half section shown in figure 8.1(b) about the system axis. The result is shown in figure 8.1(c) and with inner and outer rays in figure 8.2.

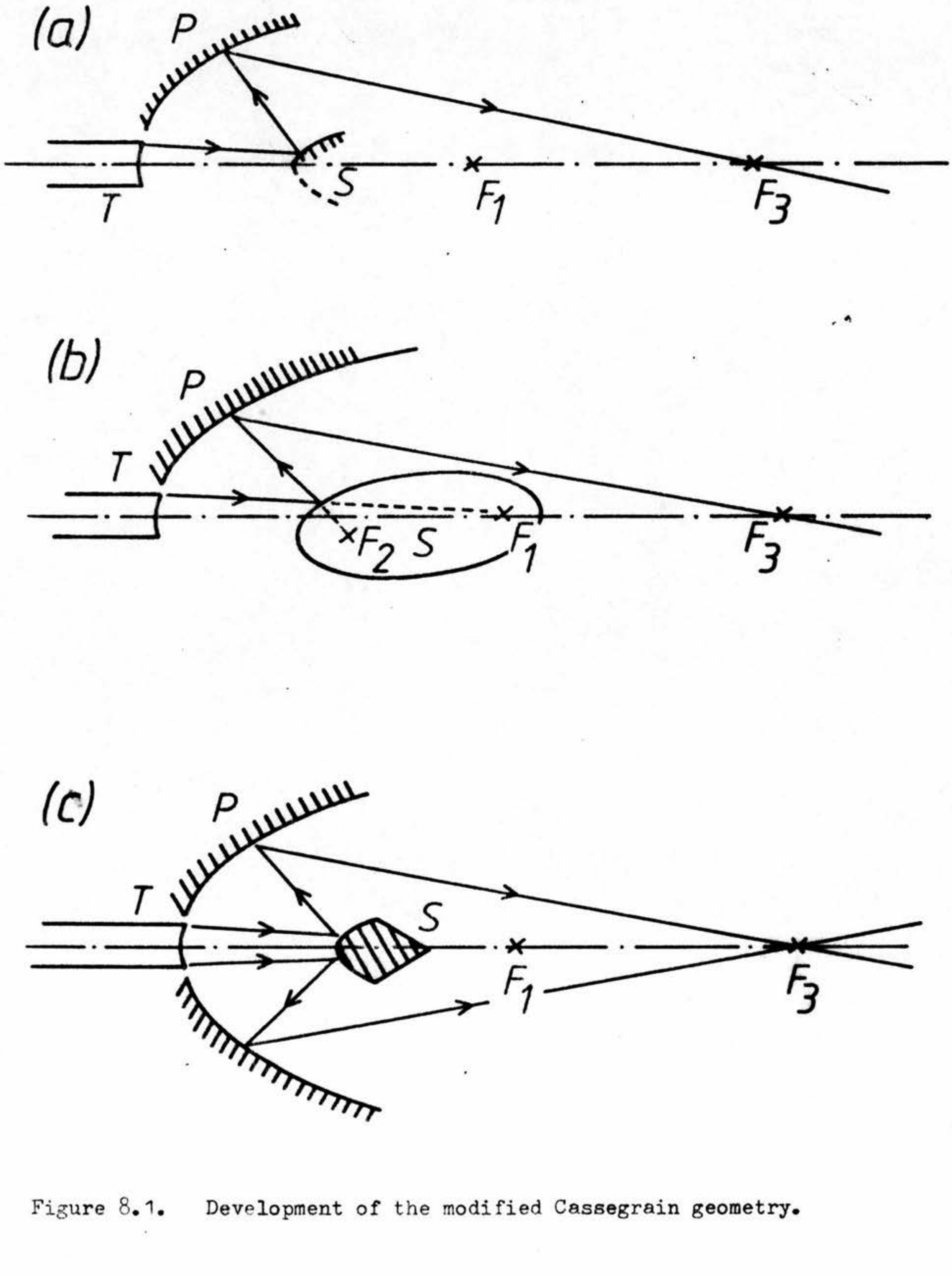

Figure 8.1. Development of the modified Cassegrain geometry.

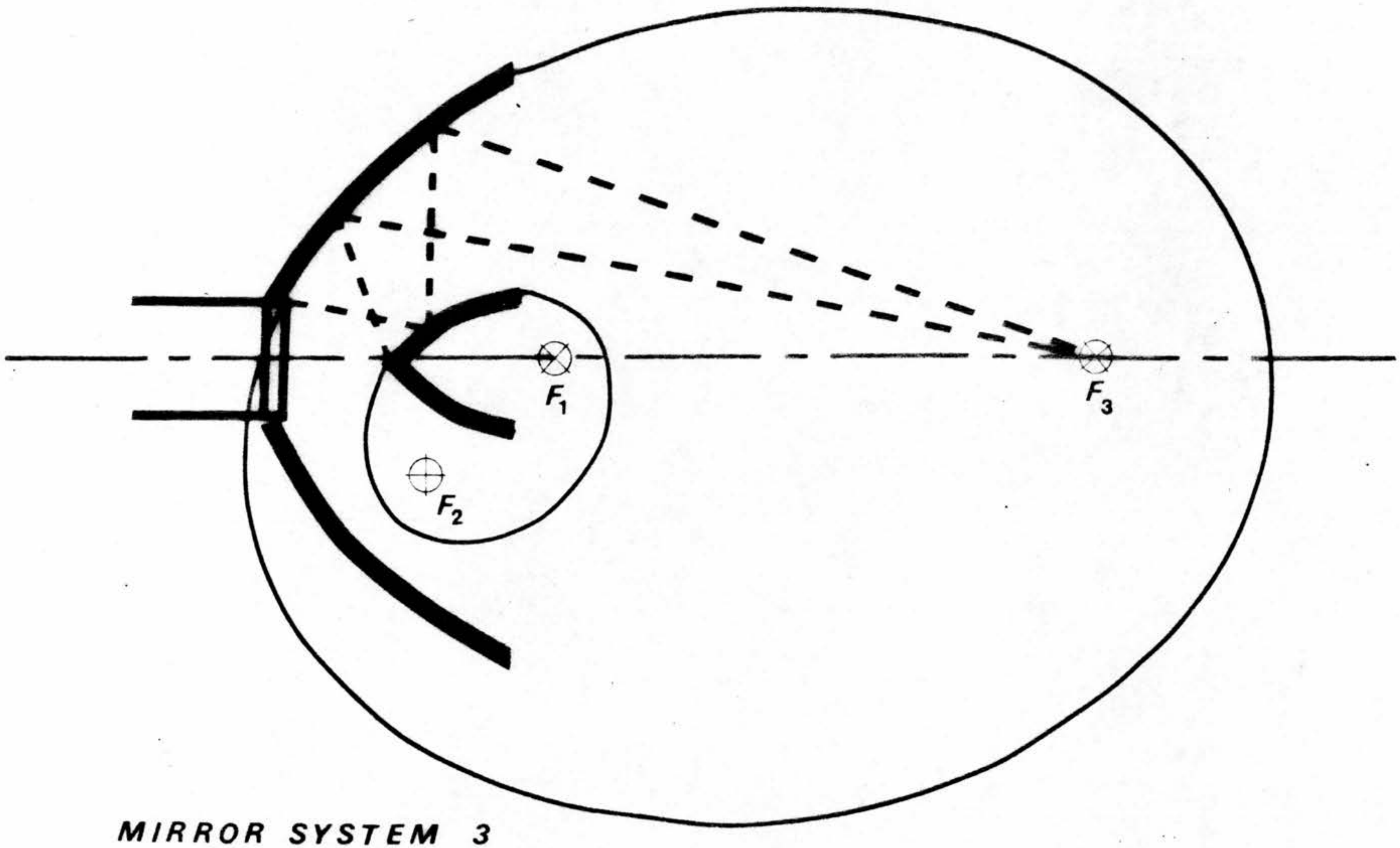

Figure 8.2. Schematic diagram of the modified Cassegrain Mirror design for a system focussing on transmission and reception with a focussed transducer.

8.1.2. Initial Design Parameters.

Practical experience with the earlier mirror was used to guide the selecting of parameters.

An effective focal length that is the distance from the transducer to the field maximum of 150 mm was chosen. This would place the focus 80 → 100 mm beyond the back of the secondary mirror and its mount.

An aperture diameter approximately 90 mm (by ray tracing) would be sought however the actual primary mirror surface would be extended to a diameter of approximately 110 mm to allow for the imperfect model of the transducer field.

The mirror surfaces required for such a device were determined by using the design program and ray tracing on the output. The result is shown in figure 8.3(a) and with inner and outer rays traced in figure 8.3(b).

The Primary Mirror is developed from an ellipse with a distance of 120 mm between the reference points. The common reference point is displaced 2.8 mm from the system axis. The semi-major axis is 91.6 mm. The aperture in the plane of F_2, the common reference point, is 104 mm diameter.

The Secondary Mirror is developed from an ellipse with 30 mm between reference points. The semi-major axis is 19.3 mm. It will spread the outer rays shown in figure 8.3(b) to a diameter of 88 mm, the inner to a diameter of 30 mm. This will adequately clear a secondary surface extended beyond the latus rectum and of sufficient thickness to absorb any unreflected signal.

8.1.3. A Reception only Mirror

An Olofsson style system was designed using the same primary. The secondary is based on a hyperbola with its external reference point

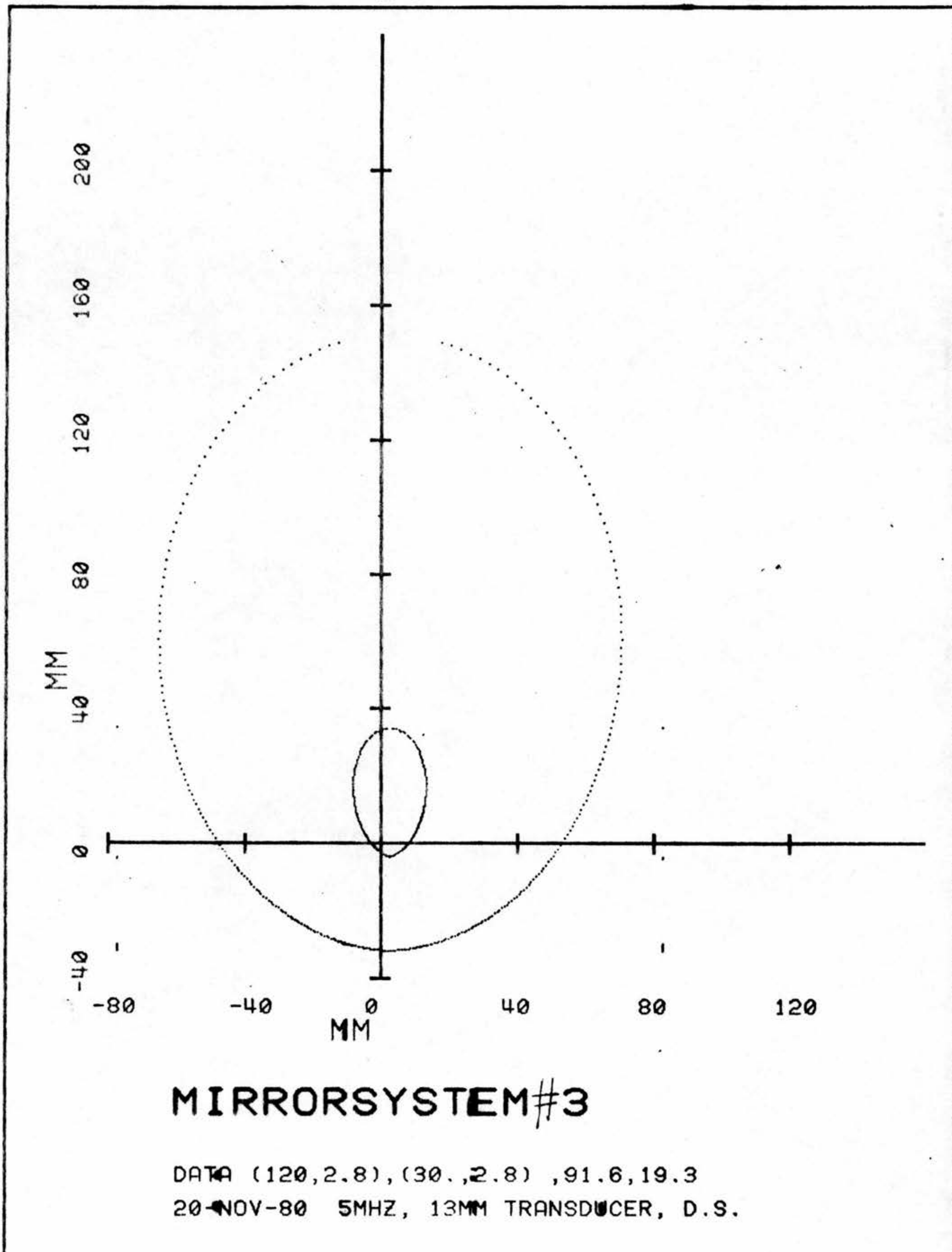

Figure 8.3(a). Design program output for modified Cassegrain system.

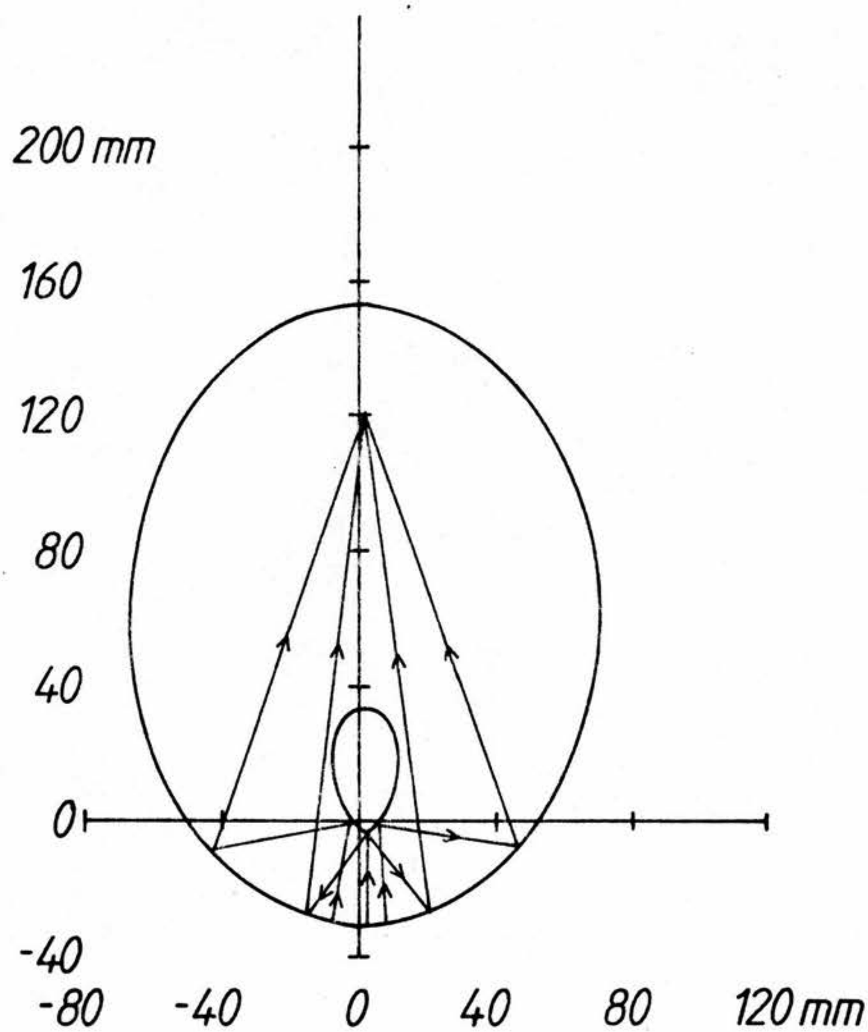

Figure 8.3(b). Final design of modified Cassegrain System. Common Reference Point 2.8 mm off-axis.

at the centre of the transducer surface. The hyperbola parameters were chosen to give the same diameter in the plane of the common reference as the ellipse based secondary. This means a distance of 30 mm between reference points and a 'semi-major axis' of -12.3 mm. The design output is shown in figure 8.4. Again the secondary surface is pointed.

8.2. Investigation of Parameters with Numerical Models.

Neither of the numerical models described in chapters 3 and 4 are able to model the modified geometry. PLOTCW permits the source to be moved only along the system axis. It would require modification to model the virtual ring focus which represents, F_2 in the design. Such a model would still idealise the representation of the transducer field and the secondary mirror. An accurate CW model would have to include a description of the secondary and of the transducer. The absence of this and the resultant spherical aberration from the calculated field is more significant to the result than the off-setting of the common reference point.

Once more both the spherical bowl and the ellipsoidal mirror models were used to describe the system. The desired focal length was investigated for outer diameters of 88 mm and 104 mm. 88 mm is the result of ray tracing; 104 mm of considering the secondary to spread the beam to a hemisphere.

Both models will help to understand the field. The spherical bowl will give the result of a uniform field converging from such an aperture. The elliptical mirror gives the more apodised field from an elliptical reflector where the field will be concentrated towards the outer edge, resulting in increased side lobes.

Even though the beam will be spread beyond the idealised limits derived from ray tracing, the resulting field across the aperture will not be the perfect distributions predicted by the models.

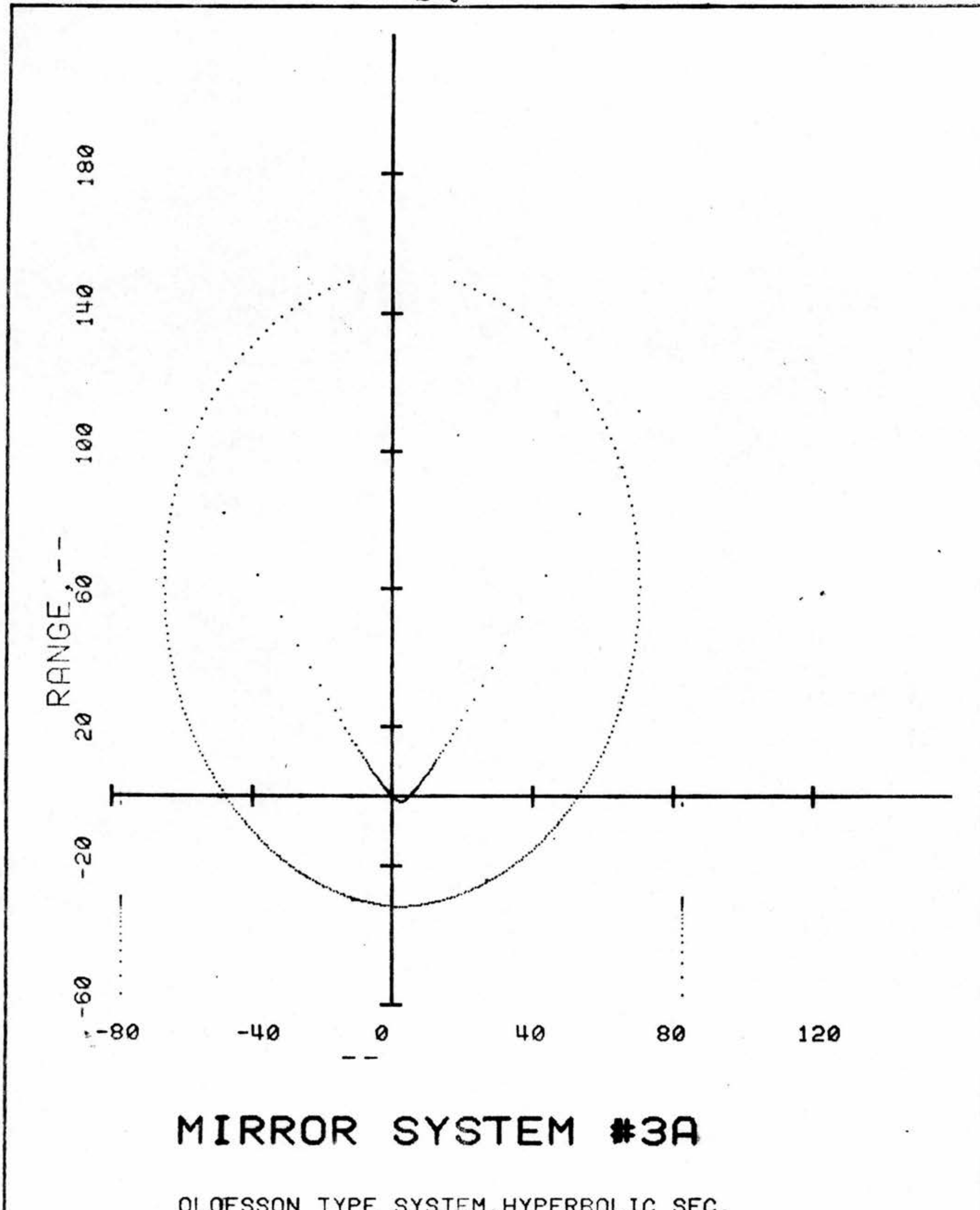

Figure 8.4. Design output for a reception only mirror.

8.2.1. The Spherical Bowl Model (PLOTBCW).

The behaviour of the model of a 88 mm diameter bowl with an increasingly large centre stop is given in Table 8.1 and shown graphically in figure 8.5 and 8.6. A 104 mm diameter bowl is shown similarly in Tables 8.2 and figures 8.7 and 8.8.

The smaller bowl's focal zone is about 15% wider and the sidelobes are only slightly more sensitive to an increasing centre stop due to the secondary.

If the idealised aperture developed from ray tracing (outer diameter = 88 mm - inner diameter 30 mm) is compared to a more realistic one (outer diameter 104 mm; inner diameter 25 mm) the difference is 14% in main lobe width and 1.85 dB in sidelobe amplitude (figure 8.9). These cases, as likely extremes, are considered again later.

An axial plot of the two outer diameters with the same apodisation is shown in figure 8.10. The 88 mm bowl gives a -12 dB (pulse-echo) focal depth of 8.7 mm; the 104 mm bowl gives 6.2 mm.

A field plot of the focal zone from PLOTCW using a spherical mirror is shown in figure 8.11.

The effect of increasing the inner diameter upon the peak pressure is shown in figure 8.12. The pressure decreases approximately with area.

8.2.2. The Ellipsoidal Mirror Model (PLOTCW).

The two sizes of aperture were also modelled by the ellipsoidal mirror. The results for the 88 mm diameter is given in Table 8.3 and graphically in figures 8.13 and 8.14. The 104 mm aperture is presented in Table 8.4 and figures 8.15 and 8.16.

As in Chapter 7 the ellipsoid model gives a much sharper focal spot and larger side lobes. The difference in main lobe width between the apertures is only 8%; in first side lobe amplitude 0.5 dB

Diameter of Apodising disc mm	Main lobe half-width mm					1st off-axis maximum	
	-3dB level	-5dB level	-6dB level	-10dB level	1st off-axis minimum	radius mm	height dB
0	0.265	0.335	0.363	0.448	0.265	0.84	-17.84
10	0.263	0.333	0.360	0.444	0.62	0.84	-16.5
20	0.258	0.325	0.352	0.433	0.60	0.84	-14.5
25	0.254	0.32	0.347	0.425	0.58	0.84	-13.5
30	0.250	0.315	0.340	0.417	0.56	0.82	-12.45
40	0.24	0.301	0.326	0.398	0.53	0.80	-10.7

Table 8.1. Behaviour of the spherical bowl model of the Modified Cassegrain System with an outer diameter of 88 mm.
Beam shape parameters.

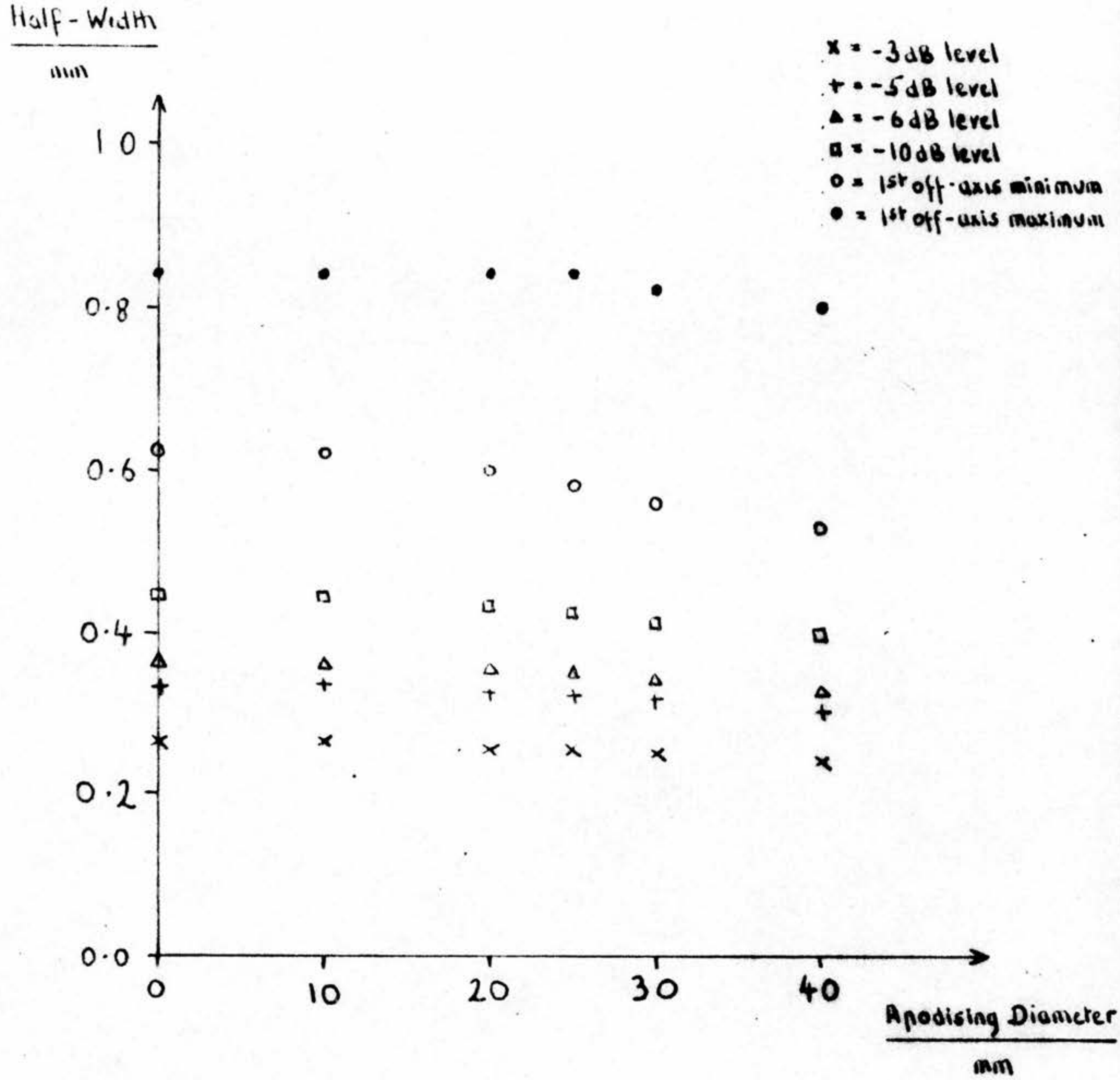

Figure 8.5: Effect of apodisation upon beam width using the spherical bowl model of the Modified Cassegrain System.
Outer diameter = 88 mm.

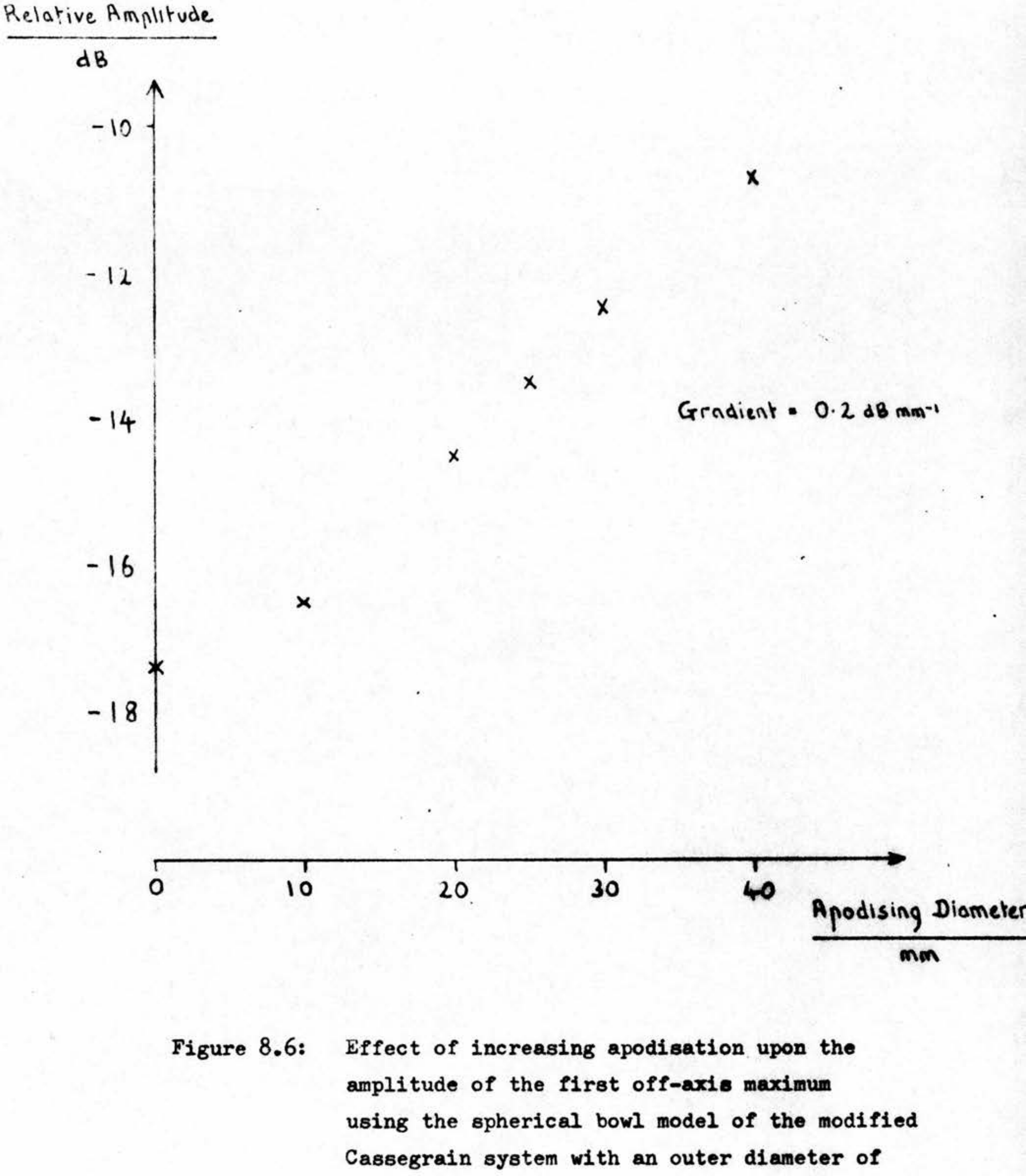

Figure 8.6: Effect of increasing apodisation upon the amplitude of the first off-axis maximum using the spherical bowl model of the modified Cassegrain system with an outer diameter of 88 mm.

Diameter of apodising disc mm	Main lobe half-width mm					1st off-axis maximum	
	-3dB level	-5dB level	-6dB level	-10dB level	1st off-axis mimimum	radius mm	amplitude dB
0	0.224	0.283	0.307	0.38	0.53	0.71	-17.3
10	0.223	0.282	0.305	0.376	0.52	0.71	-16.7
20	0.22	0.277	0.30	0.369	0.51	0.71	-15.2
25	0.217	0.274	0.297	0.365	0.50	0.71	-14.3
30	0.214	0.270	0.292	0.36	0.49	0.70	-13.4
40	0.208	0.262	0.283	0.346	0.465	0.69	-11.7

Table 8.2. Behaviour of the spherical bowl model of the modified Cassegrain system with an outer diameter of 104 mm. Beam shape parameters.

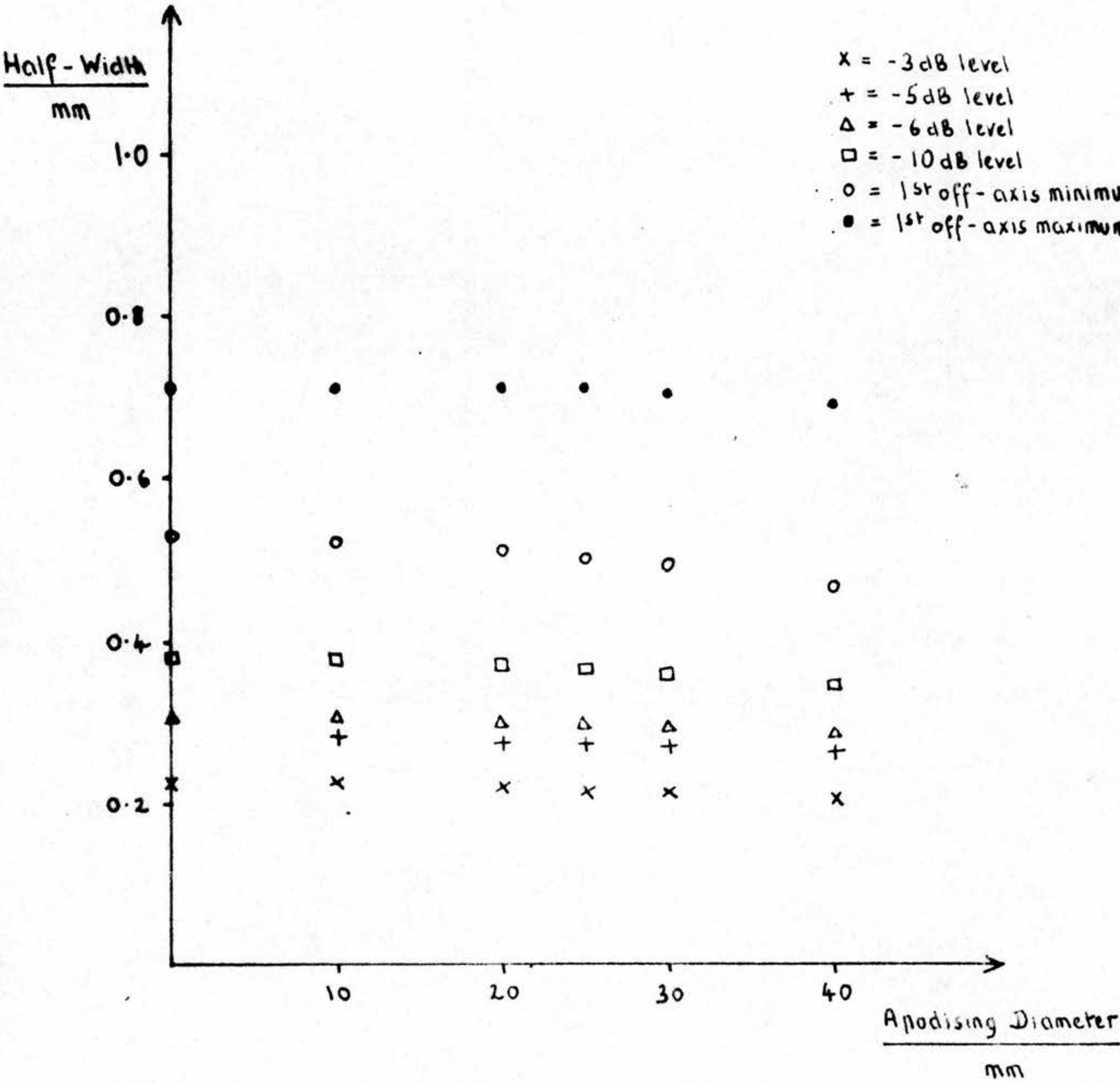

Figure 8.7: Effect of apodisation upon beam width using the spherical bowl model of the Modified Cassegrain System with outer Diameter = 104 mm.

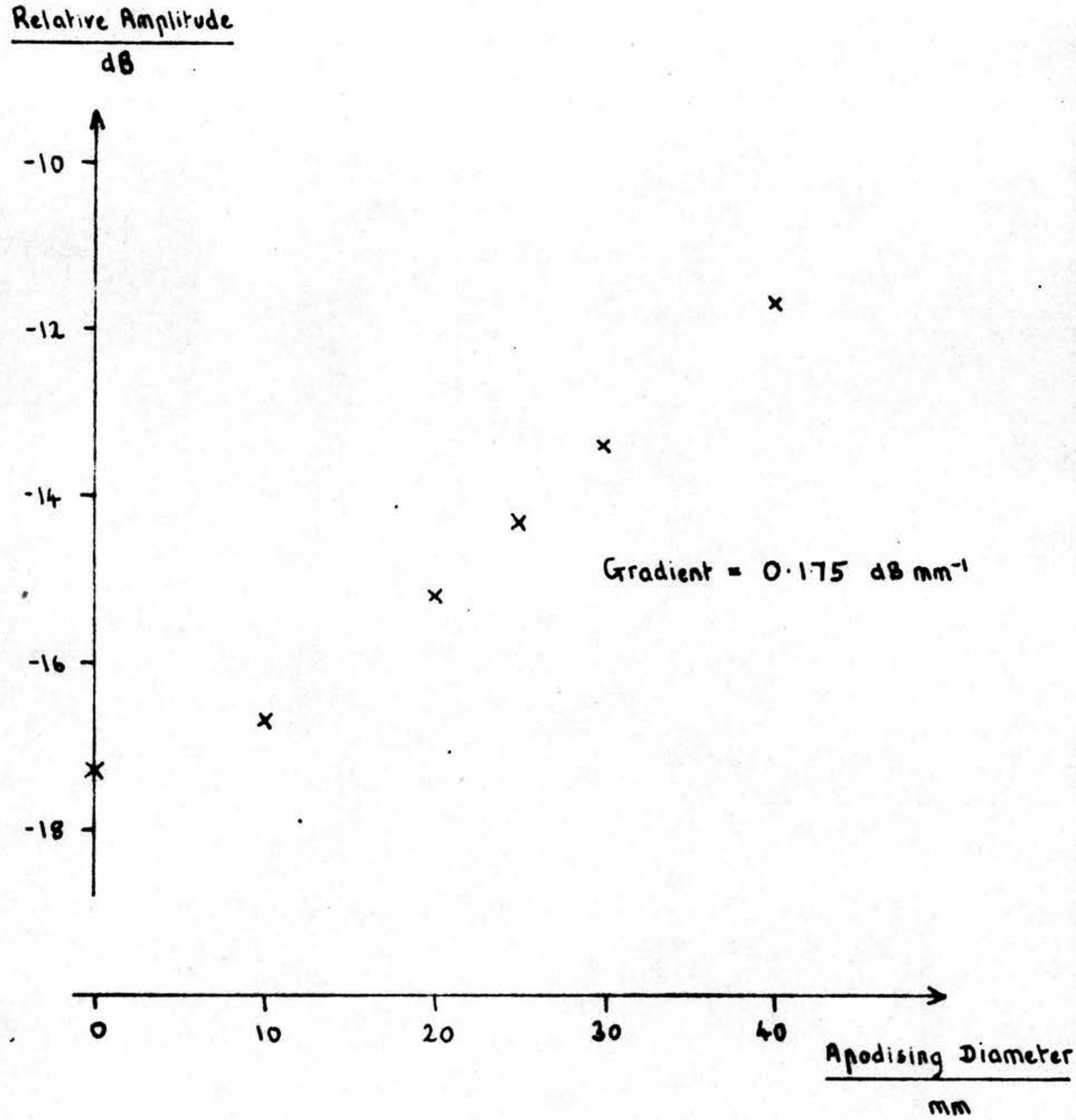

Figure 8.8: Effect of increasing apodisation upon the spherical bowl model of the modified Cassegrain System with an outer diameter of 104 mm.

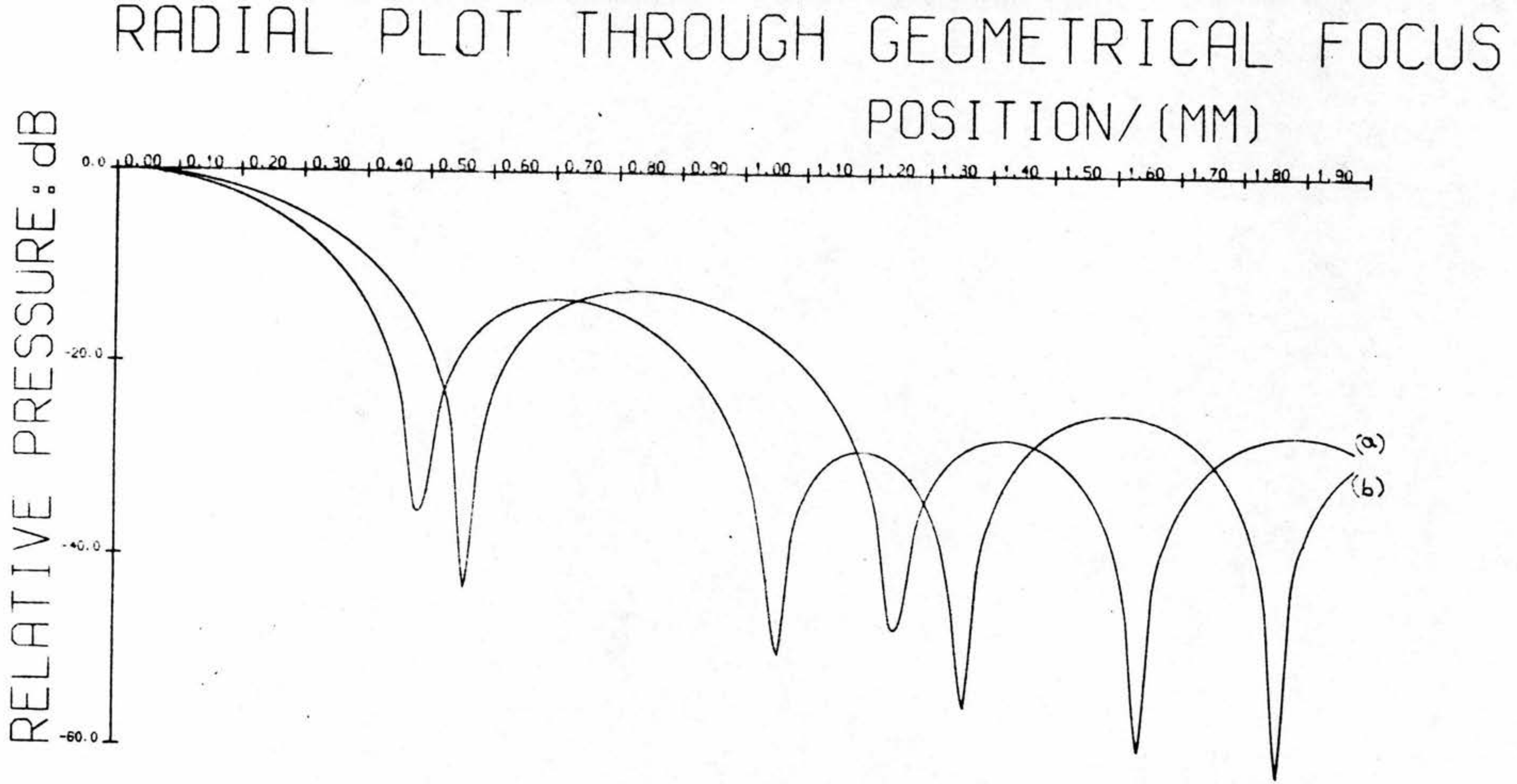

Figure 8.9. The Concave bowl fields from two apertures. (a) Outer diameter = 88mm: Inner diameter 30 mm.
(b) Outer diameter = 104mm: Inner diameter 25 mm.

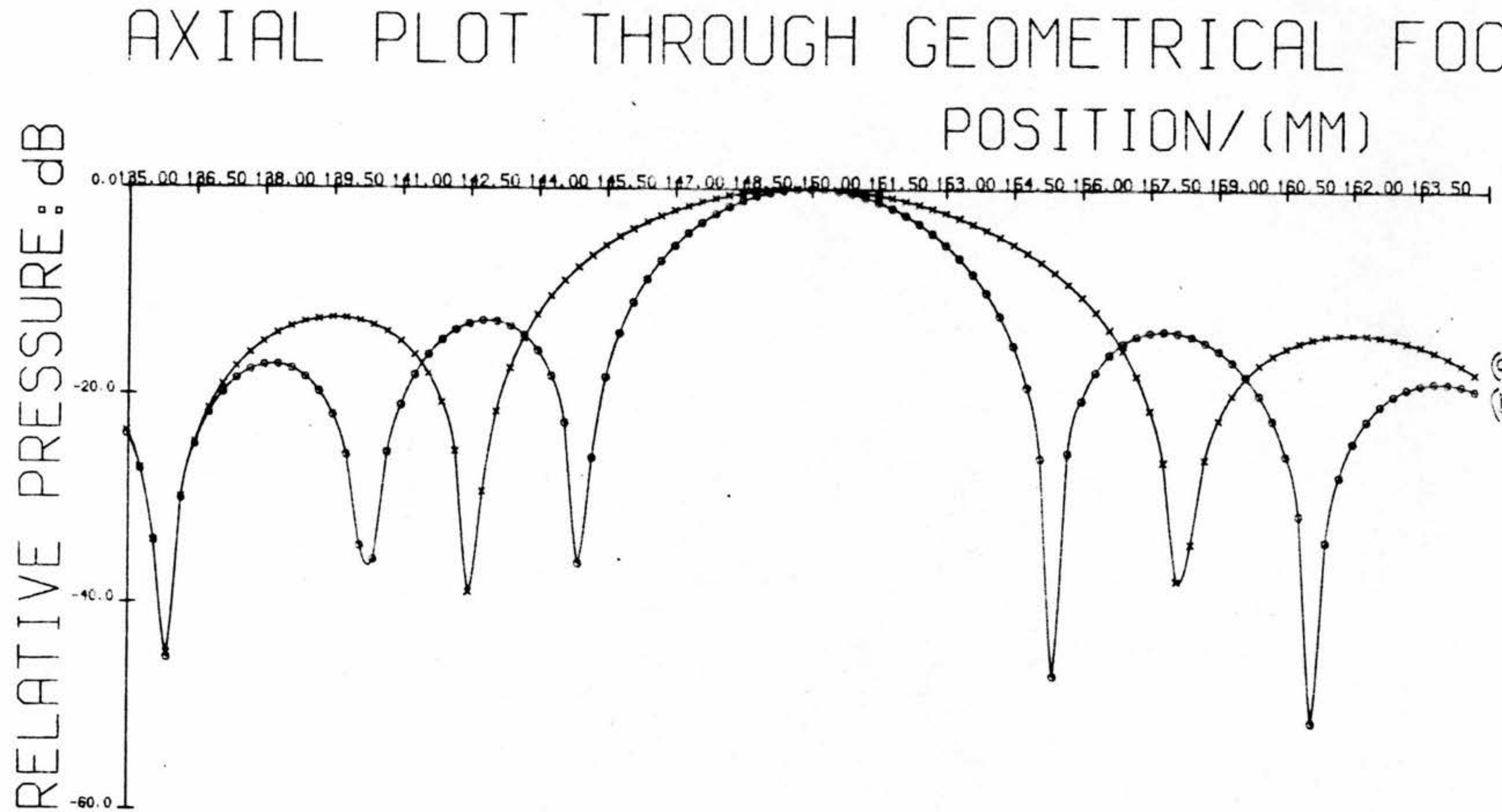

Figure 8.10. Axial plots for the concave bowl.

(a) Outer diameter 88 mm: Inner diameter 30 mm.

(b) Outer diameter 104 mm: Inner diameter 25 mm.

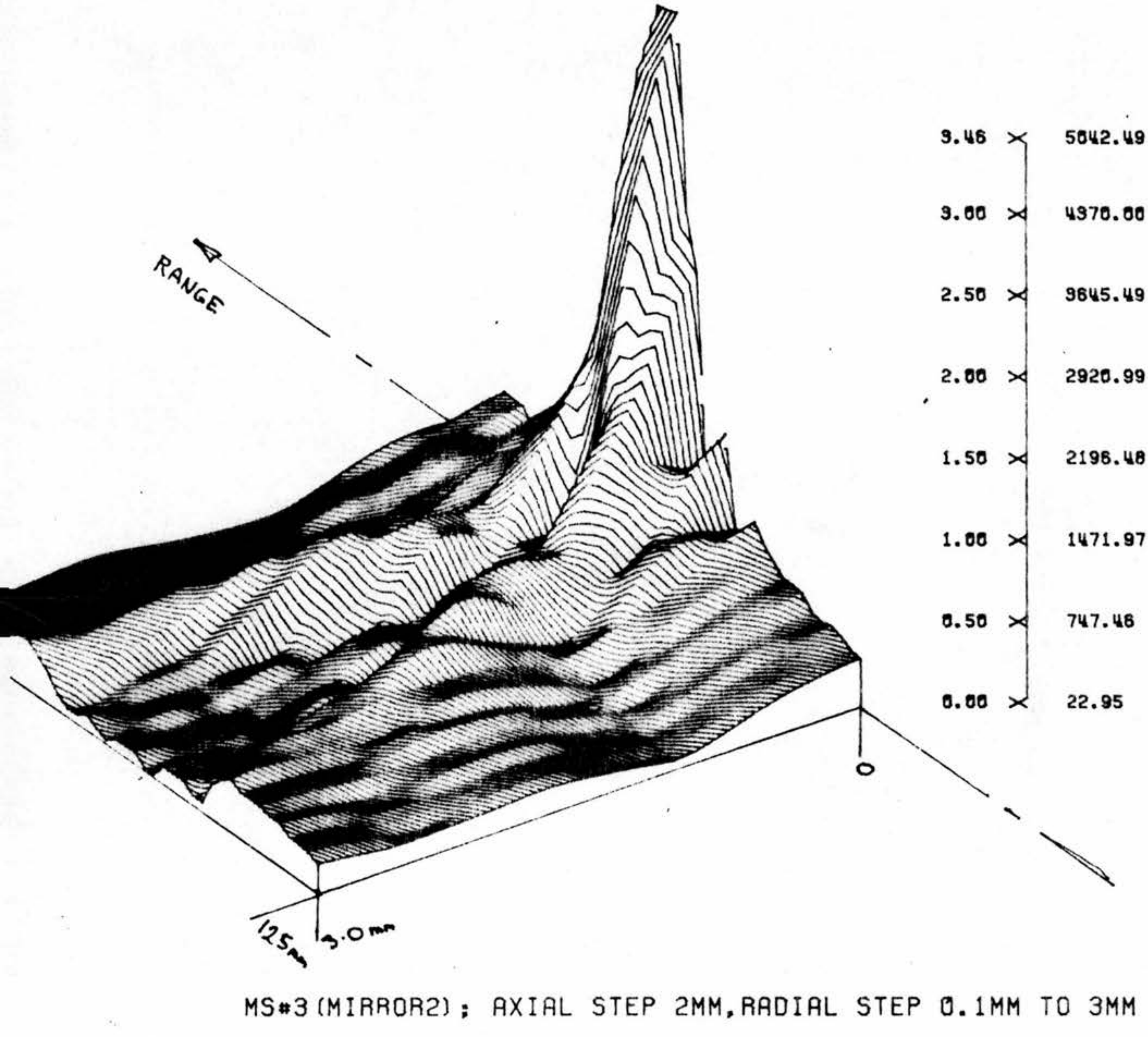

Figure 8.11. A concave spherical mirror model of the modified Cassegrain system plotted by PLOTCW.

Diameter of apodising disc mm	Main lobe half-width mm					1st off-axis maximum		2nd off-axis maximum	
	-3dB level	-5dB level	-6dB level	-10dB level	1st off-axis minimum	radius mm	Amplitude dB	radius mm	Amplitude dB
0	0.067	0.084	0.091	0.111	0.15	0.22	-11.7	0.39	-16.3
10	0.066	0.084	0.090	0.110	0.15	0.22	-11.4	0.39	-16.6
20	0.065	0.083	0.089	0.108	0.145	0.22	-10.5	0.39	-16.8
25	0.065	0.082	0.088	0.107	0.145	0.22	-10.05	0.39	-16.5
30	0.064	0.081	0.087	0.106	0.14	0.22	-9.6	0.39	-15.7
40	0.063	0.079	0.085	0.103	0.14	0.22	-8.9	0.39	-13.7

Table 8.3. Behaviour of the ellipsoidal bowl model of the modified Cassegrain system with an outer diameter of 88 mm. Beam shape parameters.

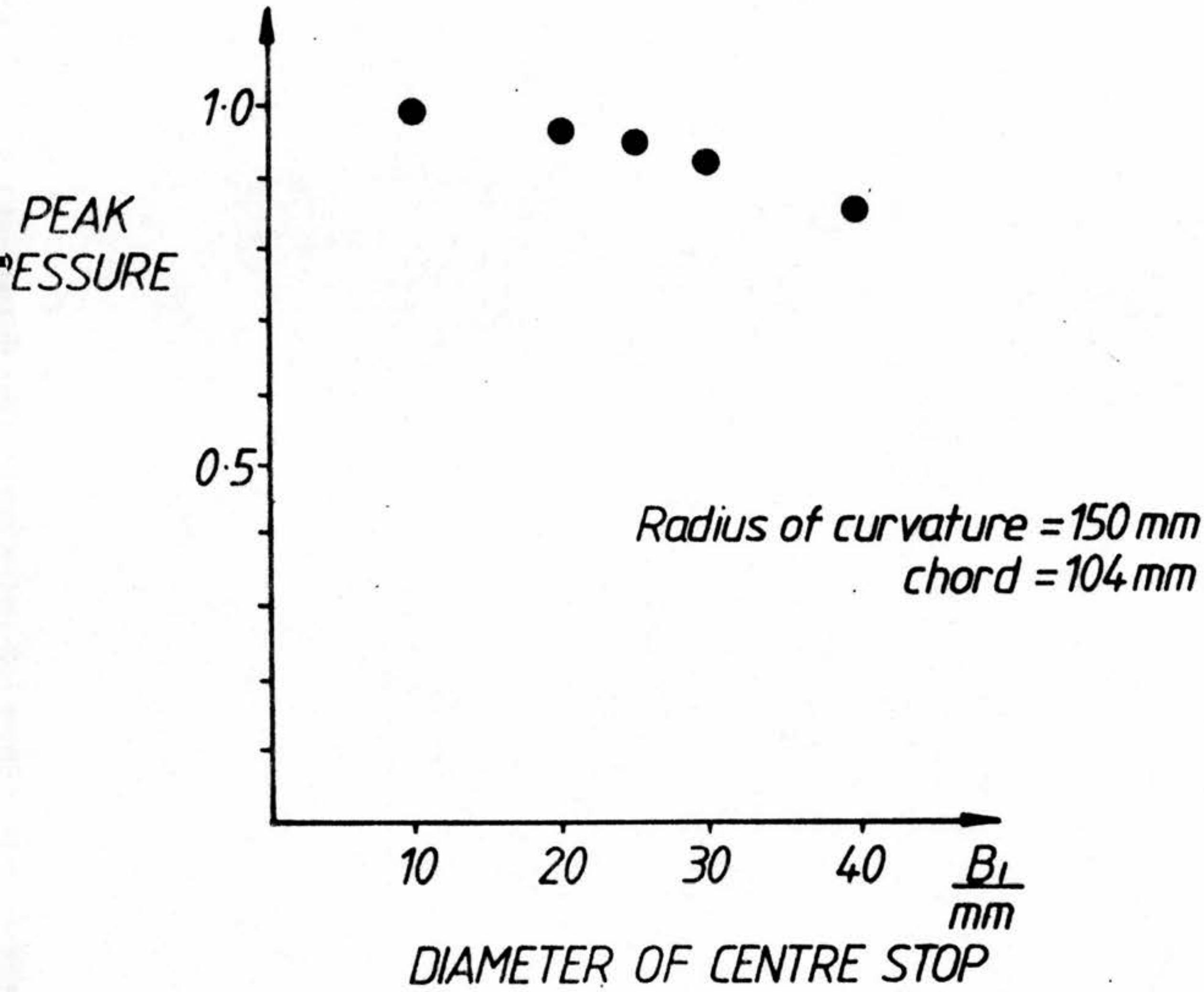

Figure 8.12. Effect of increasing size of centre stop on transmission field of concave bowl focussed at 150 mm.

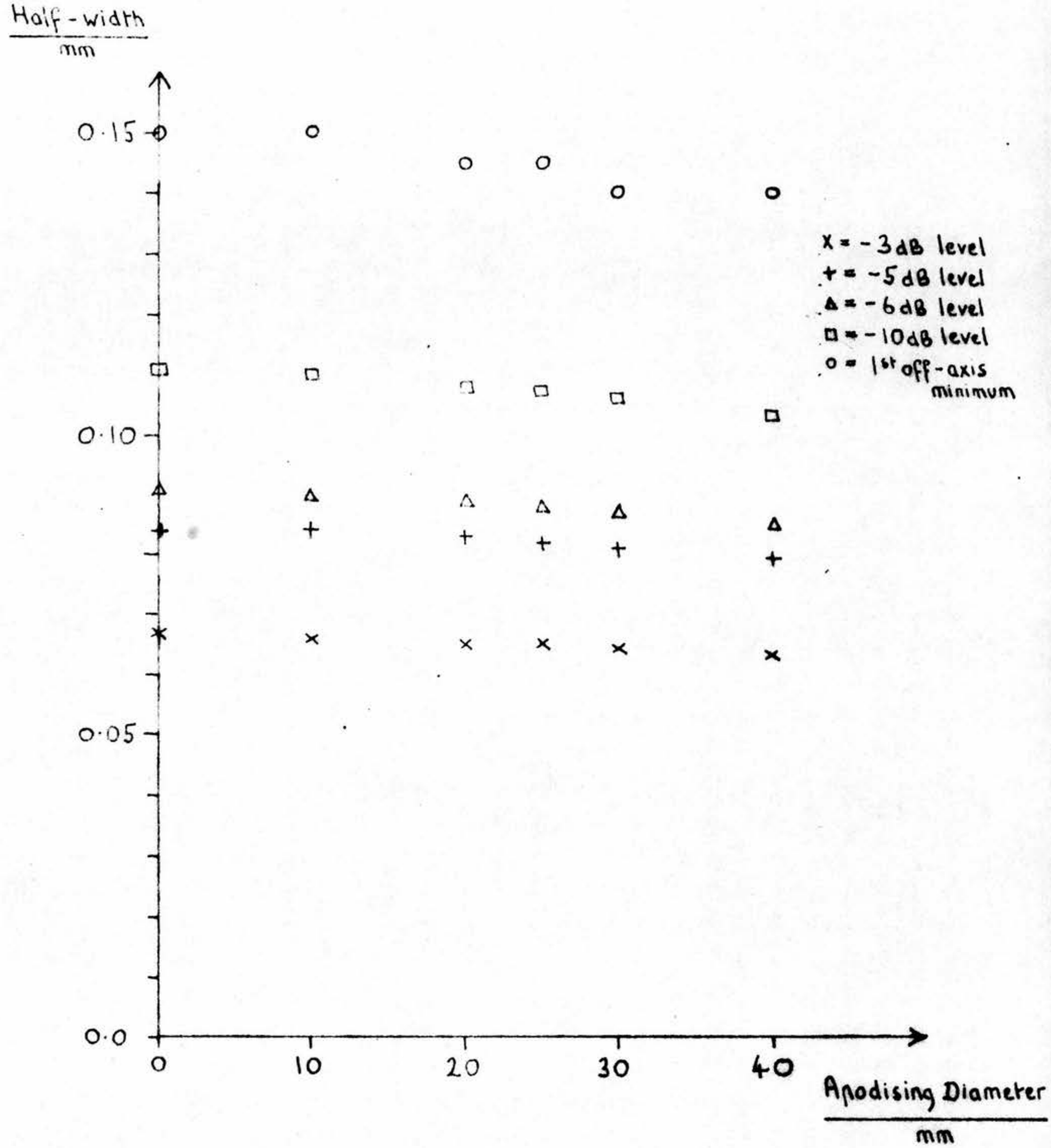

Figure 8.13: Effect of apodisation upon beam width using the elliptical mirror model of the modified Cassegrain system with outer diameter 88 mm.

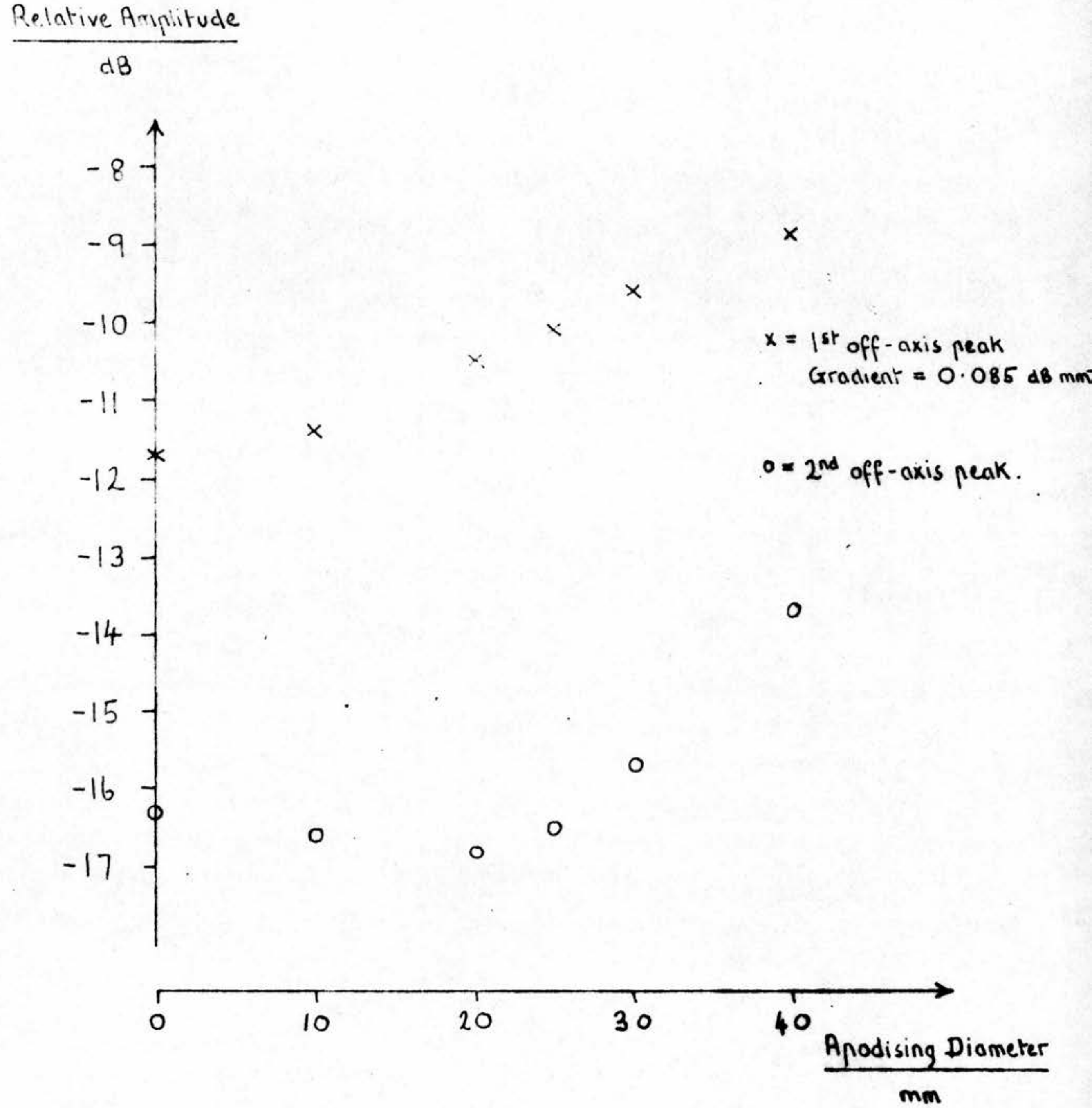

Figure 8.14: Effect of increasing apodisation upon the ellipsoidal mirror model of the modified Cassegrain system with an outer diameter of 88 mm.

Diameter of apodising disc mm	Main lobe half-width mm					1st off-axis maximum		2nd off-axis maximum	
	-3dB level	-5dB level	-6dB level	-10dB level	1st off-axis minimum	radius mm	Amplitude dB	radius mm	Amplitude dB
0	0.061	0.077	0.083	0.101	0.14	0.20	-10.4	0.365	-14.2
10	0.061	0.0764	0.0824	0.101	0.14	0.20	-10.3	0.36	-14.4
20	0.061	0.076	0.082	0.100	0.135	0.20	-9.8	0.36	-14.5
25	0.060	0.075	0.081	0.099	0.135	0.20	-9.5	0.365	-14.3
30	0.06	0.075	0.081	0.098	0.13	0.2	-9.2	0.365	-14.0
40	0.059	0.073	0.080	0.097	0.13	0.2	-8.7	0.365	-12.9

Table 8.4. Behaviour of the ellipsoidal bowl model of the modified Cassegrain system with an outer diameter of 104 mm.
Beam shape parameters.

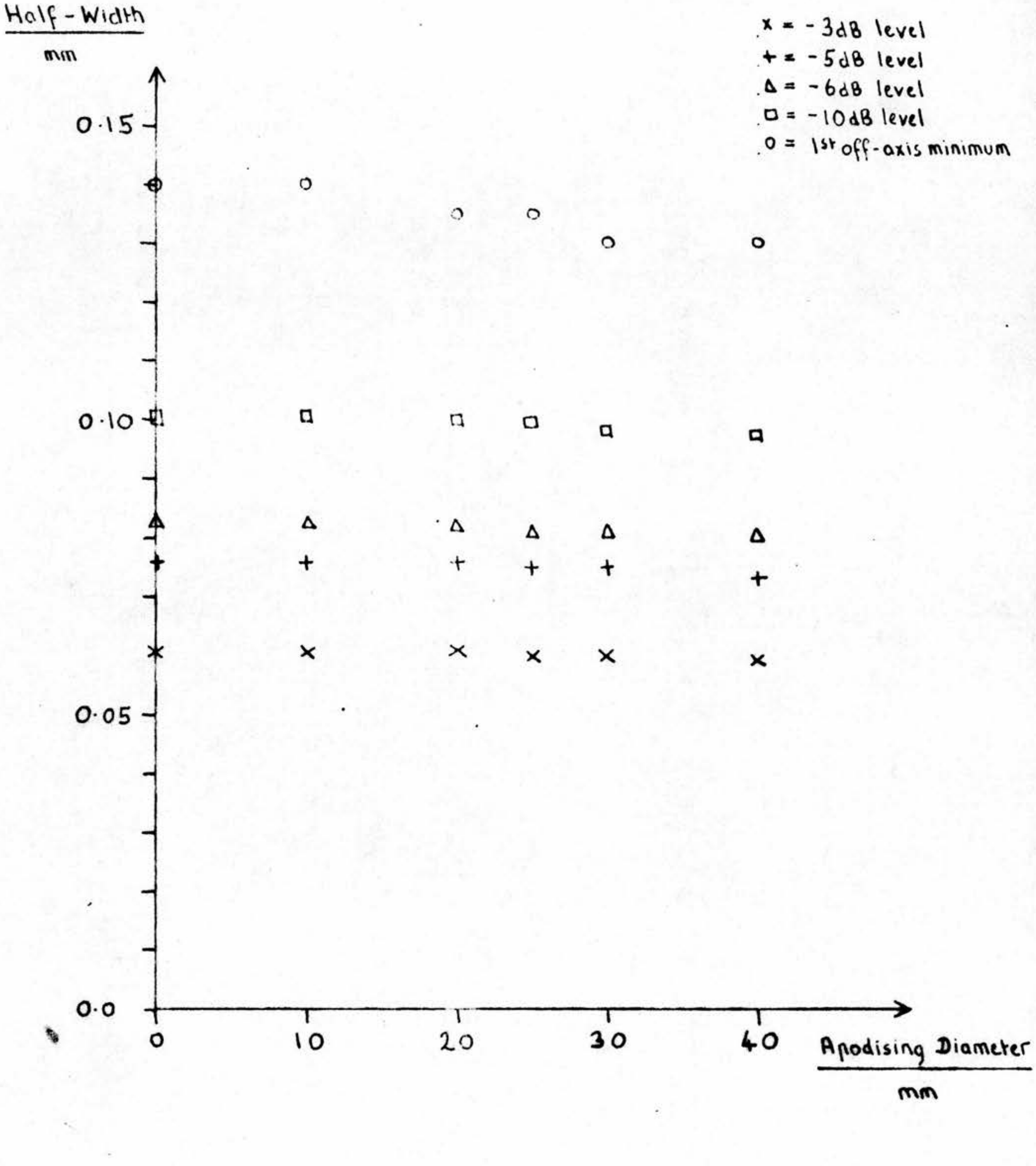

Figure 8.15: Effect of apodisation upon beam width using the elliptical mirror model of the modified Cassegrain system with outer diameter 104 mm.

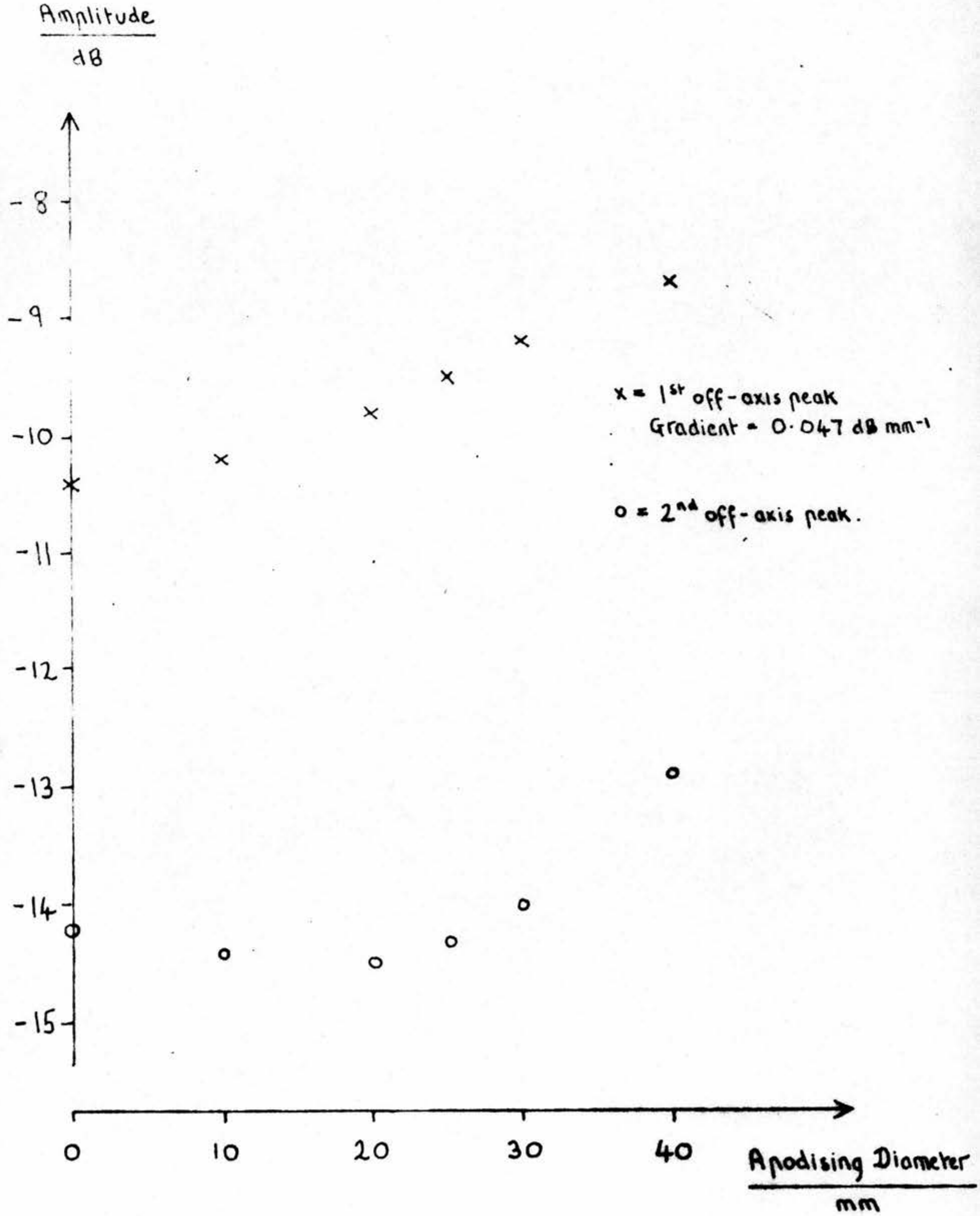

Figure 8.16: Effect of increasing apodisation upon the ellipsoidal mirror model of the modified Cassegrain system with an outer diameter of 104 mm.

and in second side lobe 2 dB.

Generally - for the same aperture dimensions - the smaller aperture has smaller first off-axis maxima but these increase more rapidly with increasing size of centre stop and above an inner diameter of 20 mm are comparable. With the very narrow main lobes and high first side lobes, the second side lobes become of interest. Their behaviour is distinctly non-linear, both apertures showing a minimum at inner diameter of 20 mm and then starting to increase quite rapidly. Again these lobes are smaller for the smaller aperture but increase more rapidly.

Comparing the same two apertures as in section 8.2.2. (88 to 30 mm and 104 to 25 mm diameters) (figure 8.17) the main lobe of the smaller bowl is 7% wider; the first side lobe is 0.1 dB larger, the second lobe 1.4 dB lower.

8.2.3. Discussion of Theoretical Results.

The models both predict an acceptable main lobe width. As expected for a device with a smaller numerical aperture than the Cassegrain Mirror discussed in Chapter 7, the difference between the two wavefronts modelled is greater. Interpreting the results in the light of Chapter 7, suggests a measurable lateral resolution of less than 1 mm. The side lobe however will be very close to the limit of what is considered acceptable, i.e., a 20 dB pulse-echo dynamic range at the focus. Kossoff et al (1976) gives the range of echoes from different tissues. Although he does not tabulate breast, the soft tissues nearly all fall within 20 dB range of each other.

8.3. Final Design and Manufacture.

The design was executed approximately as planned. The casing of the primary was made from 4½" diameter 12 gauge copper pipe, giving the reflecting surface an outer diameter of 112 mm. This mirror was more difficult to manufacture than previous designs, apparently because of the less rounded shape and slightly greater depth. This would seem to be near the limits of this manufacturing technique.

The secondary was moulded in tungsten:epoxy using the technique described in Chapter 6. This design could not be pressed in copper because of the pointed apex.

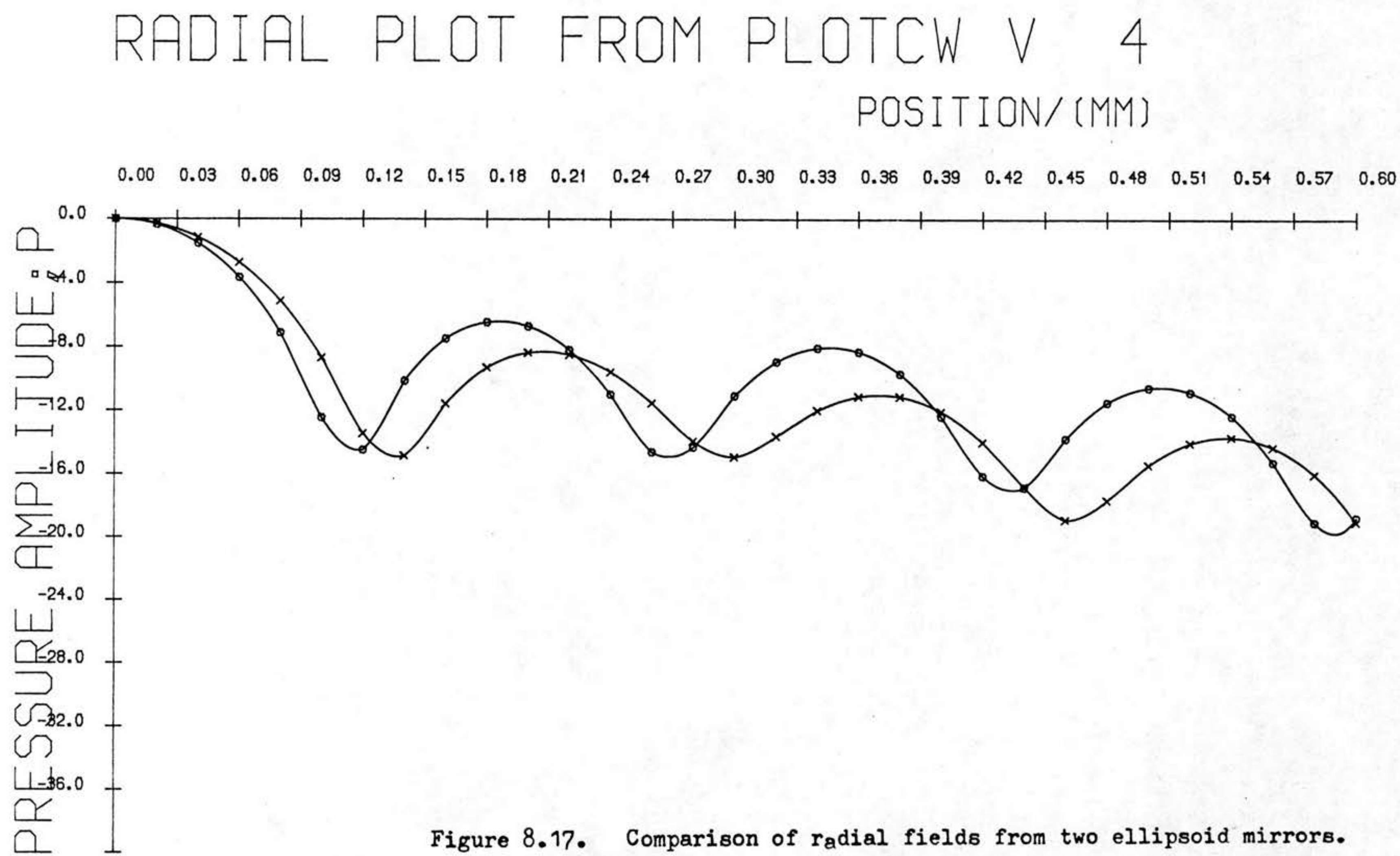

Figure 8.17. Comparison of radial fields from two ellipsoid mirrors.
X = inner diameter 30 mm; outer diameter 104 mm.
O = inner diameter 25 mm: outer diameter 88 mm.

This system proved much harder to align than the other designs. The pointed surfaces seem to be much more sensitive to angular mis-alignment of their axes than do the blunt-nosed pure conics. Placing the secondary also was difficult. The surface was extended past the plane of F_2 to a diameter of approximately 18 mm. The primary also extended beyond F_2 thus there are no axial reference points for placing the mirrors relative to one another. As explained earlier the tungsten:epoxy mix does not machine well. This is made even worse by the addition of absorber to the back of the mirror. This made machining the secondary to fit its mount difficult. There is also error in aligning the mirror axis with the lathe when doing this machining. The tilt of the primary must, therefore, be adjusted to compensate for these mounting and turning errors.

Both the optical ultrasonic alignment techniques were used with this system. Both could result in fields containing features attributable to faulty alignment. The experimental analysis (section 8.4) contains references to such effects. The target grid was used to overcome this and to speed up what was often a time consuming process. It was also helpful to place the device in the plotting tank and to adjust the tilt on the primary reflector to move the focus on to the system axis suggested by the plotting mechanism.

8.4. Experimental Results.

8.4.1. Hydrophone beam plots.

A transverse hydrophone plot through the field maximum of the system driven by the 13 mm diameter 5 MHz probe is shown in figure 8.18. Beam asymmetry is demonstrated. The half-widths refer to the main lobe. If the side lobes are included the -10 dB half-width becomes 1.52 mm. The peak is 149 mm from the transducer face. The plot is typical. Dismantling and re-aligning the system produced similar plots in terms of side lobe amplitude and beam widths although the asymmetrical effects varied.

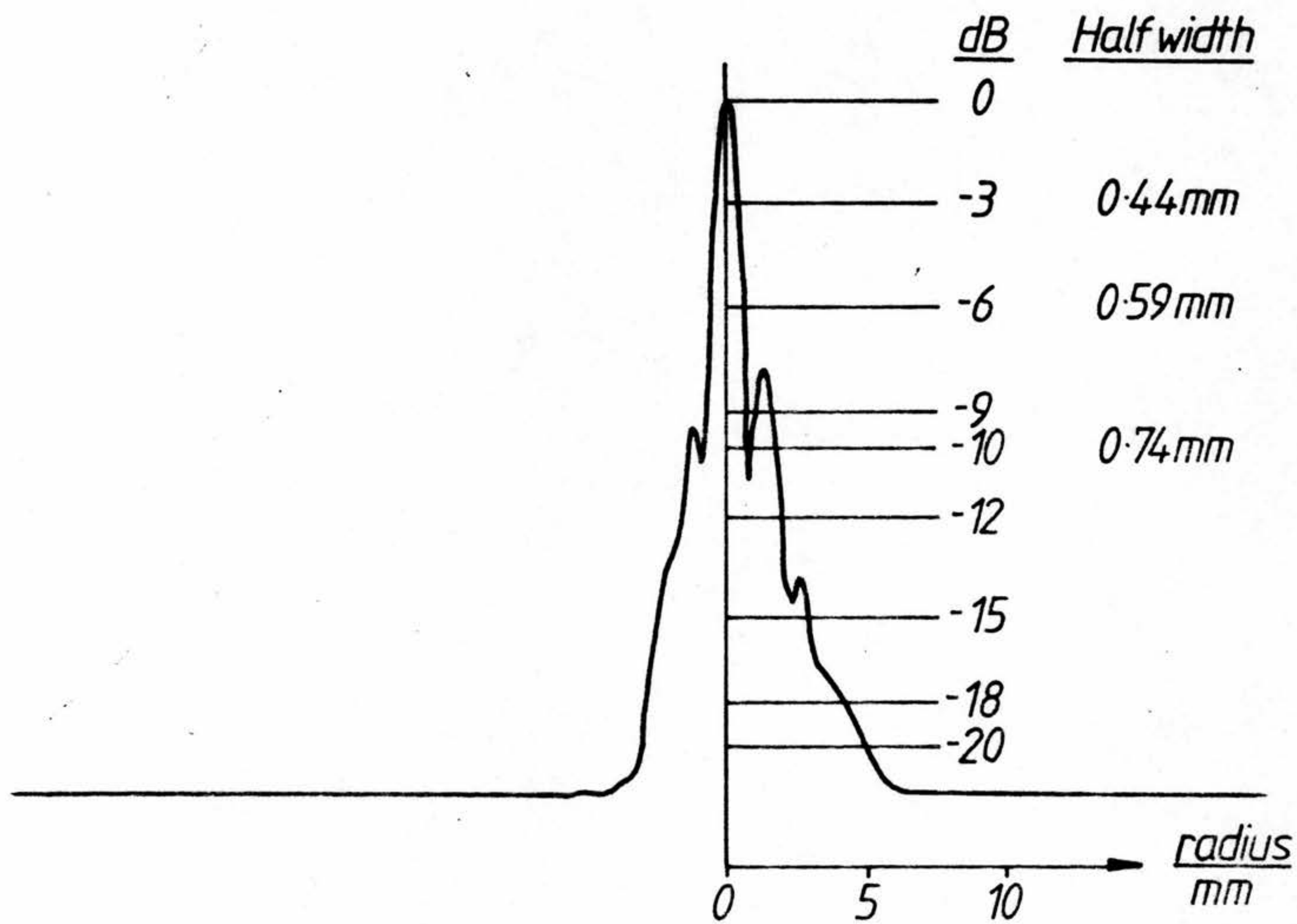

Figure 8.18. PVDF Hydrophone plot of the modified Cassegrain mirror system (T_x - 10dB)

8.4.2. Pulse-echo beam plots.

The pulse-echo transverse plot, using a 2 mm diameter stainless steel ball, matching the hydrophone plot discussed in section 8.4.1., is given in figure 8.19. The change of target has altered the appearance of the plot, especially of the side lobes.

The pulse-echo axial plot of the same alignment is given in figure 8.20. Further evidence of imperfect alignment is given by the double peak. The -12 dB depth of focus is 15.0 mm. An axial plot without this particular artifact is given in figure 8.22(a). The -12 dB beam length is 12 mm. The double axial peak can be removed by adjustment of the device. It does not, however, have any detectable adverse effect on beam width.

8.4.3. Pulse Shapes and Reverberations

The most relevant question concerning the new design was whether or not it was without the spurious echoes manifested by the Cassegrain system. Figure 8.21 shows the A-scan video trace. The first echo at S, is due to the secondary mirror. The echo marked T is due to a 2mm diameter steel ball target placed at the field maximum. The echo marked M is due to the luer needle mount of the target. There is a reverberation of echo T which occurs 35 μs late. It is only 4mV high, i.e. -63 dB.

Figure 8.22(a) is a multiple exposure photograph of the A-scan with the 2 mm ball target at varying depths in the field. Each horizontal division corresponds to 3.7 mm approximately. The peak pulse shape without the receiver connected is shown in figure 8.22(b). The second component of the echo (2.2 μs late) is derived from the mounting at the rear of the ball bearing. The -12 dB length is 12 mm.

Figure 8.23(a) is another multiple exposure A-scan. On this occasion the field shows two similarly sized axial peaks(marked B and D) following alignment. In the test tank the focus appeared on axis and the field symmetrical. The two axial peaks are the only remarkable feature. Peak B occurs at 119 mm range as before. Figure 8.23(b)

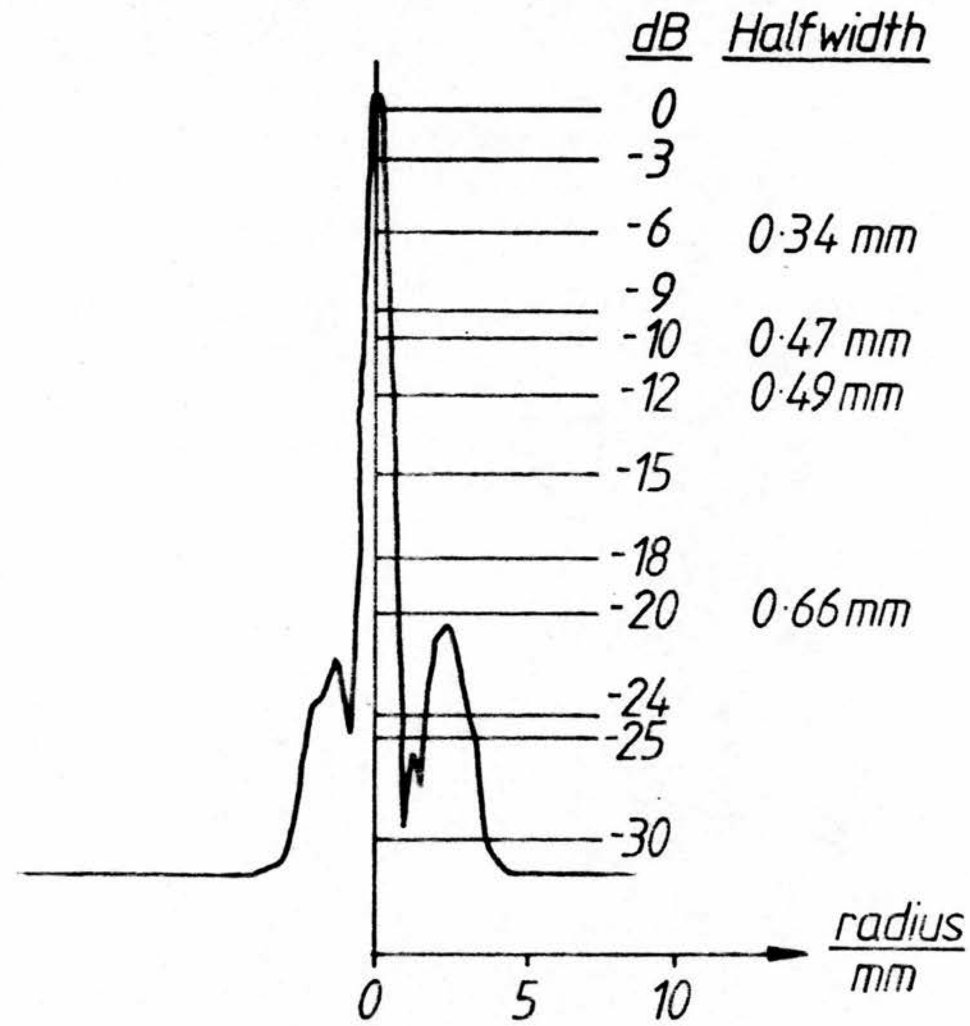

Figure 8.19. Pulse-echo plot. (2 mm diameter s.s. ball target) of the modified Cassegrain mirror system (T_x - 10 dB).

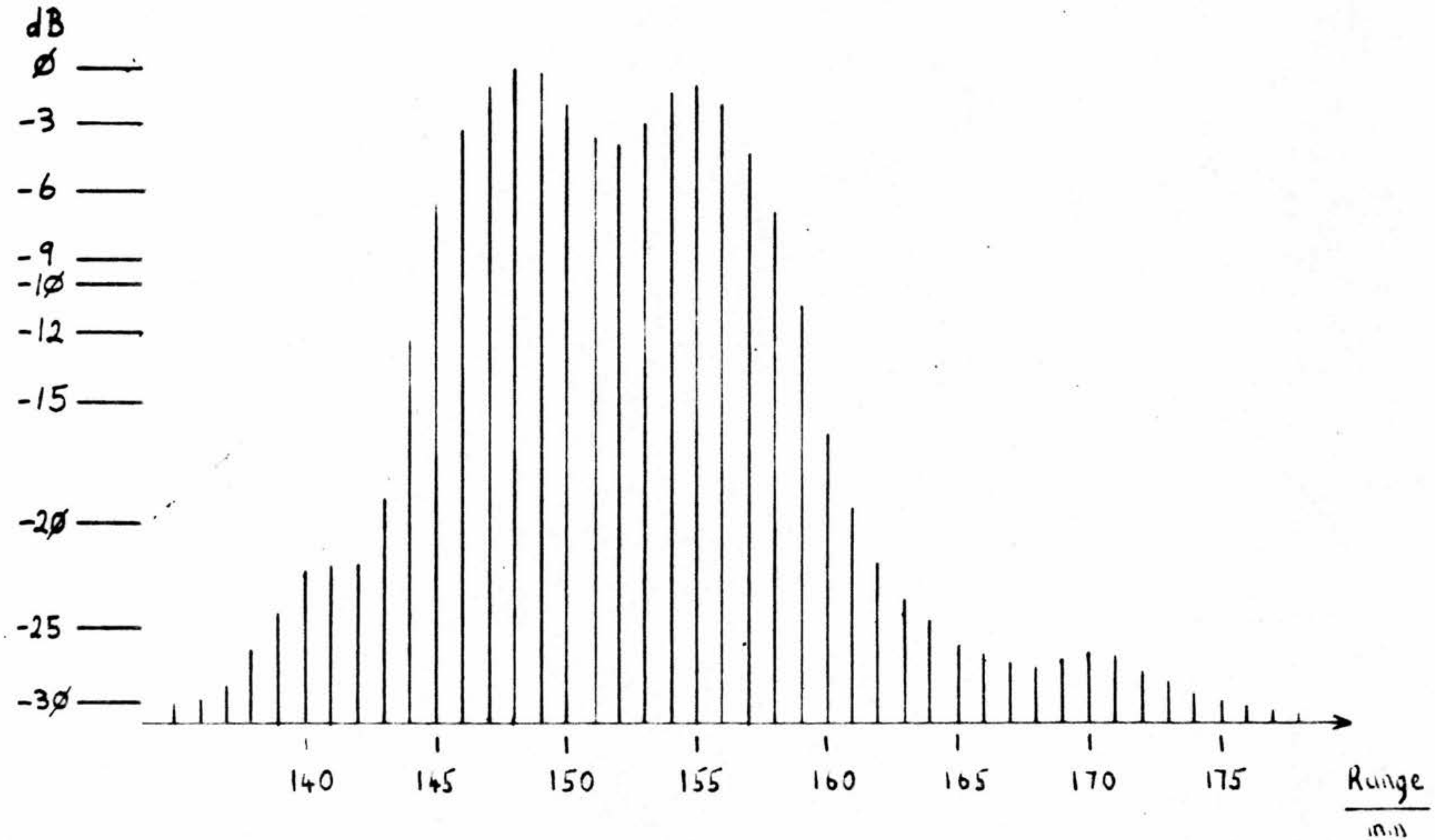

Figure 8.20. Pulse-echo axial plot of the modified Cassegrain mirror system. (Transmitter -10dB, 2 mm diameter, s.s. ball target).

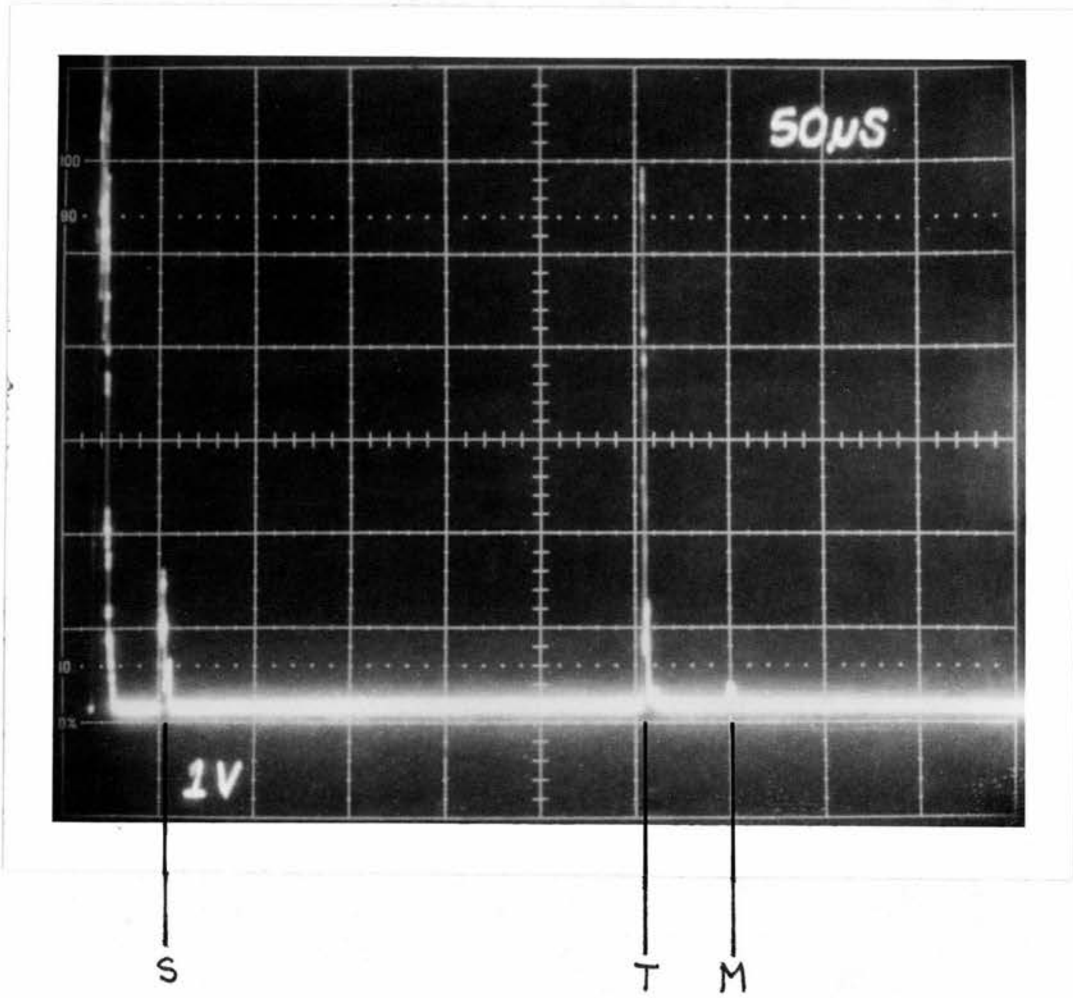

Figure 8.21. Modified Cassegrain Mirror System.
A-scan trace. 'S' marks the secondary
'T' a 2mm diameter steel ball target
at the field maximum.
'M' is due to the target mount.

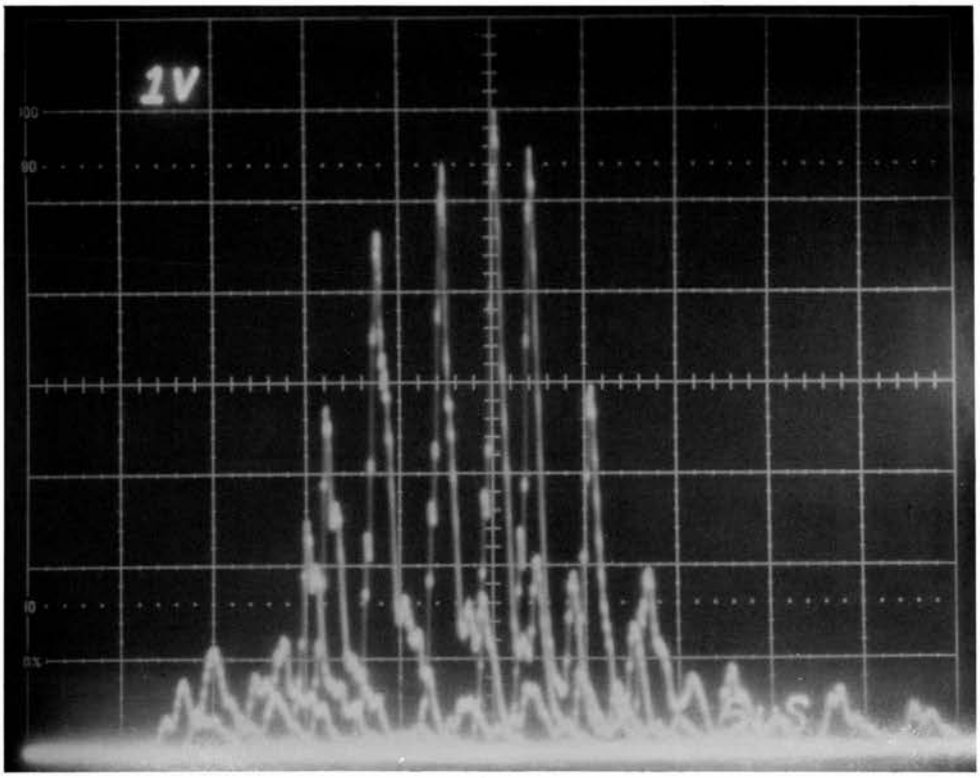

Figure 8.22(a): Axial plot of modified Cassegrain mirror system.
(Multiple exposure A-scan).

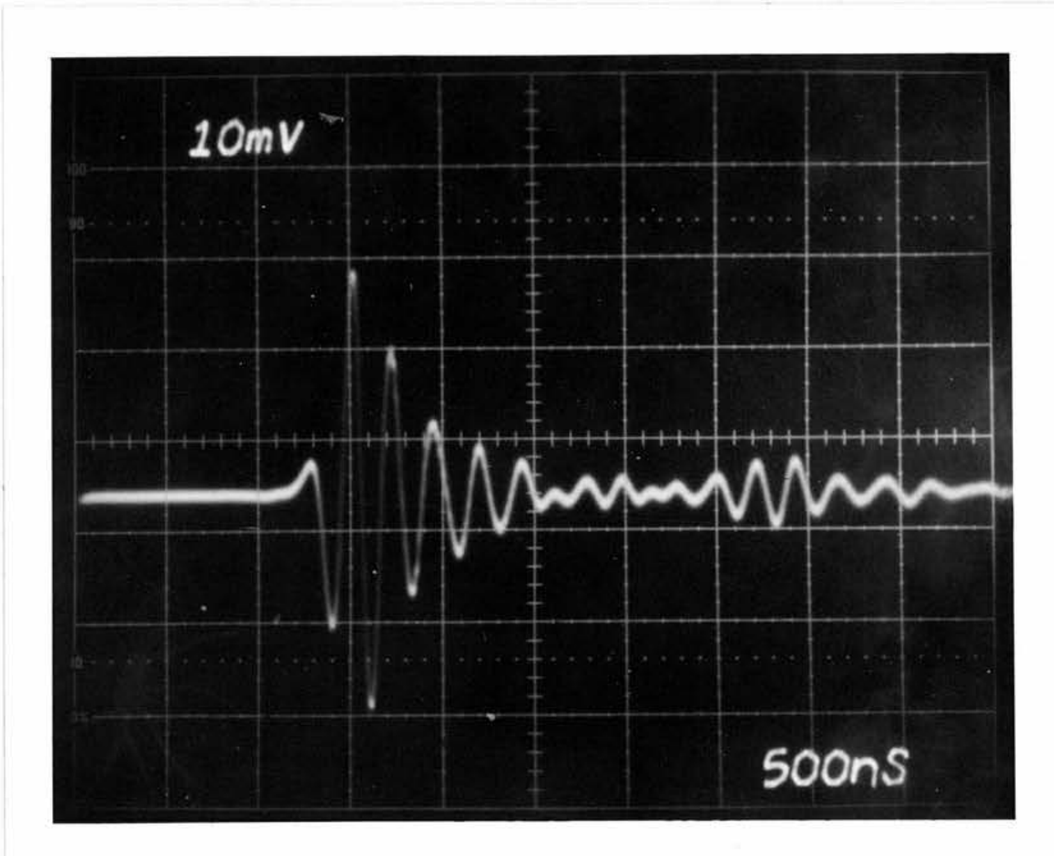

Figure 8.22(b): Echo pulse from 2mm dia. steel ball target at the field maximum of the modified Cassegrain mirror system.

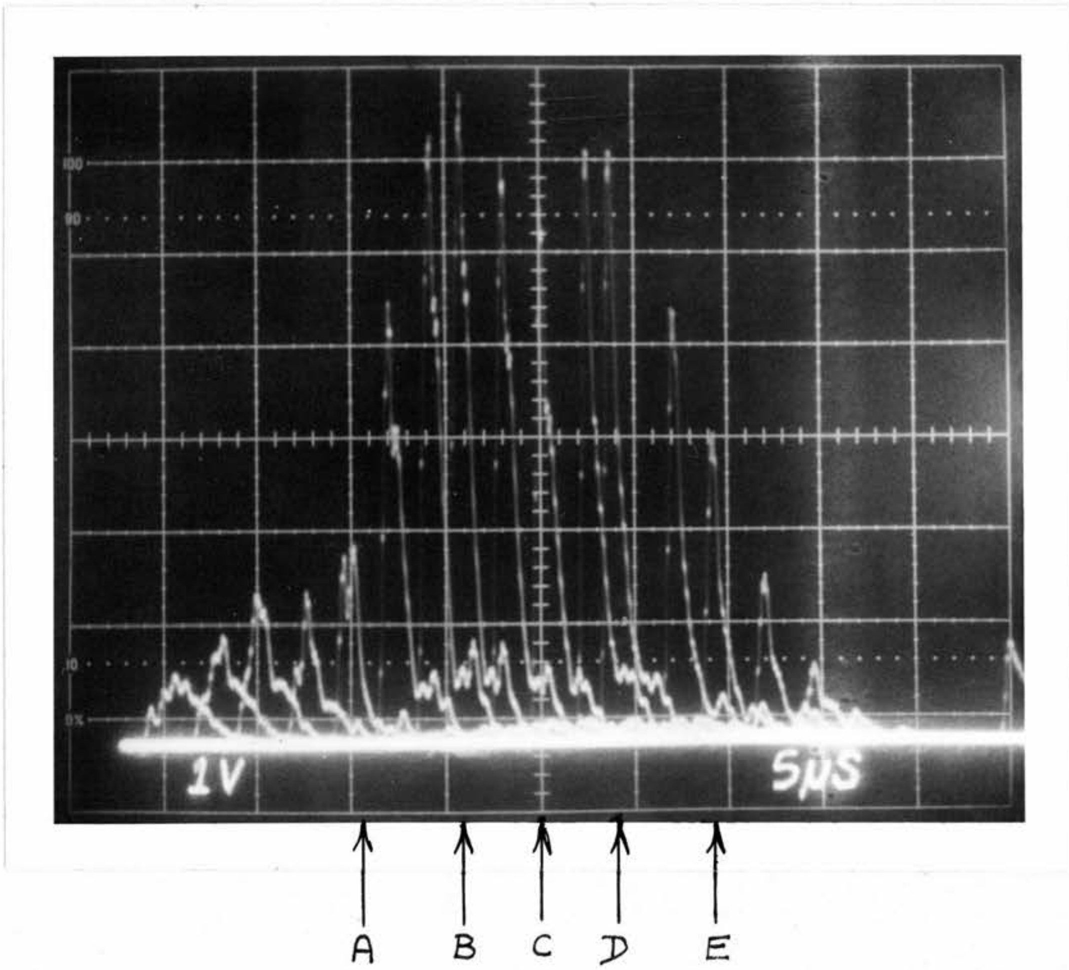

Figure 8.23(a): Axial plot of modified Cassegrain mirror system.
(Multiple exposure A-scan).

Figure 8.23(b): Pulse shapes due to 2mm dia. steel ball target on axis.

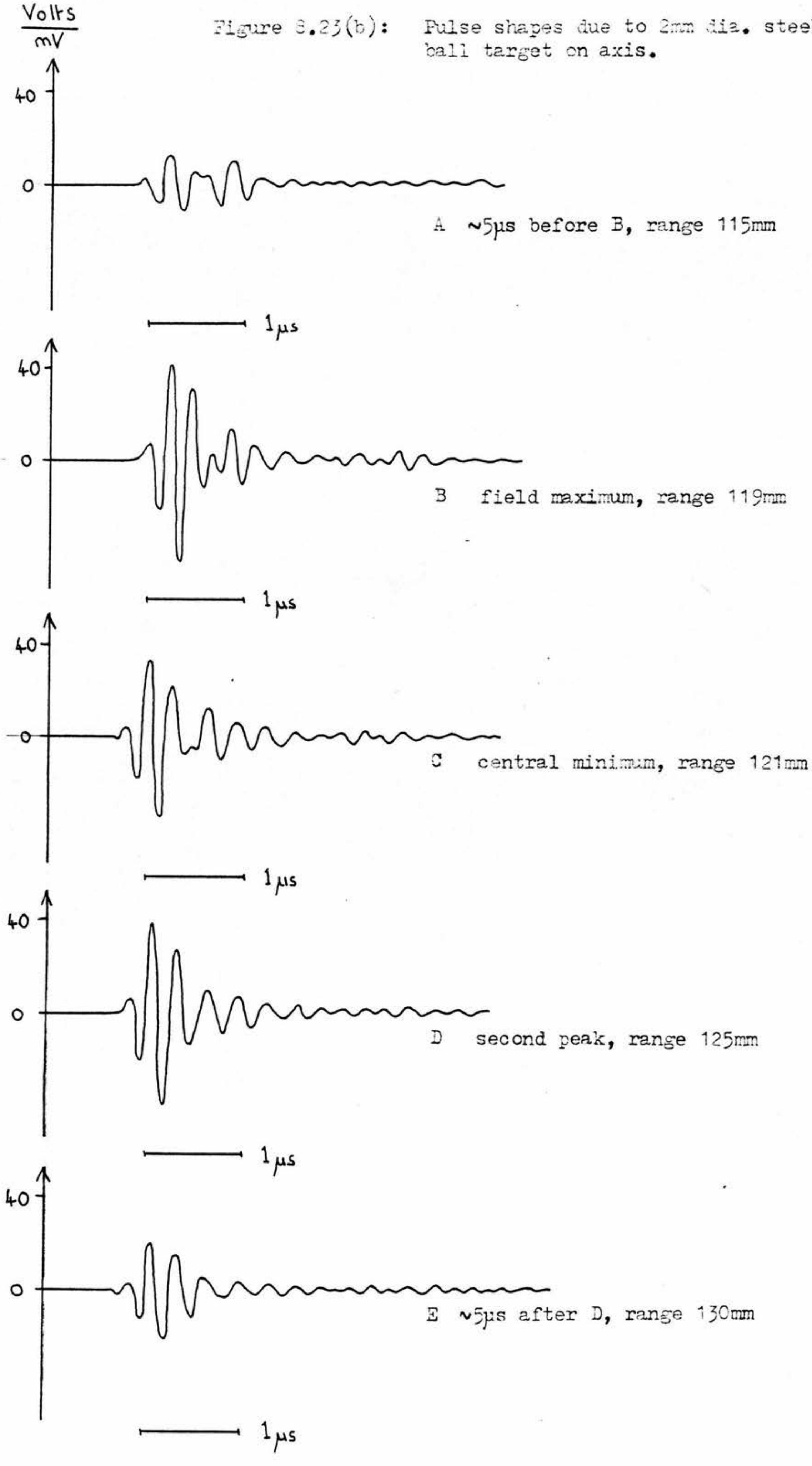

shows the echo pulse due to the 2mm ball bearing at five points through the field. The total -12 dB length is 18 mm.

The peak pulse detected by the PVDF Hydrophone is shown in figure 8.24.

8.4.4. Comparison of Theoretical and Experimental Results

The theoretical and experimental results are presented together in figure 8.25. As discussed before neither numerical model simulates the mirror geometry completely. PLOTBCW indicates the performance of a device of this numerical aperture with a centre block and a uniform spherical wavefront. PLOTCW models a similar device but with the wavefront apodised by the use of an ellipsoidal mirror but without the spherical aberration which will be present in a real system. The two models bracket the CW performance of the device if perfectly executed.

The other differences found between the CW and PW models are also seen. The PW shape is flatter topped than the CW and the sidelobes are smoothed out. The quantified association of these effects with pulse length or with target size is not possible. The results of section 5.2 suggest that the magnitude of the change in beam width could be attributed to the target alone.

8.5. Images

The mirror system was used to scan a phantom.

This was made of reticulated foam with all trapped air evacuated and replaced by water. The material contained 10 mm and 5 mm diameter voids, nylon filaments (18 and 20 swg) and a piece of 18 swg tinned copper wire. The scan shown in figure 8.26 is a composite composed of several scans collected with the focal zone at varying depths. Echoes from outside the focal zone were suppressed. The focus was moved in steps of 10 mm or 8 mm as indicated. The dark bands are due to the decrease in gain towards the edge of the focal zone.

A selection of patient breast images is given in figure 8.27.

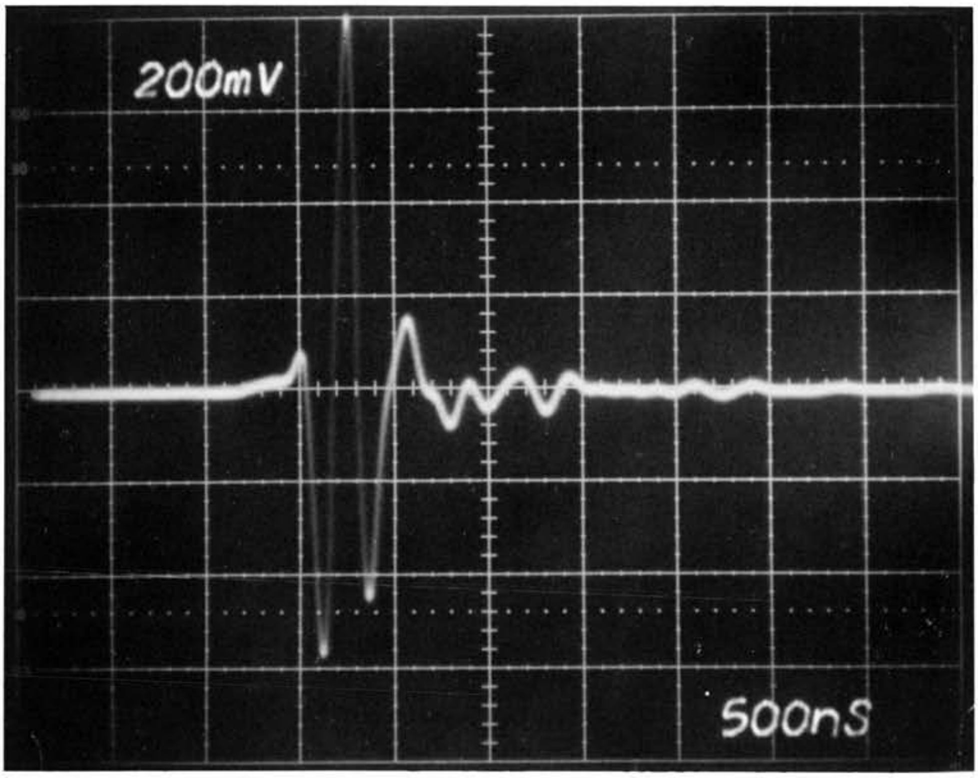

Figure 8.24. Peak pulse of modified Cassegrain Mirror system using PVDF Hydrophone.
(T_x -10dB, R_x loaded; preamp gain = 108)

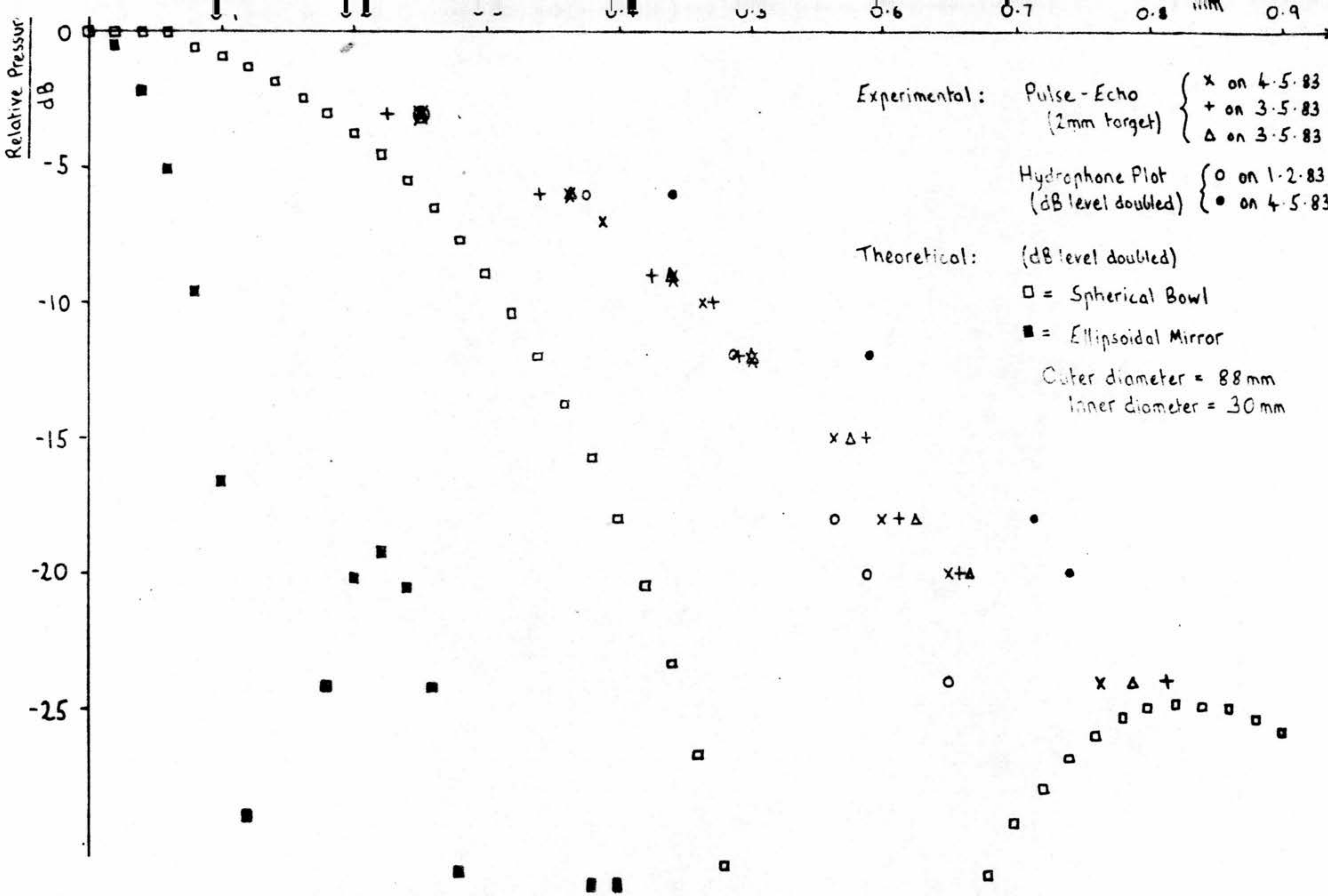

Figure 8.25: Theoretical and experimental results for the modified Cassegrain mirror system.

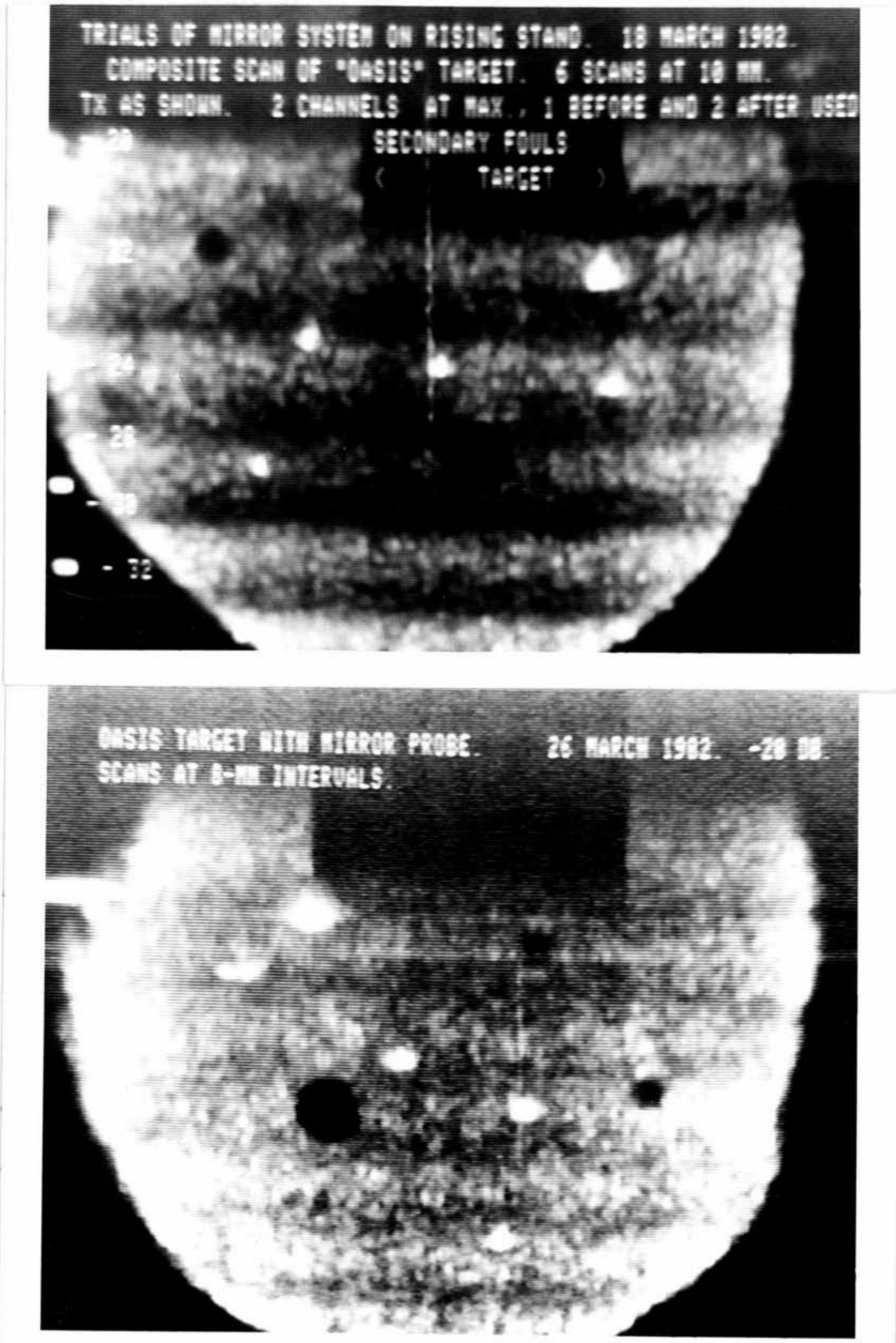

Figure 8.26: Composite images of a reticulated foam target using the modified Cassegrain mirror system.

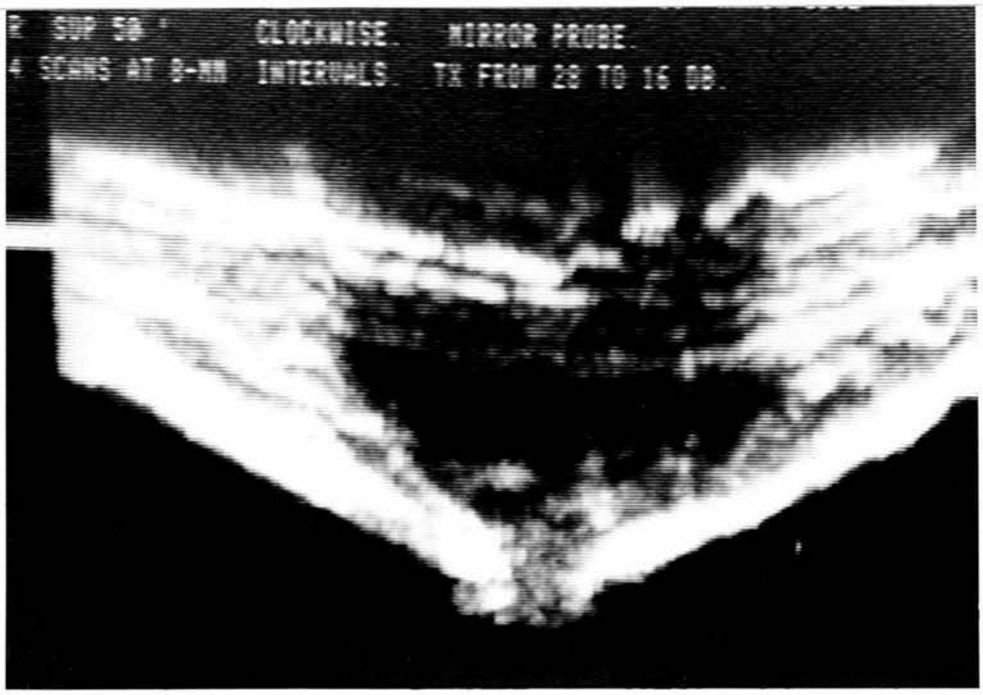

Figure 8.27: Composite breast images using the modified Cassegrain mirror system.

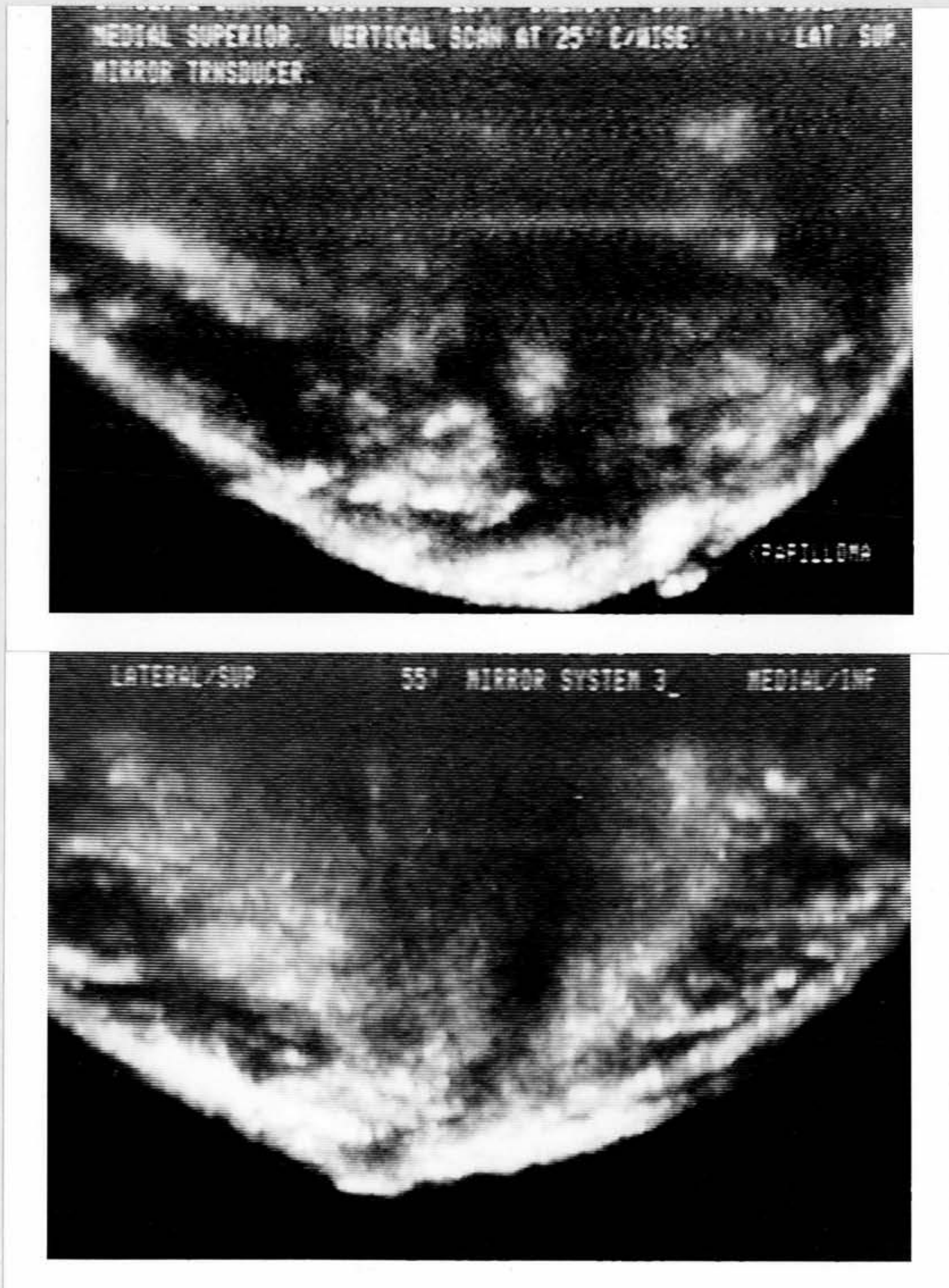

Figure 8.27: Composite breast images using the modified Cassegrain mirror system.

These images are included to demonstrate the application of the mirror system to breasts with different ultrasonic appearances. The lower image on page 252 shows clearly the central glandular tissue surrounded by fat. The speckle pattern is very fine. This is noticable if it is compared with the top image in figure 5.12. It is worth noting in this image and the lower image on page 253 there is no retro-areolar shadow. A papilloma may be seen on the skin in the upper image on page 252. The lower image on page 253 is of a small dense breast. The chest wall is demonstrated clearly behind the breast. There are few echoes from the breast parenchyma. The structure in the upper image on page 253 is more diffuse there being no clear separation of glandular and fatty tissue. Some ducts may be seen near the tip.

The breast shown in the upper image of page 252 had no disease, other than the papilloma, diagnosed. X-ray mammography of the breast shown in the upper image of page 253 showed micro-calcifications but no other evidence of disease was found. The breast contralateral to the one imaged at the bottom of page 253 was found to contain a carcinoma.

8.6. Conclusions about the modified Cassegrain System.

1. The pointed secondary design has removed the problem of reverberations.

2. The system is adequately sensitive for use on transmission and reception even although only the primary can be manufactured in air-backed copper.

3. The mirror system is a useful imaging transducer, either for demonstrating detail in a small area or for producing a composite image of a larger area. The latter procedure, however, is time consuming.

CHAPTER 9. FUTURE DEVELOPMENTS

A sensitive large aperture, highly focussed mirror system has been successfully designed and produced. As demonstrated by the many designs of optical reflector telescopes, there are many possible developments of mirror systems. The problems of ultrasonic imaging require different properties from optical systems and there are many variations in reflector design to be investigated.

Two directions for development of mirror systems are discussed here. Possible designs for smaller, more manoeuvreable systems are investigated in section 9.1 and for increasing the focal depth either by an axicon wavefront (section 9.2) or by altering the geometry to move the focal zone while scanning (section 9.3).

9.1. Arm-mounted Mirror Systems.

The mirror systems discussed in Chapters 7 and 8 had very large apertures and were heavy. The commercial transducers obtained for breast scanning (Chapter 5) had performances well below that predicted by theory and were unreliable.

The design of a small mirror system, which could be mounted on the scanning arm of the breast scanner was, therefore, investigated. The Cassegrain style of system would require two mirrors and would be relatively large and, for an outer diameter of about 50 mm, would be strongly apodised by the secondary mirror.

A different design was also considered based on the Herschelian telescope. Herschel (1738-1822) tilted the primary mirror so that its focus occurs outwith the aperture (figure 9.1), thus obviating the need for the flat secondary of Newton's design. The aperture is, therefore, unobstructed but the system is asymmetric and aberrations are difficult to control. The physical constraints of the scanner

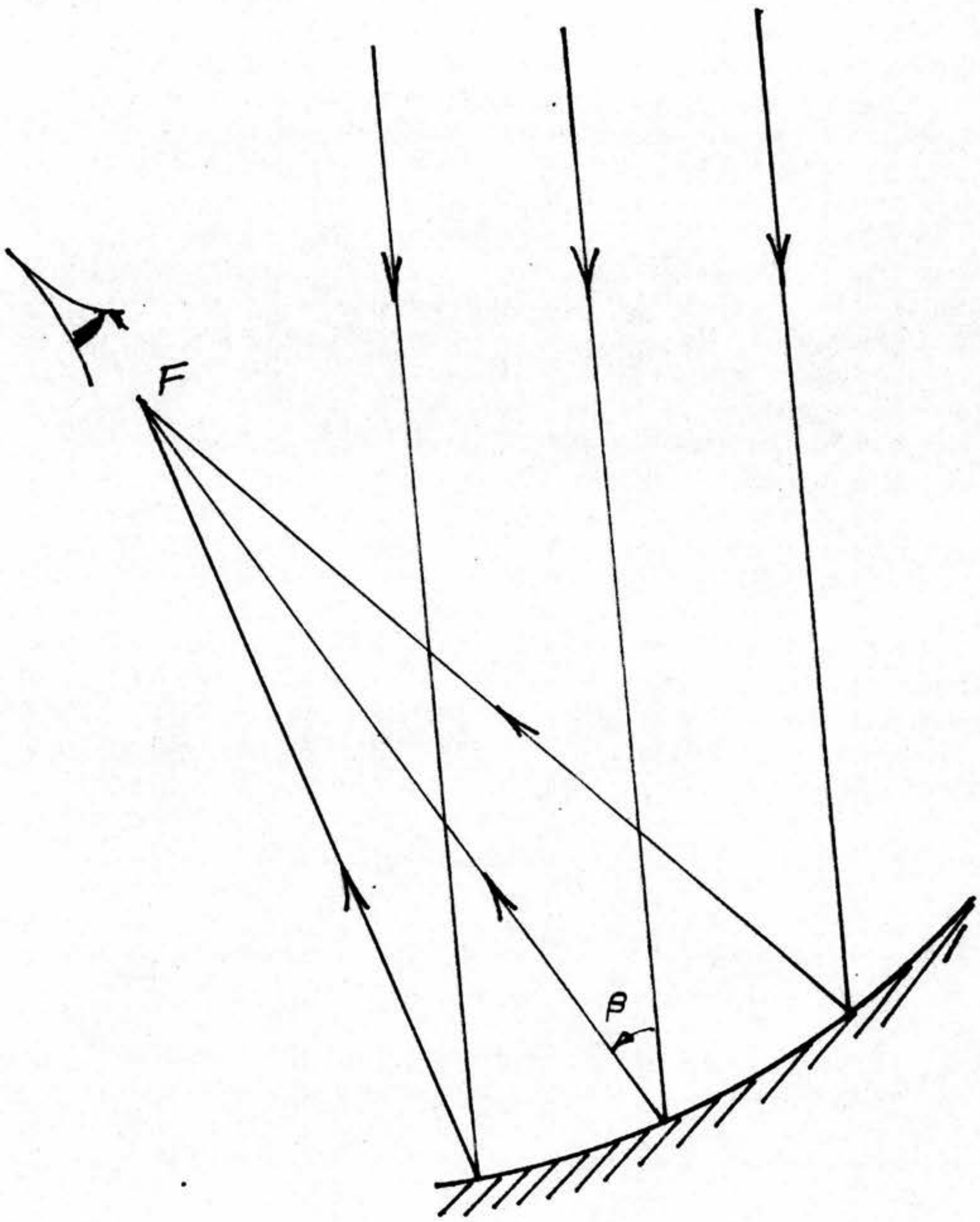

Figure 9.1: The Herschel design of reflector telescope.

will set a lower limit on the angle, β . The design requires a diverging source, the design and construction of such may not be easy.

Three small mirror systems are considered here. Two Herschel style systems, one based on an off-axis section of an ellipsoid of revolution and one based on a spherical surface are compared with a Cassegrain style system of similar dimensions.

9.1.1. Design of Herschel Mirror Systems

The design of a Herschel system is limited by the size of the scanning tank as well as arbitary constraints on transducer and mirror. The design is shown in figure 9.2.

Physical Limits

1. The nominal maximum distance from the plane of scan (marked AB) to the hub of the scanning arm and the radius of scanning about the centre of rotation, O, is 200 mm.

2. It is assumed that the largest breast to be scanned will be a 100 mm radius hemisphere, also taken as centred at O.

Mirror System Constraints.

1. Diameter of mirror (aperture) = 50 mm.

2. Focal length, /RF/ = 125 mm.

3. The distance /LR/ is limited by what diverging beams may be produced.

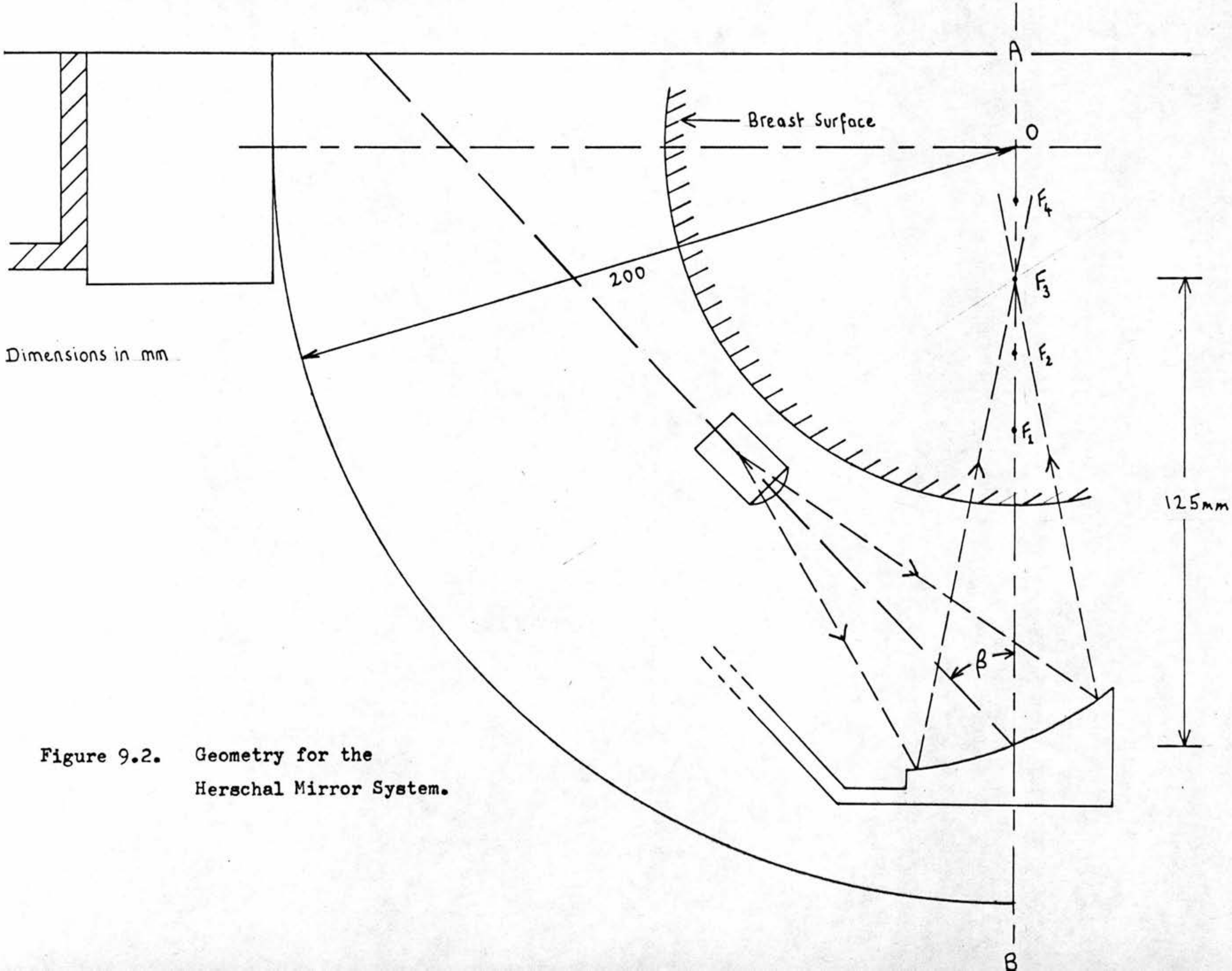

Figure 9.2. Geometry for the Herschal Mirror System.

4. The scanning arm radius should be variable in the range 140 mm → 200 mm to suit the patient being examined. Moving in 20 mm steps, this would place the focal point at F_1 (radius 75 mm), F_2 (radius 55 mm), F_3 (radius 35 mm) or F_4 (radius 15 mm).

5. The diverging transducer is taken to have a diameter ~15 mm; its back face is at the point M.

Additionally it was assumed that the minimum scan radius used with a 100 mm breast would be 160 mm. This gives a common angle β = 0.768 radians for all four diverging beams being considered.

9.1.2. <u>Diverging Sources</u>

Diverging beams were designed, based on a commercial transducer defocussed by a plano-convex lens placed against its front face.

The transducer used was a Nuclear Enterprises NE4355 (Serial No. 48673H) 5MHz, Medium Focus, 13 mm diameter.

The lenses were designed using simple, paraxial thin lens theory. A plano-convex spherical lens was relatively easy to manufacture.

The combination of a diverging beam (i.e. an imaginary source) and a convex lens surface require a refractive index (from lens to water) of greater than unity, i.e. a lens material with velocity, $C > 1520\ ms^{-1}$. This is an easy requirement. Lenses were manufactured in four materials. Lexan (Industrial Polymers Ltd, $C_1 = 2230\ ms^{-1}$). Epoxy Resin (Araldite Casting Resin CT210 + hardener HX910, $C_1 = 2550\ ms^{-1}$). Perspex ($C_1 = 2680\ ms^{-1}$) and Aluminium ($C_1 = 2400\ ms^{-1}$). (The propagation speed in Lexan and Araldite were found experimentally and have an error of $\pm$ 10 ms^{-1};

those for Perspex and Aluminium were obtained from Kaye and Laby. Other sources of acoustic properties for these materials are in reasonable agreement). Four different materials were chosen to compare attenuation between materials and to vary lens thickness. Thin lenses were desired to fulfil the thin lens approximation. Problems with ultrasound lenses have been discussed in Chapter 2.

Four different diverging beams are considered. These are shown in figure 9.3 and table 9.1. Different combinations of beam spreads and lens materials are tried to give a variety of beam shapes and lens thicknesses.

The beams were modelled theoretically using PLOTCW. A plane mirror through the origin (MIRROR6) was used to represent a circular aperture. The source is placed at a distance, i, from the aperture. With this geometry the algorithm is insensitive to whether the source is placed behind the aperture (-i) or in front of the mirror (+i). POINT6 was used since this mirror meets the small angle approximation perfectly. The quadrature routine frequently failed to achieve the required precision, although none of the failures indicated a serious error. At radii $>$ 20 mm this was occurring for some 50% of the points evaluated.

The beam width observed was of a central peak of width $\sim$ 4 mm. From this peak to a radius of 20 mm the field oscillates irregularly about 60% of the maximum. The more sharply spread the beam, the greater the oscillations. From 20 mm to 30 mm radius, the amplitude decreases.

Experimentally the beams were less promising. Plotting was unrewarding due largely to the insensitivity of the beams. At high transmitter powers, the lenses all gave reverberations. All the fields had axial maxima. Both beam width and the locations of the axial maxima depended on the transmitter power. -10db half-widths obtained were in the range 4 to 12 mm.

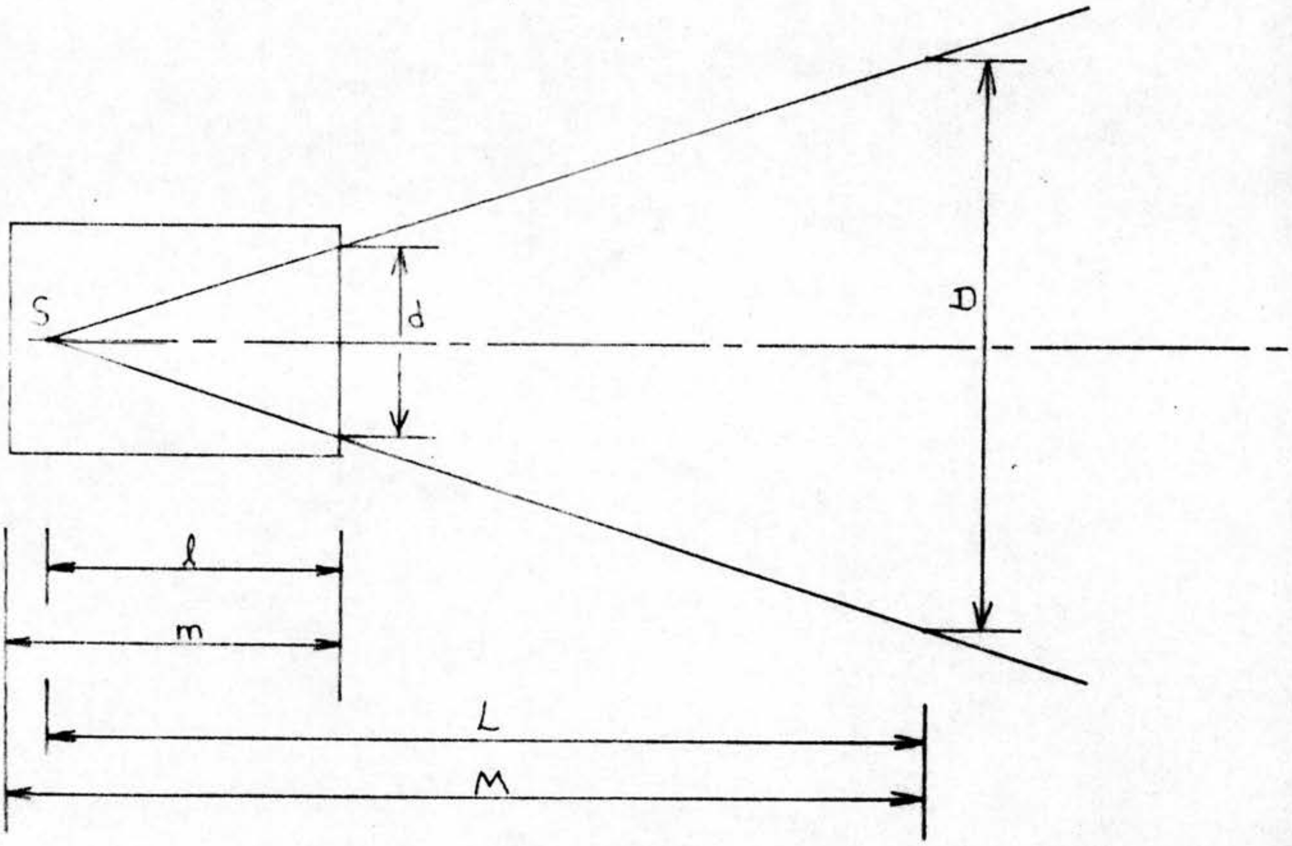

Figure 9.3: Diverging beams.

d = 13 mm
D = 50 mm
m = length of probe = 35 mm

Lens type	l / mm	i / mm	L / mm	M / mm	Manufactured in	Radius of curvature / mm
I	40	14.1	54.1	80	Aluminium	35.2
II	50	17.6	67.6	90	Araldite	8.8
III	80	28.1	108.1	120	Lexan Perspex	8.5 13.7
IV	100	35.1	135.1	140	Lexan Araldite Aluminium	9.7 14.0 41.7

Table 9.1: Diverging beams and lenses.

It seems unlikely that a successful diverging source could be obtained in this way. Alternative approaches would be (a) a convex bowl crystal; (b) a very small transducer. This might be sensitive to pulses which have not, in fact, been focussed by the mirror or (c) a large plane disc. This would be similar to the geometry shown in figure 9.1 but with F the ultrasound focus, rather than a detector.

9.1.3. Theoretical Evaluation of a Herschel System based on an Ellipsoid Reflector.

The geometry of a Herschel mirror system using an off-axis section of an ellipsoid of revolution is shown in figure 9.4. The modification of PLOTCW to study such a device is discussed in section 4.5 but the practical application is explained here.

The source is placed at S, one reference point of the ellipse and focussed to F, the other reference point. A surface approximately 50 mm x 50 mm is considered. The design program (section 6.1) was used to select the ellipsoid parameters and the subsequent angular and linear limits for the mirror. The angular limits being $\pm \frac{25\text{mm}}{h}$ as described in section 9.1.1, /RF/ = 125 mm; and /SR/ = L in figure 9.3 and table 9.1, being dependent on the source used.

The results indicate some promise. Results for Lens type II are given. The plot along the principal ray is shown in figure 9.5; a matching orthogonal plot through the intended focus, point F, in figure 9.6. Problems are easily recognised. The beam is wider than it is long, although CW estimates of beam length are pessimistic. Focal depth is less than that for an axially symmetric system. The beam is slightly skew but the first off-axis peaks are roughly similar in amplitude (-12 dB) and at the same radius (2.2 mm).

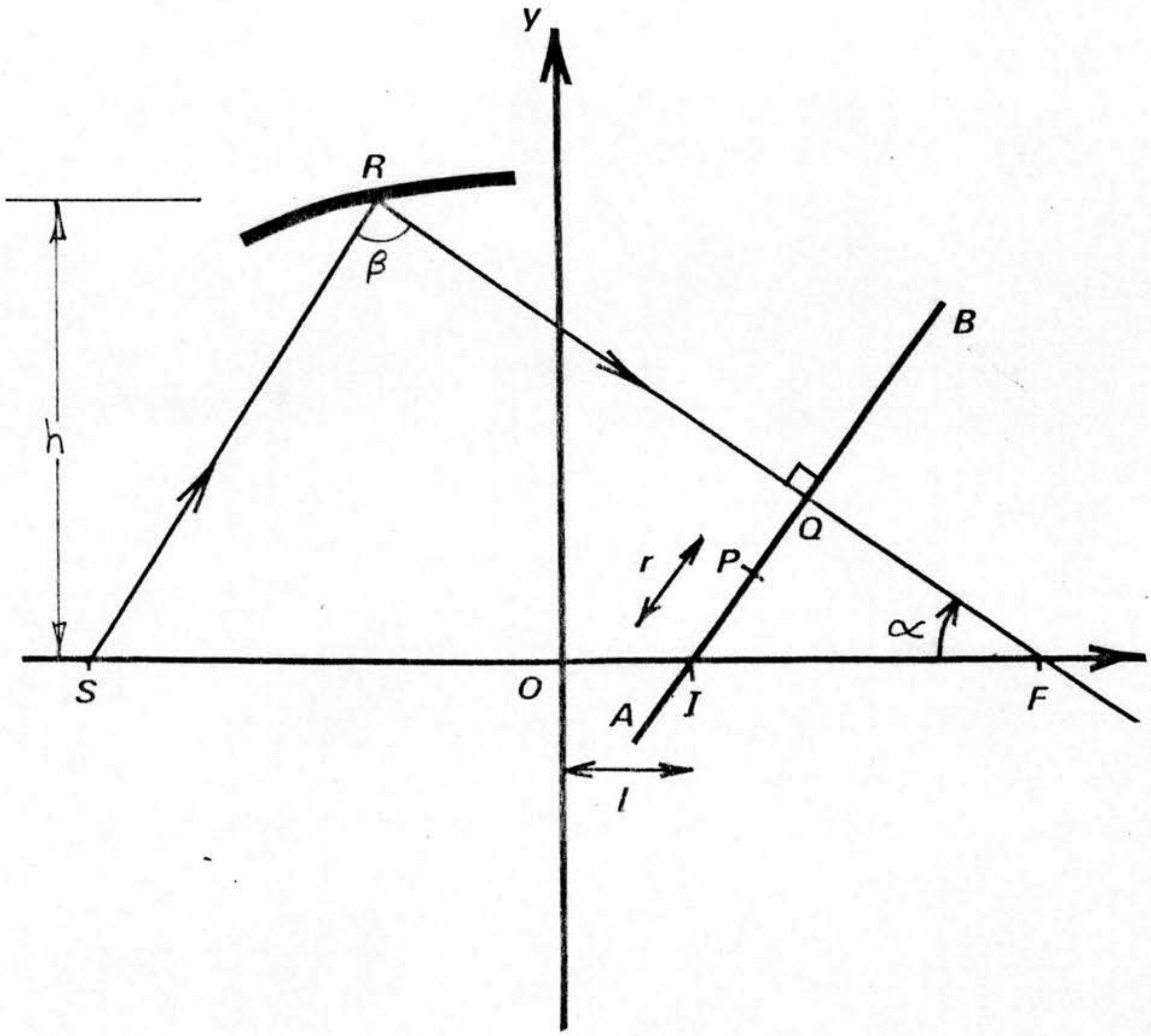

Figure 9.4: Geometry of Herschel system based on an ellipsoid. Only the principal ray is shown.

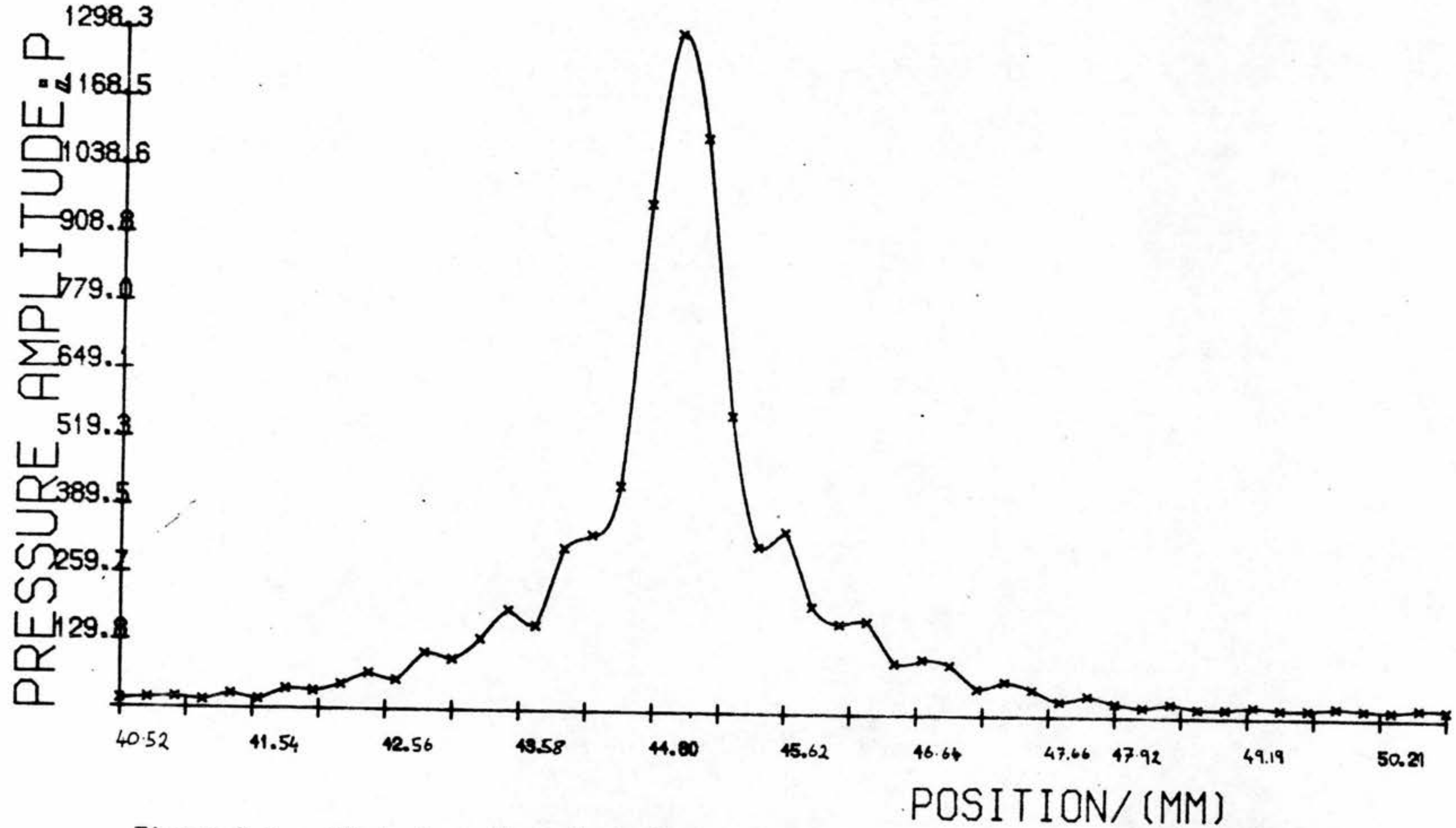

Figure 9.5. Plot along the principal ray of a Herschel system based on an ellipsoidal mirror (diverging lens type II).

BEAM LENGTHS

-3dB : 0.51 mm
-6dB : 0.72 mm
-10dB : 0.94 mm
-12dB : 1.63 mm

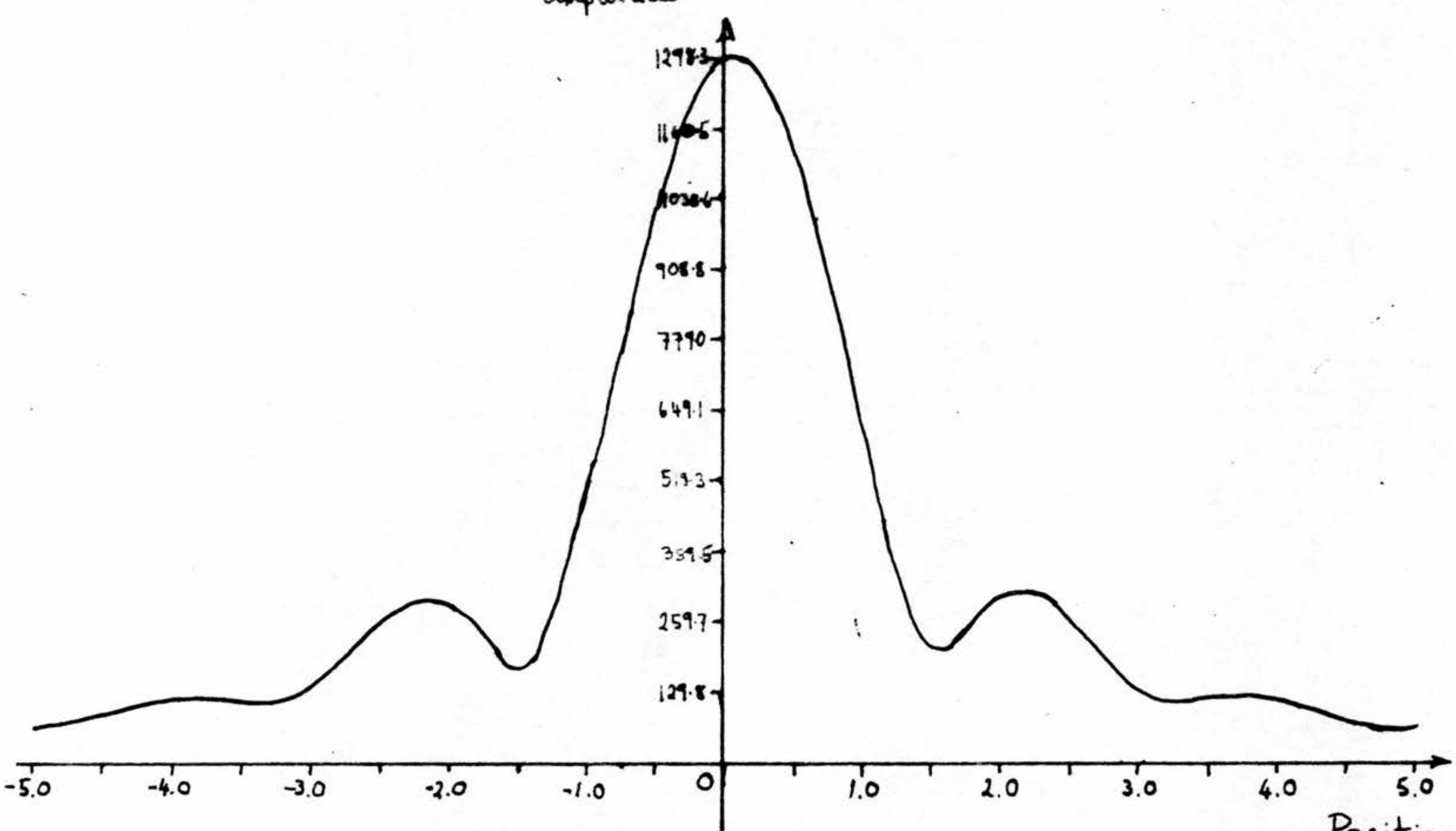

Figure 9.6. A transverse plot, orthodonal to the principal ray of the ellipsoid based Herschel Mirror System (based on diverging lens type II).

Beam widths

-3dB : 1.32 mm
-6dB : 1.82 mm
-10dB : 2.30 mm
-12dB : 2.47 mm

Further complications are indicated by the plot in figure 9.7. This is orthogonal to the principal ray (parallel to figure 9.6) but 1.7.mm closer to the mirror than the geometric focus. The vertical line marks the principal ray. The maximum is now markedly off-axis although small, -15dB compared to the point F. Such a skewed beam would lead to registration errors in an image, although this might be corrected electronically.

Interestingly, comparing plots orthogonal to the ellipse, major-axis for the sector used here and for the complete annulus, showed the same beam shape but with increased amplitude, approximately with the increase in area.

9.1.4. Theoretical Evaluation of a Herschel System based on a Spherical Reflector.

This geometry is illustrated in figure 9.8. A spherical reflector would be more easily manufactured than the off-axis section of an ellipse. Spherical aberrations will be introduced but might be compensated for by changes in off-axis aberrations.

As before, β = 0.768 radian and /RF/ = 125 mm. /SR/ = L as given in table 9.1. The constraints associated with the mirror geometry have changed. /SO/ $\neq$ /OF/. Instead $\overline{OR}$ bisects the angle $\widehat{SRF}$. With the spherical geometry, all parameters may be calculated using trigonometry.

The predicted performance for these devices is disappointing. A plot along the principal ray and a transverse plot perpendicular to it, through F, for a Herschel mirror based on lens type II (section 9.1.2.) are given in figure 9.9. The result is typical. The peak is broad, disjointed and asymmetric. The separation of sagittal and transverse focus renders the field unusable for imaging.

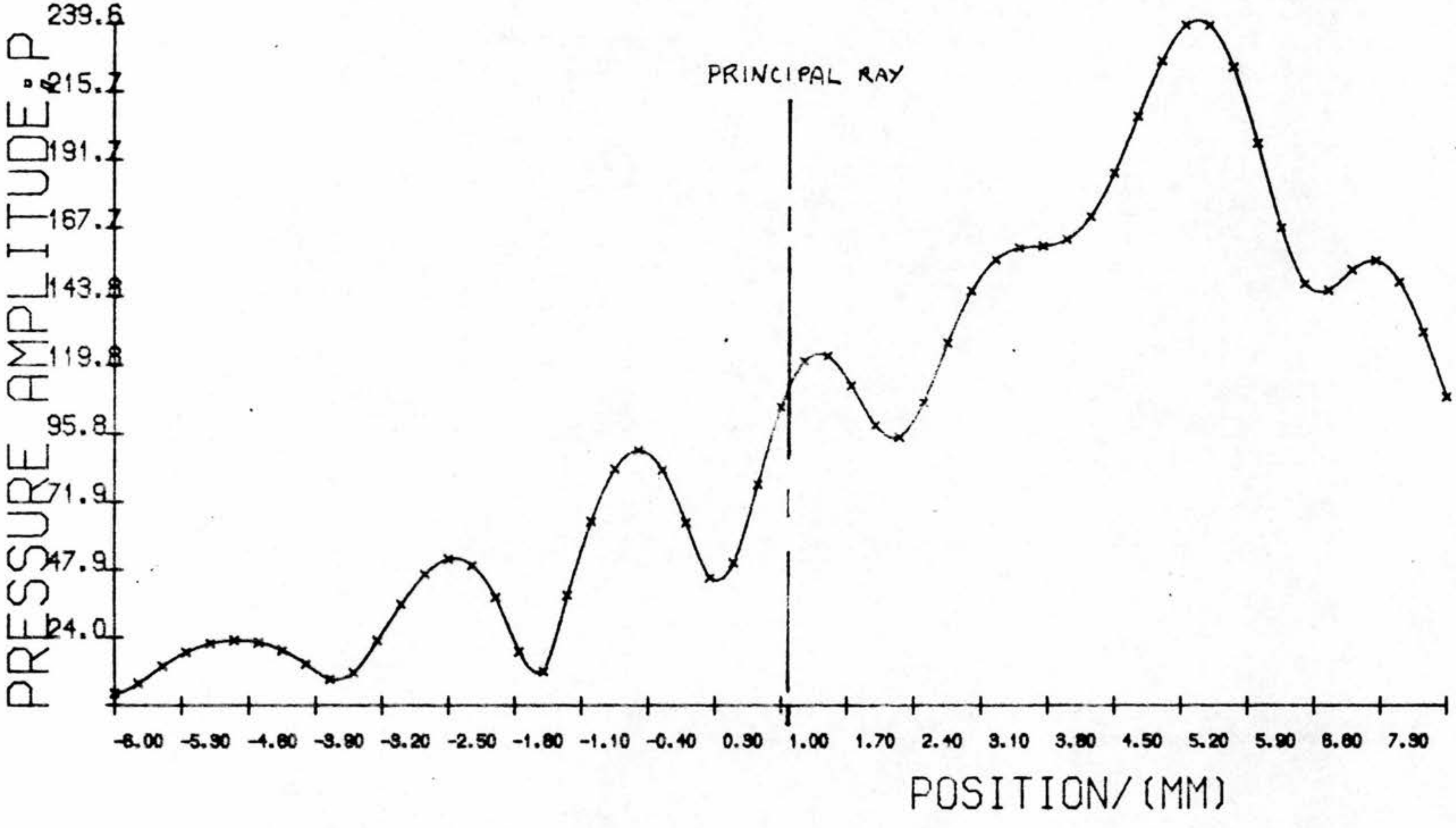

Figure 9.7. A transverse (to the principal ray) plot of Ellipsoid based Herschel Mirror. 1.05 mm closer to the mirror than the geometrical focus F

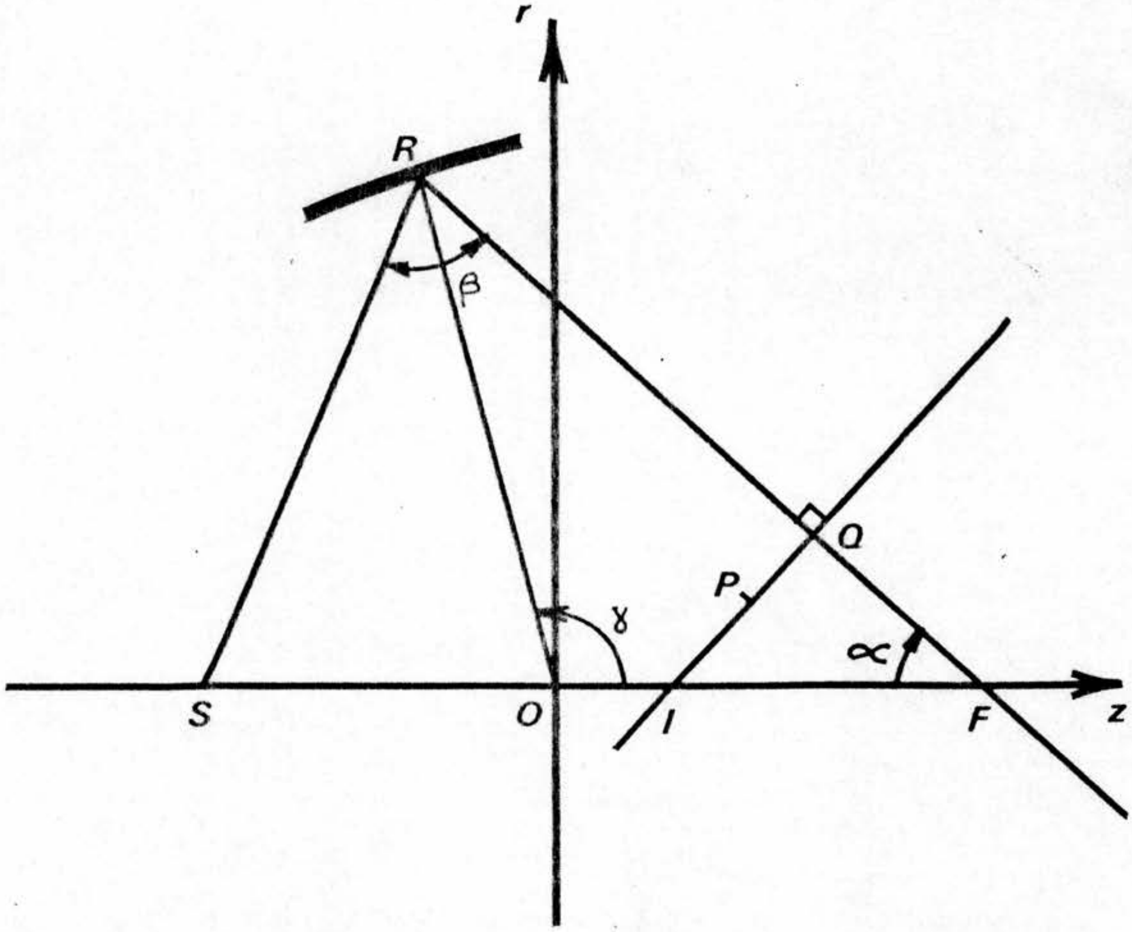

Figure 9.8: Geometry of a Herschel system based on a spherical reflector.

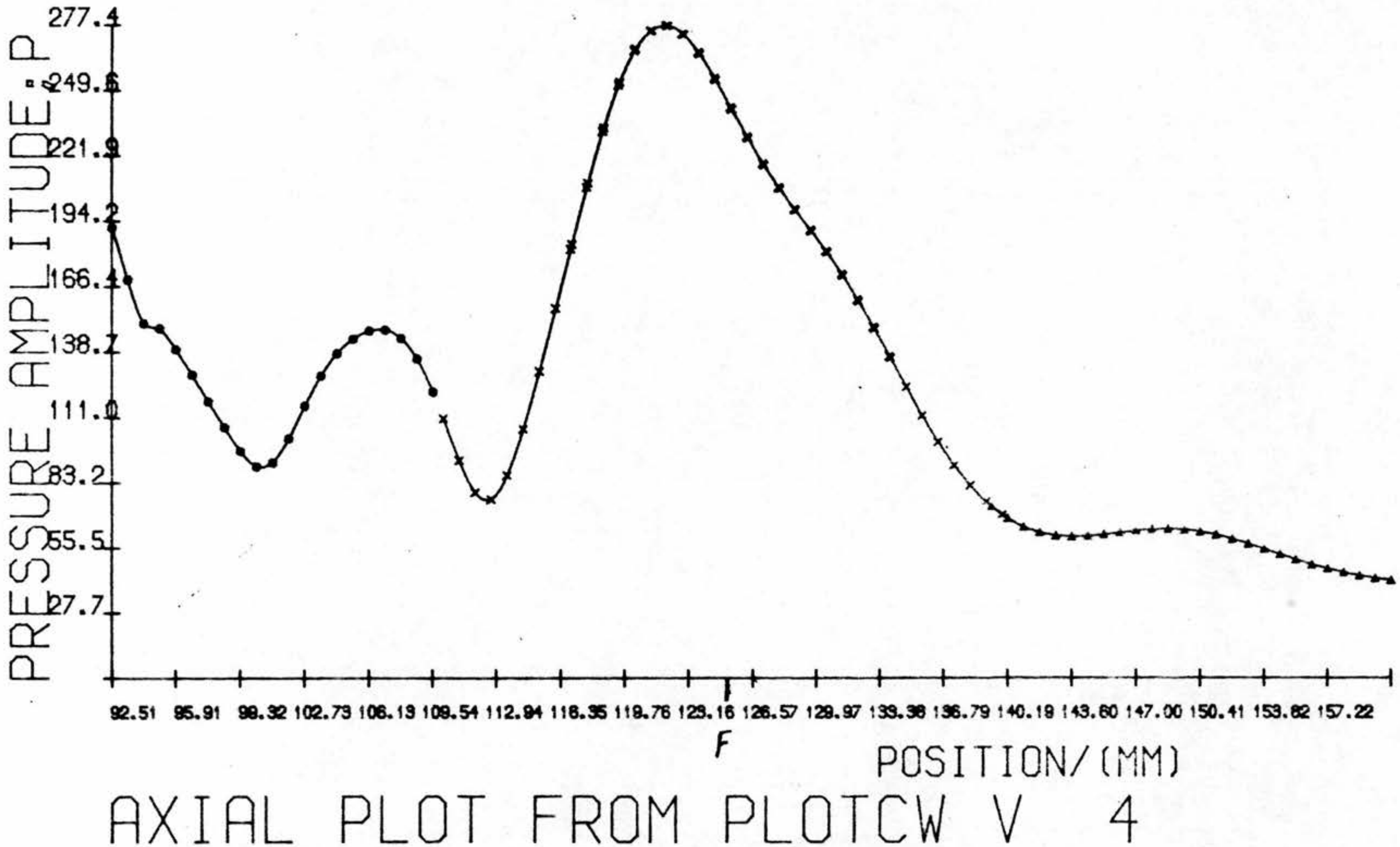

Figure 9.9(a). Typical results for a Herschel system with a spherical reflector:Axial field.

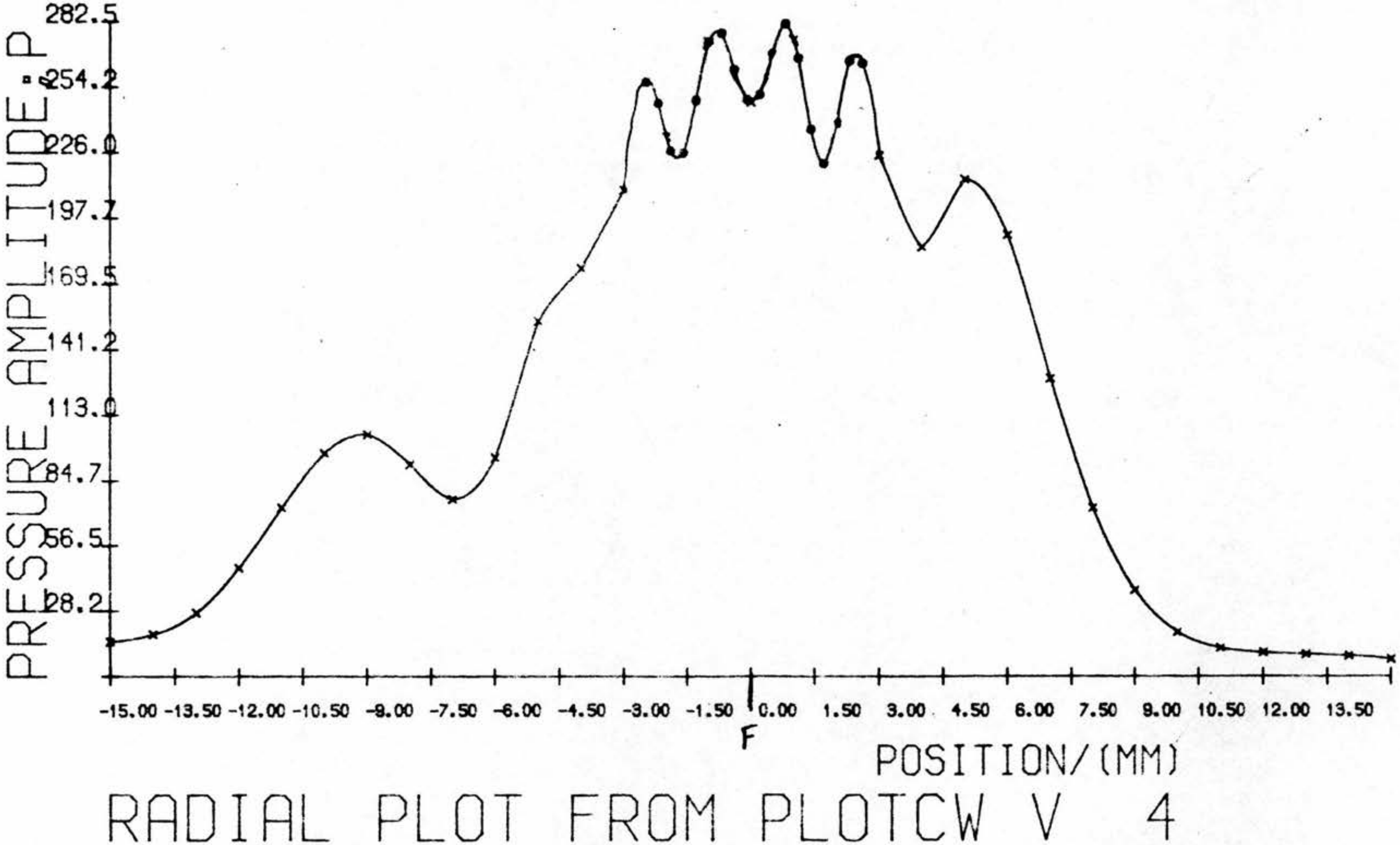

Figure 9.9(b). Typical results for a Herschel system with a spherical reflector. Transverse plot.

9.1.5. Theoretical performance of a small (50 mm diameter) apodised focussed bowl

A 50 mm diameter, 125 mm radius focussed bowl was investigated for comparison with the Herschel mirrors.

A rectilinear plot for a device apodised by a 25 mm block in the centre is shown in figure 9.10. Results for increasing apodisation are given in table 9.2 and figures 9.11 and 9.12.

A device manufactured in the modified Cassegrain design might be expected to approach this predicted field to the same degree as the system discussed in Chapter 8 approached its theoretical field. A smaller transducer might be employed to reduce the size of the centre stop.

9.1.6. Conclusions

(i) A Herschel style mirror system is desirable since it would be simple to use. It would be less bulky and less sensitive to the alignment of its components. It also has only two components.

(ii) A suitable diverging source is not currently available and would have to be developed. A large, plane disc is probably the best starting point.

(iii) A Herschel system based on a conic has some promise and also some problems. A greater length of peak along the principal ray is required. A usable system might be found if the forward radiating side lobe could be aligned along the principal ray.

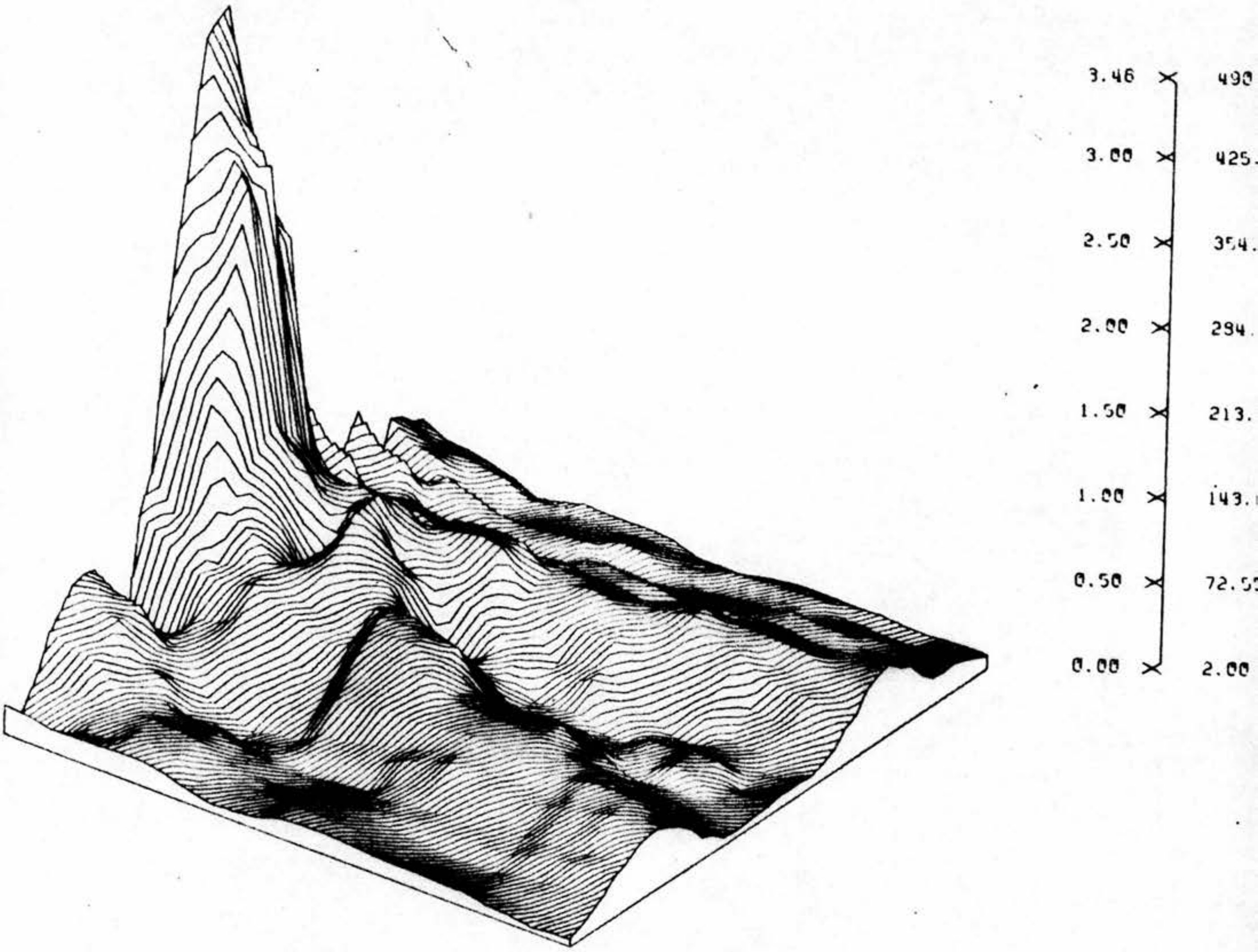

MS#6; FOCUSSED AT 125MM: AXIAL STEP 3MM, RADIAL 0.25MM

Figure 9.10. A rectlinear plot of the focal zone due to a small (50 mm diameter), Cassegrain Mirror.

Diameter of centre stop mm	Main lobe half-width mm					1st off-axis maximum		Main lobe length mm		
	-3dB level	-6dB level	-10dB level	-12dB level	1st off-axis minimum	radius mm	Amplitude dB	-6dB level	-12dB level	1st minima
0	0.39	0.53	0.66	0.70	0.92	1.25	-17.6	18.0	23.6	30.4
5	0.38	0.53	0.65	0.70	0.9	1.24	-16.9	18.3	24.0	30.4
10	0.38	0.52	0.64	0.68	0.9	1.24	-15.3	18.7	24.6	31.9
15	0.37	0.50	0.62	0.66	0.84	1.22	-13.2	19.8	26.3	33.6
20	0.361	0.49	0.59	0.64	0.80	1.20	-11.5	21.6	28.1	36.6
25	0.35+	0.46	0.56	0.60	0.76	1.16	-10.2	24.0	31.7	40.9
30	0.33	0.45-	0.54	0.58	0.71	1.12	-9.2	28.128	36.9	48.3

Table 9.2. Change of focal zone dimensions for a 50 mm diameter circular aperture apodised by a centre stop of increasing size.

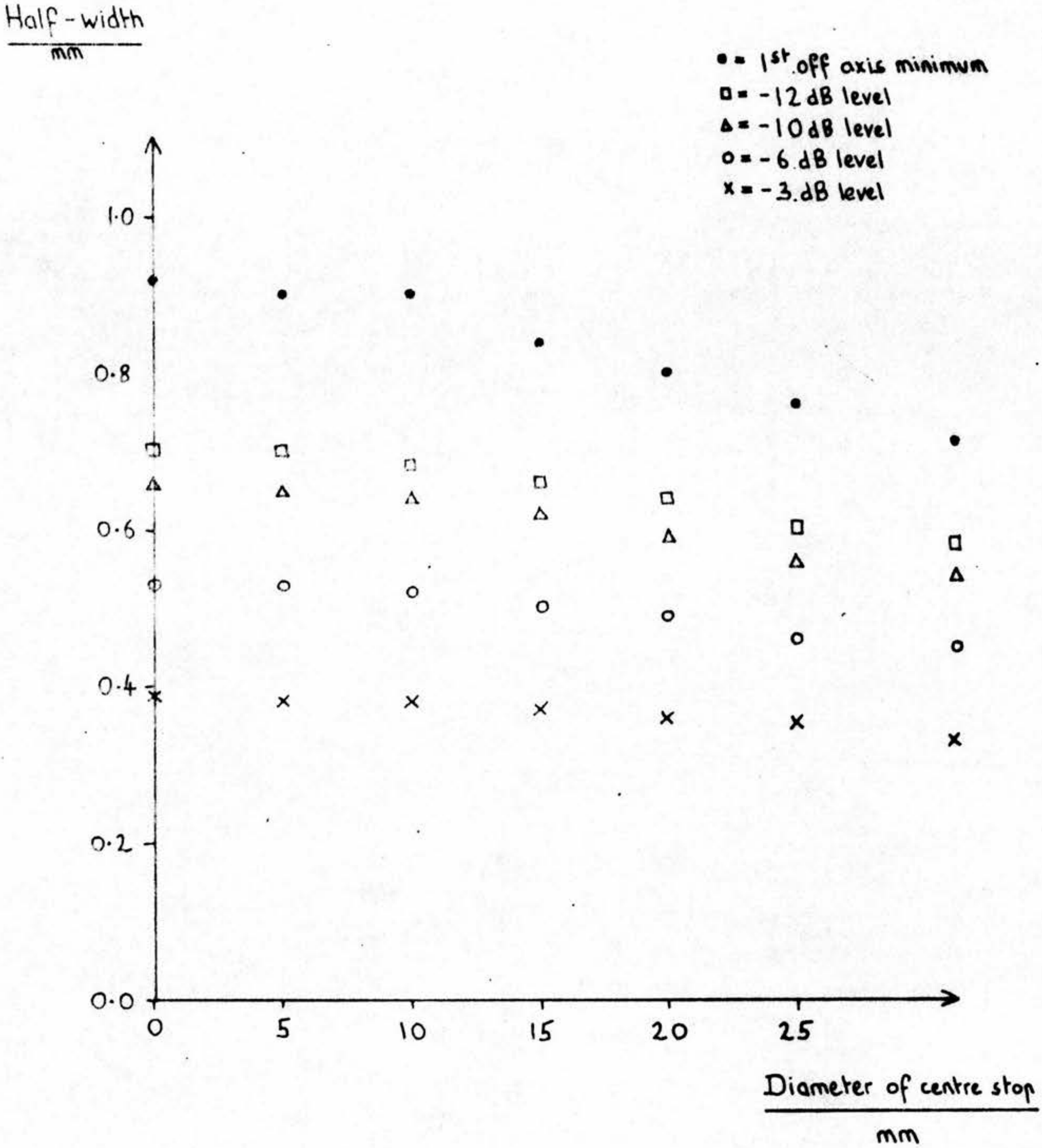

Figure 9.11(a): Behaviour of the main lobe of the beam due to a 50 mm circular aperture under increasing apodisation.

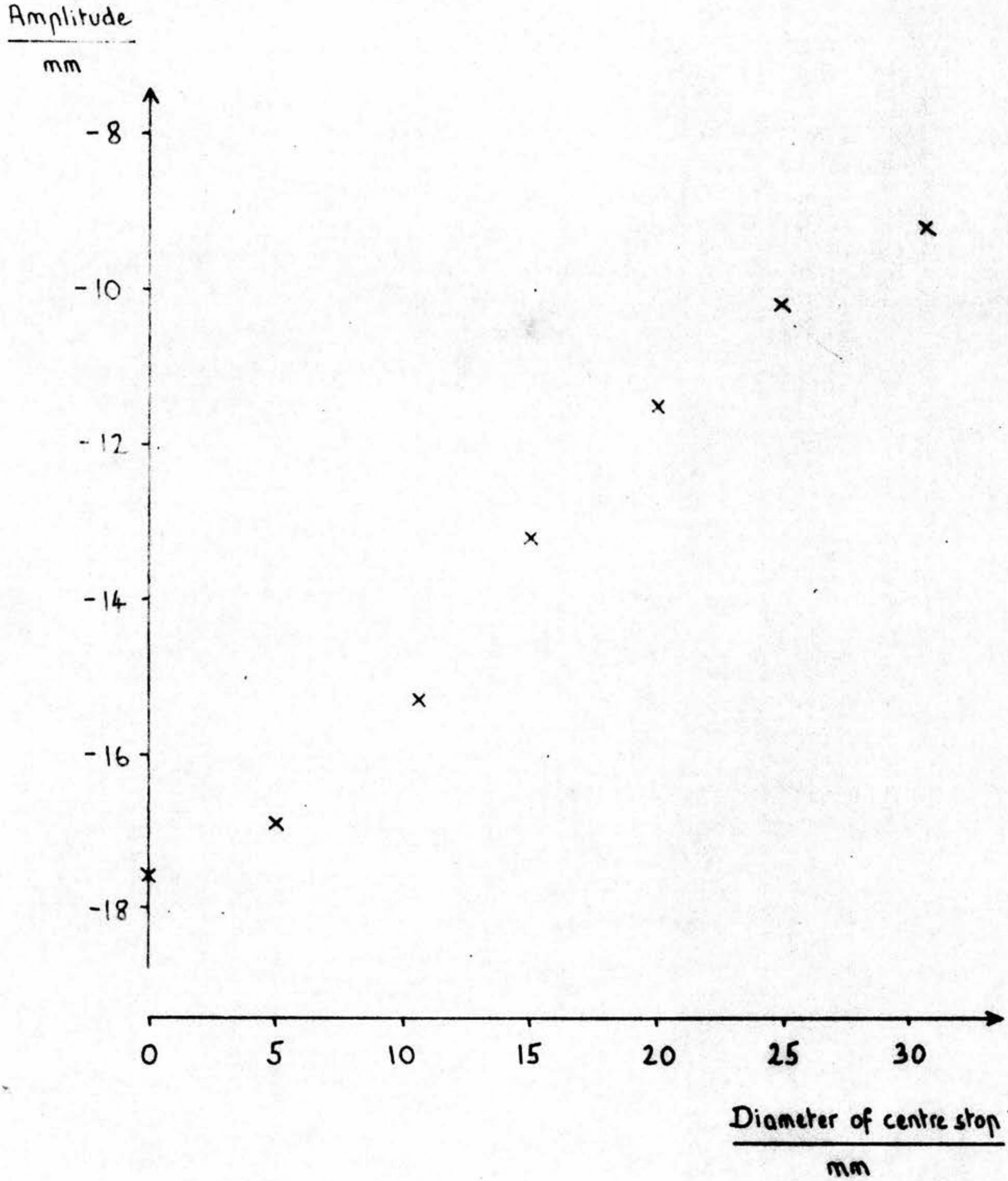

Figure 9.11(b): Behaviour of the first off-axis maximum to increasing the apodisation of a 50 mm diameter circular aperture.

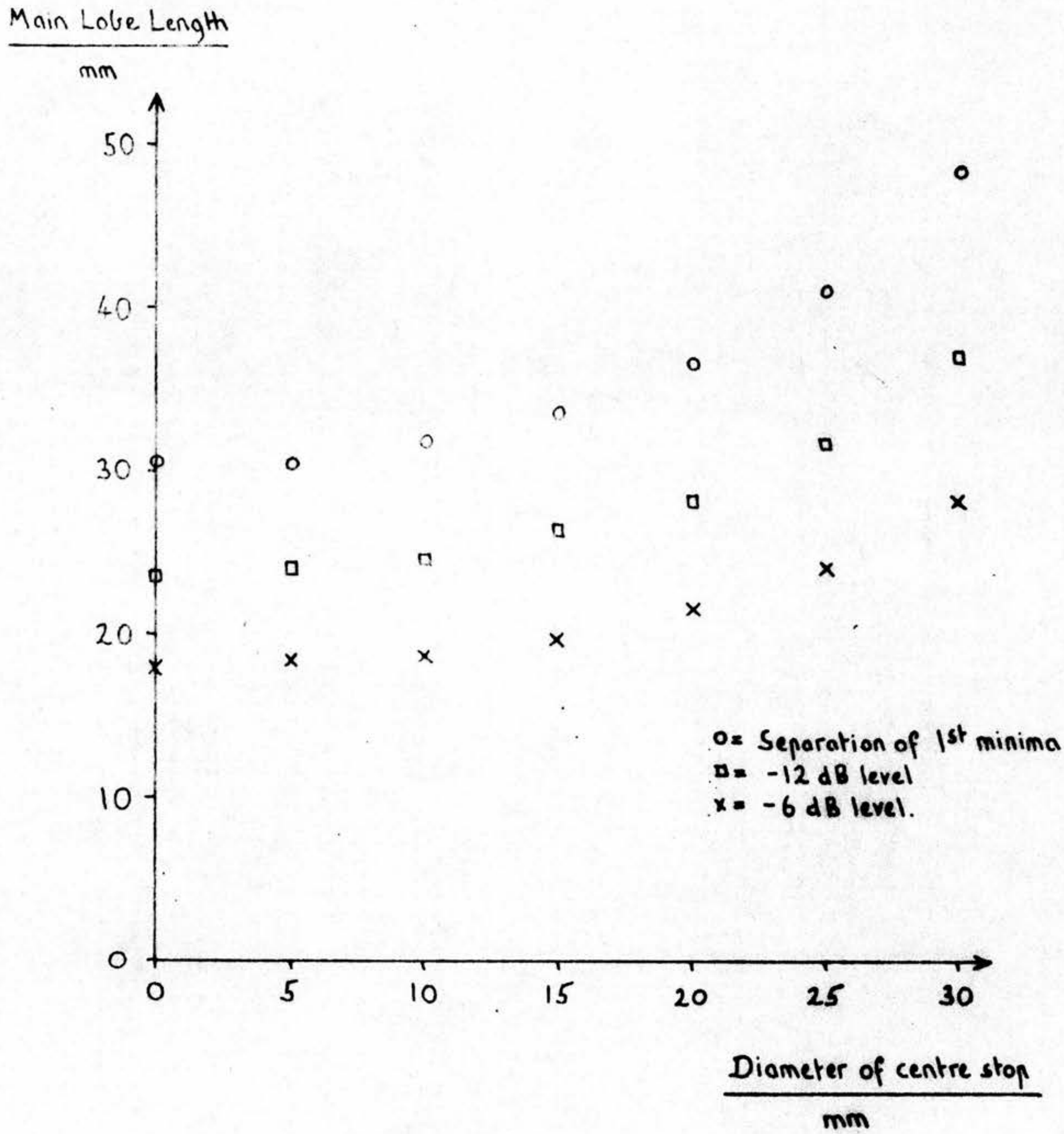

Figure 9.12: Response of main lobe length to increasing apodisation for a 500 mm diameter circular aperture.

(iv) The off-axis section of mirror does not appear to introduce additional aberrations to the focus.

(v) A Herschel system based on a spherical mirror is unusable, given the physical constraints here.

(vi) A modified Cassegrain mirror system of these dimensions has some promise but will suffer from the amplitude of side lobes, which, based on the experience of Chapter 8, will be even larger than the model predicts. Dynamic range will become more critical with longer focal length.

9.2. A modification of the Cassegrain Mirror System to give an extended focal zone.

9.2.1. Axicons

Normally wave fronts are focussed so that they converge towards a point. This gives best lateral resolution at a specific range with resolution decreasing away from that plane in either direction. Normally, therefore, lateral resolution must be sacrifised to obtain a usable depth of field.

This problem is common to all B-scanning techniques. One solution has been to shift the focal zone electronically while the pulse is travelling through the tissue being imaged (e.g. Arditi et al, 1981; Pye, 1983). These annular array techniques have been discussed briefly in section 2.2.5 and have been applied to breast scanning (Arditi et al, 1982).

Another technique is to image with a wave front, which is conically, not spherically converging. This approach originated with McLeod (1954) when he described the Axicon: a type of optical element which focusses a point on its geometric axis to a line. Examples of axicons, which he gives, are a thin annular aperture or a toroidal or a conic lens. In 1962 Fujiwara attempted to describe the field generated by such a system analytically using diffraction theory. Burckhardt et al (1977) built an ultrasound axicon mirror. However, this device suffered from high side lobes. The Toronto group have worked with a cone made from PVDF (Foster et al, 1981). They have attempted to reduce the side lobe problem by transmitting with the cone and receiving on annular array. More recently they have replaced the PVDF with a conical mirror system made from solid aluminium (Patterson and Foster, 1983). They have developed an approximation for the impulse response of a cone so that they may study the field theoretically (Patterson and Foster, 1982)

Burckhardt et al compared their experimental results with Fujiwara's theoretical predictions. They found the ratio of the first side lobe to the peak to be in agreement with the theory but the 2nd and 3rd side lobes were smaller than expected. Some points are worth noting about Fujiwara's development of the model and its application to the ultrasound device of Burckhardt. Fujiwara is concerned only with the transmitted field and comparison was made with the pulse-echo field simply by squaring the result. This would be quite reasonable if the target reproduced an identical wave front to that incident upon it. For a point target and a spherically converging wave front such circumstances might be envisaged but it seems unlikely that a conical wave front would be treated so. The assumption however worked well for Burckhardt. Fujiwara models a point source reflected in a cone but with the condition that the angle between the cone and a plane perpendicular to the axis of symmetry is very small (10^{-3} to 10^{-2} radian; $<$ 0.6 degrees) in order that he may substitute approximate expressions for the positions of the reflecting elements and for its size. Burckhardt's system does not meet this criterion. In Fujiwara's optical experiment to test his results, he used a reflecting cone with base 100 mm diameter and angle 1.5×10^{-2} radians with the object (a 1 mm diameter pinhole) and image at 20m.

Burckhardt used the same diameter aperture but focussed between 20 and 40 cm. Fujiwara's wavelength is 0.55×10^{-6}m; Burckhardt's 0.75×10^{-3}m. Also, as with the devices described here, Burckhardt's mirror system had a secondary reflector in the centre of the aperture making it annular rather than circular.

9.2.2. A Modification of the Cassegrain Geometry to give a line focus.

A conventional, conical axicon geometry is shown in figure 9.13. Seen in section two plane wave fronts converge to intersect from F to F'. When a cone is generated about the axis, this gives an axial wavefront. The main problems reported are the size of sidelobes and insensitivity.

The only general constraint of an axicon is that it is circularly symmetric (McLeod, 1954). There is no requirement that the wave fronts be plane in section; they might well be converging. Such an arrangement might increase sensitivity.

A modification of the Cassegrain geometry is shown in figure 9.14. The idea is similar to that of the modification described in Chapter 8. The difference in this design is that the external reference point (e.r.p.) of the primary ellipse is moved off-axis. The primary ellipse is shown in figure 9.14(a). The two reference points lie on the axis AA'. The extreme rays are drawn. Another axis may be chosen which intersects this converging beam over a finite length, BB'. Generation of a mirror by rotation about such an axis will give a system as shown in figure 9.14(b). A conical axicon will have a real line focus and a virtual, ring focus at infinity. This device will have a real line focus and a real ring focus generated by the external reference point (e.r.p) of the original ellipse rotating about the axis BB'.

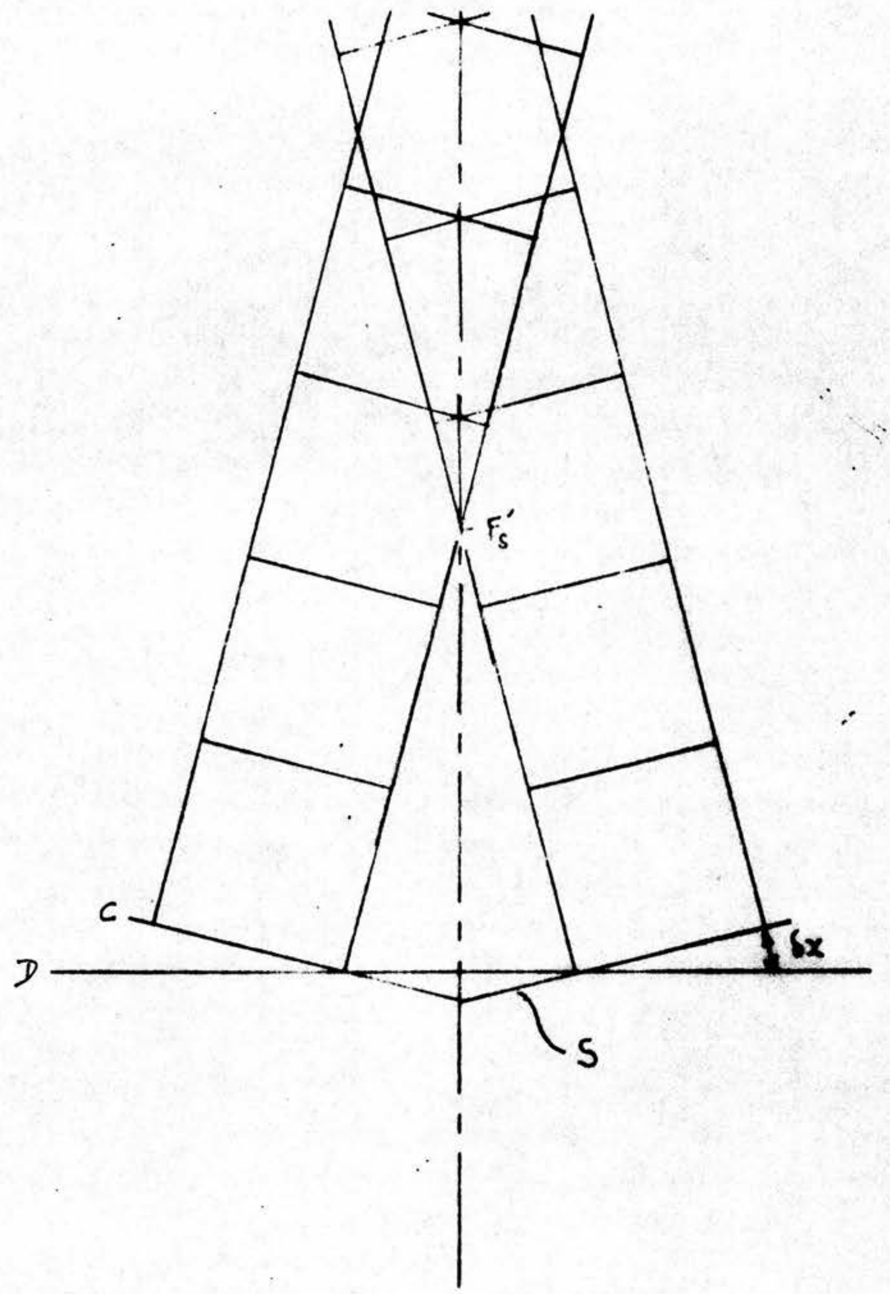

Figure 9.13: A conventional, conical axicon geometry.

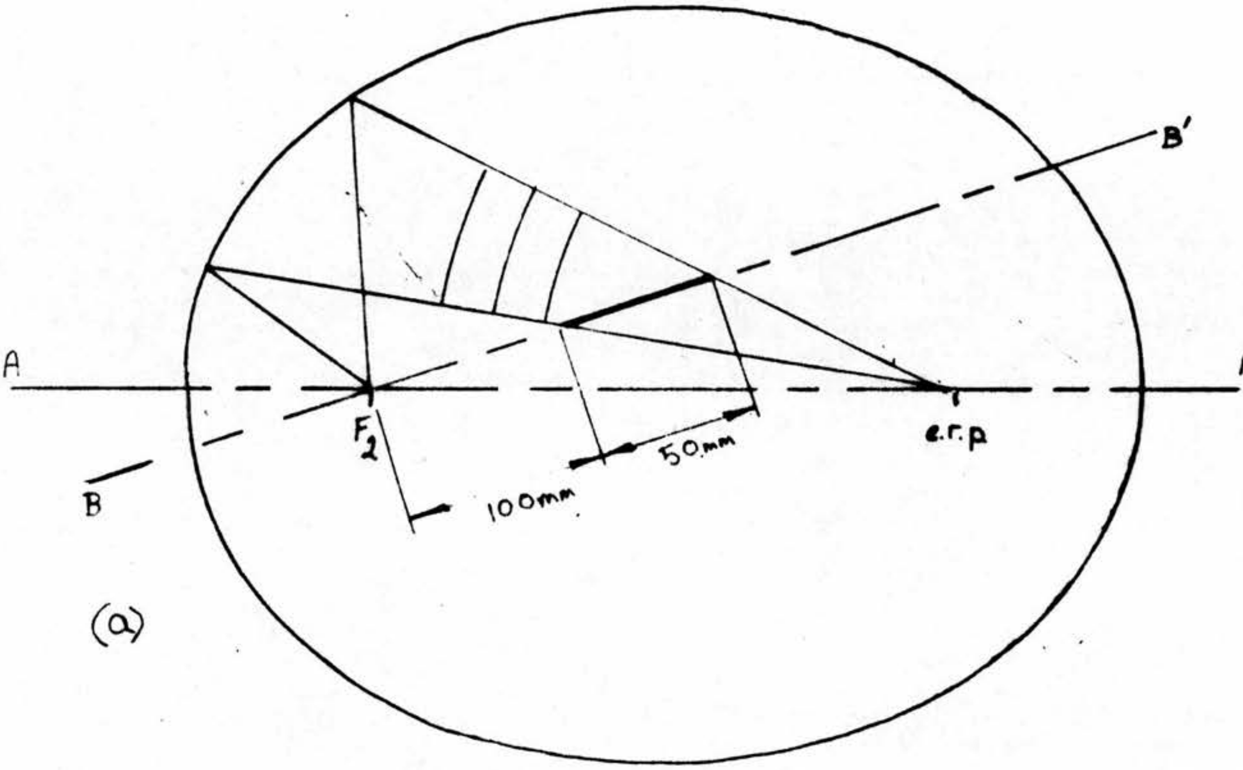

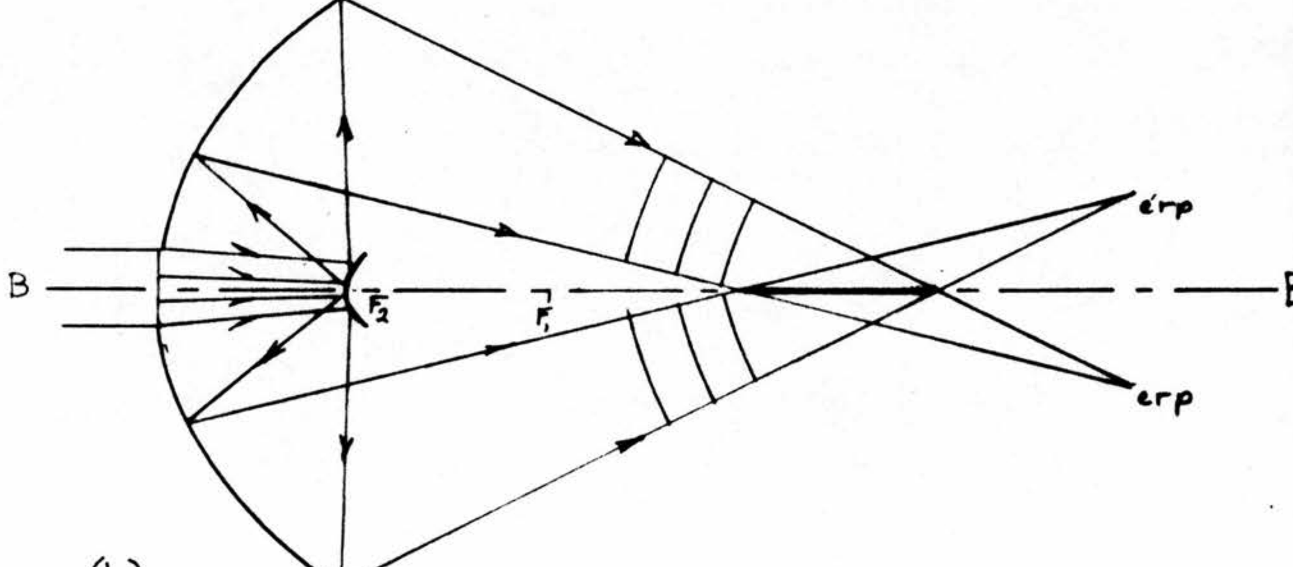

Figure 9.14. Modifying the Cassegrain geometry to give an extended focal zone.

9.2.3. Comparing Axicon Field Patterns from Pulsed Annular Arrays

The numerical model written and described by Pye (1983) was used to consider the relative effects of the two wavefronts.

The model was designed to consider design parameters for plane disc annular array transducers.

The time required to calculate the results when the model was run on a PDP-8 was one overnight run per ring. The axicon was, therefore, modelled on four rings, contiguous in an annulus. Ring widths were limited so that no significant phase differences would occur across an individual ring seen from the focal zone. Parameters used are range, Z = 100 mm: $\frac{1}{2}\lambda$ as the phase limit, wavelength : λ = 0.304 mm (5MHz at 1500 ms^{-1}) and the Fresnal zones are calculated from

$$r_{1o}{}^{2} = \left(\frac{\lambda}{2} + Z\right)^{2} - Z^{2} \qquad - 9.1$$

where r_{1o} is the outer radius of ring 1 (and the inner radius of ring 2).

This gives 4 rings.

Ring 1 radius 5.52 to 7.80 mm.
Ring 2 radius 7.80 to 9.55 mm.
Ring 3 radius 9.55 to 11.03 mm.
Ring 4 radius 11.03 to 12.33 mm.

The model always simulates a disc transducer (surface D in figure 9.13) and the effect of the conic surface (C) or another surface is simulated by altering the time of transmission from a ring to give a time difference, δt equivalent to the distance δx . These delays are calculated for the inner radius of the rings. The outer ring transmits first and the other rings transmit successively moving inwards.

The pulse considered is four cycles in a sinusoidal envelope as shown in the output.

i) <u>PW results for a conical wavefront.</u>

Delays	ring 1 :	0.200 µs
	2 :	0.146 µs
	3 :	0.083 µs
	4 :	0.000 µs

The field plot is shown in figure 9.15 and transverse sections in figure 9.16.

ii) <u>PW results for a converging wavefront.</u>

Delays	ring 1 :	0.2384 µs
	2 :	0.1445 µs
	3 :	0.069 µs
	4 :	0

These delays are calculated from the geometry shown in figure 9.17. The rays from the inner and outer rings are taken to define the axial focal length (Z_1, Z_2) and meet at the point C. The delays give a circular wave front centred on this point. Rotation about the Z-axis gives the axicon wavefront described in section 9.2.2. The delays are chosen, based on a velocity of 1520 ms^{-1} to give Z_1 = 100 mm, Z_2 = 150 mm.

The field plot for this wavefront is shown in figure 9.18 with transverse section in figure 9.19.

Using the model enables the comparison of fields due to a conical wavefront and a more sharply converging wavefront as described above. The results show that the second wavefront has advantages in sensitivity and in transverse beam shape.

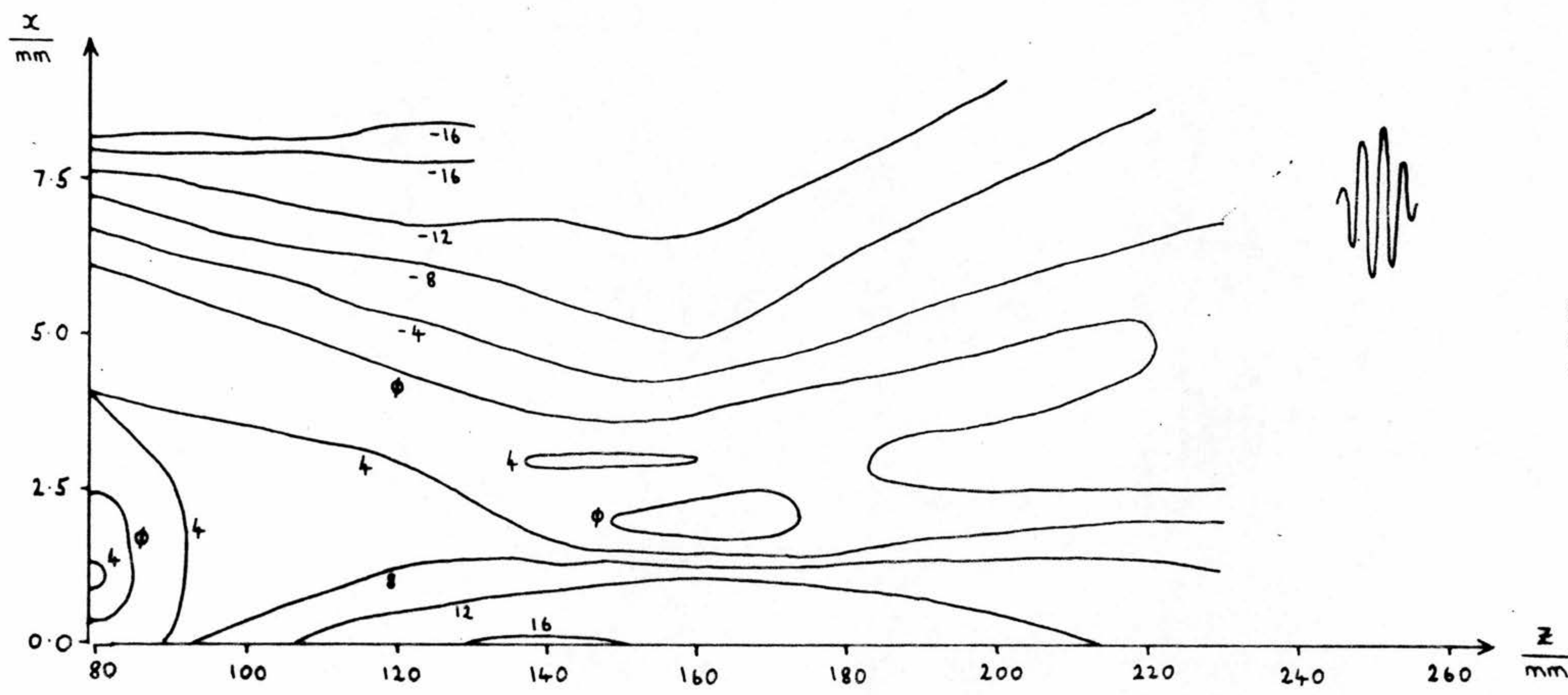

Figure 9.15. Conical axicon field plot.

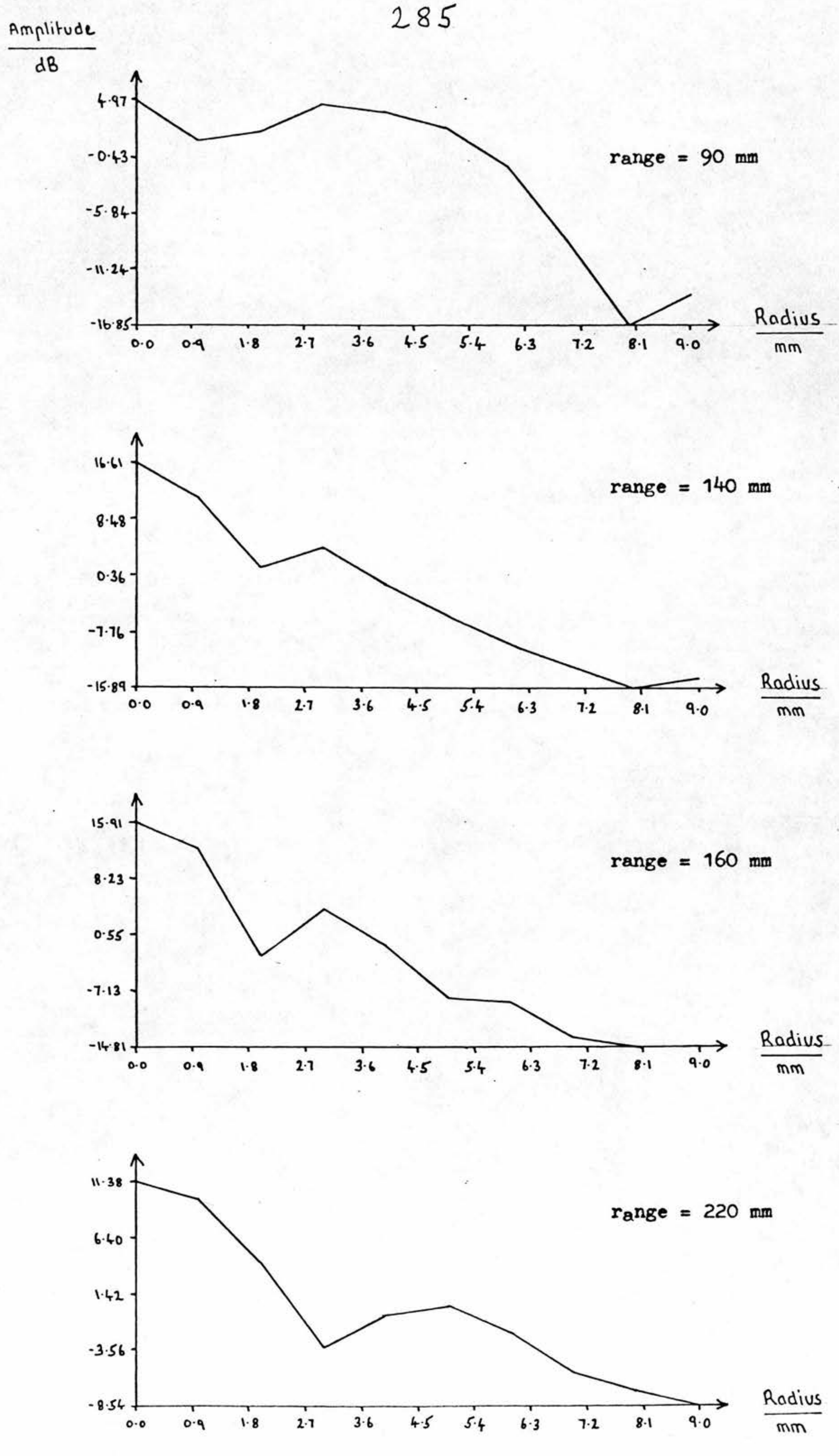

Figure 9.16. Conical axicon field transverse plots.

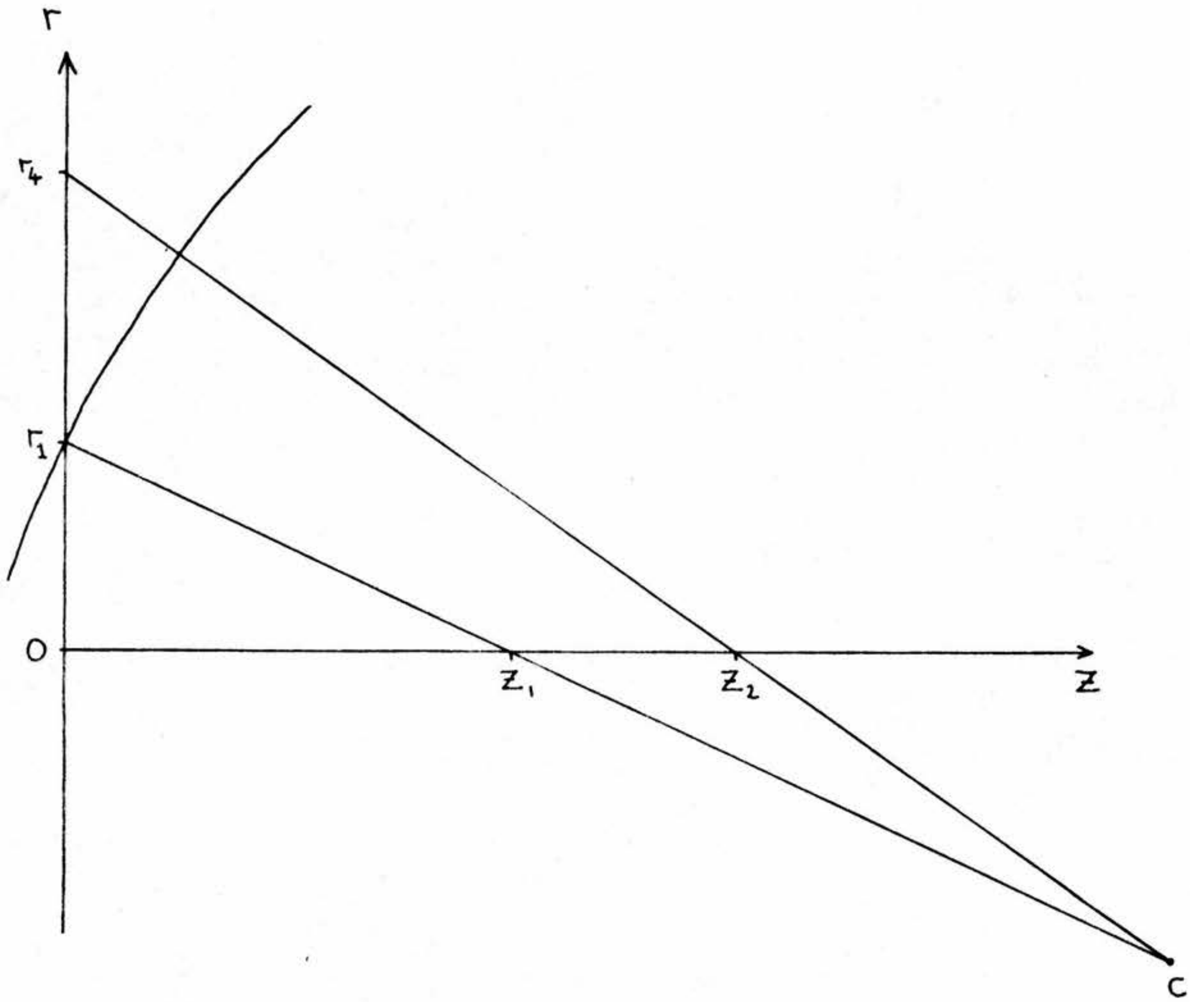

Figure 9.17. Converging axicon wavefront.

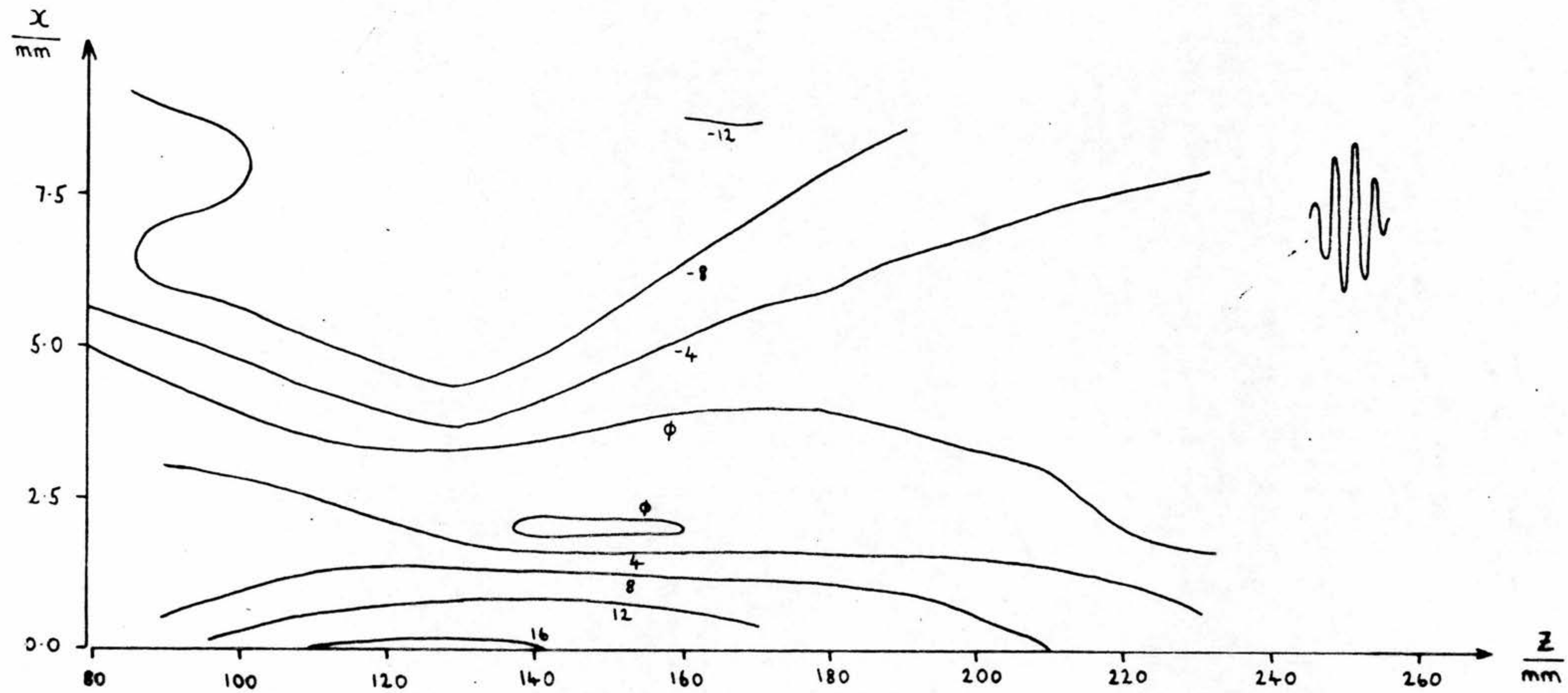

Figure 9.18. Converging axicon wavefront field plot.

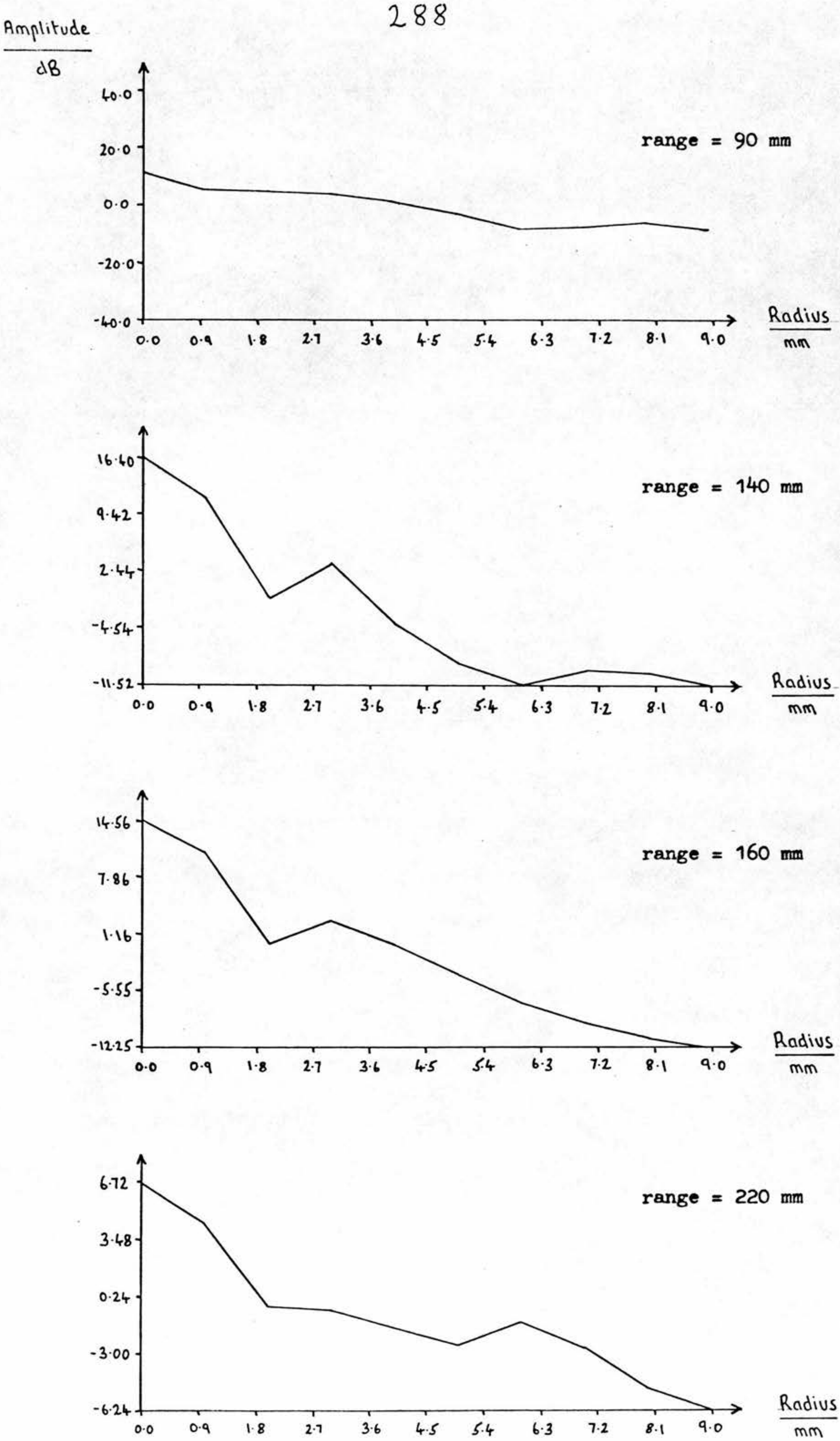

Figure 9.19. Converging axicon field: Transverse plots.

9.2.4. Final Design

The output of the design program is shown in figure 9.20.

The primary mirror has its external reference point at (198.5, -15). This gives a distance of 200 mm between the reference points. The semi-major-axis is 134.4 mm. The curve is actually described by the quadratic

$$0.449x^2 + 8.278 \times 10^{-2}xy + 0.9989y^2 - 89.03x + 6.694y - 3600 = 0$$

The secondary shown in figure 9.20 is ellipsoidal with both reference points on the system axis. As with the Cassegrain system (Chapter 7) a paraboloidal secondary may be used with an unfocussed transducer or, if the mirror is used only on reception, a hyperboloidal secondary will focus the received pulses on to a small detector. This design uses the same secondaries as the Cassegrain system described in Chapter 7.

The work of Foster et al (1981, 1983) suggests the use of a reception only axicon in conjunction with another probe may be useful for overcoming high sidelobes.

9.2.5. Experimental Results.

An experimental pulse-echo plot of the axicon mirror system is shown in figure 9.21.

The focal depth is increased but the focal zone shows considerable variation along the axis. In places, the sidelobes are large (-11 dB). At 133 mm range the peak drops to -13 dB of the field maximum. The field, however, is also promisingly narrow. At the field maximum the -10 dB full width is 1.1 mm.

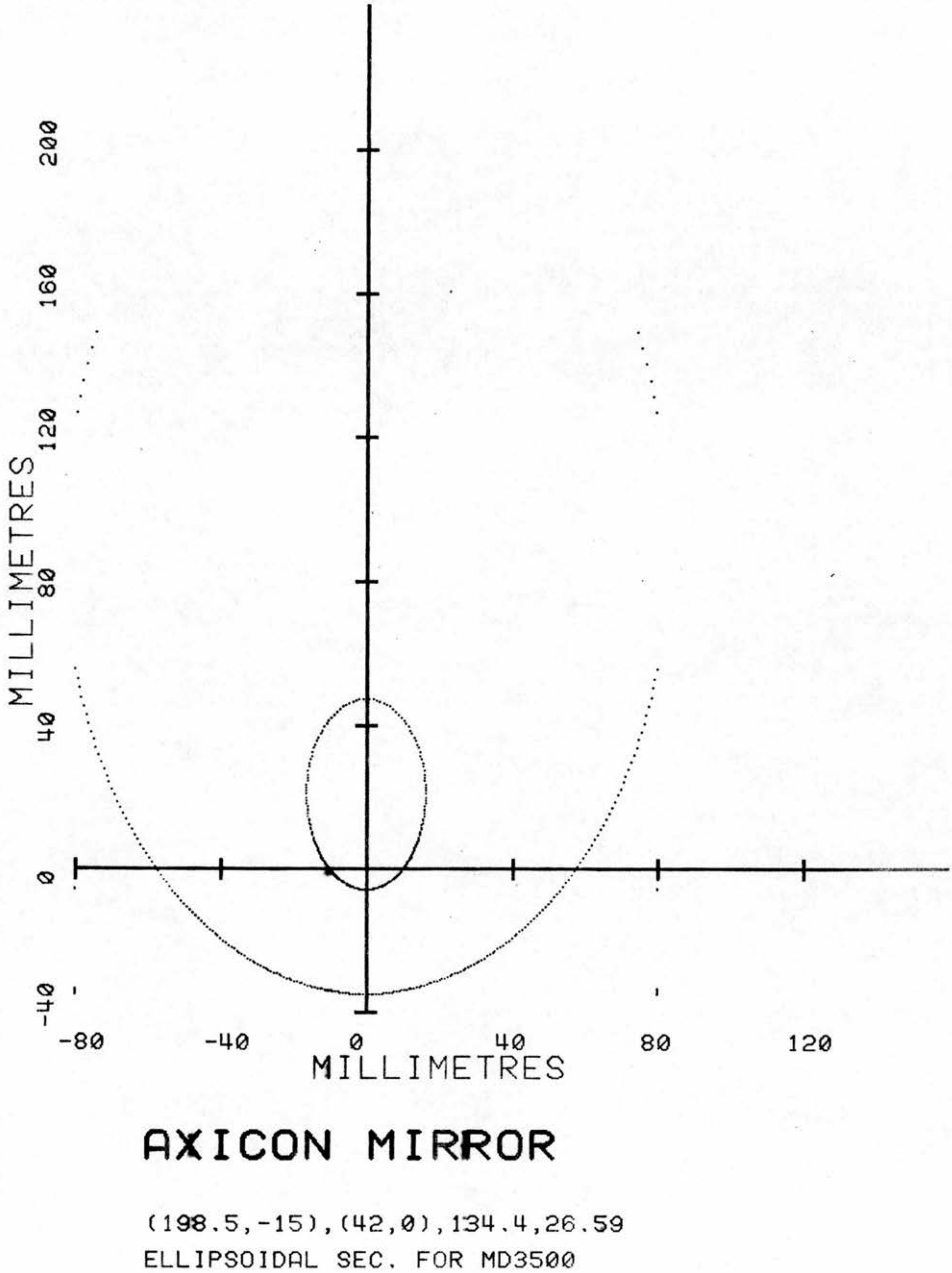

FIGURE 9.20: Design program output for a Cassegrain system modified to give an axicon wavefront.

focal spot observed. Changes in the shape of the focus were also observed.

The results are presented in tables 9.3 and 9.4, shown graphically in figures 9.23 to 9.25.

As expected the focus moves outwards as the source is moved inwards.

The field maximum amplitude is little affected by the movement. The outward movement is amplified and accompanied by a desirable increase in focal length. There is also an increase in width but this is less marked. The relative amplitude of the first sidelobe is little affected by the result. The hydrophone simulation is insensitive to the beam width charges.

9.3.2. Experiment

An outward movement of approximately 2 mm to the secondary resulted in an inward movement of approximately 10 mm. The axial field is shown in figure 9.26.

9.3.3. Conclusions and Practical Considerations.

The theoretical results are promising. The spherical mirror model suggests that the focus can be moved over a useful range. The limited experiments and experience aligning the Cassegrain mirrors support this. It is encouraging that moving the focus does not greatly degrade it. The width increases but is still useful. Importantly the amplitude of the sidelobes are not increased by this.

There is a need for more theoretical work. The effect with an ellipsoidal mirror must be investigated. Although spherical aberration is introduced by moving the source with the spherical mirror, the effect with the ellipsoid will be different. It is

9.2.6. Conclusions.

The system offers the potential of a sharp focus of depth 40 mm. The air-backed thin copper mirror again produces a system sensitive enough for use on transmission and reception.

Experimentally variations in alignment and different combinations of transducer and secondary mirror should be tried to improve the field. The reception only mirror should be tried with different probes for transmission.

Theoretically variations in mirror shape and in focal length and depth should be investigated with the CW mirror model (PLOTCW).

9.3. Moving the Focal Zone of a Cassegrain Mirror.

When aligning the Cassegrain mirror systems it was observed that although the position of the focus was influenced by small movements of the secondary mirror, its size did not seem to be appreciably affected. The possibility of positioning the focal zone by small movements of the secondary mirror was therefore investigated.

The Cassegrain system described in Chapter 7 is the subject of this study.

9.3.1. Theoretical Assessment.

The mirror system was modelled as a spherical mirror, radius of curvature 100 mm with an aperture 100 mm diameter apodised by a centre stop 20 mm diameter. MIRROR2, a circle passing through the origin, was used to simulate the reflector, the source moved about the centre of curvature and the consequent movement of the

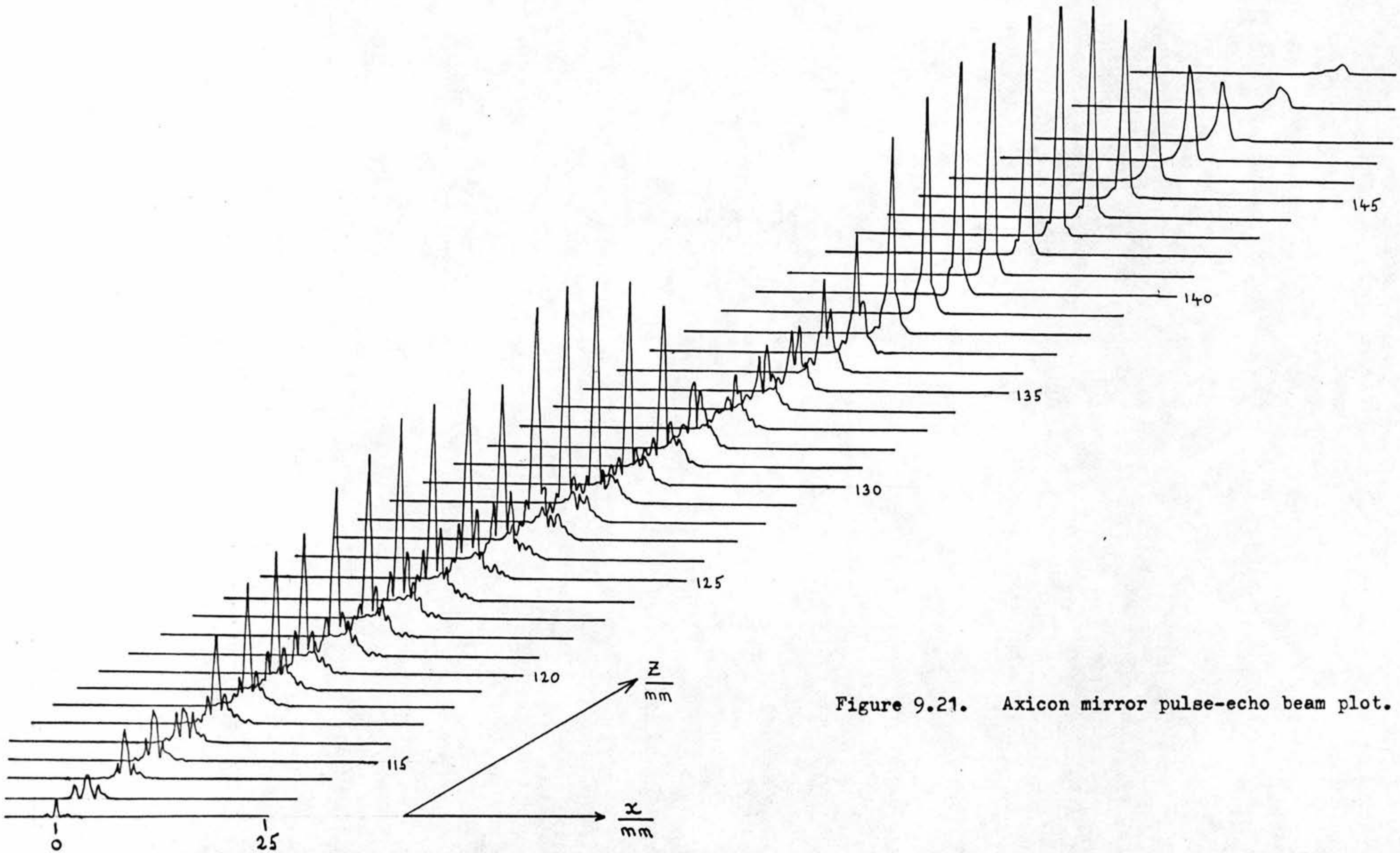

Figure 9.21. Axicon mirror pulse-echo beam plot.

Relative Position of source	Relative Position of field maximum	Length of focal zone mm					Relative amplitude of field maximums
mm	mm	-3dB level	-6dB level	-10dB level	Separation of 1st minima	Separation of 2nd maxima	
-18	+28.15	3.5	4.65	5.78	7.73	11.25	0.958
-15	+21.4	3.15	4.22	5.18	7.0	10.0	0.973
-12	+15.75	2.85	3.86	4.73	6.3	9.15	0.984
-9	+11.0	2.55	3.53	4.2	6.0	8.25	0.991
-6	+6.75	2.4	3.23	3.98	5.33	7.8	0.996
-3	+3.25	2.175	3.02	3.7	5.0	7.02	0.998
0	0	2.12	2.9	3.45	4.72	6.75	1.0
+3	-2.75	1.95	2.7	3.31	4.5	6.41	0.996
+6	-5.37	1.95	2.55	3.15	4.13	6.0	0.997

Table 9.3. Effect of moving the source upon focal position and focal length.

Relative position of source mm	Relative position of focus mm	Main lobe half-width mm				1st off-axis maximum		Theoretical Hydrophone result half-width mm		
		-3dB level	-6dB level	-10dB level	1st off-axis minimum	radius mm	amplitude dB	-3dB level	-6dB level	-10dB level
-18	+28.15	0.195	0.27	0.33	0.45	0.64	-15.2	0.43	0.55	0.66
-15	+21.4	0.18	0.255	0.31	0.44	0.6	-15.2	0.43	0.55	0.65
-12	+15.75	0.175	0.245	0.3	0.41	0.57	-15.3	0.43	0.54	0.64
-9	+11.0	0.17	0.23	0.285	0.4	0.55	-15.2	0.425	0.53	0.63
-6	+6.75	0.16	0.22	0.275	0.38	0.53	-15.3	0.43	0.53	0.63
-3	+3.25	0.16	0.215	0.265	0.36	0.51	-15.2	0.43	0.53	0.63
0	0	0.152	0.21	0.26	0.35	0.5	-15.2	0.43	0.525	0.625
+3	-2.75	0.15	0.205	0.25	0.34	0.47	-15.3	0.43	0.53	0.62
+6	-5.37	0.145	0.20	0.245	0.33	0.45	-15.3	0.43	0.525	0.62

Table 9.4. Effect of moving the source upon beam width

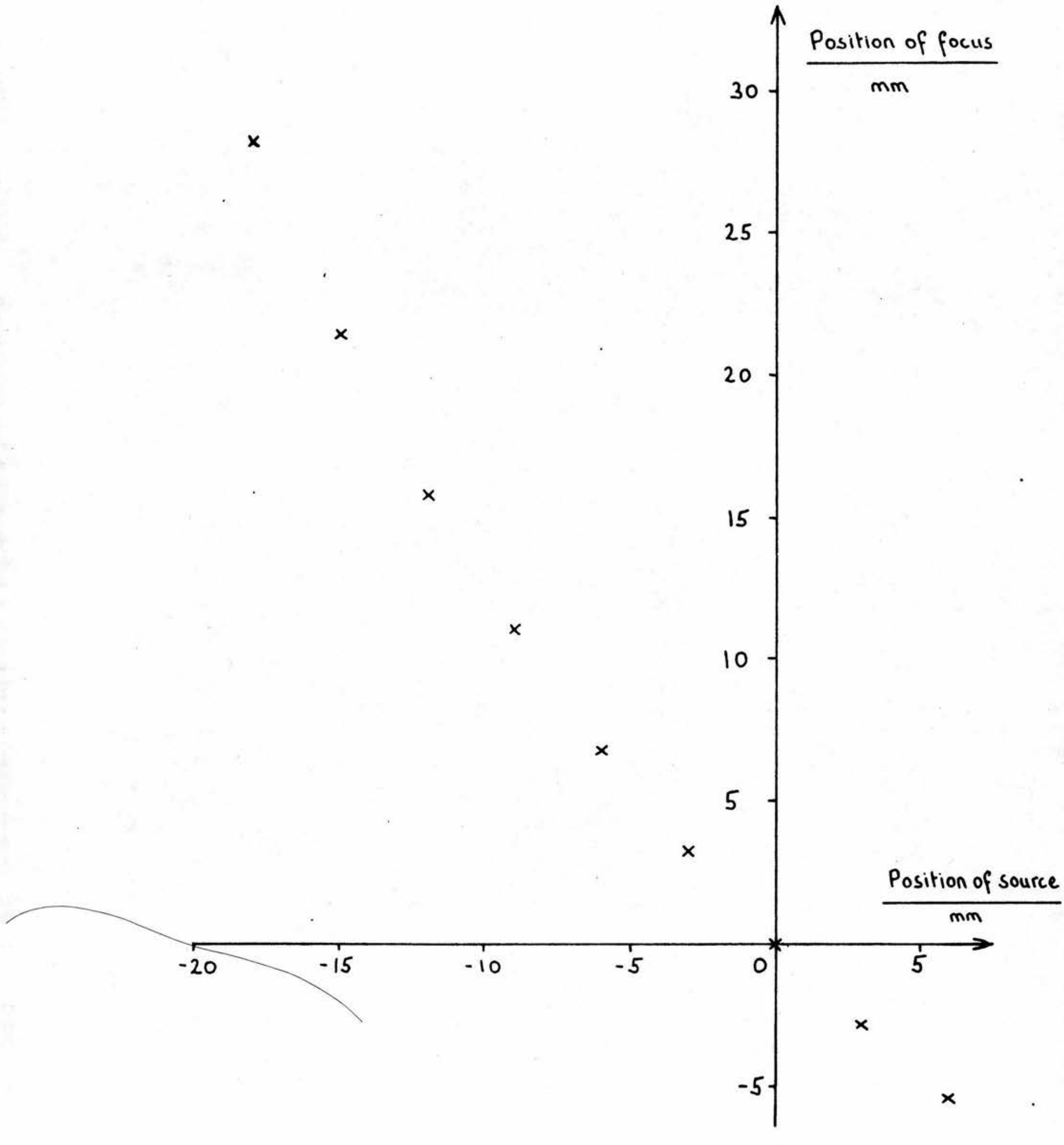

Figure 9.23. Movement of the focus in response to displacement of the source. (Spherical mirror simulation of Cassegrain Mirror: Chapter 7.)

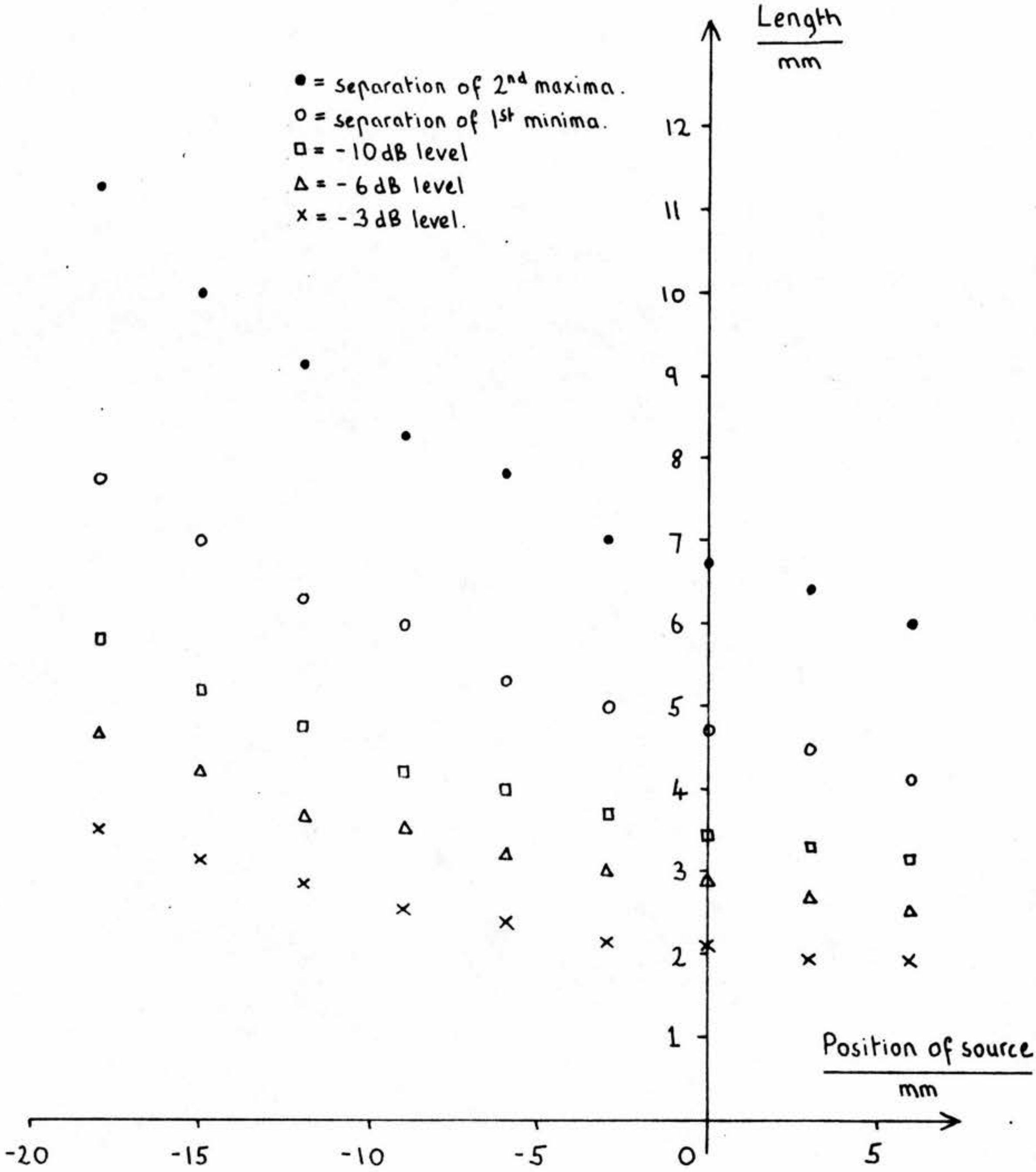

Figure 9.24. Change in focal size in response to displacement of the source.

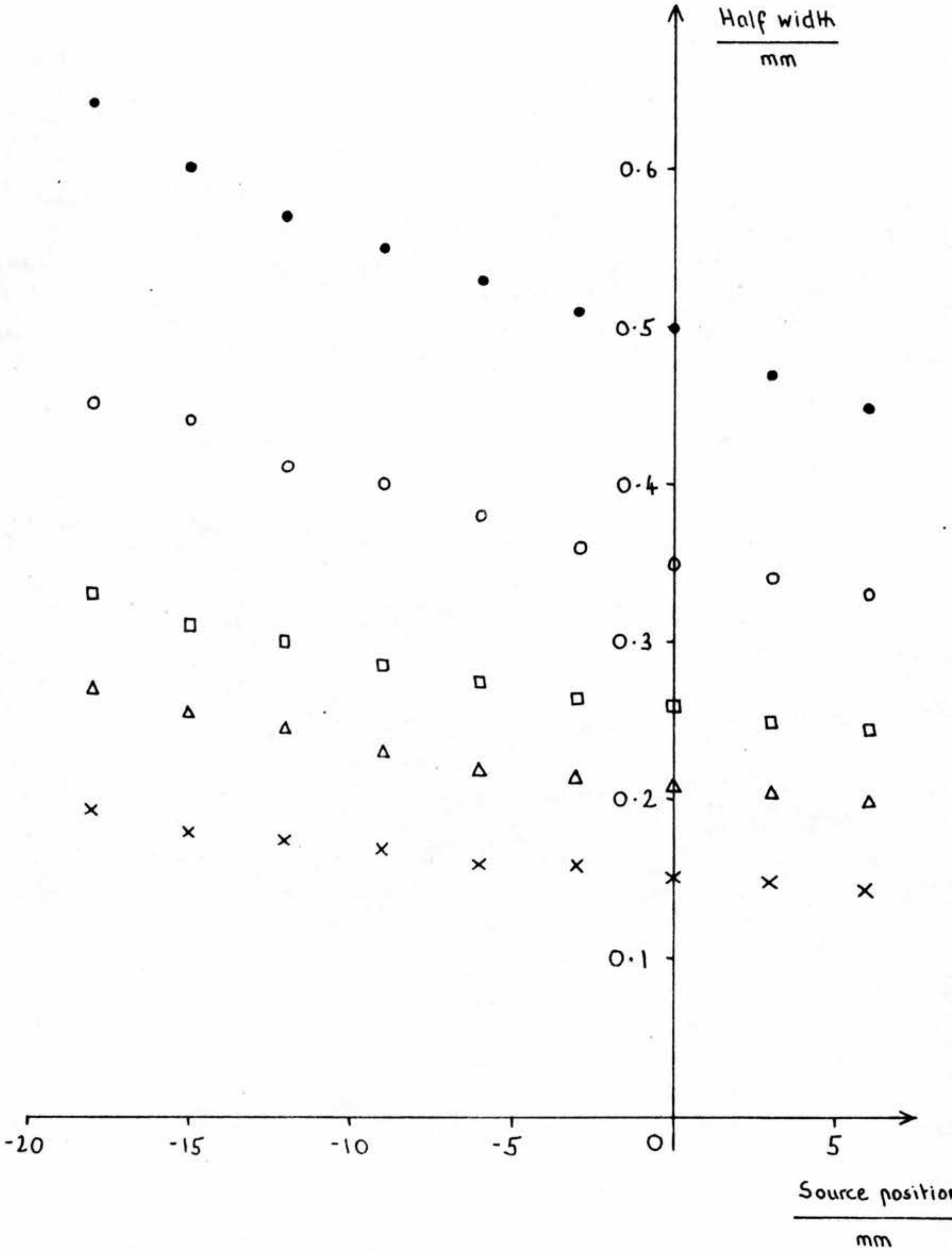

Figure 9.25. Effect of source movement upon beam width.

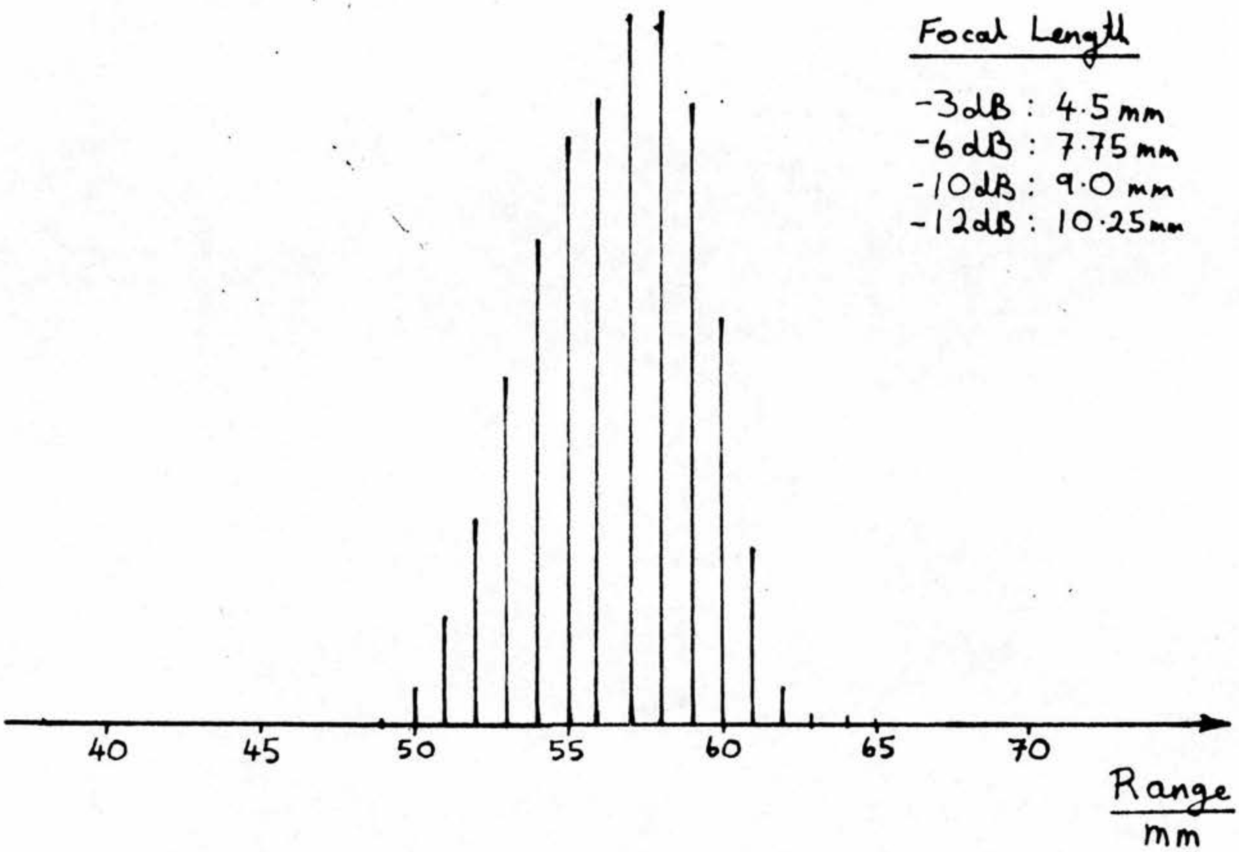

Figure 9.26. An axial plot of the Cassegrain Mirror with the secondary moved outwards by $\sim$2mm.

important to see what movements of the source will be required to move the focus over a usable range.

Experimental work needs to be done. The actual fields must be observed, as well as movement of the focal peak. Since spherical aberration caused by the axial distribution of the transducer field is a major factor in degrading the focus, the effect will be modified by the secondary moving along the transducer field. It will be altered too by the modified Cassegrain geometry (Chapter 8).

Practically there would be difficulties but these do not appear exceptional. The connection of a stepper motor drive to secondary mirror adjustment would require a new mirror mounting. The drive would require waterproofing. A slow speed drive to produce a composite image by combining bands of linear scans, such as those shown in Chapter 8) would be uncomplicated. A faster movement to build up a single line on the image before moving the mirror to generate the next line would require a better drive mechanism and a sophisticated electronic control to gate the recording of the image. This would probably require a microprocessor. The breast scanner already has a microprocessor and interface to control the scanning motors. It would be a suitable test bed for such a device.

9.4. Summary.

Ultrasound mirror systems have been investigated and found to be a practical method of producing a sharp focus in a waterbath.

A modification of the traditional Cassegrain geometry gives a system suitable for imaging. The use of pointed reflector surfaces has eliminated the problems of reverberations between components of the system. The modified geometry combines a sharply focussed beam with an adequate dynamic range for imaging in fine detail small regions of tissue. A limitation on the device is its small depth of field.

The use of thin, air-backed copper gives a mirror system of high sensitivity when used for both transmission and reception.

Continuous wave numerical models have proved a useful tool in studying and designing mirror systems. The ultrasound conditions are simplified by the use of continuous wave theory; this permits a better approach to the true geometry. The effects of geometry are important and influence the choice of design parameters. The model simulates the geometry of the primary mirror. Development could give a limited pulsed wave model or include the transducer and secondary mirror geometry - thus simulating the entire system geometry.

Mirror systems are capable of development. A Herschel system suitable for imaging might be developed. A mirror system might be designed which, while maintaining a sharp focus, has an extended focal zone, either by a modified geometry to give an axicon wavefront, as in section 9.2 or by varying the mirror geometry while imaging as in section 9.3.

Appendix 1. Definitions and Conventions used in Conic Relationships

It is not the intent to introduce new terminology. As far as possible standard terminology is followed. Where ambiguity is possible, the conventions described by Bruggemann (1968) are employed.

The use of conic mirrors requires that the definition of 'focus' be clarified. To the geometrician working with conic curves, 'focus' means the two points on the major axis, the sum of whose distances from any point on the curve, is constant. (This is true for a hyperbola as well as an ellipse if one distance is considered negative).

Generally, however, when discussing ultrasound transducers 'focus' means the point to which the sound waves converge. In figure A1 the geometrician's 'foci' are the two points where the rays A and A' cross the axis, while physically the 'foci' are defined by the distances O and I. To avoid confusion, the term 'focus' is used in the physical sense, while the term 'reference point' is used for the geometrician's 'focus'.

The mirror design program described in Chapter 6 limits the conventions that may be used to describe a conic. In particular, the usual parameters for describing an ellipse, the semi-major axis, a, and the semi-minor axis, b, may not be readily employed, since they introduce a discontinuity between the description of an ellipse and a hyperbola This is why eccentricity, e, is used in the description of the curve plotted by that program. Two conic mirrors, operating together, must have a common reference point. If this is used as the polar co-ordinate origin, the two surfaces will share the same origin. This simplifies the description of two mirror systems.

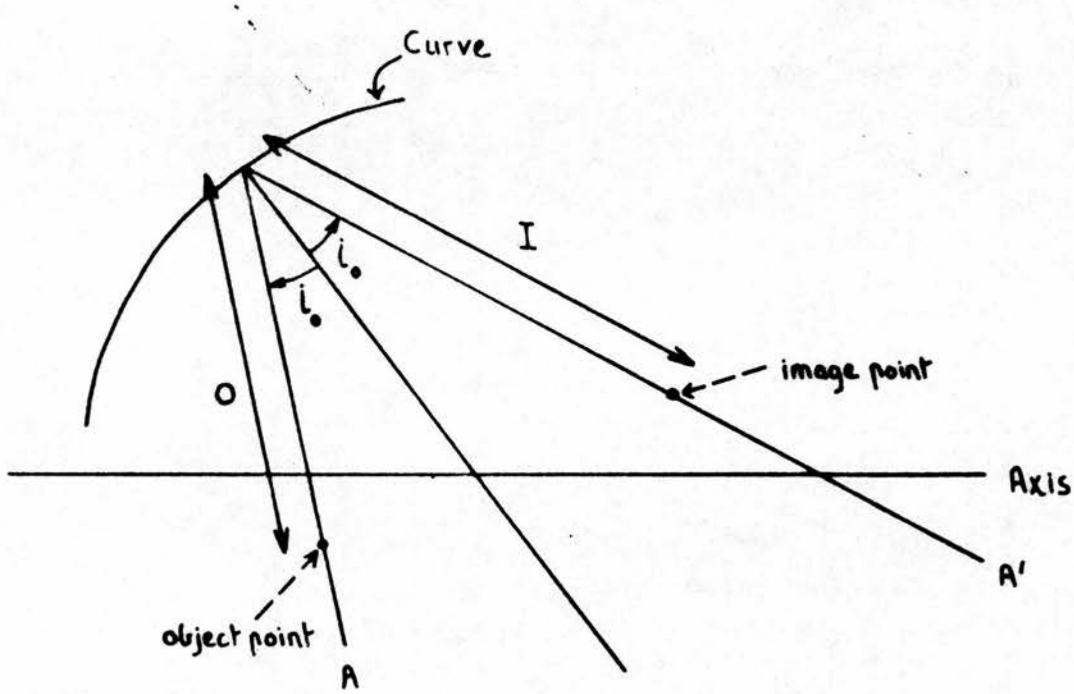

Figure A1. Surface of revolution, used as a mirror.

Appendix 2. Key Excerpts from Program Listings.

a) PLOTCW

i) Subroutine POINT1 and functions.

```
PLOTPOINT1.FT  V4A  JJN 17-FEB-81
SUBROUTINE FOR PLOTCW.FT PROGRAMS
CALCULATES PRESSURE AMPLITUDE AT POINT (L,R)
REQUIRES FUNCTIONS FUN3,FUN4,MIRROR,PHI1,PHI2
WHICH MUST BE FOUND IN THE DIRECTORY.
CCCCCCCCCCCCCCCCCCCCCCCCCCCCCCCCC
THIS POINT* NOW ACCEPTS ONLY AXIAL LIMITS
FOR THE INNER INTEGRAL AND THEREFORE MUST ONLY BE
USED WITH PLOTCW V.3J ONWARDS WHICH ALSO KNOW THIS.
CCCCCCCCCCCCCCCCCCCCCCCCCCCCCCCCCCC

SUBROUTINE POINT1 (CURVNO,I)
REAL*8 ZETA,AP,LP,K
REAL*8 FUN3,FUN4,PHI3,PHI4
REAL*8 PI2
REAL*8 ABSACC
REAL*8 AMP,AMPR,AMPI
INTEGER CURVNO,I,IFAIL,NPTS,PASS
DOUBLE PRECISION PLOTX1(100),PLOTX2(100),PLOTX3(100)
DOUBLE PRECISION PLOTY1(100),PLOTY2(100),PLOTY3(100)
COMMON PLOTX1,PLOTX2,PLOTX3,PLOTY1,PLOTY2,PLOTY3
COMMON /FUN/ ZETA,AP,LP,K
EXTERNAL FUN3,FUN4,PHI3,PHI4
DATA PI2 /6.28318530718D0/
ABSACC=0.1D-4
///
 ANS=PHI3(1.D0)
 WRITE (6,7010) ANS
 FORMAT(' PHI3=',G14.6)
 ANS=PHI4(1.D0)
 WRITE (6,7020) ANS
 FORMAT(' PHI4=',G14.6)
 /
 ALCULATE 'REAL' COMPONENT
 ASS=1
 FAIL=1
 ALL D01DAF(0.D 0,PI2,
          PHI3,PHI4,FUN3,ABSACC,AMPR,NPTS,IFAIL)

 WRITE (6,7000) PASS,AMPR,NPTS
 FORMAT(' PASS',I2,'INTEGRAL=',G14.7/' NO. OF FN EVALUATIONS=',I

 F (IFAIL) 100,100,900
 EPEAT CALL FOR 'IMAGINARY' COMPONENT
 ASS=2
 FAIL=1
 ALL D01DAF(0.D 0,PI2,
          PHI3,PHI4,FUN4,ABSACC,AMPI,NPTS,IFAIL)

 WRITE (6,7000) PASS,AMPI,NPTS

 F (IFAIL) 200,200,900
 CULATE AMPLITUDE MAGNITUDE. (!)
 MP=DSQRT(AMPR*AMPR + AMPI*AMPI) *K/PI2
 F (CURVNO.EQ.1) PLOTY1(I)=AMP
 F (CURVNO.EQ.2) PLOTY2(I)=AMP
 F (CURVNO.EQ.3) PLOTY3(I)=AMP
 ETURN

 ***************************
 ROR DETECTION
 ***************************
 ITE (6,9000) I,PASS,IFAIL
 RMAT(' ? NO CONVERGENCE I=',I3,'; PASS=',I2,',IFAIL=',I4)
  (PASS.EQ.1) GOTO 100
  (PASS.EQ.2) GOTO 200
 ITE (6,9010) PASS
 RMAT(' PASS MISCOUNT =',I4)
  OP
  D
```

```
C      FUN3.FT V2A JJN  11-NOV-81
C      FUNCTION FOR SUBROUTINE POINT
C      PROGRAM PLOTCW.FT V1
C      USES APPROXIMATION CHOICES A2 & B3 AS PER DAYBOOK
CCCCCCCCCCCCCCCCCCCCCCCCCCCCCCCCCCCCCCCCCCCCCCCCCCCCCCCCC

       DOUBLE PRECISION FUNCTION FUN3(Z,CHI)
       REAL*8 BP,CHI,Z
       REAL*8 ZETA,AP,LP,K
       COMMON /FUN/ ZETA,AP,LP,K
       REAL*8 ARCMIRROR
       EXTERNAL ARCMIRROR
C*****
C      VARIABLE NAMES CF. FUJIWARA'S EQN.
C      RHO=BP,L=AP,LDASH=LP
C*****
C/////
C       WRITE (6,7000) Z
C7000  FORMAT(' Z=',G14.6)
C/////
       BP=ARCMIRROR(Z)
       FUN3= BP*DSIN(K*(AP+(BP*BP+Z*Z)/(2*AP)+LP+
      $       (ZETA*ZETA+(BP*BP+Z*Z))/(2*LP)-(2*Z+ZETA*BP*DCOS(CHI)/LP
      $     /(ZETA*BP*DCOS(CHI)-((BP*BP+Z*Z)+AP*LP)+Z*(AP+LP))
       RETURN
       END
C      FUN4.FT V2A JJN  11-NOV-81
C      FUNCTION FOR SUBROUTINE POINT
C      PROGRAM PLOTCW.FT V1
C      USES APPROXIMATION CHOICES A2 & B3 AS PER DAYBOOK
CCCCCCCCCCCCCCCCCCCCCCCCCCCCCCCCCCCCCCCCCCCCCCCCCCCCCCCCCC

       DOUBLE PRECISION FUNCTION FUN4(Z,CHI)
       REAL*8 BP,CHI,Z
       REAL*8 ZETA,AP,LP,K
       COMMON /FUN/ ZETA,AP,LP,K
       REAL*8 ARCMIRROR
       EXTERNAL ARCMIRROR
C*****
C      VARIABLE NAMES CF. FUJIWARA'S EQN.
C      RHO=BP,L=AP,LDASH=LP
C*****
       BP=ARCMIRROR(Z)
       FUN4= BP*DCOS(K*(AP+(BP*BP+Z*Z)/(2*AP)+LP+
      $       (ZETA*ZETA+(BP*BP+Z*Z))/(2*LP)-(2*Z+ZETA*BP*DCOS(CHI)/LP)
      $     /(ZETA*BP*DCOS(CHI)-((BP*BP+Z*Z)+AP*LP)+Z*(AP+LP))
       RETURN
       END

Command:
```

ii) Subroutine POINT2 and Functions.

```
LOTPOINT2.FT  V3A  JJN  17-FEB81
UBROUTINE FOR PLOTCW.FT PROGRAMS
ALCULATES PRESSURE AMPLITUDE AT POINT (L,R)
EQUIRES FUNCTIONS FUN5,FUN6,MIRROR'N',PHI3,PHI4
HICH MUST BE FOUND IN THE DIRECTORY.
CCCCCCCCCCCCCCCCCCCCCCCCCCCCCC
IIS POINT* NOW ACCEPTS ONLY AXIAL LIMITS
JR THE INNER INTEGRAL AND THEREFORE MUST ONLY BE
SED WITH PLOTCW V.3J ONWARDS WHICH ALSO KNOW THIS.
CCCCCCCCCCCCCCCCCCCCCCCCCCCCCCCCCCCCCCCCCCCCCCCC

JBROUTINE POINT2 (CURVNO,I)
AL*8 ZETA,AP,LP,K
AL*8 FUN5,FUN6,PHI3,PHI4
AL*8 PI2
AL*8 ABSACC
AL*8 AMP,AMPR,AMPI
ITEGER CURVNO,I,IFAIL,NPTS,PASS
UBLE PRECISION PLOTX1(100),PLOTX2(100),PLOTX3(100)
UBLE PRECISION PLOTY1(100),PLOTY2(100),PLOTY3(100)
MMON PLOTX1,PLOTX2,PLOTX3,PLOTY1,PLOTY2,PLOTY3
MMON /FUN/ ZETA,AP,LP,K
TERNAL FUN5,FUN6,PHI3,PHI4
TA PI2 /6.28318530718000/
SACC=0.1D-4
/
NS=PHI3(1.D0)
RITE (6,7010) ANS
ORMAT(' PHI3=',G14.6)
NS=PHI4(1.D0)
RITE (6,7020) ANS
ORMAT(' PHI4=',G14.6)

LCULATE 'REAL' COMPONENT
SS=1
AIL=1
LL D01DAF(0.D 0,PI2,
        PHI3,PHI4,FUN5,ABSACC,AMPR,NPTS,IFAIL)

RITE (6,7000) PASS,AMPR,NPTS
ORMAT(' PASS',I2,'INTEGRAL=',G14.7/' NO. OF FN EVALUATIONS=',I(

 (IFAIL) 100,100,900
PEAT CALL FOR 'IMAGINARY' COMPONENT
SS=2
AIL=1
L D01DAF(0.D 0,PI2,
        PHI3,PHI4,FUN6,ABSACC,AMPI,NPTS,IFAIL)

ITE (6,7000) PASS,AMPI,NPTS

 (IFAIL) 200,200,900
LATE AMPLITUDE MAGNITUDE. (!)
=DSQRT(AMPR*AMPR + AMPI*AMPI) *K/PI2
 (CURVNO.EQ.1) PLOTY1(I)=AMP
 (CURVNO.EQ.2) PLOTY2(I)=AMP
 (CURVNO.EQ.3) PLOTY3(I)=AMP
 URN

 *************************
 OR DETECTION
 *************************
 TE (6,9000) I,PASS,IFAIL
 MAT(' ? NO CONVERGENCE I=',I3,'; PASS=',I2,',IFAIL=',I4)
 (PASS.EQ.1) GOTO 100
 (PASS.EQ.2) GOTO 200
 TE (6,9010) PASS
 MAT(' PASS MISCOUNT =',I4)
 P
```

```
C     FUN5.FT V1A JJN  25-MAR-81
C     FUNCTION FOR SUBROUTINE POINT2
C     PROGRAM PLOTCW.FT V2
C     USES SMALL ANGLE APPROX. (THEREFORE Z NOT BP) BUT
C     EVALUATES SQ &QP CORRECTLY.
CCCCCCCCCCCCCCCCCCCCCCCCCCCCCCCCCCCCCCCCCCCCCCCCCCCCCCCCCC

      DOUBLE PRECISION FUNCTION FUN5(Z,CHI)
      REAL*8 BP,CHI,Z
      REAL*8 ZETA,AP,LP,K
      REAL*8 DENOMR,EXPONENT,NUMATOR
      COMMON /FUN/ ZETA,AP,LP,K
      REAL*8 MIRROR,ARCMIRROR
      EXTERNAL MIRROR,ARCMIRROR
C*****
C     VARIABLE NAMES CF. FUJIWARA'S EQN.
C     RHO=BP,L=AP,LDASH=LP
C*****
C/////
C      WRITE (6,7000) Z
C7000  FORMAT(' Z=',G14.6)
C/////
      BP=ARCMIRROR(Z)
      DENOMR=ZETA*BP*DCOS(CHI)-BP*BP-Z*Z+Z*(AP+LP)-AP*LP
      EXPONENT=K*(DSQRT(BP*BP+(Z-AP)**2)+
     $          DSQRT(ZETA*ZETA+BP*BP+(LP-Z)**2-2*ZETA*BP*DCOS(CHI)))
      NUMATOR=DSIN(EXPONENT)
      FUN5= BP*NUMATOR/DENOMR
      RETURN
      END
C     FUN6.FT V1A JJN  25-MAR-81
C     FUNCTION FOR SUBROUTINE POINT2
C     PROGRAM PLOTCW.FT V2
C     USES SMALL ANGLE APPROX. (THEREFORE Z NOT BP) BUT
C     EVALUATES SQ &QP CORRECTLY.
CCCCCCCCCCCCCCCCCCCCCCCCCCCCCCCCCCCCCCCCCCCCCCCCCCCCCCCCCC

      DOUBLE PRECISION FUNCTION FUN6(Z,CHI)
      REAL*8 BP,CHI,Z
      REAL*8 ZETA,AP,LP,K
      REAL*8 DENOMR,EXPONENT,NUMATOR
      COMMON /FUN/ ZETA,AP,LP,K
      REAL*8 MIRROR,ARCMIRROR
      EXTERNAL MIRROR,ARCMIRROR
C*****
C     VARIABLE NAMES CF. FUJIWARA'S EQN.
C     RHO=BP,L=AP,LDASH=LP
C*****
C/////
C      WRITE (6,7000) Z
C7000  FORMAT(' Z=',G14.6)
C/////
      BP=ARCMIRROR(Z)
      DENOMR=ZETA*BP*DCOS(CHI)-BP*BP-Z*Z+Z*(AP+LP)-AP*LP
      EXPONENT=K*(DSQRT(BP*BP+(Z-AP)**2)+
     $          DSQRT(ZETA*ZETA+BP*BP+(LP-Z)**2-2*ZETA*BP*DCOS(CHI)))
      NUMATOR=DCOS(EXPONENT)
      FUN6= BP*NUMATOR/DENOMR
      RETURN
      END

Command:
```

iii) Subroutine POINT3 and Functions.

```
PLOTPOINT3.FT  V2A  JJN 4-AUG-81
SUBROUTINE FOR PLOTCW.FT PROGRAMS
CALCULATES PRESSURE AMPLITUDE AT POINT (L,R)
REQUIRES FUNCTIONS FUN7,FUN8,MIRROR,PHI3,PHI4
WHICH MUST BE FOUND IN THE DIRECTORY.
CCCCCCCCCCCCCCCCCCCCCCCCCCCCCCCCC

SUBROUTINE POINT3 (CURVNO,I)
REAL*8 ZETA,AP,LP,K,CHI
REAL*8 FUN7,FUN8,MIRROR,PHI3,PHI4
REAL*8 PI2
REAL*8 ABSACC,ANS
REAL*8 AMP,AMPR,AMPI
INTEGER CURVNO,I,IFAIL,NPTS,PASS
DOUBLE PRECISION PLOTX1(100),PLOTX2(100),PLOTX3(100)
DOUBLE PRECISION PLOTY1(100),PLOTY2(100),PLOTY3(100)
COMMON PLOTX1,PLOTX2,PLOTX3,PLOTY1,PLOTY2,PLOTY3
COMMON /FUN/ ZETA,AP,LP,K
EXTERNAL FUN7,FUN8,MIRROR,PHI3,PHI4
DATA PI2 /6.2831853071800D0/
ABSACC=0.1D-4
///
 ANS=PHI3(1.D0)
 WRITE (6,7010) ANS
 FORMAT(' PHI3=',G14.6)
 ANS=PHI4(1.D0)
 WRITE (6,7020) ANS
 FORMAT(' PHI4=',G14.6)
 /
 ALCULATE 'REAL' COMPONENT
 ASS=1
 FAIL=1
 ALL D01DAF(0.D0,PI2,PHI3,PHI4,FUN7,ABSACC,AMPR,NPTS,IFAIL)

 WRITE (6,7000) PASS,AMPR,NPTS
 FORMAT(' PASS',I2,'INTEGRAL=',G14.7/' NO. OF FN EVALUATIONS=',

 F (IFAIL) 100,100,900
 EPEAT CALL FOR 'IMAGINARY' COMPONENT
 ASS=2
 AIL=1
 LL D01DAF(0.D0,PI2,PHI3,PHI4,FUN8,ABSACC,AMPI,NPTS,IFAIL)

 RITE (6,7000) PASS,AMPI,NPTS

  (IFAIL) 200,200,900
 ULATE AMPLITUDE MAGNITUDE. (!)
 P=DSQRT(AMPR*AMPR + AMPI*AMPI) *K/PI2
  (CURVNO.EQ.1) PLOTY1(I)=AMP
  (CURVNO.EQ.2) PLOTY2(I)=AMP
  (CURVNO.EQ.3) PLOTY3(I)=AMP
 TURN

 ***************************
 ROR DETECTION
 ***************************
 ITE (6,9000) PASS,IFAIL
 RMAT(' ? NO CONVERGENCE PASS=',I2,',IFAIL=',I4)
  (PASS.EQ.1) GOTO 100
  (PASS.EQ.2) GOTO 200
 ITE (6,9010) PASS
 RMAT(' PASS MISCOUNT =',I4)
 P
```

```
C     FUN7.FT V2A JJN  11-NOV-81
C     FUNCTION FOR SUBROUTINE POINT3
C     PROGRAM PLOTCW.FT V2
C     USES APPROX. DIFFERENTIAL TO EVALUATE SURFACE ELEMENT BUT
C     EVALUATES SQ &QP CORRECTLY.
CCCCCCCCCCCCCCCCCCCCCCCCCCCCCCCCCCCCCCCCCCCCCCCCCCCCCCCCCCCC

      DOUBLE PRECISION FUNCTION FUN7(BP,CHI)
      REAL*8 BP,CHI,Z
      REAL*8 ZETA,AP,LP,K
      REAL*8 DELBP,DELZ
      REAL*8 DENOMR,EXPONENT,NUMATOR
      COMMON /FUN/ ZETA,AP,LP,K
      REAL*8 MIRROR
      EXTERNAL MIRROR
      DATA DELBP/5.D-5/
C*****
C     VARIABLE NAMES CF. FUJIWARA'S EQN.
C     RHO=BP,L=AP,LDASH=LP
C*****
      Z=MIRROR(BP)
      DELZ=MIRROR(BP+DELBP) - MIRROR(BP-DELBP)
      DENOMR=ZETA*BP*DCOS(CHI)-BP*BP-Z*Z+Z*(AP+LP)-AP*LP
      EXPONENT=K*(DSQRT(BP*BP+(Z-AP)**2)+
     $           DSQRT(ZETA*ZETA+BP*BP+(LP-Z)**2-2*ZETA*BP*DCOS(CHI))
      NUMATOR=DSIN(EXPONENT)
      FUN7= BP*NUMATOR/DENOMR*DSQRT(DELZ*DELZ+4*DELBP*DELBP)/(2*DELBP)
      RETURN
      END
C     FUN8.FT V2A JJN  11-NOV-81
C     FUNCTION FOR SUBROUTINE POINT3
C     PROGRAM PLOTCW.FT V2
C     USES APPROX. DIFFERENTIAL TO EVALUATE SURFACE ELEMENT BUT
C     EVALUATES SQ &QP CORRECTLY.
CCCCCCCCCCCCCCCCCCCCCCCCCCCCCCCCCCCCCCCCCCCCCCCCCCCCCCCCCCCC

      DOUBLE PRECISION FUNCTION FUN8(BP,CHI)
      REAL*8 BP,CHI,Z
      REAL*8 ZETA,AP,LP,K
      REAL*8 DELBP,DELZ
      REAL*8 DENOMR,EXPONENT,NUMATOR
      COMMON /FUN/ ZETA,AP,LP,K
      REAL*8 MIRROR
      EXTERNAL MIRROR
      DATA DELBP/5.D-5/
C*****
C     VARIABLE NAMES CF. FUJIWARA'S EQN.
C     RHO=BP,L=AP,LDASH=LP
C*****
      Z=MIRROR(BP)
      DELZ=MIRROR(BP+DELBP) - MIRROR(BP-DELBP)
      DENOMR=ZETA*BP*DCOS(CHI)-BP*BP-Z*Z+Z*(AP+LP)-AP*LP
      EXPONENT=K*(DSQRT(BP*BP+(Z-AP)**2)+
     $           DSQRT(ZETA*ZETA+BP*BP+(LP-Z)**2-2*ZETA*BP*DCOS(CHI))
      NUMATOR=DCOS(EXPONENT)
      FUN8= BP*NUMATOR/DENOMR*DSQRT(DELZ*DELZ+4*DELBP*DELBP)/(2*DELBP)
      RETURN
      END

Command:
```

iv) Subroutine POINT4 and functions.

```
'LOTPOINT4.FT  V1X  JJN 7-OCT-81
SUBROUTINE FOR PLOTCW.FT PROGRAMS
CALCULATES PRESSURE AMPLITUDE AT POINT (L,R)
REQUIRES FUNCTIONS FUN9,FUN10,MIRROR,PHI3,PHI4
WHICH MUST BE FOUND IN THE DIRECTORY.
TEST FOR POINT3: EFFECTIVE MIRROR2 ONLY!!!
CCCCCCCCCCCCCCCCCCCCCCCCCCCCCCCCC

SUBROUTINE POINT4 (CURVNO,I)
REAL*8 ZETA,AP,LP,K,CHI
REAL*8 FUN9,FUN10,MIRROR,PHI3,PHI4
REAL*8 PI2
REAL*8 ABSACC,ANS
REAL*8 AMP,AMPR,AMPI
NTEGER CURVNO,I,IFAIL,NPTS,PASS
OUBLE PRECISION PLOTX1(100),PLOTX2(100),PLOTX3(100)
OUBLE PRECISION PLOTY1(100),PLOTY2(100),PLOTY3(100)
OMMON PLOTX1,PLOTX2,PLOTX3,PLOTY1,PLOTY2,PLOTY3
OMMON /FUN/ ZETA,AP,LP,K
XTERNAL FUN9,FUN10,PHI3,PHI4
ATA PI2 /6.2831853071800D0/
BSACC=0.1D-4
//
ANS=PHI3(1.D0)
WRITE (6,7010) ANS
FORMAT(' PHI3=',G14.6)
ANS=PHI4(1.D0)
WRITE (6,7020) ANS
FORMAT(' PHI4=',G14.6)
/
ALCULATE 'REAL' COMPONENT
ASS=1
FAIL=1
ALL D01DAF(0.D 0,PI2,
         PHI3,PHI4,FUN9,ABSACC,AMPR,NPTS,IFAIL)

WRITE (6,7000) PASS,AMPR,NPTS
FORMAT(' PASS',I2,'INTEGRAL=',G14.7/' NO. OF FN EVALUATIONS=',I6)

F (IFAIL) 100,100,900
EPEAT CALL FOR 'IMAGINARY' COMPONENT
ASS=2
FAIL=1
ALL D01DAF(0.D 0,PI2,
         PHI3,PHI4,FUN10,ABSACC,AMPI,NPTS,IFAIL)

WRITE (6,7000) PASS,AMPI,NPTS

F (IFAIL) 200,200,900
CULATE AMPLITUDE MAGNITUDE. (!)
MP=DSQRT(AMPR*AMPR + AMPI*AMPI) *K/PI2
F (CURVNO.EQ.1) PLOTY1(I)=AMP
F (CURVNO.EQ.2) PLOTY2(I)=AMP
F (CURVNO.EQ.3) PLOTY3(I)=AMP
ETURN

****************************
RROR DETECTION
****************************
ITE (6,9000) PASS,IFAIL
RMAT(' ? NO CONVERGENCE PASS=',I2,',IFAIL=',I4)
 (PASS.EQ.1) GOTO 100
 (PASS.EQ.2) GOTO 200
ITE (6,9010) PASS
RMAT(' PASS MISCOUNT =',I4)
OP
D
```

```
C     FUN9.FT V2C JJN  11-NOV-81
C     FUNCTION FOR SUBROUTINE POINT4
C     EFFECTIVE ONLY IF DIFFERENTIAL FUNCTION DIFMIR
C     IS LOADED WITH MIRRORO.
C     PROGRAM PLOTCW.FT V2
C     USES  DIFFERENTIAL TO EVALUATE SURFACE ELEMENT AND
C     EVALUATES SQ &QP CORRECTLY.
CCCCCCCCCCCCCCCCCCCCCCCCCCCCCCCCCCCCCCCCCCCCCCCCCCCCCCCCCCCCC

      DOUBLE PRECISION FUNCTION FUN9(BP,CHI)
      REAL*8 BP,CHI,Z
      REAL*8 ZETA,AP,LP,K
      COMMON /FUN/ ZETA,AP,LP,K
      REAL*8 MIRROR,DIFMIR
      EXTERNAL MIRROR,DIFMIR
C*****
C     VARIABLE NAMES CF. FUJIWARA'S EQN.
C     RHO=BP,L=AP,LDASH=LP
C*****
      Z=MIRROR(BP)
      FUN9= BP*DSIN(K*(DSQRT(BP*BP+(Z-AP)**2)+
     $       DSQRT(ZETA*ZETA+BP*BP+(LP-Z)**2-2*ZETA*BP*DCOS(CHI))))
     $      /(ZETA*BP*DCOS(CHI)-BP*BP-Z*Z+Z*(AP+LP)-AP*LP)
     $      /DCOS(DATAN(DIFMIR(Z,BP)))
      RETURN
      END
C     FUN10.FT V1C JJN  11-NOV-81
C     FUNCTION FOR SUBROUTINE POINT4
C   EFFECTIVE ONLY IF DIFFERENTIAL FUNCTION DIFMIR
C     IS LOADED WITH MIRRORO.
C     PROGRAM PLOTCW.FT V2
C     USES  DIFFERENTIAL TO EVALUATE SURFACE ELEMENT AND
C     EVALUATES SQ &QP CORRECTLY.
CCCCCCCCCCCCCCCCCCCCCCCCCCCCCCCCCCCCCCCCCCCCCCCCCCCCCCCCCCCCC

      DOUBLE PRECISION FUNCTION FUN10(BP,CHI)
      REAL*8 BP,CHI,Z
      REAL*8 ZETA,AP,LP,K
      COMMON /FUN/ ZETA,AP,LP,K
      REAL*8 MIRROR,DIFMIR
      EXTERNAL MIRROR,DIFMIR
C*****
C     VARIABLE NAMES CF. FUJIWARA'S EQN.
C     RHO=BP,L=AP,LDASH=LP
C*****
      Z=MIRROR(BP)
      FUN10= BP*DCOS(K*(DSQRT(BP*BP+(Z-AP)**2)+
     $       DSQRT(ZETA*ZETA+BP*BP+(LP-Z)**2-2*ZETA*BP*DCOS(CHI))))
     $      /(ZETA*BP*DCOS(CHI)-BP*BP-Z*Z+Z*(AP+LP)-AP*LP)
     $      /DCOS(DATAN(DIFMIR(Z,BP)))
      RETURN
      END

Command:
```

v) Subroutine POINT5 and functions.

```
OTPOINT5.FT  V1A  JJN 29-OCT-81
BROUTINE FOR PLOTCW.FT PROGRAMS
LCULATES PRESSURE AMPLITUDE AT POINT (L,R)
QUIRES FUNCTIONS FUN9,FUN10,MIRROR,PHI3,PHI4
ICH MUST BE FOUND IN THE DIRECTORY.
INLY FOR USE WITH HERSCHALL SYSTEMS WHEN THE
DIAL LIMITS OF THE MIRROR CAN NOT BE EXPRESSED UNIQUELY.
CCCCCCCCCCCCCCCCCCCCCCCCCCCCCCCC

BROUTINE POINT5 (CURVNO,I)
AL*8 ZETA,AP,LP,K,CHI
AL*8 FUN13,FUN14,PHI3,PHI4
AL*8 PI2
AL*8 ABSACC,ANS
AL*8 AMP,AMPR,AMPI
TEGER CURVNO,I,IFAIL,NPTS,PASS
UBLE PRECISION PLOTX1(100),PLOTX2(100),PLOTX3(100)
UBLE PRECISION PLOTY1(100),PLOTY2(100),PLOTY3(100)
MMON PLOTX1,PLOTX2,PLOTX3,PLOTY1,PLOTY2,PLOTY3
MMON /FUN/ ZETA,AP,LP,K
TERNAL FUN13,FUN14,PHI3,PHI4
TA PI2 /6.28318530718OD0/
SACC=0.1D-4
/
NS=PHI3(1.D0)
ITE (6,7010) ANS
RMAT(' PHI3=',G14.6)
NS=PHI4(1.D0)
ITE (6,7020) ANS
RMAT(' PHI4=',G14.6)

.CULATE 'REAL' COMPONENT
SS=1
IL=1
.L D01DAF(-2.084D-1,2.084D-1,
          PHI3,PHI4,FUN13,ABSACC,AMPR,NPTS,IFAIL)

ITE (6,7000) PASS,AMPR,NPTS
RMAT(' PASS',I2,'INTEGRAL=',G14.7/' NO. OF FN EVALUATIONS=',I6)

 (IFAIL) 100,100,900
EAT CALL FOR 'IMAGINARY' COMPONENT
SS=2
IL=1
.L D01DAF(-2.084D-1,2.084D-1,
          PHI3,PHI4,FUN14,ABSACC,AMPI,NPTS,IFAIL)

ITE (6,7000) PASS,AMPI,NPTS

 (IFAIL) 200,200,900
LATE AMPLITUDE MAGNITUDE. (!)
=DSQRT(AMPR*AMPR + AMPI*AMPI) *K/PI2
 (CURVNO.EQ.1) PLOTY1(I)=AMP
 (CURVNO.EQ.2) PLOTY2(I)=AMP
 (CURVNO.EQ.3) PLOTY3(I)=AMP
URN

**************************
OR DETECTION
**************************
TE (6,9000) I,PASS,IFAIL
MAT(' ? NO CONVERGENCE I=',I3,', PASS=',I2,',IFAIL=',I4)
(PASS.EQ.1) GOTO 100
(PASS.EQ.2) GOTO 200
TE (6,9010) PASS
MAT(' PASS MISCOUNT =',I4)
P
```

```
C     FUN13.FT V1A JJN  29-OCT-81
C     FUNCTION FOR SUBROUTINE POINT5
C     EFFECTIVE ONLY IF DIFFERENTIAL FUNCTION DIFMIR
C     IS LOADED WITH MIRROR0.
C     PROGRAM PLOTCW.FT V2
C     USES  DIFFERENTIAL TO EVALUATE SURFACE ELEMENT AND
C     EVALUATES SQ &QP CORRECTLY.
CCCCCCCCCCCCCCCCCCCCCCCCCCCCCCCCCCCCCCCCCCCCCCCCCCCCCCCCCCCCCC

      DOUBLE PRECISION FUNCTION FUN13(Z,CHI)
      REAL*8 BP,CHI,Z
      REAL*8 ZETA,AP,LP,K
      COMMON /FUN/ ZETA,AP,LP,K
      REAL*8 ARCMIRROR,DIFMIR
      EXTERNAL ARCMIRROR,DIFMIR
C*****
C     VARIABLE NAMES CF. FUJIWARA'S EQN.
C     RHO=BP,L=AP,LDASH=LP
C*****
      BP=ARCMIRROR(Z)
C///////
C      WRITE (6,7000)  Z,BP
C7000  FORMAT(' Z & BP =',2G14.6)
C//////
      FUN13= BP*DSIN(K*(DSQRT(BP*BP+(Z-AP)**2)+
     $       DSQRT(ZETA*ZETA+BP*BP+(LP-Z)**2-2*ZETA*BP*DCOS(CHI)))
     $      /(ZETA*BP*DCOS(CHI)-BP*BP-Z*Z+Z*(AP+LP)-AP*LP)
     $      /(DSIN(DATAN(DIFMIR(Z,BP))))
C///////
C      WRITE (6,7010) FUN13
C7010  FORMAT (' FUN13= ',G14.6)
C///////
      RETURN
      END
C     FUN14.FT V1A   29-OCT-81
C       FUNCTION FOR SUBROUTINE POINT5
C   EFFECTIVE ONLY IF DIFFERENTIAL FUNCTION DIFMIR
C     IS LOADED WITH MIRROR0.
C     PROGRAM PLOTCW.FT V2
C     USES  DIFFERENTIAL TO EVALUATE SURFACE ELEMENT AND
C     EVALUATES SQ &QP CORRECTLY.
CCCCCCCCCCCCCCCCCCCCCCCCCCCCCCCCCCCCCCCCCCCCCCCCCCCCCCCCCCCCCC

      DOUBLE PRECISION FUNCTION FUN14(Z,CHI)
      REAL*8 BP,CHI,Z
      REAL*8 ZETA,AP,LP,K
      COMMON /FUN/ ZETA,AP,LP,K
      REAL*8 ARCMIRROR,DIFMIR
      EXTERNAL ARCMIRROR,DIFMIR
      DATA DELBP/5.D-5/
C*****
C     VARIABLE NAMES CF. FUJIWARA'S EQN.
C     RHO=BP,L=AP,LDASH=LP
C*****
      BP=ARCMIRROR(Z)
      FUN14= BP*DCOS(K*(DSQRT(BP*BP+(Z-AP)**2)+
     $        DSQRT(ZETA*ZETA+BP*BP+(LP-Z)**2-2*ZETA*BP*DCOS(CHI))))
     $      /(ZETA*BP*DCOS(CHI)-BP*BP-Z*Z+Z*(AP+LP)-AP*LP)
     *      /DSIN(DATAN(DIFMIR(Z,BP)))
      RETURN
      END

Command:
```

vi) Subroutine POINT6 and functions.

```
TPOINT6.FT  V1A  JJN 17-NOV-81
ROUTINE FOR PLOTCW.FT PROGRAMS
CULATES PRESSURE AMPLITUDE AT POINT (L,R)
UIRES FUNCTIONS FUN15,FUN16,MIRROR,PHI3,PHI4
CH MUST BE FOUND IN THE DIRECTORY.
CCCCCCCCCCCCCCCCCCCCCCCCCCCCCCC

ROUTINE POINT6 (CURVNO,I)
L*8 ZETA,AP,LP,K,CHI
L*8 FUN15,FUN16,MIRROR,PHI3,PHI4
L*8 PI2
L*8 ABSACC,ANS
L*8 AMP,AMPR,AMPI
EGER CURVNO,I,IFAIL,NPTS,PASS
BLE PRECISION PLOTX1(100),PLOTX2(100),PLOTX3(100)
BLE PRECISION PLOTY1(100),PLOTY2(100),PLOTY3(100)
MON PLOTX1,PLOTX2,PLOTX3,PLOTY1,PLOTY2,PLOTY3
MON /FUN/ ZETA,AP,LP,K
ERNAL FUN15,FUN16,MIRROR,PHI3,PHI4
A PI2 /6.28318530718OD0/
ACC=0.1D-4

S=PHI3(1.D0)
ITE (6,7010) ANS
RMAT(' PHI3=',G14.6)
S=PHI4(1.D0)
ITE (6,7020) ANS
RMAT(' PHI4=',G14.6)

CULATE 'REAL' COMPONENT
S=1
IL=1
L D01DAF(0.0 D0,PI2,
         PHI3,PHI4,FUN15,ABSACC,AMPR,NPTS,IFAIL)

ITE (6,7000) PASS,AMPR,NPTS
RMAT(' PASS',I2,'INTEGRAL=',G14.7/' NO. OF FN EVALUATIONS=',I6

(IFAIL) 100,100,900
EAT CALL FOR 'IMAGINARY' COMPONENT
S=2
IL=1
L D01DAF(0.0D 0,PI2,
         PHI3,PHI4,FUN16,ABSACC,AMPI,NPTS,IFAIL)

ITE (6,7000) PASS,AMPI,NPTS

(IFAIL) 200,200,900
LATE AMPLITUDE MAGNITUDE. (!)
=DSQRT(AMPR*AMPR + AMPI*AMPI) *K/PI2
(CURVNO.EQ.1) PLOTY1(I)=AMP
(CURVNO.EQ.2) PLOTY2(I)=AMP
(CURVNO.EQ.3) PLOTY3(I)=AMP
URN

*************************
OR DETECTION
*************************
TE (6,9000) I,PASS,IFAIL
AT(' ? NO CONVERGENCE I=',I3,',PASS=',I2,',IFAIL=',I4)
(PASS.EQ.1) GOTO 100
(PASS.EQ.2) GOTO 200
TE (6,9010) PASS
AT(' PASS MISCOUNT =',I4)
```

```
C      FUN15.FT V1A JJN  17-NOV-81
C      FUNCTION FOR SUBROUTINE POINT
C      PROGRAM PLOTCW.FT V1
C      USES SMALL ANGLE & FIRST ORDER APPROXIMATIONS.
CCCCCCCCCCCCCCCCCCCCCCCCCCCCCCCCCCCCCCCCCCCCCCCCCCCCCCCCCCCCC

       DOUBLE PRECISION FUNCTION FUN15(BP,CHI)
       REAL*8 BP,CHI,Z
       REAL*8 ZETA,AP,LP,K
       REAL*8 DENOMR,EXPONENT,NUMATOR
       COMMON /FUN/ ZETA,AP,LP,K
       REAL*8 MIRROR
       EXTERNAL MIRROR
C*****
C      VARIABLE NAMES CF. FUJIWARA'S EQN.
C      RHO=BP,L=AP,LDASH=LP
C*****
C/////
C       WRITE (6,7000) Z
C7000  FORMAT(' Z=',G14.6)
C/////
       Z=MIRROR(BP)
       FUN15= BP*DSIN(K*(AP+(BP*BP+Z*Z)/(2*AP)+LP+
      $       (ZETA*ZETA+BP*BP+Z*Z)/(2*LP)-2*Z-ZETA*BP*DCOS(CHI)/LP))
      $       /(ZETA*BP*DCOS(CHI)-BP*BP-Z*Z+Z*(AP+LP)-AP*LP)
       RETURN
       END
C      FUN16.FT V1A JJN  17-NOV-81
C      FUNCTION FOR SUBROUTINE POINT6
C      PROGRAM PLOTCW.FT V1
C      USES SMALL ANGLE & FIRST ORDER APPROXIMATIONS.
CCCCCCCCCCCCCCCCCCCCCCCCCCCCCCCCCCCCCCCCCCCCCCCCCCCCCCCCCCCCC

       DOUBLE PRECISION FUNCTION FUN16(BP,CHI)
       REAL*8 BP,CHI,Z
       REAL*8 ZETA,AP,LP,K
       REAL*8 DENOMR,EXPONENT,NUMATOR
       COMMON /FUN/ ZETA,AP,LP,K
       REAL*8 MIRROR
       EXTERNAL MIRROR
C*****
C      VARIABLE NAMES CF. FUJIWARA'S EQN.
C      RHO=BP,L=AP,LDASH=LP
C*****
       Z=MIRROR(BP)
       FUN16= BP*DCOS(K*(AP+(BP*BP+Z*Z)/(2*AP)+LP+
      $       (ZETA*ZETA+BP*BP+Z*Z)/(2*LP)-2*Z-ZETA*BP*DCOS(CHI)/LP))
      $      /(ZETA*BP*DCOS(CHI)-BP*BP-Z*Z+Z*(AP+LP)-AP*LP)
       RETURN
       END

Command:
```

vii) MIRROR Functions.

```
   LIST MIRROR+S1
C     MIRROR1.FT V1E  JJN  11-DEC-81
C     FUNCTION FOR SUBROUTINE POINT
C     DESCRIBES SHAPE OF REFLECTOR FOR PLOTCW.FT
C     ONLY ONE MIRROR SHOULD BE LOADED (AS MIRRORO)
C     AT ANY ONE TIME
C     THE AXIAL CO-ORD. IS GIVEN AS A FUNCTION OF
C     THE RADIAL (B).
C     A SIMPLE CONE.
CCCCCCCCCCCCCCCCCCCCCCCCCCCCCCCCCCCCCCCCCCCCCCCCCCCCCCCCCCC

C
C     MIRROR LABELING FUNCTION.
CCCCCCCCCCCCCCCCCCCCCCCCCCCCCCCCC

      SUBROUTINE MIRNUM(M)
      INTEGER M
      REAL*8 ALPHA
      DATA ALPHA /1.5D-3/
      M=1
      WRITE (6,1000) M,ALPHA
1000  FORMAT(' MIRROR=',I2/
     $        ' A SIMPLE CONE; APEX AT ORIGIN.'/
     $        ' ANGLE ALPHA= ',G14.6,' RADIANS.')
      RETURN
      END

C
C     MIRROR FUNCTION(AXIAL CO-ORD FROM RADIAL).
CCCCCCCCCCCCCCCCCCCCCCCCCCCCCCCCCCCCCCCCCCCCCC

      DOUBLE PRECISION FUNCTION MIRROR(BP)
      REAL*8 BP,ALPHA
      DATA ALPHA /1.5D-3/
      MIRROR=DTAN(ALPHA)* BP
      RETURN
      END



      DIFFERENTIAL OF MIRROR
CCCCCCCCCCCCCCCCCCCCCCCCCCCCCCC

      DOUBLE PRECISION FUNCTION DIFMIR(Z,BP)
      REAL*8 BP,Z
      REAL*8 ALPHA
      DATA ALPHA /1.5D-3/
      DIFMIR=DTAN(ALPHA)
      RETURN
      END

      INVERSE FUNCTION OF MIRROR
      DOUBLE PRECISION FUNCTION ARCMIRROR(Z)
      REAL*8 Z,ALPHA
      DATA ALPHA/1.5D-3/
      ARCMIRROR=Z/(DTAN(ALPHA))
      RETURN
      END

      DIFFERENTIAL OF ARCMIRROR.
CCCCCCCCCCCCCCCCCCCCCCCCCCCCCCCC

      DOUBLE PRECISION FUNCTION DIFAMIR(Z,BP)
      REAL*8 Z,BP
      REAL*8 ALPHA
      DATA ALPHA /1.5D-3/
      DIFAMIR=1.0/(DTAN(ALPHA))
      RETURN
      END

mmand:
```

```
   LIST MIRROR+S2


C     MIRROR2.FT V3A  JJN  6-NOV-81
C     FUNCTION FOR SUBROUTINE POINT
C     DESCRIBES SHAPE OF REFLECTOR FOR PLOTCW.FT
C     INCLUDES DIFFERENTIALS FOR V4.
C     ONLY ONE MIRROR SHOULD BE LOADED (AS MIRRORO)
C     AT ANY ONE TIME
C     THE AXIAL CO-ORD. IS GIVEN AS A FUNCTION OF
C     THE RADIAL (B).
C     A SPHERICAL REFLECTOR TO GIVE A WAVEFRONT CONVERGING
C     ON Z=150MM FOR COMPARISON WITH PLOTCBCW3.FT
CCCCCCCCCCCCCCCCCCCCCCCCCCCCCCCCCCCCCCCCCCCCCCCCCCCCCCCCCCCC

C
C     MIRROR LABELING FUNCTION.
CCCCCCCCCCCCCCCCCCCCCCCCCCCCCC

      SUBROUTINE MIRNUM(M)
      INTEGER M
      REAL*8 R
      DATA R / 1.D-1 /
      M=2
      WRITE (6,1000) M,R
1000  FORMAT(' MIRROR=',I2/
     $        ' SPHERICAL MIRROR; RADIUS =',G14.7/
     $        ' CENTRE AT X=RADIUS.')
      RETURN
      END

C
C     MIRRORO FUNCTION(AXIAL CO-ORD FROM RADIAL).
CCCCCCCCCCCCCCCCCCCCCCCCCCCCCCCCCCCCCCCCCCCCCCCC

      DOUBLE PRECISION FUNCTION MIRROR(BP)
      REAL*8 BP,R
      DATA R / 1.D-1 /
      MIRROR=R - DSQRT(R*R - BP*BP)
      RETURN
      END

C
C
C
C     DIFFERENTIAL OF MIRROR.
C
CCCCCCCCCCCCCCCCCCCCCCCCCCCCCCCC
      DOUBLE PRECISION FUNCTION DIFMIR (Z,BP)
      REAL*8 BP,Z,R
      DATA R / 1.D-1 /
      DIFMIR=BP/(R-Z)
      RETURN
      END
C
C     INVERSE FUNCTION OF MIRROR
C
CCCCCCCCCCCCCCCCCCCCCCCCCCCCCCCCCCCCCC

      DOUBLE PRECISION FUNCTION ARCMIRROR(Z)
      REAL*8 Z,R
      DATA R / 1.D-1 /
      ARCMIRROR=DSQRT(Z*(2*R - Z))
      RETURN
      END
C
C     DIFFERENTIAL OF ARCMIRROR
C
CCCCCCCCCCCCCCCCCCCCCCCCCCCCCCC
      DOUBLE PRECISION FUNCTION DIFAMIR(Z,BP)
      REAL*8 BP,Z,R
      DATA R / 1.D-1 /
      DIFAMIR=(R-Z)/BP
      RETURN
      END

Command:
```

```
IST MIRROR+S3

ROR3.FT V2B  JJN  8-OCT-81
CTION FOR SUBROUTINE POINT
CRIBES SHAPE OF REFLECTOR FOR PLOTCW.FT
LUDES DIFFERENTIALS FOR V4.
Y ONE MIRROR SHOULD BE LOADED (AS MIRRORO)
ANY ONE TIME
 AXIAL CO-ORD. IS GIVEN AS A FUNCTION OF
 RADIAL (B).
MARY FOR AN AXIAL FOCUS SYSTEM
PER MS#2
 FORMULAE SEE DAYBOOKS 2P88 & COMPUTING P80
CCCCCCCCCCCCCCCCCCCCCCCCCCCCCCCCCCCCCCCCCCCCCCCC

ROR LABELING FUNCTION.
CCCCCCCCCCCCCCCCCCCCCCCCC

ROUTINE MIRNUM(M)
IGER M

TE (6,1000)
MAT(' FOR MODELLING MS#2: AXICON.'/
    ' AN ELLIPSE WITH EXTERNAL REFERENCE POINT OFF AXIS.')
IRN

OR FUNCTION(AXIAL CO-ORD FROM RADIAL).
CCCCCCCCCCCCCCCCCCCCCCCCCCCCCCCCCCCCCCCCCC

LE PRECISION FUNCTION MIRROR(BP)
*8 BP
*8 AA,B,C,D,E,F
*8 G,K,N
 AA,B,C/0.4495306,8.2780008D-2,0.9968878/
 D,E/89.032354,6.6943768/
 G/-0.17856738D 1/
 K,N/0.26777507D 2,0.14460002D 5/

OR=(D-B*BP - DSQRT(G*BP*BP-K*BP+N))/(2*AA)
RN



ERENTIAL OF MIRROR.

CCCCCCCCCCCCCCCCCCCCCCCC
E PRECISION FUNCTION DIFMIR (Z,BP)
*8 BP,Z
R=(1.9937756*BP+8.2780008D-2*Z+6.6943768)
.032354-0.8990612*Z-8.2780008D-2*BP)
N


SE FUNCTION OF MIRROR
E PRECISION FUNCTION ARCMIRROR(Z)
8 Z
RROR=(-8.2780008D-2*Z-6.6943768 +
T(1.7856738*Z*Z+356.12939*Z
00.002))/1.9937756

N

RENTIAL OF ARCMIRROR

CCCCCCCCCCCCCCCCCCCCCC
E PRECISION FUNCTION DIFAMIR(Z,BP)
8 BP,Z
IR=(89.032354-0.8990612*Z-8.2780008D-2*BP)/
9937756*BP+8.2780008D-2*Z+6.6943768)

I
```

```
      LIST MIRROR+S4

C     MIRROR4.FT V1C  JJN  11-DEC-81
C     FUNCTION FOR SUBROUTINE POINT
C     DESCRIBES SHAPE OF REFLECTOR FOR PLOTCW.FT
C     INCLUDES DIFFERENTIALS FOR V4.
C     ONLY ONE MIRROR SHOULD BE LOADED (AS MIRRORO)
C     AT ANY ONE TIME
C     THE AXIAL CO-ORD. IS GIVEN AS A FUNCTION OF
C     THE RADIAL (B).
C     FOR MIRROR SYSTEM # 4; AN ELLIPSE CENTRED AT THE ORIGIN.
C     SOURCE AT (0,-C);FOCUS AT (0,C);SEMI-MAJOR AXIS A;
C     AA IS USED AS A**2;BB(SEMI-MINOR AXIS SQUARED) AS A**2-C**2
C      FOR THIS SYSTEM THE INTEGRATION LIMITS IN POINT WILL
C     BE SHORTENED TO GIVE AN ARC ~50 MM
CCCCCCCCCCCCCCCCCCCCCCCCCCCCCCCCCCCCCCCCCCCCCCCCCCCCCCCCCCCCC

C
C     MIRROR LABELING FUNCTION.
CCCCCCCCCCCCCCCCCCCCCCCCCCCCCCCCCCCCCCCCCCC

      SUBROUTINE MIRNUM(M)
      INTEGER M
      REAL*8 AA,BB,A,B
      DATA AA,BB/4.44444E-3,3.33333E-3/
      M=4
      A=DSQRT(AA)
      B=DSQRT(BB)
      WRITE (6,1000) AA,A,BB,B
1000  FORMAT(' AN ELLIPSE CENTRED AT ORIGIN'/
     $       ' AA=',G14.6/' THEREFORE SEMI-MAJOR AXIS=',G14.6/
     $       ' BB=',G14.6/' THEREFORE SEMI-MINOR AXIS=',G14.6)
      RETURN
      END

C
C     MIRROR FUNCTION(AXIAL CO-ORD FROM RADIAL).
CCCCCCCCCCCCCCCCCCCCCCCCCCCCCCCCCCCCCCCCCCCCCCCC

      DOUBLE PRECISION FUNCTION MIRROR(BP)
      REAL*8 BP
      REAL*8 AA,BB
      DATA AA,BB/4.44444E-3,3.33333E-3/
      MIRROR=DSQRT(AA*(1.D 0-(BP*BP/BB)))
      RETURN
      END

C
C
C
C     DIFFERENTIAL OF MIRROR.
C
CCCCCCCCCCCCCCCCCCCCCCCCCCCCCCCCCCCCC
      DOUBLE PRECISION FUNCTION DIFMIR (Z,BP)
      REAL*8 BP,Z
      REAL*8 AA,BB
      DATA AA,BB/4.44444E-3,3.33333E-3/
      DIFMIR=-AA*BP/(Z*BB)
      RETURN
      END

C     INVERSE FUNCTION OF MIRROR
      DOUBLE PRECISION FUNCTION ARCMIRROR(Z)
      REAL*8 Z
      REAL*8 AA,BB
      DATA AA,BB/4.44444E-3,3.33333E-3/
      ARCMIRROR=DSQRT(BB*(1.D 0-Z*Z/AA))
      RETURN
      END
C
C     DIFFERENTIAL OF ARCMIRROR
C
CCCCCCCCCCCCCCCCCCCCCCCCCCCCCCCCCCCCC
      DOUBLE PRECISION FUNCTION DIFAMIR(Z,BP)
      REAL*8 BP,Z
      REAL*8 AA,BB
      DATA AA,BB/4.44444E-3,3.33333E-3/
      DIFAMIR=-BB*Z/(AA*BP)
      RETURN
      END

Command:
```

```
   LIST MIRROR+S5
C     MIRROR5.FT V2B  JJN  11-DEC-81
C     FUNCTION FOR SUBROUTINE POINT
C     DESCRIBES SHAPE OF REFLECTOR FOR PLOTCW.FT
C     INCLUDES DIFFERENTIALS FOR V4.
C     ONLY ONE MIRROR SHOULD BE LOADED (AS MIRRORO)
C     AT ANY ONE TIME
C     FOR MIRROR SYSTEM # 5; A CIRCLE CENTRED AT THE ORIGIN.
C     RR IS USED AS R**2(RADIUS SQUARED)
C      FOR THIS SYSTEM THE INTEGRATION LIMITS IN POINT WILL
C     BE SHORTENED TO GIVE AN ARC ~50 MM
CCCCCCCCCCCCCCCCCCCCCCCCCCCCCCCCCCCCCCCCCCCCCCCCCCCCCCCCC

C
C     MIRROR LABELING FUNCTION.
CCCCCCCCCCCCCCCCCCCCCCCCCCCCCCCCCCCCCCCC

      SUBROUTINE MIRNUM(M)
      INTEGER M
      REAL*8 RR,R
      DATA RR / 6.6276D-3 /
      M=5
      R=DSQRT(RR)
      WRITE (6,1000) RR,R
1000  FORMAT(' CIRCLE CENTRED AT ORIGIN.'/
     $         ' RR=',G14.6/' THEREFORE RADIUS =',G14.6)
      RETURN
      END

C
C     MIRROR FUNCTION(AXIAL CO-ORD FROM RADIAL).
CCCCCCCCCCCCCCCCCCCCCCCCCCCCCCCCCCCCCCCCCCCCCCCCC

      DOUBLE PRECISION FUNCTION MIRROR(BP)
      REAL*8 BP
      REAL*8 RR
      DATA RR / 6.6276D-3 /
      MIRROR=-DSQRT(RR-BP*BP)
      RETURN
      END

C
C
C
C     DIFFERENTIAL OF MIRROR.
C
CCCCCCCCCCCCCCCCCCCCCCCCCCCCCCCCCC
      DOUBLE PRECISION FUNCTION DIFMIR (Z,BP)
      REAL*8 BP,Z
      REAL*8 RR
      DATA RR / 6.6276D-3 /
      DIFMIR=-BP/Z
      RETURN
      END



      INVERSE FUNCTION OF MIRROR

CCCCCCCCCCCCCCCCCCCCCCCCCCCCCCCCCCCCCCCCCCCCCCCCCC
      DOUBLE PRECISION FUNCTION ARCMIRROR(Z)
      REAL*8 Z
      REAL*8 RR
      DATA RR / 6.6276D-3 /
      ARCMIRROR=DSQRT(RR-Z*Z)
      RETURN
      END

      DIFFERENTIAL OF ARCMIRROR

CCCCCCCCCCCCCCCCCCCCCCCCCCCCCCCCC
      DOUBLE PRECISION FUNCTION DIFAMIR(Z,BP)
      REAL*8 BP,Z
      REAL*8 RR
      DATA RR / 6.6276D-3 /
      DIFAMIR=-Z/BP
      RETURN
      END

mmand:
```

```
   LIST MIRROR+S6

C     MIRROR6.FT V1A  JJN  23-NOV-81
C     FUNCTION FOR SUBROUTINE POINT
C     DESCRIBES SHAPE OF REFLECTOR FOR PLOTCW.FT
C     INCLUDES DIFFERENTIALS FOR V4.
C     ONLY ONE MIRROR SHOULD BE LOADED (AS MIRRORO)
C     AT ANY ONE TIME
C      A PLANE MIRROR THRO' THE ORIGIN IN THE Z=0 PLANE.
CCCCCCCCCCCCCCCCCCCCCCCCCCCCCCCCCCCCCCCCCCCCCCCCCCCCCCCCCCCCCC

C
C     MIRROR LABELING FUNCTION.
CCCCCCCCCCCCCCCCCCCCCCCCCCCCCCCCCCCCCCCCCC

      SUBROUTINE MIRNUM(M)
      INTEGER M
      M=6
      WRITE (6,1000)
1000  FORMAT(' A PLANE MIRROR THRO'' "O";PERPENDICULAR TO AXIS;'/
     $   ' USE POINT6. (NORMALLY).')
      RETURN
      END

C
C     MIRROR FUNCTION(AXIAL CO-ORD FROM RADIAL).
CCCCCCCCCCCCCCCCCCCCCCCCCCCCCCCCCCCCCCCCCCCCCCCCCC

      DOUBLE PRECISION FUNCTION MIRROR(BP)
      REAL*8 BP
      MIRROR=0.D 0
      RETURN
      END

C
C
C
C     DIFFERENTIAL OF MIRROR.
C
CCCCCCCCCCCCCCCCCCCCCCCCCCCCCCCCCCCC
      DOUBLE PRECISION FUNCTION DIFMIR (Z,BP)
      REAL*8 BP,Z
      DIFMIR=0.D 0
      RETURN
      END
C

Command:
```

b) PLOTCWX

i) Integration loops from main program.

```
C      SET PROGRAM TIMER
       CALL ICL9CECPUTIME(TIME1)
C
C      START OF SYMVU PLOT LOOP
C
       DO 250 J=1,ROWS
C//////
       WRITE (6,7000) J
7000   FORMAT(' ROW NUMBER=',I4)
C//////
C
C      CALCULATE RELATIVE PRESSURE FROM R1 TO R2
C
       R=R1-RSTEP
C
       DO 220 I=1,COLUMNS
C      SET AXIAL POSITION
       R=R+RSTEP
       RP=R*1.D-3
       PLOTX1(I)=R
       LP=RP
C
C      CALCULATE 'REAL' COMPONENT
       PASS=1
       IFAIL=1
       CALL D01DAF(0.D0,PI2,PHI3,PHI4,FUN11,ABSACC,AMPR,NPTS,IFAIL)
C/////
C       WRITE (6,7700) PASS,AMPR,NPTS
C7700  FORMAT(' PASS',I2,'INTEGRAL=',G14.7/' NO. OF FN EVALUATIONS=',I6)
C/////
       IF (IFAIL.GT.0) WRITE (6,9060) PASS,IFAIL,I,J
C      REPEAT CALL FOR 'IMAGINARY' COMPONENT
160    PASS=2
       IFAIL=1
       CALL D01DAF(0.D0,PI2,PHI3,PHI4,FUN12,ABSACC,AMPI,NPTS,IFAIL)
C//////
C       WRITE (6,7700) PASS,AMPI,NPTS
C//////
       IF (IFAIL.GT.0) WRITE(6,9060) PASS,IFAIL,I,J
C   CALCULATE AMPLITUDE MAGNITUDE. (!)
170    AMP=DSQRT(AMPR*AMPR + AMPI*AMPI) *K/PI2
       PLOTY1(I)=AMP
220    CONTINUE
230    WRITE (25) (PLOTY1(I),I=1,COLUMNS)
C
C      STEP RADIALLY OFF AXIS AND REPEAT PLOT
C
       ZETA=ZETA+SSTEP*1.D-3
250    CONTINUE
C
C      OUTPUT TIME TAKEN FOR INTEGRATION
```

ii) Functions.

```
C      FUN11.FT V2A JJN  2-SEP-81
C      FUNCTION PROGRAM PLOTCW.FT V5.4.2
C      USES  DIFFERENTIAL TO EVALUATE SURFACE ELEMENT AND
C      EVALUATES SQ &QP CORRECTLY.
C      CONTAINS MIRROR 2
C      LOAD WITH PLOTCW.
CCCCCCCCCCCCCCCCCCCCCCCCCCCCCCCCCCCCCCCCCCCCCCCCCCCCCCCCCCC

       DOUBLE PRECISION FUNCTION FUN11(BP,CHI)
       REAL*8 BP,CHI,Z
       REAL*8 ZETA,AP,LP,K
       REAL*8 DIFF
       REAL*8 DENOMR,EXPONENT,NUMATOR
       COMMON /FUN/ ZETA,LP
C*****
C      VARIABLE NAMES CF. FUJIWARA'S EQN.
C      RHO=BP,L=AP,LDASH=LP
C*****
C      FOR SPEED WAVENUMBER,K, IS GIVEN FOR
C      5 MHZ & 1520 M/SEC.
       DATA K /20668.373/
C#####
C      MIRROR DEPENDANT STATEMENT
       Z=1.25D-1 - DSQRT(1.5625D-2 - BP*BP)
       DIFF=(1.25D-1 - Z)/BP
C      SOURSE POSITION
       AP=1.25D-1
C#####
       FUN11= BP*DSIN(K*(DSQRT(BP*BP+(Z-AP)**2)+
      $            DSQRT(ZETA*ZETA+BP*BP+(LP-Z)**2-2*ZETA*BP*DCOS(CHI))))
      $  / (DSIN(DATAN(DIFF))*
      $      (ZETA*BP*DCOS(CHI)-BP*BP-Z*Z+Z*(AP+LP)-AP*LP))
       RETURN
       END
C      FUN12.FT V2A JJN  2-SEP-81
C      FUNCTION FOR PROGRAM PLOTCW.FT V5.4.2
C      USES  DIFFERENTIAL TO EVALUATE SURFACE ELEMENT AND
C      EVALUATES SQ &QP CORRECTLY.
C      CONTAINS MIRROR2
C      LOAD WITH PLOTCW.
CCCCCCCCCCCCCCCCCCCCCCCCCCCCCCCCCCCCCCCCCCCCCCCCCCCCCCCCCCC

       DOUBLE PRECISION FUNCTION FUN12(BP,CHI)
       REAL*8 BP,CHI,Z
       REAL*8 ZETA,AP,LP,K
       REAL*8 DIFF
       REAL*8 DENOMR,EXPONENT,NUMATOR
       COMMON /FUN/ ZETA,LP
C*****
C      VARIABLE NAMES CF. FUJIWARA'S EQN.
C      RHO=BP,L=AP,LDASH=LP
C*****
C      FOR SPEED WAVENUMBER,K, IS GIVEN FOR
C      5 MHZ & 1520 M/SEC.
       DATA K /20668.373/
C#####
C      MIRROR DEPENDANT STATEMENT
       Z=1.25D-1 - DSQRT(1.5625D-2 - BP*BP)
       DIFF=(1.25D-1 - Z)/BP
C      SOURCE POSITION
       AP=1.25D-1
C#####
       FUN12= BP*DCOS(K*(DSQRT(BP*BP+(Z-AP)**2)+
      $        DSQRT(ZETA*ZETA+BP*BP+(LP-Z)**2-2*ZETA*BP*DCOS(CHI))))
      $   / (DSIN(DATAN(DIFF)) *
      $     (ZETA*BP*DCOS(CHI)-BP*BP-Z*Z+Z*(AP+LP)-AP*LP))
       RETURN
       END
```

Appendix 3. The 'Instruction' Sets for operating PLOTCW and PLOTCWX

a) PLOTCW

PLOTCW is controlled through its instruction node. It is intended that all normal operations and alterations to the program can be made from here without leaving the program. The exception to this is changing the mirror being examined. For the reasons explained in section 4.2.2. this requires changing the object program which cannot be done while the program is running. All instructions are four characters long. They are primarily executed through subroutines, which receive data and system parameters by common blocks. EMAS commands and packages are used.

ECHO

Combines two plots to give a pulse-echo field. A tool for examining systems where transmission and reception are by different devices. It combines data from curves 1 and 2 and places the result in curve 3. It tests the imput data to check that it is compatible and gives an informative message if it is not. It is, however, up to the operator to check that the fields are positioned correctly, relative to one another; the program simply pairs successive points. Affected parameters and flags are reset to match the new curve.

EXIT

To stop the program. Any data not output will be lost. Therefore, flags set for unused data are checked and queried before the program is stopped.

GRPH

To output all calculated data in a graph plotter file. The EMAS Graphics package (Edinburgh Regional Computing Centre, 1979) is used to create this file. Channels 7Ø — 79 are used for this output into data files PLOTSTOREØ — 9. These channels are declared by the main program. The data is checked to ensure it can all be output on the same plot. The data may be altered by this subroutine. The curves may be plotted as they are or they may be scaled to give them a common peak value. Alternatively the y-scale may be set for comparison with other plots. The plots are labelled with the system parameters currently set.

HELP

Gives a list of possible instructions.

INPUT

Inputs curves from channels 15, 16 or 17. These curves will have previously been stored using the STOR instruction. The input is checked against any current curves which are protected against incompatible input. Overwriting is queried, warnings of possible risks are given and the instruction aborted if input would be fatal to the program.

LIST

Outputs a graph plotter file on a hard copy plotter. An EMAS subroutine is used to invoke the EMAS command GPLIST and any PLOTSTOREn may be listed.

LOGS

All data is converted to decibels. Normally the highest pressure of all three curves is taken as the ØdB level but the user may arbitarily select any level. As each curve is converted to logarithms, a flag is set. If the curve is already in decibels, then it is unaltered by the subroutine.

MERG

This instruction merges overlapping curves. If there is no overlap between the curves it will simply compress them together, perhaps freeing one or two curves for further calculations. If points do overlap, it will sort them in order of increasing position co-ordinate.

NNEW

To study a new system. All parameters may be reset and the current data will be overwritten. If this data has not been read in some way the instruction will be queried before execution.

NORM

The curves are rescaled to give them a common, user selected, peak value.

NUMB

Outputs the current data in a table to the interactive terminal on either the Appleton Tower (LP14) or George Square (LP4Ø) line printers using channels 14 or 4Ø respectively. Once again the channels are declared by the main program. Any single curve or all these calculated may be listed.

PHON

Simulates the output of a hydrophone of finite size plotting the beam. The beam is averaged over the diameter of the detector. The result is only approximate since the averaging is one, not two dimensional. The size of the hydrophone is input by the user.

SMLR

Runs the main program again for a system similar to the last one calculated. Any parameters may be changed and the result is stored in the first empty curve. If all three curves are full, the last one will be overwritten but only after checking with the user.

STOR

Outputs any selected curve to the file defined on channel 15, 16 or 17. The channel definitions are made outside the program, normally by a macro program run automatically at logging-on. Under these circumstances, curves may be added to the channel 15 file but 16 and 17 will only hold one curve - being overwritten if another is output. However channel definitions may be changed from EMAS command level before running the program.

TIDY

Discards any selected curve. An attempt to discard data that has never been output will be queried.

TRIM

Discards selected points from the end of curves.

TXRX

Simulates a pulse-echo field by squaring the transmission field.

VARI

Call the EMAS diagnostic routine DIAG. This will list the current values of all available variables and then continue with the program. Normally parts of the main loop will not be available as the object programs in use will have been compiled using the OPTimized parameter (See section 3.2.7).

VIEW

Invokes the EMAS command TVIEW (Emas Graphics Package, Chapter 5, ERCC 1979) to display graph plotter files on a Tektronix or Tektronix compatible Graphics VDU.

b) PLOTCWX

The primary method of controlling PLOTCWX and manipulating its date is through external programs.

NNEW

To plot another matrix. Most parameters may be reset but the source position, the frequency, the sound velocity in the medium and the size of the plotting matrix may not.

SYMV

Calls the SYMVU package and outputs the data as a three dimensional plotter file with a square grid base. The file PLOTCONTROL is used to control SYMVU. The plotter file is created with the name PLOTSYMVU.

HELP

Gives a list of possible INSTRUCTIONS.

VARI

Calls the EMAS Diagnostic routine. Normally this will be uninformative as the whole program will be compiled using the OPT parameters.

EXIT

To leave the program.

Additionally the following programs support analysis of the PLOTCWX data matrix.

The suffix 'a' indicates a run number for the program PLOTCWX. A diary is kept of run numbers and parameters set.

SYMVUDATAn and FIELDS-Sn are data files storing the results of PLOTCWX runs. As soon as possible after a run is over, the contents of PLOTDATA are copied here for safety. As the initial time and cost for calculating the data is high, all subsequent manipulations are done on SYMVUDATAn or copies of it and the copy in the partitioned file FIELDS is used only to back up SYMVUDATAn.

Storing all the data in one file, FIELDS, not only saves space but makes housekeeping of the data easy and less prone to errors.

With the data at this level, four forms of processing are possible.

SYMERGE If a plot is completed in more than one batch job, then data may be merged into one matrix. The output data files are put into channels 31-33, in order, from the axis working out. SYMERGE will put the merged data into a single file on Channel 25.

HYDROPHONE This program alters the data in Channel 25 (nominally the file PLOTDATA) to resemble the field seen by a hydrophone. This is similar to the PLOTCW Instruction 'PHON'. However, here no flag is set to say that this has been done. The data is kept in the files HYDRODATAn and FIELDS-Hn which are directly analogous to SYMVUDATAn and FIELDS-Sn and will be handled in exactly the same way by all the following programs.

PLOTSYMVU performs in exactly the same way as the instruction SYMV reading data from channel 25.

PLOTSYMn#a and PLOTHYDn#a are SYMVU plotter files as created by 'SYMV' or PLOTSYMVU; PLOTHYD being 'hydrophone' imitations. 'n' indicates the run number, 'a' a plot number since more SYMVU plots may be made after further processing. A diary is kept with the parameters used for these plots.

SYMVU on its own is limited since the plot assumes a square grid of data. To obtain a better plot, the data may be put through the SYMAP package which purports to produce a contour map on a line printer. It interpolates between points and will produce an output file specifically for input to SYMVU.

First the data must be prepared to input to SYMAP.

SYMDATA is a program which converts an unformatted data file in channel 25 to a formatted one in channel 2Ø ready for input to SYMAP. x and y co-ordinates are also required and SYMAPPT creates a file of those in channel 21. If the array being plotted is not 25 x 15, this file must be remade at the correct size.

SYMAP reads from Channels 20 and 21. It requires the file PLOTCONTROL which may be edited to alter parameters. It includes a title for the 'map' output which is normally sent to a character file. This file must be examined to obtain the matrix size of the SYMVU file. SYMAP outputs the SYMVU input file to Channel 8 which has the file name SYMVUMAP.

SYMVUMAPn and HYDROMAPn are descendants of SYMVUDATAn and HYDRODATAn respectively after processing by SYMAP. They are copied from SYMVUMAP.

SYMVU may then be used to prepare a three dimensional plotter file from SYMVUMAPn. The control file for this is VUCONTROL which is edited to give the correct matrix size, title, etc.

BIBLIOGRAPHY

ACKERMAN, L.V.; KATENSTEIN, A.L. (1977). The concept of minimal breast cancer and the pathologist role in the diagnosis of 'Early Carcinoma'. Cancer 39; 2772 - 2782.

A.I.U.M. Bio-effects Committee (1976). Biological Effects of Ultrasonic Energy on living mammals. Ultrasound in Medicine and Biology 2, 35.

ARCHER-HALL, J.A.; ALI-BASHTER, A.L.; HAZELWOOD, J.A. (1979) A means for computing the Kirchhoff surface integral for a disk radiator as a single integral with fixed limits. J. Acoust. Soc. Am. 65(6) p.p. 1568 - 1770.

ARCHER-HALL, J.A.; ALI-BASHTER, A.I. (1980). The Diffraction Pattern of Large Aperture bowl Transducers. NDT International, April, p.51 - 55.

ARCHER-HALL, J.A.; DEE, G. (1980). A Single Integral Computer Method for Axisymmetric Transducers with Various Boundary Conditions. NDT International, June, p.95 - 101.

ARDITI, M.; FOSTER, F.S.; HUNT, J.W. (1981). Transient Fields of Concave Annular Arrays. Ultrasonic Imaging 3, 37 - 61.

ARDITI, M.; TAYLOR, W.B.; FOSTER, F.S.; HUNT, J.W. (1982). An Annular Array for High Resolution Breast Echography. Ultrasonic Imaging Vol.4. Jan.

BABCOCK, P.C. (1977). Ultrasonic Scanning in the Radiotherapy Dept. Clin. Radiol. 28(3): 287 - 293 May.

BACON D.R. (1982). Characteristics of a PVDF Membrane Hydrophone for use in the range 1 - 100 MHz. IEEE Son Ul 29(1): 18 - 25.

BAILER, J.C. III. (1976) Mammography: a contrary view. Ann. Intern. Med. 84, 77.

BAILER, J.C. III. (1978). Mammographic screening: a re-appraisal of the benefits and risks. Clin. Obstet. Gynecol. 21, 1.

BAINTON, K.F.; SILK, M.G. (1980). Some Factors which affect the Performance of Ultrasonic Transducers. The British Journal of Non-Destruction Testing. January, Vol.22, No.1, p.15.

BAUM, G. (1977). Ultrasound Mammography. Radiology Vol. 122: 199 - 205. January.

BAUM, G. (1978). The need for colour coding in Ultrasound Mammography. J.C.U. 6(2): 76 - 82. April.

BEAVER, WILLIAM L. (1974). Sonic Nearfields of a Pulsed Piston Radiator. J. Acoust. Soc. Am. 56(4) p.1043 - 1048. October.

BEZ-BARDILLI, W. (1935). Uber ein Ultraschall. Total reflectometer zur Messung von Schallgeschwindigheiten sowie der elastischen Konstarten fester Korper, Zeits. f. Physik 96, 761.

BIELKE, C.; NIESWANDT, Z.; KIEFER, H.; LOCH, E.G. (1981). Real-Time Mammosonography with a Special Application Unit. 2nd Internat. Congress on the Ultrasonic Examn. of the Breast, London, June.

BLOOMBERG, T.J.; CHIVERS, T.C.; PRICE, J.L. (1981) Does Ultrasound have a Primary Screening Function for Breast Cancer? 2nd Internat. Congress on the Ultrasonic Examn. of the Breast, London, June.

BOW, C.R. (1979). Ultrasonic Visualisation in Cardiac Structure and Function. Ph.D. thesis. University of Edinburgh.

BRESLOW, L.; THOMAS, L.B.; UPTON, C.A. (1977). Final reports of the NCI ad hoc working groups on mammography in screening for breast cancer and a summary report of their joint findings and recommendations. J. Natl. Cancer Inst. 59, 467.

BREYER, B.; CEPULIC, E.; ZUNTER, F. (1982). Ultrasound Mammography without specialised equipment. Comparison with clinical examination and x-rays. Ultrasound Med. Biol. 8(4), 377 - 379.

BRUEGGEMANN, H.P. (1968). Conic Mirrors. The Focal Press (London and New York).

BURCKHARDT, C.B.; HOFFMAN, H.; GRANDCHAMP, P.A. (1973). Ultrasound Axicon: a device for focussing over a large depth. J. Acoust. Soc. Am. 54(6) 1628 - 30.

BURNS, P.N.; HALLIWELL, M.; WELLS, P.N.T.; WEBB, A.J. (1982) Ultrasonic Doppler Studies of the Breast. Ultrasound Med. Biol. 8, 127 - 143.

CALDERON, C.; WILKOMERSON, D.; HEZRICH, R.; ETZOLD, K.F.; KINGSLEY, B.; HASKIN, M. (1976). Differences in the attenuation of ultrasound by normal benign and malignant breast tissue. J. Clin. Ultrasound 4:249 - 254.

CARMEN, R.; MARTIN, M.; WILKOMERSON, D. (1981). Rapid Review of Multiple Breast Images with Reconstructions in the Coronal and Transverse Image Planes. 2nd Internat. Congress on the Ultrasonic Examn. of the Breast. London, June.

CARSON, P.L.; FISCHELLA, P.R.; OUGHTON, T.V. (1978). Ultrasound in Medicine and Biology, 3(4), 341 - 350.

CHIVERS, R.C.; PARRY, R.J. (1978). Ultrasonic velocity and attenuation in Mammalian tissues. J. Acoust. Soc. Amer. 63(3): 940 - 953. March.

CLEMENT, M.J-M. ALAIS, P. (1981). A 450 Element Toroidal Ring Array for Breast Imaging by Computerised Ultrasonic Tomography. 2nd Internat. Congress on the Ultrasonic Examn. of the Breast. London, June.

COULSON, C.A.; JEFFREY, A. (1977). WAVES - a mathematical approach to the common types of wave motion. 2nd Edit. Longman.

CRYMES, J.E. (1979). Current Status of Mammography. CRC Critical Reviews of Diagnostic Imaging, 11(3), 297 - 333.

DESILETS, C.S.; FRASER, J.D.; KINO, G.S. (1978). The Design of Efficient Broad-Band Piezoelectric Transducers. IEEE Transactions on Sonics and Ultrasonics. Vol. SU-25:3, p.115, May.

DICK, D.E.; BAY, H.P.; CARSON, P.L. (1977). Hardware Design of an Ultrasound CT Scanner. Biomedical Sciences Instrumentation, Vol. 13.

DICK, D.E.; ELLIOTT, R.D.; METZ, R.L.; ROJOHN, D.S. (1979). A new automated high resolution Ultrasound breast scanner. Ultrasonic Imaging 1, pp 368 - 377.

DIETZ, D.R.; NORTON, S.J.; LINZER, M. (1978). Wideband Annular Array Response. Proc. IEEE Ultrason. Symp. Cat. 78CH - 1344-1. SU.

DIETZ, D.R.: (1982). Apodized Conical Focussing for Ultrasound Imaging. IEEE Sonics and Ultrasonics SU-29, 3. pp 128 - 138. May.

DRISCOLL, Walter G. (1978). Handbook of Optics - Optical Society of America. McGraw-Hill.

DUCK, F.A. (1981). The Pulsed Ultrasonic Field. p.97-108 of Physical Aspects of Medical Imaging. Edit. by B.M. Moores, R.P. Parker and B.R. Pullan, John Wiley and Sons.

EISENSCHER, A. (1981). Sonoseismography. 2nd Internat. Congress on the Ultrasonic Examination of the Breast. London, June.

ELLIOT, R.D. (1981). Design of an Automated High Resolution Breast Scanner and Image Review System. 2nd Internat. Congress on the Ultrasonic Examn. of the Breast.

FARROW, S.A; Auld, B.A. (1975). An Acoustic Phase Plate Imaging Device. 6th Internat. Symposium on Acoustical Holography and Imaging, San Diego.

FEIG, S.A. et al. (1977). Analysis of Clinically Occult and Mammographically Occult Breast Tumours. Am J. Roentgenol 128(3):403-408.

FEYNMAN, R.P; LEIGHTON, R.B; SANDS, M. (1963). The Feyman Lectures on Physics, Vol. 1 Addison-Wesley.

FIELDS, S.I. (1980). Ultrasound Mammographic-Histopathologic Correlation. Ultrasonic Imaging 1, pp 150-161.

FISHER, B; SLACK, N.H; BORSS, I.D.J. and co-operating investigators. (1969). The size of breast cancer and prognosis. Cancer (Phila)24,1071.

FOSTER, F.S: HUNT, J.W. (1978). The design and characterisation of short pulse ultrasound transducers. Ultrasonics, May. pp 116-122.

FOSTER, F.S; HUNT, J.W. (1979). Transmission of Ultrasound Beams through Human Tissue - Focussing and Attenuation Studies. Ultrasound in Med. and Biol. Vol. 5, 257-268.

FOSTER, F.S; HUNT, J.W. (1978). The Focussing of Ultrasound Beams through Human Tissue. Acoustic Imaging. Vol 8, pp 709-718. Plenum Press, 1980. Proceeding of 8th Int. Symp. on Acoustical Imaging (Florida).

FOSTER, F.S; PATTERSON, M.S; ARDITI, M. (1981). The Conical Scanner: A Two Transducer Ultrasound Scatter Imaging Technique. Ultrasonic Imaging 3, 62-82

FOX, F.E; GRIFFING, V. (1949). Experimental Investigation of Ultrasonic Intensity Gain in Wager due to Concave Reflectors. J. Acoust Soc. Am 21(4), 351-359. July.

FREEDMAN, A. (1970). Sound Fields of plane or gently curved pulsed radiators. J. Acoust. Soc. Amer. 48. 221-227.

FRIEDRICH, M. (1981). Reflection Ultrasound Computed Tomography of the Breast. 2nd Internat. Congress on the Ultrasonic Examn. of the Breast. London, June.

FRUCHT, A.H. (1953). Die Schallgeschwindigkeit in Menschlichen in Menschlichen und Tierischen Geweben. Z. Gesamte. Exptl. Med. 120, 526-57.

FRY, E. KELLY; KOSSOFF, G.; GIBBON, L.V.; (1969). Characterisation of the normal female breast by Ultrasonic Visualisation Techniques: paper presented at the Meeting of the American Institute of Ultrasound in Medicine, Winnipeg.

FRY, E. KELLY; KOSSOFF, G.; HINDMAN, N.A. (1972). The potential of Ultrasound visualisation for detecting the presence of abnormal structures within the female breast.

FRY, E. KELLY; FRY, F.J.; SANGHUI, N.T.; HEIMBURGER, R.F. (1975). A combined Clinical and Research approach to the problem of Ultrasound visualisation of breast. In Ultrasound in Medicine, Vol. 1, Plenem Press, Ed. D. White pp 309-320.

FRY, E. KELLY; SANGHUI, N.T.; FRY, F.J. (1978). Frequency dependant attenuation of malignant breast tumors studies by the Fast Fourier Transform technique. In Ultrasonic Tissue Characterisation. Ed. by M. Linzer, pp 89-95. NBS Spec. Pub. 525. U.S. Govt. Printing Office.

FRY, W.J.; LEICHNER, G.H.; OKUYAMA, D.; FRY, F.J.; FRY, E.K. (1968). Ultrasound Visualisation system employing new scanning and presentation methods. J. Acoust, Soc. Amer. 44: 1324-1328.

FUJIWARA, S. (1962). Optical Properties of Conic Surfaces I Reflecting Cone. J. Opt. Soc. Amer. 52(3) p 287-92, March.

GLOVER, G.H.; SHARP, J.C.; (1977). Reconstruction of Ultrasonic Propagation Speed Distributions in Soft Tissues. IEEE Trans. Sonics Ultrasonics. SU-24. 229-234.

GOLIS, M.J. (1968) An Analysis of the Ultrasonic Zone Lens. IEEE Trans. Sonics Ultrasonics. Vol. Su-15, No.2 pp 105-10, April.

GREENLEAF, J.F.; JOHNSON, S.A.; SAMAYOA, W.F.; DUCK, F.A. (1975). Algrebraic Reconstruction of Spatral Distributions of Acoustic Velocities in Tissue from their Time-of-Flight Profiles. Acoustical Holography, 6, p.145. Plenum Press, New York.

GREENLEAF, J.F.; JOHNSON, S.A.; LENT, A.H. (1978). Measurement of spatial distribution of refractive index in tissues by Ultrasonic computer assisted tomography. Ultrasound Med. Biol. 3(4): 327-229.

GRIFFING, VIRGINIA; FOX, FRANCIS E. (1949). Theory of Ultrasonic Intensity Gain due to Concave Reflectors. J. Acoust. Soc. Am. 21(4) p.348-351, July.

GULLINO, P.M. (1977). Natural History of breast cancer. Cancer 39: 2697-2703. (June supplement).

HALLIWELL, M. (1976). On the Ultrasonic Field used in Medical Diagnosis. Ph.D. Thesis. University of Bristol.

HALLIWELL, M. (1978). Ultrasonic Beam distortion by normal female breast in VIVO. Ultrasound in Medicine 4: pp 555-6. Edit. by D.N. White and E.A. Lyons. AIUM and Plenum Press. NY.

HAMILTON-SMITH, NEIL. (Originator). (1979). ERCC Graphics Manual. Edinburgh Regional Computing Centre. (Revised Sept. 1980)

HARAN, M.E.; COOK, B.D. (1983). Distortion of Finite Amplitude Ultrasound in Lossy Media. J. Acoust. Soc. Am. 73 pp 774-779.

HARPER, A.P.; FRY, E. Kelly; NOE, J.S. (1981). Ultrasound breast imaging - the method of choice for examining the young patient. Ultrasound Med. Biol. 7(3), 231-7.

HARRIS, GERALD R. (1981). Review of transient field theory for a baffled planar piston. J. Acoust. Soc. Am. July. Vol 70(1) pp 10-20.

HAYASHI, S.; WAGAI, T.; MIYAZAWA, R.; ITO, K.; ISHIKAWA, S.; UEMATSU, K.; KIKUCHI, Y.; UCHIDA, R. (1962). Ultrasound diagnosis of breast tumor and cholelithisis. Western Journal of Surgery, Obstetrics and Gynacology, Vol. 70, 34-40.

HOLLEB, A.I.; VENET, L.; DAY, E. (1960). Breast cancer detected by routine physical examination. N.Y. State, J. Med., 60, 823.

HOWRY, D.H.; STOTT, D.A.; BLISS, W.R. (1954). Ultrasonic visualisation of carcinoma of the breast and other soft tissue structures. Cancer, N.Y. 7. 354-8.

HUNT, J.W.; ARDITI, M.; FOSTER, F.S. (1983). Ultrasound Transducers for Pulse-Echo Medical Imaging. IEEE Transaction on Biomedical Engineering, Vol. BME-30(8(pp 453-481, August.

JELLINS, J.; KOSSOFF, G.; BUDDEE, F.W.; REEVE, T.S. (1971). Ultrasonic Visualisation of the Breast. Med. J. Aust. 1: 305-

JELLINS, J.; KOSSOFF, G.; REEVE, T.S.; BARRACLOUGH, B.H. (1975). Ultrasonic, Grey-scale visualisation of breast disease. Ultrasound Med. Biol. 1(4): 373-404. March.

JELLINS, J.; KOSSOFF, G.; REEVE, T.S. (1977). Detection and classification of liquid-filled masses in the breasts by gray-scale echography. Radiology 125 (1): 205-12. October.

JENKINS, F.A.; WHITE, H.E. (1976). Fundamentals of Optics. McGraw-Hill Kogakusha Ltd. 4th Edition. IBSN 0-07-032330-5.

KAYE, G.W.C.; LADY, T.H. (1957). Tables of Physical and Chemical Constants. Longman. Velocity of sound, pp 63-4. pp 101, 171.

KINSER, L.E; FREY, P. (1965). Fundamentals of Acoustics. 2nd Editn. Wiley, New York.

KOBAYASHI, T; TAKATANI, O; HATTORI, N; KIMURA K. (1972). Study of sensitivity graded ultrasonotomography (Preliminary Report) - Evaluation upon 64 cases with breast tumor and representation 'malignant echo-like pattern' seen in two cases with fat necrosis in breast. Med. Ultrasonics 10, 38-40.

KOBAYASHI, T; TAKATANI, O; KIMURA, K; WATANBE, H; ABE, O. (1972). Clinical investigation for the differential diagnosis of breast tumor by means of the graded sensitivity method of Ultrasonotomography (2nd report) - Proposal of new differential diagnostic criteria:tadpole-tail sign with lateral shadow (benign) and acoustic middle shadow sign (malignant) and its clinical significance and evaluation. Med. Ultrasonics 10, 81-6.

KOBAYASKI, T. (1975). Review: Ultrasonic diagnosis of breast cancer. Ultrasound Med. Biol. 1(4):383-91.

KOBAYASHI, T. (1977). Gray-scale Echography for Breast Cancer. Radiology Vol. 122(1): 207-214.

KOSSOFF, G. (1966). The Effects of Backing and Matching on the Performance of Piezoelectric Ceramic Transducer. IEEE Transactions on Sonics and Ultrasonics. Vol. SU-13, No.1, March. p.20.

KOSSOFF, G; ROBINSON, D.E; GARNETT, W.J. (1968). Ultrasonic Two-dimensional Visualisation for Medical Diagnosis. J. Acoust. Soc. Am. 44. 1310-1318.

KOSSOFF, G; FRY, E. Kelly; JELLINS, J. (1973). Average velocity of Ultrasound in the human, female breast. J. Acoust. Soc. Amer. 53(6): 1730-1736. January.

KOSSOFF, G; GARROTT, W.S; CARPENTER, D.A. et al (1976) Principles and classification of soft tissues by gray-scale echography. Ultrasound Med. Biol. 2:89-105.

KOSSOFF, G. (1978). Diagnostic Ultrasound - the view fròm down ùnder. JCU 6(3):144-9. June.

LANGELAND, P. ( ). Population screening for female tumours. Acta Radiol. Suppl., 297.

LAUSTELA, E; KERMINEN, T; LIETO, J; TALA, P. (1966). Studies of Ultrasonic diagnosis of breast tumours. Annls. Chir. Gynaec. Fenn 55, 173-5.

LEES, W.R. (1981). Real-Time Compression Studies. Applicatn. in Sympomatic Women and in Screening. 2nd Internat. Congress on the Ultrasonic Examn. of the Breast.

LESTER, R.G. (1977). The risks versus benefit in breast cancer. Radiology 124, 1.

LIGHTHILL, J. (1978). Waves in Fluids. Cambridge University Press.

LOCKWOOD, J.C; WILLETTE, J.G. (1973). High speed method for computing the exact solution for the pressure variations in the nearfield of a baffled piston. J. Acoust. Soc. Am. 53, 735-741.

LYPACEWICZ, G; HILL, C.R. (1974). Choice of standard target for medical pulse-echo equipment evaluation. Ultrasound Med. Biol. 1, 287-9.

LYPACEWICZ, G; PIECHOCHI, M; POWALOWSKI, T; LUKALUSKA, K; ZOMER, J. (1981). Examns. of blood flow in breast tumours with Ultrasonic Doppler Method. Clinical Experience and Problems. 2nd Internat. Congress on the Ultrasonic Examn. of the Breast. London, June.

MACOVSKI, A; NORTON, S.J. (1975). High-Resolution B-Scan systems using a circular array. Acoustical Holography, Vol. 6. N. Booth, Ed. New York: Plenum. pp 121-143.

MATIN, R.W. (1977). Power transfer effects of backing impedance with thickness made ultrasonic transducers under complex conjugate matching. IEEE Ultrasonics Symposium Proceedings. pp 416-421.

McDICKEN, W.N. (1981). Diagnostic Ultrasound. Principles and use of instruments. 2nd Edit. Academic Press, New York.

McLEOD, J.H. (1954). The Axicon: A new type of optical element. Journal of the Optical Society of America. Vol. 44(8), pp 592-597.

McWHIRTER, R. (1948). Discussions on the treatment of Cancer of the Breast. Proc. R. Soc. Med., pp 122-129.

MINASIAN, H; BAMBER, J.C. (1982). A preliminary assessment of an ultrasonic Doppler method for the study of blood flow in human breast cancer. Ultrasound. Med. Biol. 8(4), 357-64.

MOSES, A.J. (1978). The Practising Scientists Handbook. Van Nostrand Reinhold Coy.

NAG Library Manual, Mk9. (1982). National Algorithms Group.

OLOFSSON, S. (1963). An Ultrasonic Optical Mirror System. Acustca, Vol. 13, pp 361-367.

O'NEIL, H.T. (1949). Theory of Focussing Radiators. J. Acoust. Soc. Am. 21(5), 516-26, September.

PASSMORE, R; ROBSON, J.S; Edits-in-Chief. (1968). A companion to medical studies, Vol. 1. Blackwell.

PATTERSON, M.S; FOSTER, F.S. (1982). Acoustic Fields of Conical Radiators. IEEE Transactions on Sonic and Ultrasonics. Vol. SU - 29, p83-92. March.

PATTERSON, M.S; FOSTER, F.S. (1983). The improvement and quantitative assessment of B-made images. Produced by an Annular Array/Cone Hybrid. Ultrasonic Imaging 5, p.195-213.

PATTERSON, T.N.S. (1968). Maths. Comp. Vol. 22, pp 847-856 and 877-881.

PELMORE, J.M. (1977). The Ultrasonic Properties of some filled epoxy materials. Ultrasonics International. Conference proceedings.

PATRAKIS, N.L. (1977). Genetic Factors in the Etiology of Breast Cancer. Cancer 39:2709-2715. June Supplement.

PIGGINS, J.M; McDICKEN, W.N; NICOLL, J.J. (1981). A Versatile Scanner for Ultrasonic Examination of the Breast. 2nd International Congress on the Ultrasonic Examination of the Breast.

PRESTON, R.C. (1983). Measurement and Characterisation of ultrasonic fields using hydrophones in the frequency range 0.5 MHz to 15 MHz. IEC Technical Committee 29. Electra - acoustics, sub-comm. 292. Ultrasonics Draft prepared for working group 8.

PYE, D.W. (1983). Medical Ultrasonics: Dynamic focussing in Diagnostic Imaging. Ph.D. thesis, University of Edinburgh.

QUATE, C.F. (1976). Fresnel Zone Plate as a lens in Acoustic Imaging (Ed. G. Wade). Plenum Press.

RAYLEIGH, J.W.S; (1945). The Theory of Sound. Dover, New York. Vol. II.

SCARBOROUGH, R. (1978). Proceedings of the SHARE Meeting, pp 561-567. In ERCC Library.

SCHOCH, A. (1941). Betrachtungen Uber des Schallfeld einer holbenmembran. Akoust. Z., 6, 318-326.

SEIDMAN, H. (1977). Screening for breast cancer in younger women: life expectancy gains and losses. Cancer 27, 66.

SETTE, Danielle. (1949). Ultrasonic Lenses of Plastic Materials. J. Acoust. Soc. Am. 21(4), 375-381. July.

SHAPIRO, S. (1977). Evidence on Screening for breast cancer from a randonized trial. Cancer 39:2772-2782. June Supplement.

SHOTTON, K.C; BACON, D.R; QUILLIAM, R.M. (1980). A PVDF membrane hydrophone for operation in the range 0.5 MHz to 15 MHz. Ultrasonics Vol 18, pp 123-126.

SMITH, S.M.R.S; AWOJOBI, A.O. (1979). Factors in the Design of Ultrasonic Probes. Ultrasonics, January, page 20.

SPIESBERGER, W. (1979). Mammogram Inspection by Computer. IEEE Transactions on Biomedical Engineering, Vol. BME-26(4) April, page 213.

STEPHANISHAN, P.R. (1971). Transient Radiation from Pistons in an Infinite Planar Baffle. J. Acoust. Soc. Am. 49, 1629-1638.

STEWART, H. (1980). The Management of Primary Breast Cancer - Yesterday, Today and Tomorrow. Edinburgh Medicine, September.

TARNOCZY, T. (1965). Sound Focussing lenses and Waveguides. Ultrasonics, 3. 115-27.

TEIXIDOR, H.S; KAZAM, E. (1977). Combined mammographic-sonographic evaluation of breast masses. Am. J. Reontgenol. 128(3): 403-408.

THURSTONE, F.L; McKINNEY, W.M. (1965). Focussed Transducer Arrays in an Ultrasonic Scanning System for Biological Tissue. Diagnostic Ultrasound - proceedings of the First International Conference. University of Pittsburgh. pp 191-194. (Plenum Press, New York. 1966).

VILKOMERSON, E. (1974). Acoustic imaging with thin annular apertures. Acoustical Holography, Vol. 5, P.S. Green, Ed. New York, Plenum. pp 121-143.

VILKOMERSON, D. (1981) Considerations in the Design of Ultrasonic Breast Screening Systems. 2nd Internat. Congress on the Ultrasonic Examn. of the Breast. London, June.

WAGAI, T. (1981). Echographic Differentation of Histological Structure of Breast Cancer and Enhancement of Breast Cancer. Images by Ultrasound Irradiation. 2nd Internat. Congress on the Ultrasonic Examn. of the Breast. London, June.

WEAST, R.C. (1969-70). CRC Handbook of Chemistry and Physics. 50th Edition. The Chemical Rubber Co. p.E41.

WEIGHT, J.P; HAYMAN, A.J. (1978). Observations of the propagation of very short ultrasonic pulses and their reflection by small targets. J. Acoust. Soc. Am., 63, 396-404.

WELLS, P.N.T; EVANS, K.T. (1968). An immersion scanner for two dimensional ultrasonic examination of the human breast. Ultrasonics, 6. 220-8.

WELLS, P.N.T. (1977). Biomedical Ultrasonics. Academic Press.

WEYNS, A. (1980). Radiation field calculations of pulsed ultrasonic transducers. Part 1. planar circular, square and annular transducers. Ultrasonics, July. p.183-188. Part 2. spherical disc - and ring - shaped transducers. Ultrasonics, Sept. 1980. p.219-223.

WHITE, D.N; CLEDGETT, P.R. (1978). Breast Carcinoma Detection. By Ultrasonic Doppler Signals. Ultrasound in Med. and Biol. 4(4): 329-335.

WHITING, J.F; KOCK, R; PRICE, D.C; KOJROWICZ, E; HOCKEY, G; FISHER, G; McCAFFREY, J.F. (1981). Interpretation of Breast Transmission Tomograms obtained by Reconstruction of Ultrasonic Velocity Distributions. Instrumentation, Methods and Consequences. 2nd Internat. Congress on the Ultrasonic Examn. of the Breast.

WHITTINGHAM, T.A. (1981). Real-Time Ultrasonic Scanning in Physical Aspects of Medical Imaging. Edit. by B. Moores, R. Parker, B. Pullan. Wiley and Sons.

WILD, J.J; NEAL, D. (1951). The use of high frequency ultrasonic waves for detecting changes in living tissues. Lancet, 1: 655-657.

WILD, J.J; REID, J.M. (1952). Further pilot echographic studies on the histological structure of living, intact human breast. Am. J. Path (1952) 28, p.839-61.

WOLFE, J.N. (1976). (a) Breast patterns as an index of risk for developing breast cancer. Am. J. Roentgenal, 126, 1131. (b) Risk for breast cancer development determined by mammographic parenchymal pattern. Cancer (Phila) 37, 2486.

ZEMANEK, J. (1971). Beam behaviour within the Nearfield of a Vibrating Piston. J. Acoust. Soc. Am. Vol 49, No. 1(Part 2) pp 181-91.